VESTIBULAR CONTRIBUTIONS TO HEALTH AND DISEASE, VOLUME II - DEDICATED TO BERNARD COHEN

EDITED BY: Richard Lewis and Michael Strupp
PUBLISHED IN: Frontiers in Neurology

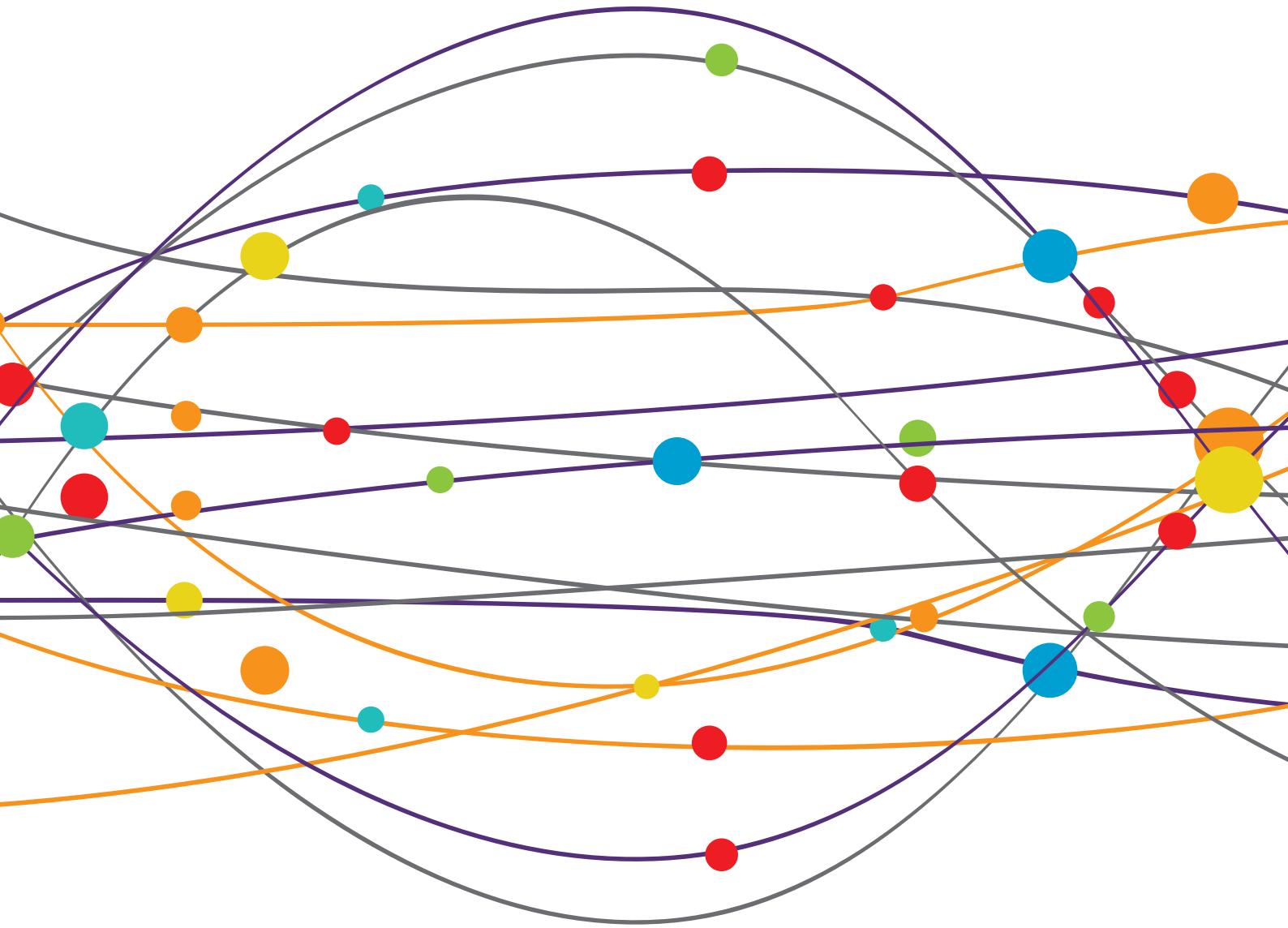

frontiers Research Topics

frontiers

ISSN 1664-8714
ISBN 978-2-88971-706-4
DOI 10.3389/978-2-88971-706-4

About Frontiers

Frontiers is more than just an open-access publisher of scholarly articles: it is a pioneering approach to the world of academia, radically improving the way scholarly research is managed. The grand vision of Frontiers is a world where all people have an equal opportunity to seek, share and generate knowledge. Frontiers provides immediate and permanent online open access to all its publications, but this alone is not enough to realize our grand goals.

Frontiers Journal Series

The Frontiers Journal Series is a multi-tier and interdisciplinary set of open-access, online journals, promising a paradigm shift from the current review, selection and dissemination processes in academic publishing. All Frontiers journals are driven by researchers for researchers; therefore, they constitute a service to the scholarly community. At the same time, the Frontiers Journal Series operates on a revolutionary invention, the tiered publishing system, initially addressing specific communities of scholars, and gradually climbing up to broader public understanding, thus serving the interests of the lay society, too.

Dedication to Quality

Each Frontiers article is a landmark of the highest quality, thanks to genuinely collaborative interactions between authors and review editors, who include some of the world's best academicians. Research must be certified by peers before entering a stream of knowledge that may eventually reach the public - and shape society; therefore, Frontiers only applies the most rigorous and unbiased reviews.
Frontiers revolutionizes research publishing by freely delivering the most outstanding research, evaluated with no bias from both the academic and social point of view. By applying the most advanced information technologies, Frontiers is catapulting scholarly publishing into a new generation.

What are Frontiers Research Topics?

Frontiers Research Topics are very popular trademarks of the Frontiers Journals Series: they are collections of at least ten articles, all centered on a particular subject. With their unique mix of varied contributions from Original Research to Review Articles, Frontiers Research Topics unify the most influential researchers, the latest key findings and historical advances in a hot research area! Find out more on how to host your own Frontiers Research Topic or contribute to one as an author by contacting the Frontiers Editorial Office: frontiersin.org/about/contact

VESTIBULAR CONTRIBUTIONS TO HEALTH AND DISEASE, VOLUME II - DEDICATED TO BERNARD COHEN

Topic Editors:
Richard Lewis, Harvard University, United States
Michael Strupp, Ludwig Maximilian University of Munich, Germany

Citation: Lewis, R., Strupp, M., eds. (2021). Vestibular Contributions to Health and Disease, Volume II - Dedicated to Bernard Cohen. Lausanne: Frontiers Media SA. doi: 10.3389/978-2-88971-706-4

Table of Contents

frontiers in Neurology

EDITORIAL
published: 01 October 2021
doi: 10.3389/fneur.2021.760822

Editorial: Vestibular Contributions to Health and Disease, Volume II-Dedicated to Bernard Cohen

Richard F. Lewis[1,2]* *and Michael Strupp*[3,4]

[1] Departments of Otolaryngology and Neurology and Harvard Medical School, Boston, MA, United States, [2] Jenks Vestibular Diagnostic and Physiology Laboratories, Massachusetts Eye and Ear, Boston, MA, United States, [3] Department of Neurology, Ludwig Maximilians University, Munich, Germany, [4] German Center for Vertigo and Balance Disorders, Munich, Germany

Keywords: vestibular, physiology, pathophysiology, labyrinth, brain, disease

Editorial on the Research Topic

Vestibular Contributions to Health and Disease, Volume II-Dedicated to Bernard Cohen

INTRODUCTION

The first volume of "Vestibular Contributions to Health and Disease," published in 2018 in *Frontiers in Neurology*, sought to "highlight some of the basic science and clinical findings that have arisen over the 1st years of the twenty-first century" with regard to central and peripheral vestibular physiology and pathophysiology (1). That collection of papers was conceived and co-edited by Bernard Cohen, M.D. (universally known as Bernie) who was the driving force behind its development and completion. Bernie had an enormous passion for this project and was jubilant when it received the Spotlight Award from *Frontiers* as the best ebook collection of the year, which led to a large, international meeting at Bernie's institution, Mount Sinai Medical School in New York City in the fall of 2019. Tragically, Bernie became ill prior to the meeting, was unable to attend it, and passed away shortly after it concluded. We (RFL and MS) and *Frontiers* felt that an appropriate memorial to Bernie's life and work would be to produce a second volume of this ebook collection in his memory and honor.

Volume II contains a number of tributes to Bernie from his colleagues and these review his scientific career in detail, so we will keep our introductory remarks relatively brief. It is difficult to overstate Bernie's importance to the vestibular field, as he was one of the giants who helped define our current understanding of the vestibular system. While his *scientific* work spanned more than five decades and covered numerous aspects of peripheral and central vestibular physiology, he is perhaps best known for his investigations on the "velocity storage" mechanism in the brain, which he elucidated in many elegant studies with his long-time collaborator Ted Raphan (2). Although velocity storage was initially identified as a mechanism that improved the brain's estimate of low-frequency angular head velocity (3), it subsequently became clear that it is a critical aspect of central vestibular function since it underlies the brain's ability to synthesize the angular velocity inputs from the semicircular canals with the gravito-inertial inputs from the otolith organs (4). This canal-otolith integration contributes significantly to our ability to estimate head motion and orientation as we move through our terrestrial environment, and may also be a key to the spatial disorientation and motion sickness experienced by patients with central or peripheral vestibular dysfunction and by astronauts in microgravity.

While he was best known for his scientific work, Bernie was an M.D. and a trained *neurologist*, and maintained a clinical practice at Mount Sinai throughout his long tenure there. Indeed,

Edited and reviewed by:
Toshihisa Murofushi, Teikyo University Mizonokuchi Hospital, Japan

***Correspondence:**
Richard F. Lewis
richard_lewis@meei.harvard.edu

Specialty section:
This article was submitted to Neuro-Otology, a section of the journal Frontiers in Neurology

Received: *18 August 2021*
Accepted: *01 September 2021*
Published: *01 October 2021*

Citation:
Lewis RF and Strupp M (2021) Editorial: Vestibular Contributions to Health and Disease, Volume II-Dedicated to Bernard Cohen. Front. Neurol. 12:760822. doi: 10.3389/fneur.2021.760822

applying scientific observations to improve understanding of clinical vestibular problems was one of the hallmarks of his career. For example, Bernie was the first to demonstrate that vestibular afferent nerves could be activated using implanted electrodes (5), work which has been fundamental to the development of the vestibular prosthesis (6, 7); he became fascinated with vestibular-autonomic interactions (8) and the possibility that the aberrant orthostatic responses that can underlie fainting could be habituated using vestibular stimulation; and he sought to understand the pathophysiology of mal de debarquement syndrome (MdDS), and with his colleagues Sergei Yakushin and the late Mingjia Dai, developed the first treatment approach for this recalcitrant disorder (9) which is currently being tested in a clinical trial.

Finally, Bernie was beloved by colleagues because of his *personal* qualities. He enjoyed an extensive network of friends and collaborators in the vestibular field around the world, many of whom contributed to the first and second editions of this ebook. While we cannot speak for the numerous colleagues who worked with him for decades, one of us (RFL) had the honor and pleasure of working with Bernie for several years as a co-editor of the first edition of this ebook collection, and found that Bernie combined two rare features—-a warm humanism evidenced by his immense generosity and loyalty; and a sharp, didactic mind that was constantly active. He was a rare individual and while his many friends and colleagues miss him greatly, we also are appreciative that we were able to share part of our professional and personal lives with him.

SECTION 1 – TRIBUTES AND HISTORICAL PAPERS

Bernie provided a heartfelt tribute (Cohen) to his long-time collaborator, Mingjia Dai, who initially come from Australia for a post-doctoral fellowship, spent his entire subsequent career working with Bernie at Mount Sinai, and died from cancer in 2019. Dai focused his research on human subjects and much of his late career was spent studying MdDS and developing a novel approach to treat patients with this intractable disorder. Guyot et al. provide a tribute to Bernie's scientific accomplishments and in particular focus on his work in the 1960's when he and Suzuki first showed that individual canal ampullary nerves could be activated with stimulation provided by electrodes implanted in the canal's ampulla (5). This work provided the foundation for the vestibular prosthesis, which has been in development for the past two-decades in animal models and has more recently moved into clinical trials (7). Maruta provides another tribute to Bernie and his scientific contributions, tracing the broad range of his research interests and contributions which touch on nearly all aspects of vestibular function. Finally, Straka et al. provides an overview of the work of Steinhausen, which previously was only available in German. They describe the pioneering work Steinhausen performed in the early 20th century in which he deduced the relationship between cupular displacement and vestibular-mediated eye movement responses.

SECTION 2 – MAL DE DEBARQUEMENT SYNDROME

Bernie focused much of his late career on mal de debarquement syndrome (MdDS), a disorder where patients continue to feel as if they are moving after they experience passive vehicular motion (10), and MdDS was therefore well-represented in Volume I of "Vestibular Disorders in Health and Disease" and at the meeting based on that volume. The three articles on MdDS in the current volume examine different aspects of this disorder's pathophysiology and potential approaches to therapy. Mucci et al. propose that neural loops between the vestibular nuclei and the cerebellar nodulus and uvula form an oscillator that cancels the postural disturbance produced by vehicular motion (e.g., in a boat) but can become pathologically potentiated and produce the persistent feeling of motion experienced by patients with MdDS. Cha et al. use functional and structural imaging in MdDS patients and found abnormalities that support aberrant sensitization of limbic structures in the brain. Based on these observations, they propose that non-invasive brain stimulation (e.g., transcranial magnetic stimulation) may be able to attenuate the synchronized oscillations in these brain regions that may underlie the persistent illusion of motion in MdDS. Yakushin et al. extend the MdDS treatment approach developed at Mount Sinai, which utilizes head motion coupled to optokinetic stimulation, to a virtual reality stimulus provided by a portable app that patients can utilize at home. In a small study, they showed promising results using this method, as all of the treated MdDS patients noted substantial symptomatic improvement after treatment.

SECTION 3 – VESTIBULAR-AUTONOMIC INTERACTIONS

The relationship between the vestibular and autonomic nervous systems has been a relatively neglected area of vestibular physiology, and Bernie became fascinated with this topic late in his career. In particular, he sought to understand the contributions of the vestibular system to orthostatic hypotension (8) and the potential susceptibility of these interactions to therapy. The current volume contains three articles that focus on vestibular-autonomic interactions. Raphan and Yakushin, both long-time collaborators of Bernie's, applied machine learning to train their model of vasovagal responses, and with this approach defined a hyperplane that segregates normal and pathologic blood pressure responses to changes in body orientation. Rice et al. activated vertical semicircular canals using infrared light and were able to modulate autonomic behaviors with this approach, indicating that the vertical canals (and not only the otolith organs) provide sensory information that is used to regulate cardiovascular responses. Bielanin et al. recorded from brainstem regions that have been proposed to use vestibular inputs to modulate cardiovascular responses (the medullary lateral tegmental field and the nucleus solitarius tract) in awake felines and found that more than a third of neurons in these regions responded to large static head tilts, implying that these

regions constitute part of the central vestibulo-sympathetic reflex pathway.

SECTION 4 – VESTIBULAR SCIENCE

Seven papers focus on other aspects of vestibular science and include physiologic and behavioral studies.

Vestibular Physiology

Curthoys provides a tribute to Yoshio Uchino, reviewing his contributions to the understanding otolith function and its clinical testing (11). Uchino elegantly demonstrated that activating hair cells that were located on different sides of the strioloa and had opposing polarizations elicited central responses that summed rather than canceled, and that utricular signals in the brain have inhibitory commissural projections that recapitulate the "push-pull" processing of central semicircular canal signals. These observations provide a context for the clinical otolith tests that utilizes sound or vibration to activate the saccules or utricles, respectively. Barmack and Pettorossi review the vestibulo-cerebellum adaptation that occurs in response to prolonged vestibular and optokinetic stimulation, and in particular, describe the relationship between behavioral (e.g., eye movement) and molecular biologic (e.g., corticotropin releasing factor) manifestations of cerebellar adaptation that contribute to postural control.

Vestibular-Mediated Behaviors

Two papers examine *eye movements* in normal human subjects and specifically investigate characteristics of the central velocity-to-position neural integrator initially demonstrated by Robinson (12). Ritter et al. describes the characteristics of gaze-evoked nystagmus and rebound nystagmus in people without otologic or neurologic disease. By quantifying these eye movement characteristics in normal subjects, they provide information which improves the ability to determine when these oculomotor findings are abnormal and indicative of underlying cerebellar disease. Lädrach et al. examined Alexander's law [slow phase velocity increases when the eyes are directed toward the nystagmus quick phase, (13)] in normal subjects by measuring post-rotatory nystagmus with the head upright or tilted. Their results support the hypothesis that Alexander's law results from an asymmetry in neural integrator function rather than a gradual adaptive process. Lackner reviewed a series of studies that demonstrate the effects of haptic stabilization introduced by light touch on *balance*. He posits the presence of a long-loop cortical reflex whereby sensory cues from the hand modulate motor activity in the legs and thereby reduce postural sway, and suggests that this mechanism is important for patients with vestibular damage and for astronauts experiencing microgravity. Two papers examined vestibular effects on *perception* and *cognition*. Wedtgrube et al. studied the effects of prolonged static tilt and optokinetic stimulation on the subjective postural vertical (e.g., the ability to align the body's longitudinal axis parallel to gravity). They found that prolonged tilt biases the subjective postural vertical in a manner that is consistent with Bayesian models since the "prior" is presumable shifted by the long-term static tilt. Dobbels et al. demonstrate that bilateral vestibular damage does not appear to affect performance on a virtual Morris water maze (vMWM) that is performed with the head stationary (e.g., a condition where no dynamic vestibular responses are elicited). This result contradicts those of a prior study (14) and suggests that visuo-spatial processing may not be affected by the absence of vestibular inputs. Conversely, an alternate explanation for their findings is that the vMWM is an inadequate assay of these visuo-spatial functions in human subjects.

SECTION 5 – VESTIBULAR DISORDERS

Eight papers examined aspects of vestibular dysfunction, including peripheral vestibular damage, central compensation, the real-world behavioral consequences of vestibular damage.

Peripheral Disorders–Meniere's Disease

Two papers examine how vestibular testing is affected by Meniere's Disease, including the primary form of the disease (etiology unknown) and the secondary form [also called delayed endolymphatic hydrops, where an initiating event can be identified, (15)]. Leng and Liu measured caloric and video head impulse tests (vHIT) in nineteen patients with delayed endolymphatic hydrops, and while the majority of patients had abnormal caloric responses, only a small minority had abnormal horizontal canal vHIT results. They suggest that this pattern of test findings may be a distinctive feature of delayed endolymphatic hydrops. Kaci et al. reviewed the literature on vHIT testing in patients with Meniere's Disease and proposed possible pathophysiologic explanations for these findings.

Peripheral Disorders–Other Etiologies

Three papers considered other types of peripheral vestibulopathies, including those caused by noise exposure, aging, and covid. Stewart et al. reviewed the effects of noise on vestibular function and described that noise can induce both peripheral and central vestibular damage in animals, particularly in the otolith organs. Much less is known about noise effects in humans, however, but saccular-collic reflexes appear to be damaged by noise, perhaps because the saccule can be activated by sound in a manner that is not recapitulated by other vestibular end-organs. Wagner et al. reviewed the effects of aging on vestibular dysfunction and its effects on balance. They indicate that the contribution of age-related vestibular damage to the imbalance associated with aging remains poorly understood and that further work is required elucidate this connection more accurately. Li et al. review the relationship between covid-19 and symptoms of dizziness and vertigo in China. They report that the etiology of dizziness shifted between the pre and per covid time frames, with an increase in benign positional vertigo and psychogenic dizziness, and a decrease in "vascular" vertigo. While these results are not readily explainable, they do support the contention that medical providers should be aware of these shifts when evaluating vestibular patients during the covid epidemic.

Central Compensation After Peripheral Damage

Two papers addressed issues related to the compensation that occurs in the brain after the vestibular periphery is damage. McGarvie et al. used vHIT to assess recovery of the vestibulo-ocular reflex (VOR) in a patient with bilateral sequential vestibular neuritis over a period of 500 days. They found that VOR recovery occurred with an exponential time course that depended on the velocity of the head motion stimulus, as responses to low-velocity head rotations had a time constant of about 100 days, but responses to high-velocity rotations improved more slowly with a time constant of about 150 days. Tarnutzer et al. examined VOR changes in patients with a unilateral vestibular schwannoma if they receive intratympanic gentamicin in the ear with the tumor prior to surgical resection of the schwannoma. As predicted, the VOR gain was reduced after intratympanic gentamicin injections, but the anterior canal was largely spared for uncertain reasons. They conclude that if gentamicin injections are provided prior to vestibular schwannoma surgery, the severity of the post-surgical vestibular deficit (e.g., vertigo, imbalance) may be reduced since a more gradual and controlled reduction in vestibular function occurred prior to surgical deafferentation of one vestibular nerve.

Real-World Consequences of Peripheral Vestibular Damage

van Leeuwen et al. provide the perspective of vestibular patients on the difficulties encountered when driving. They asked vestibular patients to complete a questionnaire about driving and from 432 responses concluded that 44% experienced difficulties driving. Furthermore, physicians rarely discussed driving issues or appropriate precautions with the vestibular patients. They opinioned that physicians should discuss driving issues with vestibular patients since these driving difficulties can limit their ability to work and perform other normal daily tasks.

CONCLUSIONS

This second edition of "Vestibular Contributions to Health and Disease" covers a wide range of vestibular topics, including normal vestibular physiology and abnormal vestibular disease processes. More specifically, Bernie's late career interests of normal (vestibulo-autonomic) and abnormal (MdDS) vestibular topics both receive considerable attention. In conclusion, Bernie's many friends and colleagues miss him greatly and we hope that this *Frontiers* ebook collection dedicated to his memory provides a small indication of the high regard he was held by all as a scientist, a clinician, and a person.

AUTHOR CONTRIBUTIONS

RL and MS contributed equally to the writing of this editorial. Both authors contributed to the article and approved the submitted version.

REFERENCES

1. Cohen B, Lewis R. Editorial: Vestibular contributions to health and disease. *Front Neurol.* (2018) 9:117. doi: 10.3389/fneur.2018.00117
2. Raphan T, Cohen B. Velocity storage and the ocular response to multidimensional vestibular stimuli.7 *Rev Oculomot Res.* (1985) 1:123–43.
3. Raphan T, Matsuo V, Cohen B. Velocity storage in the vestibulo-ocular reflex arc (VOR). *Exp Brain Res.* (1979) 35:229–48. doi: 10.1007/BF00236613
4. Wearne S, Raphan T, Cohen B. Effects of tilt of the gravito-inertial acceleration vector on the angular vestibuloocular reflex during centrifugation. *J Neurophysiol.* (1999) 81:2175–90. doi: 10.1152/jn.1999.81.5.2175
5. Cohen B, Suzuki JI, Bender MB. Eye movements from semicircular canal nerve stimulation in the cat. *Ann Otol Rhinol Laryngol.* (1964) 73:153–69. doi: 10.1177/000348946407300116
6. Lewis RF. Vestibular implants studied in animal models: clinical and scientific implications. *J Neurophysiol.* (2016) 116:2777–88. doi: 10.1152/jn.00601.2016
7. Chow MR, Ayiotis AI, Schoo DP, Gimmon Y, Lane KE, Morris BJ, et al. Posture, gait, quality of life, and hearing with a vestibular implant. *N Engl J Med.* (2021) 384:521–32. doi: 10.1056/NEJMoa2020457
8. Cohen B, Martinelli GP, Ogorodnikov D, Xiang Y, Raphan T, Holstein GR, et al. Sinusoidal galvanic vestibular stimulation (sGVS) induces a vasovagal response in the rat. *Exp Brain Res.* (2011) 210:45–55. doi: 10.1007/s00221-011-2604-4
9. Dai M, Cohen B, Smouha E, Cho C. Readaptation of the vestibulo-ocular reflex relieves the mal de debarquement syndrome. *Front Neurol.* (2014) 5:124. doi: 10.3389/fneur.2014.00124
10. Cohen B, Dai M, Smouha E, Cho C. Mal de debarquement syndrome. *Neurol Clin Pract.* (2015) 5:369–70. doi: 10.1212/01.CPJ.0000472925.22196.a2
11. Uchino Y, Kushiro K. Differences between otolith- and semicircular canal-activated neural circuitry in the vestibular system. *Neurosci Res.* (2011) 71:315–27. doi: 10.1016/j.neures.2011.09.001
12. Cannon SC, Robinson DA, Shamma S. A proposed neural network for the integrator of the oculomotor system. *Biol Cybern.* (1983) 49:127–36. doi: 10.1007/BF00320393
13. Robinson DA, Zee DS, Hain TC, Holmes A, Rosenberg LF. Alexander's law: its behavior and origin in the human vestibulo-ocular reflex. *Ann Neurol.* (1984) 16:714–22. doi: 10.1002/ana.410160614
14. Brandt T, Schautzer F, Hamilton DA, Brüning R, Markowitsch HJ, Kalla R, et al. Vestibular loss causes hippocampal atrophy and impaired spatial memory in humans. *Brain.* (2005) 128:2732–41. doi: 10.1093/brain/awh617
15. Schuknecht HF. Delayed endolymphatic hydrops. *Ann Otol Rhinol Laryngol.* (1978) 87:743–8. doi: 10.1177/000348947808700601

Conflict of Interest: The authors declare that the research was conducted in the absence of any commercial or financial relationships that could be construed as a potential conflict of interest.

frontiers in Neurology

OPINION
published: 13 December 2019
doi: 10.3389/fneur.2019.01196

Dedication to Mingjia Dai, Ph.D. for Discovery of the First Successful Treatment of the Mal de Debarquement Syndrome

Bernard Cohen[*†]

Department of Neurology, Icahn School of Medicine at Mount Sinai, New York, NY, United States

Keywords: vestibular, vestibulo-cerebellar, motion sickness, velocity storage, nodulus

INTRODUCTION

It is with deep sadness that we note the passing of Mingjia Dai, Ph.D. Assistant Professor of Neurology on February 7th, 2019, from esophageal and lung cancer. He was 71 years old.

Dai grew up in Guangzhou, China, and completed his Ph.D. in Sydney, Australia with Drs. Michael Halmagyi and Ian Curthoys. In 1989, he came to Mount Sinai to work with Dr. Cohen. Dai was an innovative, imaginative scientist who loved working with patients. He dedicated the later part of his life to studying a rare neurological disorder, the Mal de Debarquement Syndrome (MdDS). His warmth and ability to establish relationships with patients affected by MdDS made him famous in the US and all over the world.

BACKGROUND

In 1979, Drs. Raphan and Cohen at Mount Sinai (1) and Robinson at John's Hopkins (2) discovered that a process in the vestibular nuclei functioned to extend the angular velocity-related information generated in the semicircular canals. Raphan and Cohen labeled the process as a Velocity Storage Integrator, since it described the dynamic integration of the head rotation velocity. They characterized it by the time constants of the cellular activity at the beginning and end of rotation. A few years later, with Dai, they discovered that Velocity Storage acted as a gyroscope to orient the axis of eye rotation to the spatial vertical, regardless of the position of the axis of body rotation (3, 4). This led to the discovery that Velocity Storage was an integral part of the process that produced motion sickness (5), and that susceptibility to motion sickness fell along with reductions in the time constant of Velocity Storage (6). Following this with data from Solomon and Wearne that Velocity Storage was controlled by the nodulus of the vestibulo-cerebellum (7–10), they found that motion sickness could be extinguished by repeated vestibular testing that shortened the vestibular time constant (5, 6, 11).

DAI'S STUDIES THAT DETERMINED THE CAUSE OF THE MAL DE DEBARQUEMENT SYNDROME

In 2009, based on experiments in monkeys using an unusual paradigm, continuous rotation in darkness, coupled with side to side roll (roll while rotation, RWR), Dai had a brilliant insight. He reasoned that the prolonged exposure to this maneuver had produced some of the essential clinical signs in the monkey observed in patients with MdDS (12). Namely, there was positional nystagmus with upward quick phases when the head was rolled to one side. From it, he postulated that roll

OPEN ACCESS

Edited by:
Jose Antonio Lopez-Escamez, Andalusian Autonomous Government of Genomics and Oncological Research (GENYO), Spain

Reviewed by:
Eduardo Martin-Sanz, Hospital de Getafe, Spain
Vincent Van Rompaey, University of Antwerp, Belgium

***Correspondence:**
Bernard Cohen
bernardcohen999@gmail.com

[†]*Deceased*

Specialty section:
This article was submitted to Neuro-Otology, a section of the journal Frontiers in Neurology

Received: *16 August 2019*
Accepted: *28 October 2019*
Published: *13 December 2019*

Citation:
Cohen B (2019) Dedication to Mingjia Dai, Ph.D. for Discovery of the First Successful Treatment of the Mal de Debarquement Syndrome. Front. Neurol. 10:1196. doi: 10.3389/fneur.2019.01196

while rotation had caused a shift in the "eigen vector" in roll, i.e., the central representation of gravity, and that MdDS might be the result of this shift in the roll vector (13). In other experiments, neither spontaneous vestibular nystagmus, nor unusual positional nystagmus occurred in monkeys with a very short vestibular time constant, confirming that the Velocity Storage Integrator had played a critical role in producing MdDS (1, 13).

DAI'S TREATMENT OF THE MDDS

Dai then devised a treatment to reverse this vestibular maladaptation. He rolled the head back and forth at the frequency of the perceived body oscillations, while watching a slowly moving full field optokinetic stimulus moving against the vestibular imbalance as determined by the Fukuda Stepping Test (14). The OKN reoriented Velocity Storage back to the spatial vertical (15). Remarkably, the sensed body oscillations were 0.2 Hz after the sea voyages in almost all of the MdDS sufferers, indicating that the MdDS was being generated by a disordered rhythm, likely in the vestibular and vestibulo-cerebellar systems (13).

A critical aspect of the treatment was that the direction of the optokinetic stimulus had to be opposite to the direction of a vestibular imbalance that had been produced during the roll while rotation or by travel on the sea. If the movement of the OKN stripes was in the direction of the vestibular imbalance determined by the Fukuda Stepping Test, the MdDS patients became worse, and, as shown by Mucci et al. (16) if the OKN stripes did not move, the patients had no improvement.

Of note, the primary findings were in the body and limbs and not in the eyes in the Vestibulo-Ocular Reflex (VOR), and there was only rarely spontaneous nystagmus in these patients. This series of maneuvers is described in detail in a publication (of which Dai was the first author) in 2014 (17).

RESULTS

With the Dai et al. treatment, there was an immediate improvement rate of 75%, in 17 of 24 patients (17). This treatment also relieved the motion sickness susceptibility of these subjects, predominantly women (18). In about 25 percent of the MdDS patients in the 2017 study, the initial improvement of 75 percent fell back to 50 percent after 1 month, but in that 50 percent the improvement was then maintained for a year or more (18).

It should be emphasized that this was the first and only successful treatment in patients who had been suffering for up to 15 to 20 years. The successful treatment of the MdDS has been carried on by Dai's colleague, Sergei Yakushin, Ph.D., Associate Professor of Neurology. Further experiments are being performed by Dr. Yakushin to determine if the improvement after the initial treatment can be stabilized by reducing the Velocity Storage time constant. This study is based on Dai's work that showed that motion sickness is reduced by reducing the vestibular time constant that underlies Velocity Storage (15). A comprehensive review of the MdDS can be found in a paper by Van Ombergen et al. (19). Additionally, a recent study indicated that the signs and symptoms of the MdDS could be produced by the movement of subjects on an oscillating platform that generated pitch, yaw and roll at low frequencies (20). This confirms that the MdDS is generated in the vestibular system.

CONCLUSION

Dr. Dai's singular achievement in formulating the first successful treatment of the MdDS is remarkable, and I would like to have it noted by future physicians who use it to relieve its signs and symptoms. As such, I would like this treatment to be named the Dai treatment for the Mal de Debarquement Syndrome.

There is another reason to laud Dai's approach to treat MdDS. Namely, to my knowledge, this is the first medical treatment in the vestibular system that uses correction of a disordered rhythm and a return of a disordered orientation of the Eigenvector to gravity to cure a clinical condition. As such, it opens a new level of clinical treatment that could lead us to a deeper understanding of the interaction of the vestibular nuclei and the vestibulo-cerebellum, as well as to a better understanding of the neural basis of balance.

AUTHOR CONTRIBUTIONS

The author confirms being the sole contributor of this work and has approved it for publication.

ACKNOWLEDGMENTS

I thank Jun Maruta, Ph.D., Viviana Mucci, Ph.D., Sofia Moen, and Asher El Hanani for their help.

REFERENCES

1. Raphan T, Matsuo V, Cohen B. Velocity storage in the vestibulo-ocular reflex arc (VOR). *Exp Brain Res*. (1979) 35:229–48. doi: 10.1007/BF00236613
2. Robinson DA, editor. *Vestibular and Optokinetic Symbiosis: An Example of Explaining by Modeling*. Amsterdam: Elsevier (1977).
3. Dai MJ, Raphan T, Cohen B. Spatial orientation of the vestibular system: dependence of optokinetic after-nystagmus on gravity. *J Neurophysiol*. (1991) 66:1422–39. doi: 10.1152/jn.1991.66.4.1422
4. Raphan T, Cohen, B. The vestibulo-ocular reflex in three dimensions. *Exp Brain Res*. (2002) 145:1–27. doi: 10.1007/s00221-002-1067-z
5. Cohen B, Dai M, Yakushin SB, Cho C. The neural basis of motion sickness. *J Neurophysiol*. (2019) 121:973–82. doi: 10.1152/jn.00674.2018
6. Dai M, Kunin M, Raphan T, Cohen B. The relation of motion sickness to the spatial-temporal properties of velocity storage. *Exp Brain Res*. (2003) 151:173–89. doi: 10.1007/s00221-003-1479-4
7. Solomon D, Cohen, B. Simulation of the nodulus and uvula discharges velocity storage in the vestibulo-ocular reflex. *Exp Brain Res*. (1994) 102:57–68. doi: 10.1007/BF00232438

8. Wearne S, Raphan T, Cohen B. Nodulo-uvular control of central vestibular dynamics determines spatial orientation of the angular vestibulo-ocular reflex (aVOR). *Ann N Y Acad Sci*. (1996).781:348–63. doi: 10.1111/j.1749-6632.1996.tb15713.x
9. Wearne S, Raphan T, Waespe W, Cohen B. Control of the three-dimensional characteristics of the angular vestibulo-ocular reflex by the nodulus and uvula. *Prog Brain Res*. (1997) 114:321–34. doi: 10.1016/S0079-6123(08)63372-5
10. Wearne S, Raphan T, Cohen B. Control of spatial orientation of the angular vestibulo-ocular reflex by the nodulus and uvula. *J Neurophysiol*. (1998) 79:2690–715. doi: 10.1152/jn.1998.79.5.2690
11. Reason J. Motion sickness adaptation: a neural mismatch model. *J R Soc Med*. (1978) 71:819–29. doi: 10.1177/014107687807101109
12. Dai M, Raphan T, Cohen B. Adaptation of the angular vestibulo-ocular reflex (aVOR) to head movements in rotating frames of reference. *Exp Brain Res*. (2009) 195:553–67. doi: 10.1007/s00221-009-1825-2
13. Cohen B, Yakushin SB, Cho C. Hypothesis: the vestibular and cerebellar basis of the Mal de Debarquement Syndrome. *Front Neurol*. (2018) 9:28. doi: 10.3389/fneur.2018.00028
14. Fukuda T. The stepping test, two phases of the labyrinthine reflex. *Acta Otolaryngol*. (1959) 50:95–108. doi: 10.3109/00016485909129172
15. Dai M, Raphan T, Cohen B. Prolonged reduction of motion sickness sensitivity by visual-vestibular interaction. *Exp Brain Res*. (2011) 210:503–13. doi: 10.1007/s00221-011-2548-8
16. Mucci V, Perkisas T, Jillings SD, Van Rompaey V, Van Ombergen A, Fransen E, et al. (2018). Sham-controlled study of optokinetic stimuli as treatment for Mal de Debarquement Syndrome. *Front Neurol*. 9:887. doi: 10.3389/fneur.2018.00887
17. Dai M, Cohen B, Smouha E, Cho, C. Re-adaptation of the vestibulo-ocular reflex relieves the Mal de Debarquement Syndrome. *Front Neurol*. (2014) 5:124. doi: 10.3389/fneur.2014.00124
18. Dai M, Cohen B, Cho C, Shin S, Yakushin SB. Treatment of the Mal de Debarquement Syndrome: a 1-year follow-up. *Front Neurol*. (2017) 8:175. doi: 10.3389/fneur.2017.00175
19. Van Ombergen A, Van Rompaey V, Maes LK, Van de Heyning PH, Wuyts FL. Mal de Debarquement syndrome: a systematic review. *J Neurol*. (2016) 263:843–54. doi: 10.1007/s00415-015-7962-6
20. Schepermann A, Bardins S, Penkava J, Brandt T, Huppert D, Wuehr M. Approach to an experimental model of Mal de Debarquement Syndrome. *J Neurol*. (2019) 266(Suppl. 1):74–9. doi: 10.1007/s00415-019-09345-6

Conflict of Interest: The author declares that the research was conducted in the absence of any commercial or financial relationships that could be construed as a potential conflict of interest.

frontiers in Neurology

ORIGINAL RESEARCH
published: 12 May 2020
doi: 10.3389/fneur.2020.00362

Dissociation of Caloric and Video Head Impulse Tests in Patients With Delayed Endolymphatic Hydrops

*Yangming Leng and Bo Liu**

Department of Otorhinolaryngology, Union Hospital, Tongji Medical College, Huazhong University of Science and Technology, Wuhan, China

Delayed endolymphatic hydrops (DEH) represents a rare clinical entity characterized by intermittent vertigo attacks mimicking those of Ménière's disease (MD) in a patient with a prior sensorineural hearing loss. Some vestibular tests have been employed in patients with DEH. These tests provide useful diagnostic information and facilitate clinical decision-making. Here, we retrospectively studied the features of video head impulse test (vHIT) and examined its relationship with caloric test used in DEH patients. Included in this study were 17 patients with ipsilateral DEH and 2 with contralateral DEH. Among them, 73.7% (14/19) showed abnormal caloric test response (76.5% in ipsilateral DEH and 50% in contralateral DEH). Meanwhile, only 15.8% (3/19) of patients yielded abnormal horizontal vHIT results (11.8% in ipsilateral DEH and 50% in contralateral DEH). Abnormal caloric response in the presence of a preserved vHIT was common in DEH patients, especially those with ipsilateral DEH. This dissociation might be a distinctive pattern of vestibular deficit in DEH.

Keywords: delayed endolymphatic hydrops, caloric test, video head impulse test, VOR, semicircular canal

OPEN ACCESS

Edited by:
Richard Lewis,
Harvard University, United States

Reviewed by:
Adrian Priesol,
Harvard Medical School, United States
Jameson Mattingly,
Ohio State University Hospital, United States

***Correspondence:**
Bo Liu
liuboent@hust.edu.cn

Specialty section:
This article was submitted to Neuro-Otology, a section of the journal Frontiers in Neurology

Received: *07 February 2020*
Accepted: *14 April 2020*
Published: *12 May 2020*

Citation:
Leng Y and Liu B (2020) Dissociation of Caloric and Video Head Impulse Tests in Patients With Delayed Endolymphatic Hydrops. Front. Neurol. 11:362. doi: 10.3389/fneur.2020.00362

INTRODUCTION

Vestibular test is designed to assess the status of the vestibular system objectively and quantitatively. Over the last decade, vestibular test has evolved greatly, and the horizontal and vertical semicircular canals (SCC) as well as the otolith organs can be examined separately (1). Traditionally, the caloric test has been used for the assessment of the vestibulo-ocular reflex (VOR) function of horizontal SCC by using a non-physiological stimulus in a frequency ranging 0.002–0.004 Hz (2). Video head impulse test (vHIT) extends the testing range to physiological high frequency (5–7 Hz) (3). The relationship between these two VOR tests has been investigated in multiple vestibular disorders, such as Ménière's disease (MD), vestibular neuritis, vestibular migraine, benign paroxysmal positioning vertigo (BPPV), enlarged vestibular aqueduct (EVA), among others (2, 4, 5). Recently, a dissociation between caloric test and vHIT was found to be common in patients with MD (6, 7), and has therefore been suggested as an instrumental hallmark of MD (5).

Delayed endolymphatic hydrops (DEH), a rare clinical entity, is characterized by episodic vertigo of delayed onset following profound sensorineural hearing loss (SNHL), and its symptoms mimic those of MD (8). Kamei et al. for the first time, reported the association between "juvenile-onset unilateral profound deafness" and delayed onset of vertigo in 1971 (9). In 1973, when investigating the pathological features in a case of profound congenital deafness with delayed-onset vertigo, Schuknecht and Wright presumed that endolymphatic hydrops (ELH) secondary to fibrous obliteration of the vestibular aqueduct might underlie vertigo (10). Nadol et al. and Wolfson and

Leiberman also described the unilateral deafness with subsequent vertigo in 1975 (11, 12), and suggested the hydropic change due to obliteration of the vestibular aqueducts could cause this delayed-onset vertigo. Furthermore, Schuknecht proposed a hypothesis postulating that an initial labyrinthine insult leads to total disruption of cochlear but preserves vestibular function, and then results in secondary atrophy or fibrous obliteration of the endolymphatic resorptive system (13). In 1978, Schuknecht coined the term DEH to describe the delayed development of recurrent vertigo attacks in the context of a pre-existing profound SNHL, and put DEH in the category of ipsilateral and contralateral DEH (14).

Although many vestibular tests have been applied in patients with DEH, including the electronystagmography (15), caloric test (15, 16), rotatory chair (15), and vestibular evoked myogenic potentials (VEMPs) (16, 17), no study examined vHIT or the relationship between caloric test and vHIT in these patients. Our study aimed to look into the features of these two VOR tests in DEH patients, and to explore their implications in the diagnosis of ELH or hydropic ear disease.

MATERIALS AND METHODS

Study Population

A single-center retrospective study was conducted in the Department of Otorhinolaryngology, Union Hospital affiliated to Tongji Medical College, Huazhong University of Science and Technology, Wuhan, China.

Nineteen patients with DEH were diagnosed by experienced neurotologists against the diagnostic criteria formulated by the committee of the Japan Society for Equilibrium Research in 1987 (18): The ipsilateral DEH was diagnosed if (1) a prior event characterized by profound SNHL in one ear (precedent deafness); (2) delayed development of vertigo attacks without fluctuating hearing loss in the opposite ear; and (3) exclusion of central nervous system lesions, eighth nerve tumors, and other cochleovestibular diseases, such as syphilitic labyrinthitis. The diagnosis of the contralateral DEH was made if (1) a prior deafness in one ear; (2) delayed development of fluctuating hearing loss in the opposite ear that is sometimes associated with episodic attacks of vertigo; and (3) exclusion of central nervous system lesions, eighth nerve tumors, and other cochleovestibular diseases like syphilitic labyrinthitis. Profound SNHL was defined as a pure tone average of $>$90 dB over the 500, 1,000, and 2,000 Hz frequencies.

Exclusion criteria included: (1) middle or inner ear infections (otitis media, mastoiditis, labyrinthitis, etc.); (2) middle or inner ear anomaly (common cavity malformation, semicircular canal dysplasia, EVA, etc.); (3) having received previous ear surgery or intratympanic injections; (4) retro-cochlear lesions (vestibular schwannoma, internal acoustic canal stenosis, etc.); (5) head trauma; (6) systemic diseases; (7) disorders of central nervous system (vestibular migraine, multiple sclerosis, cerebellar infarction, etc); (8) having taken alcohol, caffeine or medications that would affect the results of vestibular tests (sedative, anti-depressant drugs, etc.) within 48 h before testing.

This study was conducted in strict accordance with the tenets of the Declaration of Helsinki. Informed consent was obtained from each patient and the project was approved by the ethical committee of Tongji Medical College of Huazhong University of Science and Technology, Wuhan, China.

Methods

All patients with DEH during the interictal period underwent a battery of tests, including otoscopy, audiometry, videonystagmography, caloric test, horizontal vHIT in the same day. Non-contrast magnetic resonance imaging (MRI) was routinely performed to rule out middle or inner ear infection and malformation. If retro-cochlear lesion was suspected, the patient would receive contrast-enhanced MRI.

Pure-Tone Audiometry

Pure-tone audiometry was conducted in a soundproof room, at 125, 250, 500, 1,000, 2,000, 4,000, and 8,000 Hz. Pure tone average (PTA) was calculated to be the simple arithmetic mean for frequencies of 500, 1,000, and 2,000 Hz.

Videonystagmography

Vestibular tests were performed by using an infrared videonystagmography system (Visual Eyes VNG, Micromedical Technologies, Chatham, IL, USA) in accordance with a standard test protocol, including spontaneous nystagmus test, gaze test, saccades, smooth pursuit, and optokinetic test. The Dix-Hallpike and Roll tests were also videonystagmugraphically performed.

The bithermal caloric test was conducted by using infrared videonystagmography. The subject lay supine with their head and upper trunk elevated at 30°. Each ear was irrigated alternately with a constant flow of air, with the temperature for warm or cool stimulation set at 50 and 24°C, respectively. The duration of each caloric irrigation lasted 60 s. Upon each irrigation, the maximum slow phase velocity (SPV_{max}) of caloric nystagmus was measured, and the canal paresis (CP) was calculated by using the traditional Jongkees' formula. In this study, if the asymmetry of the caloric nystagmus between the left and right ear was $\geq$25%, CP was considered significant in the horizontal SCC, indicating an abnormal caloric response. According to the published criteria (19), if the summated SPV_{max} of the nystagmus was $<$20°/s under four stimulation conditions, the caloric response is believed to indicate bilateral vestibular hypofunction. In this case, ice water irrigation (4°C, 1.0 ml) would be used to confirm the caloric unresponsiveness.

Horizontal Video Head Impulse Testing

The horizontal SCC vHIT was conducted using an ICS Impulse system (GN Otometrics, Denmark) in accordance with the manufacturer's instructions by experienced technicians. Each subject wore a pair of lightweight, tightly-fitting goggles equipped with a small video oculography camera to record and analyze the eye movement. Patient was seated upright facing the wall 1.0 m away and was instructed to fixate a static target on the wall. The patient's head was passively and randomly rotated to the left and right with a low amplitude (5∼15°) and at a high peak velocity (150∼250°/s) in an abrupt, brief and unpredictable manner. At

TABLE 1 | The clinical features and audio-vestibular data in 19 patients with delayed endolymphatic hydrops.

Patient no.	Age	Gender	Cause of deafness	Age at onset of deafness	Age at onset of vertigo	Side	Type	PTA		Caloric		Horizontal vHIT
								Right	Left	Response/ weak side	CP (%)	Response/ affected side
1	65	M	Unknown	Early childhood	40	R	ipsil-	SO	26	A/R	43	Negative
2	31	M	SSHNL	28	29	R	ipsil-	93	5	A/R	36	Negative
3	30	M	Unknown	Early childhood	27	R	ipsil-	SO	8	A/R	36	Negative
4	20	F	Unknown	Early childhood	18	L	contra-	101	78	A/R	27	Positive/R
5	60	F	Unknown	Early childhood	50	L	contra-	SO	36	N	1	Negative
6	59	F	SSHNL	44	59	R	ipsil-	SO	15	A/R	29	Negative
7	44	F	Unknown	Early childhood	33	R	ipsil-	SO	15	N	22	Negative
8	13	F	Unknown	Early childhood	11	L	ipsil-	10	91	A/L	35	Negative
9	54	F	Unknown	Early childhood	54	R	ipsil-	SO	23	A/R	54	Negative
10	26	F	Unknown	Early childhood	22	R	ipsil-	SO	13	A/R	41	Negative
11	61	F	Unknown	Early childhood	47	L	ipsil-	23	SO	A/L	26	Negative
12	22	F	Unknown	Early childhood	22	L	ipsil-	10	SO	N	22	Negative
13	29	M	Unknown	Early childhood	26	R	ipsil-	106	11	N	3	Negative
14	25	F	Unknown	5	24	L	ipsil-	15	SO	A/L	85	Negative
15	16	M	Unknown	Early childhood	10	L	ipsil-	5	105	A/L	100	Positive/L
16	58	F	Unknown	Early childhood	51	R	ipsil-	98	16	A/R	100	Negative
17	56	M	Meningitis	Early childhood	56	L	ipsil-	18	SO	A/L	84	Negative
18	56	F	SSHNL	40	46	L	ipsil-	13	SO	N	19	Negative
19	15	M	Unknown	6	15	L	ipsil-	15	100	A/R	100	Positive/R

PTA, pure tone average, which was established as the simple arithmetic mean for frequencies of 500, 1,000, and 2,000 Hz; Ipsil-, ipsilateral type; Contra-, contralateral type; CP, canal paresis; R, right side; L, left side; SO, scale out; A, abnormal; N, normal. SSNHL, sudden sensorineural hearing loss.

least 20 head impulses were delivered in each direction. Re-fixation saccades were categorized, in terms of their appearance, as covert and overt. If the velocity of the saccade exceeded 50°/s, they were deemed positive. In the present study, it was taken as abnormal if the horizontal vHIT gain < 0.8 and re-fixation saccades appeared.

RESULTS

Clinical Characteristics

Nineteen DEH patients were included (12 females, 7 males; mean age, 38.9 year; range, 13–65 year). According to the diagnostic criteria, 17 patients were diagnosed with ipsilateral DEH and two as having contralateral DEH. All 19 patients reported precedent hearing loss and episodic vertigo attacks. Fifteen patients reported profound hearing loss of unknown etiology in early childhood. In three cases, hearing loss was caused by sudden SNHL in adulthood and in one case deafness was associated with meningitis in childhood (**Table 1**). A precise latency interval between the precedent hearing loss and the hydropic symptoms (recurrent vertigo or fluctuating hearing loss) could not be obtained, since the onset time of hearing loss was uncertain in most patients. The hydropic symptoms lasted 5.3 years on average (range: 0–25 years) before inclusion into this study. The duration of vertigo attacks lasted 20 min to 10 h. The frequency of vertigo attacks varied from 3 times a week to one time in several years. Other major complaints included: tinnitus and/or aural fullness (either persistent or fluctuating). Vestibular drop attack occurred in two cases (patient No. 4 and 9). Of note, in one case (patient No. 17) of ipsilateral DEH, concurrent horizontal SCC type BPPV was diagnosed in the opposite ear, and the patient suffered from both the Ménière -like episodic vertigo lasting for over 1 h during the past several months and recurrent transient positional vertigo while lying down or getting up before presentation. No migraine symptoms or history of migraine was recorded.

Audio-Vestibular Evaluations

Audio-vestibular test results are presented in **Table 1**. All 19 patients had profound SNHL (>90 dB) in one ear. For the better-hearing ear, the PTA of 500, 1,000, and 2,000 Hz was <26 dB in 16 ears, 26–40 dB in two ears and >40 dB in 1 ear. Spontaneous nystagmus was detected in five out of 19 patients (26.3%). Among these five cases, four cases were of ipsilateral DEH type with spontaneous nystagmus beating to the affected side in one case and to the non-affected side in the other three cases, and one case was of contralateral DEH type with spontaneous nystagmus beating to the affected side. No pathological results were observed in the gaze, saccades, smooth pursuit, and optokinetic test.

In this series, 14 (73.7%) had reduced caloric response, and only three cases (15.8%) had abnormal horizontal vHIT responses. Of the 17 patients with ipsilateral DEH, abnormal CP was observed in 76.5% (13/17) of the patients and 11.8% (2/17) yielded abnormal vHIT result. In 12 cases, abnormal CP was ipsilateral in the ear with preexisting hearing loss and in one patient abnormal CP was in the opposite ear. For the two

patients with both abnormal CP and vHIT results, abnormal response occurred in the previously damaged ear in one case, and in the opposite ear in the other case. Of the two patients with contralateral DEH, abnormal CP and vHIT were detected in one case (50%), and abnormalities occurred in the ear with preexisting hearing loss. For all subjects, MRI did not reveal any retro-cochlear lesion.

Treatment and Following-Up

Lifestyle modification was recommended to the patients, including low-sodium diet, low caffeine consumption, and abstinence from stimulants. In all 19 patients, initial medication included the betahistine or diuretics, lasting for at least 3–6 months. Two patients (No. 9 and 14) received one course of intratympanic dexamesone due to unsatisfactory vertigo control. No ablative treatment was administered in this series, especially for the contralateral type of DEH. A follow-up, lasting 3 months−3.0 years, showed that, against the guidelines for MD proposed by American Academy of Otolaryngology-Head and Neck Surgery in 1995 (20), complete or substantial vertigo control (class A or B) was achieved in 16 cases and limited control (class C) in three cases. For the patient with concomitant horizontal SCC type BPPV, Gufoni maneuver successfully cured the positional vertigo.

DISCUSSION

In this study, we investigated the function of horizontal SCC VOR in patients with DEH. In our series, 73.7% (14/19) of the DEH patients showed abnormal caloric response. Meanwhile, only 15.8% (3/19) of the patients yielded abnormal horizontal vHIT results. To the best of our knowledge, this was the first study which examined the VOR function measured by vHIT and identified a discrepancy between the results of vHIT and the caloric test in patients with DEH.

Until now, two hypotheses have been put forward to explain this dissociation. First, the hydrostatic temperature dissipation hypothesis attributed the discrepancy to the different test mechanisms between caloric test and vHIT. The distended membranous duct of the horizontal SCC has been suggested to permit convective recirculation within the duct, leading to a diminished thermally- induced pressure gradient across the cupula and thus to less deflection of the cupula and hair cells and less caloric nystagmus. This assumption is supported by the observation that, in MD patients with normal vHIT results, the reduced caloric response was correlated with the severity of vestibular hydrops (as demonstrated by intravenous gadolinium-enhanced MRI of the inner-ear) (21). Second, the dual frequency hypothesis proposes that a differential activation of vestibular hair cells by stimuli with different frequencies might be responsible for the dissociation. It is believed that type II hair cells are sensitive to the low-frequency (caloric) stimulus and the type I hair cells to the high-frequency (head impulse) stimulus. Previous histological studies showed that damage was more severe in type II hair cells than in type I hair cells as MD deteriorates. This theory is recently being challenged by multiple findings (22–24). In addition, the effect of central compensation cannot be fully ruled out. Since rapid angular head movements are frequent in everyday activities, the response to rapid head movement may adapt better to vestibular hypofunction than the non-physiological caloric response.

Recently, multiple studies have demonstrated this disagreement in patients with MD (idiopathic ELH). McCaslin et al. (25) and McGarvie et al. (6) reported normal vHIT response but abnormal caloric results in patients with definite MD, respectively. A recent study by Rubin et al. (7) found that the caloric test was abnormal in 34 out of 37 MD patients, yet vHIT yielded normal gain. Jung et al. demonstrated that, apart from the patients with MD, this dissociation also occurred in patients with EVA (2). Abnormal CP was detected in four out of 10 cases and abnormal vHIT response was found only in one case. In contrast, all 19 patients with vestibular neuritis exhibited abnormal CP and 18 of them had abnormal vHIT response. Similarly, this discrepancy was also observed in patients with congenital semicircular canal malformation (common cavity formed by the vestibule and horizontal SCC), thus further supporting the dissipation theory (26). By retrospectively analyzing the conditions that show such dissociation in a non-homogenous group of patients complaining of vertigo or imbalance, Hannigan et al. (5) found that MD subjects comprised 75% (27/36) of the dissociation group. Of the 73 MD patients tested, 27 showed a dissociation and, of the 533 non-MD subjects tested, only nine showed such dissociation. Since MRI-demonstratable ELH is the common imaging feature of DEH, MD, EVA, and common cavity malformation (27), we suggest that this dissociation between the caloric test and vHIT might be a distinctive pattern of vestibular deficit in hydropic ear disease (28).

In this study, we showed that, in patients with ipsilateral DEH, 70.6% (12/17) had abnormal CP in the ear with previous cochlear damage and 5.8% (1/17) had abnormal CP in the opposite ear. Our result was in agreement with that reported by Schuknecht et al. who found that 80% of the ipsilateral DEH patients had unilateral caloric weakness in the hydropic ear and 9% had such hypofunction in the opposite ear (29). The substantially higher incidence of abnormal CP in the ear with precedent hearing loss than in the contralateral ear might be ascribed to the fact that: (1) bilateral ELH is commonly present in ipsilateral DEH patients, as demonstrated by gadolinium-enhanced MRI (30, 31), and (2) the area of ELH in the deaf ear was significantly larger than or practically equivalent to that of the better-hearing ear (31).

In the present study, 50% (1/2) of the patients with contralateral DEH showed the abnormal CP and vHIT in the previously deaf ear rather than the opposite ear. The pattern of ELH distribution and vestibular deficit is rather complicated in contralateral DEH, indicating that its pathology is more involved compared to its ipsilateral counterpart (30, 32, 33). Further studies with larger sample sizes are warranted to elucidate the pathogenesis.

We found a vHIT deficit in 15.8% and a caloric weakness in 73.7% of our DEH patients. No other studies investigated the VOR function at these high frequencies in patients with this condition. Alternatively, rotatory chair test can assess the VOR system across the low to middle frequencies (0.01–1.00 Hz). To date, only one published study has investigated the performance

of rotary chair and caloric test in DEH patients and revealed that rotatory chair test identified vestibular hypofunction in 3% while caloric test detected the hypofunction in 59% of their patients (15). More evidence is needed to verify our results.

In hydropic ear disease with fluctuating nature, the caloric response was speculated to reflect the severity of ELH more than the impairment of VOR function. Clinically, the functional assessment or therapeutic decision may be biased if based on the caloric test alone. This was in agreement of Bodmer et al. (34) and Lin et al. (35), who challenge the functional significance of CP values or caloric unresponsiveness in the prediction of long-term vertigo control, while Hone et al. found an absence of ice water response was highly predictive of adequate vertigo control and recommend a total chemical ablation of VOR function by intratympanic gentamicin treatment (36). On the contrary, vHIT allows for an objective evaluation of the actual status of angular VOR pathways by using physiological stimuli and can give clinicians a dynamic and real-time picture of the VOR function. Previous studies have proven the value of vHIT in reflecting functional fluctuation, therapeutic endpoint and vertigo recurrence in MD patients (22, 35, 37, 38). Therefore, we suggest that vHIT is an objective screening test of choice for dynamically monitoring the VOR function in patients with hydropic ear disease. This is especially necessary for those receiving ablative therapy, in whom the effective vestibular impairment should be clearly defined and the progress of functional recovery should be closely monitored.

The study had several limitations. First, the sample size was small, especially for the contralateral cases, because DEH is not a common vestibular disorder. Second, we did not perform gadolinium-enhanced MRI, which might provide further imaging evidence to account for the findings of our VOR tests. Third, this study did not perform the rotatory chair test, in which the VOR time constant has been shown to provide the most reliable assay screening fixed peripheral vestibular loss (39). Since caloric-vHIT dissociation also occurs in fixed peripheral vestibular loss, for example, during the recovery phase of vestibular neuritis (40), supplement of rotary chair test would be helpful in excluding fixed peripheral vestibular loss caused by ELH. In future, large-scale studies involving comprehensive audio-vestibular tests and contrast-enhanced MRI examinations are warranted to further understand the pathophysiology of DEH.

CONCLUSION

Abnormal caloric response in the presence of a preserved vHIT might be a distinctive pattern of vestibular deficit in patients with DEH, a rare variant of Ménière's disease. More evidence is needed to clarify the clinical implication of this dissociation in hydropic ear disease.

DATA AVAILABILITY STATEMENT

The datasets generated for this study are available on request to the corresponding author.

ETHICS STATEMENT

The studies involving human participants were reviewed and approved by Ethical committee of Tongji Medical College of Huazhong University of Science and Technology, Wuhan, China. Written informed consent to participate in this study was provided by the participants' legal guardian/next of kin.

AUTHOR CONTRIBUTIONS

BL: study conception and design, data acquisition, and critical review of the manuscript. YL: data analysis and interpretation, drafting and revision of the manuscript.

FUNDING

This work was supported by grants from the National Natural Science Foundation of China (NSFC No. 81670930), the Natural Science Foundation of Hubei Province, China (No. 2016CFB645), and Fundamental Research Funds for the Central Universities, China (No. 2016YXMS240).

REFERENCES

1. Wuyts FL, Furman J, Vanspauwen RP, de Van H. Vestibular function testing. *Curr Opin Neurol*. (2007) 20:19–24. doi: 10.1097/WCO.0b013e3280140808
2. Jung J, Suh MJ, Kim SH. Discrepancies between video head impulse and caloric tests in patients with enlarged vestibular aqueduct. *Laryngoscope*. (2017) 127:921–6. doi: 10.1002/lary.26122
3. MacDougall HG, Weber KP, McGarvie LA, Halmagyi GM, Curthoys IS. The video head impulse test: diagnostic accuracy in peripheral vestibulopathy. *Neurology*. (2009) 73:1134–41. doi: 10.1212/WNL.0b013e3181bacf85
4. Mahringer A, Rambold HA. Caloric test and video-head-impulse: a study of vertigo/dizziness patients in a community hospital. *Eur Arch Otorhinolaryngol*. (2014) 271:463–72. doi: 10.1007/s00405-013-2376-5
5. Hannigan IP, Welgampola MS, Watson SRD. Dissociation of caloric and head impulse tests: a marker of Meniere's disease. *J Neurol*. (2019) doi: 10.1007/s00415-019-09431-9. [Epub ahead of print].
6. McGarvie LA, Curthoys IS, MacDougall HG, Halmagyi GM. What does the dissociation between the results of video head impulse versus caloric testing reveal about the vestibular dysfunction in Meniere's disease? *Acta Otolaryngol*. (2015) 135:859–65. doi: 10.3109/00016489.2015.1015606
7. Rubin F, Simon F, Verillaud B, Herman P, Kania R, Hautefort C. Comparison of video head impulse test and caloric reflex test in advanced unilateral definite meniere's disease. *Eur Ann Otorhinolaryngol Head Neck Dis*. (2018) 135:167–9. doi: 10.1016/j.anorl.2017.08.008
8. Kamei T. Delayed endolymphatic hydrops as a clinical entity. *Int Tinnitus J*. (2004) 10:137–43.
9. Kamei T, Noro H, Yabe K, Makino S. Statistical observation of unilateral total deafness and characteristics of unilateral total deafness among young children with tendency toward dizziness. *Jibiinkoka*. (1971) 43:349–58.
10. Schuknecht HF, Wright JL. Pathology in a case of profound congenital deafness. *J Laryngol Otol*. (1973) 87:947–55. doi: 10.1017/S0022215100077860

11. Nadol JB Jr, Weiss AD, Parker SW. Vertigo of delayed onset after sudden deafness. *Ann Otol Rhinol Laryngol*. (1975) 84:841–6. doi: 10.1177/000348947508400617
12. Wolfson RJ, Leiberman A. Unilateral deafness with subsequent vertigo. *Laryngoscope*. (1975) 85:1762–6. doi: 10.1288/00005537-197510000-00017
13. Schuknecht HF. Pathophysiology of endolymphatic hydrops. *Arch Otorhinolaryngol*. (1976) 212:253–62. doi: 10.1007/BF00453673
14. Schuknecht HF. Delayed endolymphatic hydrops. *Ann Otol Rhinol Laryngol*. (1978) 87:743–8. doi: 10.1177/000348947808700601
15. Pollak L. Audiovestibular findings in patients with delayed and idiopathic endolymphatic hydrops: a comparative study. *Am J Otolaryngol*. (2004) 25:151–6. doi: 10.1016/j.amjoto.2003.11.009
16. Lin MC, Young YH. The use of vestibular test battery to identify the stages of delayed endolymphatic hydrops. *Otolaryngol Head Neck Surg*. (2012) 147:912–8. doi: 10.1177/0194599812452993
17. Egami N, Ushio M, Yamasoba T, Murofushi T, Iwasaki S. Indication of the side of delayed endolymphatic hydrops by vestibular evoked myogenic potential and caloric test. *ORL J Otorhinolaryngol Relat Spec*. (2010) 72:242–6. doi: 10.1159/000314696
18. Komatsuzaki A, Futaki T, Harada Y, Hozawa J, Ishii T, Kamei T. Delayed endolymphatic hydrops. The guideline for standardization of diagnostic criteria in vertiginous diseases. The Committee for Standardization of Diagnostic Criteria in 1987 16 Vertiginous Diseases. *Equilib Res*. (1987) 47:249–50.
19. Kim S, Oh YM, Koo JW, Kim JS. Bilateral vestibulopathy: clinical characteristics and diagnostic criteria. *Otol Neurotol*. (2011) 32:812–7. doi: 10.1097/MAO.0b013e31821a3b7d
20. Committee on Hearing and Equilibrium guidelines for the diagnosis and evaluation of therapy in Meniere's disease. American Academy of Otolaryngology-Head and Neck Foundation, Inc. *Otolaryngol Head Neck Surg*. (1995) 113: 181–5. doi: 10.1016/S0194-5998(95)70102-8
21. Choi JE, Kim YK, Cho YS, Lee K, Park HW, Yoon SH, et al. Morphological correlation between caloric tests and vestibular hydrops in Meniere's disease using intravenous Gd enhanced inner ear MRI. *PLoS ONE*. (2017) 12:e0188301. doi: 10.1371/journal.pone.0188301
22. Manzari L, Burgess AM, MacDougall HG, Bradshaw AP, Curthoys IS. Rapid fluctuations in dynamic semicircular canal function in early Meniere's disease. *Eur Arch Otorhinolaryngol*. (2011) 268:637–9. doi: 10.1007/s00405-010-1442-5
23. McCall AA, Ishiyama GP, Lopez IA, Bhuta S, Vetter S, Ishiyama A. Histopathological and ultrastructural analysis of vestibular endorgans in Meniere's disease reveals basement membrane pathology. *BMC Ear Nose Throat Disord*. (2009) 9:4. doi: 10.1186/1472-6815-9-4
24. Proctor LR. Results of serial vestibular testing in unilateral Meniere's disease. *Am J Otol*. (2000) 21:552–8.
25. McCaslin DL, Rivas A, Jacobson GP, Bennett ML. The dissociation of video head impulse test (vHIT) and bithermal caloric test results provide topological localization of vestibular system impairment in patients with "definite" meniere's disease. *Am J Audiol*. (2015) 24:1–10. doi: 10.1044/2014_AJA-14-0040
26. Shaw B, Raghavan RS. Dissociation between caloric and head impulse testing in patients with congenital abnormalities of the semicircular canals. *J Laryngol Otol*. (2018) 132:932–5. doi: 10.1017/S0022215118001317
27. Sone M, Yoshida T, Morimoto K, Teranishi M, Nakashima T, Naganawa S. Endolymphatic hydrops in superior canal dehiscence and large vestibular aqueduct syndromes. *Laryngoscope*. (2016) 126:1446–50. doi: 10.1002/lary.25747
28. Gurkov R. Meniere and friends: imaging and classification of hydropic ear disease. *Otol Neurotol*. (2017) 38:e539–44. doi: 10.1097/MAO.0000000000001479
29. Schuknecht HF, Suzuka Y, Zimmermann C. Delayed endolymphatic hydrops and its relationship to Meniere's disease. *Ann Otol Rhinol Laryngol*. (1990) 99:843–53. doi: 10.1177/000348949009901101
30. Iwasa YI, Tsukada K, Kobayashi M, Kitano T, Mori K, Yoshimura H, et al. Bilateral delayed endolymphatic hydrops evaluated by bilateral intratympanic injection of gadodiamide with 3T-MRI. *PLoS ONE*. (2018) 13:e0206891. doi: 10.1371/journal.pone.0206891
31. Nonoyama H, Tanigawa T, Tamaki T, Tanaka H, Yamamuro O, Ueda H. Evidence for bilateral endolymphatic hydrops in ipsilateral delayed endolymphatic hydrops: preliminary results from examination of five cases. *Acta Otolaryngol*. (2014) 134:221–6. doi: 10.3109/00016489.2013.850741
32. Fukushima M, Yokoi K, Iga J, Akahani S, Inohara H, Takeda N. Contralateral type of delayed endolymphatic hydrops may consist of two phenotypes based on a magnetic resonance imaging preliminary study. *Acta Otolaryngol*. (2017) 137:1153–7. doi: 10.1080/00016489.2017.1347825
33. Kasai S, Teranishi M, Katayama N, Sugiura M, Nakata S, Sone M, et al. Endolymphatic space imaging in patients with delayed endolymphatic hydrops. *Acta Otolaryngol*. (2009) 129:1169–74. doi: 10.3109/00016480802691143
34. Bodmer D, Morong S, Stewart C, Alexander A, Chen JM, Nedzelski JM. Long-term vertigo control in patients after intratympanic gentamicin instillation for Meniere's disease. *Otol Neurotol*. (2007) 28:1140–4. doi: 10.1097/MAO.0b013e31815aea05
35. Lin FR, Migliaccio AA, Haslwanter T, Minor LB, Carey JP. Angular vestibulo-ocular reflex gains correlate with vertigo control after intratympanic gentamicin treatment for Meniere's disease. *Ann Otol Rhinol Laryngol*. (2005) 114:777–85. doi: 10.1177/000348940511401007
36. Hone SW, Nedzelski J, Chen J. Does intratympanic gentamicin treatment for Meniere's disease cause complete vestibular ablation? *J Otolaryngol*. (2000) 29:83–7.
37. Liu H, Zhang T, Wu Q, Zhang Y, Dai C. End-point indicators of low-dose intra-tympanic gentamicin in management of Meniere's disease. *Acta Otolaryngol*. (2017) 137:136–43. doi: 10.1080/00016489.2016.1224921
38. Martin-Sanz E, Diaz JY, Esteban-Sanchez J, Sanz-Fernandez R, Perez-Fernandez N. Delayed effect and gain restoration after intratympanic gentamicin for meniere's disease. *Otol Neurotol*. (2019) 40:79–87. doi: 10.1097/MAO.0000000000001973
39. Priesol AJ, Cao M, Brodley CE, Lewis RF. Clinical vestibular testing assessed with machine-learning algorithms. *JAMA Otolaryngol Head Neck Surg*. (2015) 141:364–72. doi: 10.1001/jamaoto.2014.3519
40. Bartolomeo M, Biboulet R, Pierre G, Mondain M, Uziel A, Venail Z. Value of the video head impulse test in assessing vestibular deficits following vestibular neuritis. *Eur Arch Otorhinolaryngol*. (2014) 271:681–8. doi: 10.1007/s00405-013-2451-y

Conflict of Interest: The authors declare that the research was conducted in the absence of any commercial or financial relationships that could be construed as a potential conflict of interest.

frontiers in Neurology

OPINION
published: 27 May 2020
doi: 10.3389/fneur.2020.00452

Tribute to Bernard Cohen - Whose Pioneering Work Made the Vestibular Implant Possible

*Jean-Philippe Guyot, Nils Guinand and Angelica Perez Fornos**

Division of ENT and Head-and-Neck Surgery, Geneva University Hospitals, Geneva, Switzerland

Keywords: vestibular system, vestibular loss, vestibulopathy, electrical stimulation, vestibular implant, cochlear implant, neuroprosthesis, nystagmus

Edited by:
Michael Strupp, Ludwig Maximilian University of Munich, Germany

Reviewed by:
Ian S. Curthoys, University of Sydney, Australia
Konrad P. Weber, University of Zurich, Switzerland

****Correspondence:***
Angelica Perez Fornos
Angelica.Perez-Fornos@hcuge.ch

Specialty section:
This article was submitted to Neuro-Otology, a section of the journal Frontiers in Neurology

Received: *20 March 2020*
Accepted: *28 April 2020*
Published: *27 May 2020*

Citation:
Guyot J-P, Guinand N and Perez Fornos A (2020) Tribute to Bernard Cohen - Whose Pioneering Work Made the Vestibular Implant Possible. Front. Neurol. 11:452. doi: 10.3389/fneur.2020.00452

It is estimated that ∼1.8 million adults suffer from a severe or total bilateral vestibular deficit worldwide (1). Despite the dramatic consequences of the disease on the physical, emotional, and social functioning (2) in adults as well as its negative effects on the development of children born without vestibular function (3), there is no effective treatment for these patients (4). It was not until the mid-1990s that the idea of developing a neuroprosthesis that provides position and motion information to the brain using a concept comparable to the cochlear implant was born. Undoubtedly, this idea was based on the pioneering work of Bernard Cohen and his colleague Jun-Ichi Suzuki who, in the sixties, obtained and precisely described the reflex responses obtained by electric stimulation of the ampullary nerves in rabbits, pigeons, cats, and monkeys (5–8). Three decades later, Merfeld and Gong demonstrated that a rotation signal could be delivered to the nervous system using a piezoelectric gyroscope modulating the frequency of electrical signals according to the direction and the speed of head movements in guinea pigs (9, 10). It was time to move on to experimentation in humans.

It then seemed reasonable to us to see whether it was possible to duplicate the experiences of Cohen and Suzuki (5–8) in humans. In other words, we wanted to explore the possibility of generating vestibular reflexes upon electrical stimulation of the branches of the vestibular nerve, while at the same time limiting possible risks of hearing loss caused by the introduction of electrodes in the inner ear. Surgical approaches to the posterior and lateral ampullary nerves were developed (11) and, in 2004, the first electrical stimulation trials were performed in local anesthesia in patients undergoing surgery for cochlear implantation or suffering from Menière's disease eligible for a surgical labyrinthectomy.

These experiments showed that it was possible to access the branches of the vestibular nerve surgically without opening the labyrinth and that, not surprisingly, and in agreement with the pioneering works of Cohen and Suzuki, the nystagmic responses were aligned with the plane of the stimulated canal (12–14). Since 2007, this has led to several implantations of our vestibular implant prototypes in humans, with the demonstration of partial restoration of the vestibular function (11). Other groups in Baltimore and Washington followed with promising outcomes (15, 16).

We owe a lot to Bernard Cohen for his contribution in the field of vestibular physiology which opened the door to the development of a vestibular implant. This raises high hopes to improve the quality of life of patients suffering from a bilateral deficit. As for us, we were thrilled to present these first results at the meeting of the Association Research in Otolaryngology in Baltimore in 2011: Bernard Cohen was part of the audience. Thank you for the inspiration and encouragement, Sir !

We were sad to learn that he passed away in Mont Sinai Hospital on November 27 2019 the same hospital where he had initiated the original studies almost six decades ago.

AUTHOR CONTRIBUTIONS

J-PG, NG, and AP wrote and approved the manuscript.

REFERENCES

1. Ward BK, Agrawal Y, Hoffman HJ, Carey JP, Della Santina CC. Prevalence and impact of bilateral vestibular hypofunction: results from the 2008 US national health interview survey. *JAMA Otolaryngol Head Neck Surg.* (2013) 139:803–10. doi: 10.1001/jamaoto.2013.3913
2. Guinand N, Boselie F, Guyot JP, Kingma H. Quality of life of patients with bilateral vestibulopathy. *Ann Otol Rhinol Laryngol.* (2012) 121:471–7. doi: 10.1177/000348941212100708
3. Wiener-Vacher SR, Hamilton DA, Wiener SI. Vestibular activity and cognitive development in children: perspectives. *Front Integr Neurosci.* (2013) 7:92. doi: 10.3389/fnint.2013.00092
4. Zingler VC, Cnyrim C, Jahn K, Weintz E, Fernbacher J, Frenzel C, et al. Causative factors and epidemiology of bilateral vestibulopathy in 255 patients. *Ann Neurol.* (2007) 61:524–32. doi: 10.1002/ana.21105
5. Suzuki JI, Cohen B. Head, eye, body and limb movements from semicircular canal nerves. *Exp Neurol.* (1964) 10:393–405. doi: 10.1016/0014-4886(64)90031-7
6. Cohen B, Suzuki JI, Bender MB. Eye movements from semicircular canal nerve stimulation in the cat. *Ann Otol Rhinol Laryngol.* (1964) 73:153–69. doi: 10.1177/000348946407300116
7. Suzuki JI, Cohen B, Bender MB. Compensatory eye movements induced by vertical semicircular canal stimulation. *Exp Neurol.* (1964) 9:137–60. doi: 10.1016/0014-4886(64)90013-5
8. Cohen B, Suzuki JI. Eye movements induced by ampullary nerve stimulation. *Am J Physiol.* (1963) 204:347–51. doi: 10.1152/ajplegacy.1963.204.2.347
9. Gong W, Merfeld DM. Prototype neural semicircular canal prosthesis using patterned electrical stimulation. *Ann Biomed Eng.* (2000) 28:572–81. doi: 10.1114/1.293
10. Gong W, Merfeld DM. System design and performance of a unilateral horizontal semicircular canal prosthesis. *IEEE Trans Biomed Eng.* (2002) 49:175–81. doi: 10.1109/10.979358
11. Guyot JP, Perez Fornos A. Milestones in the development of a vestibular implant. *Curr Opin Neurol.* (2019) 32:145–53. doi: 10.1097/WCO.0000000000000639
12. Wall C III, Kos MI, Sigrist A, Delaspre O, Guyot JP. Electrical stimulation of the posterior ampularis nerve in an alert patient: preliminary results. In: *Barany Society, XXIII International Congress*. Paris (2004).
13. Wall C III, Kos MI, Guyot JP. Eye movements in response to electric stimulation of the human posterior ampullary nerve. *Ann Otol Rhinol Laryngol.* (2007) 116:369–74. doi: 10.1177/000348940711600509
14. Guyot J-P, Sigrist A, Pelizzone M, Feigl, GC, Kos MI. Eye movements in response to electric stimulation of the lateral and superior ampullary nerves. *Ann Otol Rhinol Laryngol.* (2011) 120:81–7. doi: 10.1177/000348941112000202
15. Boutros PJ, Schoo DP, Rahman M, Valentin NS, Chow MR, Ayiotis AI, et al. Continuous vestibular implant stimulation partially restores eye-stabilizing reflexes. *JCI Insight.* (2019) 4:128397. doi: 10.1172/jci.insight.128397
16. Phillips JO, Ling L, Nie K, Jameyson E, Phillips CM, Nowack AL, et al. Vestibular implantation and longitudinal electrical stimulation of the semicircular canal afferents in human subjects. *J Neurophysiol.* (2015) 113:3866–92. doi: 10.1152/jn.00171.2013

Conflict of Interest: The authors declare received research and travel grants from MED-EL Elektromedizinische Geräte GMBH (Innsbruck, Austria).

The remaining authors declare that the research was conducted in the absence of any commercial or financial relationships that could be construed as a potential conflict of interest.

frontiers in Neurology

ORIGINAL RESEARCH
published: 28 July 2020
doi: 10.3389/fneur.2020.00732

Spontaneous Recovery of the Vestibulo-Ocular Reflex After Vestibular Neuritis; Long-Term Monitoring With the Video Head Impulse Test in a Single Patient

Leigh Andrew McGarvie[1], Hamish Gavin MacDougall[2], Ian S. Curthoys[2] and Gabor Michael Halmagyi[1]*

[1] Neurology Department, Institute of Clinical Neurosciences, Royal Prince Alfred Hospital, Camperdown, NSW, Australia, [2] Vestibular Research Laboratory, School of Psychology, The University of Sydney, Sydney, NSW, Australia

Vestibular rehabilitation of patients in whom the level of vestibular function is continuously changing requires different strategies than in those where vestibular function rapidly becomes stable: where it recovers or where it does not and compensation is by catch-up saccades. In order to determine which of these situations apply to a particular patient, it is necessary to monitor the vestibulo-ocular reflex (VOR) gains, rather than just make a single measurement at a given time. The video Head Impulse Test (vHIT) is a simple and practical way to monitor precisely the time course and final level of VOR recovery and is useful when a patient has ongoing vestibular symptoms, such as after acute vestibular neuritis. In this study, we try to show the value of ongoing monitoring of vestibular function in a patient recovering from vestibular neuritis. Acute vestibular neuritis can impair function of any single semicircular canal (SCC). The level of impairment of each SCC, initially anywhere between 0 and 100%, can be accurately measured by the vHIT. In superior vestibular neuritis the anterior and lateral SCCs are the most affected. Unlike after surgical unilateral vestibular deafferentation, SCC function as measured by the VOR can recover spontaneously after acute vestibular neuritis. Here we report monitoring the VOR from all 6 SCCs for 500 days after the second attack in a patient with bilateral sequential vestibular neuritis. Spontaneous recovery of the VOR in response to anterior and lateral SCC impulses showed an exponential recovery with a time to reach stable levels being longer than previously considered or reported. VOR gain in response to low-velocity lateral SCC impulses recovered with a time constant of around 100 days and reached a stable level at about 200 days. However, in response to high-velocity lateral SCC and anterior SCC impulses, VOR gain recovered with a time constant of about 150 days and only reached a stable level toward the end of the 500 days monitoring period.

Keywords: vestibular neuritis, vestibulo-ocular reflex, VOR, vHIT, VOR recovery, temporal profile

OPEN ACCESS

Edited by:
Michael Strupp, Ludwig Maximilian University of Munich, Germany

Reviewed by:
Konrad P. Weber, University of Zurich, Switzerland
Ali S. Saber Tehrani, Johns Hopkins Medicine, United States
Jorge Kattah, University of Illinois at Chicago, United States
Alexander A. Tarnutzer, University of Zurich, Switzerland
Nicolas Perez-Fernandez, University Clinic of Navarra, Spain
Georgios Mantokoudis, Bern University Hospital, Switzerland

****Correspondence:***
Leigh Andrew McGarvie
leighm@icn.usyd.edu.au

Specialty section:
This article was submitted to Neuro-Otology, a section of the journal Frontiers in Neurology

Received: *09 April 2020*
Accepted: *15 June 2020*
Published: *28 July 2020*

Citation:
McGarvie LA, MacDougall HG, Curthoys IS and Halmagyi GM (2020) Spontaneous Recovery of the Vestibulo-Ocular Reflex After Vestibular Neuritis; Long-Term Monitoring With the Video Head Impulse Test in a Single Patient. Front. Neurol. 11:732. doi: 10.3389/fneur.2020.00732

INTRODUCTION

In humans and in animals, total surgical deafferentation of one labyrinth immediately produces a permanent, severe deficit of the angular vestibulo-ocular reflex (VOR) responses to rapid angular head accelerations in the off-direction of any semicircular canal (SCC) on the intact side. Catch-up, compensatory saccades substitute for the eye position error created by the VOR deficit; their cumulative magnitude is an index of the total VOR deficit during a head impulse. These are the fundamental principles underlying the video Head Impulse Test (vHIT) (1). If on the other hand the deafferentation is due to a reversible process, say, acute vestibular *neuritis,* then the deafferentation might not be permanent so that the VOR can recover, partly or fully, with or without treatment. Here we report the results of meticulous monitoring of the VOR over 500 days, with vHIT from each of the 6 SCCs of a single patient with acute vestibular neuritis and show that spontaneous recovery of SCC function can take longer than generally expected with consequences for the patient's recovery and rehabilitation. Our aim is to emphasize the ease and value of regular vHIT monitoring of the VOR during recovery from a peripheral vestibular lesion.

CASE HISTORY

An otherwise healthy 47 years old male presented in October 2014, 10 days after the acute onset of his first ever attack of isolated spontaneous vertigo, nausea, and vomiting. On examination he had 3°/s right-beating nystagmus suppressed by visual fixation. We diagnosed left superior vestibular neuritis. The vHIT results showed average VOR gains for the left SCCs of; lateral = 0.33; anterior = 0.02; posterior = 0.53. (**Figures 1A,B**, **2**: top row) He also had 12° leftward deviation of the subjective visual horizontal (2). Audiogram showed normal hearing. He undertook a rehabilitation exercise program and his overall balance improved to a level that he considered fully recovered.

Two and a half years later, in March 2017, he presented a week after the onset of a 2nd acute vertigo attack. He now had 2°/s left-beating nystagmus suppressed by visual fixation. Average VOR gains now showed a right superior vestibular neuritis pattern with impaired function of the right SCCs; lateral = 0.16, anterior = 0.23, posterior = 0.56. (**Figures 1A,B**, **2**: center row) He also had a 5° rightward deviation of the subjective visual horizontal. Cervical and ocular VEMPs were normal. After excluding Cogan's syndrome by slit lamp exam, and syphilis by negative serum TPHA (CSF was not examined), the clinical diagnosis was now *bilateral sequential vestibular neuritis* (3). As the patient was fit and healthy, we advised him to get as much outdoor activity as he could, especially in more challenging environments such as walking in the forest or on the beach, and one-on-one basketball. We emphasized that head movements in all planes during these activities should be maximized with a range of velocities. Subsequently, he reported that while vertigo and head turn oscillopsia lessened (particularly in the 1st month) they were ongoing at a low level over the period of testing, particularly when he was tired or stressed. The patient expressed interest in having the recovery of his vestibular function monitored and gave written informed consent in accordance with the Declaration of Helsinki to an ongoing vHIT protocol (X15-0266 HREC/11/RPAH/104) which was carried out during 12 tests over the next 500 days.

METHODS

All vHITs were carried out by the same right-handed operator (author LAM) using the same video goggles under the same lighting conditions. The patient was positioned 120 cm away from the target, an 8 mm diameter black dot set at eye level. VOR gain was calculated by an *area under the curve* algorithm from the start of the impulse until head velocity crossed zero (4). VOR gain is dependent upon head velocity (5), particularly when a large range of peak head velocity stimuli are delivered, as in the horizontal VOR gains shown in **Figure 2**. Therefore, we analyzed in detail the VOR responses to two bands of peak horizontal head velocity (80–120°/s and 180–220°/s) and to a single band of peak vertical head velocity (120–150°/s).

The data was processed by software written in LabVIEW (author HGM), which automatically detected the impulses and aligned them around peak head acceleration, into a display epoch of 600 ms. Each trace was visually checked and data displaying either artifacts or eye movements at the onset of the impulse were omitted from the final processing. VOR gain was then calculated by the software, which also processed the data into bands of peak head velocity, outputting the mean VOR gain, the standard deviation and the number of impulses within each band.

RESULTS

The first set of vHIT measurements for monitoring VOR gain changes were made 1 week after onset of the right vestibular neuritis (Test 2; Mar 2017).

The bins of head velocity used to compare VOR gains were: Low-velocity lateral SCC: 80–120°/s; High-velocity lateral SCC:180–220°/s.

All vertical bins used were for head velocities in the range 120–150°/s. (**Figures 1A,B**, **2**):

The calculated VOR gains for Test 2 were:

Right SCCs. Low-velocity lateral SCC = 0.19 ± 0.03; high-velocity lateral SCC = 0.14 ± 0.03; anterior SCC = 0.22 ± 0.04, and posterior SCC = 0.55 ± 0.03.

Left SCCs. Low-velocity lateral SCC = 0.55 ± 0.02; High-velocity lateral SCC = 0.51 ± 0.02, anterior SCC = 0.67 ± 0.07, posterior SCC = 0.53 ± 0.05.

During the 12 tests over the subsequent 500 days, the right lateral and right anterior SCC VOR gains increased at an apparently exponential rate, allowing for fluctuations. To test the validity of this assumption, single exponential curves were fitted to the data (see the **Supplementary Information** section for

fitting techniques, graphs, and equations). The results obtained from this technique were a time constant of 150 days (R^2 of fit = 0.99) for the high velocity right lateral SCC impulses, a time constant of 98 days (R^2 of fit = 0.997) for the low velocity right lateral SCC impulses and a time constant of 164 days (R^2 of fit = 0.977) for the right anterior SCC impulses. While the fitted curves give a good estimation for the lateral data, the measured anterior SCC VOR gains show more fluctuations hence the curve fitting is less representative as shown by the lower R^2 of fit value.

While left anterior SCC VOR gain and both left and right posterior SCC VOR gains were constant over the 500 days (**Figures 3–5**), right anterior SCC VOR gain increased exponentially from 0.22 to 0.69 with a temporal profile similar to that of right lateral SCC VOR gain.

Even though average left lateral SCC VOR gain remained constant over the 500 days at 0.56, the profile of its catch-up saccades changed between test 2 and test 13 (compare left lateral impulses of test 2; **Figure 1A** center panel, with test 13; **Figure 1A**; lower center panel). As average right lateral SCC VOR gain increased from 0.16 to 0.69 between tests 2 and 13 (**Figure 1B**), the profile of eye velocity correspondingly changes during the rightward "bounce-back" of the leftward lateral head impulse, producing a change in the subsequent catch-up saccades. The "bounce-back" (* on these panels of **Figure 1A**) in head velocity occurs as the operator tries to stop the leftward impulse rapidly, leading to a smaller rightward head velocity before the head actually stops. Effectively, each impulse profile in any plane comprises the intended high, ipsilateral head velocity, followed by an unintended lower velocity contralateral head braking required to bring the head to a stop.

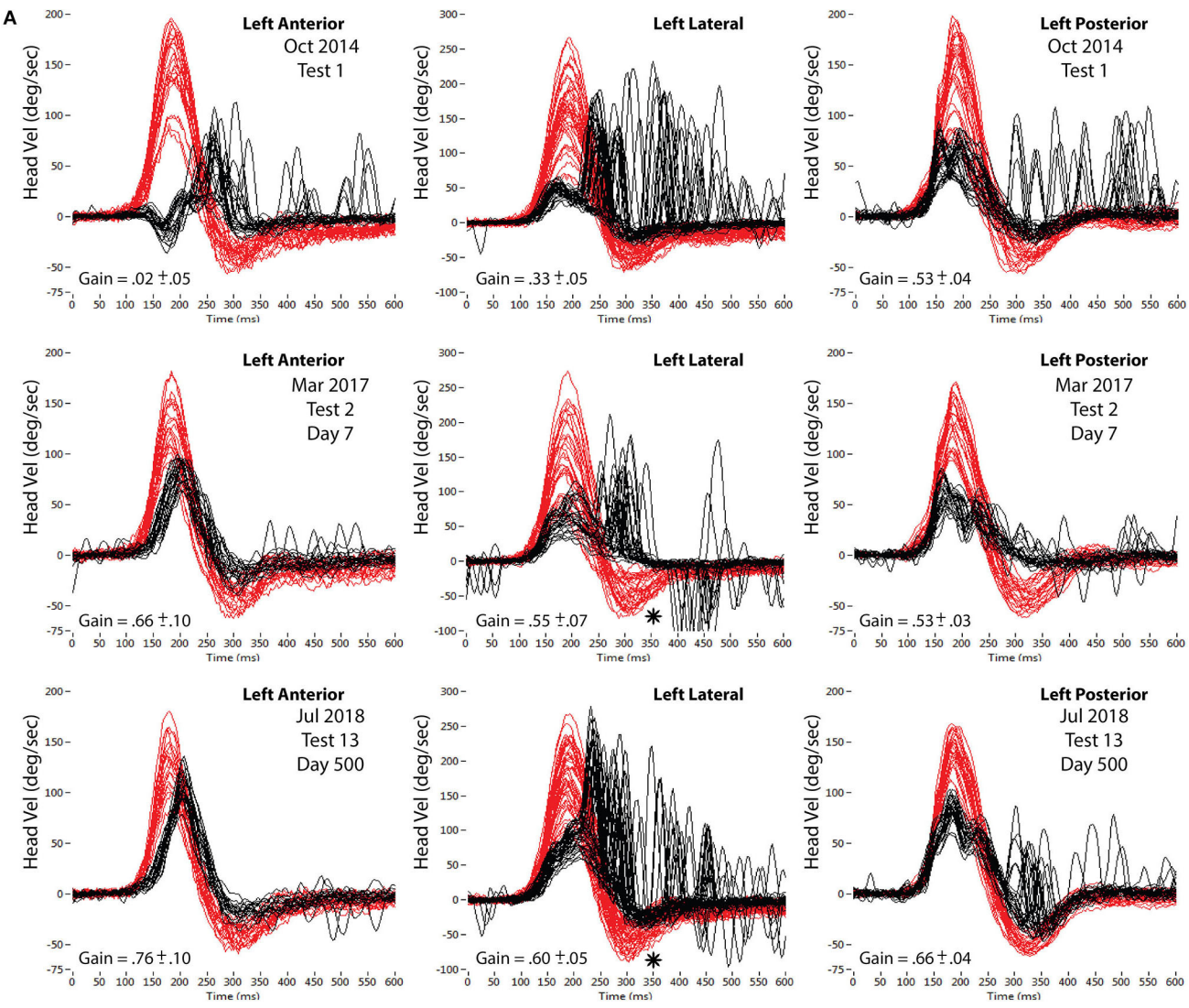

FIGURE 1 | Continued

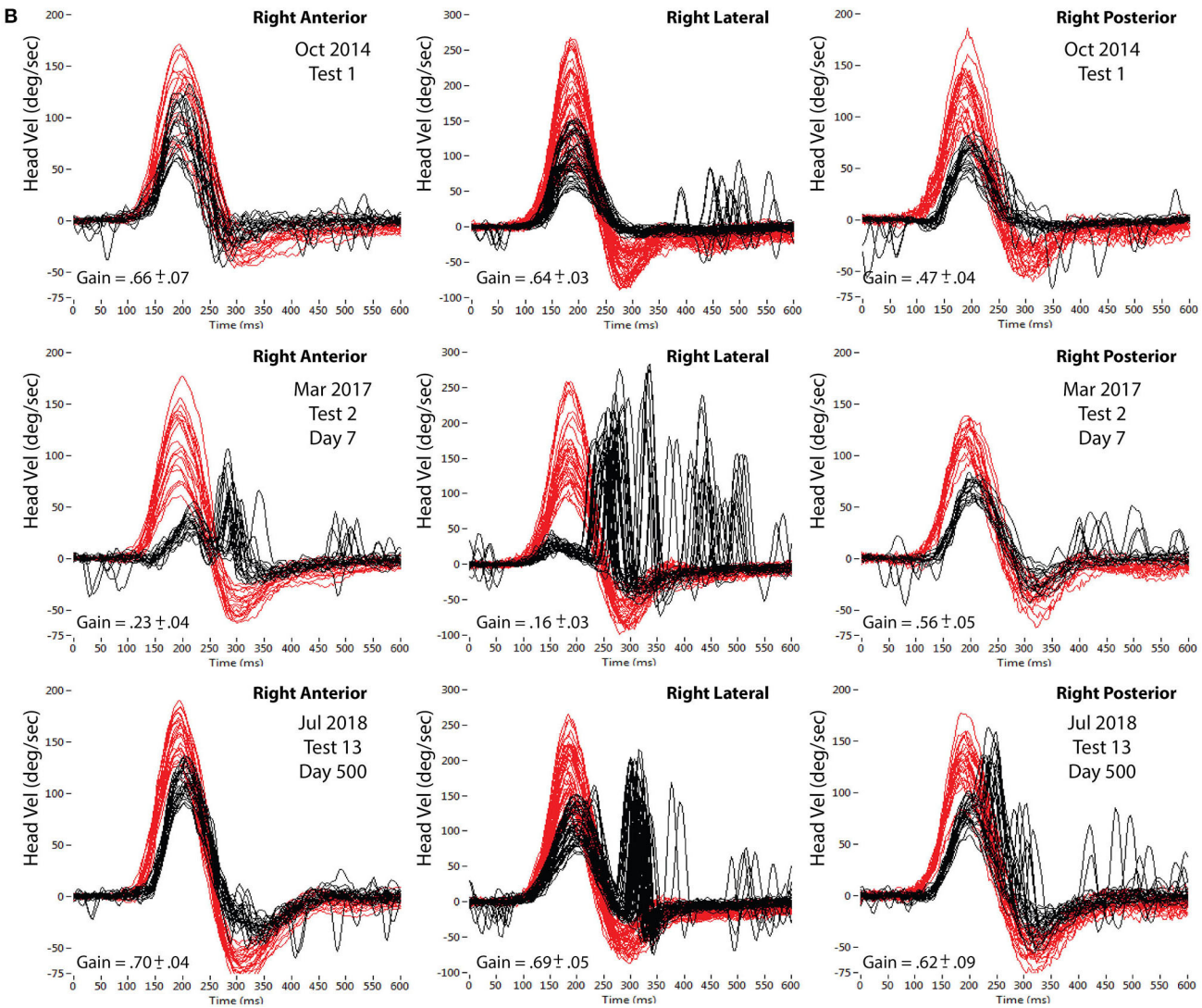

FIGURE 1 | (A) Impulsive testing of the three left SCCs on three occasions. Top row (Test 1, Oct 2014) at presentation with left vestibular neuritis. Middle row (Test 2, May 2017) at presentation with right vestibular neuritis. Bottom row (Test 13, July 2018) last test at end of the study. Superimposed head impulses of range of head velocities (in red) with VOR eye responses (in black)—inverted. Lateral velocity scale −100 to 300; Vertical velocity scale −75 to 200. VOR gain values are average values across the full head velocity range. *marks "bounce-back" discussed in text. **(B)** Impulsive testing of the three right SCCs on three occasions. Top row (Test 1, Oct 2014), at presentation with left vestibular neuritis. Middle row (Test 2, May 2017) at presentation with right vestibular neuritis. Bottom row (Test 13, July 2018) last test at end of the study. Superimposed head impulses of range of head velocities (in red) with VOR eye responses (in black) —inverted. Lateral velocity scale −100 to 300; Vertical velocity scale −75 to 200. VOR gain values are average values across the full head velocity range.

Right lateral SCC VOR gain recovered and stabilized sooner in response to low-velocity head impulses (80–120°/s), reaching a stable level at about 200 days, than in response to high-velocity head impulses (180–220°/s), which reached a stable value only after about 500 days (**Figure 3**). The effect of head velocity on VOR gain could not be accurately determined for the vertical SCCs as the maximum head velocity that can be delivered for the vertical SCCs is around 180–200°/s (**Figure 2**).

Deviation of the subjective visual horizontal at the onset of the right vestibular neuritis (Day 7) was 5.24 ± 0.45° rightward (clockwise); 20 days later it was in the normal range at 2.44 ± 0.41° and at its final value of 0.77 ± 0.36° at 50 days.

DISCUSSION

Immediately after total, permanent, surgical destruction, or deafferentation of an intact labyrinth, in an animal or human, there is an acute static vestibular syndrome with vertigo, nystagmus, and an ipsiversive ocular tilt reaction (6). Through brainstem compensation this syndrome always resolves, spontaneously and almost completely within a few days (7).

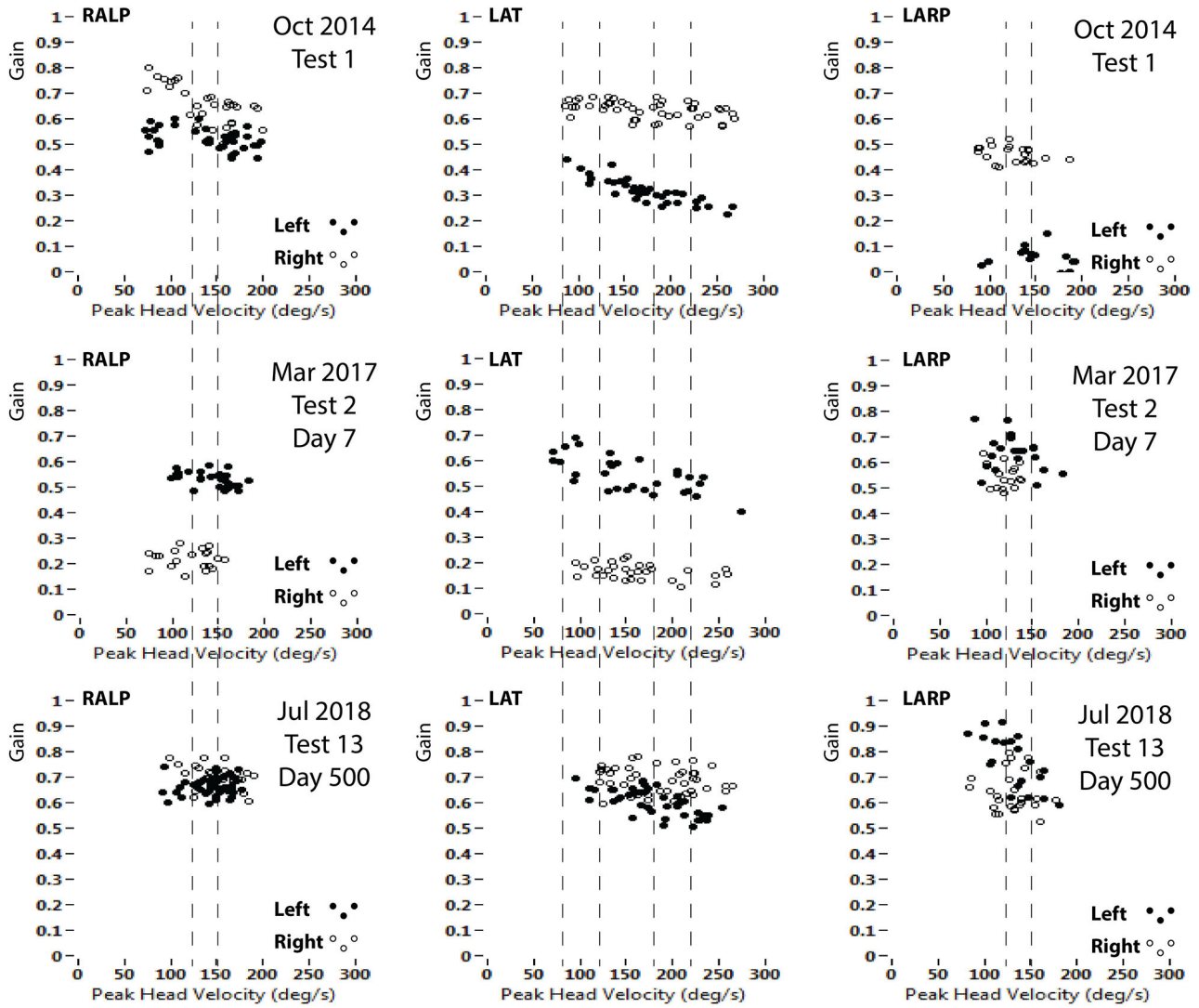

FIGURE 2 | VOR gains (area under the curve of eye/head velocity) from each of the six semicircular canals. Top row (Test 1, Oct 2014) at presentation with left vestibular neuritis. Middle row (Test 2, May 2017) at presentation with right vestibular neuritis. Bottom row (Test 13, July 2018) last test at the end of the study. Left column: RALP impulses (Right anterior-Left posterior canal plane). Center column: LAT impulses (Right Lateral-Left Lateral canal plane). Right column: LARP impulses (Left anterior-Right posterior canal plane). Head impulse velocity on horizontal axes; VOR gain on vertical axes (open circles are Left; filled circles are Right). The pairs of dashed lines indicate the head velocity ranges for analysis of VOR gains in **Figures 3**–**6**.

Unilateral vestibular deafferentiation/destruction also impairs the dynamic VOR in response to rapid angular accelerations (such as head impulses) toward any of the lesioned SCCs. In contrast to the static acute vestibular syndrome, this dynamic VOR impairment is permanent (8). From these facts it follows that if after any acute unilateral vestibular impairment (e.g., after acute vestibular neuritis) there is, as shown here, VOR recovery in response to head impulses, this recovery must be due to improvement in peripheral SCC function and not to brainstem compensation.

Acute *vestibular neuritis* is more of a clinical and pathophysiological concept than a specific disease, such as say, optic neuritis. The term covers almost any attack of acute, isolated, idiopathic, unilateral impairment of peripheral vestibular function (9). While any or all of the five vestibular sensory regions might be involved, vestibular impairment is often limited to sensory regions innervated by the superior vestibular nerve: anterior SCC, lateral SCC and utricle, so this pattern is called *superior vestibular neuritis*. If impairment is confined to regions innervated by the inferior vestibular nerve (posterior SCC and saccule) this is called *inferior vestibular neuritis* (10). Some use the term *vestibular neuronitis*, (11)—implying that the lesion involves vestibular ganglion cells. If the patient also develops Benign Positional Vertigo (BPV) the term *neurolabyrinthis* (12) is used. If the other side is involved later, then this is called *bilateral sequential vestibular neuritis*

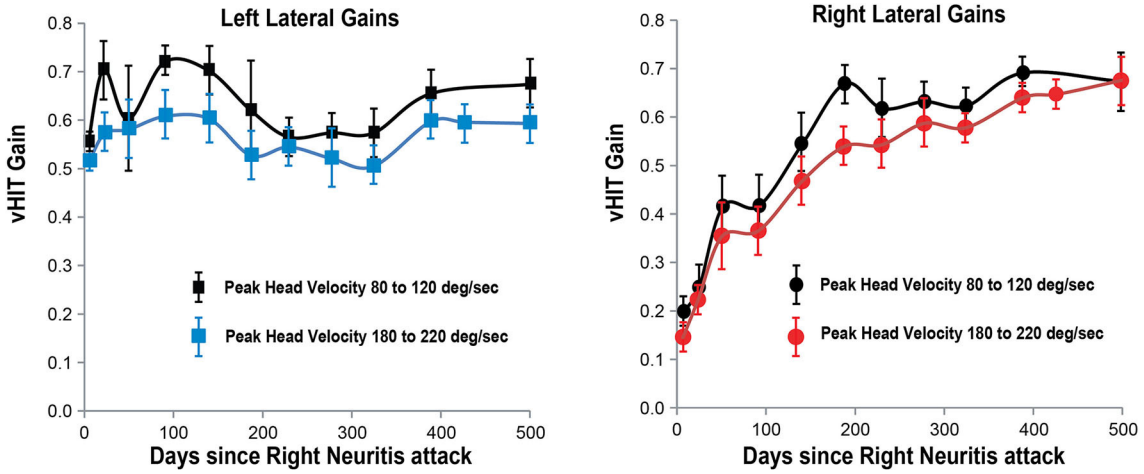

FIGURE 3 | Lateral SCC VOR gain for head velocities in the range 180–220°/s and 80–120°/s (vertical axis) as a function of days (horizontal axis) after the onset of right vestibular neuritis. High-velocity right lateral SCC VOR gain in red circles; left lateral SCC gain in blue squares; Low-velocity right lateral SCC VOR gain in black circles; left lateral SCC gain in black squares. Mean and standard deviation. Gain from the left lateral SCC stays about the same over 500 days. For the right lateral SCC high-velocity impulses, it increases exponentially from 0.14 +/– 0.03 to 0.67 +/– 0.05 with a time constant of around 150 days.

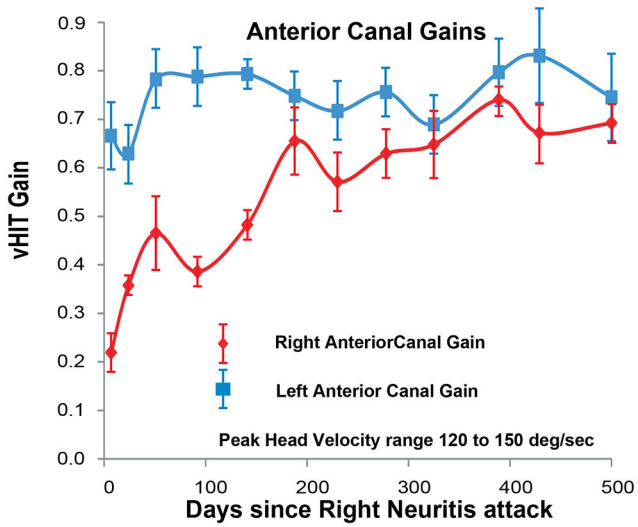

FIGURE 4 | Anterior SCC VOR gain for head velocities in the range 120–150°/s (vertical axis) as a function of days (horizontal axis) after the onset of right vestibular neuritis. Right anterior SCC VOR gain in red diamonds; left anterior SCC VOR gain in blue squares. Mean and standard deviation. For the right anterior SCC VOR gain increases exponentially from 0.22 +/– 0.04 to 0.69 +/– 0.04 with a time constant of around 100–150 days estimated from 63% of the range, or 164 days calculated from an exponential curve fitted through all the points (see **Supplementary Information**). VOR gain from the left anterior SCC stays almost constant around an average value of 0.72.

(3), if at the same time it is called *acute bilateral superior branch vestibular neuropathy* (13). If hearing is also involved then the inner ear is assumed to be the site of lesion and the diagnosis becomes *labyrinthitis* (14). [Unless the patient has herpes zoster with vestibular and cochlear and nerves involved (15)]. For some or all of these reasons some prefer the simple, non-committal term, *acute unilateral peripheral vestibulopathy* (16). Here we will continue to call it "vestibular neuritis."

The site and nature of the lesion in vestibular neuritis is uncertain. Vestibular tests, like auditory tests can lateralize a lesion but unlike auditory tests cannot localize it along the neural pathway from end-organ to brainstem nucleus. They cannot distinguish impaired vestibular function due to a disorder of vestibular hair cells from a disorder of vestibular neurons (ganglion cells, their axons, or brainstem nucleus neurons). So that while there are tests which indicate a *retro-cochlear* site of lesion for hearing loss, there are no tests to indicate *retro-labyrinthine* site of lesion for vestibular loss. Furthermore, there is no temporal bone pathology of vestibular neuritis in the acute stage; there are only a few case reports and only from temporal bones collected years after the acute event. These show loss of hair cells as well as of ganglion cells and their axons in the vestibular nerve (17).

Previous studies have shown that there usually is some spontaneous improvement of VOR gain in response to head impulses over weeks or months (18–23). In some cases there is even total recovery whereas in others there is none at all (24). If VOR recovery is incomplete then catch-up saccades, covert and overt, compensate for eye the position error produced by the deficient VOR.

In our patient with acute right vestibular neuritis, right lateral SCC VOR gain in response to high-velocity head impulses recovered spontaneously, with an exponential time constant of ~150 days. The VOR gain curves for the right anterior SCC and for both low-velocity and for high-velocity responses of the right lateral SCC, when overlaid (**Figure 6**) show similar fluctuations over time with exponential time constants of 164, 98, and 150 days, respectively (see **Supplementary Information** for curve fitting equations).

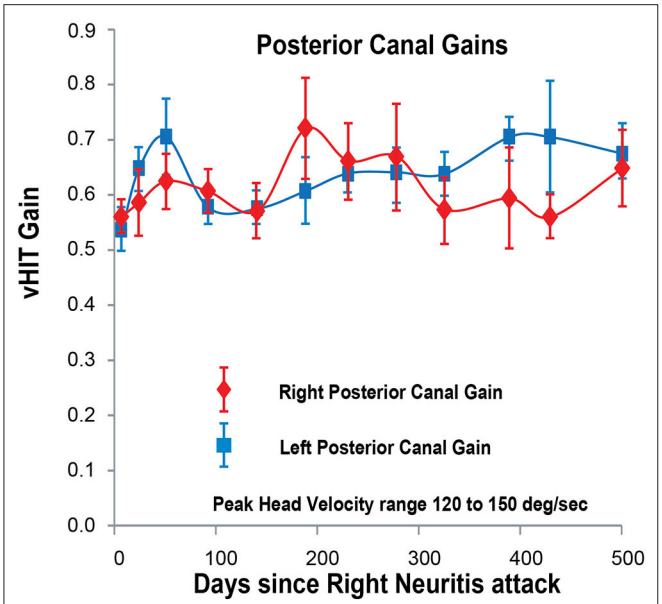

FIGURE 5 | Posterior SCC VOR gain for head velocities in the range 120–150°/s (vertical axis) as a function of days (horizontal axis) after the onset of right vestibular neuritis. Right posterior SCC VOR gain in red diamonds; left posterior SCC VOR gain in blue squares. Mean and standard deviation. Both gains stay about the same over the period of observation, averaging 0.60 for the right and 0.62 for the left.

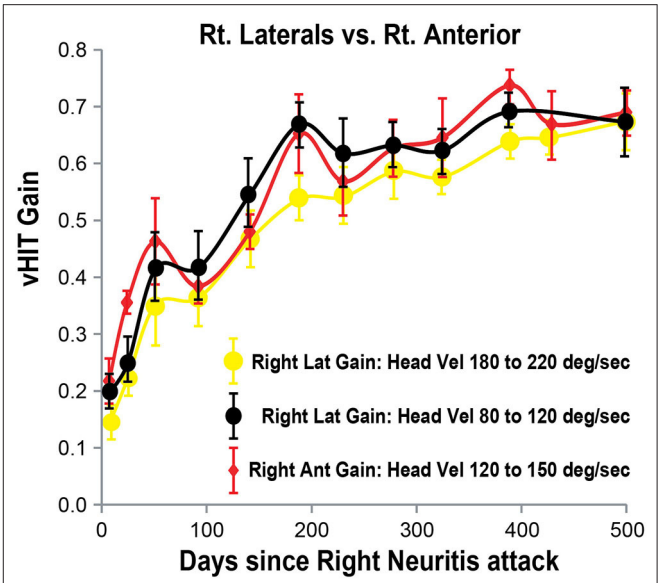

FIGURE 6 | Right lateral and anterior SCC VOR gains (vertical axis) as a function of days (horizontal axis) after the onset of right vestibular neuritis. Right lateral SCC VOR gain at higher head velocity (180–220°/s) in yellow circles. Right lateral SCC VOR gain at lower head velocity (80–120°/s) in black circles. Right anterior SCC VOR gain, at 120–150°/s head velocity, shown in red diamonds. Mean and standard deviation. Note that VOR gain increase and fluctuations from the lateral SCC at lower head velocity tends to match anterior SCC VOR gain.

During the initial steeper increase of the right SCC VOR gain over the first 3–4 weeks, the fellow left SCC VOR gains also increased, to lesser extent, and mainly at low head-velocity (**Figures 3–5**). So, as right lateral SCC high-velocity VOR gain increased from 0.14 to 0.35, left lateral SCC low-velocity VOR gain increased from 0.55 to 0.60. As right anterior SCC VOR gain increased from 0.22 to 0.47, left posterior SCC VOR gain increased from 0.53 to 0.70. These increases of the left SCC VOR gains in response to contralesional but ipsilateral leftward head impulses are, presumably, due to an increase in the crossed disinhibitory boost that the left vestibular nucleus type 1 excitatory neurons would normally receive from reduced activation of the right SCC afferents during leftward head impulses.

A salient point of this study is how long it can take for VOR gain to stabilize after acute vestibular neuritis. VOR gain at the higher horizontal head velocities took more than a year and a half to stabilize, so the patient was not be able to compensate effectively for the vestibular deficit during this period. Catch-up saccades are required to compensate when VOR gain is inadequate to stabilize gaze in space during head rotation. Once VOR gain has stabilized at any particular level, the system is able to "learn" the size of the saccades required to reorient gaze on the target for that given VOR level, with overt visually driven saccades initially correcting for any post-impulse gaze misalignment. However, while VOR gain is changing, either decreasing or increasing, then the size of the required saccades at any given head velocity also need to change so that the combined vestibular and visual system responses will be unable to accurately compensate until VOR gains stabilize.

In our patient right lateral SCC VOR gain increased slowly but steadily over a period of 500 days after the acute right vestibular neuritis, to a reach final level similar to left lateral SCC VOR gain (both about 0.65), with catch-up saccades correcting for the remaining deficit. In our view, the time-course of vestibular recovery we show here, more closely resembles the time-course of peripheral nerve conduction recovery from demyelination—as in acute inflammatory demyelination peripheral neuropathy (Guillain-Barre syndrome), than from axonal degeneration.

LIMITATIONS OF THE STUDY

This study was designed to demonstrate the value of ongoing monitoring of peripheral VOR gain during a patient's recovery period, specifically demonstrating the ease of use of the vHIT and consequently does not consider caloric or rotating chair tests. As there is only one patient studied, it cannot be extended to characterize a general time course of neuritis recovery, but rather provides an example of one potential outcome.

During the 12th test (day 429), there was insufficient time available to collect the low-velocity lateral SCC impulses in the range of 80–120°/s, and so this point is not plotted on the low-velocity lateral SCC VOR gain curves.

CONCLUSIONS

The video head impulse test enables clinicians themselves to monitor easily, accurately and regularly VOR gain from each SCC. Monitoring VOR gain could help guide rehabilitation since recovery of SCC function after acute vestibular neuritis can take longer than expected.

We emphasize that this is not meant to be a study of a particular disease. Rather it is an attempt to show how easy it is with vHIT, a method comparable in degree of difficulty to an audiogram, to monitor precisely and as often as needed, semicircular canal function over weeks, months, or years. vHIT can be used to determine whether semicircular canal function is stable or is changing, with time or with treatment. We are not specifically trying to characterize the recovery from vestibular neuritis; we are trying to show that with the correct tools, we can expand our understanding of the range of the outcomes of this and any other vestibular disorder.

DATA AVAILABILITY STATEMENT

The raw data supporting the conclusions of this article will be made available by the authors, without undue reservation.

ETHICS STATEMENT

The studies involving human participants were reviewed and approved by Royal Prince Alfred Hospital Ethics Committee approval X15-0266 HREC/11/RPAH/104. The patients/participants provided their written informed consent to participate in this study.

AUTHOR CONTRIBUTIONS

LM and GH designed the study, which was carried out by LM, and wrote the paper. HM wrote the software used by LM to analyze the data. LM, HM, IC, and GH were involved in the interpretation of the data. LM prepared the figures. All authors revised the manuscript.

ACKNOWLEDGMENTS

We dedicate this article to the memory of our friend, colleague, and mentor, Dr. Bernard Cohen of Mount Sinai Medical School, New York. Bernie was one of the greats of the vestibular world. His groundbreaking work contributed to the conceptual foundations of this study. His brilliant mind, kind demeanor and inspiring presence will live on, in our memories.

SUPPLEMENTARY MATERIAL

The Supplementary Material for this article can be found online at: https://www.frontiersin.org/articles/10.3389/fneur.2020.00732/full#supplementary-material

REFERENCES

1. Halmagyi GM, Chen L, MacDougall HG, Weber KP, McGarvie LA, Curthoys IS. The video head impulse test. *Front Neurol.* (2017) 8:258. doi: 10.3389/fneur.2017.00258
2. Karlberg M, Aw ST, Halmagyi GM, Black RA. Vibration-induced shift of the subjective visual horizontal: a sign of unilateral vestibular deficit. *Arch Otolaryngol Head Neck Surg.* (2002) 128:21–7. doi: 10.1001/archotol.128.1.21
3. Young AS, Taylor RL, McGarvie LA, Halmagyi GM, Welgampola MS. Bilateral sequential peripheral vestibulopathy. *Neurology*. (2016) 86:1454–6. doi: 10.1212/WNL.0000000000002563
4. MacDougall HG, McGarvie LA, Halmagyi GM, Curthoys IS, Weber KP. The video head impulse test (vHIT) detects vertical semicircular canal dysfunction. *PLoS ONE.* (2013) 8:e61488. doi: 10.1371/journal.pone.0061488
5. McGarvie LA, MacDougall HG, Halmagyi GM, Burgess AM, Weber KP, Curthoys IS. The video head impulse test (vHIT) of semicircular canal function – age-dependent normative values of VOR gain in healthy subjects. *Front Neurol.* (2015) 6:154. doi: 10.3389/fneur.2015.00154
6. Halmagyi GM, Weber KP, Curthoys IS. Vestibular function after acute vestibular neuritis. *Restor Neurol Neurosci.* (2010) 28:37–46. doi: 10.3233/RNN-2010-0533
7. Lacour M, Helmchen C, Vidal P-P. Vestibular compensation: the neuro-otologist's best friend. *J Neurol.* (2016) 263:S54–64. doi: 10.1007/s00415-015-7903-4
8. Halmagyi GM, Curthoys IS, Cremer PD, Henderson CJ, Todd MJ, Staples MJ, et al. The human horizontal vestibulo-ocular reflex in response to high-acceleration stimulation before and after unilateral vestibular neurectomy. *Exp Brain Res.* (1990) 81:479–90. doi: 10.1007/BF02423496
9. Strupp M, Magnusson M. Acute unilateral vestibulopathy. *Neurol Clin.* (2015) 33:669–85. doi: 10.1016/j.ncl.2015.04.012
10. Taylor RL, McGarvie LA, Reid N, Young AS, Halmagyi GM, Welgampola MS. Vestibular neuritis affects both superior and inferior vestibular nerves. *Neurology*. (2016) 87:1704–12. doi: 10.1212/WNL.0000000000003223
11. Hegemann SCA, Wenzel A. Diagnosis and treatment of vestibular neuritis/neuronitis or peripheral vestibulopathy (PVP)? open questions and possible answers. *Otol Neurotol.* (2017) 38:626–31. doi: 10.1097/MAO.0000000000001396
12. Magliulo G, Gagliardi S, Ciniglio Appiani M, Iannella G, Gagliardi M. Selective vestibular neurolabyrinthitis of the lateral and superior semicircular canal ampulla and ampullary nerves. *Ann Otol Rhinol Laryngol.* (2012) 121:640–4. doi: 10.1177/000348941212101003
13. Yacovino DA, Finlay JB, Urbina Jaimes VN, Verdecchia DH, Schubert MC. Acute bilateral superior branch vestibular neuropathy. *Front Neurol.* (2018) 9:353. doi: 10.3389/fneur.2018.00353
14. Kaya S, Schachern PA, Tsuprun V, Paparella MM, Cureoglu S. Deterioration of vestibular cells in labyrinthitis. *Ann Otol Rhinol Laryngol.* (2017) 126:89–95. doi: 10.1177/0003489416675356
15. Martin-Sanz E, Rueda A, Esteban-Sanchez J, Yanes J, Rey-Martinez J, Sanz-Fernandez R. Vestibular restoration and adaptation in vestibular neuritis and ramsay hunt syndrome with vertigo. *Otol Neurotol.* (2017) 38:e203–8. doi: 10.1097/MAO.0000000000001468
16. Uffer DS, Hegemann SC. About the pathophysiology of acute unilateral vestibular deficit—vestibular neuritis (VN) or peripheral vestibulopathy (PVP)? *J Vestib Res.* (2016) 26:311–7. doi: 10.3233/VES-160581
17. Baloh RW, Ishyama A, Wackym PA, Honrubia V. Vestibular neuritis: clinical-pathologic correlation. *Otolaryngol Head Neck Surg.* (1996) 114:586–92. doi: 10.1016/S0194-5998(96)70251-6
18. Allum JHJ, Scheltinga A, Honegger F. The effect of peripheral vestibular recovery on improvements in vestibulo-ocular reflexes and balance control

after acute unilateral peripheral vestibular loss. *Otol Neurotol*. (2017) 38:e531–8. doi: 10.1097/MAO.0000000000001477

19. Fu W, He F, Wei D, Bai Y, Shi Y, Wang X, et al. Recovery pattern of high-frequency acceleration vestibulo-ocular reflex in unilateral vestibular neuritis: a preliminary study. *Front Neurol*. (2019) 10:85. doi: 10.3389/fneur.2019.00085
20. Büki B, Hanschek M, Jünger H. Vestibular neuritis: involvement and long-term recovery of individual semicircular canals. *Auris Nasus Larynx*. (2017) 44:288–93. doi: 10.1016/j.anl.2016.07.020
21. Manzari L, Burgess AM, MacDougall HG, Curthoys IS. Objective verification of full recovery of dynamic vestibular function after superior vestibular neuritis. *Laryngoscope*. (2011) 121:2496–500. doi: 10.1002/lary.22227
22. Yoo MH, Yang CJ, Kim SA, Park MJ, Ahn JH, Chung JW, et al. Efficacy of steroid therapy based on symptomatic and functional improvement in patients with vestibular neuritis: a prospective randomized controlled trial. *Eur Arch Otorhinolaryngol*. (2017) 274:2443–51. doi: 10.1007/s00405-017-4556-1
23. Palla A, Straumann D. Recovery of the high-acceleration vestibulo-ocular reflex after vestibular neuritis. *J Assoc Res Otolaryngol*. (2004) 5:427–35. doi: 10.1007/s10162-004-4035-4
24. Manzari L, Burgess AM, MacDougall HG, Curthoys IS. Vestibular function after vestibular neuritis. *Int J Audiol*. (2013) 52:713–8. doi: 10.3109/14992027.2013.809485

Conflict of Interest: The authors declare that the research was conducted in the absence of any commercial or financial relationships that could be construed as a potential conflict of interest.

frontiers in Neurology

ORIGINAL RESEARCH
published: 11 August 2020
doi: 10.3389/fneur.2020.00710

The Virtual Morris Water Task in 64 Patients With Bilateral Vestibulopathy and the Impact of Hearing Status

Bieke Dobbels[1,2,3], Griet Mertens[1,2], Annick Gilles[1,2], Julie Moyaert[2], Raymond van de Berg[4,5], Erik Fransen[6], Paul Van de Heyning[1,2] and Vincent Van Rompaey[1,2]*

[1] Faculty of Medicine and Health Sciences, University of Antwerp, Antwerp, Belgium, [2] Department of Otorhinolaryngology and Head and Neck Surgery, Antwerp University Hospital, Edegem, Belgium, [3] Department of Otorhinolaryngology and Head and Neck Surgery, Zuyderland Medical Center, Heerlen, Netherlands, [4] Division of Balance Disorders, Department of Otorhinolaryngology and Head and Neck Surgery, Maastricht University Medical Center, Maastricht, Netherlands, [5] Faculty of Physics, Tomsk State University, Tomsk, Russia, [6] StatUa Center for Statistics, University of Antwerp, Antwerp, Belgium

Background: Previous studies have demonstrated spatial cognitive deficits in patients with bilateral vestibulopathy (BVP). However, BVP patients frequently present with a concomitant sensorineural hearing loss, which is a well-established risk factor of cognitive impairment and incident dementia. Nonetheless, previous research on spatial cognitive deficits in BVP patients have not taken hearing status into account.

Objective: This study aims to compare spatial cognition of BVP patients with healthy controls, with analyses adjusting for hearing status.

Methods: Spatial cognition was assessed in 64 BVP patients and 46 healthy controls (HC) by use of the Virtual Morris Water Task (VMWT). All statistical analyses were adjusted for hearing (dys)function, sex, age, education, and computer use.

Results: Overall, patients with BVP performed worse on all outcome measures of the VMWT. However, these differences between BVP patients and healthy controls were not statistically significant. Nonetheless, a statistically significant link between sensorineural hearing loss and spatial cognition was observed. The worse the hearing, the longer subjects took to reach the hidden platform in the VMWT. Furthermore, the worse the hearing, the less time was spent by the subjects in the correct platform quadrant during the probe trial of the VMWT.

Conclusion: In this study, no difference was found regarding spatial cognition between BVP patients and healthy controls. However, a statistically significant link was observed between sensorineural hearing loss and spatial cognition.

Keywords: spatial cognition, vestibular loss, hearing loss, hippocampus, Morris Water Maze

OPEN ACCESS

Edited by:
Michael Strupp, Ludwig Maximilian University of Munich, Germany

Reviewed by:
Shinichi Iwasaki, The University of Tokyo, Japan
Derek Alexander Hamilton, University of New Mexico, United States
Klaus Jahn, Schön Klinik, Germany

****Correspondence:***
Bieke Dobbels
bieke.dobbels@uza.be

Specialty section:
This article was submitted to Neuro-Otology, a section of the journal Frontiers in Neurology

Received: *06 April 2020*
Accepted: *10 June 2020*
Published: *11 August 2020*

Citation:
Dobbels B, Mertens G, Gilles A, Moyaert J, van de Berg R, Fransen E, Van de Heyning P and Van Rompaey V (2020) The Virtual Morris Water Task in 64 Patients With Bilateral Vestibulopathy and the Impact of Hearing Status. Front. Neurol. 11:710. doi: 10.3389/fneur.2020.00710

INTRODUCTION

A growing body of literature recognizes that the function of the vestibular system goes far beyond balance and gaze stability. Both animal and human research suggests that the vestibular system plays a critical role in cognition (1–4). According to the Diagnostic and Statistical Manual of Mental Disorders (DSM-V), cognitive functioning can be subdivided into six domains: language, learning

and memory, social cognition, attention, executive function, and visuospatial abilities (5). Of these, it seems that visuospatial abilities, which compromises spatial memory and navigation, is by far the most studied cognitive domain in animals and humans with loss of peripheral vestibular input (2, 4, 6). For example, spatial cognition has been studied in patients with vestibular loss using the Virtual Morris Water Task (VMWT) (3, 7, 8). This is a virtual version of the Morris Water Maze, considered the golden standard for assessing spatial cognition in rodents (9). Impaired spatial cognition has repeatedly been observed in patients with bilateral vestibulopathy (BVP) (3, 7). Patients with BVP suffer from a bilateral partial or complete loss of function of the vestibular structures of the inner ear, vestibular nerves, or a combination of both. BVP patients often present with oscillopsia and gait imbalance as primary complaints (10).

The link between spatial cognition and the vestibular system is of clinical importance for several reasons. First, cognitive training might yield therapeutic opportunities for BVP. Conventional treatment for patients with BVP is limited to counseling and intensive daily vestibular physical therapy to improve gaze and postural stabilization (11). However, these therapeutic strategies often remain insufficient (12). Although the utility of cognitive training has been demonstrated to enhance balance in the elderly and in patients with mild cognitive impairment and dementia, cognitive training is not included in the current treatment of BVP (13, 14). According to a recent computational model, cognitive training facilitates the central compensation process in BVP patients by increasing the knowledge about self-motion (15).

Second, interest has been directed toward the link between cognitive impairment and the vestibular system because of the rising prevalence of dementia. As in BVP patients, impaired spatial cognition is among the most frequently observed cognitive deficits in patients with dementia. One of the hallmark symptoms of Alzheimer's disease is wandering behavior and loss of topographic memory (16). The vestibular system, more than any other sensory system, makes widespread cortical projections, including to the hippocampus. The hippocampus is thought to play a key role in the neuronal substrate underlying spatial cognitive deficits in BVP patients (4). For instance, in a leading study by Brandt et al., BVP patients showed bilateral hippocampal atrophy and spatial cognitive deficits (7). Interestingly, in Alzheimer's disease, damage to the hippocampus is the most important anatomopathological feature (17).

Furthermore, several studies have found significantly poorer vestibular function in patients with dementia compared with their healthy peers (18–20).

These observations have led to the hypothesis that vestibular loss might cause cognitive decline and thus may contribute to the development of dementia. Given the rising prevalence of dementia and the lack of curative treatment, the identification of potentially modifiable risk factors is crucial (21).

In the previous literature, however, little attention has been paid to the hearing status of vestibular patients when drawing conclusions about the link between cognitive decline and the vestibular system. A systematic review pointed out that none of the studies investigating cognition in BVP patients have adjusted their analysis for the hearing status of the enrolled subjects (6). However, because of the close anatomical relationship between the vestibular system and the cochlea, hearing loss is observed in up to half of BVP patients (22, 23). Hearing loss is a well-established risk factor for dementia (24–26). Therefore, it is uncertain whether the cognitive deficits observed in BVP patients can be solely attributed to their vestibular loss as previously assumed. The frequently associated hearing loss in BVP patients might also play an essential role in their cognitive impairment (6).

The goal of this study is to compare spatial cognitive performance, assessed using the VMWT, of BVP patients with healthy controls. In contrast to previous studies, the analyses in this study were specifically designed to take the hearing loss of BVP patients into account.

METHODS

Study Design

The current study was a single-center, prospective, cross-sectional study, recruiting from October 2017 until August 2018 at the Antwerp University Hospital. The study was approved by the local ethics committee of the Antwerp University Hospital/University of Antwerp (protocol number 16/42/426) and informed consent was obtained in all study participants before the start of the study. The study was registered on ClinicalTrials.gov (NCT03690817). The majority of the enrolled participants received general cognitive assessment at another scheduled appointment on a different day. Results have been published earlier (27).

Study Participants

BVP patients were recruited from the Otorhinolaryngology, Head and Neck Surgery Department at Antwerp University Hospital, Belgium. Inclusion criteria for the BVP group were (1) BVP disease duration of more than 6 months and (2) definite diagnosis of BVP as defined by the diagnostic criteria of the Bárány Society (28):

a) Horizontal angular vestibulo-ocular reflex (VOR) gain < 0.6 measured by the video head impulse test (vHIT), and/or
b) Reduced caloric response (sum of bithermal, 30 and 44°, maximum peak slow phase velocity (SPV) on each side $<6°/s$), and/or
c) Reduced horizontal angular VOR gain < 0.1 upon sinusoidal stimulation on a rotatory chair.

Control participants were recruited by means of the population registries at the local city councils in southern Antwerp (Belgium), by advertisements in the hospital, and by approaching friends, family, and colleagues. Only control subjects with no history of vertigo, scores <5 on the Dizziness Handicap Inventory, and normal hearing thresholds at 0.25–8 kHz, based on age and sex (defined by the BS 6951:1988, EN 27029:1991, and ISO 7029-1984 standards), were enrolled in the study.

The following additional inclusion criteria were applied for both BVP patients and healthy controls: (1) age $\geq$18 years, (2) fluency in Dutch, (3) no history of neurological diseases (e.g., dementia, Parkinson's disease, cerebrovascular accident, etc.), (4)

absence of clinical signs indicating dementia or mild cognitive impairment, and (5) normal or appropriate corrected vision.

Regarding the necessity of computer use in the VMWT, all participants were asked about their frequency of computer use (daily vs. 2–5 days/week vs. seldom/never). Education of all participants was categorized as primary school, lower secondary school, upper secondary school, and college/university.

Vestibular Testing

By enrollment in the study, all BVP patients received new neuro-otological testing on site. The evaluation of the lower and mid frequencies function of the lateral semi-circular canals was performed by electronystagmography with bithermal caloric tests and rotatory chair test (Nystagliner Toennies, Germany). At our clinic, rotatory chair tests are performed using sinusoidal rotation (0.05 Hz) with a peak velocity of 60°/s (29). More detailed methodology and normative data were previously described (29). High-frequency function of all six semi-circular canals was measured by the vHIT. In the standard procedure used at our clinic, 10 valid head impulses are required for each canal. Angular head velocity was determined by three mini-gyroscopes, eye velocity by means of an infrared camera recording the right eye, all incorporated in commercially available vHIT goggles (Otometrics, Taastrup, Denmark). VOR gain was defined as the ratio of the area under the eye velocity curve to the head velocity curve from the impulse onset until the head velocity was again 0 (30).

The Virtual Morris Water Task (VMWT)

To assess spatial learning and spatial memory retrieval, the VMWT was used. This task was designed by Derek Hamilton and was inspired by the original animal research tool, which is considered the gold standard for testing spatial cognition in rodents (9, 31). A 15.6-in. PC laptop monitor was used to display the virtual environment generated by the VMWT software version 1.10 (Neuro Investigations). In this task, participants had to navigate toward a hidden platform as fast as possible. The virtual environment consisted of a round pool, located in the middle of a square room. Each wall of the room contained a different visual cue on which a participant could rely to find his way to the hidden platform. The cues were positioned in such a way that the platform could not be encountered by simply moving toward a single cue (see **Figure 1**). On the computer screen, a first-person view of the virtual environment was shown. Participants could move in the pool by using the arrow keys on the keyboard. Backward movement or up–down movement was not possible.

Before testing, all participants were given the same written instructions. Afterwards, time to ask questions to the examiner was foreseen. In both groups, four phase trials were performed:

Phase I—Exploration Trial

The first part consisted of one block of four trials with a hidden platform. Participants were familiarized with the concept of the game and the use of the key arrows. By observing the participant, the examiner checked for good understanding of the task. When necessary, supplemental explanations were given.

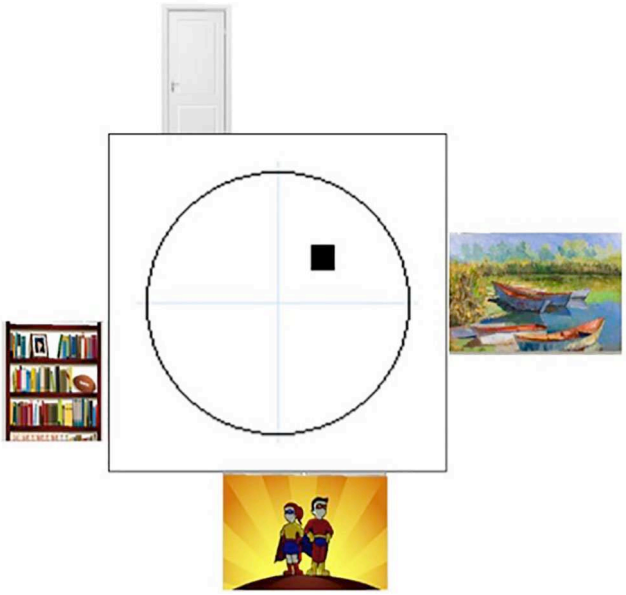

FIGURE 1 | The environment of the Virtual Morris Water Task. Overview of the virtual environment used in the Virtual Morris Water Task, with on each wall a different visual cue. The platform is indicated by the black square in the northeast quadrant of the pool.

Phase II—Hidden Trial

The test was started with 20 hidden platform trials. A virtual environment with different visual cues was used than in the exploration trial (see **Figure 2**). The hidden platform was located, in all trials, at the same spot in the northeastern quadrant of the pool. As it was submerged underneath the pool's surface, it was not visible to the participants. Starting locations during each trial were sampled pseudo-randomly from the four cardinal direction points of the pool. If participants were unable to find the hidden platform after 60 s, the platform was made visible and a message appeared prompting the participant to swim to the platform. During each of these trials, three measures were computed:

- The latency, i.e., time to reach the platform.
- The covered path length, i.e., total distance traveled, divided by the pool diameter.
- The heading error, when the participant has traveled a distance >25% of the pool diameter from the start position; the angular deviation is computed between the straight trajectory to the center of the platform and the starting position (see **Figure 3**).

Performance during these hidden platform trials represent a measure for spatial learning performance.

Phase III—Probe Trial

Subsequently, the platform was removed from the pool, unbeknownst to the participants. In this one trial, we measured the percentage of time a participant spent in the platform quadrant. A higher percentage was considered to be related to a better spatial memory retrieval of the participant.

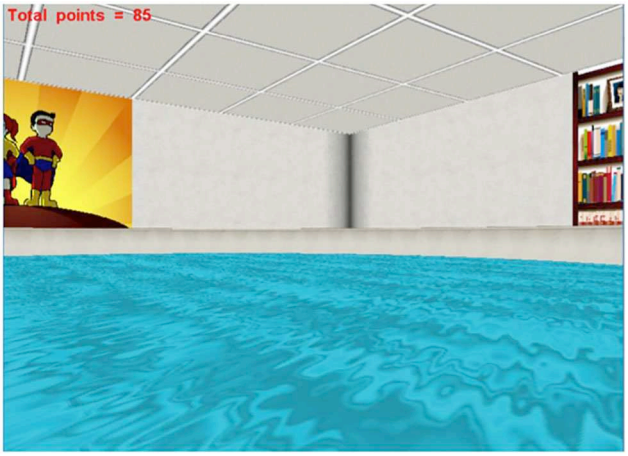

FIGURE 2 | The user's view during the Virtual Morris Water Task. Spatial cognition was assessed by the Virtual Morris Water Task. This figure shows the first-person view of the virtual environment, presented on a computer screen.

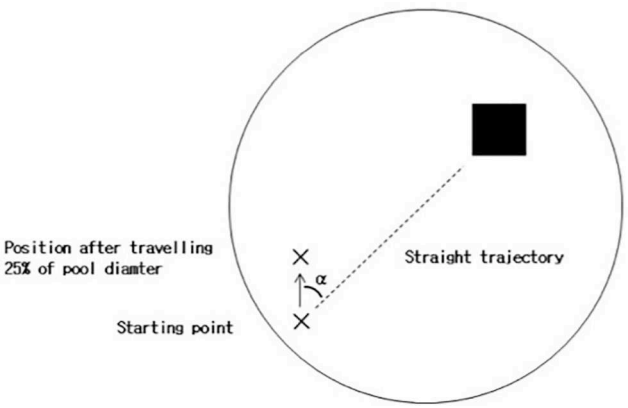

FIGURE 3 | Heading error in the Virtual Morris Water Task. During the hidden trials of the Virtual Morris Water Task, the heading error (α) is computed. When the participant first reaches a distance >25% of the pool diameter from the starting point, the angular deviation from a straight trajectory to the platform is measured. The smaller the heading error, the better the spatial orientation of the participant.

Phase IV—Visible Trials

The last part of the test represents a control task for motor condition. Participants had to perform eight visible trials in which the platform was visible and participants had to swim to the platform as soon as possible. Again, latency and path length were recorded for each trial.

Hearing Assessment

To correct cognitive outcome measures for the hearing status of the enrolled participants, a pure tone audiometry was performed. The unaided hearing thresholds were measured in a sound-isolated booth. For air conduction, hearing thresholds were determined at 125, 250, 500, 1,000, 2,000, 3,000, 4,000, 6,000, and 8,000 Hz using a two-channel Interacoustics AC-40 audiometer and insert earphones. Bone conduction thresholds were tested at 250, 500, 1,000, 2,000, 3,000, and 4,000 Hz. The high Fletcher index, which is the mean of air conduction hearing thresholds at 1, 2, and 4 kHz, was calculated for both ears. The hearing status of a participant was defined by the high Fletcher index of the better-hearing ear.

Data Collection and Statistical Analysis

Data were stored in OpenClinica LLC (Waltham, MA, USA), a secured online database for electronic data registration and data management developed for clinical research. For statistical analyses, IBMS SPSS Statistics (IBM Corp. Released 2016. Version 24.0. Armonk, NY) and "R" was used (R: A language and environment for statistical computing. Released 2013. R Foundation for Statistical Computing, Vienna, Austria).

Depending on distribution, demographic data were analyzed with either t-test and χ^2 test, or Mann–Whitney test and Fisher's exact test. Analogous to previous work, the 20 hidden platform trials were divided into three blocks: block 1 with trials 1–4, block 2 with trials 5–12, and block 3 with trials 13–20. First, for each performance variable of the hidden trial (latency, path length, and heading error), a linear mixed model was fitted. A random effect of individual was added to account for the non-independence between observations from the same individual. Fixed effects included group (BVP vs. healthy controls), time (repeated measurements during the three blocks of trials), and their interaction. The latter interaction term evaluates whether there is a difference in learning between BVP patients and healthy controls during the VMWT. In other words, a statistically significant interaction term points out that during all 20 hidden trials, one group progressively found the platform faster compared with the other group, indicating a better learning curve in this group throughout the test.

In the absence of a significant interaction, linear mixed models were fitted for all performance variables of the hidden trials, with the main factors group (BVP vs. healthy controls) and time (repeated measurements during the three blocks of trials), without interaction term and hearing status as indicated by the high Fletcher index. Using these models, we evaluated whether there was a statistically significant different performance between the two participant's groups, BVP and healthy controls, across all trial blocks. Moreover, using this model, we assessed whether there was a statistically significant main effect of the hearing status on VMWT performance. In all of these models, the following covariates were added: age, sex, computer use, and education.

To compare the spatial memory retrieval during the probe trial, a multiple linear regression model was fitted with the main factors group (BVP vs. healthy controls) and hearing status (high Fletcher index of the better-hearing ear). Again, age, sex, computer use, and education were entered as covariates.

Finally, mean path lengths and latencies during the 10 visible trials were computed and used as dependent variables in a similar multiple linear regression model.

RESULTS

Participant Characteristics

Sixty-four BVP patients with a mean age of 59 ± 14 years met the study inclusion criteria; 60% of them were male. Forty-six healthy controls with a mean age of 48 ± 17 were enrolled in the study; 44% of them were male (**Table 1**). The BVP group was gender matched to the control group. BVP patients were on average older, less educated, and had less computer experience than healthy controls ($p < 0.05$). Hearing loss was more frequent in BVP patients (High Fletcher index 58 ± 42 dB in BVP patients vs. 11 ± 12 dB in healthy controls, $p < 0.05$). To diagnose BVP, the Bárány Society criteria needed to be fulfilled (28). Forty percent of BVP patients met all Bárány Society criteria: a bilateral reduced response on caloric testing, rotatory chair test, and vHIT. In 30% of BVP patients, two out of three Bárány Society criteria were fulfilled, and in the remaining 30% of the BVP patients there was only found a vestibular hypofunction in one of the three vestibular tests (**Figure 4**). The mean gain of the left and right vHIT was, respectively, 4.2 ± 0.3 and 0.47 ± 0.3. The mean gain on the rotatory swing was 0.08 ± 0.08.

TABLE 1 | Demographic data.

	BVP patients *n* = 64	Healthy controls *n* = 46	*P*-value
Age (mean, SD)	59 (14)	48 (17)	<0.05
Sex (*n*, %)			0.1
Male	38 (60)	20 (32)	
Female	26 (33)	26 (57)	
Years of education (mean, SD)	13 (3)	17 (3)	<0.05
Computer use (*n*, %)			<0.05
Seldom/never	15 (27)	2 (6)	
2–5 days/week	10 (18)	4 (11)	
Daily	31 (55)	30 (83)	
Hearing performance: pure tone audiometry			
Fletcher index better-hearing ear (mean, SD in dB)	58 (34)	11 (12)	<0.05

BVP, bilateral vestibulopathy; dB, decibel.

An underlying cause of vestibular loss could not be identified in 33.9% of BVP patients. With a prevalence of nearly 20%, a mutation in the *COCH* gene causing DFNA9 was the most frequent underlying non-idiopathic etiology in our BVP cohort (35). In 16% of BVP patients, an infectious cause was found (e.g., meningitis, neuritis, Lyme disease). Menière's disease and head trauma accounted for, respectively, 6 and 11% of BVP causes. In four BVP patients, an ototoxic cause was suspected (three aminoglycosides antibiotics and one chemotherapy, not further specified).

Results of the VMWT

Hidden Platform Trials: Spatial Learning

First, during the hidden platform trials, a significant main effect of time was found for all outcome measurements, indicating faster determination of the hidden platform location over time (see **Table 2**). No statistically significant interaction between

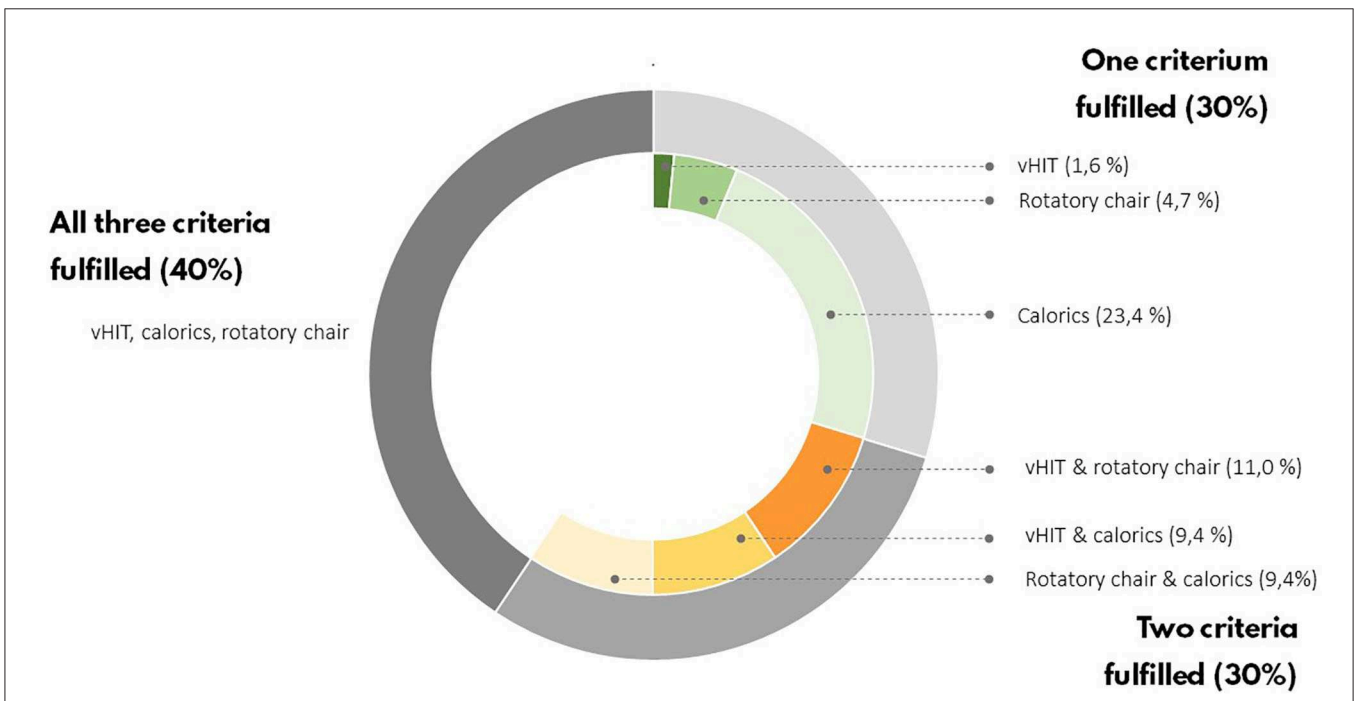

FIGURE 4 | Vestibular test results of BVP patients. According to the Bárány criteria, only one of the vestibular tests have to be bilaterally impaired to establish a BVP diagnosis.

group × time was found in any of the outcome measures. This indicates that, regardless of the absolute outcome measurements in both groups, the learning curve in BVP patients was not significantly slower than in healthy controls. This is also illustrated by a similar slope of the curves in BVP patients and controls showed in **Figures 5–7**.

Second, as shown in **Figures 5**, **6**, BVP patients took both more time and longer paths, compared with healthy controls, to reach the hidden platform during all three trial blocks (1–4, 5–12, and 13–20). Likewise, the heading error of BVP patients was larger during all three trial blocks (see **Figure 7**). Importantly, in linear mixed models no significant group effect for latency, path length, or heading error was found. In other words, the worse performance of BVP patients compared with healthy controls was not statistically significant. All these analyses were adjusted for hearing status, age, sex, computer use, and education. Third, a statistically significant association between hearing loss and spatial learning was seen. The higher the Fletcher index, the longer the latencies were during the hidden trials ($p = 0.006$, effect size 0.11). As the Fletcher index increased by 1 dB, the latency was 0.11 second longer. There was no significant effect of hearing loss on path length or heading error.

TABLE 2 | Results of the linear mixed models used for the hidden platform trials of the Virtual Morris Water Maze.

P-value (effect size if p < 0.05)	Group (BVP vs. healthy controls)	Hearing status (high Fletcher index of better-hearing ear)	Age
Latency	0.16	0.006 (0.11)	<0.001 (0.86)
Path length	0.28	0.76	0.04 (0.01)
Heading error	0.32	0.56	<0.001 (0.3)

Outcome measures for spatial learning were (1) latency, (2) path length, and (3) heading error. All analyses adjusted for age, sex, computer use, education, and hearing loss. A p < 0.05 indicates a statistically significant main effect of the examined factor.
BVP, bilateral vestibulopathy.

Probe Trial: Spatial Memory Retrieval

During the probe trial, BVP patients searched 38% (±23.3) of their time in the correct quadrant, whereas healthy controls spent 52.1% (±22.7) in the correct quadrant. However, this difference was not statistically significant between the two groups (p-value in multiple linear regression model of groups = 0.9).

Nonetheless, the analysis revealed a significant main effect of hearing loss on relative amount of time spent in the correct quadrant ($p = 0.05$, β −0.1). This indicates that the worse the hearing, the poorer the memory retrieval. The results of the probe trial are demonstrated in **Figures 8**, **9**.

Visible Trials: Motor Control Condition

No significant effects of group or hearing status were found during the visible platform trials regarding latency, path length, and heading error. This indicates that BVP patients showed no difference in their motor control condition, compared with

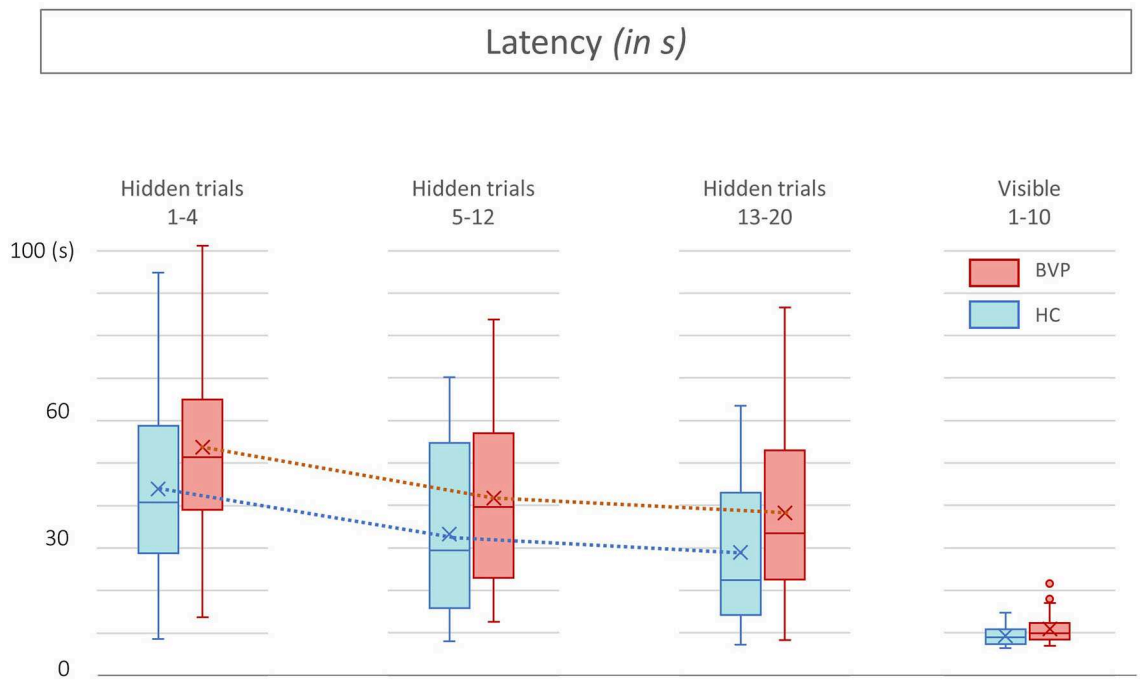

FIGURE 5 | Latencies from patients with bilateral vestibulopathy and healthy controls. This figure shows performance of patients with bilateral vestibulopathy (BVP, red) and healthy controls (HC, blue) during the 20 hidden platform trials and 10 visible platform trials of the Virtual Morris Water Maze. The latency, defined by the time in seconds needed to find the platform, is a measure for spatial learning. During all hidden platform trials, HC outperform BVP patients.

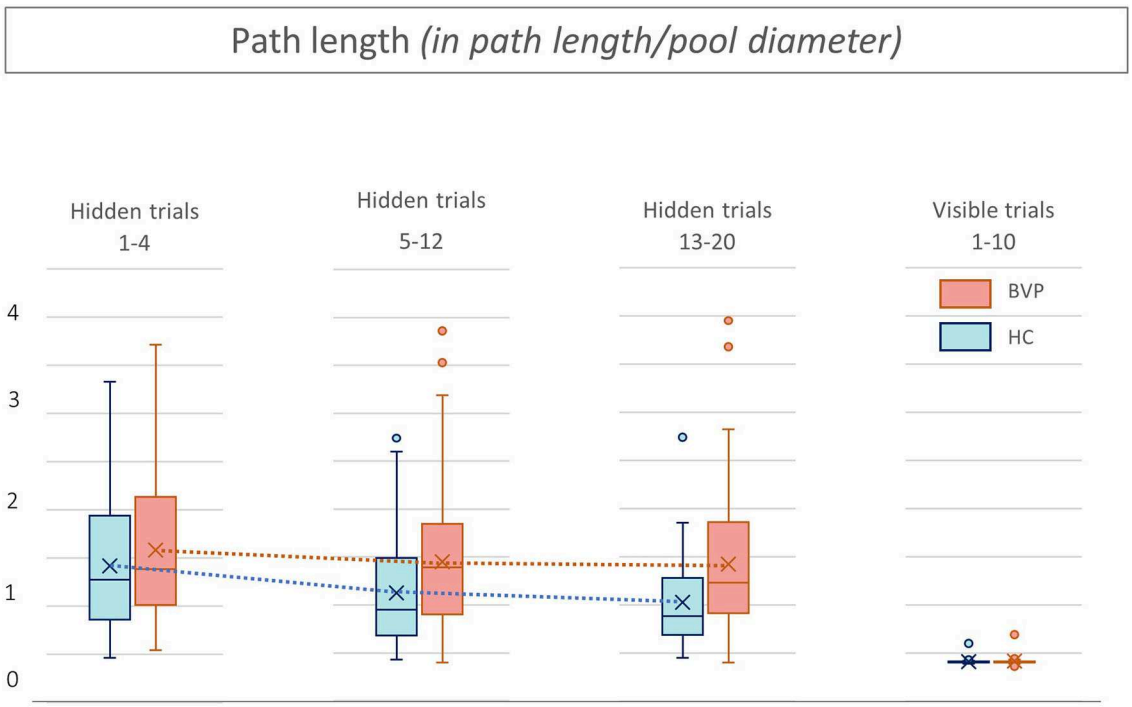

FIGURE 6 | Path length from patients with bilateral vestibulopathy and healthy controls. This figure shows performance of patients with bilateral vestibulopathy (BVP, red) and healthy controls (HC, blue) during the 20 hidden platform trials and 10 visible platform trials of the Virtual Morris Water Maze. The path length, defined by the relative distance to the pool diameter covered to reach the platform, is a measure for spatial learning. During all hidden platform trials, performance of BVP patients is worse than HC.

healthy controls. Results of the visible trials are shown in **Figures 5**–**7**.

DISCUSSION

The present study was designed to evaluate whether BVP patients suffer from spatial cognitive deficits compared with healthy controls. Furthermore, the analyses in this study were especially set out with the aim of evaluating the importance of concomitant hearing loss of BVP patients regarding the suspected relationship between cognition and the vestibular system.

In one of the largest BVP patient group so far, this study found a worse performance on all outcome measures of the VMWT in BVP patients compared with healthy controls. However, this difference was never statistically significant between the BPV group and the healthy control group. In contrast to earlier studies, all statistical analyses of this study included correction for hearing (dys)function. Although no significant group difference was observed, it seemed that, on the other hand, hearing loss was found to be statistically significantly associated with worse spatial cognition. The worse the hearing of BVP patients, the worse the spatial learning indicated by longer latencies in the hidden trial of the VMWT. Likewise, in the probe trial, hearing loss resulted in less time spent in the platform quadrant, which suggests worse spatial memory retrieval.

Vestibular Loss and Spatial Cognition

Previous studies have not dealt with the hearing status of the enrolled BVP patients when drawing conclusions about the relationship between vestibular loss and cognitive decline (6). Given the observed statistically significant effect of hearing loss on spatial cognition, this study highlights the need to correct for hearing loss when evaluating cognition in vestibular patients. Furthermore, our findings raise intriguing questions regarding the assumed link between cognition and the vestibular system. According to our results, it could be questioned whether the spatial cognitive deficits of BVP patients might be solely attributed to their hearing loss and not to their vestibular loss. However, it is important to bear in mind that the control group in this study included subjects with normal age-appropriate hearing. Hence, some of the control subjects suffered from presbyacusis, but overall the prevalence of hearing loss in the control group is low. Therefore, results should be interpreted with caution and it cannot be concluded that hearing loss is the only factor resulting in the spatial cognitive deficits of BVP patients. Vestibular loss might play an additional role. Moreover, previous studies observing spatial deficits in BVP patients included patients with complete vestibular loss. In this study, patients with BVP, as defined by the Bárány criteria, were included. This implicates that also patients with partial vestibular loss were included, for example, preserved function on vHIT in the absence of caloric function (7). Future work

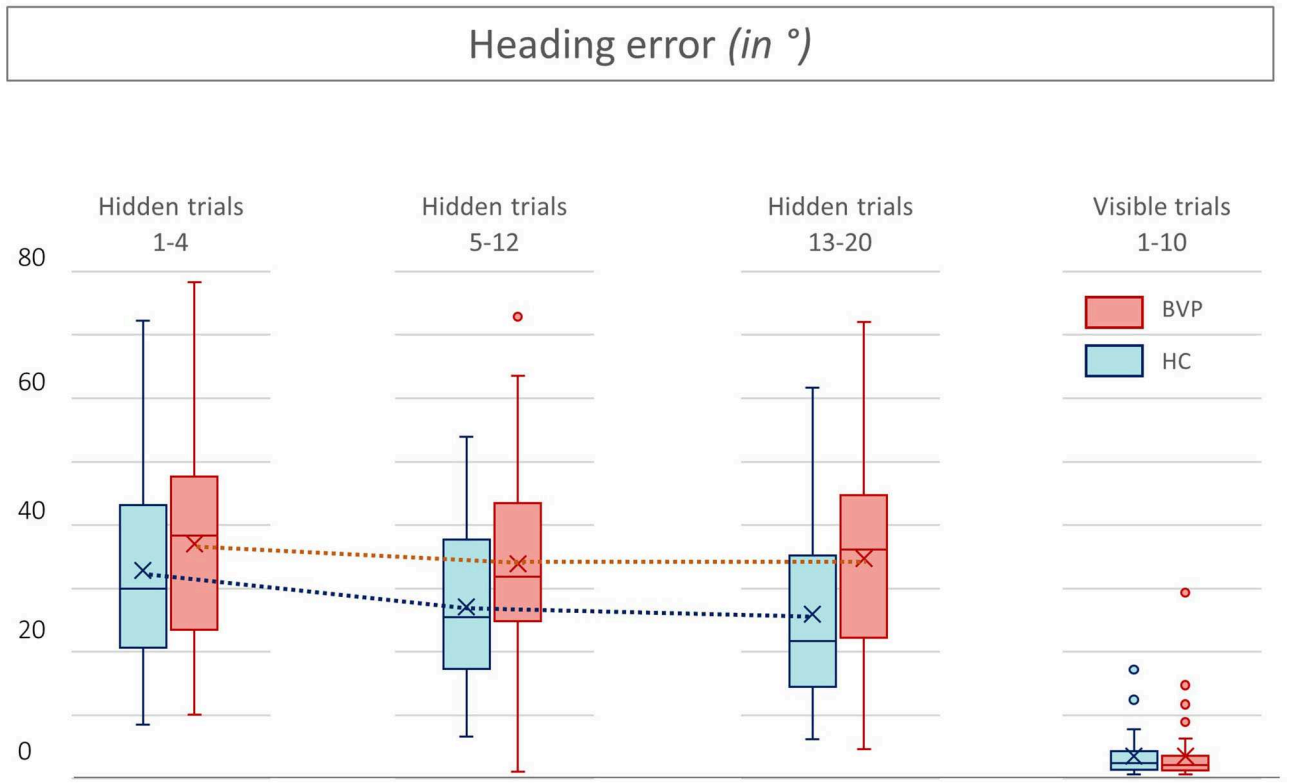

FIGURE 7 | Heading errors from patients with bilateral vestibulopathy and healthy controls. This figure shows the performance of patients with bilateral vestibulopathy (BVP, red) and healthy controls (HC, blue) during the 20 hidden platform trials and 10 visible platform trials of the Virtual Morris Water Maze. The higher the heading error, the worse the performance and thus spatial learning. In all hidden trials, the heading errors of BVP patients are higher than those of HC.

is required to further unravel the link between cognition, vestibular loss, and hearing loss. An interesting study protocol would be to compare spatial cognition between four groups: healthy controls, patients with hearing dysfunction and normal vestibular function, patients with normal hearing and vestibular dysfunction and finally, patients with both vestibular and hearing dysfunction.

Nonetheless, for all future studies investigating cognition in BVP patients, our results implicate that it is obligatory to take the hearing status of BVP patients into account.

Hearing Loss, Spatial Cognition, and the Hippocampus

In accordance with the present results, previous studies have demonstrated a link between spatial cognition and hearing loss. A recent meta-analysis showed a significant impairment of visuospatial abilities in patients with hearing loss across cross-sectional studies, using a wide variety of spatial cognitive tasks (26).

Two recent animal studies investigated spatial cognition using the Morris Water Maze (36, 37). Mice with presbyacusis were found to have worse spatial learning and spatial memory retrieval compared with mice with normal hearing (36). Likewise, mice with noise-induced hearing loss showed poorer performance during the Morris Water Maze (37). This was pointed out by longer latencies during the hidden platform trials and less time spent in the platform quadrant during a probe trial in mice with noise-induced hearing loss compared with mice with normal hearing. It is important to note that mice typically do not perform well in the Morris Water Maze and authors suggest that they might not use spatial strategy. Hence, caution should be taken to extrapolate these findings to humans (38).

The hippocampus is the area of the brain that has long been implicated in spatial memory. Animal and human studies have shown altered functioning and even atrophy of the hippocampus in subjects with vestibular loss [for review see (4)]. Interestingly, the poorer spatial performance of mice with hearing loss was also accompanied by a decrease of hippocampal neurogenesis (37). As the Morris Water Maze does not rely upon auditory function, authors hypothesize that the auditory input plays a maintenance role for hippocampal function and neurogenesis (37). However, it should be noted that exposing mice to noise trauma does not only result in hearing loss but might also induce peripheral vestibular damage (39, 40). This has not been taken into account in the study. Hence, it is possible that the decreased hippocampal neurogenesis observed in mice with noise-induced hearing loss is (partially) related to a loss of peripheral vestibular input. Vice versa, despite the extensive previous research, many questions remain about the neuroanatomical substrate underlying the association between

the vestibular system, spatial cognition, and the hippocampus. Little research has been carried out to investigate if subjects with hearing loss have altered hippocampal function and volume. Hence, it could conceivably be hypothesized that hearing loss plays a role in the assumed neuroanatomical pathways between the peripheral vestibular input and the hippocampal and cortical areas involved in spatial cognition.

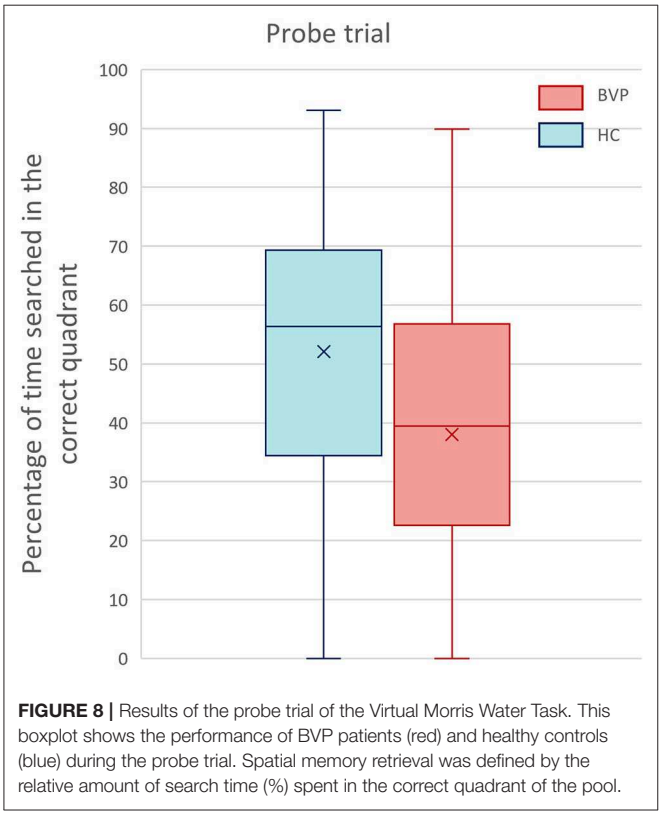

FIGURE 8 | Results of the probe trial of the Virtual Morris Water Task. This boxplot shows the performance of BVP patients (red) and healthy controls (blue) during the probe trial. Spatial memory retrieval was defined by the relative amount of search time (%) spent in the correct quadrant of the pool.

The VMWT to Assess Spatial Cognition in BVP Patients

In previous literature, the VMWT seemed to be one of the most used tools to assess spatial cognition in vestibular patients (2). In patients with complete loss of vestibular input after a bilateral vestibular neurectomy, distinct poorer performance was observed on the hidden and probe trials of the VMWT (7). In a more recent study of the same group, patients with severe but incomplete BVP showed more subtle spatial cognitive deficits (3). Likewise, in patients with a unilateral loss of vestibular input, only one of the outcome measures was impaired in patients with right unilateral vestibulopathy. In the patients with left unilateral vestibulopathy, none of the outcome measures differed significantly from controls (8). These results suggest that with increasing loss of peripheral vestibular input, the spatial cognition decreases. In our study, most BVP patients suffered from a deep but incomplete loss of vestibular function. It is possible, therefore, that the worse VMWT performance in our BVP patients did not yield statistically significance level.

Furthermore, the purely stationary set-up of the VMWT might underestimate the real-life spatial cognitive deficits of BVP patients as a result of loss of vestibular input. Previous research has established that, while navigating, an "inner neural map" is created, based on peripheral vestibular input. This neural representation of the external environment is computed in the hippocampus and entorhinal cortex and consists of several cooperative cell types: angular head velocity cells; head direction cells; place and grid cells (41). Rodent studies have demonstrated that vestibular input modulates the activity of the head direction cells and the place cells (33, 42). As the VMWT is static, the task does not rely on any vestibular input from real locomotion.

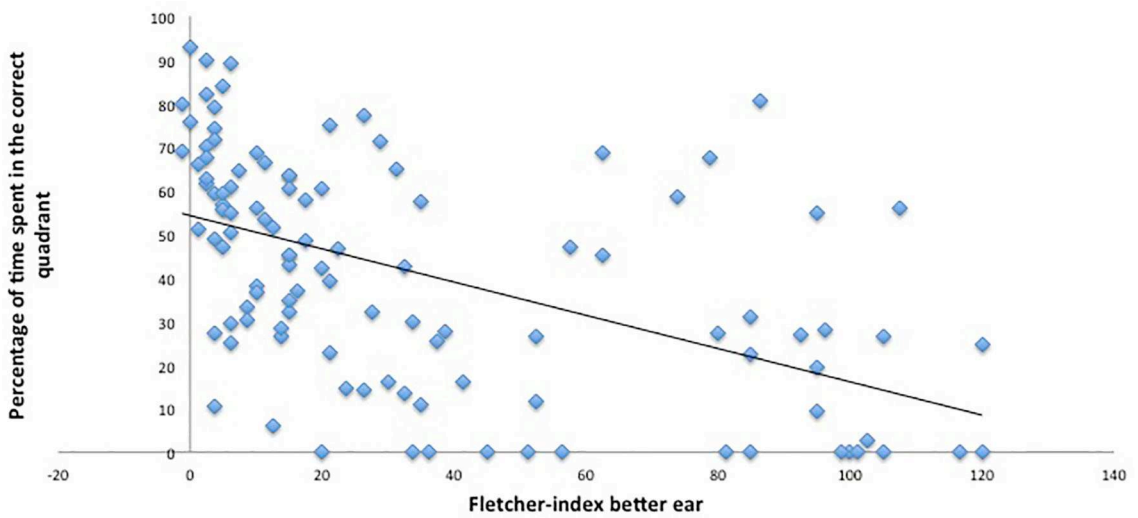

FIGURE 9 | Hearing thresholds and performance in the probe trial. This figure indicates the worse the hearing (higher hearing thresholds or Fletcher indexes), the worse the performance on the VMWT probe trial (less time spent in the correct quadrant).

Hence, it is likely that real-life navigation tasks will be more sensitive to reveal spatial cognitive deficits in BVP patients.

Moreover, attentional deficits are demonstrated in BVP patients (3, 6, 43). According to Kahneman's Capacity Model of Attention in which an individual has a limited total amount of cognitive resources available to divide among mental tasks, dual tasking might be more demanding in BVP patients because of the increased attentional need for keeping balance (34). As subjects stay seated during the VMWT, attentional resources can be fully directed toward the spatial memory task. This might be a second reason why the VMWT underestimates the real-life spatial cognitive deficits of BVP patients.

To sum up, the VMWT is a widely used method to assess spatial cognition in humans (9). Several studies have demonstrated spatial cognitive deficits in BVP patients, using the VMWT (3, 7, 8). However, previous studies have not dealt with the concomitant hearing loss of BVP patients. As hearing loss is a risk factor for dementia, this might be an important forgotten factor. This is the first study investigating spatial cognition by use of the VMWT in a BVP group as large as 64 patients, and with correction for the hearing (dys)function in all analyses. All outcome measures of the VMWT were worse in BVP patients compared with healthy controls; however, these differences were not statistically significant. Contrarily, hearing loss was statistically significantly associated with worse spatial learning and spatial memory retrieval. Regarding our study protocol with healthy controls without severe hearing loss, it is not excluded that vestibular loss has an additional effect on spatial cognition. Nonetheless, our findings confirm the negative repercussion of hearing loss on spatial cognition (26), and highlight the need to correct for hearing loss when investigating cognition in a vestibular population group.

Both vestibular and hearing dysfunction are prevalent in the elderly (32, 44, 45). Given the rising prevalence of dementia, and the current lack of therapy, future studies are needed to identify modifiable risk factors (16). Therefore, the link between cognitive decline and the hippocampus on the one hand and hearing loss and vestibular loss on the other hand needs to be further unraveled. To develop a full picture, a study protocol that would additionally include patients with normal vestibular function but different levels of sensorineural hearing loss would be interesting. Furthermore, considering the static and single task paradigm involved in the VMWT, real navigation tasks might give more insights in the potential spatial cognitive deficits related to the loss of vestibular input.

Limitations

The subjects in our HC group were not perfectly matched to BVP patients regarding age, education, and computer experience. As HC were on average younger, more educated, and more computer experienced, VMWT performance could be relatively overestimated in the HC group. Regarding the observed negative effect of hearing loss on spatial cognition (longer latencies and less time spent in the correct quadrant), it is important to bear in mind that the majority of patients with hearing loss were in the BVP group. Therefore, it is not excluded that vestibular loss plays an additional role in spatial cognition, which could not be observed in this study protocol using healthy controls with normal hearing. Second, there was a correlation with hearing loss and age. Although all models were corrected for age, it is not excluded that age might play an important role in the observed link between spatial cognition and hearing loss.

CONCLUSION

The present study assesses spatial cognitive performance in one of the largest BVP cohorts so far. The study was especially designed to determine the relative importance of hearing loss in spatial cognition of BVP patients, as this has been frequently overlooked. We found worse spatial cognitive performance on all outcome measures of BVP patients. However, these differences were not statistically significant between the BVP patients and healthy controls, when corrected for age, gender, education, level of computer use, and hearing loss. Interestingly, only hearing loss was found to be statistically significantly associated with worse spatial cognition. These findings highlight the need to correct for hearing loss in future studies investigating cognition in BVP patients. As the control group did not include subjects with severe hearing loss, an additional effect of vestibular loss on spatial cognitive performance cannot be excluded.

ADDITIONAL COMMENTS

These data have partially been presented on the 30th Bárány conference, Uppsala, June 2018.

DATA AVAILABILITY STATEMENT

The raw data supporting the conclusions of this article will be made available by the authors, without undue reservation.

ETHICS STATEMENT

The studies involving human participants were reviewed and approved by local ethics committee of the Antwerp University Hospital/University of Antwerp (protocol number 16/42/426). The patients/participants provided their written informed consent to participate in this study.

AUTHOR CONTRIBUTIONS

BD: data collection, statistical analyses, study concept, and writing manuscript. GM, RB, and PV: study concept and supervision. JM: data collection. EF: study concept and statistical analyses. VV: study concept, writing manuscript, and supervision. All authors contributed to the article and approved the submitted version.

FUNDING

The Antwerp University Hospital and Maastricht University Medical Center have received research and travel grants from MED-EL. The funders had no role in study design, data collection and analysis, decision to publish, or preparation of the manuscript.

REFERENCES

1. Smith PF, Zheng Y. From ear to uncertainty: vestibular contributions to cognitive function. *Front Integr Neurosci*. (2013) 7:84. doi: 10.3389/fnint.2013.00084
2. Bigelow RT, Agrawal Y. Vestibular involvement in cognition: visuospatial ability, attention, executive function, and memory. *J Vestib Res*. (2015) 25:73–89. doi: 10.3233/VES-150544
3. Kremmyda O, Hufner K, Flanagin VL, Hamilton DA, Linn J, Strupp M, et al. Beyond dizziness: virtual navigation, spatial anxiety and hippocampal volume in bilateral vestibulopathy. *Front Hum Neurosci*. (2016) 10:139. doi: 10.3389/fnhum.2016.00139
4. Smith PF. The vestibular system and cognition. *Curr Opin Neurol*. (2017) 30:84–9. doi: 10.1097/WCO.0000000000000403
5. Sachdev PS, Blacker D, Blazer DG, Ganguli M, Jeste DV, Paulsen JS, et al. Classifying neurocognitive disorders: the DSM-5 approach. *Nat Rev Neurol*. (2014) 10:634–42. doi: 10.1038/nrneurol.2014.181
6. Dobbels BPO, Boon B, Mertens G, Van De Heyning P, Van Rompaey V. Impact of bilateral vestibulopathy on spatial and nonspatial cognition: a systematic review. *Ear Hear*. (2018) 40:757–65. doi: 10.1097/AUD.0000000000000679
7. Brandt T, Schautzer F, Hamilton DA, Bruning R, Markowitsch HJ, Kalla R, et al. Vestibular loss causes hippocampal atrophy and impaired spatial memory in humans. *Brain*. (2005) 128:2732–41. doi: 10.1093/brain/awh617
8. Hufner K, Hamilton DA, Kalla R, Stephan T, Glasauer S, Ma J, et al. Spatial memory and hippocampal volume in humans with unilateral vestibular deafferentation. *Hippocampus*. (2007) 17:471–85. doi: 10.1002/hipo.20283
9. Hamilton DA, Driscoll I, Sutherland RJ. Human place learning in a virtual Morris water task: some important constraints on the flexibility of place navigation. *Behav Brain Res*. (2002) 129:159–70. doi: 10.1016/S0166-4328(01)00343-6
10. Lucieer F, Duijn S, Van Rompaey V, Perez Fornos A, Guinand N, Guyot JP, et al. Full spectrum of reported symptoms of bilateral vestibulopathy needs further investigation-a systematic review. *Front Neurol*. (2018) 9:352. doi: 10.3389/fneur.2018.00352
11. Fawzy M, Khater A. Bilateral vestibulopathy treatment: update and future directions. *Egypt J Otolaryngol*. (2016) 32:83–92. doi: 10.4103/1012-5574.181082
12. Hain TC, Cherchi M, Yacovino DA. Bilateral vestibular loss. *Semin Neurol*. (2013) 33:195–203. doi: 10.1055/s-0033-1354597
13. Lee YM, Jang C, Bak IH, Yoon JS. Effects of computer-assisted cognitive rehabilitation training on the cognition and static balance of the elderly. *J Phys Ther Sci*. (2013) 25:1475–7. doi: 10.1589/jpts.25.1475
14. Smith-Ray RL, Irmiter C, Boulter K. Cognitive training among cognitively impaired older adults: a feasibility study assessing the potential improvement in balance. *Front Public Health*. (2016) 4:219. doi: 10.3389/fpubh.2016.00219
15. Ellis AW, Schone CG, Vibert D, Caversaccio MD, Mast FW. Cognitive rehabilitation in bilateral vestibular patients: a computational perspective. *Front Neurol*. (2018) 9:286. doi: 10.3389/fneur.2018.00286
16. Alzheimer's A. 2016 Alzheimer's disease facts and figures. *Alzheimers Dement*. (2016) 12:459–509. doi: 10.1016/j.jalz.2016.03.001
17. Halliday G. Pathology and hippocampal atrophy in Alzheimer's disease. *Lancet Neurol*. (2017) 16:862–4. doi: 10.1016/S1474-4422(17)30343-5
18. Birdane L, Incesulu A, Gurbuz MK, Ozbabalik D. Sacculocolic reflex in patients with dementia: is it possible to use it for early diagnosis? *Neurol Sci*. (2012) 33:17–21. doi: 10.1007/s10072-011-0595-3
19. Nakamagoe K, Fujimiya S, Koganezawa T, Kadono K, Shimizu K, Fujizuka N, et al. Vestibular function impairment in Alzheimer's disease. *J Alzheimers Dis*. (2015) 47:185–96. doi: 10.3233/JAD-142646
20. Harun A, Oh ES, Bigelow RT, Studenski S, Agrawal Y. Vestibular impairment in dementia. *Otol Neurotol*. (2016) 37:1137–42. doi: 10.1097/MAO.0000000000001157
21. Livingston G, Sommerlad A, Orgeta V, Costafreda SG, Huntley J, Ames D, et al. Dementia prevention, intervention, and care. *Lancet*. (2017) 390:2673–734. doi: 10.1016/S0140-6736(17)31363-6
22. Zingler VC, Cnyrim C, Jahn K, Weintz E, Fernbacher J, Frenzel C, et al. Causative factors and epidemiology of bilateral vestibulopathy in 255 patients. *Ann Neurol*. (2007) 61:524–32. doi: 10.1002/ana.21105
23. Lucieer F, Vonk P, Guinand N, Stokroos R, Kingma H, Van De Berg R. Bilateral vestibular hypofunction: insights in etiologies, clinical subtypes, and diagnostics. *Front Neurol*. (2016) 7:26. doi: 10.3389/fneur.2016.00026
24. Claes AJ, Van De Heyning P, Gilles A, Hofkens-Van Den Brandt A, Van Rompaey V, Mertens G. Impaired cognitive functioning in cochlear implant recipients over the age of 55 years: a cross-sectional study using the repeatable battery for the assessment of neuropsychological status for hearing-impaired individuals (RBANS-H). *Front Neurosci*. (2018) 12:580. doi: 10.3389/fnins.2018.00580
25. Claes AJ, Van De Heyning P, Gilles A, Van Rompaey V, Mertens G. Cognitive performance of severely hearing-impaired older adults before and after cochlear implantation: preliminary results of a prospective, longitudinal cohort study using the RBANS-H. *Otol Neurotol*. (2018). doi: 10.1097/MAO.0000000000001936
26. Loughrey DG, Kelly ME, Kelley GA, Brennan S, Lawlor BA. Association of age-related hearing loss with cognitive function, cognitive impairment, and dementia: a systematic review and meta-analysis. *JAMA Otolaryngol Head Neck Surg*. (2018) 144:115–26. doi: 10.1001/jamaoto.2017.2513
27. Dobbels B, Mertens G, Gilles A, Claes A, Moyaert J, Van De Berg R, et al. Cognitive function in acquired bilateral vestibulopathy: a cross-sectional study on cognition, hearing, and vestibular loss. *Front Neurosci*. (2019) 13:340. doi: 10.3389/fnins.2019.00340
28. Strupp M, Kim JS, Murofushi T, Straumann D, Jen JC, Rosengren SM, et al. Bilateral vestibulopathy: diagnostic criteria consensus document of the Classification Committee of the Barany Society. *J Vestib Res*. (2017) 27:177–89. doi: 10.3233/VES-170619
29. Van Der Stappen A, Wuyts FL, Van De Heyning PH. Computerized electronystagmography: normative data revisited. *Acta Otolaryngol*. (2000) 120:724–30. doi: 10.1080/000164800750000243
30. Macdougall HG, Mcgarvie LA, Halmagyi GM, Curthoys IS, Weber KP. The video Head Impulse Test (vHIT) detects vertical semicircular canal dysfunction. *PLoS ONE*. (2013) 8:e61488. doi: 10.1371/journal.pone.0061488
31. Morris R. Spatial localization does not require the presence of local cues. *Learn Motiv*. (1981) 12:239–60. doi: 10.1016/0023-9690(81)90020-5
32. Lin FR, Thorpe R, Gordon-Salant S, Ferrucci L. Hearing loss prevalence and risk factors among older adults in the United States. *J Gerontol A Biol Sci Med Sci*. (2011) 66:582–90. doi: 10.1093/gerona/glr002
33. Yoder RM, Taube JS. The vestibular contribution to the head direction signal and navigation. *Front Integr Neurosci*. (2014) 8:32. doi: 10.3389/fnint.2014.00032
34. Bigelow RT, Semenov YR, Trevino C, Ferrucci L, Resnick SM, Simonsick EM, et al. Association between visuospatial ability and vestibular function in the Baltimore longitudinal study of aging. *J Am Geriatr Soc*. (2015) 63:1837–44. doi: 10.1111/jgs.13609
35. De Belder J, Matthysen S, Claes AJ, Mertens G, Van De Heyning P, Van Rompaey V. Does otovestibular loss in the autosomal dominant disorder DFNA9 have an impact of on cognition? A systematic review. *Front Neurosci*. (2017) 11:735. doi: 10.3389/fnins.2017.00735
36. Dong Y, Guo CR, Chen D, Chen SM, Peng Y, Song H, et al. Association between agerelated hearing loss and cognitive decline in C57BL/6J mice. *Mol Med Rep*. (2018) 18:1726–32. doi: 10.3892/mmr.2018.9118
37. Liu L, Xuan C, Shen P, He T, Chang Y, Shi L, et al. Hippocampal mechanisms underlying impairment in spatial learning long after establishment of noise-induced hearing loss in CBA mice. *Front Syst Neurosci*. (2018) 12:35. doi: 10.3389/fnsys.2018.00035
38. Whishaw IQ, Tomie J. Of mice and mazes: similarities between mice and rats on dry land but not water mazes. *Physiol Behav*. (1996) 60:1191–7. doi: 10.1016/S0031-9384(96)00176-X
39. Stewart C, Yu Y, Huang J, Maklad A, Tang X, Allison J, et al. Effects of high intensity noise on the vestibular system in rats. *Hear Res*. (2016) 335:118–27. doi: 10.1016/j.heares.2016.03.002
40. Stewart CE, Kanicki AC, Altschuler RA, King WM. Vestibular short-latency evoked potential abolished by low-frequency noise exposure in rats. *J Neurophysiol*. (2018) 119:662–7. doi: 10.1152/jn.00668.2017

41. Brandt T, Zwergal A, Glasauer S. 3-D spatial memory and navigation: functions and disorders. *Curr Opin Neurol*. (2017) 30:90–7. doi: 10.1097/WCO.0000000000000415
42. Stackman RW, Clark AS, Taube JS. Hippocampal spatial representations require vestibular input. *Hippocampus*. (2002) 12:291–303. doi: 10.1002/hipo.1112
43. Popp P, Wulff M, Finke K, Ruhl M, Brandt T, Dieterich M. Cognitive deficits in patients with a chronic vestibular failure. *J Neurol*. (2017) 264:554–63. doi: 10.1007/s00415-016-8386-7
44. Agrawal Y, Carey JP, Della Santina CC, Schubert MC, Minor LB. Disorders of balance and vestibular function in US adults: data from the National Health and Nutrition Examination Survey, 2001-2004. *Arch Intern Med*. (2009) 169:938–44. doi: 10.1001/archinternmed.2009.66
45. Agrawal Y, Van de Berg R, Wuyts F, Walther L, Magnusson M, Oh E, et al. Presbyvestibulopathy: diagnostic criteria. *J Vestibul Res*. (2018) 29:161–70. doi: 10.3233/VES-190672

Conflict of Interest: The authors declare that the research was conducted in the absence of any commercial or financial relationships that could be construed as a potential conflict of interest.

frontiers in Neurology

ORIGINAL RESEARCH
published: 18 August 2020
doi: 10.3389/fneur.2020.00814

Readaptation Treatment of Mal de Debarquement Syndrome With a Virtual Reality App: A Pilot Study

Sergei B. Yakushin[1]*, *Reilly Zink*[2,3], *Brian C. Clark*[2,4] and *Chang Liu*[2,3]

[1] Department of Neurology, Icahn School of Medicine at Mount Sinai, New York, NY, United States, [2] Ohio Musculoskeletal and Neurological Institute (OMNI), Ohio University, Athens, OH, United States, [3] School of Electrical Engineering and Computer Science, Ohio University, Athens, OH, United States, [4] Department of Biomedical Sciences, Ohio University, Athens, OH, United States

Mal de Debarquement syndrome (MdDS) is composed of constant phantom sensations of motion, which are frequently accompanied by increased sensitivity to light, inability to walk on a patterned floor, the sensation of ear fullness, head pressure, anxiety, and depression. This disabling condition generally occurs in premenopausal women within 2 days after prolonged passive motion (e.g., travel on a cruise ship, plane, or in a car). It has been previously hypothesized that MdDS is the result of maladaptive changes in the polysynaptic vestibulo-ocular reflex (VOR) pathway called velocity storage. Past research indicates that full-field optokinetic stimulation is an optimal way to activate velocity storage. Unfortunately, such devices are typically bulky and not commonly available. We questioned whether virtual reality (VR) goggles with a restricted visual field could effectively simulate a laboratory environment for MdDS treatment. A stripes program for optokinetic stimulation was implemented using Google Daydream Viewer. Five female patients (42 ± 10 years; range 26–50), whose average MdDS symptom duration was 2 months, participated in this study. Four patients had symptoms triggered by prolonged passive motion, and in one, symptoms spontaneously occurred. Symptom severity was self-scored by patients on a scale of 0–10, where 0 is no symptoms at all and 10 is the strongest symptoms that the patient could imagine. Static posturography was obtained to determine objective changes in body motion. The treatment was considered effective if the patient's subjective score improved by at least 50%. All five patients reported immediate improvement. On 2-month follow-ups, symptoms returned only in one patient. These data provide proof of concept for the limited-visual-field goggles potentially having clinical utility as a substitute for full-field optokinetic stimulation in treating patients with MdDS in clinics or via telemedicine.

Keywords: Mal de Debarquement syndrome, velocity storage, readaptation, rocking, swaying, bobbing

OPEN ACCESS

Edited by:
Michael Strupp, Ludwig Maximilian University of Munich, Germany

Reviewed by:
Floris Wuyts, University of Antwerp, Belgium
Hans van der Steen, Erasmus University Rotterdam, Netherlands

***Correspondence:**
Sergei B. Yakushin
sergei.yakushin@mssm.edu

Specialty section:
This article was submitted to Neuro-Otology, a section of the journal Frontiers in Neurology

Received: *22 May 2020*
Accepted: *29 June 2020*
Published: *18 August 2020*

Citation:
Yakushin SB, Zink R, Clark BC and Liu C (2020) Readaptation Treatment of Mal de Debarquement Syndrome With a Virtual Reality App: A Pilot Study. Front. Neurol. 11:814. doi: 10.3389/fneur.2020.00814

INTRODUCTION

Mal de Debarquement syndrome (MdDS) is a debilitating phantom sensation of motion that generally occurs within 48 h after prolonged transportation (motion triggered, MT) or with no specific motion preceding it (spontaneously occurred, SO) (1). The most frequent motion sensations are of rocking (forward back), swaying (side-to-side), bobbing, walking on a trampoline,

or gravitational pull in a specific direction. Motion sensations are frequently accompanied by psychosomatic symptoms such as brain fog, fullness of ears, heavy head and heavy leg sensations, fuzzy vision, fatigue, and high sensitivity to fluorescent lights, computer screens, and unsteadiness in crowds (2). The distinct difference between MdDS and the other vestibular disorders is that symptoms of MdDS are temporarily relieved by passive motion (1).

Head rotation is sensed by hair cells located at the ampulla of the semicircular canals of the inner ear. When the head is rotated at a constant velocity, primary vestibular afferents sense this rotation for ≈4 s from the rotation onset (3–5). At the same time, when the subject is rotated in darkness at a constant velocity, this rotation induces eye nystagmus that lasts 12–20 s (6), which is longer than the response time of the primary afferents. Thus, information about head velocity must be stored in the brain to produce such an extended eye response. In the 1970s, two groups of scientists simultaneously came to the concept that they called velocity storage mechanism (integrator) (7, 8). Despite minor differences in the two proposed models, both suggested that velocity information is temporarily stored in the brain. Because nystagmus dies away within 12–20 s, the integrator was modeled with a leak of stored velocity signal. Both models assumed that the vestibulo-ocular reflex (VOR) is composed of 3-neuronal (direct) VOR pathway that is more or less independent of the polysynaptic velocity storage (indirect) pathway.

Over the next three decades, the spatial properties of the velocity storage were intensively investigated (9–11). One of the most important findings was that velocity storage could be identically activated either by head rotation or by optokinetic stimulation (OKS) (7). If the subject is kept in darkness in the upright position after the horizontal optokinetic nystagmus (OKN) was induced, OKN is followed by horizontal optokinetic after nystagmus (OKAN), which dies away with the time constant of velocity storage (12, 13). A second important finding was that when horizontal OKN is induced with the subject tilted relative to gravity, it induces vertical or torsional OKAN components, depending on head orientation relative to gravity. As a result, when nystagmus is initiated off the vertical axis, the axis of eye rotation (eigenvector) during OKAN tends to align with the axis of gravity (12, 13).

OKN through velocity storage mechanism complements the function of the vestibular system by prolonging eye movement response to constant velocity of rotation in light (9, 10). While gain (slow-phase eye velocity/stimulus velocity) of the vestibular function is optimal at high frequencies (14–16), the gain of OKN is optimal at low frequencies and low peak velocities (17).

Lesion of the foveal area in primates did not affect the profile of slow-phase eye velocities of OKN (18). This implies that true OKN and velocity storage are generated by the visual periphery (19). As such, it is logical to assume that full-field OKN stimulation should be stronger than visual stimulation of the restricted visual field. Indeed, it has been shown that edges of the visual field affect OKN (20). Thus, OKS with restricted visual field may not be as effective as a full-field OKN. While the size of the visual field is a factor (21), however, it is less relevant for low-speed OKN, which is commonly used for MdDS treatment (22, 23). Human horizontal visual field is about ±105°, while vertical is only 50 and 70° when looking up and down, respectively (24). It was previously demonstrated that goggles with limited field (±44° horizontally and ±36° vertically) can adequately activate velocity storage (13). The visual field of our virtual reality (VR) goggles was approximately ±45° horizontally and vertically, which is comparable with what was previously used to activate velocity storage (13). Thus, the purpose of this project was to determine whether limited-field OKN produced by VR goggles could substitute for full-field OKN in successful treatment of MdDS. The velocity storage integrator is a network of neurons between left and right rostral medial and superior vestibular nuclei (25). Neurons that code velocity storage utilize $GABA_B$ as a transmitter (26–28). Their firing rate is not related to eye movement *per se* but is related to head velocity. This is why they are called vestibular-only (VO) neurons. Their firing rate, however, is modulated by OKN (29–31). VO neurons do not project directly to the oculomotor plant (32) but rather are a part of the polysynaptic (indirect) VOR pathway (31). Many of them project to the spinal cord and are part on the vestibular postural control (33).

The gain (eye velocity/head velocity) of the direct VOR can be modified (adapted) within minutes by changing the visual feedback in response to head rotation (34–36). However, induced changes are reversed back within the same time if conditions change (37, 38). VOR gain adaptation can be induced with a specific context (39–41). Contextual adaptation is more prolonged, and gain changes induced in 1 h can last for several days (42, 43).

Similar to the direct 3-neuronal VOR pathway, horizontal (yaw), vertical (pitch), and torsional (roll) components of velocity storage can be adapted (44). This is a key foundational premise for the MdDS treatment approach proposed by Dai et al. (2, 45). The full-field OKN induces a sensation of body rotation in the direction opposite to stripes' motion (vection) that is indistinguishable from actual rotation in light with stripes stationary in space (46). It was recently demonstrated that amounts of vection and velocity storage are directly correlated (47). Thus, according to VOR readaptation hypotheses, when the ship is turning relative to the coastline, it induces horizontal OKN (yaw axis rotation), if the passenger is facing the ship's direction of motion. At the same time, all ships are oscillating side-to-side at ≈0.2 Hz, which is a dominant frequency of water oscillation in the ocean (48). The ship's side-to-side oscillations induce head oscillations about the naso-occipital (roll) axis. Simultaneous head rotation about 2-axis according to Euler's rotational theorem is inducing rotation about third (pitch) axes (49). Thus, if the passenger is facing the motions, oscillations about pitch axis can be stored in the velocity storage part of the VOR pathway (44, 50). Similarly, if the patient stands sideways to the ship's long axis, oscillations in roll can be stored as a contextual learning. This stored information is interpreted by the brain as a sensation of body rocking or swaying, when the passenger steps off the ship.

It was proposed that permanent changes in VOR that occurred in MdDS patients after traveling could be reversed by activating the polysynaptic velocity storage path of VOR with a full-field

OKN, while the head is oscillated side-to-side or up–down. Head oscillations side-to-side induce cross-coupled sensations of head motion forward–back (44). Head motion up–down induces sensations of swaying side-to-side. Thus, to treat rocking, the velocity storage should be activated in the direction that is opposite to what was experienced during traveling. If the stored sensation is rocking, the head during the treatment should be oscillated side-to-side. If the sensation is side-to-side swaying, the head should be moved up–down (44). If the head is oscillated at the frequency of phantom motion, in both cases, this treatment induces sensations of motion that are out of phase with the phantom motion. As a result, the induced and stored sensations should cancel each other, and phantom sensation is reduced or cured.

METHODS

Study Participants and Study Overview

We sought to conduct a proof-of-concept study examining the utility of this limited-field OKN VR system in delivering VOR readaptation treatment to patients with MdDS. To this end, five women volunteered to undergo VOR readaptation treatment using the limited-field OKN VR system. Over the last 5 years, the Vestibular Treatment Center of Mount Sinai has provided treatment of MdDS daily, with about five to six applications each week. Patients for the present study were selected from this applicant database. Local patients were preferred because they could be called back for the original treatment if the VR goggle treatment did not work. Thus, four out of five patients in this study were local. Only female patients were considered because MdDS is more common among females than among males. All study participants reported experiencing MdDS symptoms for at least 1 month, and four of the five subjects attributed their MdDS symptoms to passive motion exposure (e.g., a cruise). Additional characteristics of the study participants are described in the results. Three of the study participants underwent four treatment sessions, one underwent seven, and another one underwent two treatment sessions. The Mount Sinai Institutional Review Board (IRB) approved the protocol, and all subjects provided written informed consent.

On the first treatment day, spontaneous nystagmus, static post-urography, and Fukuda tests were administered to determine the direction of the OKN visual stimulus and the frequency of the head oscillation as previously described (2, 45). Treatment was delivered with OKN at 5°/s.

Development and Implementation of the Limited-Field OKN VR System

We developed a limited-field OKN VR system using a mobile Google Daydream app using the Unity3D graphics engine, which we have previously described (51). This app is not currently publicly available, but researchers interested in utilizing this app can contact the Ohio Musculoskeletal and Neurological Institute at omni@ohio.edu for more information. In brief, stripes moving left, right, up, and down were implemented in four different programs. The speed of stripes could be adjusted in 5°/s increments from 0 to 20°/s. During the treatment, stripes' orientation to gravity remained unchanged despite head motions. Initially, Google Cardboard was selected as the development hardware for the intended MdDS treatment app. A prototype was implemented using Open Graphics Library for Embedded Systems (OpenGL ES) in the native Android Software Development Kit (SDK). While the prototype app was functional, we found out that many Google Cardboard goggles on the market were hard to secure firmly on one's head and had difficulty avoiding slight movement while the head was in motion. In the second phase of the project, to provide a better VR user experience, we switched to Google Daydream viewers and used Unity3D, a mobile graphic engine, to develop a Daydream VR mobile app. Key considerations in the design were (1) adjusting the environment to extend upward in an almost cone-like shape to accommodate the tendency for users to look upward when in a virtual space; (2) placing the lighting in the same position as the camera; (3) not having a "floor," such that the lines result in a sphere-like setting; (3) having a simple and easy-to-use interface; (4) developing four different applications including clockwise vertical lines, counterclockwise vertical lines, upward horizontal lines, and downward horizontal lines; and (5) accompanying audio with each speed that is easily adjustable, so the user will always be aware of the current rotation speed in degrees per second.

Google Daydream only runs on mobile phone models that are explicitly identified as Daydream-ready phones to ensure that they possess sufficient processing power in Daydream mode to reduce latency and prevent nausea. Furthermore, the 3D model used in our program is simplistic, with only simple textures and low polygon counts, much simpler than a typical mobile 3D game scene. On our test devices—Google Pixel 2 and Pixel 2 XL—there were no perceptible latency issues at all.

During some treatment sessions, patients' heads were manually passively moved side-to-side to treat the sensation of rocking (forward–backward) (45) or up–down to treat swaying (side-to-side) (2). Manual head deviation from upright in each direction was ≈20°. To maintain repeatable motion, we played metronome music, which comprised seven notes on a musical scale (heptatonic scale) played in ascending and descending order of pitch (A–B–C–D–E-F#–G#–A). During treatment, the patients sat in a stationary chair with the head in the upright position with their eyes closed. The musical metronome was started, and the head was moved when the ascending scale reached tone D. At the time of tone A, the head would be in a maximally deviated position, and as the scale went in descending order to low A, the head would reach maximal deviation from upright in the alternate direction. The metronome was programmed to play over a specific time. When the music stopped, head motions stopped too, and the patient was asked to close their eyes, while the Oculus frame was removed from the subject's head.

To determine the direction of stripes for rocking and swaying, we performed a Fukuda step test (52, 53). If the Fukuda was positive (rotation >20°), stripes were moved in the direction opposite to body rotations. Some patients reported sideways gravitational pull sensations. For these patients, the stripes were implemented in the direction opposite to the pull.

Static Post-urography and MdDS Severity

Static post-urography was obtained with eyes open and closed with feet 27 cm apart using a Wii board (Nintendo Inc.). Data were wirelessly transferred to the computer. Fast Fourier transform was used to determine the frequency of rocking and swaying (45). To compare postural stability after individual treatments, the displacement of center of pressure (COP) over a 20-s period was computed as well as the root mean square (RMS) of the postural displacement along *X*- (xRMS) and *Y*-axes (yRMS) (2).

Symptom severity was self-scored by the patients on a scale of 0–10, where 0 is no symptoms at all and 10 is the strongest symptoms that the patient could imagine (54). Symptom self-scoring was obtained before and after each treatment session. When treatment was completed, scores prior to and after the treatment were compared. We *a priori* considered that treatment would be considered successful if a patent's improvement in pretreatment and post-treatment self-scores was >50%.

Treatment Procedures

Treatment Approach for Rocking and Swaying

During the treatment, patients sat in a regular (not revolving) chair. The goggle frame was adjusted to a comfortable level prior to treatment. The software was run by the researcher. The patient was then asked to close their eyes and place the goggle frame on their head. The metronome software was run on a computer. Then the patient was asked to open their eyes while the researcher provided passive head motions at the frequency of the metronome. We first moved the head at the frequency of body oscillation. If effective, the head was also moved at lower frequencies. Typically, frequencies of 0.2 Hz for 1 min, 0.1 Hz for 3 min, and 0.05 Hz for 5 min were considered. If the body was rocking (forward–back), the head was moved side-to-side. If the body was swaying (side-to-side), the head was rocked (up–down) (44).

Treatment Approach for Sideways Gravitational Pull

During this treatment, the patient sat as described above. The head, however, remained stationary upright. If the patient complained of a sideways gravity pull, the stripes were moved in a direction opposite to the pull direction. If the patient complained of sensations of pulling backward or walking on a soft ground or a sensation that their body is too light, then stripes going upward were used. If the patient complained of being pulled forward, walking on a moving sidewalk at the airport sensation, or body heaviness, the stripes were moved down.

Statistical Analysis

For this proof-of-concept study, we sought to compare changes before and after treatment. Here, we used the Wilcoxon matched-pairs signed-rank test to compare two groups of data. The Pearson chi-square test was used for categorical data. A preset alpha level of significance of 0.05 was required for statistical significance. All statistical analyses were performed using SPSS.

TABLE 1 | Demographical data.

Patient ID	Age	Trigger	MdDS duration	Score before	Score after	Score follow-up
VRG017	50	stress	3 months	6	0	1.5
VRG018	39	cruise	1 month	4	0.5	3
VRG019	46	cruise	2 months	5	2	1
VRG020	26	boating	2 months	1–4	0–1	1–3
VRG021	48	long car ride	2 months	3–4	1	0–0.5

TABLE 2 | Phantom sensations of motion experienced by patients.

Patient ID	Rocking	Swaying	Bobbing	Trampoline walking	Gravitational pull
VRG017	+	+	–	+	Yes, right, backward
VRG018	+	+	–	+	Yes, down, forward
VRG019	–	+	–	–	Yes, back
VRG020	+	–	–	+	Yes, right
VRG021	–	+	–	+	Yes, right

RESULTS

Descriptive Characteristics of the Study Participants

Five female patients aged 42 ± 10 years (range 26–50) were treated for MdDS with VR goggles (**Table 1**). Two patients had their symptoms triggered immediately after several days on cruises, one after several hours of boarding, and one immediately after a car ride. There was no specific trigger for symptoms in a fifth subject. Diagnoses were confirmed by an ENT and neurologists in three patients. Two of the patients self-diagnosed with motion-triggered MdDS. Patients' self-scoring of their symptoms prior to treatment, on average, ranged from 3 to 6. All five patients reported improvement. On average, symptom improvement was 76% (range 60–100%). None of the patients reported any sign of motion sickness while using the device.

Among all phantom sensations of motion, bobbing is less common (2) and was not reported by any participants in this study (**Table 2**). Each patient reported a sensation of gravitational pull at least in one direction. The number of other motion symptoms did not correlate with MdDS severity. While patients VRG017 and VRG018 had all the symptoms besides bobbing, they scored their pretreatment symptom severity as 6 and 4, respectively. Patient VRG019 experienced only swaying but scored their pretreatment severity as 5. Two other patients had larger numbers of symptoms compared to those of VRG019 but had lower pretreatment scores. The same is true for post-treatment scores. While a significant improvement was reported, patient VRG019 had the highest post-treatment score compared to that of all other patients. Thus, the number of motion sensations experienced by individual patients did not correlate with symptom severity self-scores or with treatment effectiveness.

TABLE 3 | Psychosomatic symptoms reported by patients.

Patient ID	Brain fog	Fullness of ears	Heavy head	Heavy lags	Fuzzy vision	Fatigue	Sensitivity to fluorescent light	Sensitivity to computer screen	Unsteadiness in crowds
VRG017	+	+	−	−	−	+	−	−	+
VRG018	−	+	+	+	+	−	−	+	−
VRG019	−	−	−	−	−	+	−	−	+
VRG020	−	+	+	−	+	−	+	−	−
VRG021	+	+	+	+	−	+	+	+	+

In addition to phantom motion sensations, patients experienced psychosomatic symptoms (**Table 3**). The number of psychosomatic symptoms reported by patients also did not correlate with symptom severity self-scores or with treatment effectiveness.

None of the patients in this study reported vection, which is frequently reported with full-field stimulation (2, 45).

Effect of Treatment on MdDS Severity Self-Score

The average pretreatment symptom severity self-score was 4.2 ± 1.4 ranging from 1 to 6. In four patients, the severity level was consistent from day to day, and in one, it varied from 1 to 4 over the course of the day and from day to day (**Table 1**).

On the first day of examination, patient VRG017 reported sensations of rocking, swaying, and gravitational pull to the right. The patient could not maintain a standing upright posture with eyes closed; therefore, the Fukuda test could not be done. An OKN direction to the left for readaptation treatment was chosen based on gravitational pull to the right (2). The patient was first treated for gravitational pull and reported improvement after watching stripes going left for 2 min. After this treatment, post-urography revealed rocking at 0.1–0.2 Hz. The patient was treated for rocking at 0.2 Hz for 2 min and at 0.1 Hz for 3 min. After that, post-urography revealed gravitational pull back, which was treated by stripes going up for 2 min. Overall, on day 1, the patient reported significant symptom improvement from a score of 6–2 (**Figure 1A**, red circles). The next day, the patient reported that almost all symptoms returned back by 5 p.m. on day 1. Post-urography revealed small rocking at ≈0.4 Hz and swaying at ≈0.3 Hz, reduced sensation of pull to the right, and a strong pull back. The patient was treated for the backward pull for 13 min and reported significant improvement of all symptoms. Post-urography revealed small rocking at ≈0.2 Hz, and the patient was treated for that for 2 min. The patient reported some pull back, and the treatment for pull back was repeated for 5 min. Overall, the patient reported significant symptom decrease from a score of 5–1 on that day (**Figure 1A**, blue circles). On day 3, the patient reported that, regardless of all potential triggering activities that patient had on day 2, symptoms remained at score 1. Small gravitational pull back was treated for 4 and 5 min. After that, small rocking at ≈0.2 Hz was treated for 1 min. The patient reported further symptom improvement to score 0.5 on that day (**Figure 3A**, green circles). On day 4, the patient reported that symptoms stayed at a score of 0.5 since the last treatment. Post-urography revealed small rocking at ≈0.2 Hz or gravitational pull back. Treatment for pull back was performed for 5 min, and then that for rocking for 1 min. After that, the patient reported no symptoms (**Figure 1A**, pink circles). Thus, the possible reason for symptoms returning after day 1's treatments is because gravitational pull back, which was compensated by body tilting in the opposite direction, was interpreted and treated as rocking. After gravitational pull back was treated on days 2–4, symptom improvements immediately after treatment remained unaffected by daily activity (**Figure 1A**).

Patient VRG018 reported symptoms of rocking, swaying, and trampoline walking, which intensified due to prolonged traveling. The patient was treated for these symptoms and reported improvement from a score of 4–0.5 on day 1 (**Figure 1B**, red symbols). Treatment, however, remained effective only for 2 h, after which symptoms returned to the baseline. In the morning on day 2, after a good night's sleep, symptoms were reduced to a score of 2. Treatment on day 2 brought the symptoms to score 0 (**Figure 2B**, blue traces). On day 3, the patient woke up with a migraine that brought symptoms to score 3 (**Figure 1B**, green symbol). It was recommended for the patient to stay home on that day. The next day, the patient called reporting very low symptoms at score 0.5 and refused to come in for further treatments (**Figure 2B**, purple circle).

Patient VRG019 experienced swaying at 0.25–0.31 Hz and bobbing sensations. The Fukuda test was inconclusive (right 45° once out of two tests). Post-urography revealed some gravitational pull back. The patient was treated for swaying by a head up–down motion at 0.3 Hz for 1 min with no effect and then for back pull for 1 min, with some improvement reported. After that, rocking rather than swaying was observed. The patient was treated for rocking at 0.2 and 0.25 Hz for 1 min each and reported only a small pull back that was treated for 2 min. Overall, the patient reported improvement from a score of 5–3 on day 1 (**Figure 3C**, red circles). The patient came back only 6 days later, when symptoms increased to a score of 4–5. Patient reported significant swaying, rocking, and pull back. The patient was treated for pull back for 3 min first and reported less sway and less gravitational pull. Then the patient was treated for rocking for 1 min with no effect. After that, OKN direction was reversed, and the patient was treated for rocking at 0.3, 0.1, and 0.05 Hz for 1, 3, and 5 min, respectively, and reported only a small pull back sensation. After pull back treatment for 5 min, overall symptoms

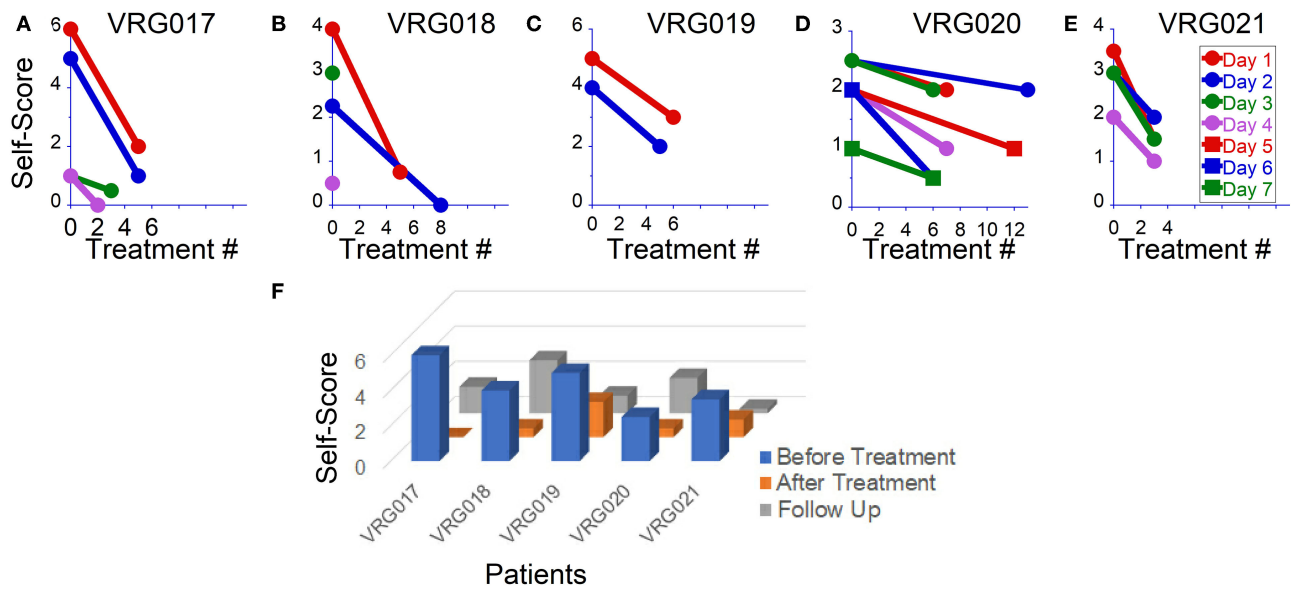

FIGURE 1 | Overall symptom severity self-scores before and after readaptation treatment in five patients. **(A–E)** Scores after individual treatments in each patient. **(F)** Overall symptoms score obtained before, after and on follow-ups.

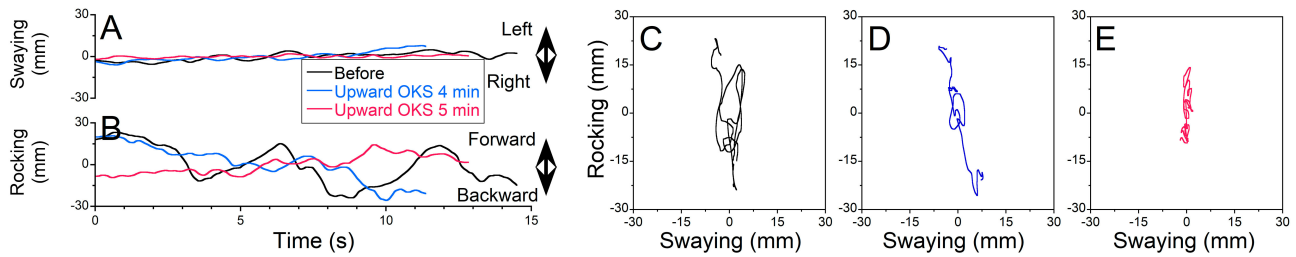

FIGURE 2 | The static post-urography obtained from patient VGR018 standing with feet apart and eyes closed over 15 s. **(A)** Swaying. **(B)** Rocking (black trace, prior to treatment; blue, after treatment 1; red, after treatment 2). **(C–E)** *X–Y* plot of posture obtained prior to treatment **(C)** and after head motion side-to-side at 0.2 Hz for 2 min **(D)** and at 0.1 Hz for 3 min **(E)**.

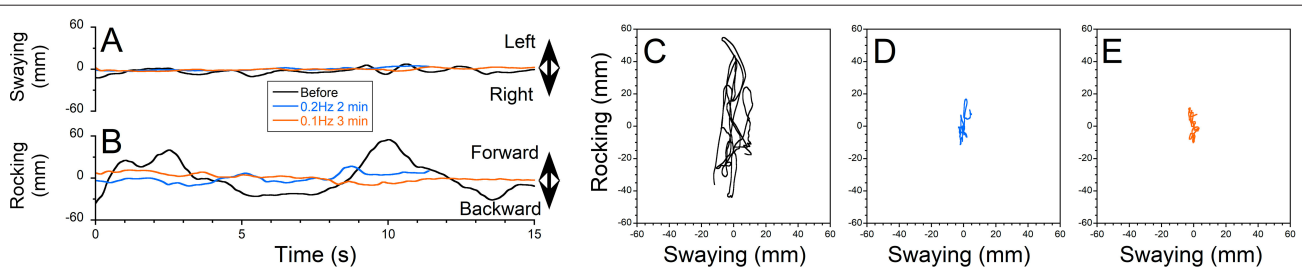

FIGURE 3 | The treatment of gravitational pull-back sensations. Patient VRG017 had experienced gravitational pull back. **(A)** Swaying and **(B)** rocking during treatment. Resistance to pull back on the trace looks like body rocking at 0.2 Hz with constant body drift backward. **(C–E)** X-Y plot of posture obtained prior to treatment **(C)**, after two treatments with upward OKN for 4 min **(D)** and 5 min **(E)**, respectively.

decreased to a score of 2. The patient never came back for more treatments (**Figure 1C**, blue circles).

On the first day of examination, patient VRG021 had mild symptoms with a score of 1 while sitting but reported sensations of the ground moving side-to-side with a score of 2–4 when walking. Additionally, the patient reported pull forward and small pull right sensations. The Fukuda test was 20° to the left in both trials. Thus, pull right and Fukuda results contradicted in terms of best OKN direction for the treatment. There were no other clues to determine the direction of OKN. Because of this,

the pull back was treated first for 1 min. After this, we treated swaying by an arbitrarily chosen OKN going left and head up–down motion at 0.2 Hz for 1 min. No changes were reported. Treatment was repeated with OKN going right. The patient reported some improvement. Treatments for swaying with OKN going right were repeated several times, and the patient reported significant improvement (**Figure 1D**, red symbols). Long driving (80 miles) back home induced some symptoms as well as an increased sensitivity to light. On day 2, treatment for pull forward was repeated three times for 2 min each. When swaying was treated with OKN to the right for 2 min, the patient's reported symptoms increased. Based on this report, OKN direction was changed to the left, and treatment for swaying was repeated nine times at frequencies 0.2 and 0.05 Hz. No improvement was reported (**Figure 1D**, blue circles). On day 3, treatment with OKN to the left was continued with no actual success (**Figure 1D**, green circles). On treatment day 4 (after the weekend), the patient reported virtually the same symptoms with the addition of a strong brain fog. Thus, OKN direction to the left was not effective. Treatment was repeated with OKN to the right, and significant improvements in brain fog and postural stability were reported (**Figure 1D**, pink circles). Treatment was continued with OKN to the right for 3 more days, with gradual symptom improvement on each sequential day (**Figure 1D**, red, blue, and green squares). Thus, OKN direction on days 1–3 was incorrect, and the treatment induced more symptoms. When OKN direction was reversed, the patient, similar to all other patients, reported gradual symptom improvement on each sequential day.

The last patient, VRG021, could not maintain a standing-upright posture with eyes closed; therefore, the Fukuda test was not done. The major symptoms on the first examination on day 1 were strong gravitational pull back and some pull to the right. The patient was treated repeatedly for pull back sensation for 2, 2, and 4 min, and improvement from a score of 3.5–1.5 was reported (**Figure 1E**, red circles). On day 2, the patient reported symptom improvement with some pull back and swaying. After 5 min of treatment for pull back, the patient reported small sway and pull right sensation. The patient was treated for both sensations consecutively and reported small symptom improvement from a score of 3–2 on that day (**Figure 1E**, blue circles). After that treatment, the patient felt improvement until a large crowd triggered some symptom back. Since the major symptom was the pull back sensation, on day 3, the patient was treated only for gravitational pull back for 10, 5, and 5 min, consecutively (**Figure 1E**, green circles). On day 4, the patient still had some gravitational pull back and a small sway. The patient was effectively treated for pull back for 10 and 5 min and in between was treated for sway with OKN going left for 1 min. The treatment for sway was not effective, but the treatment for pull back improved the patient's symptoms to a score of 1. When their average pretreatment score was compared to their last post-treatment score, all patients reported significant improvements (**Figure 1F**, blue vs. orange columns).

Treatment protocol in this study was similar to that used for readaptation treatment with full-field OKN (2). That is, we first targeted symptoms that bothered the patient the most. Typically, within one treatment day, symptoms dropped by at least 50%; however, the next day, patients may have had some symptoms rebound, although still below pretreatment levels. Improvement gradually accumulated over four treatment days.

Treatment for rocking was used 62 times for these five patients. In 35 cases (56%), patients reported symptom improvement. In 21 cases (34%), patients did not notice a difference, and in six cases (10%), patients reposted worsening of symptoms. All six worsening cases were reported by subject VRG029, when the sway sensation was treated.

The gravitational pull back sensation was treated 23 times. In 19 cases (83%), patients reported immediate improvement. In four cases (17%), patients were uncertain about the effect. The gravitational pull forward sensation was applied 10 times. In seven cases (70%), patients reported immediate improvement. In two cases (20%), there was uncertainty about treatment effect, and in one case (10%), a worsening of the symptoms was reported. The sideways pull was treated seven times. In five cases (71%), immediate improvement was reported, and in two cases (29%), patients did not note the difference.

Follow-Up Study

Prior to treatment, only patient VRG017 did not report significant changes in symptoms with any daily activity. In the other four patients, symptoms could be elevated by prolonged traveling, fluorescent lights, flickering of computer screens, use of elevators and escalators, and exposure to crowds. After the treatment, patients VRG019 and VRG021 no longer reported strong symptom fluctuations by daily activity. The scores of all three patients remained low when followed up 4 ± 1 months after the treatment (**Figure 1F**, gray columns, **Table 1**).

In patient VRG018, prior to treatment, prolonged (>1 h) driving or taking the subway intensified symptoms. After the treatment, prolonged daily traveling remained a strong trigger. The patient was invited back to the lab 7 months after VR treatment and was treated for 2 days with full-field OKN. The treatment reduced symptoms from a score of 3–0.5, although the patient experienced worsening symptoms after traveling home. When followed up 11 months after VR treatment, the patient reported symptoms with a generally low score of 0 with occasional spikes to a score of 2. The patient also reported that since the last treatment, she is limiting daily driving to short distances only.

Patient VRG020 was also invited back 3 months after VR treatment and treated for 2 days with full-field OKN. Treatment was effective on each day, but sitting at work in front of a computer screen with strong fluorescent lights on reversed the treatment effects. On the last follow-up 9 months after VR treatment, the patient reported symptom improvement. At the same time, over the last month, the patient is self-quarantined at home and completely avoids fluorescent lights and long time spent in front of a computer screen.

Thus, the treatment remained effective in three out of five patients (60%) during normal daily activity and perhaps would be effective in all patients if specific triggers were avoided.

Effect of Treatment on Static Posture

Treatment of Rocking

Figure 2 shows a typical example of rocking at ≈0.15 Hz experienced by MdDS patient VRG018 (**Figures 2A,B**, black traces). Rocking was first treated by activation of velocity storage with OKN to the left and moving the head side-to-side at 0.2 Hz for 2 min (**Figures 2A,B**, blue traces). Rocking was substantially reduced after the first treatment (**Figure 1B**). Patient was additionally treated for 3 min, while their head was moved side-to-side at 0.1 Hz (**Figure 1B**, red traces). Prior to treatment, static posturography revealed some swaying and substantial rocking (**Figure 2C**, xRMS = 3 mm, yRMS = 21, trace 20 s = 477 mm). After the first treatment at 0.2 Hz, both swaying and rocking were reduced (**Figure 2D**, xRMS = 1 mm, yRMS = 7, trace 20 s = 196 mm). The second treatment at 0.1 Hz only partially reduced body motion (**Figure 2E**, xRMS = 1 mm, yRMS = 4, trace 20 s = 180 mm). Thus, postural stability was improved by ≈65% (67, 67, and 60%) after the first treatment and 70% (67, 81, and 62%) after the second treatment. There was no further postural improvement after the second treatment ($p = 0.18$).

The postural stability was recorded on 21 occasions before and after treatment for rocking/swaying. The percentage changes in COP (xRMS, yRMS, and trace duration over 20 s) were computed and averaged. The average postural improvement was 6 ± 35% (ranging −98 to 53%).

Treatment of Gravitational Pull

Patient VRG017 reported persistent sensations of gravitational pull back. The static post-urography revealed cyclic body oscillations very similar to the rocking shown in **Figures 2**, **3**. The average body position, however, drifted backward (**Figures 3A,B**, black trace). Additionally, the *X*–*Y* plot of COP revealed that as the body resisted the pull back sensation, it had some small sway (**Figure 3C**, xRMS = 2 mm, yRMS = 11 mm, trace 20 s = 259). Pull back sensation was first treated by the upward OKN for 4 min. The sensation of pulling backward was reduced but not eliminated (**Figures 3A,B**, blue traces). This is also seen in the COP plot: while the magnitude of sway reduced, the backward drift was slower but of the same approximate magnitude (**Figure 3D**, xRMS = 1 mm, yRMS = 6 mm, trace 20 s = 199 mm). Treatment was repeated for another 5 min. No pull back sensation was reported after the second treatment (**Figures 3A,B**, red traces). The COP plot confirms great reduction of gravitational pull back (**Figure 3E**, xRMS = 2 mm, yRMS = 5 mm, trace 20 s = 163 mm). Thus, average improvement of postural stability after the first and the second treatments was 39 and 30%, respectively ($p = 0.999$). Gravitational pull back is the most common sensation among all five MdDS patients (**Table 2**). Despite the fact that gravitational pull direction varies among the patients, it was effectively treated for all patients in this group. Sensation of swaying was reported by four patients and was successfully treated with VR goggles; however, static post-urography indicates that none of the patients sway without actual rocking.

The postural stability was recorded on 10 occasions after the treatment for pull back sensations and on two occasions for pull forward sensations. The average improvement was 32 ± 27% (ranging −3 to 89%) for pull back and 28% (ranging −13 to 68%) for pull forward treatments.

TABLE 4 | Subjective vs. objective data cross-tabulation.

		Objective			
Subjective		−1	0	1	Total
	−1	0	1	1	2
	0	4	5	3	12
	1	2	4	13	19
Total		6	10	17	33

Subjective and Objective Evidence of the Treatment's Effectiveness

After 33 individual treatments for gravitational pull, the postural data and change in subjective scores were available. The subjective changes in symptoms were compared with the percentage of average postural improvement. Average postural improvement was computed as an average improvement of three values: xRMS (%), yRMS (%), and trace 20 s (%). Results were categorized as follows: category 1, improvement ≥10%; category 0, abs[improvement] <10%; and category −1, worsening of posture > −10%. Similarly, subjective score was categorized as follows: category 1, symptom improvement; category 0, no changes; category −1, symptom worsening. No correlation was found between subjective and objective changes in symptoms. Data are summarized in a cross-tabulation (**Table 4**).

Table 4 indicates that subjective and objective improvements were reported 19 and 17 times and coincide with 13 cases. Less coincidence was observed when no changes were reported and observed (5 out of 12 subjective and 5 out of 10 objective cases). Thus, in total, in 18 cases out of 33, objective and subjective symptom changes coincide. Because the sample size is too small, the chi-square test was insignificant ($p = 0.167$). Alternatively, this could be an indication of significant contribution of psychosomatic symptoms in overall scoring.

DISCUSSION

The purpose of this pilot project was to determine whether limited-field OKN produced by VR goggles may have clinical utility for treatment of MdDS. While the interpretation of the findings must be taken in the context of this not being a clinical trial, these data do suggest that further examination of a VOR readaptation protocol using VR goggles with a restricted visual field is warranted. This assertion is based on all five patients in this study showing positive responses to treatment with the limited-field OKN stimulation. Thus, limited-field OKN stimulation may be an effective stimulus for the activation of the velocity storage to the extent that it could be used for MdDS treatment.

Full-field OKN is believed to be the most efficient way to activate velocity storage (22, 55). Full-field stimulation is also the

most efficient way to induce circular vection (46). Additionally, the amount of circular vection is correlated with the duration of OKAN (56), which is directly related to the activation of velocity storage (47, 57). Furthermore, OKAN can be induced by peripheral vision, while the central (foveal) vision is blocked or lessened (18, 56). Nevertheless, the central vision also plays a role, since OKN velocities are higher if central vision is activated (18), and velocity storage cannot be activated if OKN in the foveal area is in an alternate direction with the peripheral vision (56). Thus, OKS with a restricted visual field may not be as effective as a full-field OKN. While the size of the visual field is a factor (21), it is less relevant for low-speed OKN, which is commonly used for MdDS treatment (22, 23).

In the original readaptation paper, the authors argued that the sensation of self-motion (vection) could be critical for MdDS treatment (45). Vection is generated by activation of the peripheral vision (58). In the present study, visual periphery was not activated, and none of the five patients experienced vection, yet treatment remained effective. OKN and therefore velocity storage, however, appear to have been activated by a small visual field (21, 58). Thus, vection is not likely critical for MdDS treatment. Thus, this study indicates that lack of vection and limited size of the visual field are not crucial factors, in activation of velocity storage to the limit, necessary for MdDS treatment by VOR readaptation.

Over the last 5 years, more than 600 patients had been treated for MdDS at Mount Sinai. About half of them were from New York City or in driving distance from Mount Sinai. This indicates that several thousands of patients may suffer from MdDS across the United States and suggests that more treatment options need to be available. The current equipment used for MdDS treatment at Mount Sinai is bulky and expensive and cannot be purchased for immediate use since it requires several substantial modifications. Thus, this treatment could not be easily replicated in its present form. VR goggles, however, are commercially available, are relatively inexpensive, and could provide a uniform environment for use in multiple laboratories to study the treatment effectiveness of VOR readaptation protocols for MdDS. The effectiveness of VR goggles vs. full-field OKN needs to be further investigated, though this study demonstrates the feasibility of this approach.

One of the difficulties of the proposed approach is that each patient has a unique set of symptoms, which require a unique treatment protocol. **Figure 3** demonstrate the complexity of the approach. Not only could the symptoms vary on different days or after individual treatments, but success is also dependent on whether the correct treatment is performed at the right time. The same treatment could be very effective at the beginning, but not later in the day. For example, rocking was eliminated on day 1, but gravitational pull sensation remained strong. When gravitational pull was eliminated on day 2, it had a long-lasting effect on the patient's symptoms. Some of the patients treated at Mount Sinai used an OKN web-based application to reduce their symptoms at home in case they were retriggered (http://mdds.nyc/okn-stripes-visualization/). The treatment is based on the protocol that was developed during in-lab testing. The home setup requires the computer to be connected to a large-screen TV or short-throw video projector. The effectiveness of the home treatment, however, was largely varied based on each individual home setup. The VR goggles used in this study is a promising approach for MdDS self-treatment at home.

It has been reported that scrolling on a computer screen or just watching a cellphone screen is frequently a trigger for MdDS symptoms (2). While visual sensitivity to screens was not measured in this study, it should be noted that none of the patients reported any discomfort while watching the OKN stripes in this study. However, this could be because our small sample size did not include any patients with high visual sensitivity. Thus, further testing of VR goggles is required on larger populations of MdDS patients to determine how flickering of the cell phone screen affects MdDS patients with heightened visual sensitivity.

Thus, the limitation of this study is the small and not randomly selected group of patients. Our patient group may not include all types of MdDS patients who were treated with full-field stimulation in terms of sensitivity to visual motion, sensitivity to brightness of the screen, motion sickness, anxiety, claustrophobia, etc. Due to the individual variabilities and drop-off from the study, the protocols of each patient are different. Thus, this study is lacking comparison between full-field and limited-field stimulation groups; there was no sham/placebo; there was no blinding/masking. To eliminate potential problems, a larger study of MdDS patients' treatment using VR goggles vs. full-field stimulation is required.

In conclusion, MdDS is composed of constant phantom sensations of motion, which are frequently accompanied by increased sensitivity to light, inability to walk on a patterned floor, the sensation of ear fullness, head pressure, anxiety, and depression. It has been previously hypothesized that MdDS is the result of maladaptive changes in the polysynaptic VOR called velocity storage. Past research indicates that full-field OKS is an optimal way to activate velocity storage. Unfortunately, the full-field OKS devices are typically bulky and not commonly available. We questioned whether VR goggles with a restricted visual field could effectively simulate a laboratory OKS environment for MdDS treatment. While the interpretation of our findings must be taken in the context of the limitations of the study, these data do suggest that further examination of a VOR readaptation protocol using VR goggles with a restricted visual field is warranted.

DATA AVAILABILITY STATEMENT

The raw data supporting the conclusions of this article will be made available by the authors, without undue reservation.

ETHICS STATEMENT

The studies involving human participants were reviewed and approved by Mount Sinai IRB. The patients/participants

provided their written informed consent to participate in this study.

AUTHOR CONTRIBUTIONS

SY provided patient treatment, data analyses, and wrote the initial draft of the manuscript. RZ, BC, and CL designed and developed Virtual Reality App. All authors equally contributed to writing the final version of this manuscript.

FUNDING

This study was supported by the MdDS Foundation and the NIH (NIDCD Grant DC018390).

ACKNOWLEDGMENTS

We thank Dr. Mingjia Dai for his valuable comments on the design of the application used in this study. Unfortunately, he passed away at the early stage of this project.

REFERENCES

1. Cha YH, Baloh RW, Cho C, Magnusson M, Song JJ, Strupp F, et al. Mal de Débarquement syndrome: diagnostic criteria. Consensus document of the Classification Committee of the Bárány Society. *JVR.* (2020).
2. Dai M, Cohen B, Cho C, Shin S, Yakushin SB. Treatment of the Mal de Debarquement syndrome, a one year follow up. *Front Neurol.* (2017) 8:175. doi: 10.3389/fneur.2017.00175
3. Goldberg JM, Fernandez C. Physiology of peripheral neurons innervating semicircular canals of the squirrel monkey. I. Resting discharge and response to constant angular accelerations. *J Neurophysiol.* (1971) 34:635–660. doi: 10.1152/jn.1971.34.4.635
4. Yakushin SB, Raphan T, Suzuki J-I, Arai Y, Cohen B. Dynamics and kinematics of the angular vestibulo-ocular reflex in monkey: effects of canal plugging. *J Neurophysiol.* (1998) 80:3077–99. doi: 10.1152/jn.1998.80.6.3077
5. Dai M, Klein A, Cohen B, Raphan T. Model-based study of the human cupular time constant. *J Vestib Res.* (1999) 9:293–301.
6. Hauty GT. Primary ocular nystagmus as a function of intensity and duration of acceleration. *J Exp Psychol.* (1953). 46:162–70. doi: 10.1037/h0058819
7. Raphan T, Matsuo V, Cohen B. A velocity storage mechanism responsible for optokinetic nystagmus (OKN), optokinetic after-nystagmus (OKAN), vestibular nystagmus. In Baker R, Berthoz A, editors. *Control of Gaze by Brain Stem Neurons.* Amsterdam: Elsevier/North Holland (1977). p. 37–47.
8. Robinson D. Vestibular optokinetic symbiosis: an example of explaining by modeling. In: Baker R, Berthoz A, editors. Control of Gaze by Brain Stem Neurons. Amsterdam: Elsevier/North Holland (1977). p. 49–58.
9. Raphan T, Cohen B. The vestibulo-ocular reflex in three dimensions. *Exp Brain Res.* (2002) 145:1–27. doi: 10.1007/s00221-002-1067-z
10. Cohen B, Raphan T. The physiology of the vestibuloocular reflex (VOR). In: Highstein SM, Fay RR, Popper AM, editors. *Springer Handbook of Auditory Research. The Vestibular System.* New York, NY: Springer (2004) p. 235–85. doi: 10.1007/0-387-21567-0_6
11. Raphan T. Vestibular, locomotor, and vestibulo-autonomic research: 50 years of collaboration with Bernard Cohen. *J Neurophysiol.* (2020). 123:329–345. doi: 10.1152/jn.00485.2019
12. Dai MJ, Raphan T, Cohen B. Spatial orientation of the vestibular system: dependence of optokinetic after-nystagmus on gravity. *J Neurophysiol.* (1991) 66:1422–39. doi: 10.1152/jn.1991.66.4.1422
13. Gizzi M, Raphan T, Rudolph S, Cohen B. Orientation of human optokinetic nystagmus to gravity: a model-based approach. *Exp Brain Res.* (1994) 99:347–60. doi: 10.1007/BF00239601
14. Buettner UW, Henn V, Young LR. Frequency response of the vestibulo-ocular reflex (VOR) in the monkey. *Aviat Space Environ Med.* (1981) 52:73–7.
15. Paige GD, Telford L, Seidman SH, Barnes GR. Human vestibuloocular reflex and its interactions with vision and fixation distance during linear and angular head movement. *J Neurophysiol.* (1998) 80:2391–404. doi: 10.1152/jn.1998.80.5.2391
16. Ramachandran R, Lisberger SG. Normal performance and expression of learning in the vestibulo-ocular reflex (VOR) at high frequencies. *J Neurophysiol.* (2005) 93:2028–38. doi: 10.1152/jn.00832.2004
17. Baarsma EA, Collewijn H. Vestibulo-ocular and optocinetic reaction to rotation and their interaction in the rabbit. *J.Physiol.* (1974) 238:603–25. doi: 10.1113/jphysiol.1974.sp010546
18. Büttner U, Meienberg O, Schimmelpfennig B. The effect of central retinal lesions on optokinetic nystagmus in the monkey. *Exp Brain Res.* (1983) 52:248–56. doi: 10.1007/BF00236633
19. Zee DS, Yee RD, Robinson DA. Optokinetic responses in labyrinthine-defective human beings. *Brain Res.* (1976) 113:423–8. doi: 10.1016/0006-8993(76)90955-0
20. Murasugi CM, Howard IP, Ohmi M. Optokinetic nystagmus: the effects of stationary edges, alone and in combination with central occlusion. *Vision Res.* (1986) 26:1155–62. doi: 10.1016/0042-6989(86)90049-0
21. Howard IP, Ohmi M. The efficiency of the central and peripheral retina in driving human optokinetic nystagmus. *Vision Res.* (1984) 24:969–76. doi: 10.1016/0042-6989(84)90072-5
22. Dichgans J. Optokinetic nystagmus is dependent on the retinal periphery via the vestibular nucleus. In: Baker R, Berthoz A, editors. *Control of Gaze by Brain Stem Neurons.* Amsterdam: Elsevier (1977). p. 261–7.
23. Valmaggia C, Gottlob I. Role of the stimulus size in the generation of optokinetic nystagmus in normals and in patients with retinitis pigmentosa. *Klin Monbl Augenheilkd.* (2004) 221:390–4. doi: 10.1055/s-2004-812864
24. Traquair HM. *An Introduction to Clinical Perimetry*. 1st ed. London: Henry Kimpton (1927).
25. Katz E, Dejong JMBV, Büttner-Ennever JA, Cohen B. Effects of midline medullary lesions on velocity storage and the vestibulo-ocular reflex. *Exp Brain Res.* (1991) 87:505–20. doi: 10.1007/BF00227076
26. Cohen B, Helwig D, Raphan T. Baclofen and velocity storage: a model of the effects of the drug on the vestibulo-ocular reflex in the rhesus monkey. *J. Physiol.* (1987) 393:703–25. doi: 10.1113/jphysiol.1987.sp016849
27. Holstein GR, Martinelli GP, Cohen B. Immunocytochemical visualization of l-baclofen-sensitive $GABA_b$ binding sites in the medial vestibular nucleus (MVN). *Ann N Y Acad Sci.* (1992) 656:933–36. doi: 10.1111/j.1749-6632.1992.tb25299.x
28. Holstein GR, Martinelli GP, Cohen B. L-baclofen-sensitive GABAb binding sites in the medial vestibular nucleus localized by immunocytochemistry. *Brain Res.* (1992) 581:175–80. doi: 10.1016/0006-8993(92)90361-C
29. Waespe W, Henn V. Vestibular nuclei activity during optokinetic after-nystagmus (OKAN) in the alert monkey. *Exp Brain Res.* (1977) 30:323–30. doi: 10.1007/BF00237259
30. Reisine H, Raphan T. Neural basis for eye velocity generation in the vestibular nuclei of alert monkeys during off-vertical axis rotation. *Exp Brain Res.* (1992) 92:209–26. doi: 10.1007/BF00227966
31. Yakushin SB, Raphan T, Cohen B. Spatial coding of velocity storage in the vestibular nuclei. *Front Neurol.* (2017) 8:386. doi: 10.3389/fneur.2017.00386
32. McCrea R, Gdowski G, Luan H. Current concepts of vestibular nucleus function: transformation of vestibular signals in the vestibular nuclei. *Ann N Y Acad Sci.* (2001) 942:328–44. doi: 10.1111/j.1749-6632.2001.tb03758.x
33. McCrea RA, Gdowski GT, Boyle R, Belton T. Firing behavior of vestibular neurons during active and passive head movements: vestibulo-spinal and other non-eye-movement related neurons. *J Neurophysiol.* (1999) 82:416–28. doi: 10.1152/jn.1999.82.1.416
34. Muntaseer Mahfuz M, Schubert MC, Figtree WVC, Todd CJ, Migliaccio AA. Human vestibulo-ocular reflex adaptation training: time beats quantity. *J Assoc Res Otolaryngol.* (2018) 19:729–39. doi: 10.1007/s10162-018-00689-w
35. Collewijn H, Martins AJ, Steinman RM. Compensatory eye movements during active and passive head movements: fast

adaptation to changes in visual magnification. *J Physiol (L).* (1983) 340:259–86. doi: 10.1113/jphysiol.1983.sp014762
36. Gonshor A, Melvill Jones G. Short-term adaptive changes in the human vestibulo-ocular reflex arc. *J Physiol.* (1976) 256:361–79. doi: 10.1113/jphysiol.1976.sp011329
37. Paige GD, Sargent EW. Visually-induced adaptive plasticity in the human vestibulo-ocular reflex. *Exp Brain Res.* (1991) 84:25–34. doi: 10.1007/BF00231759
38. Melvill Jones G, Davies P, Gonshor A. Long-term effects of maintained vision reversal: is vestibulo-ocular adaptation either necessary or sufficient?: in: Baker R, Berthoz A, editors. *Control of Gaze by Brain Stem Neurons. Developments in Neuroscience.* Amsterdam; New York, NY: Elsevier/North-Holland Biomedical Press. (1977). p. 59–68.
39. Lewis RF, Clendaniel RA, Zee DS. Vergence-dependent adaptation of the vestibulo-ocular reflex. *Exp Brain Res.* (2003) 152:335–40. doi: 10.1007/s00221-003-1563-9
40. Tiliket C, Shelhamer M, Tan HS, Zee DS. Adaptation of the vestibulo-ocular reflex with the head in different orientations and positions relative to the axis of body rotation. *J Vestib Res.* (1993) 3:181–95.
41. Schultheis L, Robinson DA. Directional plasticity of the vestibulo-ocular reflex in the cat. *Ann NY Acad Sci.* (1981) 374:504–12. doi: 10.1111/j.1749-6632.1981.tb30895.x
42. Yakushin SB, Palla A, Haslwanter T, Bockisch CJ, Straumann D. Dependence of adaptation of the human vertical angular vestibulo-ocular reflex on gravity. *Exp Brain Res.* (2003) 152:137–42. doi: 10.1007/s00221-003-1543-0
43. Schubert MC, Migliaccio AA, Minor LB, Clendaniel RA. Retention of VOR gain following short-term VOR adaptation. *Exp Brain Res.* (2008) 187:117–27. doi: 10.1007/s00221-008-1289-9
44. Dai M, Raphan T, Cohen B. Adaptation of the angular vestibulo-ocular reflex to head movements in rotating frames of reference. *Exp Brain Res.* (2009) 195:553–67. doi: 10.1007/s00221-009-1825-2
45. Dai M, Cohen B, Smouha E, Cho C. Readaptation of the vestibulo-ocular reflex relieves the mal de debarquement syndrome. *Front Neurol.* (2014) 5:124. doi: 10.3389/fneur.2014.00124
46. Brandt T, Dichgans J, Koenig E. Perception of self-rotation (circular vection) induced by optokinetic stimuli. *Pflugers Arch.* (1972) 332:R98.
47. Nooij SAE, Pretto P, Bülthoff HH. More vection means more velocity storage activity: a factor in visually induced motion sickness? *Exp Brain Res.* (2018) 236:3031–41. doi: 10.1007/s00221-018-5340-1
48. Munk WH. Origin and generation of waves. In: *Proceedings 1st International Conference on Coastal Engineering.* Long Beach, CA: ASCE (1950). p. 1–4. doi: 10.9753/icce.v1.1
49. Palais B, Palais R, Rodi S. A Disorienting Look at Euler's Theorem on the Axis of a Rotation. *American Mathematical Monthly.* (2009) 116:892–909. doi: 10.4169/000298909X477014
50. Cohen B, Yakushin SB, Cho C. Hypothesis: the vestibular and cerebellar Basis of the Mal de Debarquement syndrome. *Front Neurol.* (2018) 9:28. doi: 10.3389/fneur.2018.00028
51. Clark B, Yakushin SB, Dai M, Zink R, Liu C. The design of a virtual reality app for Mal de Debarquement syndrome. In*: IEEE 1st Global Conference on Life Sciences and Technologies (LifeTech).* Osaka (2019). doi: 10.1109/LifeTech.2019.8884029
52. Zhang, YB, Wang WQ. Reliability of the Fukuda stepping test to determine the side of vestibular dysfunction. *J Int Med Res.* (2011) 39:1432–7. doi: 10.1177/147323001103900431
53. Fukuda T. The stepping test: two phases of the labyrinthine reflex. *Acta Otolaryngol.* (1959). 50:95–108. doi: 10.3109/00016485909129172
54. Likert R. A technique for the measurement of attitudes. *Archiv Psychol.* (1932). 140:1–55.
55. Robinson DA, Vestibular optokinetic symbiosis: an example of explaining by modeling. In: Baker R, Berthoz A, editors. *Control of Gaze by Brain Stem Neurons* Amsterdam: Elsevier (1977). p. 49–58.
56. Brandt T, Dichgans J, Büchle W. Motion habituation: inverted self-motion perception and optokinetic after-nystagmus. *Exp Brain Res.* (1974) 21:337–52. doi: 10.1007/BF00237897
57. Raphan T, Matsuo V, Cohen B. Velocity storage in the vestibulo-ocular reflex arc (VOR). *Exp Brain Res.* (1979) 35:229–48. doi: 10.1007/BF00 236613
58. Brandt T, Dichgans JM, Koenig E. Differential effects of central versus peripheral vision of egocentric and exocentric motor perception. *Exp. Brain Res.* (1973) 16:476–91. doi: 10.1007/BF00 234474

Conflict of Interest: The authors declare that the research was conducted in the absence of any commercial or financial relationships that could be construed as a potential conflict of interest.

frontiers in Neurology

ORIGINAL RESEARCH
published: 15 October 2020
doi: 10.3389/fneur.2020.595975

Prolonged Static Whole-Body Roll-Tilt and Optokinetic Stimulation Significantly Bias the Subjective Postural Vertical in Healthy Human Subjects

Andrea Wedtgrube[1], *Christopher J. Bockisch*[1,2,3,4,5], *Dominik Straumann*[1,4,5] *and Alexander A. Tarnutzer*[1,4,5,6]*

[1] Department of Neurology, University Hospital Zurich, Zurich, Switzerland, [2] Department of Otorhinolaryngology, University Hospital Zurich, Zurich, Switzerland, [3] Department of Ophthalmology, University Hospital Zurich, Zurich, Switzerland, [4] Faculty of Medicine, University of Zurich, Zurich, Switzerland, [5] Center of Clinical Neurosciences, University Hospital Zurich, Zurich, Switzerland, [6] Neurology, Cantonal Hospital of Baden, Baden, Switzerland

OPEN ACCESS

Edited by:
Michael Strupp,
Ludwig Maximilian University of Munich, Germany

Reviewed by:
Sergei B. Yakushin,
Icahn School of Medicine at Mount Sinai, United States
Takeshi Tsutsumi,
Tokyo Medical and Dental University, Japan

***Correspondence:**
Alexander A. Tarnutzer
alexander.tarnutzer@access.uzh.ch

Specialty section:
This article was submitted to Neuro-Otology, a section of the journal Frontiers in Neurology

Received: 18 August 2020
Accepted: 07 September 2020
Published: 15 October 2020

Citation:
Wedtgrube A, Bockisch CJ, Straumann D and Tarnutzer AA (2020) Prolonged Static Whole-Body Roll-Tilt and Optokinetic Stimulation Significantly Bias the Subjective Postural Vertical in Healthy Human Subjects. Front. Neurol. 11:595975. doi: 10.3389/fneur.2020.595975

Background: Prolonged static whole-body roll-tilt has been shown to bias estimates of the direction of gravity when assessed by static paradigms such as the subjective visual vertical and the subjective haptic vertical.

Objective: We hypothesized that these shifts are paradigm-independent and thus predicted a post-tilt bias as well for self-adjustments along perceived vertical (subjective postural vertical, SPV). Likewise, rotatory optokinetic stimuli, which have been shown to shift the SPV when presented at the time of adjustments, may have an lasting effect on the SPV, predicting a shift in the perceived direction of gravity in the direction of the optokinetic rotatory stimulation.

Methods: Self-adjustments along perceived vertical by use of a motorized turntable were recorded at baseline and after 5 min of static whole-body roll-tilt (orientation = ±90°, adaptation period) in 10 healthy human subjects. During adaptation subjects were either in darkness (no OKN stimulation) or were presented a full-field rotatory optokinetic stimulus (velocity = ±60°/s). Statistical analysis of adjustment errors for the different conditions was performed using a generalized linear model.

Results: After 5 min of static whole-body roll-tilt in darkness, we observed significant ($p < 0.001$) shifts in the SPV averaging −2.8° (adaptation position: −90°) and 3.1° (+90°), respectively. Adding an optokinetic rotatory stimulus resulted in an additional, significant shift of SPV adjustments toward the direction of the previously presented optokinetic rotation (optokinetic clockwise rotation: 1.4°, $p = 0.034$; optokinetic counter-clockwise rotation: −1.3°, $p = 0.037$). Trial-to-trial variability of turntable adjustments was not significantly affected by adaptation.

Conclusions: Prolonged static roll-tilt results in a significant post-tilt bias of the perceived direction of gravity when assessed by the SPV, confirming previous findings from other vision-dependent and vision-independent paradigms. This finding emphasizes the impact of recent whole-body roll orientations relative to gravity. Such adaptational

shifts in verticality estimates may be explained in the context of Bayesian optimal observer theory with a bias of prior knowledge (i.e., expectation biased by experience). Our findings also have clinical implications, as the observed post-tilt bias may contribute to postural instability when standing up in the morning with an increasing risk for falls and fall-related injuries in humans with preexisting balance disorders.

Keywords: graviception, vestibular, Bayesian modeling, adaptation, postural vertical

INTRODUCTION

Human spatial orientation and navigation combines and weights sensory input from different end organs, including the vestibular organs [semicircular canals (SCCs) and otolith organs], pressure sensors in the skin and the visual system (1). For verticality perception, accurate, and precise adjustments have been shown for whole-body positions near upright, whereas for roll-tilted positions systematic roll over- and underestimation has been demonstrated for vision-dependent paradigms such as the subjective visual vertical (SVV) (2–4), but not for vision-independent paradigms such as the subjective haptic vertical (SHV) (5) or the subjective haptic horizontal (6). These differences emphasize the role of central integration of sensory input and also point to resulting biases.

Perceived direction of vertical also depends on the subject's recent history. Specifically, when returning back upright after prolonged static roll-tilt, a systematic bias (termed *post-tilt bias*) in the SVV can be seen (2, 7–10). This bias has exponential decay characteristics (10). It has been postulated that the sensory stimulation during the prolonged roll-tilt shifts the expectation of the body roll position toward the roll-tilt position, and this prior expectation biases perception when upright (10).

Previously, we have shown a similar pattern using a vision-independent paradigm (i.e., the SHV), proposing that this post-tilt bias most likely is of central origin (consistent with the shifting null hypothesis) (11). In most studies [including ours (10, 11)], subjects were passively brought into the roll-tilted adaptation position and back upright afterwards again. In daily life, however, self-positioning along perceived vertical is repeatedly required, e.g., when standing up in the morning after a night's sleep. Such an active task will integrate SCC input and thus differs from the SVV and the SHV task. Nevertheless, otolith input will be available for all these different tasks and thus likely will be integrated as well (12). Since the otolith organs are the only sensors that directly sense the pull of gravity (13), they are considered essential for verticality perception in all these tasks and thus may play a central role in adaptational effects in both active self-positioning in space and paradigms collected while remaining in a static whole-body roll-tilted position such as the SHV or the SVV. Thus, we predict a similar post-tilt bias when subjects are asked to align themselves along the perceived direction of vertical, a task referred to as the "subjective postural vertical" (SPV) [see (14) for review]. In addition to the proposed modulatory effect of prolonged whole-body static roll-tilt on the SPV, we hypothesized that task performance could be additionally biased by optokinetic rotatory stimuli. When presented during the SVV task, this results in a significant, roll-tilt dependent bias of perceived vertical (15), whereas only minor shifts can be seen when using a vision-independent paradigm (16). This prompted us to use this stimulus for adaptational purposes during prolonged static roll-tilt, postulating an additional modulatory effect on verticality perception when back upright. Noteworthy, for the SVV and the SHV we did not observe such a modulatory effect of optokinetic stimulation on perceived vertical when assessed immediately after returning back upright (11). This was possibly related to the fact that the SVV and the SHV task were performed in static positions, thus any adaptational effects on the percept of whole-body rotations may not have had any impact on these paradigms. In contrast, for the self-adjustments in the SPV task SCC input is also available. Hence, we predicted a modulatory effect on human self-positioning in space performance both by prolonged static roll-tilt and by rotatory optokinetic stimuli.

MATERIALS AND METHODS

Study Subjects and Ethics Statement

Six males and four females (aged between 23 and 42 years) completed the SPV paradigm and were included in the study. All participating subjects agreed to and signed a written informed consent, obtained after a meticulous explanation of the experimental procedure. The local ethics committee (Cantonal Ethics Committee Zurich, BASEC 2016-00023) approved the experimental protocol. The protocol was in accordance with the ethical standards of the 2013 Declaration of Helsinki for research involving human beings.

Experimental Setup

All data was collected on a three-axis motor-driven turntable (prototype built by Acutronic, Jona, Switzerland) and the participants were secured on the turntable with a four-point safety belt. The head was restrained using a thermoplastic mask (Sinmed, Reeuwyk, The Netherlands) which covered most of the head, thus allowing a natural straight-ahead position. The mask supported the wearing of glasses, if needed. Pillows were placed in the gaps the sides of the chair and body regions prone to unwanted movements (i.e., the shoulders, hips, and legs).

The most important organs for graviception are the otolith organs, which are located in the head. Therefore, the subjects' orientation in the roll plane will be referred as head-roll orientation, even though roll movements of the turntable were whole body. The roll axis of the motorized turntable

corresponded to the naso-occipital line passing between the subject's eyes.

The optokinetic rotatory stimulus was projected onto a sphere placed 1.5 m in front of the subject by means of a turntable-fixed video projector. The rotating optokinetic stimulus was generated with the Psychophysics Toolbox (17, 18) and GNU Octave (version 3.2.3), and consisted of randomly placed white dots on a black background (15). Three different visual-stimulus trial conditions were applied: baseline (no optokinetic stimulation), a clockwise rotating optokinetic stimulus (optokinetic CW) and a counter-clockwise rotating stimulus (optokinetic CCW). A joystick, mounted on a safety bar in front of the subject, could be tilted left or right to produce CCW and CW chair acceleration proportional to the angle of deflection, with a maximum of $30^\circ/s^2$. Turntable and joystick orientation signals were safely stored on a computer hard disk after they have been digitized at 200 Hz for further analysis.

Experimental Paradigm

In all participants, SPV control trials were obtained at the beginning of a single experimental session, followed by the adaptation trials (see **Figure 1** for illustration of the experimental paradigm). For all passive turntable movements (e.g., to reach the roll-tilted position for adaptation) we used a constant acceleration and deceleration of $\pm 10^\circ/s^2$. For all subject-guided turntable roll movements the turntable acceleration/deceleration was set to $\pm 30^\circ/s^2$. Importantly, these values were clearly above the detection thresholds of the semicircular canals (19, 20) and for self-motion perception (21). Before data collection, the participants were instructed how to use the joystick and practiced turntable roll movements, thus allowing them to perform the turntable adjustments accurately and precisely.

For the control trials, participants were brought to 90° right-ear down (RED) or 90° left-ear down (LED) position and after being roll-tilted for only 5 s, aligned themselves along perceived earth-vertical in darkness. This was performed 10 times from each starting position, in a pseudo-random order. Afterwards the adaptation trials were recorded, where subjects were roll-tilted 90°, either RED or LED and remained in these roll-tilted positions for 5 min (adaptation period) in each trial. During this period subjects were either kept in darkness (i.e., "optokinetic off" condition) or they were presented a full-field optokinetic stimulus rotating either into the clockwise ("optokinetic CW" condition) or counter-clockwise ("optokinetic CCW" condition) direction. In total, there were six different test conditions (two whole-body roll orientations, three visual stimulus conditions for each whole-body roll orientation) and each condition was recorded three times in every subject. The order of these 18 test trials was random, and after each trial another adaptation period was provided. Between trials (while upright) the lights were turned on briefly.

For both the control trials and the test trials subjects were instructed to move the turntable as quickly and as precisely as possible along the shortest path such that they are in an upright position by use of the joystick. An acoustic signal indicated the start of the subject-guided turntable movement. During these

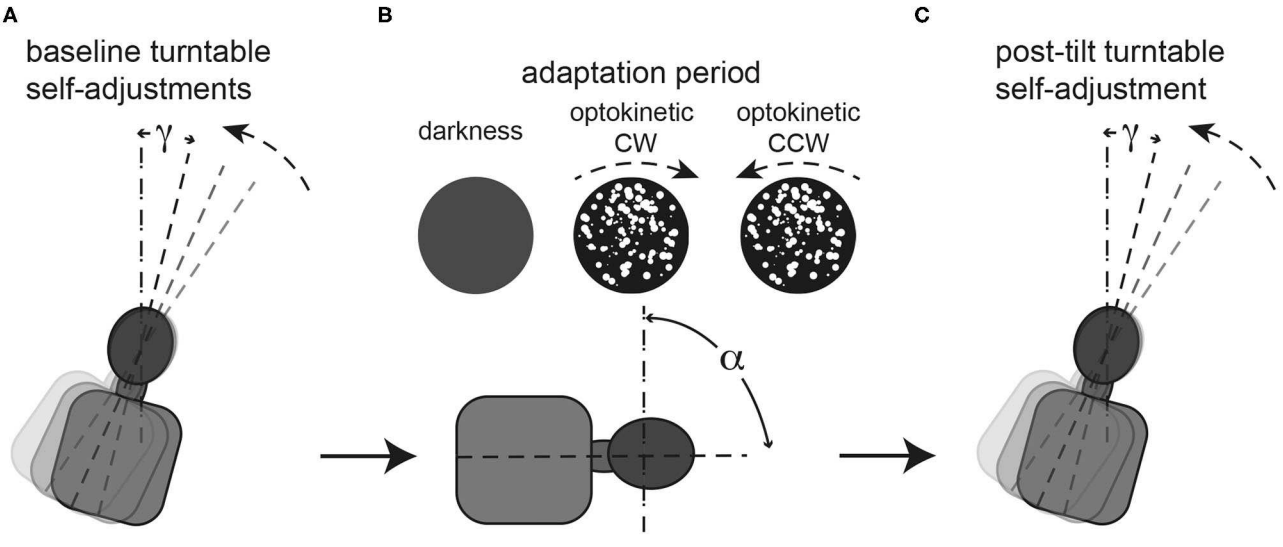

FIGURE 1 | Illustration of the required task at baseline **(A)**, during the 5-min adaptation period **(B)** and immediately afterwards **(C)**. **(A)**: repetitive baseline turntable self-adjustments starting from 90° right-ear down (RED) and 90° left-ear-down (LED) in random order (for illustrative purposes only a single trial starting from 90° RED is show) along the perceived earth-vertical are collected. Angle g represents the deviation of the turntable self-adjustments relative to earth-vertical, thus for perfect self-adjustments along earth-vertical g = 0. **(B)**: during the adaptation period, subjects remain in a static roll-tilted position (referred to as a, set to ±90°, only 90° RED shown for illustrative purposes) either in darkness ("no optokinetic stimulation" condition) or while watching an optokinetic stimulus that is rotating in either clockwise ("optokinetic CW" condition) or counter-clockwise ("optokinetic CCW" condition) direction. No self-adjustments are performed during this period. **(C)**: Single turntable self-adjustment along perceived earth-vertical in darkness (i.e., no optokinetic stimulus is shown) after the adaptation period. Again, g represents the deviation of the turntable self-adjustments relative to earth-vertical.

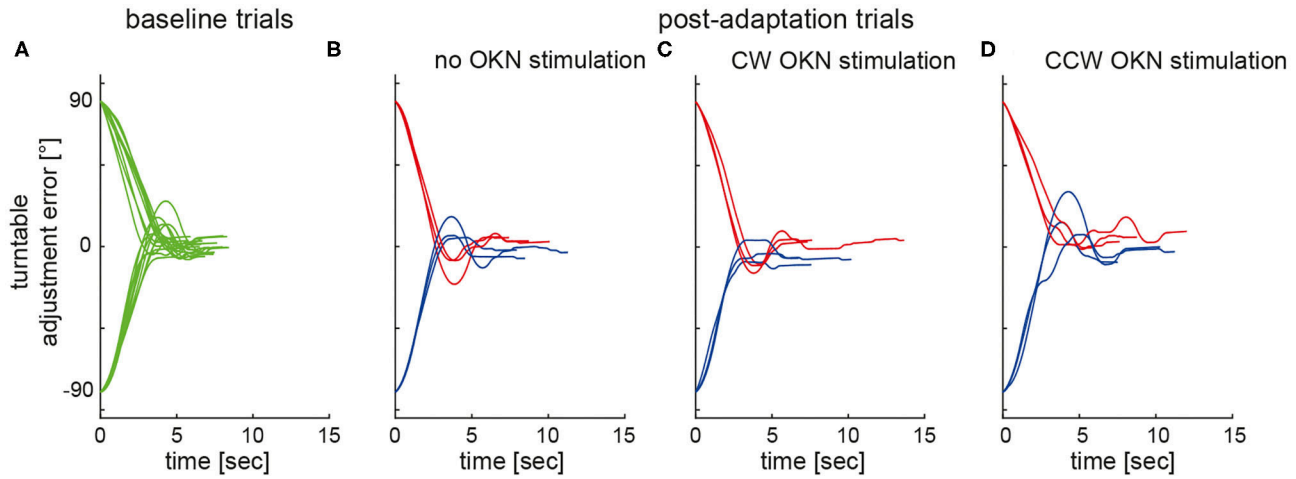

FIGURE 2 | Individual turntable adjustments relative to earth-vertical are plotted against time in a single subject (#10). Whereas, baseline trials **(A)** are shown in green, post-adaptation (test) trials (adaptation period not shown) are plotted in blue (adaptation position: 90° LED) and in red (adaptation position: 90° RED), respectively, for the different test conditions **(B–D)**.

subject-guided adjustments subjects were kept in darkness during all trial conditions. There was no specific time limit, and subjects were required to confirm the completion of adjustments by pushing a button placed next to the joystick.

Definition of Terms Frequently Used

Clockwise shifts relative to the earth-vertical axis (as seen by the subject) have positive signs, while counter-clockwise shifts have negative signs. We will use the term trial-to-trial variability when referring to the within subject standard deviation (SD). In relation to trial-to-trial variability, the term *precision* reflects the inverse, i.e., the degree of reproducibility. Furthermore, *accuracy* is defined as the magnitude of the mean adjustment error in a given paradigm. For the SPV the direction of rotation was always toward upright and defined by the starting position (either 90°RED or 90°LED).

Data Analysis

Extracted data from the SPV paradigm was sorted according to the whole-body roll orientation and the different control and test conditions using interactive programs written in Matlab 2017b (The MathWorks, Natick, MA, USA). The chair position when the subject pressed the button to confirm they were finished the adjustment was taken as perceived vertical body position for that trial.

Differences in adjustment errors and variability values for baseline trials and post-adaptation trials were calculated in all subjects. Mean values (±1 SD) were used when pooling individual data points as our data was normally distributed (tested at the level of individual trial conditions using the Jarque-Bera hypothesis test of composite normality, jbtest.m, Matlab 2017b). A generalized linear model (GLM) using SPSS 25 (IBM, Armonk, NY, USA) was applied for all statistical analyses if not specified otherwise. Main effects included the trial condition ($n = 4$; baseline vs. optokinetic off vs. optokinetic CW vs. optokinetic CCW), and the turntable adaptation position ($n = 2, \pm 90°$ roll-tilt). We kept the level of significance at a p-value of 0.05, and Fisher's least significant difference (LSD) method was used to correct for multiple comparisons when using the GLM.

The raw data supporting the conclusions of this manuscript will be made available by the authors, without undue reservation, to any qualified researcher.

RESULTS

Turntable self-adjustments were completed on average after 9.0 ± 2.3 s in all subjects. Statistical analysis yielded no main effect for the starting turntable orientation (df = 1, chi-square = 0.927, $p = 0.336$) and the trial condition (df = 3, chi-square = 7.747, $p = 0.052$) on adjustment time. Furthermore, no significant interactions (df = 3, chi-square = 1.720, $p = 0.632$) were identified.

Figure 2 illustrates single SPV adjustments in a typical subject both at baseline (panel A) and after adaptation without (panel B) and with (panels C and D) optokinetic rotatory stimulation, demonstrating a shift of adjustments toward the previous adaptation position in all test conditions.

For baseline trials, adjustment errors were small, averaging at 0.5 ± 0.7° (mean ± STD) (90°LED adaptation position) and at 0.5 ± 1.0° (90°RED adaptation position), respectively. For the different post-tilt conditions, average offsets ranged between −2.3 ± 2.1 and −5.3 ± 2.8° for 90°LED and between 3.6 ± 2.2 and 6.8 ± 2.7° for 90°RED (see **Figure 3** for details).

Post-tilt Offsets—Effect of Adaptation Position

Statistical analysis (GLM) of post-tilt adjustment errors for the SPV paradigm demonstrated significant main effects both for

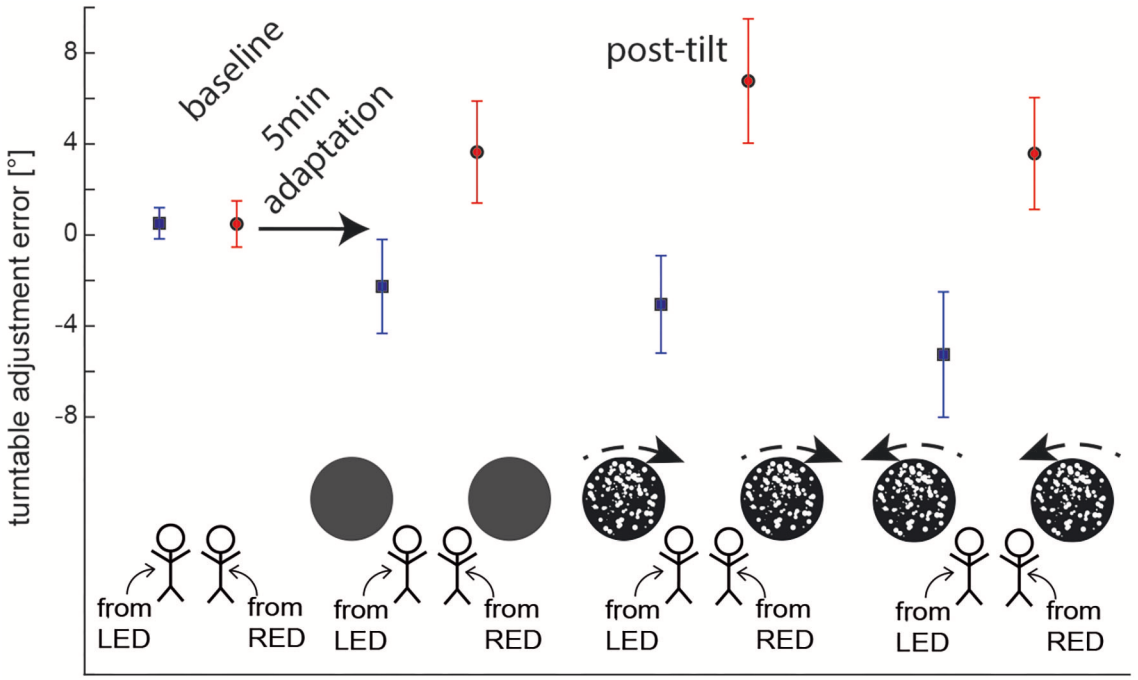

FIGURE 3 | Overall average (±1 SD) turntable adjustment errors are shown for both baseline and post-tilt conditions. For the post-tilt trials the specific adaptation condition (either 90° left-ear down (LED, lines in blue) or 90° right-ear-down (RED, lines in red) and the visual background (no optokinetic stimulus, optokinetic CW, optokinetic CCW) is illustrated. Note that in the post-tilt period all trials were collected in total darkness, i.e., no optokinetic stimulation was present.

the condition (df = 3, chi-square = 17.840, $p < 0.001$) and the adaptation position (df = 1, chi-square = 183.216, $p < 0.001$). Furthermore, a significant interaction was found between these two parameters (df = 3, chi-square = 71.751, $p < 0.001$).

Pairwise comparisons indicated significant differences in adjustment errors of the different test trials depending on the adaptation position (90°LED vs. 90°RED) and also in comparison with the control trials (without adaptation). This was true both for those post-adaptation trials without preceding optokinetic stimulation (RED vs. LED, $p < 0.001$) and for those with CW ($p < 0.001$) and CCW ($p < 0.001$) optokinetic stimulation, respectively. In contrast, there was no effect of the starting position (90°LED vs. 90°RED) on adjustment errors in the control trials ($p = 0.974$). Furthermore, adjustment errors were significantly different in post-adaptation (test) trials (with or without optokinetic rotatory stimulation) compared to the baseline trials; this was true both for LED ($p \leq 0.002$) and RED ($p \leq 0.001$). In all test conditions, deviations were toward the previous adaptation position, as shown in **Figure 3**.

Post-tilt Offsets—Effect of Optokinetic Stimulation

Pairwise comparisons were applied to further assess the observed main effect for the condition (baseline vs. no optokinetic vs. optokinetic CW vs. optokinetic CCW). They demonstrated significant shifts in adjustment errors for trials with optokinetic CW ($p = 0.034$, D = 1.4 ± 0.6°) and optokinetic CCW ($p = 0.037$, D = 1.3 ± 0.6°) stimulation compared to baseline adjustments into the direction of optokinetic stimulation. In contrast, no significant differences were observed comparing test trials without optokinetic stimulation and baseline trials (with both adaptation/starting positions pooled, $p = 0.763$, D = 0.2 ± 0.6°). Comparing the different test trials, SPV adjustments were significantly different between those two conditions with optokinetic stimulation (CW vs. CCW, $p < 0.001$) and between the optokinetic CCW conditions vs. the no optokinetic condition ($p = 0.017$). In contrast, there was no significant difference in offset when comparing the optokinetic CW condition and the no optokinetic condition ($p = 0.069$).

Pairwise comparisons found that the optokinetic stimulation effected the final vertical position only when the optokinetic stimulus moved in the same direction and the adapted title position (that is, CW when RED, and CCW when LED). For SPV adjustments after 5 min adaptation in 90° LED position, adding optokinetic stimulation during the adaptation period resulted in significantly different adjustment errors for optokinetic CCW stimulation ($p = 0.001$), but not for optokinetic CW stimulation ($p = 0.383$) in comparison to darkness (i.e., no optokinetic stimulation) during adaptation. The effect of optokinetic stimulation on turntable adjustment errors was confirmed when directly comparing optokinetic CW and optokinetic CCW conditions ($p = 0.015$).

Likewise, for SPV adjustments after 5 min of adaptation in 90° RED position, adding optokinetic stimulation during the

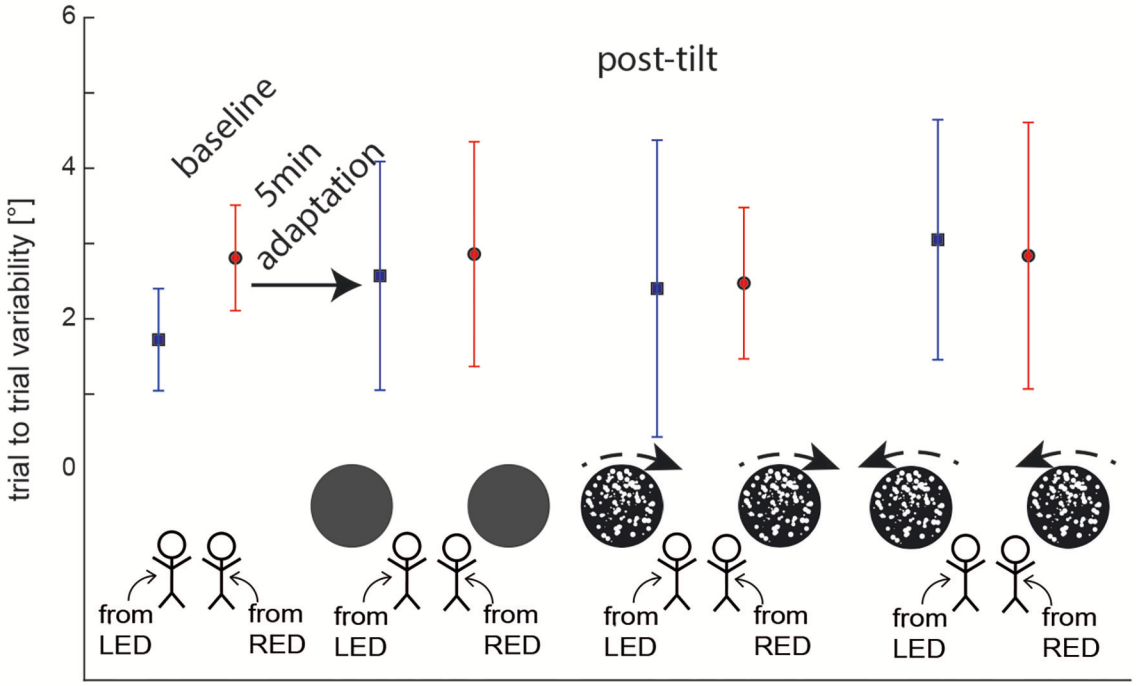

FIGURE 4 | Overall average (± 1 SD) trial-to-trial variability of turntable adjustments are shown for both baseline and post-tilt conditions. For the post-tilt trials the specific adaptation condition (either 90° left-ear down (LED, lines in blue) or 90° right-ear-down (RED, lines in red) and the visual background (no optokinetic stimulus, optokinetic CW, optokinetic CCW) is illustrated. Note that in the post-tilt period all trials were collected in darkness, i.e., no optokinetic stimuli were shown.

adaptation period resulted in significantly different adjustment errors for optokinetic CW stimulation ($p = 0.001$), but not for optokinetic CCW stimulation ($p = 0.942$) in comparison to the no optokinetic stimulation condition. Again, the effect of optokinetic stimulation on SPV adjustment errors was confirmed when directly comparing optokinetic CW and optokinetic CCW conditions ($p < 0.001$).

Trial-to-Trial Variability of SPV Adjustments

Average (±1 SD) trial-to-trial variability for the different baseline and test trials was in the range between 1.7 ± 0.7 and 3.1±1.6° as illustrated in **Figure 4**. Statistical analysis (again using a GLM) showed no main effect for the starting position (df = 1, chi-square = 1.054, $p = 0.305$) and the trial condition (df = 3, chi-square = 2.985, $p = 0.394$) on trial-to-trial variability. In addition, no significant interactions were noted (df = 3, chi-square = 2.585, $p = 0.460$).

DISCUSSION

This study was driven by the hypothesis that prolonged static whole-body roll-tilt results in a shift of the internal representation of the direction of gravity (i.e., the "null position"), termed "post-tilt bias" (22), and that visual cues presented during the adaptation period further modulate subsequent self-adjustments. Using a subjective postural vertical (SPV) paradigm, we found turntable self-adjustments to be significantly biased toward the previous adaptation position. For instance, when the subject was previously roll-tilted to the right, the SPV was tilted to the right when subjects were asked to position their body vertically. Presenting an optokinetic rotatory stimulus during the adaptation period resulted in additional offsets in verticality perception, with shifts pointing into the direction of rotation of the visual stimulus. Thus, our data confirms the presence of a post-tilt bias for the SPV paradigm and therefore emphasizes the impact of recent whole-body roll orientation on self-adjustments in the roll plane. These findings also have clinical implications as they point to systematic errors in spatial orientation after prolonged whole-body horizontal orientation, e.g., when getting up in the morning after a good night's sleep, which may contribute to falls and fall-related injuries, especially in the elderly.

The Effect of Prolonged Whole-Body Static Roll-Tilt on Self-Adjustments Along Perceived Vertical

After 5 min of static whole-body roll-tilt in darkness, we observed average shifts in the SPV of 2.8° (adaptation-position = 90° LED) and 3.1° (90° RED), respectively. Noteworthy, adjustment errors always deviated toward the previous adaptation position. To our knowledge, such adaptational effects have not been previously described for the SPV. Thus, our data demonstrates that prolonged static whole-body roll-tilt is not only affecting

static assessments of verticality perception after returning back upright [by use of e.g., the subjective visual vertical (SVV) or the subjective haptic vertical (SHV)] but is also biasing self-adjustments along perceived direction of gravity. Therefore, our findings further emphasize the impact of the subject's recent orientation relative to gravity on verticality perception.

A post-tilt bias, either toward or (less frequently) away from the previous roll-tilted position, has been previously described for the SVV (2, 7–10) and has been shown to exponentially decay with a median time constant of 71 s (10). More recently, we have demonstrated such a post-tilt bias also for the SHV, i.e., a vision-independent paradigm (11), further supporting the hypothesis that prolonged static roll-tilt results in a mostly paradigm-independent shift of the internal estimate of direction of gravity.

Changes in prior knowledge (or likelihood) in a Bayesian optimal observer model may explain such a shift in the graviceptive null position, as previously discussed by Tarnutzer et al. (10). Specifically, Bayesian optimal observer theory proposes a mechanism where the human brain combines all available sensory cues available in a weighted fashion according to their relative reliabilities and prior likelihood to generate an internal estimate of the direction of gravity (3, 4, 23–26). Thus, in subjects previously being roll-tilted, the prior will be biased toward this roll-tilted position, systematically shifting the resulting posterior probability distribution (4).

Thus, in an experimental setup, shifting prior knowledge has been shown to be a promising approach to study multisensory integration when internally estimating direction of gravity. Shifts in both the SVV, the SHV and the SPV by such adaptational paradigms emphasize the impact of prior knowledge. Noteworthy, besides the subject's roll orientation relative to gravity, also the direction of rotatory optokinetic stimuli and the resulting deviation in mean eye position from normal by an optokinetic nystagmus may bias the prior when assessed by the SPV, as discussed below.

The Effect of Optokinetic Rotatory Stimuli on Self-Adjustments Along Perceived Vertical

Interestingly, for self-adjustments to perceived vertical (performed in darkness) we observed a significant effect of rotatory optokinetic stimuli presented during the adaptation period. Specifically, SPV adjustments were shifted on average by 1.3–1.4° toward the direction of rotation of the previously presented optokinetic stimulus.

While optokinetic rotatory stimuli have been proven very powerful in biasing verticality perception when using vision-dependent paradigms such as the SVV when presented at the time of the adjustments (15, 27), minor to non-significant shifts only were observed when using other, vision-independent paradigms as the SHV to assess internal estimates of direction of gravity while presenting a rotatory stimulus (16). Noteworthy, an effect of optokinetic stimulation on the SPV, i.e., another, vision-independent paradigm assessing verticality perception, has been described by Dichgans et al. (27). Specifically, asking participants to continuously adjust their whole-body roll orientation to perceived upright while watching a rotatory stimulus, resulted in a shift of 8.5° on average. In contrast, Bisdorff et al. reported no effect of a rotatory optokinetic stimulus (velocity = 60°/s) on the SPV presented during passive whole-body rotation (28).

Furthermore, using the same rotatory optokinetic stimulus during adaptation, we have previously found no significant effect on the subsequent post-tilt bias for both vision-dependent (SVV) and vision-independent (SHV) static paradigms (11). Taking our current findings into consideration, we propose that the effect of prolonged rotatory optokinetic stimuli on verticality perception is paradigm-dependent.

We found an asymmetry in the impact of the optokinetic rotatory stimulus on the SPV. Specifically, significant shifts in turntable self-adjustment errors were noted when the static roll-tilt position and the direction of the rotatory stimulus were into the same (CW or CCW) direction. Thus, shifts were significant when adding CW optokinetic stimulation during whole-body static roll-tilt in 90° RED position (shifting perceived vertical into CW direction as well) and when adding CCW optokinetic stimulation during whole-body static roll-tilt in 90° LED position (shifting perceived vertical into CCW direction as well). In conditions when the prolonged whole-body static roll-tilt and the optokinetic stimulus point in opposite directions, no effect of optokinetic stimulation was observed in comparison to the condition with adaptation performed in darkness. This speaks against a simple additive (or subtractive) effect of these two mechanisms (i.e., the shift in verticality perception by prolonged static whole-body roll-tilt and the shift by prolonged optokinetic rotatory stimulation), but favors a more complex interaction with integration of the visual input only if the tilt direction from upright is in the same direction as the rotating visual stimulus. Thus, our findings propose that for shifting the gravitational null vestibular input is weighted more than concomitant visual input.

Previous studies have demonstrated that the SVV in patients with acute unilateral vestibular loss is strongly tilted toward the side of the lesion, whereas in the same patients the SPV was found to remained veridical, suggesting different weighting of the participating sensory systems for determining the SPV and the SVV (29). These authors concluded that the SPV is derived mainly from somatosensory input, which potentially explains why non-vestibular cues such as optokinetic stimulation had an outlasting effect in our adaptation paradigm when using the SPV but not when using the SVV or the SHV.

In a recently published study, a modulatory effect of dynamic visual stimuli on the SPV was reported (30). Specifically, in this study subjects were first presented a visual stimulus (duration = 20 s) that was moving downward along the body-longitudinal axis while subjects were roll-tilted 18° to the left side. During the subsequent passive chair rotation to the right side they had to indicate when they felt aligned with earth-vertical. Compared to control trials (without a visual stimulus), test trials with a visual stimulus that was moving downwards with constant acceleration resulted in a shift of subsequent passive SPV adjustments of 0.7° toward the previous roll-tilt position. These findings are

consistent with our observation that directed optokinetic stimuli may result in a bias of verticality perception that outlasts the duration of stimulus presentation, consistent with the concept of modulatory effects of prior knowledge in the framework of Bayesian optimal observer theory.

LIMITATIONS

Our study has several limitations, including a moderately large sample size ($n = 10$) and a limited number of trials ($n = 3$) per test condition due to the restriction to a single trial after each adaptation period. We therefore cannot make any conclusions on the decay characteristics of the post-tilt bias for self-adjustments along the perceived direction of gravity. Furthermore, calculations of trial-to-trial variability have to be taken with caution and therefore the reported non-significant differences in variability amongst different trial conditions is a preliminary finding.

CONCLUSIONS

Prolonged static whole-body roll tilt results in a significant "post-tilt" bias of perceived direction of gravity when assessed by the SPV, confirming previous findings from other paradigms including the SVV and the SHV and emphasizing the impact of recent whole-body roll orientation relative to gravity. Such adaptational shifts in verticality estimates may be explained in the context of Bayesian optimal observer theory with a bias of prior knowledge. Furthermore, the significant impact of optokinetic rotatory stimuli on subsequent self-adjustments along perceived vertical, whereas such an effect was not found for the SVV and the SHV previously, is potentially explained by differences in weighting of the sensory input available when centrally integrated. Our findings also have clinical implications, as the observed post-tilt bias may contribute to postural instability when standing up in the morning, increasing the risk for falls and fall-related injuries in patients with preexisting balance disorders.

DATA AVAILABILITY STATEMENT

The raw data supporting the conclusions of this article will be made available by the authors, without undue reservation.

ETHICS STATEMENT

The studies involving human participants were reviewed and approved by Cantonal Ethics Committee Zurich. The patients/participants provided their written informed consent to participate in this study.

AUTHOR CONTRIBUTIONS

AW: collection, analysis and interpretation of data, and drafting and revising the article critically for important intellectual content. CB: assisted in the design of the experiments, analysis and interpretation of data, and revising the article critically for important intellectual content. DS: assisted in the design of the experiments and revising the article critically for important intellectual content. AT: conception and design of the experiments, collection, analysis and interpretation of data, and revising the article critically for important intellectual content. All authors: have approved the final version of the manuscript, all persons designated as authors qualify for authorship, and all those who qualify for authorship are listed.

FUNDING

The Betty and David Koetser Foundation for Brain Research, Zurich, Switzerland; the Center of Integrative Human Physiology, University of Zurich, Switzerland; Bonizzi-Theler-Foundation, Zurich, Switzerland; Dr. Dabbous Foundation, University of Zurich, Switzerland.

ACKNOWLEDGMENTS

The authors thank Marco Penner for technical assistance.

REFERENCES

1. Cullen KE, Taube JS. Our sense of direction: progress, controversies and challenges. *Nat Neurosci.* (2017) 20:1465–73. doi: 10.1038/nn.4658
2. Lechner-Steinleitner S. Interaction of labyrinthine and somatoreceptor inputs as determinants of the subjective vertical. *Psychol Res.* (1978) 40:65–76. doi: 10.1007/BF00308464
3. De Vrijer M, Medendorp WP, Van Gisbergen JA. Shared computational mechanism for tilt compensation accounts for biased verticality percepts in motion and pattern vision. *J Neurophysiol.* (2008) 99:915–30. doi: 10.1152/jn.00921.2007
4. Tarnutzer AA, Bockisch C, Straumann D, Olasagasti I. Gravity dependence of subjective visual vertical variability. *J Neurophysiol.* (2009) 102:1657–71. doi: 10.1152/jn.00007.2008
5. Schuler JR, Bockisch CJ, Straumann D, Tarnutzer AA. Precision and accuracy of the subjective haptic vertical in the roll plane. *BMC Neurosci.* (2010) 11:83. doi: 10.1186/1471-2202-11-83
6. Wade SW, Curthoys IS. The effect of ocular torsional position on perception of the roll-tilt of visual stimuli. *Vision Res.* (1997) 37:1071–8. doi: 10.1016/S0042-6989(96)00252-0
7. Schoene H, Udo De Haes H. Perception of gravity-vertical as a function of head and trunk position. *Zeitschrift für Vergleichende Physiol.* (1968) 60:440–4. doi: 10.1007/BF00297938
8. Udo De Haes HA. Stability of apparent vertical and ocular countertorsion as a function of lateral tilt. *Percep Psychophys.* (1970) 8:137–42. doi: 10.3758/BF03210192
9. Wade NJ. Effect of prolonged tilt on visual orientation. *Q J Exp Psychol.* (1970) 22:423–39. doi: 10.1080/14640747008401916
10. Tarnutzer AA, Bertolini G, Bockisch CJ, Straumann D, Marti S. Modulation of internal estimates of gravity during and after prolonged roll-tilts. *PLoS ONE.* (2013) 8:e78079. doi: 10.1371/journal.pone.0078079
11. Wedtgrube A, Bockisch CJ, Tarnutzer AA. Effects of prolonged roll-tilt on the subjective visual and haptic vertical in healthy human subjects. *J Vestib Res.* (2020) 30:1–16. doi: 10.3233/VES-200690
12. Tarnutzer AA, Bockisch CJ, Olasagasti I, Straumann D. Egocentric and allocentric alignment tasks are affected by otolith input. *J Neurophysiol.* (2012) 107:3095–106. doi: 10.1152/jn.00724.2010
13. Schoene H. On the role of gravity in human spatial orientation. *Aerosp. Med.* (1964) 35:764–72.

14. Conceicao LB, Baggio J,a.O., Mazin SC, Edwards DJ, Santos TEG. Normative data for human postural vertical: a systematic review and meta-analysis. *PLoS ONE.* (2018) 13:e0204122. doi: 10.1371/journal.pone.0204122
15. Ward BK, Bockisch CJ, Caramia N, Bertolini G, Tarnutzer AA. Gravity dependence of the effect of optokinetic stimulation on the subjective visual vertical. *J Neurophysiol.* (2017) 117:1948–1958. doi: 10.1152/jn.00303.2016
16. Dockheer KM, Bockisch CJ, Tarnutzer AA. Effects of optokinetic stimulation on verticality perception are much larger for vision-based paradigms than for vision-independent paradigms. *Front Neurol.* (2018) 9:323. doi: 10.3389/fneur.2018.00323
17. Brainard DH. The psychophysics toolbox. *Spat Vis.* (1997) 10:433–6. doi: 10.1163/156856897X00357
18. Pelli DG. The VideoToolbox software for visual psychophysics: transforming numbers into movies. *Spat Vis.* (1997) 10:437–42. doi: 10.1163/156856897X00366
19. Shimazu H, Precht W. Tonic and kinetic responses of cat's vestibular neurons to horizontal angular acceleration. *J Neurophysiol.* (1965) 28:991–1013. doi: 10.1152/jn.1965.28.6.991
20. Diamond SG, Markham CH, Furuya N. Binocular counterrolling during sustained body tilt in normal humans and in a patient with unilateral vestibular nerve section. *Ann Otol Rhinol Laryngol.* (1982) 91:225–9. doi: 10.1177/000348948209100222
21. Lewis RF, Priesol AJ, Nicoucar K, Lim K, Merfeld DM. Dynamic tilt thresholds are reduced in vestibular migraine. *J Vestib Res.* (2011) 21:323–30. doi: 10.3233/VES-2011-0422
22. Day RH, Wade NJ. Visual spatial aftereffect from prolonged head-tilt. *Science.* (1966) 154:1201–2. doi: 10.1126/science.154.3753.1201
23. Eggert T. *Der Einfluss orientierter Texturen auf die subjektive Vertikale und seine systemtheoretische Analyse.* (Dissertation), Technical University of Munich, Munich, Germany (1998).
24. Kording KP, Wolpert DM. Bayesian integration in sensorimotor learning. *Nature.* (2004) 427:244–7. doi: 10.1038/nature02169
25. Laurens J, Droulez J. Bayesian processing of vestibular information. *Biol Cybern.* (2007) 96:405. doi: 10.1007/s00422-006-0133-1
26. Macneilage PR, Banks MS, Berger DR, Bulthoff HH. a bayesian model of the disambiguation of gravitoinertial force by visual cues. *Exp Brain Res.* (2007) 179:263–290. doi: 10.1007/s00221-006-0792-0
27. Dichgans J, Held R, Young LR, Brandt T. Moving visual scenes influence the apparent direction of gravity. *Science.* (1972) 178:1217–9. doi: 10.1126/science.178.4066.1217
28. Bisdorff A, Bronstein A, Gresty M, Wolsley C. Subjective postural vertical inferred from vestibular-optokinetic vs. proprioceptive cues. *Brain Res Bull.* (1996) 40:413–5. doi: 10.1016/0361-9230(96)00135-9
29. Anastasopoulos D, Haslwanter T, Bronstein A, Fetter M, Dichgans J. Dissociation between the perception of body verticality and the visual vertical in acute peripheral vestibular disorder in humans. *Neurosci Lett.* (1997) 233:151–3. doi: 10.1016/S0304-3940(97)00639-3
30. Tani K, Ishimaru S, Yamamoto S, Kodaka Y, Kushiro K. Effect of dynamic visual motion on perception of postural vertical through the modulation of prior knowledge of gravity. *Neurosci Lett.* (2020) 716:134687. doi: 10.1016/j.neulet.2019.134687

Conflict of Interest: The authors declare that the research was conducted in the absence of any commercial or financial relationships that could be construed as a potential conflict of interest.

frontiers in Neurology

REVIEW
published: 20 October 2020
doi: 10.3389/fneur.2020.566895

The Anatomical and Physiological Basis of Clinical Tests of Otolith Function. A Tribute to Yoshio Uchino

*Ian S. Curthoys**

Vestibular Research Laboratory, School of Psychology, The University of Sydney, Sydney, NSW, Australia

Otolithic receptors are stimulated by gravitoinertial force (GIF) acting on the otoconia resulting in deflections of the hair bundles of otolithic receptor hair cells. The GIF is the sum of gravitational force and the inertial force due to linear acceleration. The usual clinical and experimental tests of otolith function have used GIFs (roll tilts re gravity or linear accelerations) as test stimuli. However, the opposite polarization of receptors across each otolithic macula is puzzling since a GIF directed across the otolith macula will excite receptors on one side of the line of polarity reversal (LPR at the striola) and simultaneously act to silence receptors on the opposite side of the LPR. It would seem the two neural signals from the one otolith macula should cancel. In fact, Uchino showed that instead of canceling, the simultaneous stimulation of the oppositely polarized hair cells enhances the otolithic response to GIF—both in the saccular macula and the utricular macula. For the utricular system there is also commissural inhibitory interaction between the utricular maculae in each ear. The results are that the one GIF stimulus will cause direct excitation of utricular receptors in the activated sector in one ear as well as indirect excitation resulting from the disfacilitation of utricular receptors in the corresponding sector on the opposite labyrinth. There are effectively two complementary parallel otolithic afferent systems—the sustained system concerned with signaling low frequency GIF stimuli such as roll head tilts and the transient system which is activated by sound and vibration. Clinical tests of the sustained otolith system—such as ocular counterrolling to roll-tilt or tests using linear translation—do not show unilateral otolithic loss reliably, whereas tests of transient otolith function [vestibular evoked myogenic potentials (VEMPs) to brief sound and vibration stimuli] do show unilateral otolithic loss. The opposing sectors of the maculae also explain the results of galvanic vestibular stimulation (GVS) where bilateral mastoid galvanic stimulation causes ocular torsion position similar to the otolithic response to GIF. However, GVS stimulates canal afferents as well as otolithic afferents so the eye movement response is complex.

Keywords: vestibular, otolith, utricular, saccular, vemp

OPEN ACCESS

Edited by:
Richard Lewis,
Harvard University, United States

Reviewed by:
Faisal Karmali,
Harvard Medical School,
United States
Bryan Kevin Ward,
Johns Hopkins University,
United States

***Correspondence:**
Ian S. Curthoys
ian.curthoys@sydney.edu.au

Specialty section:
This article was submitted to Neuro-Otology, a section of the journal Frontiers in Neurology

Received: *28 May 2020*
Accepted: *18 September 2020*
Published: *20 October 2020*

Citation:
Curthoys IS (2020) The Anatomical and Physiological Basis of Clinical Tests of Otolith Function. A Tribute to Yoshio Uchino. Front. Neurol. 11:566895. doi: 10.3389/fneur.2020.566895

INTRODUCTION

The canals and the otolithic sensory regions of the inner ear function as an integrated system—in response to head movements, otolith signals interact with canal signals to generate appropriate sensations, eye movements, and postural responses (1). Loss of otolith function disrupts that neural interaction and causes patient reports of disorientation as well as postural unsteadiness (2). Many patients arrive at clinics complaining of dizziness, vertigo, postural unsteadiness but tests in these patients may show all semicircular canals have normal function (2).

In parallel with the aim of clinical testing of the semicircular canals, clinical tests of otolith function seek to identify the level of otolith function in each ear and whether there is unilateral loss of otolith function. However, the structure of the otoliths is unusual and, as we show below, tests which *prima facie* appear that they should be indicators of the level of otolith function in each ear do not provide clinically useful data about asymmetry of otolith function. In particular, the opposite polarization of receptors across each otolithic macula is puzzling since a gravitoinertial force (GIF) stimulus directed across the otolith macula will excite receptors on one side of the line of polarity reversal (LPR at the striola) and simultaneously act to silence receptors on the opposite side of the LPR. It would seem the two neural signals from the one otolith macula should cancel. In fact, Uchino's detailed physiology in the VN show exactly the opposite!—that instead of canceling, the simultaneous stimulation of the oppositely polarized hair cells enhances the otolithic response to GIF—both in the saccular macula and the utricular macula.

In the labyrinth of each ear the otolithic receptors are laid out on two sheets of cells called maculae—the utricular macula and the saccular macula—and the receptors and afferents within each macula form two complementary otolithic systems—the sustained system concerned with signaling low frequency GIFs and the transient system which is activated by high frequency stimuli such as sounds and vibration (1). Tests of the sustained otolith system do not show unilateral loss reliably, whereas tests of transient (dynamic) otolith function do show unilateral otolithic loss.

A good example of a test using the sustained system is the response to maintained head tilt. **Figure 1** shows a side-on view of the utricular macula of a guinea pig—the white layer being the otoconia adhering to the upper surface of the otolithic membrane. The human utricular macula is similar. During a roll head tilt, gravity displaces the crystals (the otoconia) and so stimulates the otolith utricular receptors (**Figure 2A**) and causes both eyes to roll around the line of sight and to maintain a rolled position during the maintained head tilt. A roll head tilt, left ear down, causes both eyes to roll so the upper pole of both eyes is rolled in the orbit by a few degrees to the right. This response is termed ocular torsion or ocular counterrolling (OCR). It has been presumed that loss of the otoliths in one labyrinth should result in asymmetrical OCR for the two directions of lateral head tilt, just as unilateral loss of the semicircular canals results in asymmetrical horizontal vestibulo-ocular responses. At the acute stage roll head tilts to the affected side do show reduced OCR, but that is not the case in patients with long term unilateral loss—there is no systematic asymmetry in OCR responses for roll-tilts to the left or right (7). However, tests of the transient otolith system, do show unilateral otolithic loss acutely and chronically. In this review we examine the peripheral anatomy and physiology of the otoliths underlying these very different and puzzling outcomes.

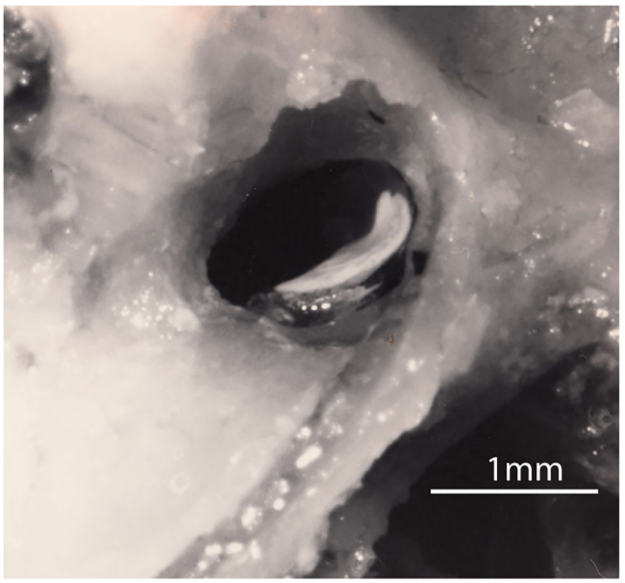

FIGURE 1 | A lateral view of the right utricular macula in a guinea pig. The white layer is the otoconia adhering to the upper surface of the gelatinous otoconial membrane (OM) on the macula. The upturn is at the rostral end of the macula where it is attached to bone and where the afferent neurons leave. The rest of the macula (the flat plate) rests on a membrane stretched across the labyrinth (the *membrana limitans*) so that most of the utricular macula effectively floats on fluid (3–5). Figure reproduced with permission of the Aerospace Medical Association from Curthoys (3).

Summary of Otolith Anatomy and Physiology

Vestibular Receptor Hair Cells

In the human there are around 33,000 receptors in each utricular macula [synapsing on around 6,000 afferents (8)] and 18,000

Abbreviations: ACS, air conducted sound; BCV, bone-conducted vibration; OM, otolithic membrane; GIF, gravitoinertial force—the effective stimulus for otolithic receptors; HSV, horizontal slow phase eye velocity; VSV, vertical slow phase eye velocity; TSV, torsional slow phase eye velocity; SCD, semicircular canal dehiscence; LPR, line of polarity reversal; type I, excitatory neurons in the vestibular nucleus; type II, inhibitory neurons in the vestibular nucleus; VN, vestibular nucleus; ABD, abducens nucleus; GVS, galvanic vestibular stimulation; VEMP, vestibular evoked myogenic potential; oVEMP, ocular vestibular evoked myogenic potential; cVEMP, cervical vestibular evoked myogenic potential; Fz, the midline of the forehead at the hair line; OCR, ocular counterrolling—torsion of the eye in a direction opposite to the gravitoinertial force; OTR, the ocular tilt reaction. A triad of ipsilesional roll head tilt, ipsilesional ocular torsion and skew deviation with the ipsilesional eye lower in the orbit; ipsilesional, on the same side as the loss or lesion; contralesional, on the opposite side to the loss or lesion (in other words, the healthy side).

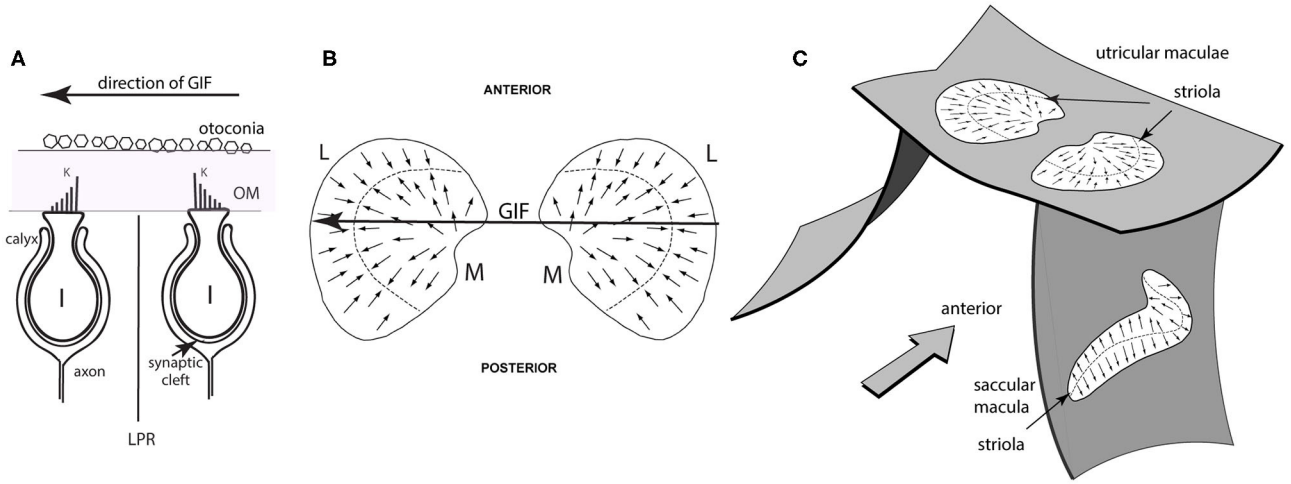

FIGURE 2 | Simplified schematic diagrams of otolithic type I receptors, the line of polarity reversal and the spatial organization of the utricular and saccular maculae. **(A)** Showing two type I receptors on either side of the line of polarity reversal (LPR). The primary afferent neuron forms a calyx ending which envelops the whole amphora-shaped receptor cell body. Other receptors are barrel shaped and are called type II receptors. The kinocilium is the longest cilium and is identified by the letter K in this schematic. A gravitoinertial force directed from right to left (such as a roll tilt of the head left ear down) will displace the otoconia above the macula which will deflect the hair bundles of the receptors and so facilitate the type I receptor on the right because the cilia of that receptor will be deflected toward the kinocilium, but simultaneously disfacilitate the receptor on the left whose cilia will be deflected away from the kinocilium. **(B)** Schematic representations of the view looking straight down on the two utricular maculae during a laterally directed GIF to the left (shown by the large arrow). The small arrows represent the preferred directions of receptors on the maculae and the systematic change in preferred direction and the opposite polarization on either side of the line of polarity reversal (LPR—dashed line) are shown. The two utricular maculae are mirror images of one another. The medial sectors are identified by the letter M and the lateral sectors by the letter L. The GIF (large arrow) simultaneously facilitates left medial and disfacilitates left lateral receptors. **(C)** Showing the approximate spatial configuration of the utricular and saccular maculae in the head. The band of receptors adjacent to the line of polarity reversal is called the striola. In the utricular macula the receptors point toward the LPR, whereas in the saccular macula the receptors point away from the LPR [from Curthoys (6), Copyright © 2020 Karger Publishers, Basel, Switzerland].

receptors in each saccular macula (9) [synapsing on around 4,000 saccular afferents (8)]. Projecting from each otolithic receptor cell are hair-like cilia and deflections of these hair bundles stimulate the receptor. The hair bundles project into the gelatinous otoconial membrane (OM), the upper surface of which is covered by otoconia (**Figures 1**, **2A**). Each receptor has one distinct cilium (the kinocilium, K) which serves as a unique feature which identifies the preferred direction of stimulation of that receptor—its "morphological polarization" or directional preference (10). Intracellular recording from isolated receptors has shown that for all receptors, deflections of the receptor hair bundle toward the kinocilium are facilitatory (excitatory), deflections away from the kinocilium are disfacilitatory (11–13) (**Figure 2A**). There is a systematic change in the directional preference of the individual receptors around the utricular macula (9). This structural organization is shown schematically in **Figures 2B,C** as small arrows on the surface of the maculae, representing the different preferred directions of receptors all over the macula. This spatial ordering of the directional preference of receptors in the otolithic maculae (**Figure 2C**) contrasts with the uniform directional preference of all receptors on each semicircular canal crista (9). Each otolithic maculae is divided into two sectors in which the hair cells have exactly opposite directional preferences (9) (**Figures 2B,C**).

The line dividing the two sectors is called the line of polarity reversal (LPR) and the thin band of receptors on either side of the LPR is called the striola.

Gravity is usually the stimulus generating hair bundle deflection. A gravitoinertial force in one direction displaces the dense crystals of the otoconia of the otolith organs, and so the hair bundles of the otolithic receptor hair cells, embedded in the otoconial membrane, tuned to that direction are deflected and activated. Recently it has been shown that sound and vibration are very effective stimuli for one class of otolithic receptors and afferents—those with irregular resting discharge originating from receptors at the striola (14). Other stimuli [small electric currents called galvanic vestibular stimulation (GVS) delivered by surface electrodes on the mastoids] activate all vestibular receptors and afferent neurons on the side of the cathode electrode and inhibit afferents on the side of the anode electrode (15–17). Each one of these stimuli has been used in possible clinical tests of otolithic function and they are discussed below after considering the anatomy and physiology of the otoliths.

The receptor organization of the otolithic maculae means that in response to the one GIF stimulus, some otolithic receptors and afferents have an increased activation (facilitation) whereas others in the same macula have decreased activation (disfacilitation) to exactly the same stimulus (**Figure 2B**). It seems that these two opposite responses should cancel. In fact the opposite is true—Uchino's results have shown that because of interposed inhibitory neurons, their simultaneous stimulation acts to enhance the response to the GIF in a manner analogous to the enhancement to angular acceleration by bilateral inhibitory interaction in processing of semicircular canal neural

information (18–20). In the semicircular canal system this is called mutual commissural inhibitory interaction and it has been shown to enhance the neural response of single VN neurons to angular acceleration (19) (see **Figure 3**). In the following I show how Uchino's results apply in the otolithic system, but some general features of vestibular afferents and physiological conventions in this area need to be clarified.

Sustained and Transient Otolithic Systems

As well as providing information about the direction of the GIF, the afferents from each otolithic macula provide information about different temporal aspects of the stimulus. As a simplification these different neural channels are characterized as the sustained and the transient systems (14, 21, 22). They are most likely extremes of a continuum.

Afferents arising from the striola which have irregular resting activity and constitute the origin of the transient system—they prefer high frequency GIF stimuli and are activated by sound or vibration. In the otolithic maculae the striola is a comparatively thin band with a small number of receptors and afferents, and it is afferents from this band which respond to vibration [see (23) for a review]. The thin band can be seen by inspection of whole mount preparations of the maculae (14, 24). There are many more receptors and afferents in the extra-striolar area, and afferents from the extra-striolar area have regular resting discharge and constitute the sustained system. The sustained afferents prefer maintained or low frequency GIFs stimuli and do not respond to sound or vibration at physiological levels (22, 25–27). Afferents in the two systems have different responses to stimulus onset, different thresholds for activation by electrical stimulation and different adaptation rates to maintained stimulation (6). This differential receptor and afferent organization of the otoliths is analogous to the organization of the retina with 1,000,000 cones concentrated at the fovea specialized to detect fine detail but 125,000,000 receptors in the rest of the retina (28).

In the present paper the focus is on the sustained system since diagrams in Uchino's papers show that his results probably originated mainly from isolated electrical stimulation of the extra-striolar macula areas (29, 30) from where the sustained afferents mainly originate. The physiology of the transient system and the clinical testing of it have been extensively reviewed recently (1, 21, 23, 31, 32) and so they will be covered only briefly in this paper.

Otolith Physiology—General

The opposite polarization of receptors across each macula is puzzling since a GIF directed across the utricular macula will excite receptors on one side of the LPR and simultaneously act to disfacilitate (silence) receptors on the opposite side of the LPR (**Figure 2B**). It would seem the two neural signals from the one utricular macula should cancel. In fact, detailed physiology in the VN show exactly the opposite—that instead of canceling, the simultaneous stimulation of the oppositely polarized hair cells, both in the saccular macula and the utricular macula, enhances the otolithic response to the GIF similar to the enhancement shown above for the semicircular canals. Uchino called this phenomenon cross-striolar inhibitory interaction. In the case of the utricular macula this enhanced response is further complemented by inhibitory interaction between the two labyrinths which Uchino called commissural inhibitory interaction (29). Below I discuss how cross-striolar inhibition works and then I address commissural inhibitory interaction. The following shows how Uchino's results operate in the VN, using schematic figures derived from Uchino's representations. These patterns of response organization were shown by intracellular recording of single neurons in the VN and measuring their response to isolated electrical stimulation of distinct locations on each otolithic macula and measuring the excitatory or inhibitory responses in VN neurons to such stimulation [summarized in (29, 33)].

The naming convention used to describe the response of central semicircular canal neurons is used here to describe otolithic neurons. Specifically type I neurons are excitatory neurons in the VN receiving monosynaptic afferent projections from primary otolithic afferent neurons and having multiple central projections. Type II neurons are inhibitory neurons in the VN which are activated by an axon branch from a type I neuron projecting to, and so inhibiting, other type I neurons. The schematic figures [redrawn from the schematic figures used by Uchino (29, 33, 34)], depict exemplars of these neural types and their established connections to show how these neural types are activated and interact. These principles operate for a limited number of otolithic neurons—many otolithic neurons are outside the interactive "loops" described below.

Cross-Striolar Inhibition in the Saccular System

This section explains how cross-striolar inhibitory interaction works within each saccular macula. **Figure 4** shows a schematic representation of the saccular macula with receptors projecting to the VN. Receptors in the ventral sector (b) are activated by the GIF—the force of gravity (thick arrow)—and facilitate the primary afferent neurons (p) which in turn project to and activate the neuron in the VN labeled type I (c) whose firing rate accordingly increases. Simultaneously receptors in the dorsal sector of the saccular macula (a) are deflected away from the kinocilium, so they disfacilitate their primary afferent neurons (dashed lines) and so disfacilitate the type I neurons in the VN labeled d. An axon branch from the facilitated type I neuron (c) projects to an inhibitory VN neuron [type II (e) shown with a—sign] which inhibits the VN neuron receiving input from the dorsal sector (d)—further silencing this disfacilitated neuron. In turn this disfacilitated VN type I neuron exerts less drive to the inhibitory type II neuron (f) which exerts less inhibition on the activated type I neurons. Less inhibition from (f) is equivalent to activation of (c)—this release from inhibition is called disinhibition. So, the type I neuron (c) receives both direct excitation from the ventral sector of the saccular macula and also additional excitatory drive by disinhibition from receptors in the dorsal sector. The outcome of the cross-striolar inhibitory interaction is an enhanced neural signal with the difference in firing between the two opposing sectors being greater than would be the case without the inhibitory interaction. So instead of

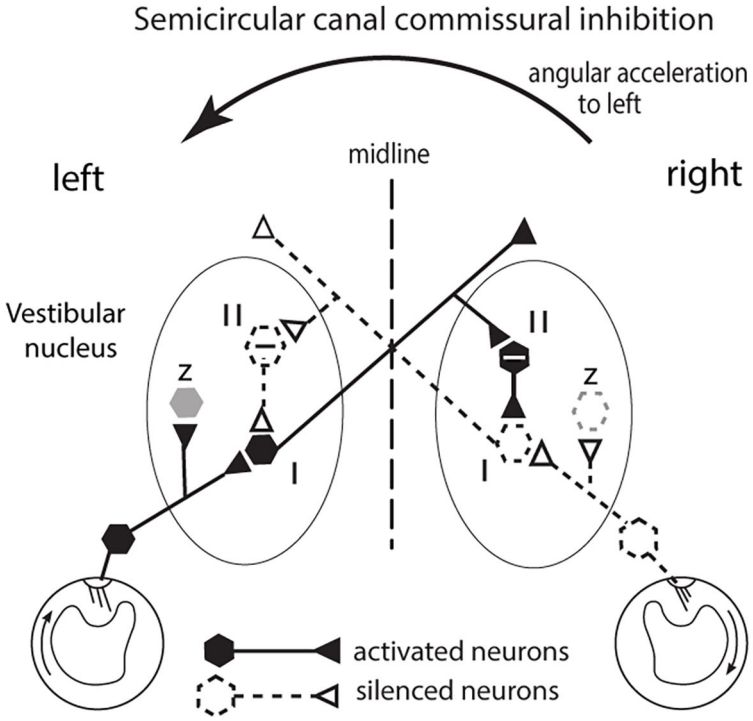

FIGURE 3 | The commissural inhibitory interaction of the semicircular canals to angular acceleration during a leftward head turn. The figure represents a view looking down on the horizontal canals and the vestibular nuclei of the brainstem. The primary afferents from the horizontal canal on the side to which the head is turned (left in this example) are facilitated (activated) and in turn they activate VN type I neurons (excitatory neurons receiving afferent input). Simultaneously the corresponding primary afferents on the opposite (right) side are silenced (disfacilitated) because the fluid flow deflects the cilia away from the kinocilium and so the VN neurons they serve are disfacilitated [Conventions: solid lines and hexagons—neurons which are activated; dashed lines and hexagons—neurons whose activity (firing rate) is reduced or silenced; hexagons containing a—sign are inhibitory neurons]. The result is that the angular acceleration causes an imbalance in the neural activity of type I neurons in the two VN. That imbalance is enhanced by an axon branch from the activated left type I projecting to the right side, activating an inhibitory neuron (type II) and the increased inhibition it exerts on its target type I neuron further silences the type I neuron on the right side. In this way the imbalance occurring at the periphery is further enhanced. In turn the silencing of those right VN type I neurons acts to reduce inhibition on the left VN type I neuron and so acts to increase its firing and so further enhance the difference in neural activity between the two VN. That release from inhibition is called disinhibition. Note that this "closed loop" depicts the activity of only a small group of canal neurons in the VN: other VN neurons (shown as z in the figure and shown as light gray) are outside this closed loop. These data are based on results by Shimazu and Precht (18); Markham et al. (19).

canceling, the effect of the cross-striolar inhibitory interaction between the oppositely polarized sectors is to enhance the neural response to the stimulus. Once again it should be noted that this "closed loop" is only part of the story—the afferents from each sector project to other VN neurons outside this loop (z) which are grayed out in this and the following figures.

Uchino referred to this whole process as cross-striolar inhibition, and it applies in both saccular and utricular maculae. He reported that more than 61% of saccular neurons tested in the VN showed cross-striolar inhibitory interaction, but cross-striolar inhibitory interaction is not as widespread in the utricular macula (it was only seen in 30% of utricular neurons tested) (29, 30). The two saccular maculae function largely independently since there is virtually no bilateral interaction between the two saccular maculae in each labyrinth—no commissural inhibition (34) —whereas utricular neurons receive commissural inhibition (as shown below) as well as this cross-striolar inhibition (30).

Cross-Striolar Inhibition in the Utricular System

The analysis for the utricular macula is identical to that given above for the saccular system. Consider a GIF stimulus directed across the left utricular macula from right to left (**Figure 5**). It will activate receptors in the left medial sector which project to and activate a type I neuron in the VN (c). Simultaneously receptors in the left lateral sector (a) will be disfacilitated. These project to a type I in the VN (d), and so its activity will be reduced. An axon branch from the facilitated type I (c) projects to an inhibitory (type II) VN neuron (e shown with a—sign) which inhibits the VN type I neuron (d) receiving input from the lateral sector—further silencing the disfacilitated neuron. In turn this disfacilitated VN type I neuron (d) exerts less drive and so less inhibition via the type II neuron (e) on the activated type I neuron (c). So, the activated type I neuron (c) receives both direct excitation from the medial sector of the utricular macula and additional excitatory drive by disinhibition from receptors

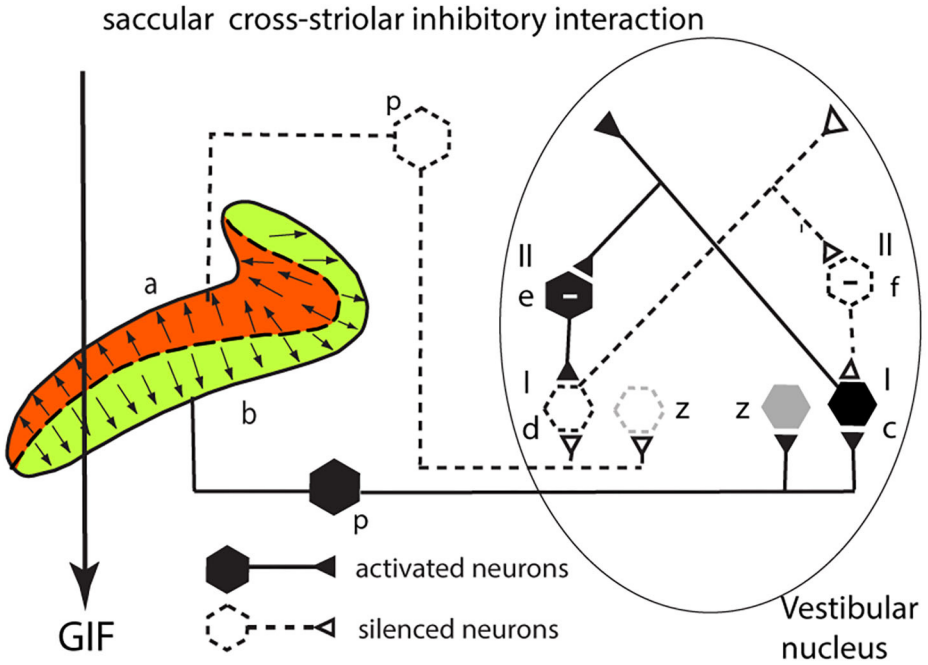

FIGURE 4 | Cross-striolar inhibition in the saccular macula—see text for full explanation.

in the lateral sector. The outcome of the cross-striolar inhibitory interaction is an enhanced neural signal with the difference in firing between the two sectors being greater than would be the case without the inhibitory interaction. In summary: in both the utricular and saccular maculae, cross-striolar inhibitory interaction serves to enhance the response to the GIF stimulus.

Commissural Inhibition in the Utricular System

Medial Sectors

The utricular system also receives an additional enhancement due to inhibitory interaction between the two labyrinths which Uchino called commissural inhibitory interaction (30). Consider a GIF directed from right to left across a subject's head, during a roll head tilt to the left [see the schematic representation of both utricular maculae (**Figure 6**)]. This stimulus will activate (facilitate) receptors in the medial sector of the left utricular macula (labeled b) because the direction of the stimulus is aligned with the preferred directions of medial sector utricular receptors on the left. It will simultaneously act to disfacilitate receptors in the medial sector of the contralateral right utricular macula (labeled c) because the direction of the stimulus is opposite to the preferred direction of receptors in the right medial sector. The afferents from these excited left medial sector receptors project to and activate neurons in the ipsilateral (left) VN (type I neurons) (labeled k in **Figure 6**). The axon of that neuron projects to a contralateral inhibitory type II neuron (s) on the right side, increasing its firing and so increasing the inhibition exerted by s onto the type I neuron (f) in the right VN which is receiving disfacilitated afferent input from the medial sector of the right utricular macula. These afferents and type I neurons on the right are already firing at a reduced firing rate (shown as dashed lines) since the stimulus direction is opposite to their preferred direction, and so the stimulus itself is acting to disfacilitate the receptors and afferents. In turn the reduced firing of the right sided type I (f) will reduce the inhibition from the left side via the inhibitory neuron type II (u) acting on the left type I (k) allowing it to fire at an even higher rate (disinhibition).

The outcome is that the stimulus—a roll head tilt left ear down—will cause an imbalance in neural activity between the two VN—a high firing rate for type I neurons on the left and a low firing rate for type I neurons on the right. In this way, commissural inhibitory interaction between the corresponding medial sectors on each side acts to enhance the imbalance in the neural activity in response to the stimulus. Once again, the otolithic neural response depends on two sources of facilitation—direct facilitation from the ipsilateral activated otolithic receptors and reduced inhibition (disinhibition) originating from the contralateral disfacilitated receptors. Again, other VN neurons (gray) are outside this loop.

Commissural Inhibition in the Utricular System

Lateral Sectors

There is comparable mutual inhibitory interaction in the VN between afferents from the two lateral sectors of the utricular macula (a and d) (**Figure 7**), but now for the same GIF directed from right to left it is the right lateral sector which is activated and the left lateral sector which is disfacilitated. Inspection of response of the medial and the lateral circuits in **Figure 7** raises

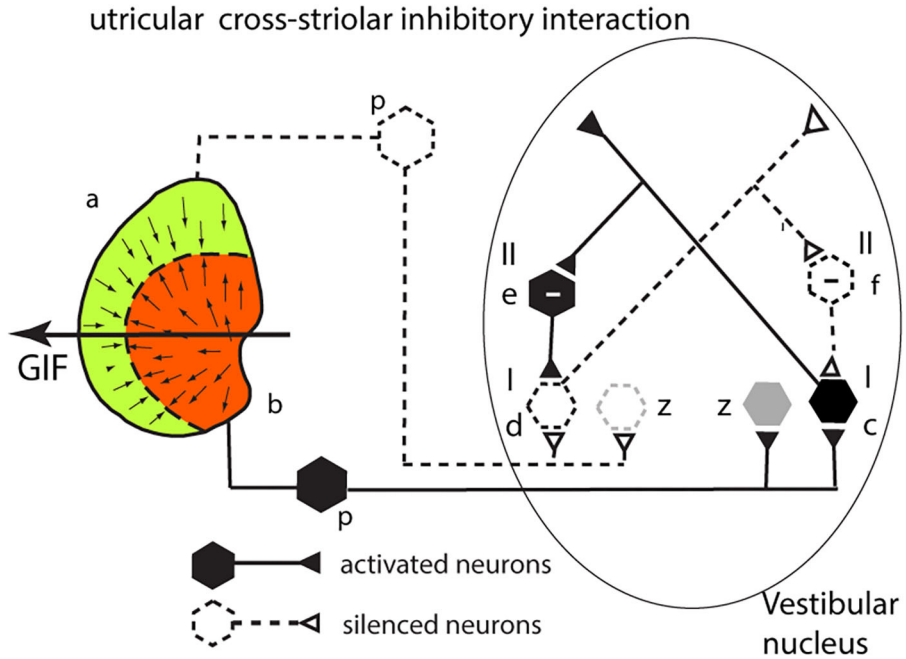

FIGURE 5 | Cross-striolar inhibition in the utricular macula—see text for full explanation.

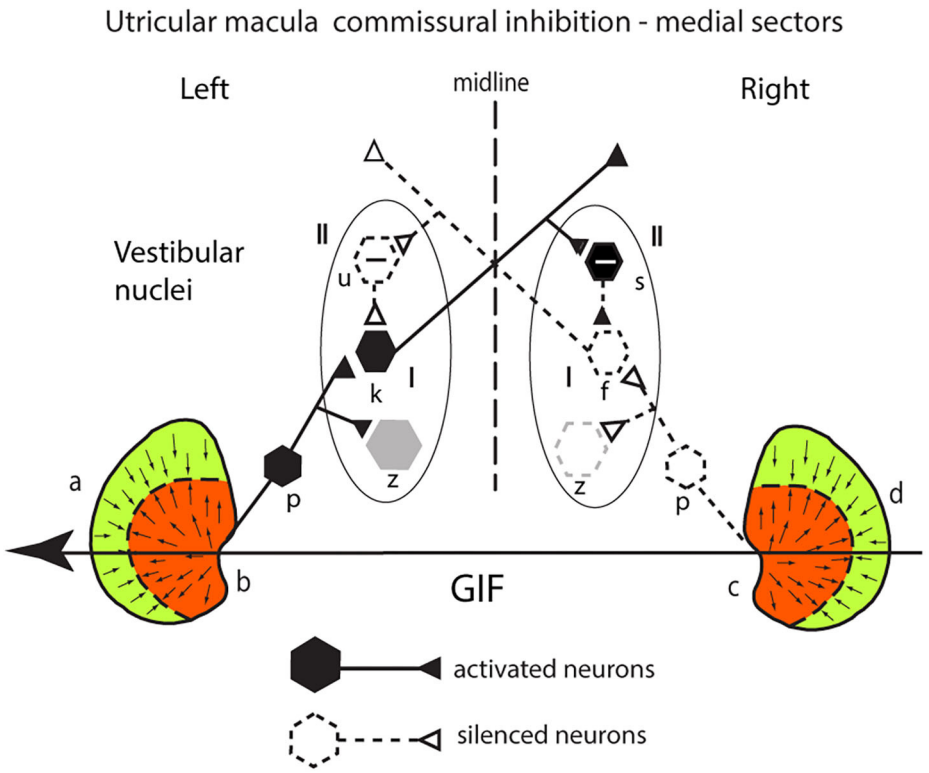

FIGURE 6 | Commissural inhibition in the utricular macula—see text for full explanation.

the question—why doesn't the right lateral sector activation simply cancel out the left medial sector activation so there is no imbalance in activity between type I neurons in the two vestibular nuclei? Don't they just cancel centrally? The following are three reasons that the response from the left medial sector predominates:

1. the area of the medial sector (and so the number of afferents) is larger than the area of the lateral sector (35).
2. cross-striolar inhibition favors the medial sector (60% of neurons tested) vs. lateral sector (30% of neurons tested) (30).
3. commissural inhibition is more frequent for medial sector afferents (56%) than for lateral sector afferents (44%).

So, taking all of this together, the left medial response is larger because both cross-striolar and commissural inhibition favor the medial sector. Confirmation of the medial sector predominance comes from recordings of VN neurons to roll-tilt, which shows more VN neurons activated by medial sector stimulation (48% by ipsilateral ear down tilt) than are activated by lateral sector stimulation (26% contralateral ear down tilt) (36).

A final consideration is that anatomical evidence indicates that the medial and lateral sectors of the utricular macula have different projections. Both project to the brainstem and cerebellum (37) but the lateral sector projection to the cerebellum is greater.

OTOLITH STIMULATION AND RESPONSES

This section relates the basic neurophysiology of the peripheral otolith system to potential clinical tests of otolithic function by gravity or low frequency linear acceleration and so testing predominantly the sustained system. The effect on otolith function by such procedures as unilateral vestibular loss, selective otolith ablation, and galvanic stimulation on responses in sensory, oculomotor and postural control systems are discussed. There are extensive literatures about the response of each of these systems to otolithic stimulation or manipulation, and here I note general principles which are of interest for the development of clinical otolithic tests, rather than presenting an exhaustive review. Most clinical tests of otolith function have focused on measuring eye movements to otolithic stimulation, in particular to stimuli such as roll-tilt. Whilst ocular torsion has usually been measured it is important to note that each quadrant of the utricular macula projects to different eye muscles (38).

Tests of the Sustained System of Otolith Function

Responses to Roll Head Tilt in Healthy Subjects and After Unilateral Vestibular Loss

At rest the central otolithic neuronal signals in the VN from the bilateral medial utricular maculae are presumed to be in equilibrium. However, stimulation or unilateral loss will upset that balance and generate responses. The oculomotor response to roll-tilt consists of mainly ocular torsion (also called counterrolling—OCR). In response to the increasing lateral GIF across the utricular macula as the head rolls, the eyes roll with the upper poles of both eyes being displaced in the orbit in a direction opposite to the GIF (39–44). The OCR is usually a very small fraction of the roll-tilt angle (about 8–10 deg maximum in healthy people). Increasing the roll-tilt stimulus systematically increases the magnitude of the GIF vector across the medio-lateral sector of the maculae and so progressively increases the neural imbalance between utricular neurons in the two nuclei. As roll-tilt increases there is a non-monotonic increase in OCR which is likely mainly due to utricular stimulation, although there is evidence for a small contribution to OCR from the saccular macula at large roll-tilt angles (45, 46). Direct electrical stimulation of the utricular nerve in cats (47) caused torsion of both eyes with the upper poles of the eyes rolled away from the side being electrically stimulated. This torsion occurred primarily because of utricular activation of the contralateral inferior oblique and ipsilateral superior oblique muscles (48). Additionally, there were small horizontal and vertical components.

Complementing the results of increasing roll-tilt stimulation is the evidence that unilateral section of the vestibular nerve causes both eyes of human patients to adopt a maintained rolled eye position (49–51), rolled toward the operated side (**Figure 8**). This result follows from the physiological analysis above. In a healthy individual if one labyrinth is suddenly silenced, for example by surgical removal or severe neuritis then the equilibrium between the two VN is lost with otolithic type I neurons in the VN on the lesioned side being silenced and otolithic type I neurons on the intact side presumably having normal resting activity. Such an imbalance corresponds to the utricular neural response to roll head tilt to the healthy side which causes a small OCR toward the opposite (lesioned) ear. Such an imbalance of utricular otolithic neural activity corresponds to the imbalance of semicircular canal neural activity after unilateral loss in the semicircular canal system (52–54). Acutely in the case of the semicircular canals the imbalance results in nystagmus and vertigo. Acutely, in the case of the utricular maculae the imbalance is equivalent to a large roll-tilt and drives the head and eyes to roll toward the lesioned side and to maintain this rolled position (49, 55). There are simultaneous postural changes—head tilt to the affected side, falling to the affected side. This loss-induced torsion and postural change reduce over time in the process called vestibular compensation (20). It is argued that this maintained ocular torsion position is probably an otolithic response rather than a canal response because canal loss induces a change in eye velocity (nystagmus) rather than a maintained eye position and because isolated loss of the utricular macula with canals intact in guinea pigs caused similar responses (56).

In patients weeks or months after unilateral vestibular loss there remains a small ocular torsion which is usually only a few degrees, but it causes a small systematic bias of the perceived orientation of a horizontal (or vertical) visible line in an otherwise darkened room so that the line no longer appears to be horizontal (or vertical) (20, 49, 57) (**Figure 9**). This perceptual error occurs because the ocular torsional position is rolled by a few degrees toward the affected ear and the orientation of the retina is a major determinant of visually perceived vertical or horizontal in an otherwise darkened room (43). This small perceptual error is called the visual bias (49, 58, 59). It occurs

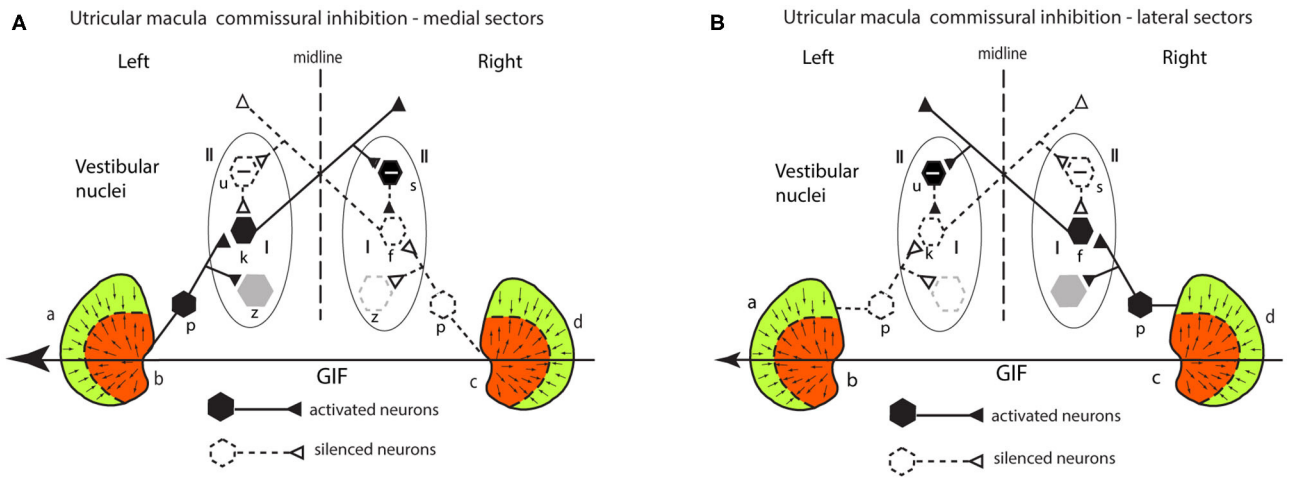

FIGURE 7 | (A,B) Schematic representation of the two utricular maculae and examples of afferent neurons projecting from the medial sector of each macula **(A)** and lateral sectors **(B)** of each utricular macula to synapse on central excitatory otolithic neurons (hexagons) in the VN. The figure shows the commissural interaction in the medial **(A)** and lateral **(B)** sectors.

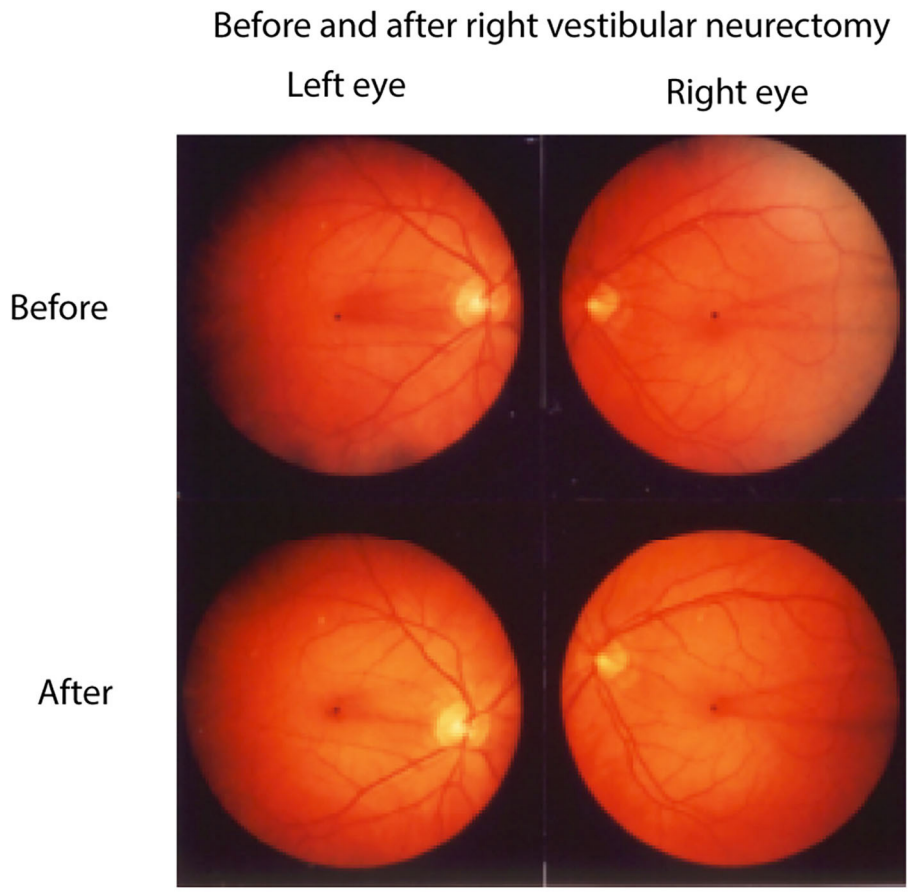

FIGURE 8 | Fundus photographs of the left and right eyes of a patient before and 1 week after a neurectomy of the right vestibular nerve showing the unique pattern of retinal blood vessels in each eye. The blood vessel patterns show very clearly that after unilateral vestibular neurectomy both eyes adopt a maintained roll eye position, rolled toward the patient's lesioned (right) side. Reprinted by permission from Springer Nature, Curthoys et al. (49) © 2020.

with horizontal lines [subjective visual horizontal (SVH)] or vertical lines [subjective visual vertical (SVV)]. Although they are not large, the ocular torsion position angle and the visual bias appear to be an almost permanent legacy of probable otolithic origin after unilateral vestibular loss (49, 60). Over time this ocular torsion and the visual bias decrease but never completely vanish. The visual bias is a simple useful clinical indicator of asymmetric sustained otolithic function (49, 61, 62) (**Figure 9**). Why does the maintained roll of the eye persist? It appears that the reduced afferent input from the affected utricular macula results in permanently slightly reduced neural input projecting to the ipsilateral superior oblique and contralateral inferior oblique eye muscles so that the eye adopts a rolled eye position—rolled toward the affected ear. It should be noted that maintained ocular torsion is not necessarily a specific indicator of peripheral otolithic loss—it can occur with central lesions along the pathway from the otolithic receptors to the eye muscles (63). Ocular pathology can also cause changes in SVV.

One other otolith oculomotor response after unilateral peripheral vestibular loss is skew deviation which refers to vertical misalignment of the two eyes after unilateral vestibular loss with the ipsilesional eye being lower in the orbit than the contralesional eye. This is usually a very small effect which can be identified clinically by alternately covering each eye and identifying if a vertical refixation is needed. However, lesions of central vestibular pathways also generate skew (63).

Acutely after unilateral vestibular loss the OCR response to maintained roll-tilt stimulation shows a temporary reduction in OCR for roll-tilts to the affected ear (64, 65), but testing OCR to roll-tilt in chronic patients weeks after unilateral loss shows there is no asymmetry of OCR—it fails to identify which side is affected (7, 40, 66, 67). The empirical result is that measuring OCR to left and right roll-tilt does not reliably indicate the affected side after unilateral loss in chronic patients, whereas the visual bias shows the affected side in acute and chronic patients. It appears that vestibular compensation is acting to nullify the initial asymmetrical OCR response.

Unilateral Centrifugation

Another way of generating sustained GIF stimulus depends on the fact that the two otoliths are around 3.6 cm from the midline of the head (68, 69). As a result, a constant velocity rotation of a patient on a rotating chair with the center of the head positioned exactly over the axis of rotation induces a GIF across each utricular macula. This is called unilateral centrifugation (70, 71). At high rotational velocities (e.g., 300 deg/s) this GIF achieves a reasonable magnitude but in healthy people being directed outward, it is opposite in each labyrinth, so the effects of the opposite GIFs cancel, and no systematic torsion occurs (71). However, if the subject's head is displaced 3.6 cm laterally so that one labyrinth is exactly over the axis of rotation, the GIF during high velocity rotation [300 deg/s at 7 cm generates about 0.2*g* laterally (70)] and so stimulates the utricular macula in the "off-axis" ear causing torsion and perceptual responses, so the utricular function of that ear can be measured (70). This unilateral centrifugation test shows unilateral loss both acutely and in chronic patients (70–72). The rotational velocities required are very high (around 300 deg/s and so potentially dangerous), the resulting torsion is small (just a few degrees), variable between patients (71) and difficult to measure so this method has not proved to be a widely used practical clinical test of unilateral otolith function.

Oculomotor Response to Linear Translation

A lateral translation of the head causes deflection of the utricular receptor hair bundles because of inertia. The otoconia, attached to the upper surface of the otoconial membrane, tend to stay in place and so drag the hair bundles of utricular receptors opposite to the lateral translation (**Figure 10A**). In this way lateral translation should cause OCR opposite to the translation direction, and that result has been reported in humans (73) and chinchillas (74). There were also small horizontal eye movements—lateral translation to the left causes both eyes to move horizontally to the right (75, 76), depending on many factors such as fixation direction and distance (77). This compensatory horizontal eye movement response is due in part to utricular afferents which project to ipsilateral abducens nucleus (33, 78, 79), but other cerebellar pathways probably contribute (77).

This horizontal eye movement to lateral linear acceleration (80) has been used to try to identify the unilateral utricular loss, by analogy with the success of the horizontal eye movement to angular acceleration identifying the side of unilateral semicircular canal loss (81). A horizontal angular acceleration toward the affected ear results in a reduced horizontal compensatory eye velocity response and so permanently identifies the affected semicircular canal (82). That result occurs essentially because of the uniform receptor organization on the crista in each horizontal canal, and the projections from the canals to the contralateral abducens nuclei (20). Corresponding to that canal result is the evidence that acutely after unilateral loss linear head translations toward the affected ear cause reduced compensatory horizontal eye movements (80). But in contrast to the permanent reduced response for angular acceleration stimulation of the affected canal, the reduced horizontal eye velocity response for ipsilesional lateral accelerations is very short-lived and testing 6 weeks after loss, shows there is no detectable reduction in the horizontal eye velocity to lateral translation toward the affected ear (80). Two other factors should be noted: the whole body lateral linear accelerations were very small stimuli—about 0.24 *g* (80), with very long rise time (so jerk was small), and had a very long latency around 35–45 ms (80) compared to a latency of about 7 ms for the horizontal eye velocity response to semicircular canal stimulation (82, 83).

Whilst the reduced horizontal eye velocity for linear accelerations toward the affected ear seems consistent with the reduced horizontal eye velocity response for angular acceleration of the canal after unilateral loss—both giving reduced horizontal eye movement responses for stimuli directed to the affected side—the result for linear accelerations after unilateral loss in fact is not readily explicable by the receptor organization of the utricular maculae and their neural projections! This conundrum is shown in **Figure 10B**—the linear acceleration of the head toward the affected ear causes the otoconia to

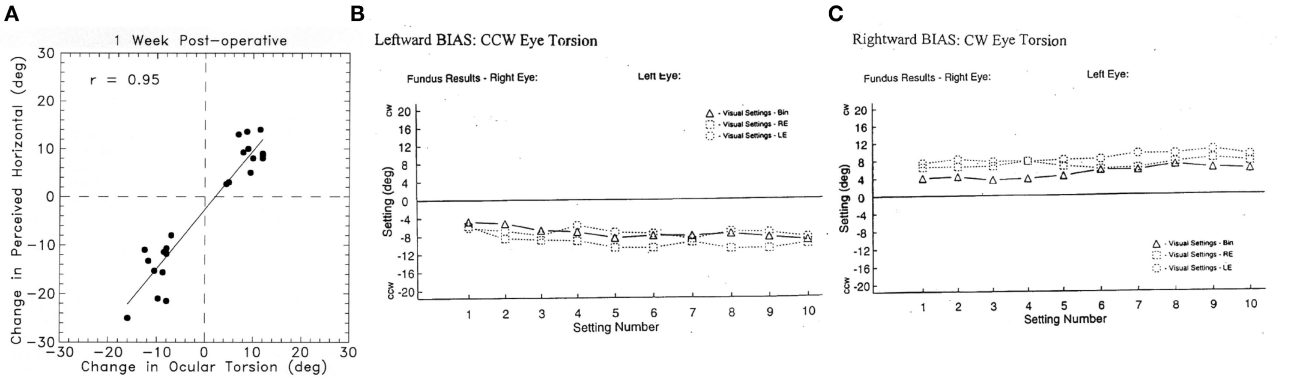

FIGURE 9 | (A) To show the very close relationship between the change in ocular torsional position after unilateral vestibular neurectomy and the corresponding change in the setting of a visual line to the subjective visual horizontal (49) in patients after unilateral vestibular loss. This setting is called the visual bias test. This close correspondence justifies the use of the perceptual result to indicate the torted position of the eye. Reprinted by permission from Springer Nature, Curthoys et al. (49) © 2020. **(B)** Results of the visual bias clinical test of otolith function in a patient with a left side loss. The patient made 30 successive settings to where they judged the gravitational horizontal to be: 10 settings with binocular viewing (BIN), 10 with left eye only (LE), and 10 with right eye only (RE). CCW, counterclockwise from the patient's point of view (i.e., the line is set so the left side is below the true gravitational horizontal); CW, clockwise from the patient's point of view. The results show a very consistent shift of the perceived horizontal so after left unilateral loss, the visual bar is set left side down from the patient's point of view, which corresponds to the rolled horizontal meridian of the eye, as shown in **Figure 8**. **(C)** Similar results from a patient with a right-side vestibular loss which causes the visual line to be set so that the right side of the line is set down, corresponding to the rolled horizontal meridian of the eye. Most subjects and patients can perform this task with very small variability as shown here (Settings consistently >2° are outside the normal range).

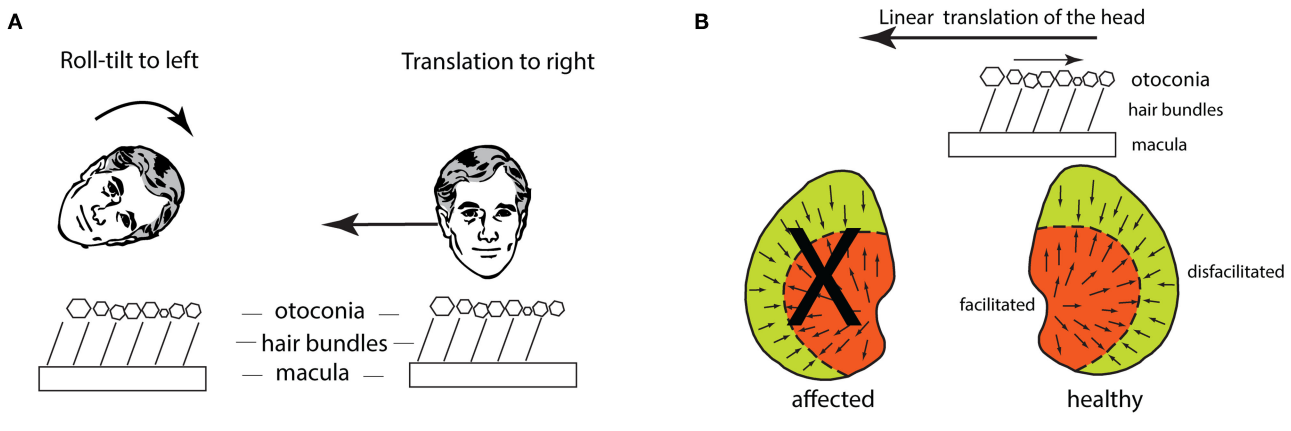

FIGURE 10 | (A) Schematic figures to show how the hair bundles of utricular receptors are deflected identically for a roll-tilt left ear down and a horizontal head translation to the person's right. **(B)** The effect of lateral linear acceleration toward the affected ear in a patient with unilateral vestibular loss (the X shows the affected utricular macula). The linear acceleration directed toward the affected ear causes the otoconia to remain in place because of inertia and so the hair bundles of all the utricular receptors are deflected opposite to the linear acceleration. This direction of hair bundle deflection is an excitatory stimulus for receptors in the medial sector of the utricular macula, and an inhibitory stimulus for receptors in the lateral sector. The medial excitation would be expected to generate a compensatory horizontal eye velocity response, however in human patients there is instead a (temporary) reduced horizontal eye velocity response for linear accelerations directed to the affected ear.

remain in place because of inertia, so the hair bundles of the receptors on the remaining utricular macula are deflected opposite to the direction of the linear translation. As shown in **Figure 10B**, because of their respective polarizations, that means that receptors in the medial sector of the healthy macula are excited, while those in the lateral sector are inhibited. However, excitation of the medial sector receptors should cause an increased oculomotor response (as it does for the torsional response to lateral roll-tilt of the head) but the empirical result for horizontal eye velocity to lateral linear accelerations in patients is exactly the opposite—the linear acceleration toward the affected ear causes a reduced compensatory horizontal eye movement response (80). To accommodate this puzzling result, Lempert suggested that it must be receptors in the lateral sector of the utricular maculae which generate compensatory horizontal eye velocity responses to lateral linear accelerations (80). In the case of unilateral loss, the receptors in the lateral sector would be inhibited by the lateral linear acceleration stimulus to the affected

ear and so their inhibition would cause a reduced horizontal eye movement response, as is observed. Further compounding the puzzle is the fact that the projections from the utricular macula to abducens are from utricular macula to ipsilateral abducens nucleus (78, 79) so utricular activation would generate an ipsilateral eye rotation for ipsilateral utricular stimulation (23, 84), although the precise origin of these projections from the utricular macula (medial or lateral sectors) to the ipsi lateral abducens is unknown. We can best summarize the story of lateral linear accelerations by noting the logical and empirical problems which the results of linear acceleration on horizontal eye movements after unilateral loss have shown (77, 85). This puzzling result has not been explained. The long latency for the horizontal component to lateral linear accelerations suggests the involvement of indirect pathways, such as via the cerebellum. Indeed, Maklad et al. have shown that afferents from the two sectors of the utricular macula have different projection patterns—in the mouse afferents from the medial sector project mainly to the brainstem and afferents from the lateral sector project mainly to the cerebellum (37).

In summary clinical tests based on asymmetry of ocular responses to roll-tilt or to lateral translation do not provide a reliable indicator of the side of unilateral otolithic loss in long term patients, so using these tests, the clinician cannot reliably determine whether the left or right utricular macula has been compromised. The visual bias test and unilateral centrifugation are indicators of sustained otolith function which do show the affected side in chronic patients.

Tests of the Transient System of Otolith Function

Returning to the peripheral otolithic sense organs—each otolithic macula contains a band, a stripe, around the LPR and the band is called the striola. In this band the receptors and afferents are structurally and functionally specialized. The hair bundles are shorter and stiffer than those in the extrastriola area and they are only tenuously attached to the otolithic membrane [see (9, 14, 23)]. Recordings from primary afferents originating from this region with irregular resting activity show they are activated and are even phase locked up to high frequencies of sound and vibration (e.g., 500 Hz and up to 3,000 Hz) (14, 22, 26, 86). That result means that each otolithic sense organ has two modes of responding—for low frequency GIFs and low frequency vibration the otolithic macula responds as an accelerometer, but for high frequency stimuli it responds as a seismometer (23, 83, 85, 86). How can that dual mode of responding occur? At low frequencies the otoconia and hair bundles move relative to the receptor cell body, but at high frequencies the receptor cell body moves relative to the otoconia and hair bundles. In both cases the hair bundles are deflected relative to the receptor cell body, so the receptor is activated, but the dynamics of that deflection are completely different (87).

The response of the otolithic receptors to sound and vibration seems at odds with what is regarded as the usual response of otoliths to gravity and low frequency linear acceleration. Evolution provides an insight. Fish do not have cochleas but have otolithic maculae. Fish primary otolithic neurons are activated by to vibration and show precise phase locking up to high frequencies (88) and show directional tuning (89). It appears that these features of otolithic processing have been transferred to mammals. This high frequency mode is particularly important since the myogenic responses triggered by the high frequency activation of these receptors at the striola do show unilateral otolithic loss in both acute and chronic patients (90) which is in sharp contrast to the failure of the low frequency otolithic stimuli (testing mainly the sustained system) to detect the affected side as we have shown. The two main measures of the transient system are short latency vestibular evoked myogenic potentials (VEMPs)—the ocular VEMPs from beneath the eyes recording primarily utricular functional status and the cervical VEMPs recording primarily the saccular functional status (2, 21, 87, 91) (**Figure 11**). The evidence for the ability of VEMPs to detect unilateral loss was shown first by Colebatch and Halmagyi for cVEMPs (94) and Iwasaki et al. for oVEMPs (90), and both results have been confirmed in many studies since, so that these tests are now standard clinical tests of unilateral otolith function as is covered in the recent reviews devoted to VEMPs noted above.

The sustained and transient modes of otolithic operation have an interesting consequence—that there could be a dissociation between the results of the low frequency and high frequency tests. That has been confirmed in healthy subjects by Zalewski et al. (95) who found no correlation between ocular torsion (bias) (low frequency) and oVEMPs (high frequency), indicating the two types of tests are probing different functions. In the case of patients, complete unilateral loss of otolith function abolishes both high and low frequency responses, but in other patients, one or the other of the high frequency or low frequency response modes could be affected whilst leaving the other mode intact. Cherchi has reported exactly this dissociation between tests of sustained and transient utricular function after vestibular neuritis (96). It will likely also occur in patients after treatment with the ototoxic antibiotic gentamicin which preferentially attacks the type I receptors at the striola (97, 98) and so would degrade the transient system but leave the sustained system functioning. It would be expected that some such patients would have reduced or absent oVEMPs (transient function) but preserved ocular counterrolling to roll-tilt stimulation (sustained function).

In summary, Short latency myogenic responses to sound or vibration stimulation of the otoliths do show clinically important clear permanent response asymmetries after unilateral vestibular loss, due to loss of the transient system originating from receptors at the striola of the utricular and saccular macula.

Effect of Isolated Otolithic Macula Loss

In animal studies it has been possible to carry out selective lesions restricted to the utricular macula or to the saccular macula (56, 99). In guinea pigs isolated loss of just the utricular macula in one labyrinth causes strong postural changes at the acute stage (yaw head turn, head roll-tilt toward the affected side) (99). These are similar to the responses found with complete unilateral vestibular loss since isolated unilateral utricular loss will upset the bilateral balance between the two VN just as a total unilateral loss does. These responses diminish over time in vestibular compensation. Comparable data from isolated utricular loss in human patients is rare (2). One patient inadvertently received what was probably

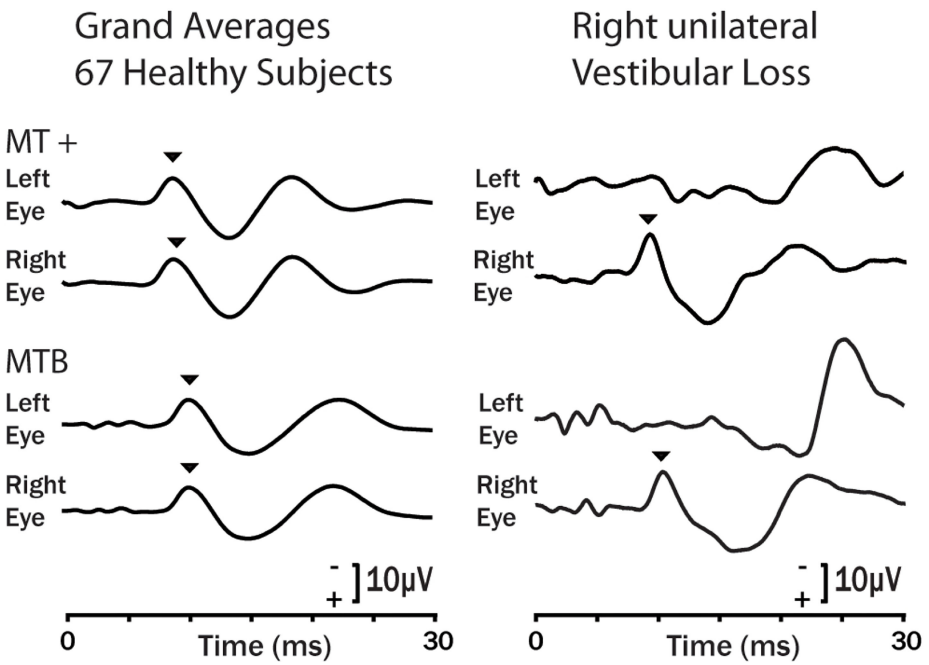

FIGURE 11 | Examples of the oVEMP response of healthy subjects (grand means left column) and a typical patient with right side unilateral vestibular loss in response to bone conducted vibration stimulation (92) on the forehead at Fz using the 4810 Mini-Shaker driven by a condensation click (MT +) and 6 ms tone bursts at 500 Hz (MTB). Bone conducted vibration delivered at Fz stimulates both ears about equally and results in small symmetrical oVEMP n10s (arrow heads) beneath both eyes (93). The response is similar for a single tap (MT +) or a brief tone burst (MTB). For the patient the asymmetrical response is clear: the n10 component of the oVEMP (arrowhead) is absent under the eye ***contralateral*** to the patient's affected ear because the oVEMP is a crossed response (90).

an isolated utricular loss and was described as showing an "ocular tilt reaction" (61). The patient showed ipsilesional maintained torsional eye position, roll head tilt toward the affected ear and skew deviation with the ipsilesional eye being lower in the orbit.

In total unilateral vestibular loss, the saccular macula is destroyed as well as the utricular macula, but the interaction in the saccular system is predominantly between opposing sectors within each macula (cross-striolar inhibitory interaction within each macula) with very little commissural inhibitory interaction. Thus, the removal of one saccular macula in a unilateral labyrinthectomy should remove both opposing sectors and so not cause a bilateral imbalance of saccular activity. In guinea pigs, selective unilateral removal of just the saccular macula had little measurable effect on posture or oculomotor responses (56, 99). Such a result is consistent with cross-striolar inhibition because both interacting sectors within the one saccular macula are removed so there is no imbalance of saccular activity. There is a remaining saccular macula in the opposite labyrinth to signal GIF.

Galvanic Vestibular Stimulation (GVS)

All vestibular receptors and afferents from both canals and otoliths are activated by small cathodal and inhibited by small anodal currents (15), which in human subjects are usually passed between electrodes on the mastoids. This is bilateral Galvanic Vestibular Stimulation (GVS) and it usually consists of low current (5–10 mA or less) cathodal stimulation of one mastoid and simultaneous anodal stimulation of the opposite mastoid using surface electrodes with large surface areas [small area electrodes cause discomfort and even skin burns (100)]. With maintained (DC) stimulation this bilateral stimulus causes both eyes to adopt a rolled eye position, rolled away from the cathode. Since the response is a maintained torsional eye position rather than an eye velocity response it is held to be of otolithic origin. However, it is important to emphasize that GVS activates both canal and otolith receptors and afferents (15–17, 101). Neural recordings from all vestibular sensory regions show that GVS is not a specific otolithic stimulus—so caution is needed in interpreting the results of GVS as purely otolithic, although there is a clear otolithic component. The canal contribution becomes clear if the GVS is delivered in darkness where, in addition to the torsion, nystagmus is seen (**Figure 12**). Vision usually suppresses the GVS-induced nystagmus, as shown in **Figure 12** it reduces the eye velocity response to GVS. Transient GVS stimulation has been proposed as a clinical test of peripheral function and it is affected in Meniere's Disease (103–105).

This mainly torsional eye movement response to GVS is in accord with the physiology discussed above. Cathodal galvanic stimulation of the left mastoid will activate all afferents from both sectors of the left utricular macula, and simultaneous anodal stimulation of the right mastoid will disfacilitate all afferents from both sectors of the right macula. As a result, afferents from

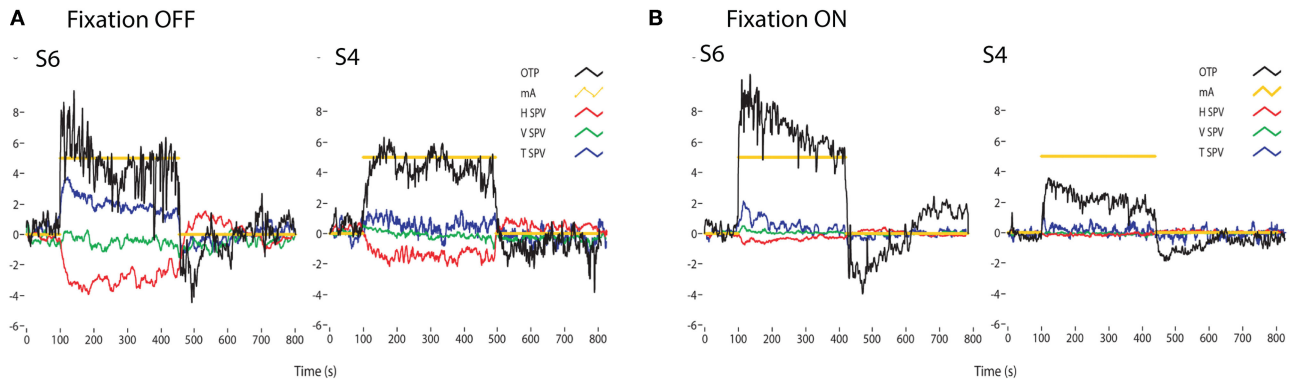

FIGURE 12 | Time series of the eye movements of two healthy subjects (S1 and S2) to a square wave of bilateral galvanic stimulation with fixation off **(A)** and on **(B)**, showing the current (mA), the ocular torsion position (OTP) and horizontal (HSV), vertical (VSV) and torsional (TSV) eye velocity. The ordinate for each graph is degrees (for OTP) or degrees/sec for the eye velocity records. GVS causes large changes in torsion position, with and without fixation. In darkness the eye velocity responses are clear, confirming that GVS activates all semicircular canals as well as the otoliths. However, the importance of vision is shown by how the eye velocity responses are greatly reduced in the presence of a fixation point [from Figure 5 of (102)]. There is considerable variability between subjects for the same GVS stimulus. Reprinted by permission from Springer Nature, MacDougall et al. (102) © 2020.

the left medial sector will be facilitated, and those from the right medial sector will be disfacilitated, just as occurs during a real roll tilt of the head left ear down—toward the cathodal side. The result will be activation of afferents from the left utricular macula and simultaneous reduction of commissural inhibition from the right side since the afferents from the medial sector on the right have a reduced firing rate. This bilateral stimulus should cause maintained rolled ocular torsion opposite to the cathode because the stimulus pattern for the two medial sectors is comparable to that caused by a real roll-tilt to the left ear. The left lateral sector afferents will be activated, and the right lateral sector afferents will be silenced by the anodal current to the right mastoid. But just as discussed above for real roll-tilt, the contribution of the lateral sectors is apparently outweighed by the contribution from the medial sectors. It seems that during the GVS the activation of afferents from the lateral sectors (and their commissural interaction) should just cancel the effect of the stimulation of the medial sectors. One argument has been that this cancellation does not happen because the macula areas of the opposing receptors are not equal (9, 35). Another consideration is the very differential projections of the medial and lateral sectors shown by Maklad et al. (37). Afferents from the lateral sector project extensively to the cerebellum.

Unilateral galvanic stimulation causes smaller but clear eye movement responses. Unilateral cathodal stimulation of one mastoid will activate afferents from both sectors of the left utricular macula and so activate ipsilateral type I neurons from the medial sector and so cause both eyes to roll away from the cathodal side. Unilateral anodal stimulation of the right mastoid will disfacilitate the afferents from both sectors of the right utricular macula and so reduce the activity of the all afferents from the right including the right medial type I VN neuron. In turn that disfacilitation will reduce the inhibition acting on the left VN neuron, resulting in increased activation of the left VN neuron (via disinhibition) and so an ocular torsion response of both eyes. The enhanced activation should drive the response so the eyes should tort toward the anodal side. Both of these results have been reported (100, 102, 106).

For the saccular system left cathodal stimulation and right anodal stimulation will simultaneously facilitate afferents from dorsal and ventral sectors of the left saccular macula, and disfacilitate afferents from both sectors of the right saccular macula. Since there is little commissural interaction in the saccular system there should be little or no contribution from the saccular macula on the opposite side.

SUMMARY

Acutely after unilateral loss there are asymmetrical ocular responses to roll-tilt and to lateral linear acceleration. However, these asymmetries reduce over time such that long term patients (6–10 weeks) show no consistent asymmetry to roll-tilt stimuli (7). Similarly, patients 6 weeks after surgery show no asymmetry for linear lateral translations (81, 107). This is in sharp contrast to the semicircular canal system where response asymmetries after unilateral loss are permanent as shown by the head impulse test (108–110). Clinical tests based on asymmetry of oculomotor responses to roll-tilt or lateral translation do not show a reliable difference for the two opposite directions of gravitoinertial force so using these tests the clinician cannot determine whether the left or right utricular macula has been compromised. The clinical value of VEMPs is that they do allow identification of the affected side in unilateral loss and even allow the clinician to gauge whether it is the utricular or saccular macula (or both) which are affected in both acute and chronic patients. It seems that over time vestibular compensation takes place—and so except for the visual bias,

unilateral centrifugation and VEMPs—the asymmetry between the two sides is reduced.

This review shows how the inhibitory interactions in the vestibular nuclei (VN) between neurons receiving afferents from the otolithic maculae [as summarized by (29, 33)] explain the results of several clinical and experimental tests of otolith function. Uchino has shown that inhibitory interaction in the vestibular nuclei (VN) is fundamental for the operation of the peripheral otolithic system (29). That within each macula there is inhibitory interaction across the striola (called cross-striolar inhibition) and in the case of the utricular macula there is additionally inhibitory interaction between the afferents from each labyrinth (commissural inhibitory interaction). The essential outcome of inhibitory interaction is that the one GIF stimulus will cause two sources of excitation of neurons in the vestibular nuclei (VN)—from both direct facilitation of some utricular receptors in one sector complemented by indirect excitation resulting from the disfacilitation from utricular receptors in the opposing sector. Utricular mutual commissural inhibitory interaction parallels the commissural inhibitory interaction between afferent input from the two horizontal semicircular canals to angular acceleration. It is important to emphasize the neurons showing this inhibitory interaction are only a small proportion of all the otolithic neurons—many otolithic neurons are outside the inhibitory interaction loops. There are effectively two complementary otolithic systems—the sustained system concerned with signaling low frequency GIF stimuli and the transient system which is activated by high frequency stimuli such as sounds and vibration (1). Most clinical tests of the sustained otolith system using low frequency GIF stimuli do not show unilateral loss reliably, whereas tests of transient otolith function do show unilateral otolithic loss. The transient otolithic system has been reviewed extensively recently (1, 21), so in this paper the focus has been on the sustained otolithic system.

AUTHOR'S NOTE

This review is dedicated to Bernard Cohen who made so many pioneering contributions to understanding vestibular function. It is a tribute to honor the great work that Yoshio Uchino carried out over so any years, illuminating the operation of the otoliths.

AUTHOR CONTRIBUTIONS

The author confirms being the sole contributor of this work and has approved it for publication.

FUNDING

This work was supported by a grant L2907 RP557 from the Garnett Passe and Rodney Williams Memorial Foundation.

ACKNOWLEDGMENTS

I thank Ann Burgess for her help in preparing this paper and for her excellent help over so many years in the research reported here. Much of the work reported here has been supported by the Garnett Passe and Rodney Williams Memorial Foundation, and I am very grateful for their continued support and for that of the National Health and Medical Research Foundation of Australia. I thank Wally Grant, Michael Halmagyi, Leigh McGarvie, Leonardo Manzari, Chris Pastras, Aaron Camp, Laura Fröhlich, Jorge Rey-Martinez, and Julia Dlugaiczyk for their helpful comments.

REFERENCES

1. Curthoys IS, MacDougall HG, Vidal PP, de Waele C. Sustained and transient vestibular systems: a physiological basis for interpreting vestibular function. *Front. Neurol.* (2017) 8:117. doi: 10.3389/fneur.2017.00117
2. Curthoys IS, Burgess AM, Manzari L. The evidence for selective loss of otolithic function. *Semin Neurol.* (2020) 40:33–9. doi: 10.1055/s-0039-3402064
3. Curthoys IS. Eye movements produced by utricular and saccular stimulation. *Aviat. Space. Environ. Med.* (1987) 58:A192–7.
4. Mukherjee P, Cheng K, Curthoys I. Three-dimensional study of vestibular anatomy as it relates to the stapes footplate and its clinical implications: an augmented reality development. *J. Laryngol. Otol.* (2019) 133:187–91. doi: 10.1017/S0022215119000239
5. Uzun-Coruhlu H, Curthoys IS, Jones AS. Attachment of the utricular and saccular maculae to the temporal bone. *Hear. Res.* (2007) 233:77–85. doi: 10.1016/j.heares.2007.07.008
6. Curthoys IS. Concepts and physiological aspects of the otolith organ in relation to electrical stimulation. *Audiol. Neurootol.* (2020) 25:25–34. doi: 10.1159/000502712
7. Otero-Millan J, Trevino C, Winnick A, Zee DS, Carey JP, Kheradmand A. The video ocular counter-roll (vOCR): a clinical test to detect loss of otolith-ocular function. *Acta Otolaryngol.* (2017) 137:593–7. doi: 10.1080/00016489.2016.1269364
8. Bergstrom B. Morphology of vestibular nerve. 2. Number of myelinated vestibular nerve fibers in man at various ages. *Acta Otolaryngol.* (1973) 76:173–9. doi: 10.3109/00016487309121496
9. Lindeman HH. Studies on the morphology of the sensory regions of the vestibular apparatus with 45 figures. *Ergeb. Anat. Entwicklungsgesch.* (1969) 42:1–113. doi: 10.1007/978-3-662-24992-5
10. Flock A. Structure of macula utriculi with special reference to directional interplay of sensory responses as revealed by morphological polarization. *J. Cell Biol.* (1964) 22:413–31. doi: 10.1083/jcb.22.2.413
11. Hudspeth A. How the ear's works work: mechanoelectrical transduction and amplification by hair cells. *C R Biol.* (2005) 328:155–62. doi: 10.1016/j.crvi.2004.12.003
12. Shotwell SL, Jacobs R, Hudspeth AJ. Directional sensitivity of individual vertebrate hair-cells to controlled deflection of their hair bundles. *Ann. N. Y. Acad. Sci.* (1981) 374:1–10. doi: 10.1111/j.1749-6632.1981.tb30854.x
13. Hudspeth AJ. The cellular basis of hearing - the biophysics of hair-cells. *Science.* (1985) 230:745–52. doi: 10.1126/science.2414845
14. Curthoys IS. The new vestibular stimuli: sound and vibration-anatomical, physiological and clinical evidence. *Exp. Brain Res.* (2017) 235:957–72. doi: 10.1007/s00221-017-4874-y
15. Kim J, Curthoys IS. Responses of primary vestibular neurons to galvanic vestibular stimulation (GVS) in the anaesthetised guinea pig. *Brain Res. Bull.* (2004) 64:265–71. doi: 10.1016/j.brainresbull.2004.07.008

16. Dlugaiczyk J, Gensberger KD, Straka H. Galvanic vestibular stimulation: from basic concepts to clinical applications. *J. Neurophysiol.* (2019) 121:2237–55. doi: 10.1152/jn.00035.2019
17. Gensberger KD, Kaufmann AK, Dietrich H, Branoner F, Banchi R, Chagnaud BP, et al. Galvanic vestibular stimulation: cellular substrates and response patterns of neurons in the Vestibulo-Ocular Network. *J. Neurosci.* (2016) 36:9097–110. doi: 10.1523/JNEUROSCI.4239-15.2016
18. Shimazu H, Precht W. Inhibition of central vestibular neurons from contralateral labyrinth and its mediating pathway. *J. Neurophysiol.* (1966) 29:467–92. doi: 10.1152/jn.1966.29.3.467
19. Markham CH, Yagi T, Curthoys IS. Contribution of contralateral labyrinth to 2nd order vestibular neuronal-activity in cat. *Brain Res.* (1977) 138:99–109. doi: 10.1016/0006-8993(77)90786-7
20. Curthoys IS, Halmagyi GM. Vestibular compensation: a review of the oculomotor, neural, and clinical consequences of unilateral vestibular loss. *J. Vestib. Res.* (1995) 5:67–107.
21. Curthoys IS, Grant JW, Burgess AM, Pastras CJ, Brown DJ, Manzari L. Otolithic receptor mechanisms for vestibular-evoked myogenic potentials: a review. *Front. Neurol.* (2018) 9:366. doi: 10.3389/fneur.2018.00366
22. Curthoys IS, Vulovic V. Vestibular primary afferent responses to sound and vibration in the guinea pig. *Exp. Brain Res.* (2011) 210:347–52. doi: 10.1007/s00221-010-2499-5
23. Curthoys IS, Grant JW, Pastras CJ, Brown DJ, Burgess AM, Brichta AM, et al. A review of mechanical and synaptic processes in otolith transduction of sound and vibration for clinical VEMP testing. *J. Neurophysiol.* (2019) 122: 259–76. doi: 10.1152/jn.00031.2019
24. Watanuki K, Schuknecht HF. Morphological-study of human vestibular sensory epithelia. *Arch. Otolaryngol. Head Neck Surg.* (1976) 102:583–8. doi: 10.1001/archotol.1976.00780150051001
25. Curthoys IS, Vulovic V, Burgess AM, Sokolic L, Goonetilleke SC. The response of guinea pig primary utricular and saccular irregular neurons to bone-conducted vibration (BCV) and air-conducted, sound (ACS). *Hear. Res.* (2016) 331:131–43. doi: 10.1016/j.heares.2015.10.019
26. Curthoys IS, Vulovic V, Sokolic L, Pogson J, Burgess AM. Irregular primary otolith afferents from the guinea pig utricular and saccular maculae respond to both bone conducted vibration and to air conducted sound. *Brain Res. Bull.* (2012) 89:16–21. doi: 10.1016/j.brainresbull.2012.07.007
27. Zhu H, Tang X, Wei W, Mustain W, Xu Y, Zhou W. Click-evoked responses in vestibular afferents in rats. *J. Neurophysiol.* (2011) 106:754–63. doi: 10.1152/jn.00003.2011
28. Rodieck RW. *The Vertebrate Retina*. San Francisco, CA: W. H. Freeman (1973).
29. Uchino Y. Role of cross-striolar and commissural inhibition in the vestibulocollic reflex. *Prog. Brain Res.* (2004) 143:403–9. doi: 10.1016/S0079-6123(03)43038-0
30. Ogawa Y, Kushiro K, Zakir M, Sato H, Uchino Y. Neuronal organization of the utricular macula concerned with innervation of single vestibular neurons in the cat. *Neurosci. Lett.* (2000) 278:89–92. doi: 10.1016/S0304-3940(99)00909-X
31. Curthoys IS, Dlugaiczyk J. Physiology, clinical evidence and diagnostic relevance of sound-induced and vibration-induced vestibular stimulation. *Curr. Opin. Neurol.* (2020) 33:126–35. doi: 10.1097/WCO.0000000000000770
32. Rosengren SM, Colebatch JG. The contributions of vestibular evoked myogenic potentials and acoustic vestibular stimulation to our understanding of the vestibular system. *Front. Neurol.* (2018) 9:481. doi: 10.3389/fneur.2018.00481
33. Uchino Y, Kushiro K. Differences between otolith- and semicircular canal-activated neural circuitry in the vestibular system. *Neurosci. Res.* (2011) 71:315–27. doi: 10.1016/j.neures.2011.09.001
34. Uchino Y, Sato H, Suwa H. Excitatory and inhibitory inputs from saccular afferents to single vestibular neurons in the cat. *J. Neurophysiol.* (1997) 78:2186–92. doi: 10.1152/jn.1997.78.4.2186
35. Fernandez C, Goldberg JM, Abend WK. Response to static tilts of peripheral neurons innervating otolith organs of the squirrel monkey. *J. Neurophysiol.* (1972) 35:978–87. doi: 10.1152/jn.1972.35.6.978
36. Xerri C, Gianni S, Manzoni D, Pompeiano O. Central compensation of vestibular deficits.1. Response characteristics of lateral vestibular neurons to roll tilt after ipsilateral labyrinth deafferentation. *J. Neurophysiol.* (1983) 50:428–48. doi: 10.1152/jn.1983.50.2.428
37. Maklad A, Kamel S, Wong E, Fritzsch B. Development and organization of polarity-specific segregation of primary vestibular afferent fibers in mice. *Cell Tissue Res.* (2010) 340:303–21. doi: 10.1007/s00441-010-0944-1
38. Szentágothai J. Pathways and synaptic articulation patterns connecting vestibular receptors and oculomotor nuclei. In: Bender MB, editor. *The Oculomotor System*. New York, NY: Hoeber Medical Division. Harper & Row (1962). p. 205–23.
39. Diamond SG, Markham CH, Simpson NE, Curthoys IS. Binocular counter-rolling in humans during dynamic rotation. *Acta Otolaryngol.* (1979) 87:490–8. doi: 10.3109/00016487909126457
40. Diamond SG, Markham CH. Binocular counterrolling in humans with unilateral labyrinthectomy and in normal controls. *Ann. N. Y. Acad. Sci.* (1981) 374:69–79. doi: 10.1111/j.1749-6632.1981.tb30861.x
41. Diamond SG, Markham CH. Ocular counterrolling as an indicator of vestibular otolith function. *Neurology.* (1983) 33:1460–9. doi: 10.1212/WNL.33.11.1460
42. Schmid-Priscoveanu A, Straumann D, Bohmer A, Obzina H. Vestibulo-ocular responses during static head roll and three-dimensional head impulses after vestibular neuritis. *Acta Otolaryngol.* (1999) 119:750–7. doi: 10.1080/00016489950180379
43. Wade SW, Curthoys IS. The effect of ocular torsional position on perception of the roll-tilt of visual stimuli. *Vision Res.* (1997) 37:1071–8. doi: 10.1016/S0042-6989(96)00252-0
44. Miller EF, Graybiel A. A comparison of ocular counter-rolling movements between normal persons and deaf subjects with bilateral labyrinthine defects. *Ann. Otol. Rhinol. Laryngol.* (1963) 72:885–93. doi: 10.1177/000348946307200402
45. DeGraaf B, Bos JE, Groen E. Saccular impact on ocular torsion. *Brain Res. Bull.* (1996) 40:321–6. doi: 10.1016/0361-9230(96)00126-8
46. MacDougall HG, Curthoys IS, Betts GA, Burgess AM, Halmagyi GM. Human ocular counterrolling during roll-tilt and centrifugation. *Ann. N. Y. Acad. Sci.* (1999) 871:173–80. doi: 10.1111/j.1749-6632.1999.tb09183.x
47. Suzuki JI, Tokumasu K, Goto K. Eye movements from single utricular nerve stimulation in the cat. *Acta Otolaryngol.* (1969) 68:350–62. doi: 10.3109/00016486909121573
48. Suzuki JI, Goto K, Tokumasu K, Cohen B. Implantation of electrodes near individual vestibular nerve branches in mammals. *Ann. Otol. Rhinol. Laryngol.* (1969) 78:815–26. doi: 10.1177/000348946907800414
49. Curthoys IS, Dai MJ, Halmagyi GM. Human ocular torsional position before and after unilateral vestibular neurectomy. *Exp. Brain Res.* (1991) 85:218–25. doi: 10.1007/BF00230003
50. Dai MJ, Curthoys IS, Halmagyi GM. Linear acceleration perception in the roll plane before and after unilateral vestibular neurectomy. *Exp. Brain Res.* (1989) 77:315–28. doi: 10.1007/BF00274989
51. Wolfe GI, Taylor CL, Flamm ES, Gray LG, Raps EC, Galetta SL. Ocular tilt reaction resulting from vestibuloacoustic nerve surgery. *Neurosurgery.* (1993) 32:417–20. doi: 10.1097/00006123-199303000-00013
52. Smith PF, Curthoys IS. Neuronal activity in the ipsilateral medial vestibular nucleus of the guinea pig following unilateral labyrinthectomy. *Brain Res.* (1988) 444:308–19. doi: 10.1016/0006-8993(88)90939-0
53. Smith PF, Curthoys IS. Neuronal activity in the contralateral medial vestibular nucleus of the guinea pig following unilateral labyrinthectomy. *Brain Res.* (1988) 444:295–307. doi: 10.1016/0006-8993(88)90938-9
54. Smith PF, Curthoys IS. Mechanisms of recovery following unilateral labyrinthectomy—a review. *Brain Res. Rev.* (1989) 14:155–80. doi: 10.1016/0165-0173(89)90013-1
55. Toczek S, Hyde JE. Effect of vestibular nerve section on torsion and on evoked rotatory movements. *Exp. Neurol.* (1963) 8:143–54. doi: 10.1016/0014-4886(63)90041-4
56. de Waele C, Graf W, Josset P, Vidal PP. A radiological analysis of the postural syndromes following hemilabyrinthectomy and selective canal and otolith lesions in the guinea-pig. *Exp. Brain Res.* (1989) 77:166–82. doi: 10.1007/BF00250579
57. Tribukait A, Bergenius J, Brantberg K. Subjective visual horizontal during follow-up after unilateral vestibular deafferentation with gentamicin. *Acta Otolaryngol.* (1998) 118:479–87. doi: 10.1080/00016489850154595

58. Friedmann G. The judgement of the visual vertical and horizontal with peripheral and central vestibular lesions. *Brain.* (1970) 93:313–28. doi: 10.1093/brain/93.2.313
59. Friedmann G. The influence of unilateral labyrinthectomy on orientation in space. *Acta Otolaryngol.* (1971) 71:289–98. doi: 10.3109/00016487109125366
60. Curthoys IS, Dai MJ, Halmagyi GM. Human otolithic function before and after unilateral vestibular neurectomy. *J. Vestib. Res.* (1990) 1:199–209.
61. Halmagyi GM, Gresty MA, Gibson WP. Ocular tilt reaction with peripheral vestibular lesion. *Ann. Neurol.* (1979) 6:80–3. doi: 10.1002/ana.410060122
62. Curthoys IS, Wade SW. Ocular torsion position and the perception of visual orientation. *Acta Otolaryngol. Suppl.* (1995) 520(Pt 2):298–300. doi: 10.3109/00016489509125254
63. Newman-Toker DE, Curthoys IS, Halmagyi GM. Diagnosing stroke in acute vertigo: the HINTS family of eye movement tests and the future of the "eye ECG". *Semin. Neurol.* (2015) 35:506–21. doi: 10.1055/s-0035-1564298
64. Nelson JR, Cope D. Otoliths and ocular countertorsion reflex. *Arch. Otolaryngol.* (1971) 94:40–50. doi: 10.1001/archotol.1971.00770070076008
65. Kanzaki J, Ouchi T. Measurement of ocular counter-torsion reflex with fundoscopic camera in normal subjects and in patients with inner-ear lesions. *Arch. Otorhinolaryngol.* (1978) 218:191–201. doi: 10.1007/BF00455553
66. Schmid-Priscoveanu A, Straumann D, Bohmer A, Obzina H. Is static ocular counterroll asymmetric after vestibular neuritis? In: Claussen CF, Haid CT, Hofferberth B, editors. *Equilibrium Research, Clinical Equilibriometry and Modern Treatment*. International Congress Series. Amsterdam: Elsevier (2000). p. 442.
67. Wuyts FL, Van Der Stappen A, Hoppenbrouwers M, Van Dyck D, Schor RH, Furman JM, et al. Otolith function after acoustic neuroma surgery. *Acta Otolaryngol.* (2001):170–3. doi: 10.1080/000164801750388379
68. Nowe V, Wuyts FL, Hoppenbrouwers M, Van de Heyning PH. The interutricular distance determined from external landmarks. *J. Vestib. Res.* (2003) 13:17–23.
69. Curthoys IS, Blanks RH, Markham CH. Semicircular canal functional anatomy in cat, guinea pig and man. *Acta Otolaryngol.* (1977) 83:258–65. doi: 10.3109/00016487709128843
70. Clarke AH, Schönfeld U, Helling K. Unilateral examination of utricle and saccule function. *J. Vestib. Res.* (2003) 13:215–25.
71. Wetzig J, Hofstetterdegen K, Maurer J, Vonbaumgarten RJ. Clinical verification of a unilateral otolith test. *Acta Astronaut.* (1992) 27:19–24. doi: 10.1016/0094-5765(92)90169-j
72. Clarke AH, Schonfeld U, Hamann C, Scherer H. Measuring unilateral otolith function via the otolith-ocular response and the subjective visual vertical. *Acta Otolaryngol.* (2001):84–7. doi: 10.1080/000164801750388180
73. Lichtenberg BK, Young LR, Arrott AP. Human ocular counter-rolling induced by varying linear accelerations. *Exp. Brain Res.* (1982) 48:127–36. doi: 10.1007/BF00239580
74. Hageman KN, Chow MR, Roberts D, Boutros PJ, Tooker A, Lee K, et al. Binocular 3D otolith-ocular reflexes: responses of chinchillas to prosthetic electrical stimulation targeting the utricle and saccule. *J. Neurophysiol.* (2020) 123:259–76. doi: 10.1152/jn.00883.2018
75. Bronstein AM, Gresty MA, Brookes GB. Compensatory otolithic slow phase eye movement responses to abrupt linear head motion in the lateral direction. Findings in patients with labyrinthine and neurological lesions. *Acta Otolaryngol. Suppl.* (1991) 481:42–6. doi: 10.3109/00016489109131341
76. Ramat S, Zee DS. Ocular motor responses to abrupt interaural head translation in normal humans. *J. Neurophysiol.* (2003) 90:887–902. doi: 10.1152/jn.01121.2002
77. Angelaki DE. Eyes on target: what neurons must do for the vestibuloocular reflex during linear motion. *J. Neurophysiol.* (2004) 92:20–35. doi: 10.1152/jn.00047.2004
78. Schwindt PC, Richter A, Precht W. Short latency utricular and canal input to ipsilateral abducens motoneurons. *Brain Res.* (1973) 60:259–62. doi: 10.1016/0006-8993(73)90867-6
79. Imagawa M, Isu N, Sasaki M, Endo K, Ikegami H, Uchino Y. Axonal projections of utricular afferents to the vestibular nuclei and the abducens nucleus in cats. *Neurosci. Lett.* (1995) 186:87–90. doi: 10.1016/0304-3940(95)11288-8
80. Lempert T, Gianna C, Brookes G, Bronstein A, Gresty M. Horizontal otolith-ocular responses in humans after unilateral vestibular deafferentation. *Exp. Brain Res.* (1998) 118:533–40. doi: 10.1007/s002210050309
81. Tian JR, Ishiyama A, Demer JL. Effect of unilateral vestibular deafferentation on the initial human vestibulo-ocular reflex to surge translation. *Exp. Brain Res.* (2007) 176:575–87. doi: 10.1007/s00221-006-0636-y
82. Aw ST, Halmagyi GM, Haslwanter T, Curthoys IS, Yavor RA, Todd MJ. Three-dimensional vector analysis of the human vestibuloocular reflex in response to high-acceleration head rotations. II. Responses in subjects with unilateral vestibular loss and selective semicircular canal occlusion. *J. Neurophysiol.* (1996) 76:4021–30. doi: 10.1152/jn.1996.76.6.4021
83. Curthoys IS, Grant JW. How does high-frequency sound or vibration activate vestibular receptors? *Exp. Brain Res.* (2015) 233:691–9. doi: 10.1007/s00221-014-4192-6
84. Goto F, Meng H, Bai RS, Sato H, Imagawa M, Sasaki M, et al. Eye movements evoked by the selective stimulation of the utricular nerve in cats. *Auris. Nasus. Larynx.* (2003) 30:341–8. doi: 10.1016/j.anl.2003.07.003
85. Grant W, Curthoys I. Otoliths - accelerometer and seismometer; implications in Vestibular Evoked Myogenic Potential (VEMP). *Hear. Res.* (2017) 353:26–35. doi: 10.1016/j.heares.2017.07.012
86. Curthoys IS, Burgess AM, Goonetilleke SC. Phase-locking of irregular guinea pig primary vestibular afferents to high frequency (>250 Hz) sound and vibration. *Hear. Res.* (2019) 373:59–70. doi: 10.1016/j.heares.2018.12.009
87. Curthoys IS. A critical review of the neurophysiological evidence underlying clinical vestibular testing using sound, vibration and galvanic stimuli. *Clin. Neurophysiol.* (2010) 121:132–44. doi: 10.1016/j.clinph.2009.09.027
88. Lu Z, Xu Z, Buchser WJ. Coding of acoustic particle motion by utricular fibers in the sleeper goby, Dormitator latifrons. *J. Comp. Physiol. A Neuroethol. Sens. Neural. Behav. Physiol.* (2004) 190:923–38. doi: 10.1007/s00359-004-0550-3
89. Popper AN, Hawkins AD. The importance of particle motion to fishes and invertebrates. *J. Acoust. Soc. Am.* (2018) 143:470–88. doi: 10.1121/1.5021594
90. Iwasaki S, McGarvie LA, Halmagyi GM, Burgess AM, Kim J, Colebatch JG, et al. Head taps evoke a crossed vestibulo-ocular reflex. *Neurology.* (2007) 68:1227–9. doi: 10.1212/01.wnl.0000259064.80564.21
91. Colebatch JG, Rosengren SM. Investigating short latency subcortical vestibular projections in humans: what have we learned? *J. Neurophysiol.* (2019) 122:2000–15. doi: 10.1152/jn.00157.2019
92. Iwasaki S, Smulders YE, Burgess AM, McGarvie LA, Macdougall HG, Halmagyi GM, et al. Ocular vestibular evoked myogenic potentials in response to bone-conducted vibration of the midline forehead at Fz. A new indicator of unilateral otolithic loss. *Audiol. Neurootol.* (2008) 13:396–404. doi: 10.1159/000148203
93. Iwasaki S, Smulders YE, Burgess AM, McGarvie LA, Macdougall HG, Halmagyi GM, et al. Ocular vestibular evoked myogenic potentials to bone conducted vibration of the midline forehead at Fz in healthy subjects. *Clin. Neurophysiol.* (2008) 119:2135–47. doi: 10.1016/j.clinph.2008.05.028
94. Colebatch JG, Halmagyi GM. Vestibular evoked potentials in human neck muscles before and after unilateral vestibular deafferentation. *Neurology.* (1992) 42:1635–6. doi: 10.1212/WNL.42.8.1635
95. Zalewski CK, Ackley RS, McCaslin DL, Clark MD, Hanks WD, Brewer CC. Examination of utricular response using oVEMP and unilateral centrifugation rotation testing. *Ear Hear.* (2018) 39:910–21. doi: 10.1097/AUD.0000000000000552
96. Cherchi M. Utricular function in vestibular neuritis: a pilot study of concordance/discordance between ocular vestibular evoked myogenic potentials and ocular cycloposition. *Exp. Brain Res.* (2019) 237:1531–8. doi: 10.1007/s00221-019-05529-8
97. Lue JH, Day AS, Cheng PW, Young YH. Vestibular evoked myogenic potentials are heavily dependent on type I hair cell activity of the saccular macula in guinea pigs. *Audiol. Neurootol.* (2009) 14:59–66. doi: 10.1159/000156701
98. Lyford-Pike S, Vogelheim C, Chu E, Della Santina CC, Carey JP. Gentamicin is primarily localized in vestibular type I hair cells after intratympanic administration. *J. Assoc. Res. Otolaryngol.* (2007) 8:497–508. doi: 10.1007/s10162-007-0093-8

99. Curthoys IS, Smith PF, Darlington CL. Postural compensation in the guinea pig following unilateral labyrinthectomy. *Prog. Brain Res.* (1988) 76:375–84. doi: 10.1016/S0079-6123(08)64524-0
100. Watson SRD, Brizuela AE, Curthoys IS, Colebatch JG, MacDougall HG, Halmagyi GM. Maintained ocular torsion produced by bilateral and unilateral galvanic (DC) vestibular stimulation in humans. *Exp. Brain Res.* (1998) 122:453–8. doi: 10.1007/s002210050533
101. Curthoys IS, Macdougall HG. What galvanic vestibular stimulation actually activates. *Front. Neurol.* (2012) 3:117. doi: 10.3389/fneur.2012.00117
102. MacDougall HG, Brizuela AE, Burgess AM, Curthoys IS. Between-subject variability and within-subject reliability of the human eye-movement response to bilateral galvanic (DC) vestibular stimulation. *Exp. Brain Res.* (2002) 144:69–78. doi: 10.1007/s00221-002-1038-4
103. Aw ST, Aw GE, Todd MJ, Halmagyi GM. Enhanced vestibulo-ocular reflex to electrical vestibular stimulation in Meniere's disease. *J. Assoc. Res. Otolaryngol.* (2013) 14:49–59. doi: 10.1007/s10162-012-0362-z
104. Aw ST, Todd MJ, Halmagyi GM. Latency and initiation of the human vestibuloocular reflex to pulsed galvanic stimulation. *J. Neurophysiol.* (2006) 96:925–30. doi: 10.1152/jn.01250.2005
105. Aw ST, Todd MJ, Lehnen N, Aw GE, Weber KP, Eggert T, et al. Electrical vestibular stimulation after vestibular deafferentation and in vestibular schwannoma. *PLoS ONE*. (2013) 8:e82078. doi: 10.1371/journal.pone.0082078
106. MacDougall HG, Brizuela AE, Curthoys IS. Linearity, symmetry and additivity of the human eye-movement response to maintained unilateral and bilateral surface galvanic (DC) vestibular stimulation. *Exp. Brain Res.* (2003) 148:166–75. doi: 10.1007/s00221-002-1289-0
107. Lempert T, Gresty MA, Bronstein AM. Horizontal linear vestibulo-ocular reflex testing in patients with peripheral vestibular disorders. *Ann. N. Y. Acad. Sci*. (1999) 871:232–47. doi: 10.1111/j.1749-6632.1999.tb09188.x
108. Halmagyi GM, Curthoys IS, Cremer PD, Henderson CJ, Todd MJ, Staples MJ, et al. The human horizontal vestibulo-ocular reflex in response to high-acceleration stimulation before and after unilateral vestibular neurectomy. *Exp. Brain Res.* (1990) 81:479–90. doi: 10.1007/BF02423496
109. Halmagyi GM, Curthoys IS. A clinical sign of canal paresis. *Arch. Neurol.* (1988) 45:737–9. doi: 10.1001/archneur.1988.00520310043015
110. Halmagyi GM, Chen LK, MacDougall HG, Weber KP, McGarvie LA, Curthoys IS. The video head impulse test. *Front. Neurol.* (2017) 8:258. doi: 10.3389/fneur.2017.00258

Conflict of Interest: The author declares that the research was conducted in the absence of any commercial or financial relationships that could be construed as a potential conflict of interest.

frontiers in Neurology

ORIGINAL RESEARCH
published: 22 October 2020
doi: 10.3389/fneur.2020.547015

Prevalence and Characteristics of Physiological Gaze-Evoked and Rebound Nystagmus: Implications for Testing Their Pathological Counterparts

Michelle Sari Ritter[1,2,3†], *Giovanni Bertolini*[1,2,3,4†], *Dominik Straumann*[1,2,3,4] *and Stefan Yu Bögli*[1,2,3,4*]

[1] Department of Neurology, University Hospital Zurich, Zurich, Switzerland, [2] University of Zurich, Zurich, Switzerland, [3] Clinical Neuroscience Center, Zurich, Switzerland, [4] Swiss Concussion Center, Schulthess Clinic, Zurich, Switzerland

OPEN ACCESS

Edited by:
Michael Strupp, Ludwig Maximilian University of Munich, Germany

Reviewed by:
Jeong-Yoon Choi, Seoul National University Bundang Hospital, South Korea
Fatema Ghasia, Cleveland Clinic, United States

***Correspondence:**
Stefan Yu Bögli
stefanyu.boegli@usz.ch

†*These authors have contributed equally to this work and share first authorship*

Specialty section:
This article was submitted to Neuro-Otology, a section of the journal Frontiers in Neurology

Received: *30 March 2020*
Accepted: *17 August 2020*
Published: *22 October 2020*

Citation:
Ritter MS, Bertolini G, Straumann D and Bögli SY (2020) Prevalence and Characteristics of Physiological Gaze-Evoked and Rebound Nystagmus: Implications for Testing Their Pathological Counterparts. Front. Neurol. 11:547015. doi: 10.3389/fneur.2020.547015

Objective: Cerebellar diseases frequently affect the ocular motor neural velocity-to-position integrator by increasing its leakiness and thereby causing gaze-evoked nystagmus (GEN) and rebound nystagmus (RN). Minor leakiness is physiological and occasionally causes GEN in healthy humans. We aimed to evaluate the characteristics of GEN/RN in healthy subjects for better differentiation between physiological and pathological GEN/RN.

Methods: Using video-oculography, eye position was measured in 14 healthy humans at straight ahead eye position before and after, and during 30 s of ocular fixation at 4 horizontal eccentric targets between 30° and 45°. We determined the eye drift velocity and the prevalence of nystagmus before/during/after eccentric fixation.

Results: Eye drift velocities during (range: 0.62 ± 0.53°/s to 1.78 ± 0.69°/s) and after eccentric gaze (range: 0.28 ± 0.52°/s to 1.48 ± 1.02°/s) increased with the amount of gaze eccentricity (30°-45°). During continuous eccentric gaze, eye drift velocities decreased by 0.41 ± 0.18°/s at 30°, and 0.84 ± 0.38°/s at 45° gaze eccentricity. GEN was elicited in 71% of subjects at 30° gaze eccentricity. Twenty-one percent showed RN thereafter. This prevalence increased to 100% (GEN)/72% (RN) at 45° gaze eccentricity. RN found after 30° gaze eccentricity was of low velocity (0.82 ± 0.21°/s) and occurred after minor drift velocity decrease during prior eccentric gaze (0.43 ± 0.15°/s).

Conclusion: GEN and RN should be tested using horizontal gaze eccentricities of <30°, since most healthy subjects physiologically show GEN and RN at higher eccentricities. In case of an uncertain result, both the reduction of eye drift velocity during eccentric gaze and the velocity of RN can be analyzed to distinguish physiological from pathological nystagmus.

Keywords: video-oculography, nystagmus, cerebellum, gaze-holding, clinical examination, gaze-evoked nystagmus, rebound nystagmus

INTRODUCTION

Cerebellar diseases frequently affect the ocular motor neural velocity-to-position integrator. This is a neural network within the brainstem and the cerebellum that generates the position command for the ocular motor neurons to enable stable eccentric gaze (1–4). Already in its normal state, it exhibits some "leakiness" as indicated by centripetal drifts occurring in darkness in healthy individuals attempting eccentric gaze (5, 6). Cerebellar loss-of-function (such as due to drug/alcohol toxicity, malnutrition or cerebellar neurodegeneration/deficits) causes an increase of integrator leakiness thereby leading to gaze-evoked nystagmus (GEN) (1–4, 7–9) and rebound nystagmus (RN) (10–12). GEN is a centrifugal nystagmus occurring at eccentric eye positions, while RN describes a centripetal nystagmus that appears upon the return of gaze to the primary position (straight ahead) after prolonged eccentric gaze.

In clinical neurologic examination, GEN and RN are tested by asking the patient to visually fixate a horizontal eccentric target at roughly 20–30° for up to 20 s (to check for GEN) before asking the patient to look at a subsequent target at primary position (to check for RN). Video-oculography is frequently used for quantification of GEN and RN.

GEN is commonly seen as a clinical sign of a cerebellar lesion, which helps to identify patients with acute vestibular syndrome due to deficits of central vestibular pathways (8, 13). Yet, GEN has frequently been described in healthy subjects with a prevalence of up to 21% already at 10° horizontal gaze eccentricity, increasing up to 93% at extreme lateral gaze (14, 15). RN is also seen as a sign of cerebellar disease. In fact, RN can emerge before any other signs of cerebellar disease are detectable and therefore brain MR-imaging has been recommended in any unexplained case of RN (12, 16). Like GEN, RN has been described in healthy subjects, albeit most commonly only after continuous gaze at larger eccentric gaze angles between 40° and 60° (17–19).

While RN is often examined in daily clinical practice, only few studies have described the characteristics of physiological RN and its relation to physiological GEN. Thus, the aim of this study was to evaluate physiological GEN and RN in healthy human subjects before, during, and after prolonged gaze at different horizontal eccentricities using video-oculography. The results can ease distinguishing physiological GEN or RN from their pathological counterparts.

METHODS

The study protocol was approved by the local ethics committee (cantonal ethics commission Zurich, KEK-ZH-2012-0150) and was in accordance with the ethical standards laid down in the 2013 Declaration of Helsinki for research involving human subjects. Written informed consent was obtained from each subject. Participants with neurologic/psychiatric disease, and subjects who were regularly taking medication were excluded. In total, 14 healthy participants (seven male/seven female, aged 29.7 ± 13.3 years) were included.

Abbreviations: GEN, gaze-evoked nystagmus; RN, rebound nystagmus.

Experimental Setup

All recordings were obtained with the participant seated on a chair with their head being stabilized in upright position using a thermoplastic mask (Sinmed, BV, Reeuwijk, Netherlands). Visual targets were generated by LEDs mounted on a hemispherical screen at 1.5 m distance or a laser projecting to this screen at eye level of the participant. Aside from these visual stimuli, the experiment was conducted in complete darkness. Binocular horizontal eye movements were recorded at 220 Hz with two head-mounted infrared cameras (EyeSeeCam, Munich, Germany). At all times, the left eye was covered using a lens filter, preventing binocular vision but still allowing for recording by the infrared camera. Participants were asked to fixate a flashing red target (20 ms every 2 s, to allow for staying eccentrically without being able to fixate) without moving their head. A total of four trials was conducted per subject. Each trial consisted of three parts. First, "baseline" eye position at the straight ahead horizontal eye position (primary position) was measured for 5 s (step A). Then eye position during 30 s of eccentric gaze was assessed (termed "induction phase," step B). Immediately afterwards, eye position was measured again at the straight ahead eye position for 10 s (step C). After step C the light in the room was turned on for 60 s to prevent contamination of the following trial from prior testing. In each of the four trials the gaze angle of step B was changed (30°, 35°, 40°, and 45° temporally of the viewing eye), while steps A and C were measured at the straight ahead horizontal eye position. In case of interruption during step B or step C (e.g., missing the target position), the trial was repeated.

Data Analysis

Data analysis was performed using custom-written interactive programs in MATLAB Version R2016b (The Mathworks, Natick, MA, USA). Velocity traces were obtained as the derivative of horizontal eye position traces. The appearance of GEN and RN was assessed by extracting the occurrence of at least 3 consecutive saccades (within 10 s) in centrifugal (for GEN) or centripetal (for RN) direction with preceding eye drifts in the opposite direction.

Eye drift velocity for steps A and C was calculated as the median eye velocity over a time window of 2–5 s (average of 3.12 ± 1.16 s) after gaze reached the target position (identified by visual inspection). This time window was interactively adjusted depending on data quality and depending on the duration and vigor of the eye drift. This time window was defined for each participant once, and remained the same for all parts of all trials of the same participant. For each trial, the data from both eyes (viewing and non-viewing eye) were pooled as validated by previous works (6, 20). In addition, the median eye velocity at the beginning and the end of eccentric gaze fixation period (step B) was extracted using the same time window as described above (i.e., with a time window of, e.g., 3 s the median of the first 3 s and the one of the last 3 s of the eye drift velocity during step B was calculated). Statistical testing was conducted using SPSS (IBM, Armonk, NY, USA). The data is shown as mean ± standard deviation. One-way repeated measures ANOVA was used to determine the dependence of the eye movements on the

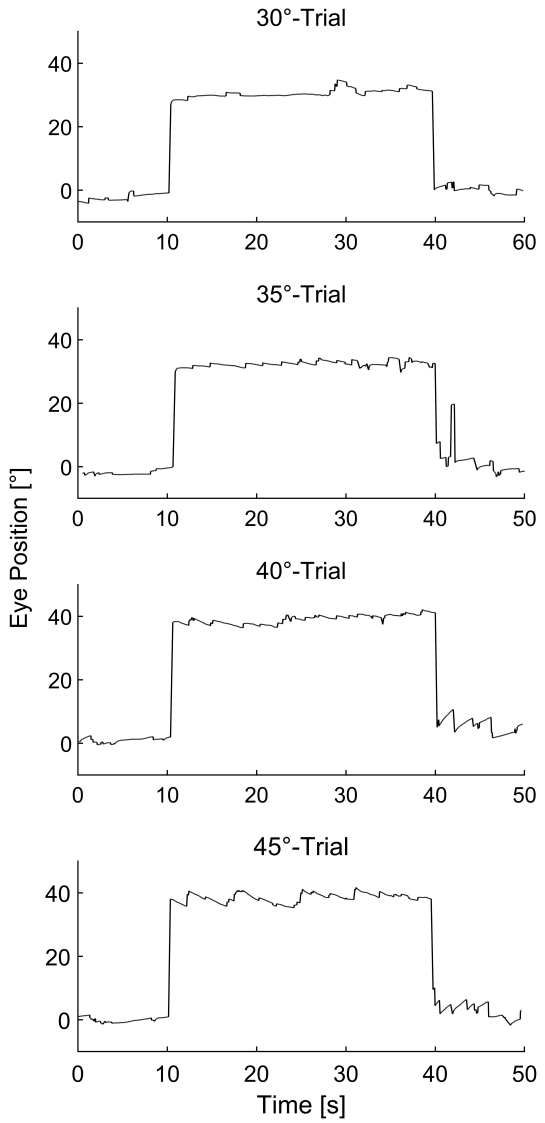

FIGURE 1 | Representative eye movement traces of a single subject before, during, and after sustained eccentric gaze at 30°, 35°, 40°, and 45° respectively.

TABLE 1 | Absolute eye drift velocity at the beginning, during and after the induction phase.

Eccentricity of the induction phase	Absolute eye drift velocity		
	At the beginning of the induction phase	During the induction phase (reduction of eye drift velocity)	After the induction phase at 0°
30°	0.62 ± 0.53°/s	0.41 ± 0.18°/s	0.28 ± 0.52°/s
35°	0.82 ± 0.72°/s	0.58 ± 0.26°/s	0.61 ± 0.61°/s
40°	1.22 ± 0.83°/s	0.70 ± 0.30°/s	0.96 ± 0.65°/s
45°	1.78 ± 0.69°/s	0.84 ± 0.38°/s	1.48 ± 1.02°/s

eccentricity of the induction phase. The *p*-values were corrected for multiple comparison using Bonferroni adjustment. Principal component analysis was used to evaluate correlations between dependent variables providing the goodness-of-fit (R^2-value), the *p*-value, and the slope of the fit including the 95% confidence interval (CI).

RESULTS

In this study, we evaluated the appearance of eye drift and physiological nystagmus before, during, and after prolonged horizontal eccentric gaze between 30° and 45° (induction phase) in healthy human subjects. Eye movement traces showing horizontal eye position before, during, and after prolonged eccentric gaze at all tested eccentricities in a representative subject are depicted in **Figure 1**. Physiological GEN was elicited in all 14 subjects, while physiological RN could only be elicited in 11 subjects. At 30° physiological GEN manifested in 10 participants, while physiological RN only manifested in three participants. These values increased to 10/6 at 35°, 13/11 at 40°, and 14/10 at 45° for physiological GEN and RN, respectively.

The mean eye drift velocity at 0° during baseline measurements (i.e., before the induction phase) was 0.03 ± 0.28°/s. The eye drift velocities found at the beginning, during and after the induction phase are summarized in **Table 1**. Using one-way repeated measure ANOVA statistically significant changes in eye drift velocity could be shown for both the velocity at the beginning of the induction phase [$F_{(1,954,25.407)} = 26.508$, $p < 0.001$] as well as thereafter [$F_{(3,39)} = 16.921$, $p < 0.001$]. *Post hoc* analysis revealed the eye drift velocities to increase depending on the eccentricity of the induction phase (**Figure 2**).

During prolonged eccentric gaze, the eye drift velocity decreased (**Table 1**). Yet, physiological GEN persisted during the continuous eccentric gaze holding in 7 (64%), 8 (80%), 13 (100%), 13 (93%) subjects for eccentric gaze at 30°/35°/40°/45°, respectively. Using principal component analysis, a strong relationship between the drop of eye drift velocity during the induction phase and the subsequent emergence of centrifugal eye drift when returning gaze to the primary position was observed in all our subjects [$R^2 = 0.82$, $p < 0.001$, slope = 0.52 (95%–CI = 0.43–0.67)].

Eye drift did not always result in nystagmus. Therefore, we decided to separately pool subjects who displayed nystagmus and subjects who did not. Subjects who displayed physiological GEN had significantly higher eye drift velocities (1.33 ± 0.75°/s) at the beginning of the induction phase in comparison to those who did not (0.35 ± 0.25°/s, unpaired *t*-test, $p < 0.001$). Furthermore, those subjects who displayed physiological RN showed a significantly higher reduction of eye drift velocity during the induction phase (beginning minus end of induction phase, 0.79 ± 0.33°/s) in comparison to those who did not (0.45 ± 0.20°/s, unpaired *t*-test, $p < 0.001$). In the subjects, in whom physiological RN was elicited already at 30° of eccentric gaze, we measured a RN eye drift

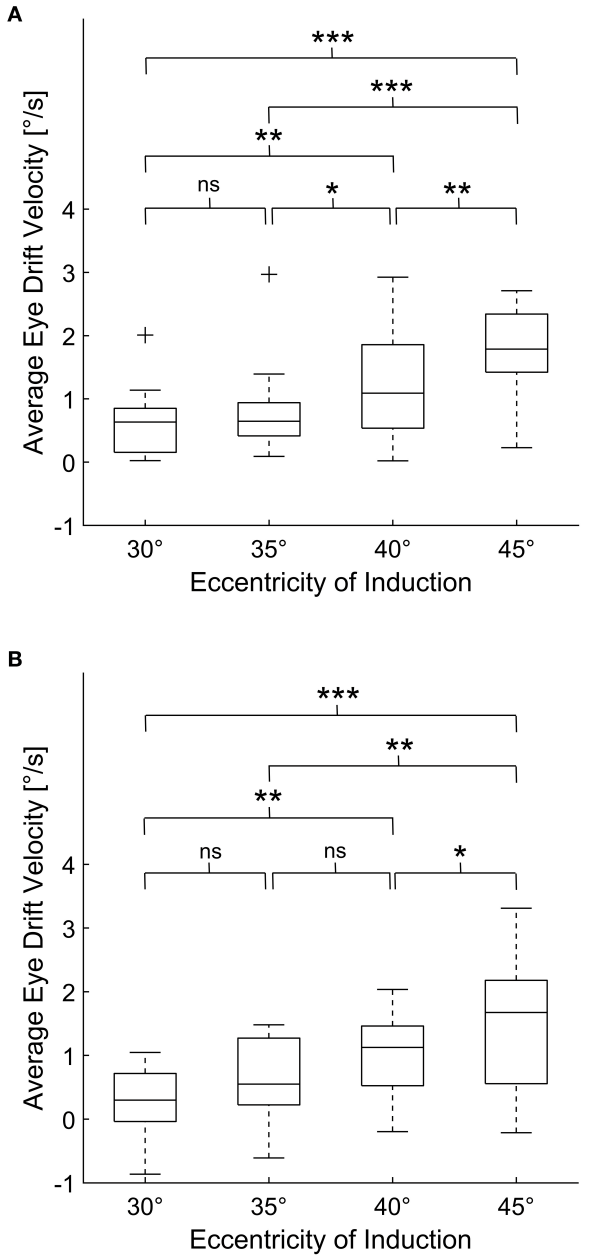

FIGURE 2 | Average eye drift velocities of all subjects during 30 s of eccentric gaze **(A)** and after subsequent return to primary position **(B)**. For each box, the central line indicates the median value. The bottom and top of the box indicate the 25th and 75th percentiles, while the whiskers extend to the most extreme data points that are not considered outliers. The outliers are marked with "+." One-way repeated measures ANOVA demonstrated statistically significant changes in eye drift velocity depending on the eccentricity of the induction phase for both eye drift during and after 30 s of eccentric gaze. The *p*-values, corrected for multiple comparison using Bonferroni adjustment, are shown in each panel (ns for $p > 0.05$, * for $p \leq 0.05$, ** for $p \leq 0.01$, *** for $p \leq 0.001$).

velocity of 0.82 ± 0.21°/s which corresponded to the small decrease of eye drift velocity during the induction phase (0.43 ± 0.15°/s).

DISCUSSION

This study provides a quantitative description of eye drift and physiological RN/GEN before, during, and after prolonged horizontal eccentric gaze at 30–45° in healthy human subjects.

In our study, physiological GEN could be elicited in all tested subjects with the prevalence being dependent on eccentricity (71% at 30° up to 100% at 40–45°). While the prevalence found at extreme eccentric gaze matches prior studies (15, 21, 22), the prevalence at lower eccentricities such as 30–35° was higher [71% in our study vs. 0–58% in prior studies (14, 15, 19)]. Eye drift velocities of physiological GEN were rarely reported. Furthermore, the reported values had large variabilities ranging from as low as 0.26°/s up to 28°/s (6, 21, 22), in comparison to our mean values of 0.62 ± 0.53°/s to 1.78 ± 0.69°/s. Similar to previously reported, velocities of eye drift decreased during continuous eccentric gaze, thus increasing gaze stability (23). Unlike physiological GEN, physiological RN was only found with a prevalence of 21% after eccentric gaze at 30°. The prevalence increased with the eccentricity of prior gaze up to 79% after extreme lateral gaze. This is in contrasts to most prior studies that only described physiological RN after eccentric gaze of 40° or more (17–19, 24), while confirming a single study of five subjects that also found physiological RN after eccentric gaze at 30° (25). Velocities were rarely reported, but if so, ranged between 0.3 and 6.8°/s (24, 25) in comparison to our range of 0.28 ± 0.52°/s to 1.48 ± 1.02°/s.

In comparison to studies performed in patients with cerebellar disease, GEN eye drift velocities found in our study were at the low end of reported velocities (1–24°/s) (9, 11, 23, 26, 27). Eye drift velocities of RN in patients with cerebellar disease were rarely reported. However, the values found in our study were largely lower in comparison to the previously reported range of 2.29–30°/s (23, 28).

Studies on cerebellar disease commonly included patients by mere appearance of nystagmus disregarding the actual drift velocities or a possible correlation between GEN and RN. This is similar to routine clinical examination. Eye drift velocity cannot directly be quantified by eye. Accordingly, the amount of saccades and the repetitive occurrence thereof (which is easily quantifiable) is commonly used for the evaluation of nystagmus. The weakness of this procedure is evident if one considers that GEN already occurred in 71% of subjects at a relatively low eccentricity of 30°. We demonstrate that even persistence of GEN over time is not a solid sign for being pathological. While prior reports described GEN to be pathological if persistent over 20 s (27, 29), we observed that (although the velocity of drift decreased during prolonged eccentric gaze) GEN commonly persisted for the duration of 30 s (in 64–100% of subjects depending on gaze eccentricity). Furthermore, while the velocities found in our study were generally at the low end of ranges presented in prior studies in patients, these results still indicate that certain cases might have been wrongly identified as pathological.

Similar to physiological GEN, physiological RN was also elicited using all induction eccentricities tested. However, this

study demonstrates differences that can be used to distinguish physiological from pathological RN. In those cases where physiological RN was elicited after eccentric gaze at 30°, velocities were largely lower than in patients [average of 0.82 ± 0.21°/s in our study vs. previously reported range of 2.29–30°/s (23, 28)]. Secondly, the amount of adaptation that occurred prior to the appearance of physiological RN during eccentric gaze may be an important sign to be observed, as it was much lower than the values reported in a previous study using a similar methodology in patients with cerebellar disease (average of 0.43 ± 0.15°/s in our study vs. 2.40°/s) (23).

The exact mechanism of RN and its relation to GEN are unknown. In this study, we found a high correlation between the decrease of physiological GEN and subsequent physiological RN. This finding supports current hypothesis suggesting that during sustained eccentric gaze, different adaptive mechanisms alter the neural integrator to enhance gaze stability at this eccentric gaze position by decreasing the centripetal eye drift by a change of the set-point (gaze angle with least eye drift), which then causes a gaze-instability at primary position (23–25), altogether suggesting that RN and GEN are physiological phenomena of the same neural integrator that are exacerbated by cerebellar disease.

LIMITATIONS

Our study has several limitations. Firstly, we only tested 14 subjects, which is a rather small sample size. Secondly, parameters used during our study are different from parameters that are generally used during bedside examination. These include the duration of eccentric gaze (this study: 30 s, bedside: maximally 20 s), the horizontal eccentricity of gaze (this study: 30–45°, bedside: 20–30°), the prevention of fixation (this study: experiment conducted in darkness with one eye covered, bedside: binocular vision in a lit room) and the fixation target (this study: flashing target appearing for 20 ms every 2 s, bedside: continuously visible target). Thus, no direct correlation to the clinical examination is possible. However, the parameters used in this study are known to provoke occurrence of nystagmus. The occurrence of only minor physiological RN after eccentric gaze at 30° for 30 s is thus of high importance. The results improve the significance of any RN that is found during general clinical examination with parameters that are easier (e.g., less gaze eccentricity, reduced duration of eccentric gaze, improved fixation) than in this study. Lastly, methods used during the testing were similar, however not the same as in prior reports, thus comparisons have to be made cautiously. Direct comparisons can only be made with one study (23) that used the same methods testing patients with cerebellar degeneration. In the future further studies directly comparing patients and matched healthy subjects using the same paradigms are necessary.

CONCLUSIONS

Our study provides an in-depth description of eye drift and physiological nystagmus before, during, and after prolonged eccentric gaze at eccentricities between 30° and 45° in healthy. We provide values for physiological eye drift velocities that can and should be expected during an examination of eye movements/nystagmus using video-oculography. Furthermore, our results show that GEN and RN should be tested at eccentricities of <30° using video-oculography, as higher eccentricities lead to significant gaze drift and physiological nystagmus (most commonly GEN) in healthy subjects, while pathological nystagmus can often already be elicited at lower eccentricities (4, 9, 11, 23). In case of an uncertain result both the reduction of GEN drift velocity (adaptation) during eccentric gaze and the drift velocity of RN can be analyzed to distinguish physiological from pathological nystagmus, while the occurrence and persistence of GEN during continuous eccentric gaze are not *per se* pathological.

DATA AVAILABILITY STATEMENT

The raw data supporting the conclusions of this article will be made available by the authors, without undue reservation.

ETHICS STATEMENT

The studies involving human participants were reviewed and approved by Kantonale Ethikkommission Zürich Stampfenbachstrasse 121, 8090 Zürich, Switzerland. The patients/participants provided their written informed consent to participate in this study.

AUTHOR CONTRIBUTIONS

GB, DS, and SB conceived and designed the study. MR and SB performed the experiments and acquired the data. MR, GB, and SB analyzed the data. MR and SB drafted the manuscript. All authors interpreted the data and revised the manuscript for intellectual content and approved the submitted version.

FUNDING

This work was supported by the Betty and David Koetser Foundation for Brain Research (Zurich, Switzerland), the Hartmann Müller Foundation (Zurich, Switzerland), and the EMDO Foundation (Zurich, Switzerland).

REFERENCES

1. Robinson DA. The effect of cerebellectomy on the cat's vestibulo-ocular integrator. *Brain Res.* (1974) 71:195–207. doi: 10.1016/0006-8993(74)90961-5

2. Zee DS, Yamazaki A, Butler PH, Gucer G. Effects of ablation of flocculus and paraflocculus of eye movements in primate. *J Neurophysiol.* (1981) 46:878–99. doi: 10.1152/jn.1981.46.4.878

3. Cannon SC, Robinson DA. Loss of the neural integrator of the oculomotor system from brain stem lesions in monkey. *J Neurophysiol*. (1987) 57:1383–409. doi: 10.1152/jn.1987.57.5.1383
4. Versino M, Hurko O, Zee DS. Disorders of binocular control of eye movements in patients with cerebellar dysfunction. *Brain*. (1996) 119:1933–50. doi: 10.1093/brain/119.6.1933
5. Becker W, Klein HM. Accuracy of saccadic eye movements and maintenance of eccentric eye positions in the dark. *Vision Res*. (1973) 13:1021–34. doi: 10.1016/0042-6989(73)90141-7
6. Bertolini G, Tarnutzer AA, Olasagasti I, Khojasteh E, Weber KP, Bockisch CJ, et al. Gaze holding in healthy subjects. *PLoS ONE*. (2013) 8:e61389. doi: 10.1371/journal.pone.0061389
7. Baier B, Dieterich M. Incidence and anatomy of gaze-evoked nystagmus in patients with cerebellar lesions. *Neurology*. (2011) 76:361–5. doi: 10.1212/WNL.0b013e318208f4c3
8. Tarnutzer AA, Berkowitz AL, Robinson KA, Hsieh YH, Newman-Toker DE. Does my dizzy patient have a stroke? A systematic review of bedside diagnosis in acute vestibular syndrome. *CMAJ*. (2011) 183:E571–92. doi: 10.1503/cmaj.100174
9. Tarnutzer AA, Weber KP, Schuknecht B, Straumann D, Marti S, Bertolini G. Gaze holding deficits discriminate early from late onset cerebellar degeneration. *J Neurol*. (2015) 262:1837–49. doi: 10.1007/s00415-015-7773-9
10. Hood JD, Kayan A, Leech J. Rebound nystagmus. *Brain*. (1973) 96:507–26. doi: 10.1093/brain/96.3.507
11. Zee DS, Yee RD, Cogan DG, Robinson DA, Engel WK. Ocular motor abnormalities in hereditary cerebellar ataxia. *Brain*. (1976) 99:207–34. doi: 10.1093/brain/99.2.207
12. Lin CY, Young YH. Clinical significance of rebound nystagmus. *Laryngoscope*. (1999) 109:1803–5. doi: 10.1097/00005537-199911000-00015
13. Kattah JC, Talkad AV, Wang DZ, Hsieh YH, Newman-Toker DE. HINTS to diagnose stroke in the acute vestibular syndrome: three-step bedside oculomotor examination more sensitive than early MRI diffusion-weighted imaging. *Stroke*. (2009) 40:3504–10. doi: 10.1161/STROKEAHA.109.551234
14. Abel LA, Parker L, Daroff RB, Dell'osso LF. End-point nystagmus. *Invest Ophthalmol Vis Sci*. (1978) 17:539–44.
15. Whyte CA, Petrock AM, Rosenberg M. Occurrence of physiologic gaze-evoked nystagmus at small angles of gaze. *Invest Ophthalmol Vis Sci*. (2010) 51:2476–8. doi: 10.1167/iovs.08-3241
16. Huang CC, Young YH. Vertigo with rebound nystagmus as an initial manifestation in a patient with basilar artery occlusion. *Eur Arch Otorhinolaryngol*. (2005) 262:576–9. doi: 10.1007/s00405-004-0874-1
17. Shallo-Hoffmann J, Schwarze H, Simonsz HJ, Muhlendyck H. A reexamination of end-point and rebound nystagmus in normals. *Invest Ophthalmol Vis Sci*. (1990) 31:388–92.
18. Wild F, Shallo-Hoffmann J, Muhlendyck H. [Physiologic and pathologic rebound nystagmus. Description and comparison]. *Fortschr Ophthalmol*. (1991) 88:73–7.
19. Levo H, Aalto H, Hirvonen TPJO. Nystagmus measured with video-oculography: methodological aspects and normative data. *J Otorhinolaryngol Relat Spec*. (2004) 66:101–4. doi: 10.1159/000079327
20. Romano F, Tarnutzer AA, Straumann D, Ramat S, Bertolini G. Gaze-evoked nystagmus induced by alcohol intoxication. *J Physiol*. (2017) 595:2161–73. doi: 10.1113/JP273204
21. Schmidt D, Kommerell G. [End position nystagmus caused by prolonged lateral gaze. (author's transl)]. *Albrecht Von Graefes Arch Klin Exp Ophthalmol*. (1976) 198:17–24. doi: 10.1007/BF00411440
22. Eizenman M, Cheng P, Sharpe JA, Frecker RC. End-point nystagmus and ocular drift: an experimental and theoretical study. *Vision Res*. (1990) 30:863–77. doi: 10.1016/0042-6989(90)90055-P
23. Bögli SY, Straumann D, Schuknecht B, Bertolini G, Tarnutzer AA. Cerebellar rebound nystagmus explained as gaze-evoked nystagmus relative to an eccentric set point: implications for the clinical examination. *Cerebellum*. (2020). doi: 10.1007/s12311-020-01118-6. [Epub ahead of print].
24. Otero-Millan J, Colpak AI, Kheradmand A, Zee DS. Rebound nystagmus, a window into the oculomotor integrator. *Prog Brain Res*. (2019) 249:197–209. doi: 10.1016/bs.pbr.2019.04.040
25. Gordon SH, Hain TC, Zee DS, Fetter M. Rebound nystagmus. *Soc Neuroscience*. (1986) 12:1091.
26. Buttner U, Grundei T. Gaze-evoked nystagmus and smooth pursuit deficits: their relationship studied in 52 patients. *J Neurol*. (1995) 242:384–9. doi: 10.1007/BF00868394
27. Yetiser S, Ince D, Yetiser B. Optokinetic analysis in patients with spontaneous horizontal gaze-evoked nystagmus without radiological neuropathology. *Ear Nose Throat J*. (2019) 98:420–4. doi: 10.1177/0145561319840902
28. Hood JD. Further observations on the phenomenon of rebound nystagmus. *Ann N Y Acad Sci*. (1981) 374:532–9. doi: 10.1111/j.1749-6632.1981.tb30898.x
29. Strupp M, Kremmyda O, Adamczyk C, Bottcher N, Muth C, Yip CW, et al. Central ocular motor disorders, including gaze palsy and nystagmus. *J Neurol*. (2014) 261 (Suppl. 2):S542–58. doi: 10.1007/s00415-014-7385-9

Conflict of Interest: The authors declare that the research was conducted in the absence of any commercial or financial relationships that could be construed as a potential conflict of interest.

frontiers in Neurology

MINI REVIEW
published: 29 October 2020
doi: 10.3389/fneur.2020.581527

Usefulness of Video Head Impulse Test Results in the Identification of Meniere's Disease

Brahim Kaci[1,2], *Mujda Nooristani*[1,2], *Tamara Mijovic*[3] *and Maxime Maheu*[1,2]*

[1] Vestibulab, School of Speech Language Pathology and Audiology, University of Montreal, Montreal, QC, Canada, [2] Centre de Recherche Interdisciplinaire en Réadaptation - Institut Universitaire sur la Réadaptation en Déficience Physique de Montréal (IURDPM), Pavillon Laurier, CIUSSS du Centre-Sud-de-l'Île-de-Montréal, Montreal, QC, Canada, [3] Department of Otolaryngology-Head and Neck Surgery, Royal Victoria Hospital, Montreal, QC, Canada

Meniere's disease (MD) is an inner ear disorder inducing tinnitus, aural fullness, sensorineural hearing loss, and vertigo episodes. In the past few years, efforts have been made to develop objective measures able to distinguish MD from other pathologies. Indeed, some authors investigated electrophysiological measures, such as electrocochleography and vestibular evoked myogenic potentials or imaging techniques. More recently, the video head impulse test (vHIT) was developed to assess the vestibulo-ocular reflex (VOR). In the last few years, authors aimed at identifying how vHIT may help to identify MD. The objective of this manuscript is to review the different vHIT results in MD patients. We will discuss the usefulness of these findings in the identification of MD, how these results may be explained by pathophysiological mechanisms associated with MD, and finally provide directions for future studies.

Keywords: Meniere disease, vestibular system, endolymphatic hydrops, caloric, vHIT

OPEN ACCESS

Edited by:
Michael Strupp, Ludwig Maximilian University of Munich, Germany

Reviewed by:
Tadashi Kitahara, Nara Medical University, Japan
Dario Andres Yacovino, Dr. César Milstein Hospital, Argentina

***Correspondence:**
Maxime Maheu
maxime.maheu.1@umontreal.ca

Specialty section:
This article was submitted to Neuro-Otology, a section of the journal Frontiers in Neurology

Received: *09 July 2020*
Accepted: *28 September 2020*
Published: *29 October 2020*

Citation:
Kaci B, Nooristani M, Mijovic T and Maheu M (2020) Usefulness of Video Head Impulse Test Results in the Identification of Meniere's Disease. Front. Neurol. 11:581527. doi: 10.3389/fneur.2020.581527

INTRODUCTION

Meniere's disease (MD) is an inner ear pathology that induces episodes of vertigo, ear fullness, tinnitus, and fluctuating sensorineural hearing loss. A commonly accepted pathophysiological mechanism of MD is endolymphatic hydrops (EH) (1). Indeed, EH is a disorder where the endolymph accumulates in the cochlea and in the vestibular organs (2) and is revealed to be a frequent finding in histopathological and imaging studies of the inner ear of MD patients (3). The American Academy of Otolaryngology—Head and Neck Surgery (AAO-HNS) (4) has defined the diagnostic criteria that are based on the presence/absence and duration of the different symptoms described above allowing the classification of patients in different MD categories, such as probable, possible, definite, and certain. These criteria and the classification have been reviewed in 2015 with the idea to improve diagnosis, leaving only probable and definite MD (5). However, the diagnosis of MD remains difficult probably due to the lack of a gold standard test.

In the past few years efforts have been made to develop an objective test able to accurately identify MD. Previous studies aimed at identifying MD markers either at the cochlear level or at the vestibular level using, respectively, electrocochleography and vestibular evoked myogenic potentials. No consensus could be reached from these studies regarding their efficacy in the identification of MD [for review, see (6–8)]. More recently, the video head impulse test (vHIT) was developed to assess the vestibulo-ocular reflex (VOR), and efforts have been made to understand

how MD influences vHIT results. However, studies are sometimes contradictory as some found reduced VOR results, whereas others found enhanced VOR results. Moreover, contradictory findings have been observed between vHIT and caloric test, both assessing horizontal canal function. The objective of this manuscript is to review the different vHIT results in MD patients. We will discuss the usefulness of these findings in the identification of MD, how these seemingly contradictory results may be unified, and how they relate to the pathophysiological mechanisms associated with MD. Finally, we will provide directions for future studies.

VIDEO HEAD IMPULSE RESULTS IN MENIERE

Video Head Impulse Test

The vHIT is a recently developed tool allowing the assessment of high-frequency VOR function of all six semicircular canals (9). It uses a gyroscope and an infrared camera mounted on goggles to record, respectively, head and eye velocity. With these parameters, it is possible to calculate VOR gain (eye/head) and to detect catch-up saccades during fast and passively applied head impulses (10). During these impulses, participants are required to maintain gaze on an earth-fixed target. It is assumed that when VOR is normal, the eyes will move at the same velocity as the head but in the opposite direction generating a perfect VOR gain of 1.0. However, when VOR is abnormal, the eyes will follow the head's movement reducing the VOR gain and requiring catch-up saccades to bring gaze back on target (10).

Reduced VOR Function in MD

Some of the previous studies investigated the distribution of the abnormal results across all six semicircular canals in the quiescent phase (interictal) and found divergent results (**Table 1**). In 2014, Zulueta-Santos et al. (13) studied 36 participants with definite MD and revealed that the most frequently affected canal in MD participants was the posterior (40%), followed by the superior (22.8%) and the lateral (14.2%). More recently, Sobhy et al. (14) studied 40 patients with definite MD and observed the exact opposite classification. This group observed that the most frequently affected canal was the lateral (20%), followed by the superior (7.5%) and the posterior (5%). The possible differences observed between these studies could be, at least in part, due to two methodological differences in the definition of abnormal values. First, Zulueta-Santos et al. (13) used only the VOR gain to classify results as abnormal (normal if VOR gain was: <0.8 for lateral canals and <0.7 for vertical canals). On the other hand, Sobhy et al. (14) as well used VOR gain (absolute and asymmetry) but also included the presence of catch-up saccades to classify results as normal or abnormal. The latter method is in line with the results reported by Jerin et al. (17). This group studied 54 participants with certain MD and found that the vast majority (74%) of the participants showed normal VOR gain but presented catch-up saccades. These saccades were present in <50% of the trials in 14 out of 54 participants and in at least 50% of the trials in 33 out of 54 participants. Therefore, it seems that catch-up saccades are an important component to take into consideration and it could influence the categorization of a normal or abnormal VOR function. Second, another methodological discrepancy

TABLE 1 | Comparison of the reviewed reports that investigated the influence of MD on vHIT results (gain and saccades).

MD diagnosis and duration	*N*	Normative values (vHIT)	Results	Moment of evaluation	References
Diagnosis: definite MD[a] Duration: 0.5–4 years	24	Lateral: 0.88–1.27 Anterior: 0.75–1.29 Posterior: 0.77–1.13	Irritative/recovery phase: reduced gain in 37% Paretic phase: reduced gain in 79%	Ictal phase (irritative/recovery and paretic phases)	(11)
Diagnosis: N/A Duration: 2 years	1	N/A	Paretic phase: reduced gain Interictal: gain returned to baseline	Ictal phase (paretic phase) Outside the ictal phase	(12)
Diagnosis: definite MD[b] Duration: 4–9 years	36	Lateral: >0.8 Anterior: >0.7 Posterior: >0.7	Lateral: 14.2% Anterior: 22.8% Posterior: 40%	Outside the ictal phase	(13)
Diagnosis: definite MD[b] Duration: 3 months−15 years	40	Lateral: 1.03 ± 0.12 Anterior: 0.95 ± 0.11 Posterior: 1.03 ± 0.18	Lateral: normal 80%/enhanced 7.5%/reduced 12.5% Anterior: normal 95%/reduced 7.5% Posterior: normal 92.5%/reduced 5%	Outside the ictal phase	(14)
Case 1 Diagnosis: probable MD[a] Duration: 5 years *Case 2* Diagnosis: definite MD[a] Duration: 10 years	2	N/A	Case 1: enhanced VOR gain Case 2: enhanced VOR gain	Case 1: N/A Case 2: 10 days after the last episode	(15)
Diagnosis: definite MD[a] Duration: 1–11 years	10	Lateral: >0.8 or <1.11	Interictal: no difference between affected and unaffected, controls Ictal: reduced gain between affected and unaffected/controls	Outside the ictal phase Ictal phase (initial, peak, recovery) Post-attack	(16)

[a] *Bárány Society criteria (2015).* [b] *American Academy of Otolaryngology—Head and Neck surgery criteria (1995) (AAO-HNS).*

between these two studies could be the normative gain value applied. Indeed, contrary to Zulueta-Santos et al. (13), Sobhy et al. (14) did not specify their cut-off value for normal and abnormal VOR gain limiting possible comparisons.

Fluctuation of VOR Function in MD

As MD being an episodic disorder, some authors measured VOR parameters at different moments of the MD episodes (before, during, or in between episodes) (**Table 1**). The vHIT findings seemed to fluctuate depending on the moment of the evaluation. Yacovino and Finlay (12) followed up a 64-year-old patient with MD over a 12-month period. They measured vHIT during and between episodes of vertigo. They noticed that during the episodes, VOR gain was reduced, and saccades were present on the affected side. When tested between episodes, patients showed normal gain and either fewer or no catch-up saccades. The contralateral side remained stable over time. This fluctuation in VOR gain was also observed in a 54-year-old patient known for MD. They measured VOR gain and saccades using vHIT before, during, and after an MD episode. They found similar results (reduced gain during an episode and a return to normal after a crisis) but only for the superior canal of the affected ear (18). Yacovino et al. (16) recently demonstrated this variation in the different phases of MD episodes (initial, peak, and recovery) in 10 patients. They showed a significant reduction in VOR gain between the affected and unaffected ears for all three different phases. However, no gain differences were observed between the affected and unaffected ears between episodes (interictal) and post-attack. Interestingly, these studies reveal different results as opposed to Rey-Martinez et al. (15), who report enhanced VOR gain in two patients known with MD. This group described the case of a 74-year-old male with probable MD and the case of a 45-year-old female with definite bilateral MD. The first case described was a male subject followed up for a period of 5-years, and they found systematically enhanced VOR gain. In this case, the authors did not report if the assessment was done during or between crisis. The second case was evaluated once, 10 days following the episode, and they also found an enhanced VOR gain.

vHIT vs. CALORIC

Caloric Stimulation

VOR can be examined using different methods, such as vHIT and caloric test. vHIT is known to evaluate VOR at frequencies between 5 and 7 Hz (19, 20) and caloric between 0.003 and 0.008 Hz (21). Caloric test is thought to induce an endolymphatic movement in the horizontal semicircular canal. It consists of increasing or decreasing the temperature of the external auditory canal, using air or water, to induce a movement of the endolymph in the horizontal semicircular canal. This movement modulates the spontaneous firing rate of the peripheral vestibular system and creates an asymmetry in the plane of the horizontal semicircular canal (21).

Discrepancies Between Caloric Test and vHIT in Meniere's Disease

Over the past few years, there has been a growing interest in observing how caloric test and vHIT are differently affected by MD as these two tests evaluate the function of the horizontal semicircular canals but tend to show opposing results in MD. As demonstrated in **Table 2**, it has been noticed by previous studies that even though caloric test usually demonstrates an asymmetry toward the affected ear, vHIT parameters are usually preserved in definite MD (22–30). Some authors tried to evaluate if this discrepancy in the results may be in relation to the duration or the stage of MD but failed to find a significant relationship (25, 27, 29). Limviriyakul et al. (29) went further and assessed if this discrepancy was related to patients being in the active or inactive phase according to the Shea classification of MD (31). These authors separated the participants into two groups, either active (symptoms within the past 3 months) or inactive (symptom free for at least 3 months). However, this study failed to reveal any significant difference between these two groups regarding the number of participants with and without caloric/vHIT discrepancies.

There seems to have a higher prevalence of caloric/vHIT discrepancy in MD patients as opposed to controls when the diagnosis is based on the criteria proposed by AAO-HNS (1995) (4) or on the Classification Committee of the Bárány Society (2015) (5). This leads to propose that the presence of an abnormal caloric response in the presence of a normal vHIT results may be used as a marker in the diagnosis of MD. However, a recent study raised doubts as they failed to find an association between caloric/vHIT discrepancy and the pathophysiological marker of MD, namely, EH (28). They used an inner ear MRI to classify MD patients based on the presence or absence of a positive sign of EH. They sought to compare the number of patients with opposing caloric and vHIT results in each group and found that a positive finding of EH demonstrated by inner ear MRI did not always indicate a caloric/vHIT discrepancy in an MD group. More precisely, they observed that out of 29 patients who showed a discrepancy in caloric and vHIT results, 15 showed a positive sign of EH as opposed to 14 who had a negative sign of EH. Instead, they found that the discrepancy between caloric and vHIT results was strongly associated with vestibular herniation into the semicircular canals (protrusion of part of the vestibular labyrinth into the semicircular canals).

DISCUSSION

This review aimed at presenting the different vHIT findings observed in MD. The results of the reviewed studies may seem to be heterogeneous as some demonstrated that VOR is well-preserved, whereas others reported a reduced VOR gain with saccades or even an enhanced VOR gain. However, we propose that these results may be unified, at least in part, when considering the moment of assessment relative to the ictal phase or the duration of the disease.

First, MD, being an episodic disease, comprises two phases, either ictal (during MD episode) or outside the ictal. It is

TABLE 2 | Comparison of the reviewed reports that investigated the discrepancy of caloric and vHIT results in MD.

MD diagnosis and duration	*N*	Normative values (caloric)	Normative values (vHIT)	*N* (%) CV	Moment of evaluation	References
Definite MD[a] Mean duration: N/A	3	Abnormal: unilateral weakness (UW) >22% and directional preponderance (DP) >28%	Abnormal: VOR gain <0.7 and/or saccades	3 (100%)	No indication of patients' state (ictal or outside the ictal phase) during vestibular assessment nor MD stages	(22)
Definite MD[b] Mean duration: 3 years	32	Abnormal: sum of slow phase velocity (SPV) of one ear (cold and warm) <5°/s (unilateral) or sum of SPV (cold and warm) of both ears <12°/s (bilateral)	Abnormal: presence of saccades and/or VOR gain <0.8 for lateral SCCs VOR gain <0.75 for vertical SCCs	17 (43.6%)	Outside the ictal phase: at least 72 h after MD crisis	(23)
Definite MD[b] Mean duration: 7 years	37	Abnormal: UW ≥20%	Abnormal: presence of saccades or VOR <0.78 for lateral SCCs VOR <0.64 for vertical SCCs	Total: 34 (91.9%) Patients outside MD crisis: 31 (94%) Patients just after MD crisis: 3 (75%)	Outside the ictal phase: 33 patients Just after an MD crisis (irritative/recovery phase): 4 patients	(24)
Definite MD[a] Mean duration: 5 ± 6.2 years	87	Abnormal: vestibular preponderance >22% or DP >28% or Irrigation response V_{max} <15°/s	Abnormal: VOR gain <0.8 and saccades	132 ears (86.8%)	Outside the ictal phase	(25)
Definite MD[a] Mean duration: 3 ± 2.3 years	88	Abnormal: UW >20% and DP >28%	Abnormal: VOR gain <0.8 for lateral SCCs VOR gain <0.7 for vertical SCCs and saccades	Lateral canal: 40 (45.6%) All 6 canals: 16 (18.2%)	Outside the ictal phase	(26)
Definite MD[b] Mean duration: N/A	73	Abnormal: UW ≥30% or Bilateral slow phase velocity responses were ≤10°/s	Abnormal if VOR <0.8	27 (37.0%)	Outside the ictal phase	(27)
MD classification not indicated[b] Mean duration: N/A	20 (15 unilateral, 5 bilateral; total: 25 ears)	Abnormal: ENG response ≤10°/s.	Abnormal: VOR gain <0.8 for lateral SCCs or VOR gain <0.8 and saccades	14/25 ears (56%) 14/20 MD patients (70%)	No indication of patients' state (during or after crisis) during vestibular assessment	(28)
Definite MD[a] Mean duration: N/A	51	Abnormal: UW >25%	Abnormal: VOR gain <0.8 for lateral SCCs VOR <0.7 for vertical SCCs or Presence of overt and covert saccades for >50% of trials	Active: 16 (40%) Inactive: 6 (54.6%)	Shea classification of MD: Active (symptoms within the past 3 months): 40 Inactive (symptom free for at least 3 months): 11	(29)

[a] *American Academy of Otolaryngology—Head and Neck surgery criteria (1995) (AAO-HNS).* [b] *Bárány Society criteria (2015).*

documented that the ictal phase could be subcategorized into three phases: (1) irritative, (2) paretic, and (3) recovery. The irritative and recovery phases are characterized by spontaneous nystagmus that beats toward the affected ear as opposed to the paretic phase that is characterized by a nystagmus beating toward the unaffected ear (32). Based on the studies reported in this review, when patients are tested during the ictal paretic phase, the VOR gain associated with the affected ear is usually reduced (11, 12). However, when patients are assessed during either the irritative or recovery phase of the ictal period or assessed outside the ictal period, the majority of the MD patients demonstrate a normal VOR gain. These results associated to the different phases of MD are supported by animal model of EH. Indeed, EH has been associated with increase in perilymph potassium concentration (33). In animal models, induction of potassium within the tympanic cavity revealed similar irritative and paretic phases seen in MD patients (34). Therefore, these pathophysiologic evidences support that

the fluctuations in VOR gain measured by vHIT could be an indicator of EH.

Second, even though no association between duration of the disease and VOR gain was revealed in the reviewed studies (25), previous literature suggests an interaction between duration of the disease and moment of the evaluation (ictal phase or outside the ictal phase). Indeed, Maire and Van Melle (35) observed a dissociation of VOR response between early (<12 months) and late (>12 months) MD participants using a rotary chair. They found that early and late MD participants showed opposite results during the ictal phase. While early MD revealed enhanced VOR, late MD showed reduced VOR gain. This may explain differences with van Esch et al.'s (25) study that assessed participants between MD episodes (outside the ictal phase). To our knowledge, no studies using vHIT assessed the relationship between MD phase and MD duration. Therefore, it would be of great interest for future studies to investigate vHIT results in early and late MD for all six semicircular canals and separate groups in relation to the MD phase (during or between MD episodes). This could help to advance our understanding of the pathophysiology of MD and its influence on vHIT results.

The present manuscript also reviewed research that studied the caloric/vHIT discrepancy, which seems to be a promising indicator of MD. However, some questions remain unanswered. One question that future studies would need to assess is if this discrepancy occurs only at a certain moment in the progression of MD. Indeed, as described by Sugimoto et al. (36), vestibular herniation is thought to explain the discrepancy between caloric and vHIT results and is associated with the progression of EH. This could lead to hypothesize that the discrepancy between caloric test and vHIT may more frequently occur only at a certain stage/duration of the disease. To our knowledge, no previous studies investigated this question, and therefore, future studies should examine this hypothesis by analyzing the ratio of caloric and vHIT discrepancy in relation to the different stages and durations of MD. Furthermore, the differences between the caloric/vHIT discrepancies may be related to the phase of MD. When analyzed closely, the percentage of patients showing caloric/vHIT discrepancy is higher when they were assessed outside the ictal phase than when they were assessed during the ictal phase (**Table 2**). This could be related to the previous observation that during the ictal paretic phase, VOR gain is decreased that may reduce the percentage of MD patients showing caloric/vHIT discrepancy.

In the past few years, several theories have been put forward to explain how the pathophysiology of MD may explain the caloric/vHIT discrepancy. One of the theories, well-described in McCaslin et al. (22), states that MD differently affects regular and irregular afferents. Indeed, a significant loss of type II hair cells in the crista with MD has been reported, suggesting that MD specifically damages regular afferents. This theory is based on the fact that peripheral zones of the crista are characterized by afferents that are most sensitive to low-frequency movements (regular afferents) as opposed to afferents located centrally that are most sensitive to higher frequencies (irregular afferents). Therefore, as described earlier, the caloric test (low frequency) will stimulate the regular afferent of the semicircular canal that responds to sustained stimulation as opposed to the transient high acceleration head impulses delivered during vHIT examination, which will mostly stimulate the irregular afferents (37, 38). However, some doubts are raised about the fact that MD affects specifically regular afferents as a study found that both type I and type II hair cells were equally affected in MD (39). A second theory was put forward by Mcgarvie et al. (40). This theory is based on the physiology of the canal and the impact of EH. Mcgarvie et al. (40) suggest that the caloric weakness observed in MD is due to the hydropic expansion of the lateral canal membranous duct. The enlargement of the canal would reduce the hydrostatic drive, normally provided by a change in endolymph temperature, by inducing local convection flows and thus reducing slow phase eye velocity when the affected canal is being stimulated with the caloric test. However, the hydrops would not reduce the endolymphatic flow generated following head acceleration and, therefore, would not affect VOR gain. This theory recently received support from Fukushima et al.'s (41) study that observed that endolymphatic volume affects caloric response but is independent of the vHIT results. Therefore, this theory states that the discrepancy between the results may be due to the physical enlargement of the labyrinth due to EH.

Some important points may limit the comparisons of the studies reviewed here and need to be highlighted. First, the lack of description of the inclusion/exclusion criteria related to medication/treatment. This is of great importance as the spectrum of possible treatment for MD varies a lot and may have different impacts on vestibular measures [for a review of possible treatments, see (42)]. Future studies should always report the medication/treatment received by the participants. Second, an important variation in the normative criteria used to identify a vestibular dysfunction between studies was noted. More specifically, the normative caloric asymmetry ratio used by the different studies reviewed varied between 20 and 30%. This variation seems to be associated with the variation of caloric/vHIT discrepancies. Generally, greater cut-off values are associated with lower discrepancy ratios, and inversely, higher discrepancy ratios are observed with lower cut-off values. Further research should aim at identifying the optimal cut-off values for caloric test and vHIT to improve the accuracy of the discrepancy between these two tests before suggesting this approach as a diagnostic indicator of MD.

Finally, recent evidence reported in this review cannot support the sole use of vHIT in the identification of MD. However, it would be of great interest for future studies to assess the high-frequency VOR fluctuation in seriated measures as opposed to only cross-sectional. Future studies will also need to determine the optimal parameters (gain vs. saccades) and moments of evaluation (ictal vs. outside the ictal). However, for now, vHIT is a valuable complement in the evaluation of MD along with the caloric test as the dissociation between these two tests is a promising indicator in the identification of MD.

AUTHOR CONTRIBUTIONS

BK, MN, and MM reviewed the literature. BK, MN, TM, and MM wrote the paper. All authors discussed the results and implications and commented on the manuscript at all stages.

REFERENCES

1. Merchant SN, Adams JC, Nadol JB. Pathophysiology of Ménière's syndrome: are symptoms caused by endolymphatic hydrops? *Otol Neurotol.* (2005) 26:74–81. doi: 10.1097/00129492-200501000-00013
2. Nakashima T, Pyykkö I, Arroll MA, Casselbrant ML, Foster CA, Manzoor NF, et al. Meniere's disease. *Nat Rev Dis Primers.* (2016) 2:16028. doi: 10.1038/nrdp.2016.28
3. Ishiyama G, Lopez IA, Sepahdari AR, Ishiyama A. Meniere's disease: histopathology, cytochemistry, and imaging. *Ann N Y Acad Sci.* (2015) 1343:49–57. doi: 10.1111/nyas.12699
4. Committee on Hearing and Equilibrium guidelines for the diagnosis and evaluation of therapy in Menière's disease. American Academy of Otolaryngology-Head and Neck Foundation, Inc. *Otolaryngol Head Neck Surg.* (1995) 113:181–5. doi: 10.1016/S0194-5998(95)70102-8
5. Lopez-Escamez JA, Carey J, Chung W-H, Goebel JA, Magnusson M, Mandalà M, et al. Diagnostic criteria for Menière's disease. *J Vestibul Res.* (2015) 25:1–7. doi: 10.3233/ves-150549
6. Ziylan F, Smeeing DPJ, Stegeman I, Thomeer HGXM. Click stimulus electrocochleography versus MRI with intratympanic contrast in Ménière's disease. *Otol Neurotol.* (2016) 37:421–7. doi: 10.1097/mao.0000000000001021
7. Hornibrook J. Tone burst electrocochleography for the diagnosis of clinically certain Meniere's disease. *Front Neurosci.* (2017) 11:301. doi: 10.3389/fnins.2017.00301
8. Maheu M, Alvarado-Umanzor JM, Delcenserie A, Champoux F. The clinical utility of vestibular-evoked myogenic potentials in the diagnosis of Ménière's disease. *Front Neurol.* (2017) 8:415. doi: 10.3389/fneur.2017.00415
9. Strupp M, Feil K, Dieterich M, Brandt T. Bilateral vestibulopathy. *Handb Clin Neurol.* (2016) 137:235–40. doi: 10.1016/b978-0-444-63437-5.00017-0
10. Macdougall HG, Weber KP, Mcgarvie LA, Halmagyi GM, Curthoys IS. The video head impulse test: diagnostic accuracy in peripheral vestibulopathy. *Neurology.* (2009) 73:1134–41. doi: 10.1212/wnl.0b013e3181bacf85
11. Lee S-U, Kim H-J, Choi J-Y, Koo J-W, Yang X, Kim J-S. Evolution in the findings of head-impulse tests during the attacks of Menière's disease. *Otol Neurotol.* (2020) 41:e744–50. doi: 10.1097/mao.0000000000002645
12. Yacovino DA, Finlay JB. Intra-attack vestibuloocular reflex changes in Ménière's disease. *Case Rep Otolaryngol.* (2016) 2016:2427983. doi: 10.1155/2016/2427983
13. Zulueta-Santos C, Lujan B, Manrique-Huarte R, Perez-Fernandez N. The vestibulo-ocular reflex assessment in patients with Ménière's disease: examining all semicircular canals. *Acta Otolaryngol.* (2014) 134:1128–33. doi: 10.3109/00016489.2014.919405
14. Sobhy OA, Elmoazen DM, Abd-Elbaky FA. Towards a new staging of Ménière's disease: a vestibular approach. *Acta Otorhinolaryngol Ital.* (2019) 39:419–28. doi: 10.14639/0392-100x-2461
15. Rey-Martinez J, Burgess AM, Curthoys IS. Enhanced vestibulo-ocular reflex responses on vHIT is it a casual finding or a sign of vestibular dysfunction? *Front Neurol.* (2018) 9:866. doi: 10.3389/fneur.2018.00866
16. Yacovino DA, Schubert MC, Zanotti E. Evidence of large vestibulo-ocular reflex reduction in patients with Menière attacks. *Otol Neurotol.* (2020) 41:e1133–9. doi: 10.1097/MAO.0000000000002746
17. Jerin C, Maxwell R, Gürkov R. High-frequency horizontal semicircular canal function in certain Menière's disease. *Ear Hear.* (2018) 1:128–34. doi: 10.1097/aud.0000000000000600
18. Martinez-Lopez M, Manrique-Huarte R, Perez-Fernandez N. A puzzle of vestibular physiology in a Meniere's disease acute attack. *Case Rep Otolaryngol.* (2015) 2015:460757. doi: 10.1155/2015/460757
19. Halmagyi GM, Curthoys IS. A clinical sign of canal paresis. *Arch Neurol.* (1988) 45:737–9. doi: 10.1001/archneur.1988.00520310043015
20. Weber KP, Aw ST, Todd MJ, McGarvie LA, Curthoys IS, Halmagyi GM. Horizontal head impulse test detects gentamicin vestibulotoxicity. *Neurology.* (2009) 72:1417–24. doi: 10.1212/WNL.0b013e3181a18652
21. Shepard NT, Jacobson GP. The caloric irrigation test. *Handb Clin Neurol.* (2016) 137:119–31. doi: 10.1016/B978-0-444-63437-5.00009-1
22. McCaslin DL, Rivas A, Jacobson GP, Bennett ML. The dissociation of video head impulse test (vHIT) and bithermal caloric test results provide topological localization of vestibular system impairment in patients with "definite" Ménière's disease. *Am J Audiol.* (2015) 24:1–10. doi: 10.1044/2014_AJA-14-0040
23. Oliveira LNDR, Oliveira CLDA, Lopes KDC, Ganança FF. Diagnostic assessment of patients with Meniere's disease through caloric testing and the video-head-impulse test. *Braz J Otorhinolaryngol.* (2019). doi: 10.1016/j.bjorl.2019.10.008. [Epub ahead of print].
24. Rubin F, Simon F, Verillaud B, Herman P, Kania R, Hautefort C. Comparison of video head impulse test and caloric reflex test in advanced unilateral definite Menière's disease. *Eur Ann Otorhinolaryngol Head Neck Dis.* (2018) 135:167–9. doi: 10.1016/j.anorl.2017.08.008
25. van Esch BF, Abolhosseini K, Masius-Olthof S, van der Zaag-Loonen HJ, van Benthem PPG, Bruintjes TD. Video-head impulse test results in patients with Menière's disease related to duration and stage of disease. *J Vestib Res.* (2018) 28:401–7. doi: 10.3233/VES-190654
26. Cordero-Yanza JA, Arrieta Vázquez EV, Hernaiz Leonardo JC, Mancera Sánchez J, Hernández Palestina MS, Pérez-Fernández N. Comparative study between the caloric vestibular and the video-head impulse tests in unilateral Menière's disease. *Acta Otolaryngol.* (2017) 137:1178–82. doi: 10.1080/00016489.2017.1354395
27. Hannigan IP, Welgampola MS, Watson SRD. Dissociation of caloric and head impulse tests: a marker of Meniere's disease. *J Neurol.* (2019). doi: 10.1007/s00415-019-09431-9. [Epub ahead of print].
28. Kitano K, Kitahara T, Ito T, Shiozaki T, Wada Y, Yamanaka T. Results in caloric test, video head impulse test and inner ear MRI in patients with Ménière's disease. *Auris Nasus Larynx.* (2020) 47:71–8. doi: 10.1016/j.anl.2019.06.002
29. Limviriyakul S, Luangsawang C, Suvansit K, Prakairungthong S, Thongyai K, Atipas S. Video head impulse test and caloric test in definite Ménière's disease. *Eur Arch Otorhinolaryngol.* (2020) 277:679–86. doi: 10.1007/s00405-019-05735-8
30. Blödow A, Heinze M, Bloching MB, Von Brevern M, Radtke A, Lempert T. Caloric stimulation and video-head impulse testing in Ménière's disease and vestibular migraine. *Acta Otolaryngol.* (2014) 134:1239–44. doi: 10.3109/00016489.2014.939300
31. Shea JJ Jr. Classification of Menière's disease. *Am J Otol.* (1993) 14:224–9.
32. Bance M, Mai M, Tomlinson D, Rutka J. The changing direction of nystagmus in acute Menieres disease. *Laryngoscope.* (1991) 101:197–201. doi: 10.1288/00005537-199102000-00017
33. Kakigi A, Salt AN, Takeda T. Effect of artificial endolymph injection into the cochlear duct on perilymph potassium. *ORL.* (2009) 71:16–8. doi: 10.1159/000265118
34. Hozawa J, Fukuoka K, Usami S, Ikeno K, Fukushi E, Shinkawa H, et al. The mechanism of irritative nystagmus and paralytic nystagmus. A histochemical study of the guinea pig's vestibular organ and an autoradiographic study of the vestibular nuclei. *Acta Otolaryngol Suppl.* (1991) 481:73–6. doi: 10.3109/00016489109131349
35. Maire R, Van Melle G. Vestibulo-ocular reflex characteristics in patients with unilateral Ménière's disease. *Otol Neurotol.* (2008) 29:693–8. doi: 10.1097/mao.0b013e3181776703
36. Sugimoto S, Yoshida T, Teranishi M, Kobayashi M, Shimono M, Naganawa S, et al. Significance of endolymphatic hydrops herniation into the semicircular canals detected on MRI. *Otol Neurotol.* (2018) 39:1229–34. doi: 10.1097/mao.0000000000002022
37. Hullar TE, Minor LB. High-frequency dynamics of regularly discharging canal afferents provide a linear signal for angular vestibuloocular reflexes. *J Neurophysiol.* (1999) 82:2000–5. doi: 10.1152/jn.1999.82.4.2000
38. Hullar TE. Responses of irregularly discharging chinchilla semicircular canal vestibular-nerve afferents during high-frequency head rotations. *J Neurophysiol.* (2005) 93:2777–86. doi: 10.1152/jn.01002.2004
39. Mccall AA, Ishiyama GP, Lopez IA, Bhuta S, Vetter S, Ishiyama A. Histopathological and ultrastructural analysis of vestibular endorgans in Meniere's disease reveals basement membrane pathology. *BMC Ear Nose Throat Disord.* (2009) 9:4. doi: 10.1186/1472-6815-9-4
40. Mcgarvie LA, Curthoys IS, Macdougall HG, Halmagyi GM. What does the dissociation between the results of video head impulse versus

caloric testing reveal about the vestibular dysfunction in Ménière's disease? *Acta Otolaryngol.* (2015) 135:859–65. doi: 10.3109/00016489.2015.1015606

41. Fukushima M, Oya R, Nozaki K, Eguchi H, Akahani S, Inohara H, et al. Vertical head impulse and caloric are complementary but react opposite to Meniere's disease hydrops. *Laryngoscope.* (2019) 129:1660–6. doi: 10.1002/lary.27580
42. Nevoux J, Barbara M, Dornhoffer J, Gibson W, Kitahara T, Darrouzet V. International consensus (ICON) on treatment of Ménière's disease. *Eur Ann Otorhinolaryngol Head Neck Dis.* (2018) 135:S29–32. doi: 10.1016/j.anorl.2017.12.006

Conflict of Interest: The authors declare that the research was conducted in the absence of any commercial or financial relationships that could be construed as a potential conflict of interest.

frontiers in Neurology

HYPOTHESIS AND THEORY
published: 10 November 2020
doi: 10.3389/fneur.2020.576860

Mal de Debarquement Syndrome: A Matter of Loops?

Viviana Mucci[1,2]*, *Iole Indovina*[2,3], *Cherylea J. Browne*[1,4], *Franco Blanchini*[5], *Giulia Giordano*[6], *Lucio Marinelli*[7,8] and *Bruno Burlando*[9]

[1] School of Science, Western Sydney University, Penrith, NSW, Australia, [2] Laboratory of Neuromotor Physiology, Istituto di Ricovero e Cura a Carattere Scientifico Fondazione Santa Lucia, Rome, Italy, [3] Department of Biomedical and Dental Sciences and Morphofunctional Imaging, University of Messina, Messina, Italy, [4] Translational Neuroscience Facility, School of Medical Sciences, UNSW Sydney, Sydney, NSW, Australia, [5] Department of Mathematics, Computer Science and Physics, University of Udine, Udine, Italy, [6] Department of Industrial Engineering, University of Trento, Trento, Italy, [7] Department of Neuroscience, Rehabilitation, Ophthalmology, Genetics, Maternal and Child Health (DINOGMI), University of Genova, Genova, Italy, [8] Division of Clinical Neurophysiology, Department of Neurosciences, Istituto di Ricovero e Cura a Carattere Scientifico (IRCCS) Ospedale Policlinico San Martino, Genova, Italy, [9] Department of Pharmacy, University of Genova, Genova, Italy

OPEN ACCESS

Edited by:
Michael Strupp, Ludwig Maximilian University of Munich, Germany

Reviewed by:
Sung-Hee Kim, Kyungpook National University, South Korea
Takeshi Tsutsumi, Tokyo Medical and Dental University, Japan
Floris Wuyts, University of Antwerp, Belgium
Andreas Sprenger, University of Lübeck, Germany

***Correspondence:**
Viviana Mucci
viviana.mucci@gmail.com

Specialty section:
This article was submitted to Neuro-Otology, a section of the journal Frontiers in Neurology

Received: *27 June 2020*
Accepted: *05 October 2020*
Published: *10 November 2020*

Citation:
Mucci V, Indovina I, Browne CJ, Blanchini F, Giordano G, Marinelli L and Burlando B (2020) Mal de Debarquement Syndrome: A Matter of Loops? Front. Neurol. 11:576860. doi: 10.3389/fneur.2020.576860

Introduction: Mal de Debarquement Syndrome (MdDS) is a poorly understood neurological disorder affecting mostly perimenopausal women. MdDS has been hypothesized to be a maladaptation of the vestibulo-ocular reflex, a neuroplasticity disorder, and a consequence of neurochemical imbalances and hormonal changes. Our hypothesis considers elements from these theories, but presents a novel approach based on the analysis of functional loops, according to Systems and Control Theory.

Hypothesis: MdDS is characterized by a persistent sensation of self-motion, usually occurring after sea travels. We assume the existence of a neuronal mechanism acting as an oscillator, i.e., an adaptive internal model, that may be able to cancel a sinusoidal disturbance of posture experienced aboard, due to wave motion. Thereafter, we identify this mechanism as a multi-loop neural network that spans between vestibular nuclei and the flocculonodular lobe of the cerebellum. We demonstrate that this loop system has a tendency to oscillate, which increases with increasing strength of neuronal connections. Therefore, we hypothesize that synaptic plasticity, specifically long-term potentiation, may play a role in making these oscillations poorly damped. Finally, we assume that the neuromodulator Calcitonin Gene-Related Peptide, which is modulated in perimenopausal women, exacerbates this process thus rendering the transition irreversible and consequently leading to MdDS.

Conclusion and Validation: The concept of an oscillator that becomes noxiously permanent can be used as a model for MdDS, given a high correlation between patients with MdDS and sea travels involving undulating passive motion, and an alleviation of symptoms when patients are re-exposed to similar passive motion. The mechanism could be further investigated utilizing posturography tests to evaluate if subjective perception of motion matches with objective postural instability. Neurochemical imbalances that would render individuals more susceptible to developing MdDS could be investigated through hormonal profile screening. Alterations in the connections between vestibular nuclei and cerebellum, notably GABAergic fibers, could be explored by

neuroimaging techniques as well as transcranial magnetic stimulation. If our hypothesis were tested and verified, optimal targets for MdDS treatment could be found within both the neural networks and biochemical factors that are deemed to play a fundamental role in loop functioning and synaptic plasticity.

Keywords: mal de debarquement syndrome, brain derived neurotrophic factor, calcitonin gene related peptide, functional loops, synaptic plasticity, systems and control theory

INTRODUCTION

Mal de Debarquement Syndrome is a condition characterized by a subjective sensation of self-motion (i.e., rocking, swaying, bobbing), which persists after an initial exposure to passive motion, usually after sea travel but occasionally after air or overland trips. Commonly, many people report this condition in its temporary form, "*Mal de Debarquement*" (MdD), with symptoms usually subsiding within 48 h, or in the worse cases a few weeks (1). However, a small subset of these individuals do not recover, and experience chronic symptoms for months, up to years, after the initial onset due to passive motion exposure, thus developing "*Mal de Debarquement Syndrome*" (MdDS) (2). The prevalence of the syndrome in the population is currently unknown, while a neurotology clinic survey reported that 1.3% of patients were diagnosed annually (3). Despite the lack of precise epidemiological data, MdDS is considered a rare pathological condition with associated psychosocial and economic impacts (4). In addition to its most recognized primary symptoms (i.e., chronic self-motion perception and postural instability), there are a series of secondary symptoms such as brain fog, migraine, visual sensitivity, and associated mood disorders (4). The underlying pathophysiology is still not clear; consequently, there are limited therapeutic and experimental options. In addition to this, low awareness regarding MdDS in the medical community has contributed to high misdiagnosis rates (4, 5), which potentially increases the perceived rarity of the condition.

Emerging research has concluded that the typical contemporaneous MdDS patient is female (though MdDS has been reported in males, the current female to male ratio is 8:2) (6), in the 5–6th decade of life, having been exposed to passive motion, usually cruise ship travels (7). As mentioned, the onset cause of the condition, in a typical MdDS patient is related to the exposure to passive motion and symptoms began after disembarking; those triggered in this way are termed Motion-Triggered (MT) MdDS patients. Interestingly, a similar symptom profile can also be present in individuals that cannot attribute their symptom onset to a passive motion exposure, but rather to a non-motion trigger (non-motion triggered onset MdDS). These cases without any clear trigger are also referred to as Spontaneous Onset (SO) MdDS (4). The classification of SO MdDS remains under review. SO MdDS may be re-classified to come under another central vestibular disorder called Persistent Postural-Perceptual Dizziness (PPPD) (8), given that these two disorders present overlapping symptoms. The distinguish feature so far identified between SO-MdDS and PPPD is that individuals with PPPD do not report the typical temporal relief of symptoms described by patients with MdDS when re-exposed to passive motion (*e.g., being passenger in a driving vehicle*). Thus, this partial and temporal alleviation from symptoms when re-exposed to passive motion has now been described as a key feature in identifying MdDS patients (4). Thus, more research is needed to assess the possibility that SO MdDS and MT MdDS include similar symptom manifestation of differing underlying pathophysiological mechanisms. The theory presented in this manuscript will solely focus on MT MdDS, indicated hereafter as "MdDS" in this manuscript.

A series of hypotheses have been formulated to explain the pathogenesis of this condition. It has been proposed that MdDS is the result of Vestibular Ocular Reflex (VOR) maladaptation (9), involving velocity storage (VS), a central vestibular mechanism that increases the time constant of the VOR with respect to that of semicircular canal (SCC) afferents. In this hypothesis, the authors propose that a cross-axis-coupled stimulus (e.g., roll while pitching, a type of stimulation that can be experienced by passengers on a boat) may alter the VS of the VOR (9). The VS circuit is thought to be located in vestibular-only (VO) neurons, which are found in the medial and superior vestibular nuclei (VN) of the brainstem (10), and has been investigated in non-human primates (11). This study demonstrated that monkeys without VS, and thus having a very short VOR time constant, did not develop abnormal responses to roll while rotating. A similar mechanism was hypothesized to be present in humans (9). VO neurons are γ-aminobutyric acid (GABA) neurons and their axons decussate in the brainstem, where information is then projected to the reticulospinal and vestibulospinal pathways (12).

Cohen and colleagues proposed that the cause for the appearance of MdDS symptoms could potentially be a maladaptive response to the typical oscillatory frequencies experienced during air or sea navigation, which ranges between 0.2 and 0.3 Hz, and activates the lower limbs into compensatory rocking and swaying movements for balance maintenance (13). In MdDS, VO neurons, on both sides of the brainstem, are theorized to persistently oscillate at these frequencies after disembarking (9), and these oscillations may have originated in the nodulus of the vestibulocerebellum, which has control over the VS (9, 13, 14). Indeed, such activity was observed in the nodulus of the rabbit (15), suggesting that a similar mechanism may be possible and present in humans. Moreover, additional symptoms which are a part of MdDS manifestations, such as brain fog, anxiety, depression, and sensitivity to sound and light, may be the result of the inability to "turn off" these incessant oscillations (9). Cortical changes also seem to contribute to MdDS (16). In particular it has been

theorized that MdDS is a disorder of the central mechanism that generates a memory for an internal representation of passive movement (17). Accordingly, in MdDS patients a decrease in functional connectivity has been reported in different brain regions, including visual-vestibular processing areas (e.g., middle temporal visual area [V5]), the brain's default mode network (that includes the cingulate cortex), somatosensory network (including the postcentral gyrus), and central executive network including the dorsolateral prefrontal cortex (2, 17, 18). Resting-state functional Magnetic Resonance Imaging (fMRI) studies have also shown variations in functional connectivity involving the left entorhinal cortex (EC)/amygdala, with increased connectivity to posterior visual and vestibular processing areas, and decreased connectivity to multiple prefrontal areas (17). Also, high-density Electroencephalogram (EEG) studies have shown that MdDS patients have a higher synchronicity during periods of higher symptom severity, specifically in vestibular projections to the limbic system (1, 19). While abnormalities in the limbic system are correlated to abnormal motion perception (17, 18), the EC is known to also play a role in keeping the hippocampus active during sleep for memory consolidation (20). This has been hypothesized as why in some MdDS patients symptoms present after a night's sleep and not immediately after landing/disembarking (2, 16). Following this hypothesis, a series of experimental treatment protocols have been developed to treat MdDS sufferers with the use of neuromodulation techniques targeting these regions (21, 22).

In addition to neutrally-centered hypotheses, which may not be mutually exclusive, a new hypothesis was formulated which proposed that gonadal hormones may influence MdDS pathophysiology (7). Correlations between MdDS and hormonal factors have been reported, driven by the fact that MdDS patients are mostly females and that the average onset age matches with the perimenopausal phase (23). It is known that hormones play an important role in various vestibular pathologies such as vestibular migraine, and Meniere's disease (24), and that there are correlations between hormonal fluctuations and various inner ear symptoms such as vertigo, instability, tinnitus, hearing loss and intra-aural pressure (25). Additionally, it is well-known from animal studies and human clinical data that hormonal changes also influence neurochemical pathways that are linked to depression (26). As for migrainous patients, a recent pilot study showed that pregnant MdDS patients reported an alleviation of symptoms during the first two trimesters (27). Following these preliminary observations, hormones were theorized to play a role in aggravating patient symptoms as well as in rendering an individual more susceptible to developing the disorder *per se* (7, 23). Specifically, it was theorized that patients who developed MdDS may have had, at the time when onset occurred, significant decreases in estrogen levels which altered their GABAergic system, as well as Calcitonin Gene-Related Peptide (CGRP) levels (7). Recently, CGRP has been implicated in the pathophysiology of migraine and depression, which are also comorbidity factors of MdDS (2, 7, 28). It is known to support vestibular function and, more specifically, to strengthen the VOR (29, 30). Accordingly, CGRP positive neurons have been found in VN and the vestibulocerebellum (30). In addition, CGPR could be overlooked for its role in neuroplasticity, e.g., influencing neurotransmitters such as the brain-derived neurotrophic factor (BDNF) (31, 32). Despite the above hypotheses, knowledge about the comprehensive mechanisms of MdDS is still lacking, thereby hindering the possibility of developing resolutive treatments for the condition. Therefore, this manuscript aims to combine the relevant aspects and ideas from these theories and review them within a theoretical model based on **Systems and Control Theory**. This is an interdisciplinary field combining mathematics and engineering to study the functioning and the emergent behavior of systems arising both in nature and in engineering. Although most of its subsequent developments are aimed at designing and managing human-made systems, such as processes and machines, the discipline was originally inspired by the study of living processes and is particularly well-suited to model and analyse phenomena in physiology and biology (33). One of the main topics of Systems and Control Theory is the study of feedback loops that accomplish a specific function. Accordingly, our hypothesis provides a pathophysiological mechanism of MdDS involving the interaction of functional loops at various levels, including neural networks and intracellular biochemical pathways.

THE HYPOTHESIS

Our model is based on the hypothesis that, to ensure adaptation to an external oscillatory stimulus, an internal oscillatory behaviors must be activated by a neural network (34). The internal generation of oscillatory behaviors most likely relies on a loop-based arrangement, due to the presence of negative feedback loops containing inhibitory interactions (35). Specifically, our hypothesis relies on **Systems and Control Theory,** whose mathematical formalism was mainly developed in engineering but has been widely applied to biological systems since its origin (33, 36). Following this Theory, a perfect adaptation to an external periodic perturbation (*like a wave*), can only occur thanks to the activation of an "internal model" that cancels the perturbation. In our case, the internal model is a neuronal oscillator that generates a signal of the same type but opposing the forcing input (37). According to this fundamental principle, it could be hypothesized that what has been previously described as the presence of a brain oscillator in MdDS may be part of this mechanism (2). Hence, MdDS could be the pathological permanence of such a compensatory mechanism, after the external perturbation has vanished.

However, no clear evidence is available about the neural site of this hypothetical oscillator. In the first theory described previously, MdDS pathophysiology is attributed primarily to the VN in the brainstem, receiving input from SCC and generating vestibulo-ocular, vestibulocollic, vestibulospinal, and vestibulo-thalamo-cortical pathways (13). As already mentioned, it has been proposed that MdDS is driven by an oscillation between VO neurons on each side of the brainstem at frequencies of 0.2–0.3 Hz, controlled by output from cerebellar nodular neurons (13, 38). Interestingly, similar oscillatory behavior has been experimentally induced in the vestibulocerebellum of rabbits

through a rolling about the longitudinal axis (15). In these experiments, 5% of climbing fibers in the uvula and nodulus started firing periodically at the same frequency after the sinusoidal vestibular stimulation had stopped, persisting for 200–300 s (15). Although obtained in animal studies, these results were believed to provide a potential neural basis for oscillations at 0.2 and 0.3 Hz manifesting as rocking, swaying, and bobbing in MdDS patients (13, 14, 39).

Besides identifying a brain oscillator, in order to understand the pathogenesis of MdDS a mechanism converting the adaptation to environmental oscillations into a permanent noxious condition must be found. According to Systems and Control Theory, positive loops are a common distinctive feature of multi-stationary systems that can undergo transitions among different equilibrium points (35, 40). These kinds of transitions are thought to operate also in processes of pathogenesis, and therefore, the identification of a positive loop could be a key step in the understanding of MdDS onset. As shown below, we identify this multi-stationary positive loop with an intracellular biochemical pathway involved in synaptic rearrangement.

Biomechanical Analysis

In order to formulate a hypothesis regarding the mechanisms implicated in MdDS pathophysiology, we first consider a biomechanical analysis of body posture from the standpoint of **Systems and Control Theory**.

The considered mechanical system that governs body posture, labeled as **P** in **Figure 1**, is composed of two loops:

- One, labeled as **C** in **Figure 1**, is the well-studied **stabilizing posture control mechanism** (41, 42), whose function is of ensuring the correct angle (the angle between main body axis and gravity axis).
- The second, labeled as **A** in **Figure 1**, which we consider as the **adaptation mechanism,** has the function of adapting the posture in the presence of a persistent sinusoidal disturbance (wave motion, craft fluctuations, or similar).

Both the stabilization loop **C** and the adaptation loop **A** are **negative loops** (having one inhibitory step) because their action is in **opposition**, respectively, to destabilizing gravity and to the external disturbance signal. The following considerations are based on well-known physical laws.

In addition to this, in order to fully understand the loop theory, few more points must be considered:

- The **stabilization loop C** must compensate the discrepancies between the position, the posture angle, and the angular speed, namely the derivative of the angle. For doing this, the stabilization loop requires a feedback of the proportional-derivative type, which compensates for both posture and angle errors and their derivatives.
- The **adaptation loop A** is activated to ensure perfect adaptation. For example, it is able to cancel a persistent disturbance whenever it comes into play.
- **Perfect (or semi-perfect) adaptation** requires the generation of a signal **that cancels the** external disturbance, hence it needs to have the same frequency as the disturbance, but needs to be in phase opposition, so that the sum of the two signals is almost zero.
- To be synchronized with the disturbance (in particular, in phase opposition), the compensating signal must be generated by a **feedback loop,** otherwise it is impossible to robustly generate a signal of the same frequency and synchronization.
- To achieve perfect adaptation, the **adaptation loop** must therefore include an oscillator capable of producing a signal having the same frequency as the external disturbance, an assertion supported by the Internal Model Principle (37, 43). Remarkably, the idea of an internal model has been invoked also for MdDS and firstly mentioned by Hain and Helminski (44).

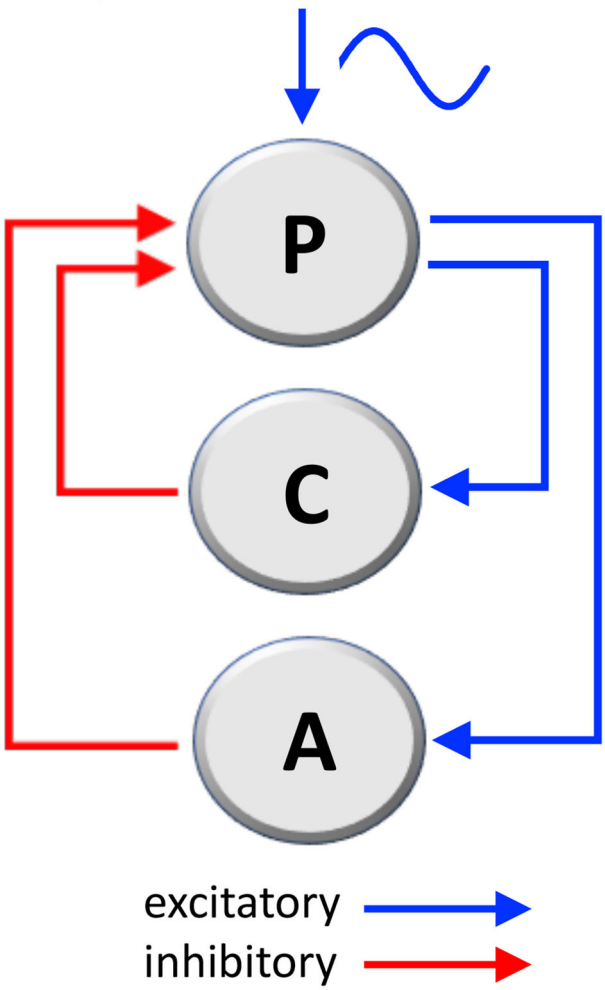

FIGURE 1 | Mechanical loops involved in the stabilization of body's posture and the adaptation to a periodic disturbance, such as passive environmental movements experienced by travelers aboard. P, posture mechanism; C, posture-stabilizing feedback control; A, adaptation mechanism (C and A are negative feedback loops; see **Supplementary Materials** for a mathematical analysis).

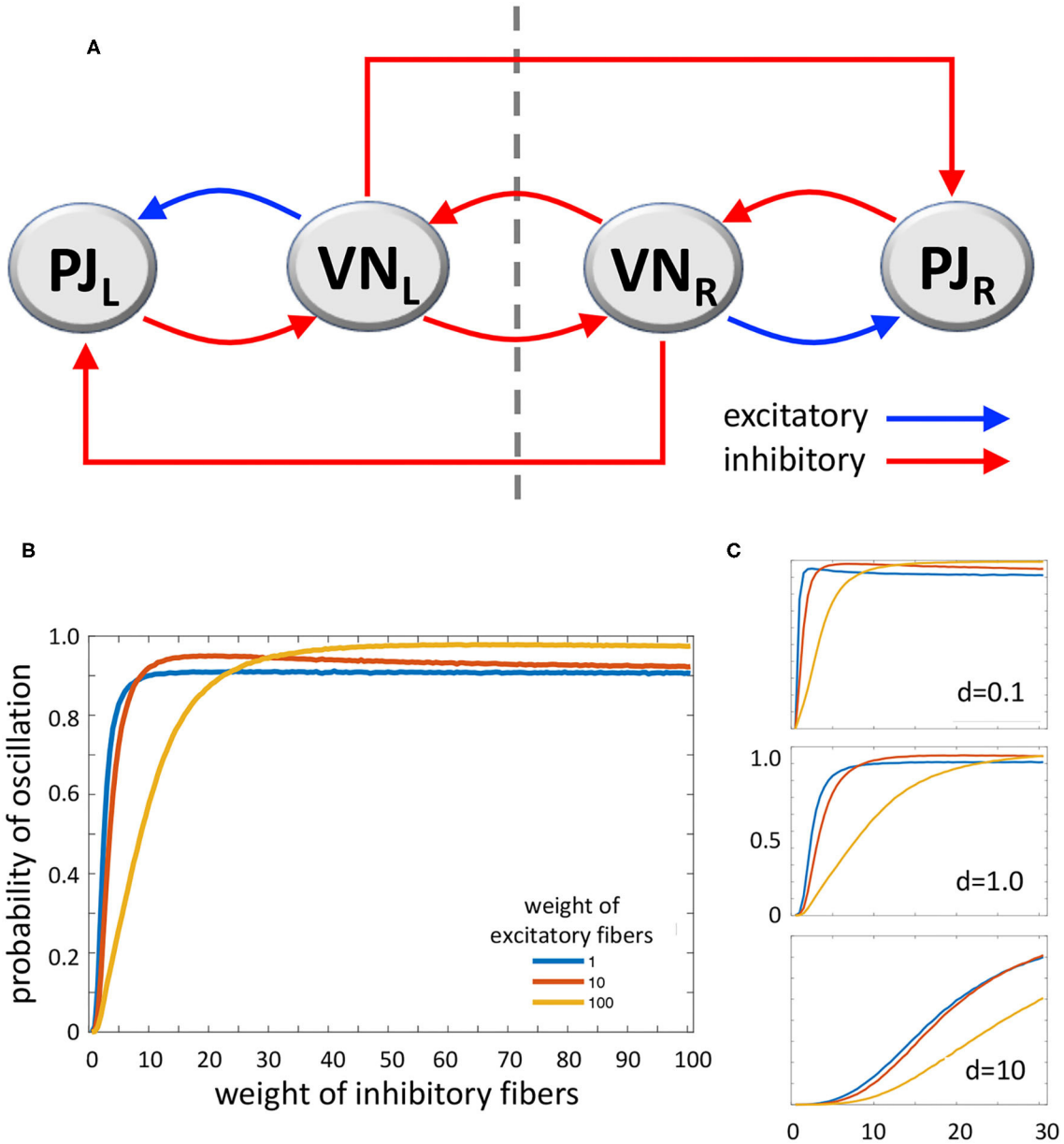

FIGURE 2 | (A) Diagram of the loop system envisaged for vestibulocerebellar neural circuits, consisting of two ipsilateral negative loops, a central, contralateral, double-negative loop, and two contralateral vestibulocerebellar connections. PJ, Purkinje cell; VN, vestibular nuclei; R and L, subscripts refer to right and left sides of the brainstem; dashed line, brainstem midline. **(B)** MatLab analysis of the above system yielding the probability of oscillation (i.e., the fraction of Jacobian matrices associated to the loop system with positive-real-part complex eigenvalues, out of 100,000 randomly generated Jacobian matrices). The curves represent the variation of oscillation probability when the weight of inhibitory connections varies in the range 1–100, in arbitrary units, and the weight of excitatory connections is 1 (blue curve), 10 (red curve), and 100 (yellow curve). The weight of self-inhibitory connections (matrix diagonal entries) is always set to 1. **(C)** Probability of oscillation calculated as above, when the weight of inhibitory connections varies in the range 1–30, the weight of excitatory connections is 1 (blue), 10 (red), and 100 (yellow), and the weight of self-inhibitory connections (d) is 0.1 (top), 1.0 (middle), and 10 (bottom). Plot axes as in B.

Within our hypothesis, if the external signal is removed (disembarking), then the oscillator in the adaptation loop **A** could remain active for a time under normal conditions, or for longer time under pathological status (when developing MdDS). This oscillator is not capable of destabilizing the posture, since the main stabilizing loop **C** prevails. Yet, the effect of the oscillator persists in generating phantom sensations, possibly at a frequency very close to the initial forcing disturbance. This phenomenon manifests in the patients as a sensation of self-motion (*bobbing, swaying and rocking*). The mathematical description of the above loop system can be found as **Supplementary Materials**.

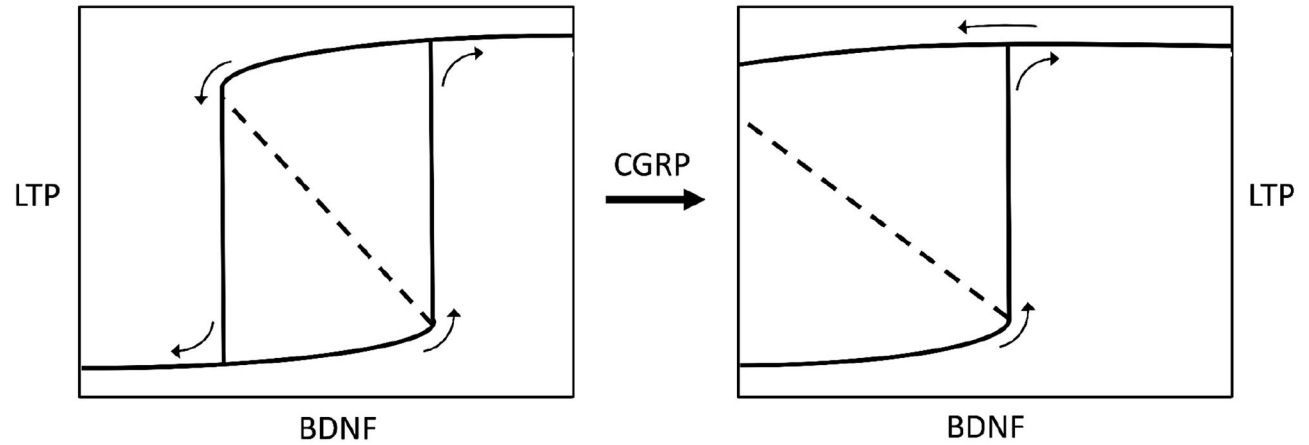

FIGURE 3 | Bistable hysteretic model of synaptic plasticity depicted by a stimulus-response curve. The stimulus is represented by variations of brain-derived neurotrophic factor levels (BDNF) in the central nervous system. The response is a biochemical pathway arranged as a positive loop (not shown here) leading to synaptic long-term potentiation (LTP), according to Hao et al. (68). If the loop has a lower strength (left chart) the stimulus-response curve shows a bifurcation generating bistability and hysteresis. Bistability means the occurrence of two equilibrium points, i.e., low or high (excess) LTP. Hysteresis means that for some given values of BDNF there are two possible values of LTP, and the status assumed by the system will depend on its previous history, i.e., it will be low LTP for increasing BDNF, or high LTP for decreasing BDNF (see small arrows on charts). If the BDNF-induced, biochemical positive loop that produces LTP is progressively strengthened by calcitonin gene-related peptide (CGRP), the bistability region widens until hysteresis switches to irreversibility (right chart), meaning that once LTP is developed, after BDNF rise, it becomes permanent even if BDNF decreases to zero. The model has been envisaged according to data reported by Buldyrev et al. (31). Small arrows on charts indicate the evolution of the system for increasing or decreasing BDNF values.

Physiological Analysis

We consider now the possibility of establishing a link between the **mechanical loop system** of **Figure 1** and **vestibular neural networks**, by using a neuroanatomical representation.

In the mechanical loop system, the **stabilization loop C** can be easily matched to a postural reflex that corrects postural bias. This element can be identified with vestibulocollic (VCR) and vestibulospinal (VSR) reflexes that are realized by VN and induce compensatory movements maintaining head and postural stability and preventing falls (45). The VCR and VSR involve SCC, otolith, neck proprioception, and visual afferences to the VN, where they become processed through commissural inhibition and ipsilateral integration and filtering (46, 47). One mechanism involved in the processing and fine-tuning of the final reflexes is the VS mechanism, which is particularly relevant when considering head rotation movements (angular acceleration). This mechanism is believed to prolong the SCC afferent signal, by extending the VOR time constant with respect to the SCC signal time constant, and then improving compensatory responses to low-frequency rotations of the head (48, 49). Similarly to this, there is another mechanism (gravity estimator) which processes linear acceleration movements, by integrating SCC and otolith inputs, and estimates head tilt (50). Both mechanisms act as integrators provided with negative loops avoiding error accumulation due to afferent signal noise (50).

A correspondence between these mechanisms and vestibular pathways can be found in the scheme proposed by Galiana and Outerbridge for bilateral VOR pathways in the cat (51). This scheme shows a commissural inhibitory circuit between the two contralateral VN, which is connected on each side to two ipsilateral circuits spanning between VN and the cerebellum. According to the viewpoint of Systems and Control Theory, the central commissural circuit is a double negative loop, i.e., it has an even number of inhibitory steps (two) and therefore it is a candidate multi-stationary system with at least two stable equilibrium points. The two lateral elements are negative loops, i.e., they have an odd number of inhibitory steps (one) and therefore they are candidate oscillators (35, 40). These circuits could be at least partially overlapped with vestibular networks that are regarded to be relevant in MdDS pathophysiology, such as VOR and VS. Specifically, the external negative loops could correspond to the noise correction mechanisms described for the integrators of SCC and otolith afferences, while it is known that cutting the commissural fibers connecting the contralateral VN permanently destroys the VS mechanism (52).

According to Systems and Control Theory, a model which includes a **triple loop chain** with a core positive loop flanked by two negative loops could generate oscillations upon alternate stimulation of the two sides. The two lateral negative loops, behaving as oscillators, would induce the central loop to toggle between its two stable states (53) (**Figure 2A**). However, VN also project as GABAergic fibers to the inferior olive that in turn projects as glutamatergic climbing fibers to the contralateral cerebellar flocculonodular lobe, altogether realizing contralateral inhibitory pathways (54). Mossy fibers are also derived from VN to cerebellum, which could participate to the network; however, experimental recording of periodical firing at the same frequency of sinusoidal vestibular stimulation was recorded in climbing fibers (see above) (15). The complete system (**Figure 2A**), consisting of the triple loop discussed above with the further addition of two contralateral inhibitory connections, can still produce oscillations, depending on the values of the parameters

that regulate the interactions among the elements of the system. Therefore, a main role in the tendency to oscillate could be played by the relative strength of excitatory and inhibitory pathways.

In order to evaluate the capability of this system to yield sustained oscillations, we studied it by using MatLab (*The MathWorks, Inc., Natick, MA, USA*). We computed the oscillation probability as a function of the strength of excitatory and inhibitory pathways. In particular, given the graph in **Figure 2A**, with the addition of stabilizing self-inhibitions for each functional agent, we randomly generated instances of the associated Jacobian matrix (see **Supplementary Materials**):

$$J = \begin{bmatrix} -\alpha & \mu & -\nu & 0 \\ -\kappa_1 & -\beta & -\sigma & 0 \\ 0 & -\varphi & -\gamma & -\kappa_2 \\ 0 & -\tau & \xi & -\delta \end{bmatrix} \quad (1)$$

where each non-zero entry, denoted by a Greek letter, is generated as a random number with absolute value between 0 and 1, multiplied by a scaling coefficient that can be chosen differently for: (i) diagonal entries associated with self-inhibitory connections ($\alpha, \beta, \gamma, \delta$), (ii) entries associated with excitatory connections (μ, ξ), and (iii) entries associated with inhibitory connections ($\nu, \kappa_1, \sigma, \varphi, \kappa_2, \tau$), so as to modulate their relative strength. Then, we computed the eigenvalues of each randomly generated Jacobian matrix *J*, to evaluate the fraction of Jacobian matrices having strictly complex eigenvalues with positive real part; the presence of this type of eigenvalues is associated with persistent oscillations. **Figure 2B** shows the probability of oscillation (*precisely, the fraction of matrices with positive-real-part complex eigenvalues out of 100,000 randomly generated matrices*) when (i) the weight of self-inhibitory connections is set to 1 in arbitrary units, (ii) the weight of inhibitory connections grows from 1 to 100, and (iii) the weight of excitatory connections is chosen as 1 (*blue curve*), 10 (*red curve*) and 100 (*yellow curve*). In **Figure 2C** the same curves are shown, with the weight of inhibitory connections growing from 1 to 30, and the weight of self-inhibitory connections (*i.e., the matrix diagonal entries*) set to 0.1, 1.0, and 10.

The results of our numerical study show that, if the **strength of inhibitory connections** is low (*i.e. their weight equals about 0–20 in arbitrary units*), the tendency to produce contralateral oscillations is inversely correlated with the strength of excitatory connections. Conversely, if the strength of inhibitory connections is intermediate (*about 20–40*), then the tendency to produce oscillations is high and almost independent of the strength of excitatory connections. Finally, if the **strength of inhibitory connections is high** (*about 40–100*) **the effect of excitatory connections is reversed, since higher values of the latter induce a higher tendency to produce oscillations** (**Figure 2B**). As for the role of self-inhibitory connections *(i.e., the matrix diagonal entries, associated with weight d*), **Figure 2C** shows that oscillations are more likely when the strength of these connections is lower (*as expected, given their stabilizing effect*); however, irrespective of their strength, the trend of the curves is always qualitatively similar (*in **Figure 2C** plots, the axes and the curve colors have the same meaning as in **Figure 2B***). Taken together, these data show that our loop system can generate oscillations, and moreover, the tendency to oscillate increases together with the increasing strength of inhibitory connections, reaching its highest when both inhibitory and excitatory connections are strong.

Given its ability to realize oscillations, the loop system depicted in **Figure 2A** could be hypothesized to be the **adaptation loop A,** i.e., the internal model, of the mechanical loop system (**Figure 1**). Specifically, during adaptation to external stimulation, the circuit alternatively activates and inhibits VN neurons located on the right and left side of the brainstem. This model of course is a simplified schematic representation of the actual neural networks, while other components could contribute to the adaptive mechanism. For instance, in agreement with studies on the role of efference copy and feed-forward loop in postural adaptation to environmental disturbance (55), a feed-forward loop could help make the system faster and more accurate. However, the feedback loop system is to be considered the key component of the oscillator.

Active Scenario

Having this basis aforementioned, we are now able to consider the passive motion and environmental stimuli (active scenario). In the presence of an oscillatory movement, where the individual is exposed to passive motion, such as being passenger in a boat or plane, the VN are stimulated from side to side by their various afferents, i.e., vestibular sensors, proprioceptors, and visual inputs. This stimulation corresponds to the sinusoidal external disturbance applied to the mechanical loop system (***Figure 1***). If the **adaptation A (internal model)** circuit were absent, the **stabilization C (postural reflex)** circuit would continuously stimulate the proprioceptors and the muscle tone to correct the posture. However, we assume that the **adaptation loop** becomes entrained by this kind of external stimulation, thereby undergoing an oscillatory behavior that cancels the environmental stimulation and abolishes the need of postural correction. This scenario fits the previously commented assumption that in ship travelers VO neurons are entrained to oscillate at frequencies of about 0.2–0.3 Hz, (under control of cerebellar nodulus neurons) (38). Hence, in this scenario the individual exposed to passive motion is going through natural adaptation and compensatory mechanisms of passive motion.

Thereafter, when the individual is disembarking (returning to a stable environment), the oscillatory external stimulus ceases, and the **adaptation loop** system is expected to stop its compensatory work. However, it can be shown through mathematical analysis (see **Supplementary Materials**) that the adaptation mechanism has poorly damped oscillations for a reasonably wide range of its parameters, possibly explaining the above-mentioned, temporary MdD condition that can be experienced after a ship travel. Conversely, in MdDS the adaptation loop seems to persist beyond any possible delayed damping, thus becoming a permanent oscillator that provides an undesired input to the **stabilization mechanism**. Consequently, this creates a sensation of postural unbalance (phantom sensation of bobbing, rocking, swaying). This interpretation of MdDS seems confirmed by the notion that patients report a feeling

of **phantom motion** when in a stable environment (*e.g., on land*), but they find a temporal relief while re-exposed to passive motion. This would happen by being re-exposed to the dominant frequencies of their postural swaying that match fairly with passive motion (*around 0.2–0.3 Hz*) (4).

Hence, a remaining open question concerns the causes of the over-synchronization affecting the neural network that generates MdDS. The mathematical analysis of our neural loop system shows that the tendency to oscillate increases for increasing strength of inhibitory pathways, while it reaches its maximum when the strength of both inhibitory and excitatory pathways is high. Such a result strongly suggests that the **over-synchronization of the internal oscillator may be found in synaptic plasticity** (56), which can induce variations of connection strength in the neural loop system. Most notably, a typical example of this kind of neuronal rearrangement is long-term potentiation (**LTP)** (57). Synaptic plasticity has been shown to occur in Purkinje cells of the flocculonodular cerebellum, as well as in their interconnected vestibular circuit (58, 59). Hence, it can be hypothesized that LTP may occur in these neurons during passive motion (*e.g., when in/on a vehicle*), due to continuous, alternate stimulations from sensory inputs. The distinction between MdD (*rapid healing)* and MdDS (*recalcitrant healing*), could be due to differences in the strength of synaptic plasticity. Therefore, excess synaptic plasticity could be the essential element that switches a physiological mechanism (*internal model*) into a pathological condition.

The involvement of excessive synaptic plasticity has been reported for various disorders, e.g., diminished LTP and long term depression (LTD) in schizophrenia (60), dopamine-driven synaptic facilitation in drug addiction (61), or unbalanced excitatory and inhibitory stimuli on fusiform cells of the dorsal cochlear nuclei in tinnitus (62). Even closer to MdDS, maladaptive cortical plasticity is involved in the pathophysiology of focal dystonia, such as writer's cramp and spasmodic torticollis, where repetitive sensory input reaches cortical sensory areas that show excessive plastic adaptation characterized by increased motor output, excessive muscle contractions, abnormal postures, and involuntary movements (63–66). Similarly, we suggest that in MdDS abnormal plasticity occurs in vestibular and Purkinje neurons. This is strongly supported by the above results from MatLab computational analysis of the loop system modeling the vestibulocerebellar connections in the brainstem. These findings show that an increase in the strength of inhibitory connections renders the loop more incline to oscillate, suggesting that excess LTP in GABAergic fibers could strengthen the vestibulocerebellar oscillator, thus rendering it recalcitrant to vanish when the environmental stimulus ceases (*stable environment*).

If excess synaptic plasticity is responsible for the insurgence of MdDS, we have now to explain why it occurs in some individuals at a certain time. Taking this into account, we aim at a unifying paradigm between vestibular sensory processing and Systems and Control Theory, according to the approach advocated by Burlando (67). Based on this theoretical view, a transition from health to disorder can be always reconducted to a positive loop showing a bifurcation that creates the possibility of shifting from one steady state equilibrium point to another one. Interestingly, LTP has been described as a shift in gene expression due to the activity of a biomolecular positive loop undergoing bifurcation (68). Moreover, a relevant property of dynamic systems showing bifurcation and bistability is hysteresis, meaning that it is easier to maintain the system in one stable state, or equilibrium point, than to make it jump to another stable state by applying or removing a stimulus. In addition, if the strength of the positive loop increases, the system develops irreversibility, i.e., the impossibility of returning to a former equilibrium point by complete removal of the stimulus (69). It has been shown that different cellular and biomolecular processes can be modeled through bistability and hysteresis (70), while positive feedback loops are starting to be taken into consideration also for mechanisms of pathogenesis (e.g., Alzheimer's' Disease) (71). In our model of adaptation to an oscillating environment, the occurrence of synaptic plasticity in the vestibulocerebellar circuit (***Figures 1***, ***2***) could be modulated from normal to excessive by the strength of a biomolecular positive loop, thus determining a variable degree of persistence of the internal model after disembarkation. Normal synaptic plasticity could be converted into excessive synaptic plasticity by a predisposing factor expressed in some individuals. This is a point of convergence of our hypothesis with the theory of MdDS hormonal and neurochemical predisposition published in 2018 (7). As known, hormonal changes at the luteal phase of pre-menstrual syndrome, or in perimenopause, can influence the brain levels of CGRP, whose expression is regulated by gonadal hormones (7, 72, 73). CGRP has been reported as an LTP promoter (32), while its expression is closely correlated with that of the BDNF (31), which is the key element of bifurcation in the above-mentioned positive feedback loop that generates LTP (68).

BDNF is not only influenced by CGRP but also by gonadal hormones (74), possibly indicating that a particular hormonal state may induce neurochemical changes. In addition to this, CGRP is known to strengthen the VOR reflex (29), confirming the role of this neuromodulator in modifying the activity of vestibular neural networks, and being consistent with the correlation between CGRP brain levels and the severity of MdDS symptoms (34). Hence, by putting it all together, we can theorize that some gonadal imbalance, correlated with high CGRP brain levels, potentially affects other modulators, like BDNF, thereby leading to excessive synaptic plasticity and ultimately causing symptom chronicity in MdDS (**Figure 3**).

In summary, by our hypothesis MdDS is not only regarded as a maladaptation of the VOR, but upstream to it, as a malfunctioning of a vestibulocerebellar network that realizes an oscillatory loop system. According to this new approach, we have shown how this **loop system** could be entrained to oscillate by environment movements, thereby leading to MdDS through its over-synchronization. While undergoing synaptic plasticity, this process could become excessive in individuals experiencing an impairment in the brain levels of specific hormones and neuromodulators (*possibly including low levels of estrogen, as well as high levels of CGRP and BDNF*). This would render the internal oscillator noxiously persistent after disembarking from a vehicle, thereby leading to the constant perceptions of self-motion that we know as MdDS. This theory may also explain why

MdDS patients experience a temporary relief of symptoms when exposed to passive motion, as mentioned before, because their over-synchronized loop would be working in its perfect status of canceling the external stimuli.

COMPARISON WITH PREVIOUS THEORIES

In the herein proposed hypothesis, feedback loop dynamics are invoked as an explanatory umbrella for a series of ailments of increasing severity going from MdD to MdDS. The hypothesis is innovative in the framework of MdDS studies, but to some extent it is also a synthesis of different ideas that have been previously formulated about this syndrome. As discussed above, the most significant synergism can be established between our hypothesis and the hormone theory of MdDS (7). However, a close connection can also be found with the idea of an over-synchronization of brain networks caused by entrainment due to the exposure to passive motion (18, 21). The proposed treatments that follow this kind of analysis, such as transcranial Direct Current Stimulation (tDCS) (75) and repetitive Transcranial Magnetic Stimulation (rTMS) (21), are consistent with our hypothesis since they could disorganize an excessive neural network connection (21), but the success rate reported by patients is considered poor (22), suggesting that more refined targets and modalities of treatment are needed.

The theory concerning VOR and VS maladaptation (9, 76) is also somewhat consistent with our hypothesis, given that the neural circuits of these mechanisms are presumed to be, at least in part, coincident with our oscillating loop system. Following this theory, patients were exposed to a full-field optokinetic (OKN) stimulus during head rotation, obtaining an improvement of symptoms in 70% of cases (14), even though there was a slight decline in the success rate over time (9). Similar results were obtained in a recent study which involved a sham protocol for MdDS patients undergoing OKN stimulation, while it was speculated that OKN stimulation worked in re-adapting the so-called maladapted VOR (77). To date, the success rate of the OKN treatment is higher for those with MT MdDS compared to the SO patients (22), further research is needed to understand why this is the case. These studies considered the relationship between VOR and OKN reflexes, knowing that the VOR response can adapt and accommodate sensory arrangements, as shown in a study by Draper (78). The authors hypothesized that a disrupted VOR leads to a disrupted VS and VSR, which consequently leads to poor postural control (9). The results from this study (77) support Dai's theory that the OKN stimulation and head roll is able to induce a VOR adaptation process by altering the performance of the OKN reflex through visual anomalies. However, a striking difference with our hypothesis is that this VOR maladaptation would be a downstream consequence of MdDS, not a triggering effect, i.e., the cause-effect relationship between MdDS pathogenesis and VOR would be inverted. Nevertheless, the OKN treatment fits well also under our hypothesis, since a strong stimulation of the VOR could partially alleviate the excessive synaptic plasticity that we presume to be present in MdDS patients. In addition to this, as reported in the sham study (77), the OKN treatment could be just one part of the treatment process for MdDS subjects, since most subjects also continued to report associated symptoms such as migraine (7, 77) following a postural improvement.

HOW TO VALIDATE THE HYPOTHESIS

Our hypothesis is, for now, only a theoretical model and a series of studies have to be developed and executed in order to validate it. Specific clinical protocols and tests will have to be developed according to a suitable, hypothesis-driven experimental design based on the herein proposed model, thus collecting data specifically suitable to prove or disprove the model.

One of the first aspects to consider is the assessment of the internal model, such as verifying that MdDS is triggered in the presence of a regular wave with a single (*or strongly dominant*) sinusoidal component (*boat or plane*); rather than in the presence of noise (*car or train*). Such a result has been partially achieved in a retrospective study on a large number of MdDS patients, showing that the disease is mainly triggered by boat travels (4). However, additionally, the mechanism could be further investigated with the use of computerized posturography tests under static or moving conditions at different frequencies of oscillations, to evaluate if subjective perception of motion matches with objective postural instability.

Secondly, to specifically prove the over-synchronization of an oscillatory neural loop system the use of neuroimaging techniques could be a suitable approach. By employing high-resolution functional magnetic resonance imaging (fMRI)/18F-fludeoxyglucose positron-emission tomography (18F-FDG–PET) scans, and electroencephalogram (EEG) it would be possible to explore variations in functional connectivity between VNs and the flocculonodular lobe. This kind of analysis could be done on controls and patients without previous treatment or after different exposures, including various kinds of vestibular stimulation, hence showing possible differences in vestibulocerebellar connectivity consistent with the hypothesized model. If the vestibulocerebellar connectivity pattern would show higher correlation in patients with respect to controls, selectively at the internal oscillator frequencies, this will confirm that the internal oscillator would have become undesirably persistent in MdDS. This would potentially provide a neuroimaging biomarker allowing to distinguish MdDS from other central vestibular disorders, especially SO MdDS, which might be falling more clearly into the PPPD diagnostic sphere.

In addition, as posed in the hypothesis, MdDS patients may develop this permanent form due to a neurochemical imbalance that would render them more susceptible to this maladaptation, hence their hormonal status and history should be taken into account (*e.g., perimenopausal, low testosterone or estrogen, and usage of steroids or hormonal replacement therapy)* (23).

Another method of exploring altered connections between VN and cerebellum, potentially affecting the functioning of VS, VOR, and other vestibular circuits, could be the use of transcranial magnetic stimulation (TMS), a technique that has contributed significantly to the understanding and treatment

of several neurological and psychiatric disorders (79, 80). TMS can be used with single and paired pulses over the primary cortex (M1), allowing to trace excitatory and inhibitory pathways (79). For instance, paired-pulse TMS can induce short-interval intracortical inhibition (SICI) by involving $GABA_A$ receptors (79, 81). TMS has been also used in combination with drugs (82), showing that benzodiazepine (*a positive modulator of* $GABA_A$) enhances SICI (79), while long-interval intracortical inhibition (LICI) and cortical silent period (CSP), which are measures of long-lasting inhibition, increase with the $GABA_B$ receptor agonists tiagabine (*working on* LICI) (83), and baclofen (*working on* CSP) (84). These techniques have been used to study the pathophysiology of motor system disorders such as amyotrophic lateral sclerosis, Parkinson's disease, Tourette syndrome, and altered motor cortex $GABA_B$ function in concussed athletes (79, 80).

Despite that MdDS may not be a motor disorder, TMS could allow researchers to understand if a GABAergic alteration is characteristic of MdDS patients. Studying pharmacological changes with TMS allows for an indirect measure of excitatory and inhibitory mechanisms and their implications in neurotransmitters modulation. It has also been proposed that TMS could be used with *in vivo* proton magnetic resonance spectroscopy (1H-MRS), thus measuring the levels of GABA during different phases of the menstrual cycle and aligning these data with symptom intensity in MdDS patients (7). 1H-MRS would allow the detection and quantification of different neurometabolites besides GABA, such as myoinositol, N-acetylaspartate, and glutamate (79, 85).

A recent study utilized transcranial direct current stimulation (tDCS) to ease MdDS symptoms, with promising results (75). This novel neuromodulation technique would be advantageous for patients since it can be performed at home in a remote setting, reducing or eliminating long commutes which are known to cause discomfort for those with MdDS. Another technique used to test vestibular-spinal control system is Galvanic Vestibular Stimulation (GVS) (86). In a recent study on PPPD patients, GVS allowed the stimulation of vestibular afferents without head motion on either side separately, showing higher instability with higher intensity GVS (range from low to high, 0.8–2.8 mA) and closed eyes, consistent with the greater visual dependency in controlling posture of these subjects (86). A similar experiment could be performed on MdDS patients to examine their sensory reweighting.

Finally, the aforementioned postural, neuroendocrine, neurochemical, neuroimaging and transcranial stimulation data has the potential to contribute partial confirmations of our hypothesis, however their amassing has the ability to ultimately validate the hypothesis.

CONCLUSIONS

MdDS remains a challenging problem for healthcare professionals. Due to unclear underlying mechanisms and the lack of definitive biomarkers, the diagnostic process is typically long and costly, while treatment options are experimental and limited. Our hypothesis provides an innovative vision into this syndrome, by proposing that dynamic loops are involved in brain adaptive responses to oscillatory passive motion. Our hypothesis does not reject previous theories on MdDS pathogenesis, but it rather embodies elements of these in a comprehensive mechanism, based on Systems and Control Theory. The main elements of our hypothesis are the following:

- Starting from an essential biomechanical analysis of posture, we derived the notion that perfect adaptation to an external oscillatory disturbance needs the **activation of an adaptation loop including an internal oscillator able to cancel disturbance** (Internal Model Principle).
- Thereafter, starting from available neuroanatomical and physiological knowledge of the vestibulocerebellar region we identified **a bilateral neural network arranged** as a **triple loop with two further contralateral connections**, involving the VNs and the cerebellar flocculonodular lobe.
- By using computational simulation, we proved the tendency of the **neural network to behave as an oscillator with the increasing strength of inhibitory connections**, reaching its highest when both inhibitory and excitatory connections are strong.
- We therefore assumed that the identified neural loop system becomes entrained by exposure to passive motion, e.g., those experienced onboard of a vehicle, thus activating an adaptive internal model.
- Finally, given that such entrainment is likely to involve synaptic LTP, and by assuming that synaptic plasticity is triggered by a biomolecular positive loop, we envisaged that under some unbalance of neuromodulators like CGRP and BDNF, during peculiar gonadal hormonal phases, the transition to LTP becomes irreversible. This would maintain the internal oscillator after the removal of the external stimulus (e.g., after disembarkation), thereby producing MdDS.

If this hypothesis were tested and verified, then optimal targets for MdDS treatment could be found inside the neural networks and biochemical factors that play a fundamental role in loop functioning and synaptic plasticity. We proposed a few studies to address this theory, such as: the use of dynamic posturography for exposing patients at different frequencies and evaluate their self-perception of motion; perform specific neuroimaging studies to explore variations in functional connectivity between VNs and the flocculonodular lobe in MdDS patients vs. healthy controls; assess patient's hormonal status and history and observe if specific hormonal imbalances or conditions are characterizing of MdDS patients; using TMS to study SICI and LICI by involving the use of medications and their effect on the patient's GABAergic system, evaluating if altered GABAergic system is present in MdDS patients, this could also be combined with 1H-MRS, thus measuring the levels of GABA during different phases of the menstrual cycle and aligning these data with symptom intensity in MdDS patients.

As a corollary, our hypothesis falls into a wider theory of the organism's physiology (67, 87), based on the assumption that dynamic loops are an essential trait for all processes and

transitions that occur in the organism, notably transitions from physiological to pathological status. Therefore, this hypothesis can be taken as a basis for theoretical analysis and novel experimental models of other neurological disorders.

DATA AVAILABILITY STATEMENT

All datasets generated for this study are included in the article/**Supplementary Materials**.

AUTHOR CONTRIBUTIONS

VM is the primary author, she contributed to the formation of the team to collaborate and to the scientific basis for implementing the theory. II reviewed the hypothesis and contributed to the reviewing of the manuscript. CB reviewed the hypothesis and the manuscript. FB provided the mathematical model and contributed to the formation of the hypothesis. GG provided the mathematical model and contributed to the formation of the hypothesis. LM contributed to the validation of the hypothesis with clinical studies. BB contributed to the formation of the hypothesis and developed a pathophysiological model of MdDS. All authors contributed to the article and approved the submitted version.

FUNDING

This work was supported by the Italian Ministry of Health (Ricerca corrente, IRCCS Fondazione Santa Lucia, PE-2013-02355372) and by the generous donors of the CrowdScience campaign (Research into the Pathophysiology and Therapy Options of Mal de Debarquement Syndrome - https://crowd.science/campaigns/research-into-the-pathophysiology-and-therapy-options-of-mal-de-debarquement-syndrome/) launched by VM.

ACKNOWLEDGMENTS

We would like to dedicate this work to Prof. Cohen, and Dr. Dai in their memory. We also would like to thank Natalie Jonk from CrowdScience, for the help provided with our crowdfunding campaign which has been able to support the current work. We would also like to express our gratitude to all the donors, who have contributed to the CrowdScience MdDS initiative.

SUPPLEMENTARY MATERIAL

The Supplementary Material for this article can be found online at: https://www.frontiersin.org/articles/10.3389/fneur.2020.576860/full#supplementary-material

REFERENCES

1. Van Ombergen A, Van Rompaey V, Maes LK, Van de Heyning PH, Wuyts FL. Mal de debarquement syndrome : a systematic review. *J Neurol.* (2016) 263:843–54. doi: 10.1007/s00415-015-7962-6
2. Cha Y-H. Mal de debarquement syndrome: new insights yoon-Hee. *Ann N Y Acad Sci.* (2015) 1343:63–8. doi: 10.1111/nyas.12701
3. Cha Y. Less common neuro-otologic disorders. *Contin.* (2012) 18:1142–57. doi: 10.1212/01.CON.0000421623.56525.11
4. Mucci V, Canceri JM, Brown R, Dai M, Yakushin S, Watson S, et al. Mal de debarquement syndrome: a survey on subtypes, misdiagnoses, onset and associated psychological features. *J Neurol.* (2018) 265:486–99. doi: 10.1007/s00415-017-8725-3
5. Cha YH, Cui YY, Baloh RW. Comprehensive clinical profile of mal de debarquement syndrome. *Front Neurol.* (2018) 9:261. doi: 10.3389/fneur.2018.00261
6. Hain TC, Cherchi M. Mal de d ebarquement syndrome. *Handb Clin Neurol.* (2016) 137:391–395. doi: 10.1016/B978-0-444-63437-5.00028-5
7. Mucci V, Jacquemyn Y, Van Ombergen A, Van de Heyning PH, Browne CJ. A new theory on GABA and calcitonin gene-related peptide involvement in mal de debarquement syndrome predisposition factors and pathophysiology. *Med Hypotheses.* (2018) 120:128–34. doi: 10.1016/j.mehy.2018.08.024
8. Staab JP, Eckhardt-Henn A, Horii A, Jacob R, Strupp M, Brandt T, et al. Diagnostic criteria for persistent postural-perceptual dizziness (PPPD): consensus document of the committee for the classification of vestibular disorders of the bárány society. *J Vestib Res.* (2017) 27:191–208. doi: 10.3233/VES-170622
9. Dai M, Cohen B, Cho C, Shin S, Yakushin SB. Treatment of the mal de debarquement syndrome : a 1-year follow-up. *Front Neurol.* (2017) 8:1–10. doi: 10.3389/fneur.2017.00175
10. Cohen B, Dai M, Yakushin SB, Raphan T. Baclofen, motion sickness susceptibility and the neural basis for velocity storage. *Prog Brain Res.* (2008) 171:543–53. doi: 10.1016/S0079-6123(08)00677-8
11. Cohen B, Kozlovskaya I, Raphan T, Solomon D, Helwig D, Cohen N, et al. Vestibuloocular reflex of rhesus monkeys after spaceflight. *J Appl Physiol.* (1985) 73:121S—31. doi: 10.1152/jappl.1992.73.2.S121
12. Holstein GR, Martinelli GP, Wearne S, Cohen B. Ultrastructure of vestibular commissural neurons related to velocity storage in the monkey. *Neuroscience.* (1999) 93:155–70. doi: 10.1016/S0306-4522(99)00142-6
13. Cohen B, Yakushin SB, Cho C. Hypothesis : the vestibular and cerebellar basis of the mal de debarquement syndrome. *Front Neurol.* (2018) 9:28. doi: 10.3389/fneur.2018.00028
14. Dai M, Cohen B, Smouha E, Cho C. Readaptation of the vestibulo-ocular reflex relieves the mal de debarquement syndrome. *Front Neurol.* (2014) 5:124. doi: 10.3389/fneur.2014.00124
15. Barmack NH, Shojaku H. Vestibularly induced slow oscillations in climbing fiber responses of purkinje cells in the cerebellar nodulus of the rabbit. *Neuroscience.* (1992) 50:1–5. doi: 10.1016/0306-4522(92)90376-D
16. Mucci V, Cha YH, Wuyts FL, Van Ombergen A. Perspective : stepping stones to unraveling the pathophysiology of mal de debarquement syndrome with neuroimaging. *Front Neurol.* (2018) 9:42. doi: 10.3389/fneur.2018.00042
17. Cha Y, Chakrapani S, Craig A, Baloh R. Metabolic and functional connectivity changes in mal de debarquement syndrome. *PLoS ONE.* (2012) 7:e49560. doi: 10.1371/journal.pone.0049560
18. Cha YH, Chakrapani S. Voxel based morphometry alterations in mal de debarquement syndrome. *PLoS ONE.* (2015) 10:e0135021. doi: 10.1371/journal.pone.0135021
19. Van Ombergen A, Wuyts FL, Cha YH. Letter to the Editor : comment and erratum to Mal de debarquement syndrome : a systematic review. *J Neurol.* (2016) 263:855–60. doi: 10.1007/s00415-016-8102-7
20. Dupret D, Csicsvari J. The medial entorhinal cortex keeps up. *Nat Neurosci.* (2012) 15:1471–2. doi: 10.1038/nn.3245
21. Cha YH, Cui Y, Baloh RW. Repetitive transcranial magneti stimulation for mal de debarquement syndrome. *Otol Neurotol.* (2013) 34:175–9. doi: 10.1097/MAO.0b013e318278bf7c
22. Canceri JM, Brown R, Watson SR, Browne CJ. An examination of current treatments and symptom management strategies utilized by mal de debarquement syndrome patients. *Front Neurol.* (2018) 9:943. doi: 10.3389/fneur.2018.00943
23. Mucci V, Canceri JM, Brown R, Dai M, Yakushin SB, Watson S, et al. Mal de debarquement syndrome : a retrospective online questionnaire on the

influences of gonadal hormones in relation to onset and symptom fluctuation. *Front Neurol.* (2018) 9:362. doi: 10.3389/fneur.2018.00362
24. Monaghan S. Ménière's disease in women – can the cyclical nature of symptoms in some women provide insights into its mechanism of action? (2016) 6–9. Available online at: https://www.menieres.org.uk/files/pdfs/Monaghan.pdf
25. Elkind-Hirsch KE, Stoner WR, Stach B, Jerger JF. Estrogen influences auditory brainstem responses during the normal menstrual cycle. *Hear Res.* (1992) 60:143–8. doi: 10.1016/0378-5955(92)90016-G
26. Albert PR. Why is depression more prevalent in women? *J Psychiatry Neurosci.* (2015) 40:219–21. doi: 10.1503/jpn.150205
27. Mucci V, Canceri JM, Jacquemyn Y, Ombergen AV, Maes LK, Van de Heyning PH, et al. Pilot study on patients with mal de debarquement syndrome during pregnancy. *Futur Sci OA.* (2019) 5:FSO377. doi: 10.4155/fsoa-2018-0109
28. Balaban CD, Jacob RG, Furman JM. Neurologic bases for comorbidity of balance disorders, anxiety disorders and migraine : neurotherapeutic implications. *Expert Rev Neurother.* (2011) 11:379–94. doi: 10.1586/ern.11.19
29. Luebke AE, Holt JC, Jordan PM, Wong YS, Caldwell JS, Cullen KE. Loss of α-calcitonin gene-related peptide (αCGRP) reduces the efficacy of the vestibulo-ocular reflex (VOR). *J Neurosci.* (2014) 34:10453–8. doi: 10.1523/JNEUROSCI.3336-13.2014
30. Ohno K, Takeda N, Tanaka-Tsuji M, Matsunaga T. Calcitonin gene-related peptide in the efferent system of the inner ear : a review. *Acta Otolaryngol.* (2016) 6489:1651—2251. doi: 10.3109/00016489309126206
31. Buldyrev I, Tanner NM, Hsieh HY, Dodd EG, Nguyen LT, Balkowiec A. Calcitonin gene-related peptide enhances release of native brain-derived neurotrophic factor from trigeminal ganglion neurons. *J Neurochem.* (2006) 99:1338–50. doi: 10.1111/j.1471-4159.2006.04161.x
32. Wu X, Zhang JT, Liu J, Yang S, Chen T, Chen JG, et al. Calcitonin gene-related peptide erases the fear memory and facilitates long-term potentiation in the central nucleus of the amygdala in rats. *J Neurochem.* (2015) 135:787–98. doi: 10.1111/jnc.13246
33. von Bertalanffy L. *General System Theory: Foundations, Development, Applications*. New York, NY: George Braziller Inc. (1968)
34. Thut G, Schyns PG, Gross J. Entrainment of perceptually relevant brain oscillations by non-invasive rhythmic stimulation of the human brain. *Front Psychol.* (2011) 2:170. doi: 10.3389/fpsyg.2011.00170
35. Blanchini F, Franco E, Giordano G. A structural classification of candidate oscillatory and multistationary biochemical systems. *Bull Math Biol.* (2014) 76:2542–69. doi: 10.1007/s11538-014-0023-y
36. Wiener N. *Cybernetics: Or Control and Communication in the Animal and the Machine*. Cambridge, MA: MIT Press (1961). doi: 10.1037/13140-000
37. Sontag ED. Adaptation and regulation with signal detection implies internal model. *Syst Control Lett.* (2003) 50:119–26. doi: 10.1016/S0167-6911(03)00136-1
38. Yakushin SB, Raphan T, Cohen B. Coding of velocity storage in the vestibular nuclei. *Front Neural Circ Neural Circ.* (2017) 8:386. doi: 10.3389/fneur.2017.00386
39. Hain TC, Hanna PA, Rheinberger MA. Mal de debarquement. *Arch Otolaryngol Head Neck Surg.* (1999) 125:615–20. doi: 10.1001/archotol.125.6.615
40. Blanchini F, Franco E, Giordano G. Structural conditions for oscillations and multistationarity in aggregate monotone systems. In: *2015 54th IEEE Conference on Decision and Control (CDC)*. Osaka. (2015). p. 609–14. doi: 10.1109/CDC.2015.7402296
41. Alexandrov AV, Frolov AA, Horak FB, Carlson-Kuhta P, Park S. Feed-back equilibrium control during human standing. *Biol Cybern.* (2005) 93:309322. doi: 10.1007/s00422-005-0004-1
42. Morasso P, Cherif A, Zenzeri J. Quiet standing: the single inverted pendulum model is not so bad after all. *PLoS ONE.* (2019) 14:e0213870. doi: 10.1371/journal.pone.0213870
43. Huang J, Isidori A, Marconi L, et al. (2019) Internal Models in Control, Biology and Neuroscience. *IEEE Conference on Decision and Control (CDC)*, Miami Beach, FL (2018).
44. Moeller L, Lempert T. Mal de debarquement: Pseudo-hallucinations from vestibular memory? *J Neurol*. (2007) 254:813. doi: 10.1007/s00415-006-0440-4
45. Hain T, Helminski J. Anatomy and physiology of the normal vestibular system. In: Herdman S. editor *Vestibular Rehabilitation*, 3rd ed. F.A Davis Company, Philadelphia. (2007) 1–18.
46. Uchino Y, Kushiro K. Differences between otolith- and semicircular canal-activated neural circuitry in the vestibular system. *Neurosci Res.* (2011) 71:315–27. doi: 10.1016/j.neures.2011.09.001
47. Kathleen EC. The vestibular system: multimodal integration and encoding of self-motion for motor control. *Trends Neurosci.* (2014) 23:1–7. doi: 10.1016/j.tins.2011.12.001
48. Bertolini G, Ramat S, Laurens J, Bockisch CJ, Marti S, Straumann D, et al. Velocity storage contribution to vestibular self-motion perception in healthy human subjects. *J Neurophysiol.* (2011) 105:209–23. doi: 10.1152/jn.00154.2010
49. Raphan T, Matsuo V, Cohen B. Velocity storage in the vestibulo-ocular reflex arc (VOR). *Exp Brain Res.* (1979) 35:229–48. doi: 10.1007/BF00236613
50. Laurens J, Angelaki DE.Laurens J, Angelaki DE. The functional significance of velocity storage and its dependence on gravity. *Exp Brain Res.* (2011) 210:407–22. doi: 10.1007/s00221-011-2568-4
51. Galiana HL, Outerbridge JS. A bilateral model for central neural pathways in vestibuloocular reflex. *J Neurophysiol.* (1984) 51:210–41. doi: 10.1152/jn.1984.51.2.210
52. Katz E, Vianney de Jong JM, Buettner-Ennever J, Cohen B. Effects of midline medullary lesions on velocity storage and the vestibulo-ocular reflex. *Exp Brain Res.* (1991) 87:505–20. doi: 10.1007/BF00227076
53. Samaniego CC, Franco E, Giordano G. Design and analysis of a biomolecular positive-feedback oscillator. *Proc IEEE Conf Decis Control 2018-Decem.* Miami Beach, FL (2018). p. 1083–88. doi: 10.1109/CDC.2018.8619738
54. Barmack NH, Shojaku H. Vestibular and visual climbing fiber signals evoked in the uvula-nodulus of the rabbit cerebellum by natural stimulation. *J Neurophysiol.* (1995) 74:2573–89. doi: 10.1152/jn.1995.74.6.2573
55. Bos JE, Bles W. Theoretical considerations on canal–otolith interaction and an observer model. *Biol Cybern.* (2002) 86:191–207. doi: 10.1007/s00422-001-0289-7
56. Stampanoni Bassi M, Iezzi E, Gilio L, Centonze D, Buttari F. Synaptic plasticity shapes brain connectivity: implications for network topology. *Int J Mol Sci.* (2019) 20:6193. doi: 10.3390/ijms20246193
57. Takeuchi T, Duszkiewicz AJ, Morris RG. The synaptic plasticity and memory hypothesis: encoding, storage and persistence. *Philos Trans R Soc L B Biol Sci.* (2014) 369:20130288. doi: 10.1098/rstb.2013.0288
58. Boyden ES, Katoh A, Raymond JL. Cerebellum-dependent learning: the role of multiple plasticity mechanisms. *Annu Rev Neurosci.* (2004) 27:581–09. doi: 10.1146/annurev.neuro.27.070203.144238
59. Gittis AH, du Lac S. Intrinsic and synaptic plasticity in the vestibular system. *Curr Opin Neurol.* (2006) 16:385–90. doi: 10.1016/j.conb.2006.06.012
60. Keshavan MS, Mehta UM, Padmanabhan JL, Shah JL. Dysplasticity, metaplasticity, and schizophrenia: implications for risk, illness, novel interventions. *Dev Psychopathol.* (2015) 27:615-635. doi: 10.1017/S095457941500019X
61. Berke D, Hyman S. Addiction, dopamine, and the molecular mechanisms of memory. *Neuron.* (2000) 25:515–32. doi: 10.1016/S0896-6273(00)81056-9
62. Thanos Tzounopoulos. (2008). Mechanisms of synaptic plasticity in the dorsal cochlear nucleus: plasticity-induced changes that could underlie tinnitus. *Am J Audiol.* (2018) 17:S170–5. doi: 10.1044/1059-0889(2008/07-0030)
63. Conte A, Rocchi L, Latorre A, Belvisi D, Rothwell JC, Berardelli A. Ten-Year reflections on the neurophysiological abnormalities of focal dystonias in humans. *Mov Disord.* (2019) 34:1616–28. doi: 10.1002/mds.27859
64. Weise D, Schramm A, Stefan K, Wolters A, Reiners K, Naumann M, et al. The two sides of associative plasticity in writer's cramp. *Brain.* (2006) 129:2709–21. doi: 10.1093/brain/awl221
65. Münchau A, Bronstein AM. Role of the vestibular system in the pathophysiology of spasmodic torticollis. *J Neurol Neurosurg Psychiatr.* (2001) 71:285–8. doi: 10.1136/jnnp.71.3.285
66. Kanovský P, Bares M, Streitová H, Klajblová H, Daniel P, Rektor I. Idiopathic spasmodic torticollis is not associated with abnormal kinesthetic perception

from neck proprioceptive and vestibular afferences. *J Neurol.* (2003) 250:546–55. doi: 10.1007/s00415-003-1034-z
67. Burlando B. Loopomics: a new functional approach to life. *J Appl Physiol.* (2017) 123:1011–3. doi: 10.1152/japplphysiol.00173.2017
68. Hao L, Yang Z, Lei J. Underlying mechanisms of cooperativity, input specificity, and associativity of long-term potentiation through a positive feedback of local protein synthesis. *Front Comput Neurosci.* (2018) 12:25. doi: 10.3389/fncom.2018.00025
69. Xiong W, Ferrell JE. Erratum: a positive-feedback-based bistable "memory module" that governs a cell fate decision. *Nature*. 426:460–5. doi: 10.1038/nature02089
70. Angeli D, Ferrell JE, Sontag ED. Detection of multistability, bifurcations, and hysteresis in a large class of biological positive-feedback systems. *Proc Natl Acad Sci USA*. (2004) 101:1822–7. doi: 10.1073/pnas.0308265100
71. Doig AJ. Positive feedback loops in alzheimer's disease: the alzheimer's feedback hypothesis. *J Alzheimers Dis.* (2018) 66:25–36. doi: 10.3233/JAD-180583
72. Wang D, Zhao J, Wang J, Li J, Yu S, Guo X. Deficiency of female sex hormones augments PGE 2 and CGRP levels within midbrain periaqueductal gray. *J Neurol Sci.* (2014) 346:107–11. doi: 10.1016/j.jns.2014.08.002
73. Labastida-Ramirez A, Rubio-Beltran E, Villanon MC, Maassen Van Den Brink A. Gender aspects of CGRP in migraine. *Cephalalgia.* (2019) 39:435–44. doi: 10.1177/0333102417739584
74. Jezierski MK, Sohrabji F. Region- and peptide-specific regulation of the neurotrophins by estrogen. *Mol Brain Res.* (2000) 85:77–84. doi: 10.1016/S0169-328X(00)00244-8
75. Cha YH, Urbano D, Pariseau N. Randomized single blind sham controlled trial of adjunctive home-Based tDCS after rTMS for mal de debarquement syndrome: safety, efficacy, and participant satisfaction assessment. *Brain Stimul.* (2016) 9:537–44. doi: 10.1016/j.brs.2016.03.016
76. Dai M, Kunin M, Raphan T, Cohen B. The relation of motion sickness to the spatial-temporal properties of velocity storage. *Exp Brain Res.* (2003) 151:173–89. doi: 10.1007/s00221-003-1479-4
77. Mucci V, Perkisas T, Jillings SD, Van Rompaey V, Van Ombergen A, Fransen E, et al. Sham-controlled study of optokinetic stimuli as treatment for mal de debarquement syndrome. *Front Neurol.* (2018) 9:887. doi: 10.3389/fneur.2018.00887
78. Draper MH. The effects of image scale factor on vestibulo-ocular reflex adaptation and simulator sickness in head-coupled virtual environments. *Sage J.* (2015) 42:1481–5. doi: 10.1177/154193129804202104
79. Tremblay S, Beaulé V, Proulx S, de Beaumont L, Marjanska M, Doyon J, et al. Relationship between transcranial magnetic stimulation measures of intracortical inhibition and spectroscopy measures of GABA and glutamate+glutamine. *J Neurophysiol.* (2013) 109:1343–9. doi: 10.1152/jn.00704.2012
80. Chen R, Cros D, Curra A, Di Lazzaro V, Lefaucheur JP, Magistris MR, et al. The clinical diagnostic utility of transcranial magnetic stimulation: report of an IFCN committee. *Clin Neurophysiol.* (2008) 119:504-532. doi: 10.1016/j.clinph.2007.10.014
81. Kujirai T, Caramia MD, Rothwell JC, Day BL, Thompson PD, Ferbert A, et al. corticocortical inhibition in human motor cortex. *J Physiol.* (1993) 471:501–19. doi: 10.1113/jphysiol.1993.sp019912
82. Teo JTH, Terranova C, Swayne OB, et al. Europe PMC funders group differing effects of intracortical circuits on plasticity. *Exp Brain Res.* (2009) 193:555–63. doi: 10.1007/s00221-008-1658-4
83. McDonnell MN, Orekhov Y, Ziemann U. The role of GABA(B) receptors in intracortical inhibition in the human motor cortex. *Exp Brain Res.* (2006) 173:86-93. doi: 10.1007/s00221-006-0365-2
84. Werhahn KJ, Kunesch E, Noachtar S, Benecke R, Classen J. Different effects on motorcortical inhibition induced by blockage of GABA uptake in humans. *J Physiol.* (1999) 517:591–597. doi: 10.1111/j.1469-7793.1999.0591t.x
85. Mescher M, Merkle H, Kirsch J, Garwood M, Gruetter R. Simultaneous *in vivo* spectral editing and water suppression. *NMR Biomed.* (1998) 11:266–72. doi: 10.1002/(SICI)1099-1492(199810)11:6<266::AID-NBM530>3.0.CO;2-J
86. Woll J, Sprenger A, Helmchen C. Postural control during galvanic vestibular stimulation in patients with persistent perceptual–postural dizziness. *J Neurol.* (2019) 266:1236–49. doi: 10.1007/s00415-019-09255-7
87. Burlando B, Blanchini F, Giordano G. Loop analysis of blood pressure/volume homeostasis. *PLoS Comput Biol.* (2019) 15:e1007346. doi: 10.1371/journal.pcbi.1007346

Conflict of Interest: The authors declare that the research was conducted in the absence of any commercial or financial relationships that could be construed as a potential conflict of interest.

frontiers in Neurology

ORIGINAL RESEARCH
published: 23 November 2020
doi: 10.3389/fneur.2020.604502

Alexander's Law During High-Speed, Yaw-Axis Rotation: Adaptation or Saturation?

*Claudia Lädrach[1], David S. Zee[2], Thomas Wyss[1], Wilhelm Wimmer[3], Athanasia Korda[1], Cinzia Salmina[1], Marco D. Caversaccio[1] and Georgios Mantokoudis[1]**

[1] Department of Otorhinolaryngology, Head and Neck Surgery, Inselspital Bern, Bern, Switzerland, [2] Department of Neurology, Johns Hopkins University School of Medicine, Baltimore, MD, United States, [3] Hearing Research Laboratory, ARTORG Center, University of Bern, Bern, Switzerland

Objective: Alexander's law (AL) states the intensity of nystagmus increases when gaze is toward the direction of the quick phase. What might be its cause? A gaze-holding neural integrator (NI) that becomes imperfect as the result of an adaptive process, or saturation in the discharge of neurons in the vestibular nuclei?

Methods: We induced nystagmus in normal subjects using a rapid chair acceleration around the yaw (vertical) axis to a constant velocity of 200°/second [s] and then, 90 s later, a sudden stop to induce post-rotatory nystagmus (PRN). Subjects alternated gaze every 2 s between flashing LEDs (right/left or up/down). We calculated the change in slow-phase velocity (ΔSPV) between right and left gaze when the lateral semicircular canals (SCC) were primarily stimulated (head upright) or, with the head tilted to the side, stimulating the vertical and lateral SCC together.

Results: During PRN AL occurred for horizontal eye movements with the head upright and for both horizontal and vertical components of eye movements with the head tilted. AL was apparent within just a few seconds of the chair stopping when peak SPV of PRN was reached. When slow-phase velocity of PRN faded into the range of 6–18°/s AL could no longer be demonstrated.

Conclusions: Our results support the idea that AL is produced by asymmetrical responses within the vestibular nuclei impairing the NI, and not by an adaptive response that develops over time. AL was related to the predicted plane of eye rotations in the orbit based on the pattern of SCC activation.

Keywords: Alexander's law, nystagmus, vestibulo-ocular reflex, gaze-dependent nystagmus, eye-velocity-to-position integrator

OPEN ACCESS

Edited by:
Richard Lewis, Harvard University, United States

Reviewed by:
Matthew Crowson, Harvard Medical School, United States
Adrian Priesol, Harvard Medical School, United States

****Correspondence:***
Georgios Mantokoudis
georgios.mantokoudis@insel.ch

Specialty section:
This article was submitted to Neuro-Otology, a section of the journal Frontiers in Neurology

Received: *09 September 2020*
Accepted: *02 October 2020*
Published: *23 November 2020*

Citation:
Lädrach C, Zee DS, Wyss T, Wimmer W, Korda A, Salmina C, Caversaccio MD and Mantokoudis G (2020) Alexander's Law During High-Speed, Yaw-Axis Rotation: Adaptation or Saturation? Front. Neurol. 11:604502. doi: 10.3389/fneur.2020.604502

INTRODUCTION

Alexander's law (AL) is commonly shown by patients with spontaneous nystagmus (SN) due to a vestibular imbalance. The nystagmus is more intense, with a higher velocity of the slow phase, when patients gaze in the direction of the quick phase (1). Two main hypotheses have been invoked to account for AL.

First, AL has been attributed to a slowly developing, adaptive mechanism that lessens the slow-phase velocity of a pathological SN when gaze is in the direction of the slow phase (2). According to this hypothesis, the neural circuit for eccentric gaze holding is "purposefully" impaired, causing the eyes to drift centripetally so that in one direction of gaze a bias from the centripetal drift opposes and diminishes the SN. Normally eccentric gaze is held steady by a neural network called the ocular motor neural integrator (NI) (3). How well the NI performs is judged by its time constant (TcNI, [seconds, s]) of decay when an input is no longer present. The more perfect the integrator the higher the value of the time constant being in the range of 20–40 s (4). When the TcNI is low, making the NI "leaky," the eyes drift centripetally on eccentric gaze so when a patient with SN looks in the direction of the slow phase, the SN is reduced, gaze is better stabilized, images move less on the retina, and vision is improved (2, 5).

Alternative hypotheses suggest that AL arises as an epiphenomenon from a non-linear interaction in the vestibular nuclei (6, 7) or in the ocular motor nuclei (8), when processing activity for the vestibulo-ocular reflex (VOR). One difficulty in arriving at a more definitive explanation for AL are the different types of stimuli (caloric, one ear vs. both ears stimulation, total body vs. head only rotations), stimulus characteristics (frequency, intensity, duration, stimulus profiles) and subject populations (healthy vs. pathological) that have been used to investigate AL. The aim of this study was to buttress one or the other of these hypotheses. We examined the influences on AL of a high-speed, constant-velocity, chair rotation in *healthy subjects* to induce a prolonged nystagmus as a surrogate for SN in patients. We particularly focused on (1) the onset of AL relative to the onset of nystagmus, (2) the effect of the magnitude of the SPV of nystagmus on AL, and (3) the effect of stimulating different patterns of the semicircular canals on AL.

MATERIALS AND METHODS

Subjects

We tested nine healthy subjects from 24 to 54 years of age (mean 33.2 years, SD ± 10.9 years), four women and five men. Subjects had no history of vestibular, ocular, or neurologic dysfunction, and had normal vision and normal ocular motor function. All included subjects had a normal rotational velocity step test including a normal time constant. Subjects had no spontaneous nystagmus (SN) at rest.

Rotational Chair Stimuli

We used a yaw-axis, rotational chair paradigm (Mini Torque, DIFRA, France) in complete darkness with acceleration to a constant velocity of 200°/s within 1 s. We used the same pattern of alternating rotational directions for all subjects to compare systematically right/left and up/down gaze. The rotation period lasted 90 s and was followed by a sudden deceleration of 200°/s^2 to an abrupt stop.

All subjects were tested in two head positions, (1) upright primary head position with head pitched 30° downward, maximally stimulating the lateral SCCs (**Figure 1A**) and (2) head rolled (tilted) 45° to the left, stimulating both the lateral and vertical SCCs (**Figures 1B,C**). One other subject was tested with the head upright (**Figure 1A**) at two rotational velocities (100 and 200°/s).

Video-Oculography (VOG)

We recorded horizontal and vertical eye movements at a frame rate of 200 Hz using the video-oculography (VOG) device with a single infrared camera mounted on a goggle frame (Eyeseecam, EyeSeeTec, Munich), therefore tracking the movement of one eye, leaving the other covered (avoiding double vision or vergence). The VOG device was calibrated for horizontal and vertical eye positions using its built-in calibration system with laser projections on the wall at 1.5 m distance.

Flashing Light Targets

To compare AL with different target locations on separate trials subjects were asked to look at LEDs positioned in the goggles to the right and left (±18°, **Figures 1A,B**) or diagonally (up and down ±13°, **Figure 1C**), during and after rotation. The LEDs were flashed every second for 20 ms. Subjects were cued every second to alternate the direction of their gaze to the other LED by a beep heard through headphones.

SPV and Alexander's Law

The slow-phase velocity (SPV) of the nystagmus was calculated using custom MATLAB software scripts by differentiating eye positions (EPos) after a de-saccading procedure using median filters. Data quality was checked and outliers including remaining saccades removed. Data points around the center gaze position (-10 *to* $+10°$) were excluded from analysis. SPV>100°/s or slow phases in the wrong direction were considered outliers. We recorded and analyzed the PRN and the nystagmus at rest prior to stimulation. We calculated the time constant of the VOR (TcVOR) for each gaze position. The decay of SPV during PRN was fitted with a negative exponential curve function $y = A^*e^{\wedge}[b^*(-t)]$ to calculate the peak SPV (A) and TcVOR (b) over time (t). TcVOR indicated the time when SPV declined to 63% of its peak value. At each gaze interval of 2 s, the instantaneous difference between the opposing eye positions at peak SPV (ΔEPos = left EPos – right EPos), and the instantaneous difference in SPV between right and left gaze (ΔSPV = left gaze SPV – right gaze SPV) were calculated. The corresponding values of the time constant (TcNI), which reflects the fidelity of the NI for holding positions of gaze, was calculated as follows:

$$\mathrm{TcNI} = \Delta\mathrm{EPos}/\Delta\mathrm{SPV}$$

We also determined the time between when the chair stopped, and the SPV of PRN reached its peak. We estimated by eye when the TcNI began to return to its normal value by choosing the time point during PRN at a clear inflection point (e.g., **Figure 2D**, arrow) and its corresponding mean SPV.

Statistics

Differences in outcome measures were estimated using separate linear mixed-effects models for each stimulation condition (head

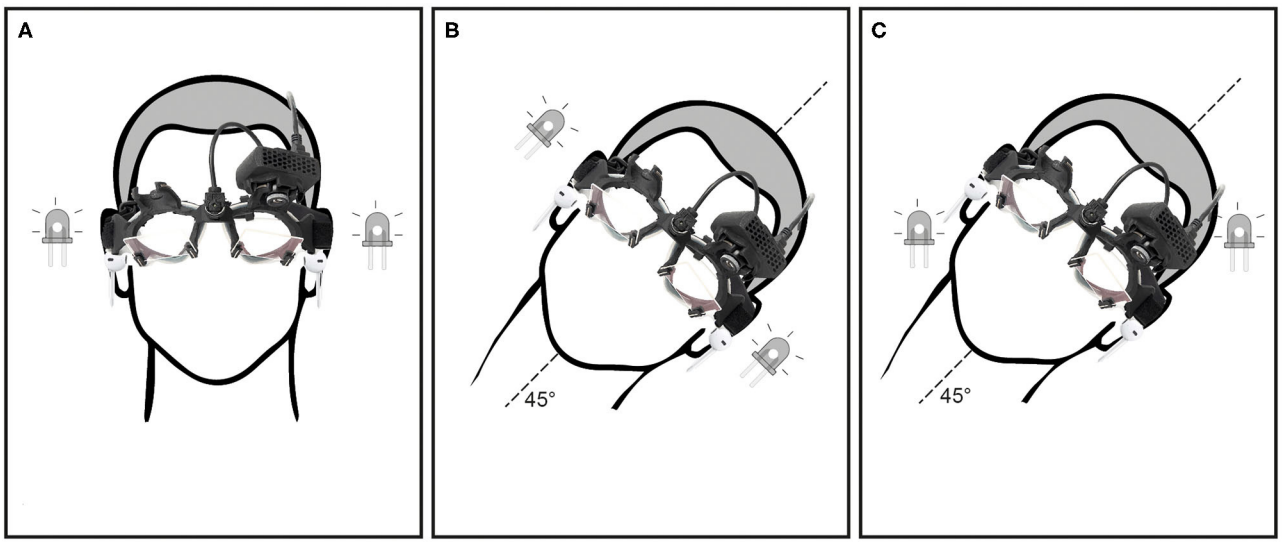

FIGURE 1 | Showing different head and LED positions: **(A)** head upright, LED positioned for horizontal eye movements in the orbit, **(B)** head tilt 45° to the left, LED positioned for horizontal eye movements in the orbit and **(C)** head tilt 45° to the left, LED positioned for oblique (combined horizontal and vertical) eye movements in the orbit.

upright vs. head tilted) and for horizontal and vertical eye movements separately. We evaluated SPV at peak velocity (A) and the TcVOR (b) separately as well.

We used gaze direction (right vs. left or up vs. down) as fixed effects and a subject-level random effect to account for paired measurements. To compare horizontal ΔSPV between the two stimulations, we included the test condition (head upright vs. head tilted) interacting with the gaze direction. We used general linear hypothesis testing with two-tailed tests and Holm correction for *post-hoc* comparisons among the test conditions (9). A significance level of 0.05 was used for all comparisons. The statistical analysis was performed with the R environment (v3.4, R Core Team) (10).

RESULTS

We excluded trial runs when datasets did not meet pre-defined quality criteria. The main reasons for excluding data were poor VOG eye tracking due to eyelid artifacts or blinking, and inability to maintain eye position at the locations of interest. For the assessment of AL in horizontal eye positions, eight datasets fulfilled the inclusion criteria for lateral SCC stimulation, and seven for combined stimulation. For vertical eye positions, six data sets fulfilled the inclusion criteria.

Mean TcNI for eccentric right and left gaze before rotation was 21 s (±8.2). **Figure 2** shows an example for horizontal SPV of PRN at both right and left gaze in the head upright position (**Figure 1**, condition A). There is a stronger PRN in left gaze than in right gaze, thus following AL. Panel D in **Figure 2** depicts how the TcNI varied over time. AL appeared virtually immediately, at least within the resolution of our measurements (onset at ∼3 s after chair rotation). For all subjects, at peak SPV, the difference in amplitude between right and left gaze (ΔSPV = 20.4°/s) was significant for horizontal PRN (p = 0.0065) in the head upright paradigm (**Figure 1A**) and the TcNI was low (1.1 s, **Table 1**). When TcNI began to recover (TcNI > 5 s), the SPV of PRN had diminished into the range of 6–18°/s (mean 12°/s) and AL was no longer present despite the residual PRN.

In the head tilted paradigm (combined horizontal/vertical SCC stimulation, **Figure 1B**) for all subjects the difference in the amplitude of the horizontal eye component of PRN (ΔSPV) between right and left gaze at peak SPV was 18.7°/s (p = 0.00882) corresponding to a TcNI of 1.3 s. Examining the vertical component in the head tilted paradigm (**Figure 1C**), the ΔSPV between up and down gaze at peak SPV was 20.3°/s (p = 0.00303) corresponding to a TcNI of 1.0 s. There was, however, no significant difference for the vertical component of the PRN at peak SPV (3 s time interval) in left or right gaze (p = 0.87). Likewise, there was no significant difference in the time constant of the decay (TcVOR) (p = 0.26) of PRN in up- and downward gaze.

Figure 3 illustrates the fitted negative exponential curves from all subjects derived from the parameters of the mixed effects model and the corresponding time constants (TcNI) for horizontal and combined horizontal and vertical SCC stimulations. **Table 1** shows the aggregate results of all three tested conditions using the mixed effects model. There is statistically no difference in the TcVOR in any condition between left and right gaze or up and down gaze (range 8.1–11 s). In other words, TcVOR, reflected in the decay of PRN was not different between head orientations or eye positions in the orbit.

For one subject, we rotated the subject head upright at two different chair rotation velocities, 100°/s and 200°/s (**Figures 4A,B**). The two SPV curves overlapped, decaying

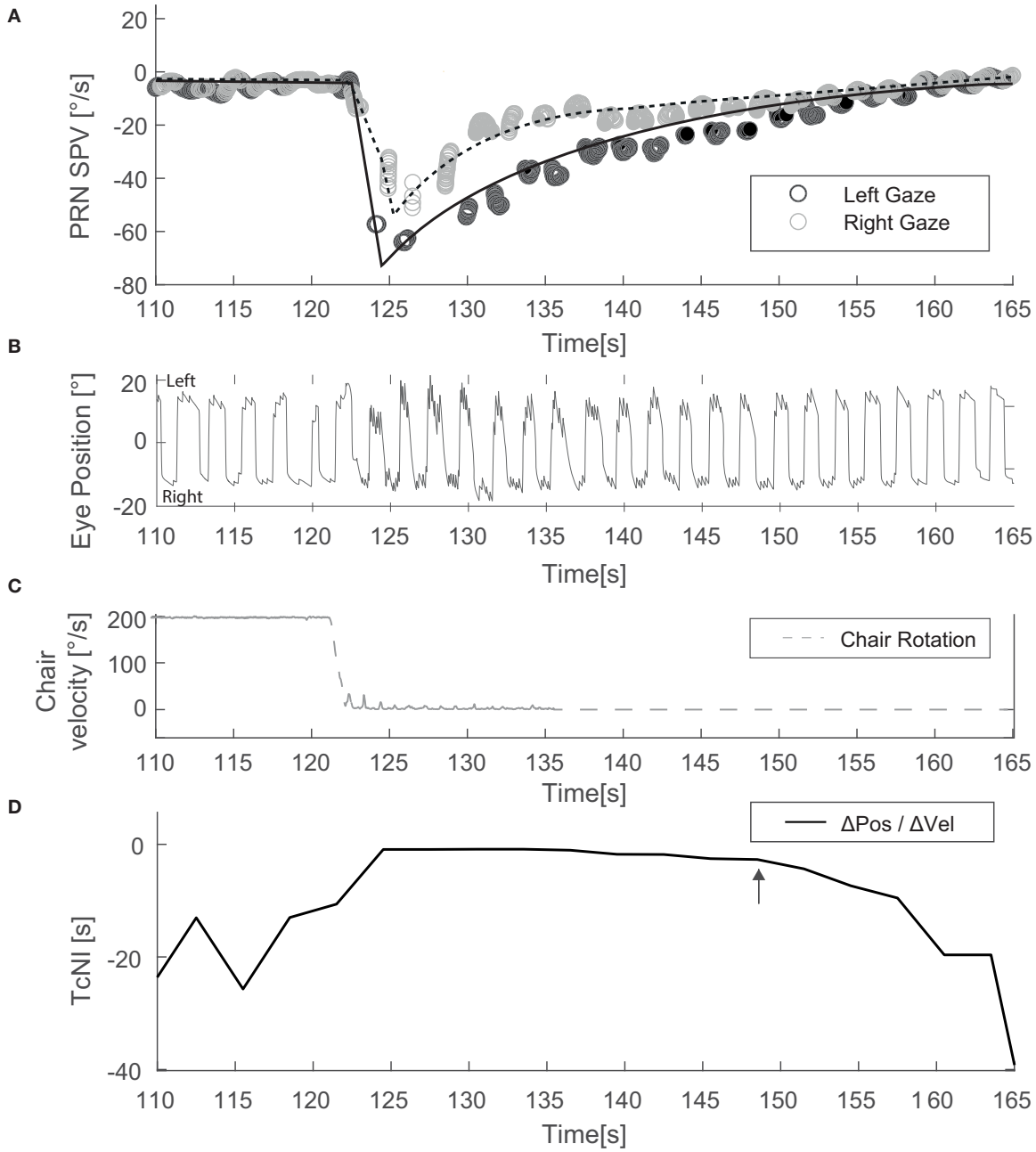

FIGURE 2 | Example of an experiment with the head upright and alternating horizontal gaze (Condition **Figure 1A**). **(A)** Depicts SPV over time just before and after the chair has stopped. **(B)** Illustrates the corresponding eye position data. **(C)** Shows the rotational stimulus used (chair velocity). **(D)** Shows TcNI as a function of time. The arrow indicates the estimated point when the TcNI began to recover toward normal.

at the same rate. In both paradigms the TcNI was initially decreased and then began to rise again when SPV dropped to comparable values: 21°/s at 3.5 s after peak velocity for the 100°/s rotation, vs. 18°/s at 12 s after peak velocity for the 200°/s rotation. In other words, the TcNI began to return toward normal when slow-phase velocity decreased to a range of values, rather than at the same time point in the decay of PRN.

DISCUSSION

The main findings of our study were 3-fold. AL was apparent almost immediately at the onset of PRN. AL began to fade when PRN reached a value in the 6–18°/s range. AL was present for pure horizontal and for mixed horizontal/vertical SCC stimulation. We will discuss possible mechanisms for these findings.

TABLE 1 | SPV, TcVOR, and TcNI for all three conditions.

SCC stimulation and target configuration	*n*	Gaze	Peak SPV amplitude (°/s)	TcVOR (s)	*P*-value right vs. left TcVOR	ΔSPV (°/s) at peak SPV (*p*-value)	TcNI (s) at peak SPV
Horizontal (**Figure 1A**)	9	Right	60.6	9.9	0.4141	20.4 (0.00655)	1.1
		Left	81.0	11.0			
Combined Horizontal/Vertical (**Figure 1B**)	8	Right	55.6	8.8	0.948	18.7 (0.00882)	1.3
		Left	74.3	8.9			
Combined Horizontal/Vertical (**Figure 1C**)	6	Down	48.7	8.1	0.257	20.3 (0.00303)	1.0
		Up	69.0	10.7			

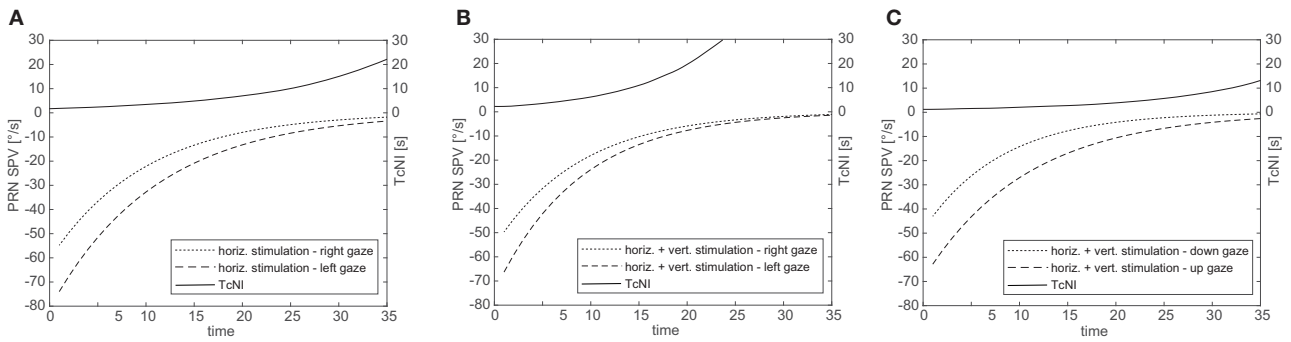

FIGURE 3 | Aggregate results for all subjects for SPV decay over time for right and left gaze **(A,B)** and up and down gaze **(C)**. The solid line illustrates the corresponding TcNI. Note that the TcNI begins to return toward normal when SPV drop to the range of 8–16°/s.

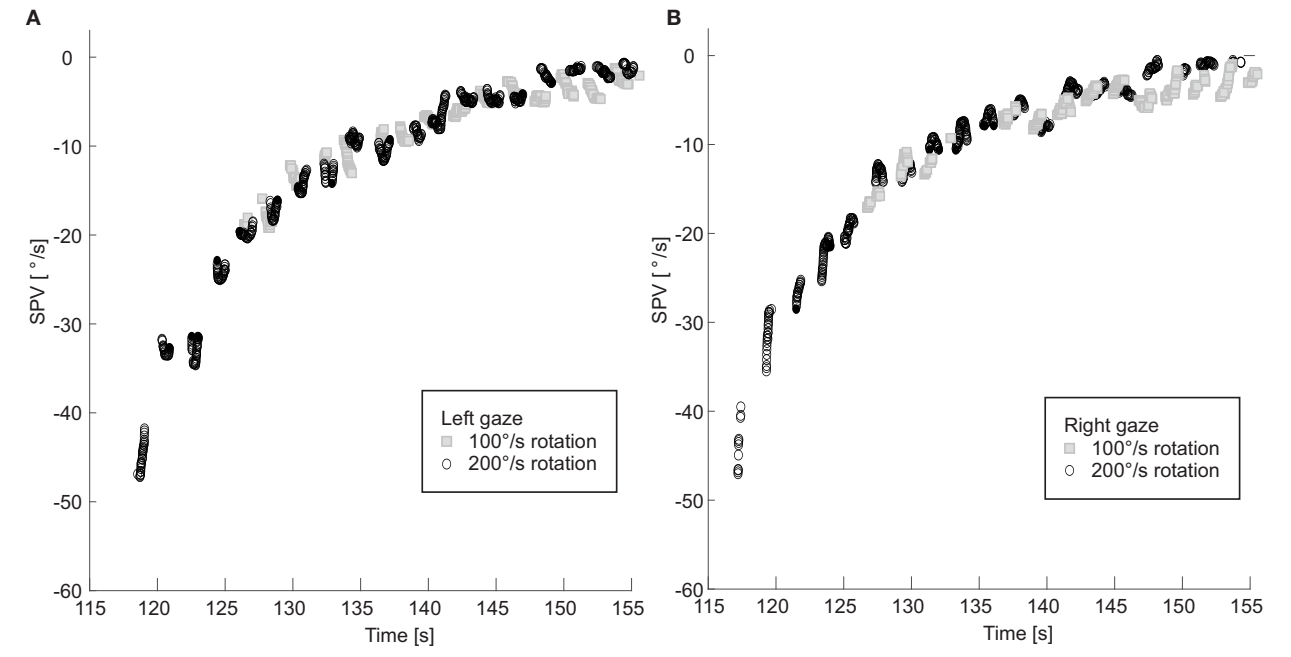

FIGURE 4 | SPV is shown for rotations at 100 and 200°/s with right **(A)** and left **(B)** gaze. Note the two right and left SPV curves still overlap even when the initial slow phase velocities are different.

Is AL an Adaptive Response?

Is AL a goal-driven, "*adaptive*" response to a *pathological* vestibular imbalance? The idea is that one can counteract the unwanted bias of a pathological SN by purposefully impairing the function of the ocular motor neural integrators (NI) that provide the signals to hold steady eccentric positions of gaze (2). By making the NI "leaky," the nystagmus can be diminished or even nullified by moving the eyes to a position in the orbit in the direction of the slow phase of the SN. This concept reflects the general idea that the effect of persistent integration (perseveration) of unwanted biological noise—in this case the sustained pathological bias of SN—can be lessened by disabling neural integrator circuits. An analogous argument can be made for the gradual decrease (habituation) of the time constant of the velocity-storage integrator of the VOR when faced with the recurring nystagmus produced with repetitive constant-velocity (low frequency) chair rotations (2). The repetitive per- and post-rotatory nystagmus induced by this paradigm is interpreted as arising from a lesion, and hence the integrating (perseverating) circuits are disabled. Our results, however, suggest that the change in the TcNI was not time dependent. If it were adaptive it would more likely be time dependent.

Is AL a Result of the Non-linear Properties of Neuronal Discharge Rates in the Vestibular Nuclei?–Results in Normal Subjects With Normal Patterns of Stimulation

The alternative hypothesis suggests that AL develops from the inherent physiological properties of the brainstem nuclei that process information both for the vestibulo-ocular reflex and for normal gaze holding. Particularly cogent arguments have been made for this view by the Zurich group (7, 11) and our results are largely in accord with their interpretation. First, using the decaying response of PRN as was induced in our rotatory chair paradigm, we confirmed that AL occurs in normal individuals, and when there is a natural reciprocal pattern of stimulation of both labyrinths. AL does not require that the sustained nystagmus be pathological as in a patient with loss of function in one labyrinth, nor produced with an unnatural stimulus in a normal individual as occurs with unilateral caloric stimulation. Future studies should investigate AL behavior in patients with unilateral vestibular loss or with vestibulocerebellar lesions.

Does AL Take Time to Develop?

Within the limits of the capabilities of our experimental paradigms, AL appeared to begin promptly after the PRN began. There certainly could not have been a delay of more than a few seconds after the slow-phase velocity of the PRN reached its peak. We also showed a similar delay in the several subjects in whom we analyzed the earliest stage of their per-rotatory nystagmus. AL was already apparent once slow-phase velocity had reached its peak indicating that the prompt appearance of AL in the post-rotatory phase was not a result of the immediately preceding per-rotatory stimulus. Furthermore, we showed that the dissipation of AL as the PRN lessened was related to dropping to a specific range of values of slow-phase velocity (discussed further below), rather than the specific time during the decay of the PRN. In other words, we found no evidence of a delay in when AL is implemented by the brain once a substantial spontaneous nystagmus appeared, nor any relation of the AL effect to the duration of PRN.

On the other hand, our results do not exclude that other parameters of stimulation, such as the frequency content of the stimulus, the degree of eccentricity of eye positions during vestibular stimulation or the values of head acceleration or head velocity, influence the implementation of AL. For example, Anagnostou and Anastasopoulos (12, 13) showed no AL effect in normal subjects during horizontal or vertical head impulse testing (which is a high frequency, high acceleration stimulus). Similarly, Robinson et al. showed no AL effect for natural sinusoidal rotations (0.5 Hz) but the velocities were relatively low (peak velocity $< 30^{\circ}$/s) (2).

Is AL Related to the Amplitude of the Velocity Bias Created by a Sustained Nystagmus?

We showed a clear lessening of the AL effect over time in individual trials when the overall SPV of the PRN declined to a specific range of values. For all subjects at a mean value of 12.1°/s (range 6.4–18.1°/s) the inferred calculation of the TcNI increased relatively abruptly and soon reached a plateau at its previous normal high value. This finding is in accord with the result shown in Figure 4C of Bockisch et al. (14) in which the AL effect was greater for a higher SPV. This can be interpreted as the higher the SPV, the more likely the circuits that implement the VOR will show the non-linear effects of saturation, in which (1) neurons lose their ability to fire at higher rates in their excitatory direction and, (2) because of the effects of inhibitory cutoff at higher speeds of rotation, neurons can no longer decrease their discharge in a reciprocal fashion. The values for cutoff may be less in patients with unilateral hypofunction (15) since in these situations AL appears for even lower velocities of SN than we found in our normal subjects in our rotational chair paradigm.

Khojasteh et al. (11) developed a control systems model based on the known physiology of vestibular neurons in the face of asymmetrical inputs, and was able to simulate much of the known empirical data about AL. It is important to remember that the gaze-holding networks of the ocular motor NI for control of eye position are closely intertwined with the networks that generate the slow-phase velocities of the VOR. In the case of horizontal eye movements, for example, both functions are accomplished by shared neurons in the medial vestibular nucleus and the nucleus pre-positus hypoglossi (16). The saturation or inhibition effects of a high-velocity vestibular imbalance can be reflected in the effects of eye position on slow-phase velocity of the nystagmus, i.e., AL. In other words, as in the formulation of Khojasteh et al. (11), AL does not reflect changes in the function of the NI *per se*, but are driven by the direct effects of a vestibular imbalance on the same neurons in the vestibular nuclei that generate both the VOR and gaze-holding commands. Thus, neither a bias alone (e.g., Doslak et al. (6) and Jeffcoat et al. (8))

nor a change in the integrator alone (e.g., Robinson et al. (2)) explains AL.

As another result of our experiments, we noted that the AL effects were similar following both stimulation of the lateral SCC alone and of the lateral and vertical SCC together. The interaction between simultaneous horizontal and vertical stimulation had no impact on the AL effect nor on the overall TcVOR of either the horizontal or the vertical components of the PRN. Likewise, we showed that the AL effect was not directly related to vertical vs. horizontal eye positions in the orbit but rather to the direction of the vertical and horizontal eye movements produced relative to the requirements dictated by the pattern of stimulation of the SCC (17).

Caveats and Limitations

We cannot exclude a small delay in the onset of AL, because our paradigm led to a strong nystagmus at the onset and offset of chair rotation, often causing artifacts due to blinks or imprecise gaze directions and thus decreased the amount of usable early data. Nystagmus might have been partially suppressed due to fixation on the blinking LEDs (20 ms) and potentially led to a smaller AL effect overall or at different times in the period of fading nystagmus. However, the relatively high speed of the nystagmus and the extremely brief period of exposure (20 ms) to the LED would lead to only a small amount of retinal image motion, equivalent to just a few degrees every 2 s that would not effectively drive visual suppression of the PRN.

Small suppression effects by head pitched downwards might have biased our results, however, these effects were considered negligible at 30° tilt compared to the traditional tilt suppression test with 90° head tilt (18).

The eccentric gaze positions and the timing of changing them in our paradigms were limited and symmetric. It is possible that our results would have been different if we used larger or smaller eccentric eye positions or different patterns of the timing of change in position. For example, effects like those that underlie rebound nystagmus might have influenced the estimates of the time constant of the neural integrator if there had been some asymmetry in the eccentric eye positions (19). In addition, we never measured the influence of AL on other aspects of function of the NI such as its direct effects on the phase of the VOR (20). More scrutiny of both the rise and the decay patterns of per- and post-rotatory nystagmus with a more sensitive recording technique such as with scleral search coils might reveal subtle deviations from the expected pattern from a simple exponential decay, and a more precise measure of the thresholds of the appearance and decay of AL. While the choice of the threshold when the TcNI began to recover was qualitative and by visual inspection the results were consistent among subjects.

CONCLUSIONS

Even with its limitations our results strongly support the idea that AL develops because of the effects of the non-linear discharge properties of neurons within the common circuits that mediate the horizontal VOR and horizontal gaze-holding. Furthermore, stimulation of both vertical and horizontal SCC showed that AL was related to the predicted plane of rotation of the eyes based on the pattern of activation of the SCC.

DATA AVAILABILITY STATEMENT

The original contributions presented in the study are included in the article/supplementary materials, further inquiries can be directed to the corresponding author.

ETHICS STATEMENT

The studies involving human participants were reviewed and approved by Kantonale Ethikkommission, KEK-Gesuchs-Nr.: 047/14, PB_2016-00680. The patients/participants provided their written informed consent to participate in this study.

AUTHOR CONTRIBUTIONS

CL: subject recruitment, data collection, data analysis, and drafting the article. DZ: conceptualization, supervision, methodology, data analysis, and drafting the article. TW: software, data analysis, and critical revision of the article. WW: data analysis and critical revision of the article. AK: data collection, database setup, and critical revision of the article. CS: database setup and critical revision of the article. MC: supervision, funding acquisition, and critical revision of the article. DZ, TW, WW, AK, CS, and MC: final approval of the version to be published. GM: conceptualization, supervision, methodology, data analysis, drafting the article, supervision, project administration, and funding acquisition. All authors contributed to the article and approved the submitted version.

FUNDING

GM was supported by the Swiss National Science Foundation (Grant #320030_173081). DZ was supported by a Guest Professorship Grant, Inselspital Bern, University of Bern.

ACKNOWLEDGMENTS

We thank Jorge Otero-Millan, Johns Hopkins University School of Medicine, for his valuable technical support.

REFERENCES

1. Alexander G. Die Ohrenkrankheiten im Kindesalter. In: Pfaundler M, Schlossmann A, editors. *Handbuch der* Kinderheilkunge. Vogel: Leipzig (1912). p. 84–96.
2. Robinson DA, Zee DS, Hain TC, Holmes A, Rosenberg LF. Alexander's law: its behavior and origin in the human vestibulo-ocular reflex. *Ann Neurol.* (1984) 16:714–22. doi: 10.1002/ana.410160614
3. Robinson DA. Eye movement control in primates. *Science.* (1968) 161:1219–24. doi: 10.1126/science.161.3847.1219

4. Bertolini G, Tarnutzer AA, Olasagasti I, Khojasteh E, Weber KP, Bockisch CJ, et al. Gaze holding in healthy subjects. *PLoS ONE*. (2013) 8:e61389. doi: 10.1371/journal.pone.0061389
5. Hess K, Reisine H. Counterdrifting of the eyes: additional findings and hypothesis. *ORL J Otorhinolaryngol Relat Spec*. (1984) 46:1–6. doi: 10.1159/000275677
6. Doslak MJ, Dell'Osso LF, Daroff RB. A model of Alexander's law of vestibular nystagmus. *Biol Cybern*. (1979) 34:181–6. doi: 10.1007/BF00336969
7. Khojasteh E, Bockisch CJ, Straumann D, Hegemann SC. A dynamic model for eye-position-dependence of spontaneous nystagmus in acute unilateral vestibular deficit (Alexander's Law). *Eur J Neurosci*. (2013) 37:141–9. doi: 10.1111/ejn.12030
8. Jeffcoat B, Shelukhin A, Fong A, Mustain W, Zhou W. Alexander's law revisited. *J Neurophysiol*. (2008) 100:154–9. doi: 10.1152/jn.00055.2008
9. Holm S. A simple sequentially rejective multiple test procedure. *Scand J Stat*. (1979) 6:65–70.
10. R Core Team. *A Language and Environment for Statistical Computing*. Vienna: R Foundation for Statistical Computing (2018).
11. Khojasteh E, Bockisch CJ, Straumann D, Hegemann SC. A mechanism for eye position effects on spontaneous nystagmus. *Conf Proc IEEE Eng Med Biol Soc*. (2012) 2012:3572–5. doi: 10.1109/EMBC.2012.6346738
12. Anastasopoulos D, Anagnostou E. Invariance of vestibulo-ocular reflex gain to head impulses in pitch at different initial eye-in-orbit elevations: implications for Alexander's law. *Acta Otolaryngol*. (2012) 132:1066–72. doi: 10.3109/00016489.2012.682120
13. Anagnostou E, Heimberger J, Sklavos S, Anastasopoulos D. Alexander's law during high-acceleration head rotations in humans. *Neuroreport*. (2011) 22:239–43. doi: 10.1097/WNR.0b013e3283451769
14. Bockisch CJ, Khojasteh E, Straumann D, Hegemann SCA. Eye position dependency of nystagmus during constant vestibular stimulation. *Exp Brain Res*. (2013) 226:175–82. doi: 10.1007/s00221-013-3423-6
15. Hegemann S, Straumann D, Bockisch C. Alexander's law in patients with acute vestibular tone asymmetry–evidence for multiple horizontal neural integrators. *J Assoc Res Otolaryngol*. (2007) 8:551–61. doi: 10.1007/s10162-007-0095-6
16. Cannon SC, Robinson DA. Loss of the neural integrator of the oculomotor system from brain stem lesions in monkey. *J Neurophysiol*. (1987) 57:1383–409. doi: 10.1152/jn.1987.57.5.1383
17. Bockisch CJ, Hegemann S. Alexander's law and the oculomotor neural integrator: three-dimensional eye velocity in patients with an acute vestibular asymmetry. *J Neurophysiol*. (2008) 100:3105–16. doi: 10.1152/jn.90381.2008
18. Hain TC, Zee DS, Maria BL. Tilt suppression of vestibulo-ocular reflex in patients with cerebellar lesions. *Acta Otolaryngol*. (1988) 105:13–20. doi: 10.3109/00016488809119440
19. Otero-Millan J, Colpak AI, Kheradmand A, Zee DS. Rebound nystagmus, a window into the oculomotor integrator. *Prog Brain Res*. (2019) 249:197–209. doi: 10.1016/bs.pbr.2019.04.040
20. Skavenski AA, Robinson DA. Role of abducens neurons in vestibuloocular reflex. *J Neurophysiol*. (1973) 36:724–38. doi: 10.1152/jn.1973.36.4.724

Conflict of Interest: The authors declare that the research was conducted in the absence of any commercial or financial relationships that could be construed as a potential conflict of interest.

frontiers in Neurology

REVIEW
published: 25 November 2020
doi: 10.3389/fneur.2020.593919

Effects of Noise Exposure on the Vestibular System: A Systematic Review

Courtney Elaine Stewart[1,2]*, *Avril Genene Holt*[3,4], *Richard A. Altschuler*[1,2], *Anthony Thomas Cacace*[5], *Courtney D. Hall*[6,7], *Owen D. Murnane*[8,9], *W. Michael King*[1] and *Faith W. Akin*[8,9]

[1] University of Michigan Department of Otolaryngology/Head-Neck Surgery, Kresge Hearing Research Institute, Ann Arbor, MI, United States, [2] VA Ann Arbor Healthcare System, Research Service, Ann Arbor, MI, United States, [3] Department of Ophthalmology Visual and Anatomical Sciences, Wayne State University School of Medicine, Detroit, MI, United States, [4] John D. Dingell VA Medical Center, Molecular Anatomy of Central Sensory Systems Laboratory, Research Service, Detroit, MI, United States, [5] Department of Communication Sciences and Disorders, Wayne State University, Detroit, MI, United States, [6] Department of Rehabilitative Sciences, Doctor of Physical Therapy Program, East Tennessee State University, Johnson City, TN, United States, [7] Gait and Balance Research Laboratory, James H. Quillen VA Medical Center, Mountain Home, TN, United States, [8] Department of Audiology and Speech-Language Pathology, East Tennessee State University, Johnson City, TN, United States, [9] Vestibular Research Laboratory, James H. Quillen VA Medical Center, Mountain Home, TN, United States

Despite our understanding of the impact of noise-induced damage to the auditory system, much less is known about the impact of noise exposure on the vestibular system. In this article, we review the anatomical, physiological, and functional evidence for noise-induced damage to peripheral and central vestibular structures. Morphological studies in several animal models have demonstrated cellular damage throughout the peripheral vestibular system and particularly in the otolith organs; however, there is a paucity of data on the effect of noise exposure on human vestibular end organs. Physiological studies have corroborated morphological studies by demonstrating disruption across vestibular pathways with otolith-mediated pathways impacted more than semicircular canal-mediated pathways. Similar to the temporary threshold shifts observed in the auditory system, physiological studies in animals have suggested a capacity for recovery following noise-induced vestibular damage. Human studies have demonstrated that diminished sacculo-collic responses are related to the severity of noise-induced hearing loss, and dose-dependent vestibular deficits following noise exposure have been corroborated in animal models. Further work is needed to better understand the physiological and functional consequences of noise-induced vestibular impairment in animals and humans.

Keywords: vestibular system, noise-induced vestibular loss, saccule and utricle, semicircular canals, impulse noise, continuous noise, vestibular nuclear complex

OPEN ACCESS

Edited by:
Michael Strupp, Ludwig Maximilian University of Munich, Germany

Reviewed by:
Leonardo Manzari, MSA ENT Academy Center, Italy
Ian S. Curthoys, The University of Sydney, Australia

***Correspondence:**
Courtney Elaine Stewart
cestewar@med.umich.edu

Specialty section:
This article was submitted to Neuro-Otology, a section of the journal Frontiers in Neurology

Received: *11 August 2020*
Accepted: *28 September 2020*
Published: *25 November 2020*

Citation:
Stewart CE, Holt AG, Altschuler RA, Cacace AT, Hall CD, Murnane OD, King WM and Akin FW (2020) Effects of Noise Exposure on the Vestibular System: A Systematic Review. Front. Neurol. 11:593919. doi: 10.3389/fneur.2020.593919

INTRODUCTION

It is well-established that noise overstimulation has the potential to cause temporary or permanent damage to sensory cells in the cochlea and the afferent neurons innervating them, resulting in temporary or permanent loss of hearing [for review see: (1, 2)]. Less known and considerably less understood are the effects of noise on vestibular and balance function. Similar to the cochlea, the vestibular sensory end organs are housed within the temporal bone and membranous labyrinth of the inner ear. Hair cells, the sensory cells of the inner ear, share similar morphology in

the vestibular end organs and in the organ of Corti; they both transduce displacement of hair-bundles into neural activity through the shared vestibulocochlear nerve (CN VIII). Five peripheral vestibular end organs (three semicircular canal cristae and two otolith organs) provide sensory input to vestibular nuclei as well as the vestibular cerebellum and contribute to vestibulo-ocular and vestibulo-spinal reflexes (VOR and VSR; **Figure 1**). Although a primary role of the mammalian vestibular system is to maintain gaze and postural stability, neurophysiological studies demonstrate that, like the cochlea, the vestibular end organs, and the saccule and utricle (otolith organs) in particular, are sensitive to sound [e.g., (3–5) for reviews see (6, 7)]. Large diameter afferents with calyceal terminations are characterized by phase-locking and an irregularly discharging firing rate (8–10), high sensitivity to linear forces (11), and increased firing in response to air-conducted sound or bone-conducted vibration (3, 4, 12). The properties of irregular vestibular afferents have been described in detail [(13); for reviews see (6, 14)]. Their physiological properties and sound-sensitivity put these afferents at greater risk for noise-induced damage. Specifically, since irregular vestibular afferents can be activated by sound, it follows that this population may be over-stimulated by sound, and therefore susceptible to noise-induced damage. Noise exposures can be grouped into one of two types—impulse or continuous noise. Continuous noise occurs over an extended period of time, whereas impulse noise occurs rapidly, and generally at a considerably higher sound pressure level (SPL). Both types of noise exposures will be explored in this review with a description of the anatomical, neurophysiological, and functional evidence for noise-induced damage to the vestibular system.

ANATOMICAL EVIDENCE FOR NOISE-INDUCED DAMAGE TO THE VESTIBULAR PERIPHERY

Continuous Noise Exposure

Similar to the auditory system, animal models of continuous noise exposure have revealed that damage to the vestibular periphery is dependent on characteristics of the noise, including: duration, frequency, level, and time course. The duration of noise exposure varies across experiments ranging from <1 h to more than 1 day and likely contributes to the level of tissue damage observed across studies. In an early study, Mangabeira-Albernaz et al. (15) used a wide range of frequencies (170–50,000 Hz) and durations (5–160 min) at high SPLs (118–133 dB), and then allowed 0–133 days of recovery before tissue collection. Across all of the tissue analyzed, saccular collapse was observed in approximately one third of the samples and utricular rupture was observed in approximately one third of the samples. Saccular rupture was identified in ∼25% of the samples, and utricular collapse was least commonly observed, in ∼15% of samples. When this damage is categorized by frequency, saccular rupture was most prevalent with 0.5–2 kHz noise exposure (142–150 dB SPL, 1–4 min), and saccular collapse was most prevalent with 4 kHz noise exposure (150–163 dB SPL, 1–2 min). Utricular rupture was most prevalent with 1–4 kHz, and 40–50 kHz (142–163 dB SPL, 1–4 min and 140–144.5 dB, 2–4 min, respectively), and utricular collapse did not appear to occur at a specific frequency. Interestingly, rupture of the saccule was not changed with post-noise exposure recovery time, but rupture of the utricle became less common as post-noise exposure recovery time increased. Conversely, utricular collapse was not impacted by post-noise exposure recovery time, but saccular collapse was more common as post-noise exposure recovery time increased. This study laid the groundwork for more recent work and provided early evidence of noise-induced damage to the vestibular periphery.

Hsu et al. (16) demonstrated the impact of duration of noise exposure on tissue damage by delivering a broadband noise of identical intensity (115 dB SPL) to guinea pigs for either 30 min or 40 h. Assessment of general morphology using light and electron microscopy showed no signs of saccular disruption 1 week after noise exposure with the short term 30-min exposure. The long-term 40-h exposure resulted in otolithic membrane disruption, as well as atrophy and vacuolization in type I saccular hair cells. There was little damage to type II hair cells or supporting cells and the vestibular nerve was intact 1 month after noise exposure (16).

The time course of noise exposure also influences the potential for peripheral vestibular damage. Akdogan et al. (17) compared vestibular changes in guinea pigs exposed to an intense (120 dB SPL) 6-h 4 kHz octave band (continuous) noise vs. a group exposed to intermittent noise (1-h exposure followed by a 1-h break, alternating for 12 h). Damage was identified in the continuous, but not the intermittent noise exposure group. This damage included large vacuoles and enlarged mitochondria with crystolysis in epithelial cells from saccular maculae and apoptosis of non-sensory cells (stromal cells and osteocytes). This study suggests that intermittent noise exposure is less damaging to the vestibular system than continuous noise exposure. In a similar study, rats were exposed to a continuous 6-h intense (120 dB SPL) 1.5 kHz 3-octave band noise. **Figure 2** shows significant decrease in calretinin immunolabeled calyceal endings observed in rat saccular maculae following a 28-day recovery period; however, hair cell loss was not observed in this study (18). Following a 3-h 116 dB SPL broadband noise exposure, damage to stereocilia bundles without qualitative observation of hair cell loss (absence of scarring where hair-bundles were missing in sensory epithelia) was significant through most of the vestibular labyrinth (saccule, utricle, and anterior and horizontal semicircular canals), with the greatest effect observed in the otolith organs in tissue collected 7 days after noise exposure [(19); **Figure 3**].

The sound levels used to study the effects of continuous noise on the vestibular periphery have ranged from 70 to 150 dB SPL with even higher levels used in impulse noise exposure paradigms. Exposure to lower sound levels over a long time period can produce signs of peripheral vestibular injury (20), whereas higher sound levels can produce damaging effects within minutes (21). Tamura et al. (20) observed a reduction in the number of vestibular hair cells and increased oxidative stress in mice exposed to a relatively low sound level (70 dB SPL) for 1 month. In contrast, a 20-min exposure to a much higher sound level (136 to 150 dB SPL) band-limited noise produced saccular collapse, destruction of otolithic membrane,

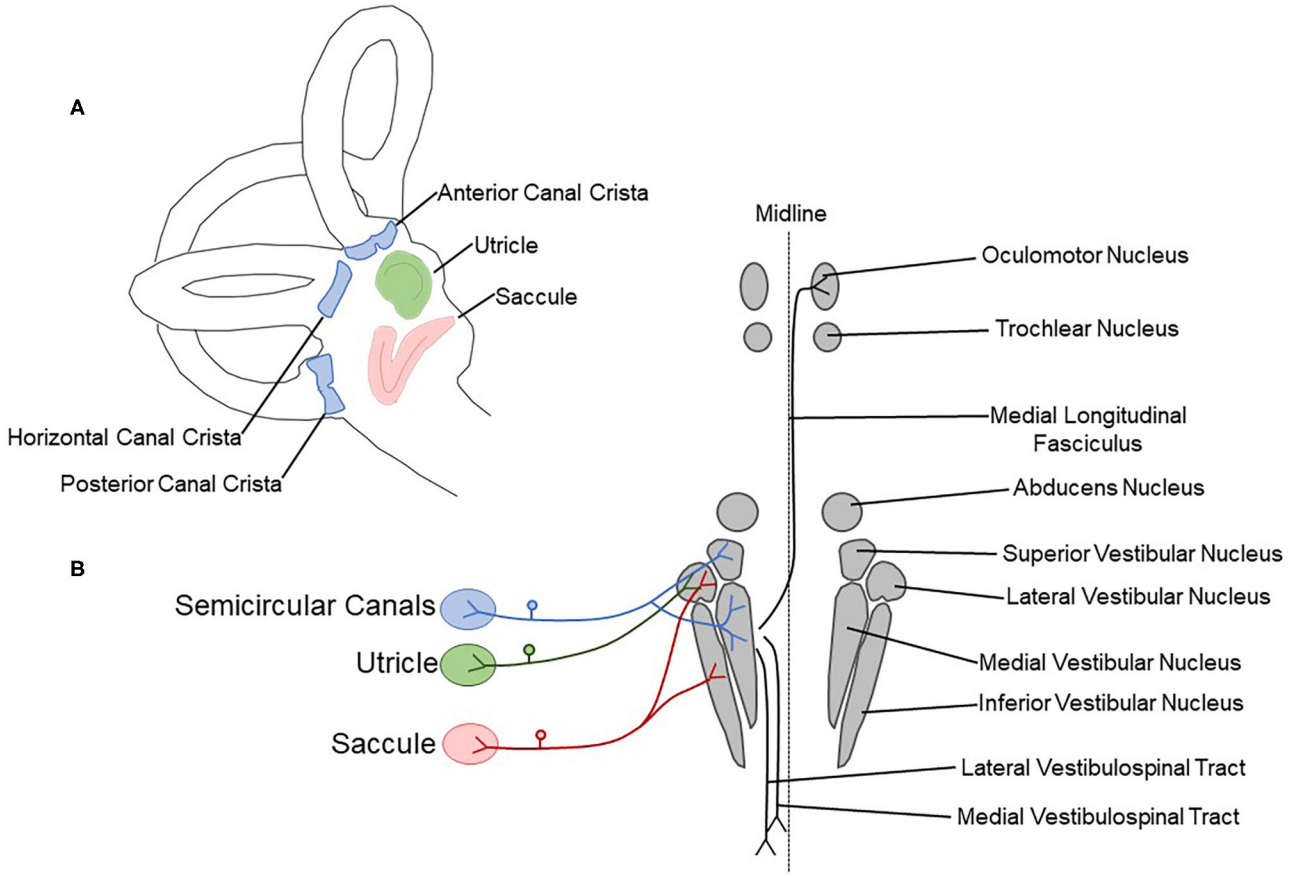

FIGURE 1 | Schematic drawing showing peripheral vestibular sensory organs and central pathways. **(A)** The vestibular labyrinth contains three semicircular canal cristae (anterior, horizontal, and posterior; blue) and two otolith organs (saccule, red; utricle, green). **(B)** The semicircular canal cristae, utricle, and saccule are innervated by the vestibulocochlear nerve (CN VIII). Afferent fibers terminate in the vestibular nuclear complex, containing the superior, lateral, medial, and inferior vestibular nuclei. The medial longitudinal fasciculus, lateral vestibulospinal tract, and medial vestibulospinal tract are critical central components of vestibular reflex pathways.

and detached macular sensory cells (21). It should be noted, however, that in this study the non-saccular vestibular end organs were not affected by the noise exposure.

Evidence for frequency-dependent noise-induced damage has also been described. Tamura et al. (20) examined otolith organs collected from mice that were chronically exposed to low-intensity (70 dB SPL), low-frequency (0.1 kHz) noise. They identified fewer vestibular hair cells and elevated markers of oxidative stress including D-beta-aspartic acid and oxidized phospholipids compared to control animals. Interestingly, damage was not observed in animals exposed to the same duration and level of high-frequency (16 kHz) noise. These results are consistent with the finding that vestibular afferents are most sensitive to low-frequency sound stimulation [e.g., (3)].

The studies reviewed in this section have outlined the consequences of continuous noise exposure and mechanisms underlying damage to the vestibular periphery. Although noise-induced vestibular damage is attributed to excitotoxicity (especially when type I hair cells and calyceal afferents are preferentially impacted) and to direct mechanical trauma, ischemia and free-radical production also contribute to noise-induced damage observed in the vestibular periphery. Using quench-assisted magnetic resonance imaging (QUEST MRI) to measure excessive free radical production *in vivo*, Kühl et al. (22) identified noise-induced free radical production not only in the cochlea, but also in the vestibular aspect of the inner ear of rats exposed to 118 dB SPL, 10 kHz-centered 1/3 octave band noise for 4 h. When compared to normal hearing controls and ears protected from noise exposure by silicone elastomer, the unprotected cochlea of noise exposed rats exhibited elevated MRI R1 values. These increased MRI R1 values were "quenched" by anti-oxidant treatment, indicating the presence of noise induced free radicals. Measurement of MRI R1 values *in vivo* within vestibular related regions of the inner ear in these same animals suggest increased free radical levels after noise exposure (**Figure 4**). Other studies have used post-life measures of noise-induced free radical production. Fetoni et al. (23) exposed guinea pigs to a 6 kHz pure tone at 120 dB SPL for 1 h and identified hair cell loss, a large, progressive increase in vascular endothelial growth factor (VEGF), and a small increase in 4-hydroxynonenal

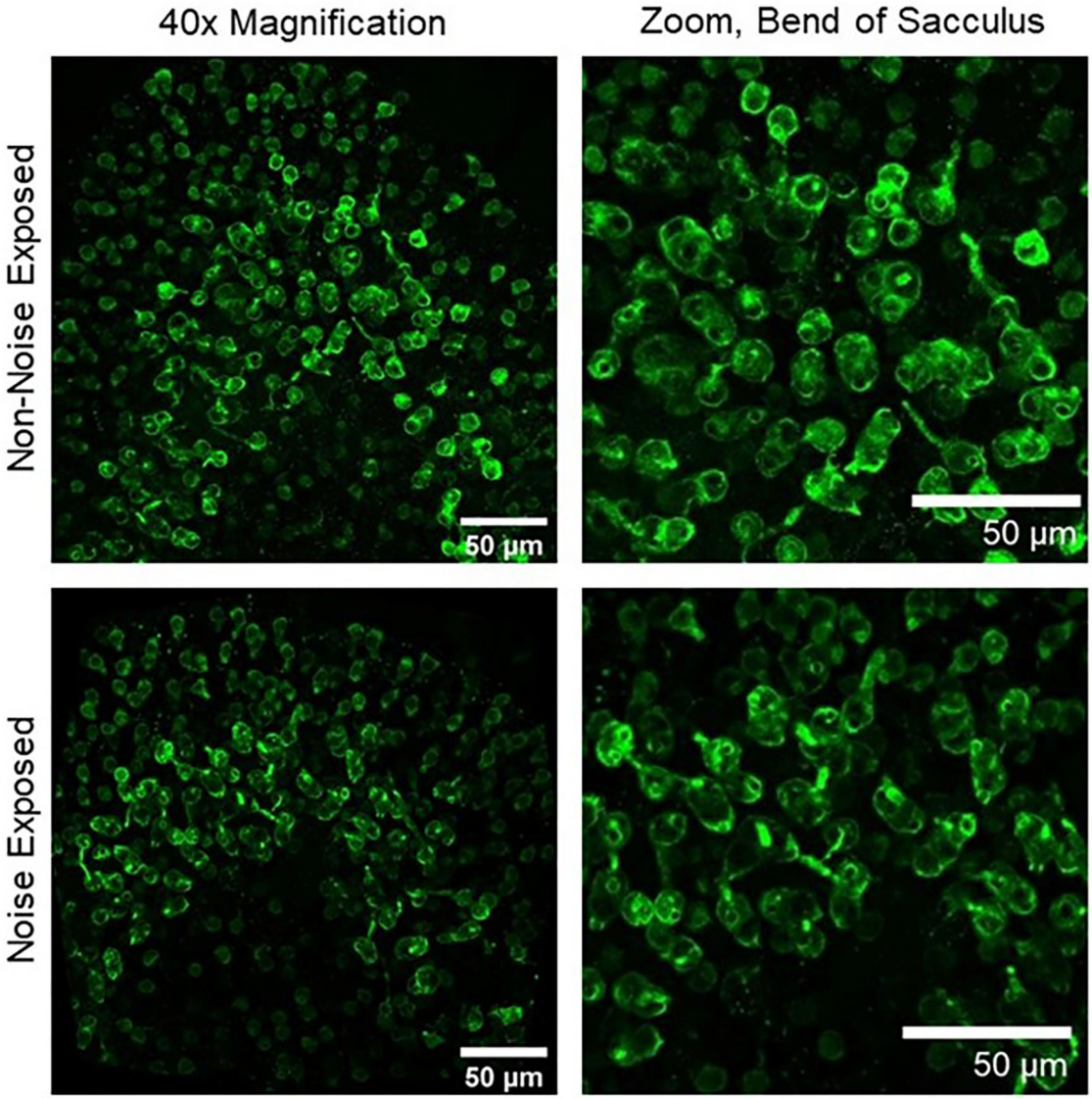

FIGURE 2 | Upper left, 40× magnification image of a non-noise exposed sacculus labeled with calretinin, a marker of calyx-only afferent terminals. Upper right, zoomed image of the bend of the sacculus showing numerous well-labeled calyces in non-noise-exposed tissue. Lower left, 40× magnification image of a noise-exposed sacculus. Lower right, zoomed image of the bend of the sacculus showing a reduction in the number of calretinin-labeled calyces 28 days after noise exposure (18).

(4-HNE). 4-HNE is a product of lipid peroxidation and used as a marker of oxidative stress. VEGF is primarily viewed as an angiogenic factor; it has been suggested that it is also protective against apoptosis (24, 25) and is upregulated in noise-induced hearing loss (26–28). It is possible that VEGF is induced by ischemia (24) and related to the production of reactive oxygen species (29). Tamura et al. (20) exposed mice to a continuous 0.1 kHz noise at 70 dB SPL for 1 month. After noise exposure, the inner ears were paraffin-embedded and sectioned. In sections of the vestibule that contained the otolith organs, hair cell loss and elevated levels of oxidative stress were observed. Oxidative stress was determined as elevated presence of oxidized phospholipids and D-beta-aspartic acid. Both studies suggest that noise exposure can lead to production of free-radicals; however, differences in the identification of free-radicals by Tamura et al. (20) and Fetoni et al. (23) are likely due to differences in the animal model, the selection of antibody targets, and the duration of post-noise recovery prior to tissue analyses. It is also possible that a long duration or a low frequency noise exposure produces the greatest damage, a finding that is relevant to environmental health and workplace safety.

In summary, these studies suggest that both brief exposure to an elevated sound level and sustained exposure to low-frequency continuous sound at more moderate levels can have

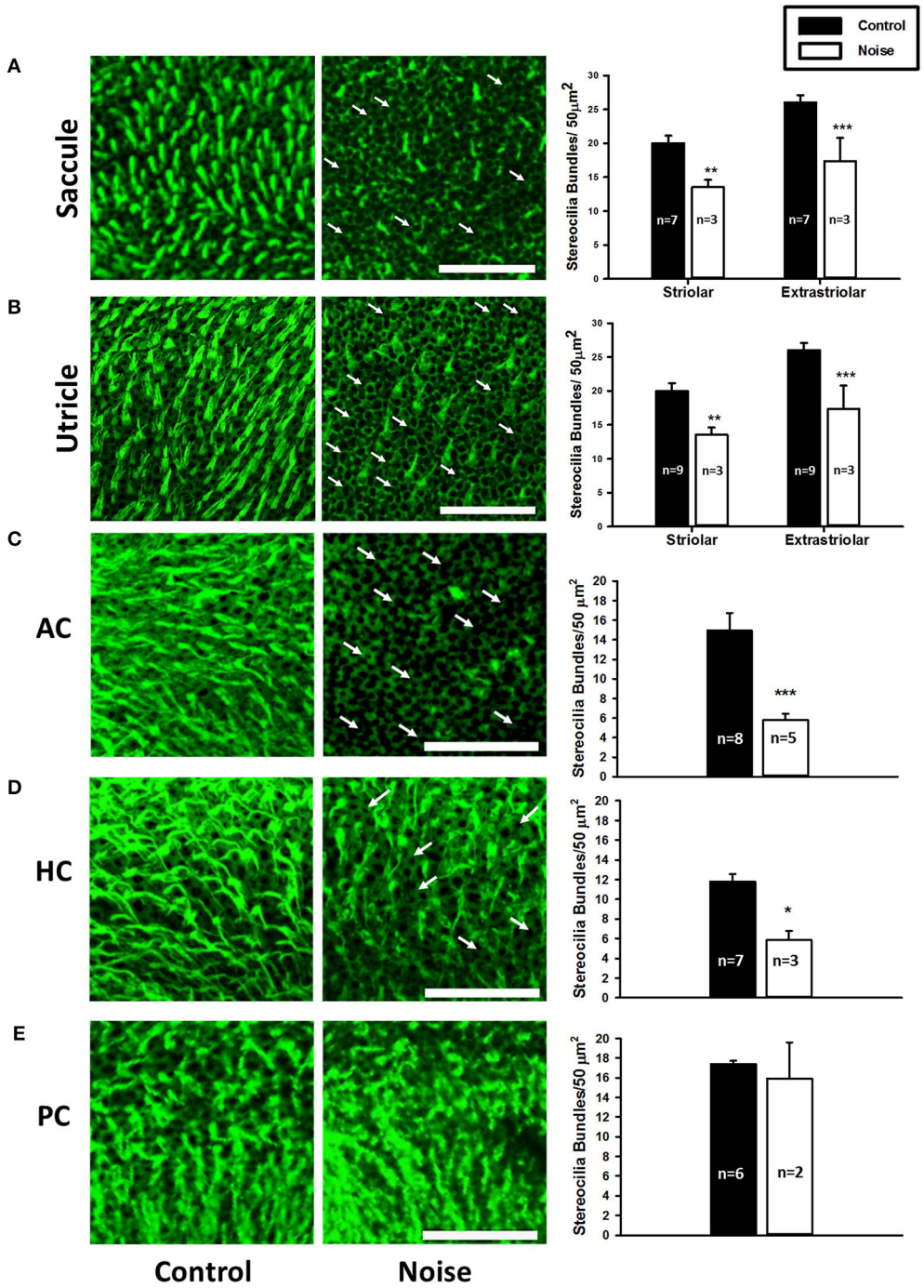

FIGURE 3 | (A,B) Representative images of the saccular macula and the utricular macula stained with phalloidin from control (left panels) and noise-exposed rats (right panels). Arrows indicate intact cuticular plates with missing stereocilia bundles. Scale bar is 50 μm. Noise exposure decreases stereocilia bundle density in both the striolar and extra-striolar regions of the saccules and the utricles (**$P < 0.01$; ***$P < 0.0005$). **(C–E)** Representative images of the anterior (AC), horizontal (HC), and posterior (PC) semicircular canal cristae stained with phalloidin from control (left panels) and noise-exposed rats (right panels). Arrows indicate missing stereocilia bundles. Scale bar is 50 μm. Noise exposure decreases stereocilia bundle density in the AC and HC, but not the PC (*$P < 0.05$; ***$P < 0.0005$). Adapted from (19).

a damaging impact on the vestibular periphery. Comparisons across studies are difficult due to differences in frequency range, duration, sound level, time course, and even animal models; however, it is clear that vestibular damage is measurable following noise exposure. Animal models have revealed cellular and anatomical changes to the vestibular periphery associated

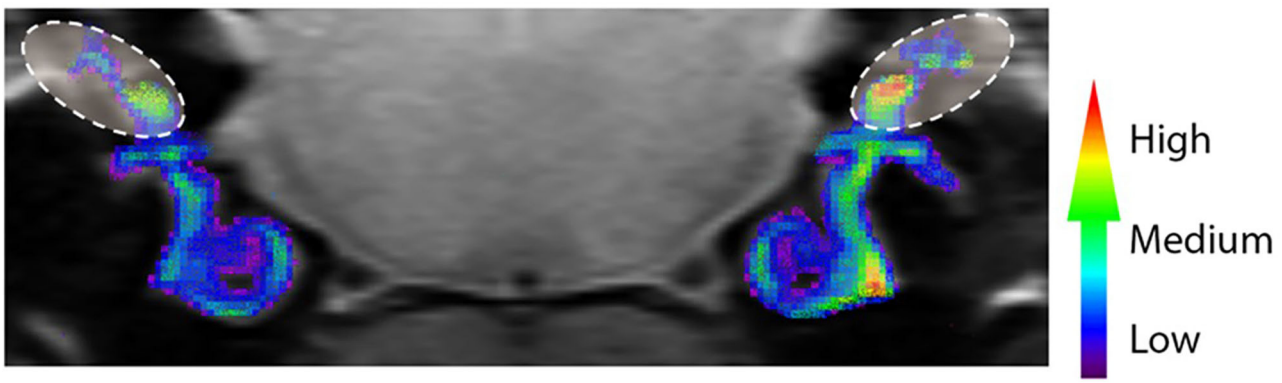

FIGURE 4 | Noise-evoked inner ear oxidative stress measured *in vivo* with QUEST MRI. R1 (1/T1) maps were generated and used to compare protected (plugged ear) and unprotected vestibular end organs and cochleae. Scale bar is a graded colorimetric representation of R1 values. High values are represented as a gradient from red to yellow and low values are represented from blue to purple. Vestibular regions–area within ovals with dashed lines. The R1 values were collected *in vivo* from 400 μm MRI scans. Scans through the cochlear and vestibular ducts were sampled and analyzed from caudal to rostral. Therefore, the coronal image in **Figure 4**, provides views of the regions of interest from caudal to rostral (e.g., the right cochlea is viewed on the right side of the image). Adapted from (22).

with noise overstimulation. Continuous noise-induced damage has been identified with markers of oxidative stress and ischemia; fewer calyceal terminals, loss of stereocilia bundles, hair cell loss, and, with sufficient sound pressure, a complete collapse of the saccule, and destruction of the otoconial matrix overlaying this structure. Most of the research on the effects of continuous noise on the vestibular periphery has examined the impact on the otolith organs, and the saccule is likely the most susceptible to noise-induced damage due to the anatomical proximity of the saccule to the stapes footplate (30) [e.g., (17, 19, 21)]. In contrast, fewer studies have examined noise-induced damage to the semicircular canals (19).

Impulse Noise Exposure

To our knowledge, there is no report that has examined the vestibular aspect of the human temporal bone after continuous or impulse noise exposure. Kerr and Byrne (31), however, examined temporal bones of two victims killed in a Northern Ireland restaurant bombing and their histological examination revealed rupture of the saccule, utricle and basilar membranes following a close-proximity blast.

In guinea pigs exposed to impulse noise from 90 to 300 rifle shots with a peak level of 158 dB SPL at 1.1 kHz, Ylikoski (32) found that the most severe damage occurred in ampullary cristae and the cochlea. This damage was characterized as a separation of sensory epithelium from underlying connective tissue and damage to sensory cells. With this noise exposure condition, epithelial separation occurred less frequently and was less severe in utricular and saccular maculae than in cristae (32). In contrast, Lien and Dickman (33) exposed mice to 63 kPa peak blast waves and observed stereocilia bundle loss in the utricular maculae and horizontal semicircular canal cristae (the sacculus and vertical semicircular canals were not measured), suggesting a broader effect of blast exposure than is seen in other noise exposure paradigms.

Kumagami (34) reported that moderate to extensive endolymphatic hydrops occurred 1 year after exposure to firecracker explosion in Albino guinea pigs. According to the author, from 6 months to 1-year post-exposure, the vestibule and semicircular canals showed slight to moderate endolymphatic hydrops without overt damage to the sensory maculae contained within these structures. In this temporal trajectory, three prominent post-traumatic events occurred: (1) after 4 months, degeneration of the endolymphatic sac was observed, (2) endolymphatic hydrops developed after disappearance of the Preyer reflex in ∼50% of the animals studied, and (3) damage to cochlear hair cells preceded degeneration of epithelial cells in the endolymphatic sac. In summary, these studies suggest that impulse noise may have a broad impact, damaging the ampullary cristae, otolith organ maculae, and endolymphatic sac; however, literature on the impact of impulse noise on tissue damage in the vestibular periphery is limited.

ANATOMICAL EVIDENCE FOR NOISE-INDUCED DAMAGE TO CENTRAL VESTIBULAR PATHWAYS

There is some anatomical evidence for central vestibular pathway damage following exposure to continuous and impulse noises. A gas chromatography mass spectrometry (GC/MS)-based metabolomics platform has been used to show changes in neurotransmitter-related metabolites after exposing rats unilaterally for 1 h to a 16 kHz 110 dB SPL tone (35). After 6 months, increases in glutamic acid were found in both the vestibular nuclear complex (VNC) and the cerebellum. There were also significant increases in the relative abundance of cysteine, urea, and inosine in the VNC while glycine, 3-hydroxybutyrate, and myo-inositol concentrations were elevated in the cerebellum. These chronic changes in metabolites are

suggestive of changes in neuronal activity and the balance between excitation and inhibition (i.e., increased endocytosis).

Kaur et al. (36) evaluated the cerebellar cortex of rats in response to blast exposure. When examined 4 to 7 days after the blast exposure, ultrastructural analysis using electron microscopy revealed neurons with darkened dendrites (dark appearance of cytoplasm within dendritic processes). Darkened dendrites can indicate that neurons are in an atrophic state due to trauma and have been reported following axotomy and exposure to neurotoxins (37, 38). Additionally, microglia at this same time point exhibited morphological changes and proliferation, suggesting a massive inflammatory response mediated by microglia. Microglia were observed near and sometimes even wrapping around some of the darkened dendritic processes. At 21–28 days after the blast, however, no darkened dendrites were observed, and the morphological characteristics and numbers of microglia had returned to pre-blast levels. The data suggest that these proliferating microglia removed, at least a portion of, the affected dendrites. The authors postulated that acute changes in affected neurons and activation of microglia may have resulted in a prolonged atrophic state and/or release of factors that caused other chronic effects (e.g., changes in neuronal activity, increased endocytosis).

Although some morphological changes were acute as reported by Kaur et al. (36), studies in other animal models showed persistent effects. The impact of mild repetitive blast (3 blasts 20–30 min apart ranging from 15–19 psi = 107–133 kPa) on brain microstructure and volume was examined using magnetic resonance imaging (MRI) in Sprague Dawley rats, at two time points (7 and 90 days) after exposure (39). At 90 days post-trauma, localized reductions in volume were observed in the cerebellum and the VNC. Microstructural changes in the cerebellum were observed at 7 days and persisted through the 90-day time point. The specific details surrounding the morphological changes were not reported. Although ipsilateral vs. contralateral damage was discussed, neither damage of specific subnuclei nor localization within subnuclei were described (i.e., rostro-caudal, dorso-ventral, or medio-lateral). Another question is whether particular neuronal phenotypes were disproportionately affected (e.g., excitatory vs. inhibitory). Other studies have addressed the differential impact of continuous noise on neurons within vestibular nuclei. Specifically, in Barker et al. (40), neurons in the lateral vestibular nucleus (LVN) of the rat project to the dorsal cochlear nucleus (DCN). Combining tract tracing and immunohistochemistry 5 days after a noise trauma (15 kHz, 110 dB SPL for 6 h), synaptic terminals originating from LVN neurons were shown to be more numerous in the DCN when compared to sham noise-exposed control animals. They further determined that the synaptic terminals were glutamatergic, immunolabeling for vGLUT2 (vesicular glutamate transporter 2), a protein responsible for loading glutamate into synaptic vesicles. Others have postulated that neuropathic pain and inflammatory processes induced by noise may underlie the increased excitatory vGLUT2 neurite outgrowth from the LVN into the cochlear nucleus [e.g., (41)]. These new synaptic terminals could be evidence of cross-modal plasticity and contribute to an increase in spontaneous neuronal activity that is sometimes observed following loud noise exposure and could be associated with the perception of tinnitus and/or hyperacusis.

ELECTROPHYSIOLOGICAL EVIDENCE FOR NOISE-INDUCED DAMAGE TO THE VESTIBULAR SYSTEM

Neurophysiological studies have focused primarily on otolith organ pathways in examination of the impact of noise exposure on vestibular function. The majority of animal studies have used the vestibular short latency evoked potential (VsEP) to study changes in central and peripheral activity after noise exposure [(18, 42–45) for review of VsEPs see: (46)]. VsEPs have predominantly been recorded from experimental animals in response to brief linear acceleration impulses applied to the skull using an electrodynamic shaker that is bolted or clamped to the animal's skull [**Figure 5**; e.g., (47)]. VsEPs remain intact following cochlear extirpation whereas the response is abolished following damage to the vestibule or eighth nerve or the administration of neural blocking agents [e.g., (48)]. Further, the use of air conduction masking does not eliminate the VsEP response (48, 49). For a review of the vestibular specificity of the VsEP, see Brown et al. (50). The VsEP reflects the synchronous compound field potential of peripheral and/or central vestibular neurons in response to the onset of head/body motion (jerk). The VsEP is well-validated and used to evaluate the effects of noise exposure on irregular otolithic afferents. It is known that irregular afferents that contribute to central vestibular reflex pathways are sound sensitive [e.g., (3); for review see (6)]. Furthermore, it has been demonstrated that damage to this population of afferents (**Figure 2**; calretinin-positive calyx-only afferent terminals) is associated with loss or reduction of the VsEP response (18, 45). In summary, the VsEP is an appealing metric to evaluate the vestibular consequences of noise exposure in animal models; however, due to challenges in recording VsEPs in humans, the impact of noise exposure on the human VsEP has not been examined.

To examine the impact of noise on the human vestibular system, most laboratories have used vestibular evoked myogenic potentials (VEMPs; **Figure 6**). VEMPs are short-latency myogenic potentials arising from vestibular afferents that are responsive to air-conducted sound or bone-conducted vibration (51). Cervical VEMPs (cVEMPs; **Figure 6A**), a measure of the sacculo-collic pathway, are recorded from surface electrodes over the sternocleidomastoid muscle. Ocular VEMPs (oVEMPs; **Figure 6B**), a measure of utricular/superior vestibular nerve function, are recorded from surface electrodes over the inferior oblique extraocular muscle. cVEMPs are mediated by an ipsilateral reflex pathway originating in the saccule and projecting to motoneurons of the sternocleidomastoid muscle via the inferior vestibular nerve, vestibular nuclei and descending medial vestibulospinal tract [for review, see (6)]. oVEMPs are mediated by a contralateral reflex pathway originating in the utricle and projecting to motoneurons of the inferior oblique muscle via the superior vestibular nerve, vestibular nuclei, medial

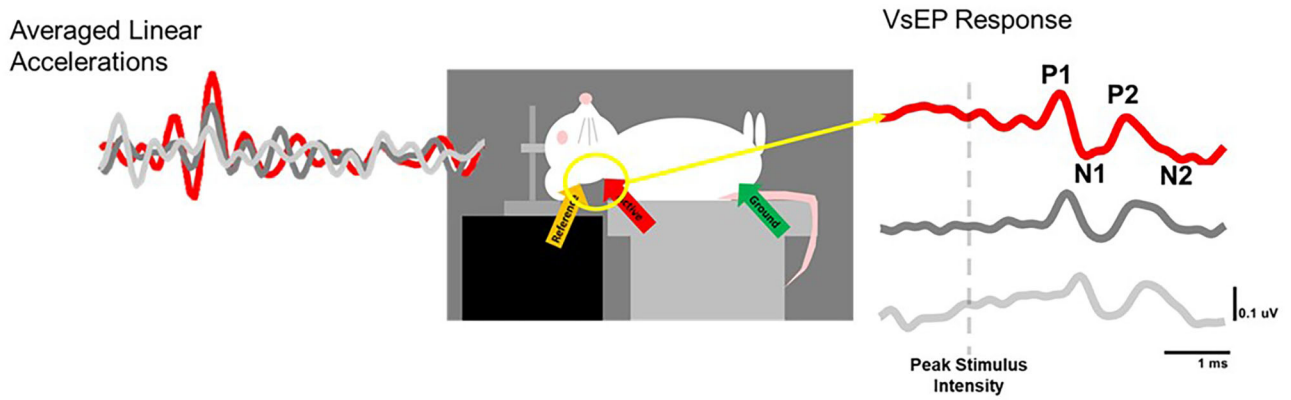

FIGURE 5 | VsEP recording set-up. The skull of an anesthetized rat is fixed to the arm of an electrodynamic transducer (ET-132-203, Labworks, Inc.) and linear head-jerks (left) are delivered in the naso-occipital plane to elicit responses (right) with characterisitic P1N1 and P2N2 waveforms that can be measured before and after noise exposure to track vestibular loss and recovery over time.

longitudinal fasciculus, and the oculomotor nucleus [for review, see (52)].

Otolith Organ Pathways

Vestibular Short-Latency Evoked Potentials (VsEPs)

Animal studies using VsEPs have demonstrated changes in VsEP characteristics following noise exposure. Perez et al. (44) observed a reduction in VsEP amplitude elicited by a ∼3 g/ms head-jerk in rats following exposure to impulse noise (10 gunshots at ∼160 dB SPL). Six weeks after noise exposure, the VsEP amplitude recovered but the latency did not, suggesting an incomplete recovery. Similarly, Stewart et al. (45) reported a reduction in VsEP amplitude in rats exposed to high-intensity (120 dB SPL) low-frequency (0.5–4 kHz) continuous noise for 6 h. Unlike the Perez et al. (44) study, the initial reduction in VsEP amplitude using head-jerk stimuli up to 1.2 g/ms did not recover 3 weeks post-noise exposure (**Figure 7**). In a follow-up study that used the same noise exposure paradigm, larger head jerk stimuli were used to elicit VsEP responses and track recovery for 28 days post-noise exposure (18). Even with larger head-jerk stimuli, the post-noise exposure response amplitudes were severely attenuated and exhibited longer latencies than those obtained from the non-noise exposed animals. In fact, these deficits showed minimal recovery 28 days after noise exposure [(18); **Figure 8**]. It is likely that differences between the results of Perez et al. (44) and Stewart et al. (18, 45) were related, at least in part, to differences in the level and duration of the noise exposure paradigms. In the Perez et al. (44) study, the impulses delivered to the rats were 40 dB SPL greater than in the continuous noise paradigm used by Stewart et al. (18, 45). However, the effect of continuous noise delivered over 6 h was considerably more severe and more persistent. In contrast to the work of Stewart et al. (18, 45) and Perez et al. (44), two studies reported that continuous 113 dB SPL white noise did not induce a deficit in VsEP responses in intact animals (42, 43). No significant changes were observed in VsEP amplitude or latency after a 1-h exposure or after 3 weeks of daily 12-h noise exposures (42). Although this result is surprising, the relatively moderate level combined with the broadband frequency content of the noise exposures might explain the lack of vestibular loss observed in the Sohmer et al. (42) and Biron et al. (43) studies, compared to the high-level impulse noise used by Perez et al. (44), and the low-frequency high-level noise used by Stewart et al. (18, 45). Neurophysiological studies are consistent with anatomical studies that suggest the site, degree, and duration of damage observed in the vestibular periphery (temporary vs. permanent) is impacted by the level, frequency, and duration of noise exposure.

Cervical Vestibular Evoked Myogenic Potentials (cVEMPs)

The approach to determining noise-related damage to the human vestibular system has primarily focused on recording air-conducted sound cVEMPs in individuals with noise-induced hearing loss (NIHL). NIHL is characterized by an audiometric notch or "noise-notch" (decrease in hearing sensitivity at or near 4 kHz) and serves as a biomarker for noise-related damage to the cochlea. cVEMPs are absent in individuals with NIHL with an incidence ranging from 20 to 58% (53–60). Akin et al. (53) examined cVEMPs in 43 military veterans (mean age = 52 years) with a history of noise exposure greater in one ear than the other and asymmetric NIHL (defined as a noise notch at 4 kHz of ≥35 dB HL in the poorer hearing ear with a minimum interaural asymmetry of 20 dB HL at the affected frequencies). cVEMPs were absent in 24% of the poorer-hearing ears (**Figure 9**). In contrast, cVEMPs were present in most (97.5%) of the better-hearing ears of the noise-exposed group and present and symmetrical in the age-matched controls. Other studies have reported a decrease in cVEMP amplitudes and longer latencies in individuals with NIHL compared to individuals without noise exposure (54, 56, 59). Similarly, cVEMP thresholds were higher (poorer) in military veterans with NIHL than in age-matched controls (53). There is evidence that a diminished vestibular response is associated with the

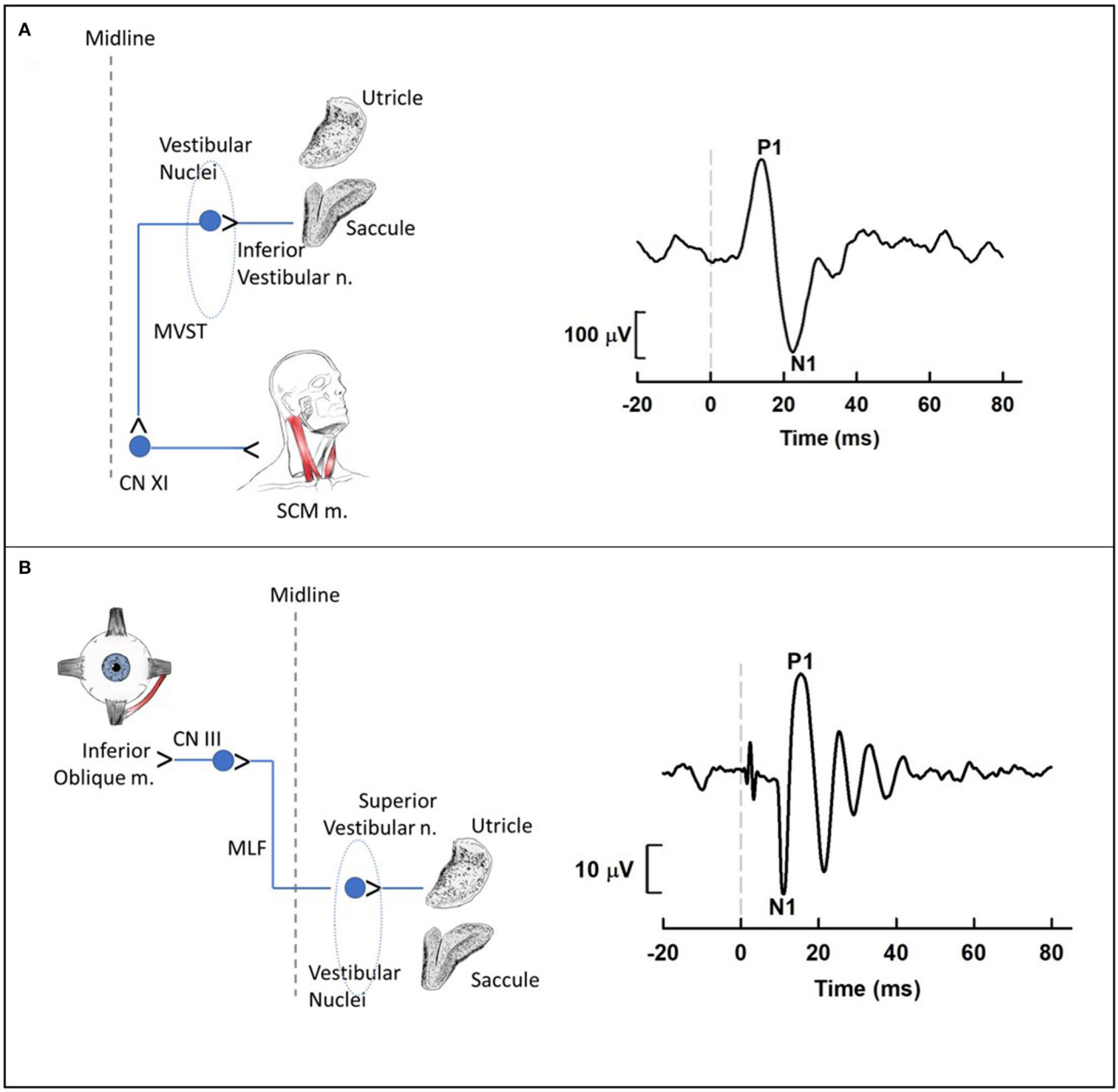

FIGURE 6 | Cervical **(A)** and ocular **(B)** vestibular-evoked myogenic potential (VEMP) pathways and waveforms. **(A)** Cervical VEMPs (cVEMPs) are mediated by an ipsilateral reflex pathway originating in the saccule and projecting to motoneurons of the sternocleidomastoid muscle (SCM m.) via the inferior vestibular nerve, vestibular nuclei and descending medial vestibulospinal tract. The cVEMP waveform was obtained using air conduction 500-Hz tone bursts (95 dB nHL) during activation of the SCM m. with a lateral head turn. **(B)** Ocular VEMPs (oVEMPs) are mediated by a contralateral reflex pathway originating in the utricle and projecting to motoneurons of the inferior oblique muscle via the superior vestibular nerve, vestibular nuclei, medial longitudinal fasciculus, and the oculomotor nucleus. The oVEMP waveform was obtained using bone conduction 500-Hz tone bursts (Brüel & Kjær Model 4,810 mini-shaker applied to the midline forehead; 145 dB peak force level) during upward gaze. For each waveform, the dashed vertical line at 0 ms indicates stimulus onset. Medial Vestibulospinal Tract, MVST; Accessory Nerve, CNXI; Sternocleidomastoid, SCM; Oculomotor Nerve, CNIII; Medial Longitudinal Fasciculus, MLF.

degree of NIHL. In military veterans with bilateral asymmetric NIHL, Akin et al. (53) observed that the poorer hearing ear of NIHL subjects with absent cVEMPs had a greater degree of high-frequency hearing loss than the poorer hearing ear of NIHL subjects with present cVEMPs (**Figure 10**). Similarly, in 30 industrial workers with NIHL, cVEMP latency increased and amplitude decreased as a function of a four-frequency pure-tone average (55). Wang et al. (57) examined hearing improvement following acoustic trauma in 20 patients and reported that absent cVEMP responses or abnormally prolonged cVEMP

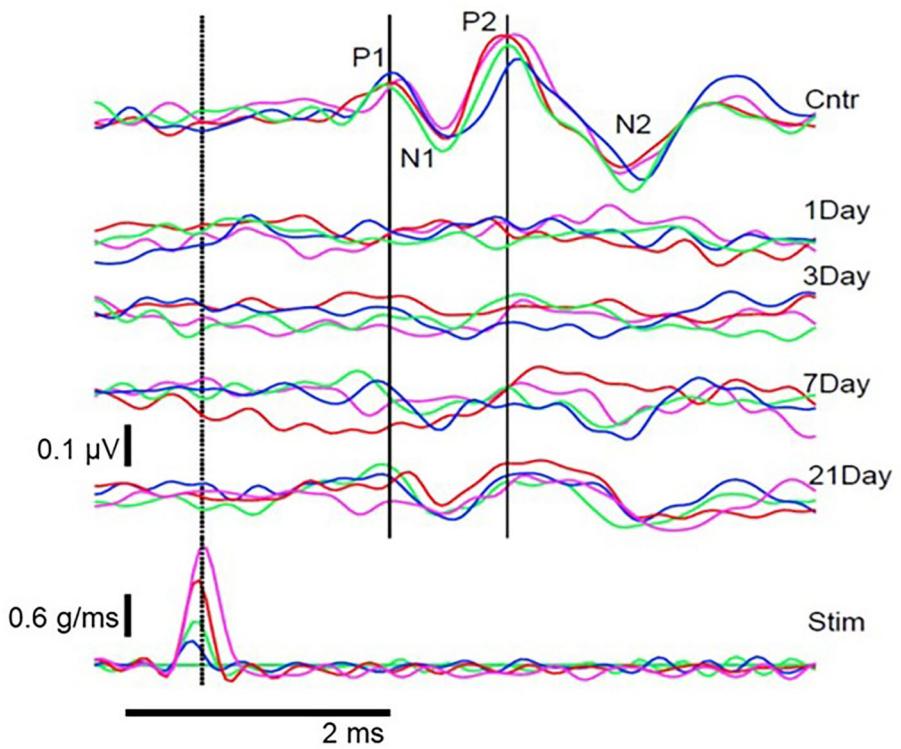

FIGURE 7 | Pre- and post-noise exposure VsEP waveforms for 1 animal at 4 stimulus intensities. **(Bottom row)** stimulus waveforms at 4 intensities (blue, 0.2 g/ms; green, 0.4 g/ms; red, 0.7 g/ms; magenta, 1.2 g/ms). **(Top)** Pre-exposure (Cntr) and post-exposure (Day 1–21) VsEP waveforms for each stimulus intensity and the identified P1N1 and P2N2 components. VsEP is abolished immediately after noise exposure and partially recovers 3–21 days after exposure. Dotted vertical line marks peak stimulus intensity and was used as the reference (0 ms) to calculate latency. Originally published in (45).

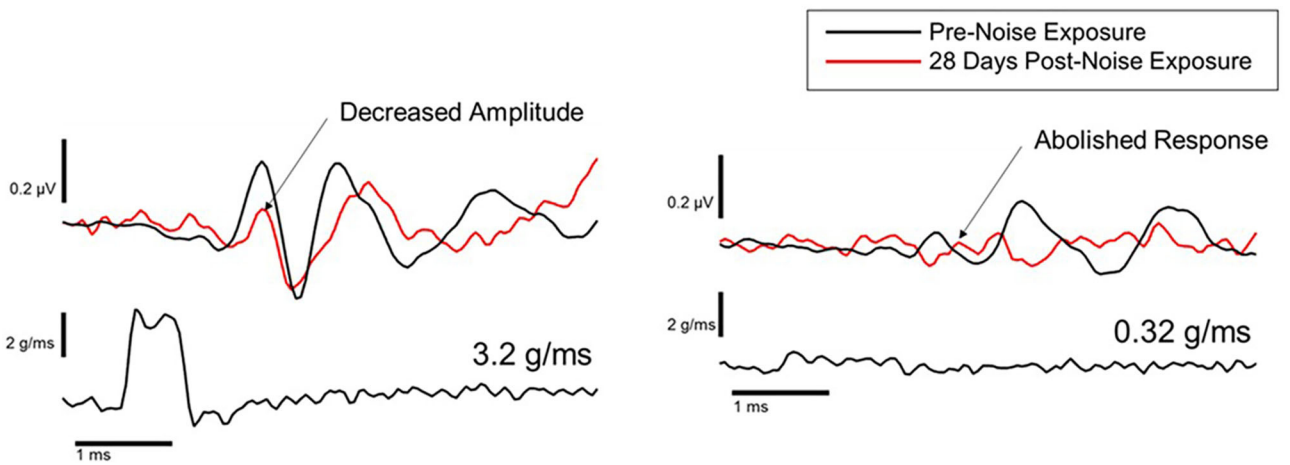

FIGURE 8 | Representative VsEP waveforms in response to a 3.2 g/ms stimulus (left), and a 0.32 g/ms stimulus (right), at baseline (black traces) and 28 days after noise exposure (red traces) (18).

latency indicated poor prognosis for hearing recovery. Indeed, absent cVEMP or prolonged cVEMP latency predicted acoustic trauma hearing outcome with a sensitivity of 44% and specificity of 100%.

cVEMP findings in humans are consistent with morphological studies in animals that suggest the sacculus is particularly susceptible to noise-related damage. Human studies are limited, however, by a lack of histopathological data and difficulty

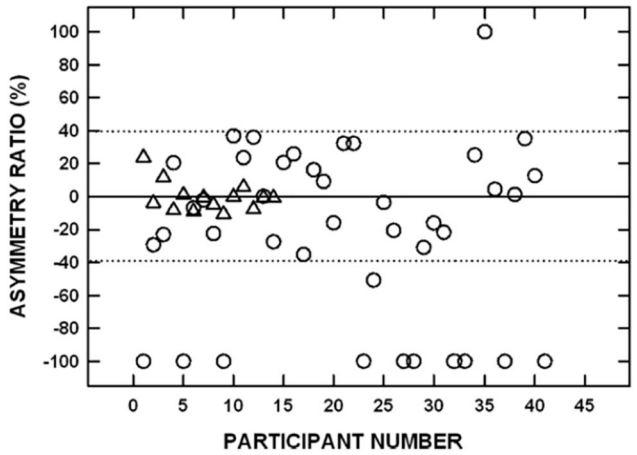

FIGURE 9 | Signed interaural amplitude asymmetry ratio for cervical vestibular evoked myogenic potentials in 14 age-matched controls (triangles) and 41 participants with bilateral asymmetric noise-induced hearing loss (circles). For the noise-exposed group, −100% indicates the cVEMP was absent from the poorer-hearing ear, whereas 100% indicates the cVEMP was absent from the better-hearing ear. For the control group, negative values indicate that the P1-N1 amplitude was greater on the left side and positive values indicate that the P1-N1 amplitude was greater on the right side. The area between the dotted horizontal lines indicates asymmetry ratios within normal limits. Two noise-exposed participants had cVEMPs absent bilaterally and are not shown. Adapted from (53).

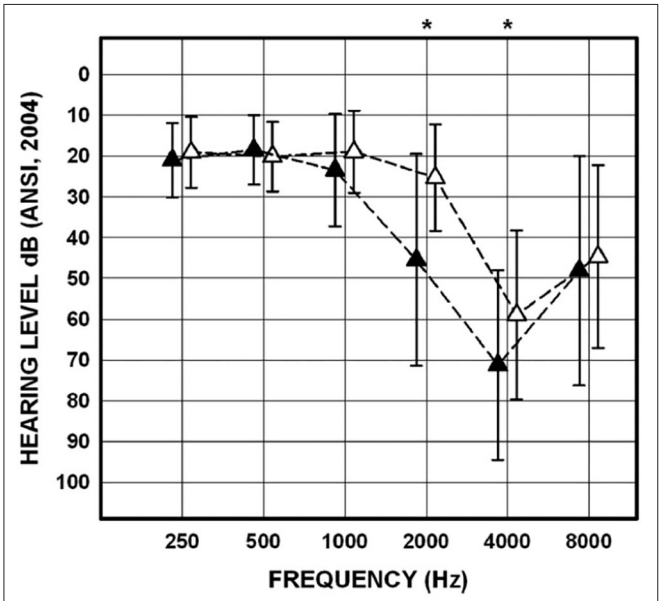

FIGURE 10 | Mean and SDs for pure-tone thresholds for the poorer-hearing ear of noise-exposed participants ($n = 43$) with cVEMPs present ($n = 29$; open triangles) and for the poorer-hearing ear of noise-exposed participants with cVEMPs absent ($n = 14$; filled triangles). Asterisks indicate significant *post-hoc* comparisons. Adapted from (53).

quantifying noise exposure across a lifespan. Additionally, the human cVEMP is somewhat limited as an estimate of peripheral vestibular function as the response is recorded from the motoneurons of muscles at the end of a reflex pathway that includes central components. These limitations have been partially addressed by the work of Hsu et al. (16) in which cVEMPs were measured in guinea pigs following short-term vs. long-term noise exposure. In this study, a "normal" cVEMP was defined as the presence of a biphasic waveform at a latency of 6- to 9-ms, with a peak-to-peak amplitude of 5–20 μV. When a peak was not observed in the latency range of 6- to 9-ms, or was smaller than 5 μV, the cVEMP response was considered 'abnormal'. Hsu et al. (16) observed recovery of vestibular function (return of normal cVEMP responses) following short-term (30 min) exposure to continuous broadband noise at 114 dB SPL. In contrast, abnormal cVEMP responses persisted for at least 30 days in most guinea pigs (78%; $n = 18$) following exposure to 40 h of continuous broadband noise. These findings are consistent with anatomical findings described earlier and suggest that permanent physiological damage to the sacculo-collic pathway is more likely following long vs. short-duration noise exposures.

Semicircular Canal Pathways

The studies that have examined the horizontal semicircular canal and VOR pathways have yielded inconsistent findings in individuals with NIHL. For example, Man et al. (61) observed a caloric weakness in only one of 176 patients with NIHL, whereas other studies have revealed a caloric weakness in up to 25% of individuals with NIHL (56, 57, 62). Using slow harmonic acceleration, Shupak et al. (63) found that VOR gain was significantly lower in industrial workers and military personnel with NIHL compared to a control group with normal hearing.

Recently, Yilmaz et al. (64) used the video head impulse test to measure VOR gain for all six semicircular canals in 36 industrial workers (mean age = 44 years) with high frequency hearing loss and four or more years working the steel and metal industry. They reported canal deficits (a decrease in VOR gain in at least one canal) in 55.5% of noise exposed participants compared with 6.6% of control participants. Decreased gain was reported more frequently in the horizontal semicircular canals (47%) than in the vertical canals (8%), with two noise-exposed participants demonstrating decreased VOR gain in more than one canal. Interpretation of these data is limited because NIHL was defined according to the degree of hearing loss at 4,000 Hz rather than a characteristic noise notch.

In contrast to cVEMP findings that suggest greater sacculo-collic pathway damage associated with more severe NIHL, the relationship between damage to the horizontal semicircular canal/VOR pathways and the degree of NIHL is less clear. Shupak et al. (63) observed significant correlations between pure-tone average, VOR gain, and caloric lateralization. Golz et al. (62), however, found no correlation between the severity of hearing loss and abnormal caloric test findings. It is worth noting, however, that the caloric response is a very low frequency response and may be independent of central zone hair cells and afferents that might be sensitive to pressure wave disturbances.

To examine the impact of noise exposure across multiple vestibular pathways, Tseng and Young (56) performed bithermal calorics and cVEMPs and oVEMPs using bone-conducted vibration on 30 individuals with NIHL related to chronic occupational noise exposure. Their findings revealed that cVEMPs were most frequently abnormal (70%) followed by oVEMPs (57%) and calorics (33%) consistent with other studies that suggest the saccule is more susceptible to acoustic trauma than other vestibular sensory organs. These findings are also consistent with anatomical findings that show the saccule is most susceptible to noise-induced damage, followed by the utricle, and then the semicircular canals (19).

VsEPs have also been used to assess semicircular canal function by replacing the linear head-jerk stimulus with an angular acceleration stimulus [A-VsEP; (42, 44)]. Perez et al. (44) delivered a 15,000°/s^2 (1–3 ms rise time) stimulus to provoke A-VsEPs to assess semicircular canal function in sand rats (*Psammomys obesus*) exposed to impulse-noise (160 dB SPL, 10 impulses). This work found no change in A-VsEP amplitude, and only a transient (2–4-h) post-noise increase in A-VsEP latency that recovered by 1-week post-noise. In another study, the same stimulus was used to assess the effect of a short (1 h) or extended and repeated noise exposure (12 h per day for 21 days). There was no effect of noise exposure on the A-VsEP with either noise exposure paradigm (42). Furthermore, there was no effect of noise exposure on the linear VsEP following 113 dB SPL white noise exposure (42). It should be noted that there was a 7-day rest interval between the last 12-h noise exposure and the post-noise VsEP measurement. It is possible that if measurements had been taken shortly after the last noise exposure, a transient deficit might have been detected.

Single unit extracellular recording can be used to assess regular and irregular vestibular afferent activity arising from all five vestibular end organs. In a report characterizing changes in vestibular nerve activity, 116 dB SPL broadband white noise was delivered unilaterally to rats for 3 h on a single day. Seven days later, changes in hearing (ABR) and vestibular nerve activity (single unit extracellular recording from the superior vestibular nerve) on the noise exposed side was evaluated (19). Recordings from the superior aspect of the vestibular nerve included anterior and horizontal semicircular canal afferents as well as otolithic afferents (utricle and 1/3 of the saccule). Although there was no change in spontaneous firing rate in irregular superior vestibular nerve afferents, spontaneous firing rates were significantly reduced in regular superior vestibular nerve afferents originating from the anterior semicircular canal crista and the otolith organs. Furthermore, there were extensive changes in the gain and phase of regular horizontal and anterior canal afferents but a minimal effect of the 116 dB SPL broadband noise exposure on the irregular canal afferents. As discussed earlier, a post-exposure examination of vestibular sensory epithelia reflected broad damage to the hair bundles in all end organs innervated by the superior vestibular nerve (utricle, saccule; anterior and horizontal semicircular canal cristae). This work identified noise-induced damage to regular afferents and highlights a limitation of VsEP measurements: VsEPs only measure activity arising from irregular afferents.

Central Vestibular Pathways

Using chronically implanted micro-electrode arrays, Ordek et al. (65) evaluated cerebellar neuronal activity after mild blast exposure (100–130 kPa). Behavioral testing 24 h and 7 days after blast (ladder climbing, roto-rod, ladder walking) and immunohistochemistry for the number of calbindin and caspase-3 (markers of Purkinje cells, oxidative stress, and apoptosis) positive cells showed no differences from controls. In contrast, evoked potentials after blast exposure demonstrated sustained changes beginning 24 h after injury. Potentials related to mossy fiber discharges exhibited increased amplitudes and latencies while potentials related to climbing fiber activity exhibited decreased amplitudes and decreased latencies. They concluded that neuronal activity may be more effective than behavioral tests or immunolabeling for neuronal loss in identifying early onset of subtle injury after mild blast exposure.

Other studies have made use of manganese enhanced MRI (MEMRI) to examine noise-induced changes in neuronal activity in animal models *in vivo* (66–68). Manganese is a paramagnetic ion that can be visualized using MRI. Manganese ions act as calcium ion surrogates and enters active neurons via voltage gated calcium channels. Differential uptake of manganese is used to identify changes in neuronal activity within vestibular-related brain regions at acute (48 h, **Figure 11**) and chronic time points (10 months, not shown) after noise exposure. Increased manganese uptake presumed to reflect increased neuronal activity, was found in the cerebellar paraflocculus and the primary visual cortex (68, 69). Although vestibular pathways were not a focus, this study provides a basis for future MEMRI studies that follow the impact of noise on temporal changes in neuronal activity within vestibular pathways *in vivo*.

FUNCTIONAL EVIDENCE FOR NOISE-INDUCED VESTIBULAR DAMAGE

Loss of vestibular function can result in vertigo (the illusion of movement), oscillopsia (blurred vision during head movement), postural instability, and/or motion intolerance. Several studies in humans demonstrate a significant relationship between NIHL and postural stability. A limitation of these studies is a lack of vestibular function testing; thus, the mechanism underlying the association between NIHL and postural stability is not clear. An early study of iron workers (mean age = 53.3 years) with chronic noise exposure (70) demonstrated a significant relationship between auditory thresholds and postural stability as measured by sway velocity during static balance testing on a firm surface with eyes open and closed. Service members with NIHL (mean age = 44.6 years) due to chronic impulse noise exposure had greater postural sway (i.e., greater instability), especially in the medial-lateral direction, during static balance testing with eyes open and closed than controls with normal hearing and no noise exposure (mean age = 40.7 years) (71, 72). Guest et al. (73) showed a small reduction in voluntary limits of stability as measured by the functional reach test in military personnel with noise and solvent exposure (n = 601) compared to controls (no exposure: n = 391; noise exposure only,

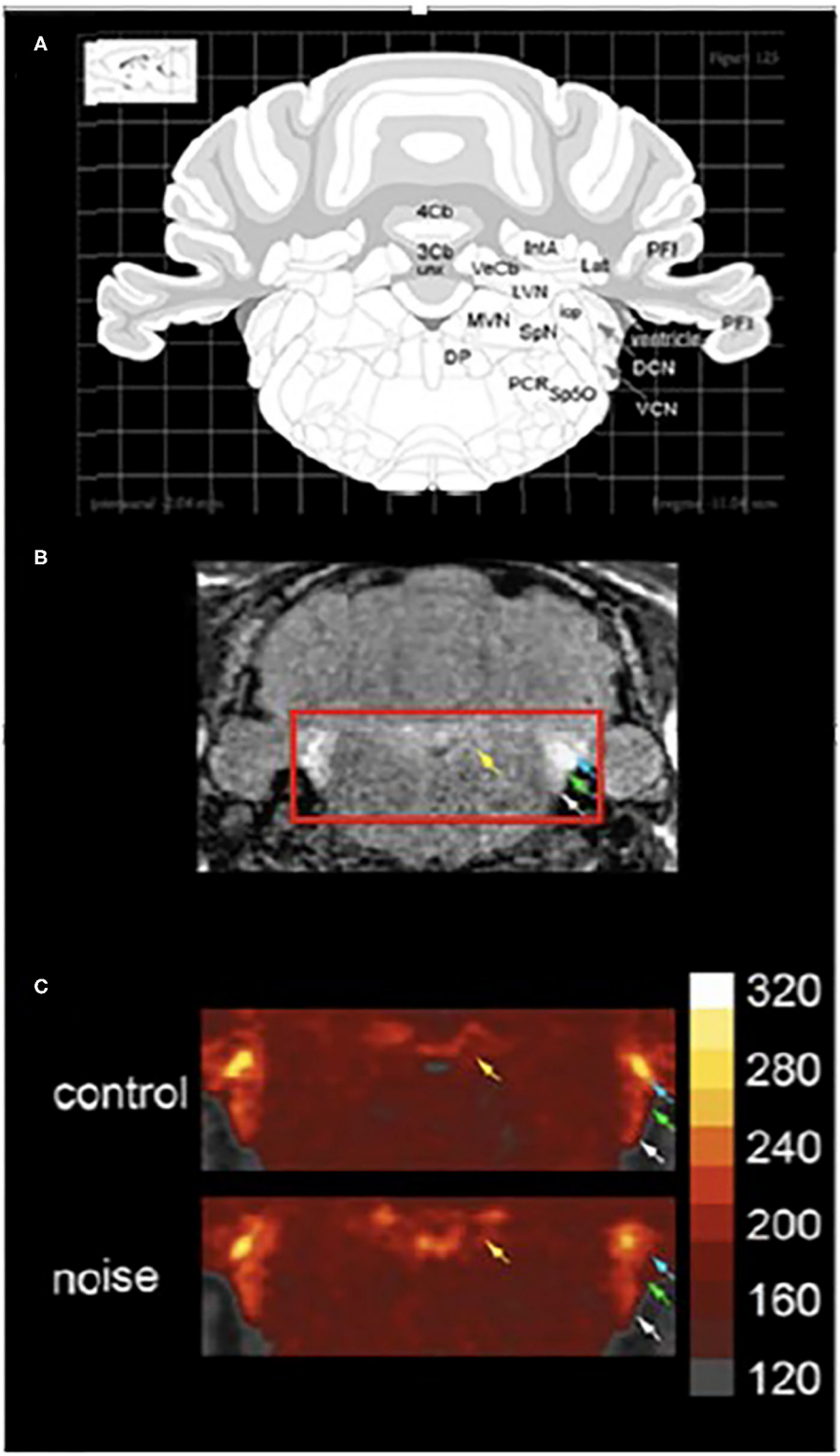

FIGURE 11 | MEMRI (manganese enhanced magnetic resonance imaging) of the vestibular nuclear complex and cochlear nucleus 48 h. After noise exposure (10 kHz, 1/3 octave, 118 dB SPL, 4 h). **(A)** A schematic of a coronal section through the brainstem taken from a rat atlas showing brain regions of interest. **(B)** The T1-weighted image shows brain regions of interest *in vivo*. Yellow arrows indicate the vestibular nuclear complex while white, green, and blue arrows indicate auditory regions. **(C)** When noise-exposed animals are compared to controls 48 h. After the exposure there is increase in manganese uptake in the vestibular and auditory regions. Colorimetric scale bar–gray indicates lowest Mn2+ uptake while white indicates the highest level of Mn2+ uptake. Adapted from (68).

$n = 500$). Moreover, there was a significant inverse corelation between low-frequency auditory thresholds and functional reach, such that higher (poorer) thresholds were associated with lower functional reach.

Two studies failed to demonstrate a significant relationship between NIHL and postural stability (74, 75). Pyykkö et al. found equivalent postural sway velocity between Finnish soldiers ($n = 54$) with acute hearing loss due to firearm noise exposure (mean age = 27 years) and two control groups (soldiers with no acute noise trauma and age-matched civilians). Participants were tested within 5 days of the onset of hearing loss under a variety balance conditions: eyes open and closed on firm and foam surfaces, with and without calf muscle vibration, and with neck extended backwards. The lack of a significant relationship between NIHL and postural stability may be due to acute noise exposure (vs. chronic exposure in the previous studies) or the younger age of the subjects. Prasher et al. (75) examined postural control in four exposure groups: noise only (n = 153; mean age = 53.3 years), solvents only (n = 13; mean age = 49.6 years), noise and solvents (n = 174; mean age = 47.4 years) and controls with no noise or solvent exposure (n = 39; mean age = 47.6 years). As expected, the noise exposed group exhibited significantly poorer pure-tone thresholds than the other groups, but had normal postural stability as measured by computerized posturography during static balance with eyes open and closed on firm and foam surfaces. It is not clear why these findings conflict with the previous studies.

There is a paucity of data on the effects of noise exposure on agility and motor function in animal models. Tamura et al. (20) observed balance and gait changes in mice subjected to moderate level, low-frequency continuous noise for a one-month time period. Specifically, low-frequency noise-exposed mice exhibited impaired rotarod performance and imbalance, as well as shorter strides and a winding gait pattern that persisted for 4 weeks post-exposure vs. controls or high-frequency noise-exposed mice. These deficits were associated with reduced calbindin labeling of hair cells, and with elevated oxidative stress marker labeling when compared to control and high-frequency noise-exposed mice (20).

CONCLUSIONS

This review has examined the current literature on noise-induced vestibular loss, the differences in characteristics of noise exposure, and how these differences might contribute to variability in reported noise-induced vestibular deficits. Early studies suggested that the vestibular system was susceptible to noise over-exposure. More recently, morphological studies have confirmed and extended this early work, showing cellular damage throughout the peripheral vestibular system, particularly in the otolith organs; however, there is still a paucity of data on the effect of noise exposure on human vestibular end organs. Other work has identified evidence of free-radical production in the vestibular labyrinth following noise exposure, which suggests a mechanism that may contribute to morphological observations. There are limited data on the effects of noise on the central vestibular system, especially following exposure to continuous noise. Physiological studies have corroborated morphological studies by demonstrating disruption across vestibular pathways with otolith-mediated pathways (VEMPs and linear VsEPs) impacted more frequently than semicircular canal-mediated pathways. Similar to the temporary threshold shifts observed in the auditory system, physiological studies in animals have suggested a capacity for recovery following noise-induced vestibular damage. Human studies have demonstrated that diminished VEMP responses are related to the severity of noise-induced hearing loss, and dose-dependent vestibular deficits following noise exposure have been corroborated in animal models. In contrast to the anatomical and neurophysiologic evidence, less is known about the relationship among noise-induced damage to the inner ear, physiological changes associated with this damage, and functional measures of vestibular impairment (e.g., balance and gait) in animals and humans.

AUTHOR CONTRIBUTIONS

CS reviewed the animal anatomical, physiological, and functional vestibular literature, drafted and revised the review. RA reviewed the anatomical literature and provided feedback on the entire review. AC drafted the blast-related hydrops section of the review and provided feedback on the entire review. CH drafted the human functional section of the review. AH drafted the central vestibular sections of the review and provided feedback on the entire review. OM reviewed physiological and functional literature, and revised the entire review. WK reviewed physiological literature and revised the entire review. FA reviewed the human anatomical, physiological, and functional literature, drafted and revised the review. All authors contributed to the article and approved the submitted version.

FUNDING

This work was supported by Grant support: VA: 1I01RX001986*, 1IK2RX003271, E3367R*, 1I01RX001095*; NIDCD: DC018003-01, DC015097, DC017063-01, DC000011. This material is based upon work supported (or supported in part) by the Department of Veterans Affairs, Veterans Health Administration, Office of Research and Development.

ACKNOWLEDGMENTS

Maverick Dunavan for help with medical illustration.

REFERENCES

1. Dinh CT, Goncalves S, Bas E, Van De Water TR, Zine A. Molecular regulation of auditory hair cell death and approaches to protect sensory receptor cells and/or stimulate repair following acoustic trauma. *Front Cell Neurosci.* (2015) 9:96. doi: 10.3389/fncel.2015.00096
2. Henderson D, Hamernik RP, Dosanjh DS, Mills JH. *Effects of Noise on Hearing*. New York, NY: Raven Press (1976).
3. McCue MP, Guinan JJ. Acoustically responsive fibers in the vestibular nerve of the cat. *J Neurosci.* (1994) 14:6058–70. doi: 10.1523/JNEUROSCI.14-10-06058.1994
4. Zhu H, Tang X, Wei W, Mustain W, Xu Y, Zhou W. Click-evoked responses in vestibular afferents in rats. *J Neurophysiol.* (2011) 106:754–63. doi: 10.1152/jn.00003.2011
5. Murofushi T, Curthoys IS, Topple AN, Colebatch JG, Halmagyi GM. Response of guinea pig primary vestibular neurons to clicks. *Exp Brain Res.* (1995) 103:174–8. doi: 10.1007/BF00241975
6. Curthoys IS, MacDougall HG, Vidal PP, de Waele C. Sustained and transient vestibular systems: a physiological basis for interpreting vestibular function. *Front Neurol.* (2017) 8:117. doi: 10.3389/fneur.2017.00117
7. Halmagyi GM, Curthoys IS, Colebatch JG, Aw ST. Vestibular responses to sound. *Ann N Y Acad Sci.* (2005) 1039:54–67. doi: 10.1196/annals.1325.006
8. Goldberg JM, Fernandez C. Conduction times and background discharge of vestibular afferents. *Brain Res.* (1977) 122:545–50. doi: 10.1016/0006-8993(77)90465-6
9. Baird RA, Desmadryl G, Fernandez C, Goldberg JM. The vestibular nerve of the chinchilla. II. Relation between afferent response properties and peripheral innervation patterns in the semicircular canals. *J Neurophysiol.* (1988) 60:182–203. doi: 10.1152/jn.1988.60.1.182
10. Lysakowski A, Minor LB, Fernandez C, Goldberg JM. Physiological identification of morphologically distinct afferent classes innervating the cristae ampullares of the squirrel monkey. *J Neurophysiol.* (1995) 73:1270–81. doi: 10.1152/jn.1995.73.3.1270
11. Fernandez C, Goldberg JM. Physiology of peripheral neurons innervating the otolith organs of the squirrel monkey. II. Directional selectivity and force-response relations. *J Neurophysiol.* (1976) 39:985–95. doi: 10.1152/jn.1976.39.5.985
12. Curthoys IS, Vulovic V. Vestibular primary afferent responses to sound and vibration in the guinea pig. *Exp Brain Res.* (2011) 210:347–52. doi: 10.1007/s00221-010-2499-5
13. Songer JE, Eatock RA. Tuning and timing in mammalian type I hair cells and calyceal synapses. *J Neurosci.* (2013) 33:3706–24. doi: 10.1523/JNEUROSCI.4067-12.2013
14. Goldberg JM. Afferent diversity and the organization of central vestibular pathways. *Exp Brain Res.* (2000) 130:277–97. doi: 10.1007/s002210050033
15. Mangabeira-Albernaz PL, Covell WP, Eldredge DH. Changes in the vestibular labyrinth with intense sound. *Laryngoscope.* (1959) 69:1478–93. doi: 10.1288/00005537-195912000-00002
16. Hsu WC, Wang JD, Lue JH, Day AS, Young YH. Physiological and morphological assessment of the saccule in guinea pigs after noise exposure. *Arch Otolaryngol Head Neck Surg.* (2008) 134:1099–106. doi: 10.1001/archotol.134.10.1099
17. Akdogan O, Selcuk A, Take G, Erdogan D, Dere H. Continuous or intermittent noise exposure, does it cause vestibular damage?: An experimental study. *Auris Nasus Larynx.* (2009) 36:2–6. doi: 10.1016/j.anl.2008.03.003
18. Stewart CE, Bauer DS, Kanicki AC, Altschuler RA, King WM. Intense noise exposure alters peripheral vestibular structures and physiology. *J Neurophysiol.* (2020) 123:658–69. doi: 10.1152/jn.00642.2019
19. Stewart C, Yu Y, Huang J, Maklad A, Tang X, Allison J, et al. Effects of high intensity noise on the vestibular system in rats. *Hear Res.* (2016) 335:118–27. doi: 10.1016/j.heares.2016.03.002
20. Tamura H, Ohgami N, Yajima I, Iida M, Ohgami K, Fujii N, et al. Chronic exposure to low frequency noise at moderate levels causes impaired balance in mice. *PLoS ONE.* (2012) 7:e39807. doi: 10.1371/journal.pone.0039807
21. McCabe BF, Lawrence M. The effects of intense sound on the non-auditory labyrinth. *Acta Otolaryngol.* (1958) 49:147–57. doi: 10.3109/00016485809134738
22. Kühl A, Dixon A, Hali M, Apawu AK, Muca A, Sinan M, et al. Novel QUEST MRI *in vivo* measurement of noise-induced oxidative stress in the cochlea. *Sci Rep.* (2019) 9:16265. doi: 10.1038/s41598-019-52439-4
23. Fetoni AR, Ferraresi A, Picciotti P, Gaetani E, Paludetti G, Troiani D. Noise induced hearing loss and vestibular dysfunction in the guinea pig. *Int J Audiol.* (2009) 48:804–10. doi: 10.3109/14992020903023140
24. Storkebaum E, Lambrechts D, Carmeliet P. VEGF: once regarded as a specific angiogenetic factor, now implicated in neuroprotection. *BioEssays.* (2004) 26:943–54. doi: 10.1002/bies.20092
25. Zachary I. Neuroprotective role of vascular endothelial growth factor: signalling mechanisms, biological function, and therapeutic potential. *Neurosignals.* (2005) 14:207–21. doi: 10.1159/000088637
26. Zou J, Pyykkö I, Sutinen P, Toppila E. Vibration induced hearing loss in guinea pig cochlea: expression of TNF-alpha and VEGF. *Hear Res.* (2005) 202:13–20. doi: 10.1016/j.heares.2004.10.008
27. Picciotti PM, Fetoni AR, Paludetti G, Wolf FI, Torsello A, Troiani D, et al. Vascular endothelial growth factor (VEGF) expression in noise-induced hearing loss. *Hear Res.* (2006) 214:76–83. doi: 10.1016/j.heares.2006.02.004
28. Selivanova O, Heinrich UR, Brieger J, Feltens R, Mann W. Fast alterations of vascular endothelial growth factor (VEGF) expression and that of its receptors (Flt-1, Flk-1 and Neuropilin) in the cochlea of guinea pigs after moderate noise exposure. *Eur Arch Otorhinolaryngol.* (2007) 264:121–8. doi: 10.1007/s00405-006-0154-3
29. Kuroki M, Voest EE, Amano S, Beerepoot LW, Takashima S, Tolentino M, et al. Reactive oxygen intermediates increase vascular endothelial growth factor expression *in vitro* and *in vivo*. *J Clin Invest.* (1996) 98:1667–75. doi: 10.1172/JCI118962
30. Backous DD, Aboujaoude ES, Minor LB, Nager GT. Relationship of the utriculus and sacculus to the stapes footplate: anatomic implications for sound- and/or pressure-induced otolith activation. *Ann Otol Rhinol Laryngol.* (1999) 108:548–53. doi: 10.1177/000348949910800604
31. Kerr AG, Byrne JE. Concussive effects of bomb blast on the ear. *J Laryngol Otol.* (1975) 89:131–43. doi: 10.1017/S002221510008018X
32. Ylikoski J. Impulse noise induced damage in the vestibular end organs of the guinea pig. A light microscopic study. *Acta Otolaryngol.* (1987) 103:415–21.
33. Lien S, Dickman DJ. Vestibular injury after low-intensity blast exposure. *Front Neurol.* (2018) 9:297. doi: 10.3389/fneur.2018.00297
34. Kumagami H. Endolymphatic hydrops induced by noise exposure. *Auris Nasis Larynx.* (1992) 19:94–105. doi: 10.1016/S0385-8146(12)80097-6
35. He J, Zhu Y, Aa J, Smith PF, De Ridder D, Wang G, et al. Brain metabolic changes in rats following acoustic trauma. *Front Neurosci.* (2017) 11:148. doi: 10.3389/fnins.2017.00148
36. Kaur C, Singh J, Lim MK, Ng BL, Yap EPH, Ling EA. The response of neurons and microglia to blast injury in the rat brain. *Neuropathol Appl Neurobiol.* (1995) 21:369–77. doi: 10.1111/j.1365-2990.1995.tb01073.x
37. Ling EA, Shieh JY, Wen CY, Chan YG, Wong WC. Degenerative changes of neurons in the superior cervical ganglion following an injection of ricinus communis agglutinin into the vagus nerve in hamsters. *J Neurocytol.* (1990) 19:1–9. doi: 10.1007/BF01188435
38. Ling EA, Wong WC, Yick TY, Leong SK. Ultrastructural changes in the dorsal motor nucleus of monkey following bilateral cervical vagotomy. *J Neurocytol.* (1986) 15:1–15. doi: 10.1007/BF02057900
39. Badea AK, Anderson RJ, Calabrese E, Long JB, Denes V. Repeated mild blast exposure in young adult rats results in dynamic and persistent microstructural changes in the brain. *Neuroimage Clin.* (2018) 18:60–73. doi: 10.1016/j.nicl.2018.01.007
40. Barker M, Solinski HJ, Hashimoto H, Tagoe T, Pilati N, Hamann M. Acoustic overexposure increases the expression of VGLUT-2 mediated projections from the lateral vestibular nucleus to the dorsal cochlear nucleus. *PLoS ONE.* (2012) 7:e35955. doi: 10.1371/journal.pone.0035955
41. Manohar S, Dahar K, Adler HJ, Dalian D, Salvi R. Noise-induced hearing loss: neuropathic pain via Ntrk1 signaling. *Mol Cell Neurosci.* (2016) 75:101–12. doi: 10.1016/j.mcn.2016.07.005

42. Sohmer H, Elidan J, Plotnik M, Freeman S, Sockalingam R, Berkowitz Z, et al. Effect of noise on the vestibular system – vestibular evoked potential studies in rats. *Noise Health*. (1999) 5:41–51.
43. Biron A, Freeman S, Sichel JY, Sohmer H. The effect of noise exposure in the presence of canal fenestration on the amplitude of short-latency vestibular evoked potentials. *Arch Otolaryngol Head Neck Surg*. (2002) 128:544–8. doi: 10.1001/archotol.128.5.544
44. Perez R, Freeman S, Cohen D, Sohmer H. Functional impairment of the vestibular end organ resulting from impulse noise exposure. *Laryngoscope*. (2002) 112:1110–4. doi: 10.1097/00005537-200206000-00032
45. Stewart CE, Kanicki AC, Altschuler RA, King WM. Vestibular short-latency evoked potentials abolished by low-frequency noise exposure in rats. *J Neurophysiol*. (2018) 119:662–7. doi: 10.1152/jn.00668.2017
46. Jones TA, Jones SM. Vestibular evoked potentials. In: *Auditory Evoked Potentials: Basic Principles and Clinical Application*, edited by Burkard RF, Eggermont JJ, Don M. Philadelphia, PA: Lippincott Williams & Wilkins. (2007).
47. Jones SM, Subramanian G, Avniel W, Guo Y, Burkard RF, Jones TA. Stimulus and recording variables and their effects on mammalian vestibular evoked potentials. *J Neurosci Methods*. (2002) 118:23–31. doi: 10.1016/S0165-0270(02)00125-5
48. Jones TA, Jones SM. Short latency compound action potentials from mammalian gravity receptor organs. *Hear Res*. (1999) 136:75–85. doi: 10.1016/S0378-5955(99)00110-0
49. Plotnik M, Elidan J, Mager M, Sohmer H. Short latency vestibular evoked potentials (VsEPs) to linear acceleration impulses in rats. *Electroencephalogr Clin Neurophysiol*. (1997) 104:522–30. doi: 10.1016/S0168-5597(97)00062-2
50. Brown DJ, Pastras CJ, Curthoys IS. Electrophysiological measurements of peripheral vestibular function-a review of electrovestibulography. *Front Syst Neurosci*. (2017) 11:34. doi: 10.3389/fnsys.2017.00034
51. Curthoys IS, Vulovic V, Sokolic L, Pogson J, Burgess AM. Irregular primary otolith afferents from the guinea pig utricular and saccular maculae respond to both bone conducted vibration and to air conducted sound. *Brain Res*. (2012) 89:16–21. doi: 10.1016/j.brainresbull.2012.07.007
52. Dlugaiczyk J. Ocular vestibular evoked myogenic potentials: where are we now? *Otol Neurotol*. (2017) 38:e513–21. doi: 10.1097/MAO.0000000000001478
53. Akin FW, Murnane OD, Tampas JW, Clinard C, Byrd S, Kelly JK. The effect of noise exposure on the cervical vestibular evoked myogenic potential. *Ear Hear*. (2012) 33:458–65. doi: 10.1097/AUD.0b013e3182498c5f
54. Giorgianni C, Spatari G, Tanzariello MG, Gangemi S, Brecciaroli R, Tanzariello A. Cervical vestibular evoked myogenic potential (c-VEMPs) assessment in workers with occupational acoustic trauma. *Health.* (2015) 7:456–8. doi: 10.4236/health.2015.74053
55. Kumar K, Vivarthini CJ, Bhat JS. Vestibular evoked myogenic potential in noise-induced hearing loss. *Noise Health*. (2010) 12:191–4. doi: 10.4103/1463-1741.64973
56. Tseng CC, Young YH. Sequence of vestibular deficits in patients with noise-induced hearing loss. *Eur Arch Otorhinolaryngol*. (2013) 270:2021–6. doi: 10.1007/s00405-012-2270-6
57. Wang YP, Hsu WC, Young YH. Vestibular evoked myogenic potentials in acute acoustic trauma. *Otol Neurotol*. (2006) 27:956–61. doi: 10.1097/01.mao.0000231590.57348.4b
58. Wang YP, Young YH. Vestibular-evoked myogenic potentials in chronic noise-induced hearing loss. *Otolaryngol Head Neck Surg*. (2007) 137:607–11. doi: 10.1016/j.otohns.2007.05.005
59. Wu CC, Young YH. Ten-year longitudinal study of the effect of impulse noise exposure from gunshot on inner ear function. *Int J Audiol*. (2009) 48:655–60. doi: 10.1080/14992020903012481
60. Zuniga MG, Dinkes RE, Davalos-Bichara M, Carey JP, Schubert MC, King WM, et al. Association between hearing loss and saccular dysfunction in older individuals. *Otol Neurotol*. (2012) 33:1586–92. doi: 10.1097/MAO.0b013e31826bedbc
61. Man A, Segal S, Nagaan L. Vestibular involvement in acoustic trauma. *J Laryngol Otol*. (1980) 94:1395–400. doi: 10.1017/S0022215100090228
62. Golz A, Westerman ST, Westerman LM, Goldenberg D, Netzer A, Wiedmyer T, et al. The effects of noise on the vestibular system. *Am J Otolaryngol*. (2001) 22:190–6. doi: 10.1053/ajot.2001.23428
63. Shupak A, Bar-El E, Podoshin L, Spitzer O, Gordon CR, Ben-David J. Vestibular findings associated with chronic noise induced hearing impairment. *Acta Otolaryngol*. (1994) 114:579–85. doi: 10.3109/00016489409126109
64. Yilmaz N, Ila K, Soylemez E, Ozdek A. Evaluation of vestibular system with vHIT in industrial workers with noise-induced hearing loss. *Eur Arch Oto-Rhino-Laryngol.* (2018) 275:2659–65. doi: 10.1007/s00405-018-5125-y
65. Ordek G, Asan AS, Cetinkaya E, Skotak M, Kakulavarapu VR, Chandra N, et al. Electrophysiological correlates of blast-wave induced cerebellar injury. *Sci Rep*. (2018) 8:13633. doi: 10.1038/s41598-018-31728-4
66. Yu X, Wadghiri YZ, Sanes DH, Turnbull DH. *In vivo* auditory brain mapping in mice with Mn-enhanced MRI. *Nat Neurosci*. (2005) 8:961–8. doi: 10.1038/nn1477
67. Brozoski TJ, Ciobanu L, Bauer CA. Central neural activity in rats with tinnitus evaluated with manganese-enhanced magnetic resonance imaging (MEMRI). *Hear Res*. (2007) 228:168–79. doi: 10.1016/j.heares.2007.02.003
68. Holt AG, Bissig D, Mirza N, Rajah G, Berkowitz B. Evidence of key tinnitus-related brain regions documented by a unique combination of manganese-enhanced MRI and acoustic startle reflex testing. *PLoS ONE*. (2010) 5:e14260. doi: 10.1371/journal.pone.0014260
69. Brozoski TJ, Wisner KW, Odintsov B, Bauer CA. Local NMDA receptor blockade attenuates chronic tinnitus and associated brain activity in an animal model. *PLoS ONE*. (2013) 8:e77674. doi: 10.1371/journal.pone.0077674
70. Kilburn KH, Warshaw RH, Hanscom B. Are hearing loss and balance dysfunction linked in construction iron workers? *Br J Industrial Med*. (1992) 49:138–41. doi: 10.1136/oem.49.2.138
71. Juntunen J, Matikainen E, Ylikoski J, Ylikoski M, Ojala M, Vaheri E. Postural body sway and exposure to high-energy impulse noise. *Lancet*. (1987) 2:261–4. doi: 10.1016/S0140-6736(87)90840-3
72. Ylikoski J, Juntunen J, Matikainen E, Ylikoski M, Ojala M. Subclinical vestibular pathology in patients with noise-induced hearing loss from intense impulse noise. *Acta Otolaryngol*. (1988) 105:558–63. doi: 10.3109/00016488809119520
73. Guest M, Boggess M, E'Este C, Attia J, Brown A. An observed relationship between vestibular function and auditory thresholds in aircraft-maintenance workers. *J Occ Environ Med*. (2011) 53:146–52. doi: 10.1097/JOM.0b013e318204fa7f
74. Pyykko I, Aalto H, Ylikoski J. Does impulse noise induce vestibular disturbances? *Acta Otolaryngol.* (1989) 468:211–6. doi: 10.3109/00016488909139048
75. Prasher D, Al-Hajjaj H, Aylott S, Aksentijevic A. Effect of exposure to a mixture of solvents and noise on hearing and balance in aircraft maintenance workers. *Noise Health*. (2005) 7:31–9. doi: 10.4103/1463-1741.31876

Conflict of Interest: The authors declare that the research was conducted in the absence of any commercial or financial relationships that could be construed as a potential conflict of interest.

frontiers in Neurology

ORIGINAL RESEARCH
published: 18 December 2020
doi: 10.3389/fneur.2020.620817

Responses of Neurons in the Medullary Lateral Tegmental Field and Nucleus Tractus Solitarius to Vestibular Stimuli in Conscious Felines

*John P. Bielanin[1], Nerone O. Douglas[1], Jonathan A. Shulgach[1], Andrew A. McCall[1], Derek M. Miller[1], Pooja R. Amin[1], Charles P. Murphey[1,2], Susan M. Barman[3] and Bill J. Yates[1,2]**

[1] Department of Otolaryngology, University of Pittsburgh School of Medicine, Pittsburgh, PA, United States, [2] Department of Neuroscience, University of Pittsburgh, Pittsburgh, PA, United States, [3] Department of Pharmacology and Toxicology, Michigan State University, East Lansing, MI, United States

OPEN ACCESS

Edited by:
Michael Strupp,
Ludwig Maximilian University of Munich, Germany

Reviewed by:
Andrei V. Derbenev,
Tulane University, United States
Sergei B. Yakushin,
Icahn School of Medicine at Mount Sinai, United States

***Correspondence:**
Bill J. Yates
byates@pitt.edu

Specialty section:
This article was submitted to Neuro-Otology, a section of the journal Frontiers in Neurology

Received: 23 October 2020
Accepted: 30 November 2020
Published: 18 December 2020

Citation:
Bielanin JP, Douglas NO, Shulgach JA, McCall AA, Miller DM, Amin PR, Murphey CP, Barman SM and Yates BJ (2020) Responses of Neurons in the Medullary Lateral Tegmental Field and Nucleus Tractus Solitarius to Vestibular Stimuli in Conscious Felines. Front. Neurol. 11:620817. doi: 10.3389/fneur.2020.620817

Considerable evidence shows that the vestibular system contributes to adjusting sympathetic nervous system activity to maintain adequate blood pressure during movement and changes in posture. However, only a few prior experiments entailed recordings in conscious animals from brainstem neurons presumed to convey baroreceptor and vestibular inputs to neurons in the rostral ventrolateral medulla (RVLM) that provide inputs to sympathetic preganglionic neurons in the spinal cord. In this study, recordings were made in conscious felines from neurons in the medullary lateral tegmental field (LTF) and nucleus tractus solitarius (NTS) identified as regulating sympathetic nervous system activity by exhibiting changes in firing rate related to the cardiac cycle, or cardiac-related activity (CRA). Approximately 38% of LTF and NTS neurons responded to static 40° head up tilts with a change in firing rate (increase for 60% of the neurons, decrease for 40%) of ∼50%. However, few of these neurons responded to 10° sinusoidal rotations in the pitch plane, in contrast to prior findings in decerebrate animals that the firing rates of both NTS and LTF neurons are modulated by small-amplitude body rotations. Thus, as previously demonstrated for RVLM neurons, in conscious animals NTS and LTF neurons only respond to large rotations that lead to changes in sympathetic nervous system activity. The similar responses to head-up rotations of LTF and NTS neurons with those documented for RVLM neurons suggest that LTF and NTS neurons are components of the vestibulo-sympathetic reflex pathway. However, a difference between NTS/LTF and RVLM neurons was variability in CRA over time. This variability was significantly greater for RVLM neurons, raising the hypothesis that the responsiveness of these neurons to baroreceptor input is adjusted based on the animal's vigilance and alertness.

Keywords: vestibular, cardiovascular regulation, vestibulo-sympathetic responses, rostral ventrolateral medulla, nucleus tractus solitarius (NTS), lateral tegmental field, sympathetic nervous system, reticular formation

INTRODUCTION

The neural pathways through which baroreceptor and other inputs affect sympathetic nervous system activity have been determined in a variety of mammalian species (1–3). A caveat is that most neurophysiologic experiments examining changes in activity of neurons in key brainstem areas that participate in regulating cardiovascular function were conducted in anesthetized or decerebrate animals (4). An exception is the rostral ventrolateral medulla (RVLM), an area of the reticular formation that plays a key role in controlling the firing rate of sympathetic preganglionic neurons that regulate heart rate and constriction of vascular smooth muscle (5, 6). Three studies reported the activity of RVLM neurons in conscious felines and how it differs from that in decerebrate animals (7–9). These studies showed that RVLM neurons whose activity is correlated with the cardiac cycle, and presumably participate in controlling sympathetic nervous system activity, have spontaneous firing rates that vary over time. They also compared peak and trough firing rates of RVLM neurons between cardiac cycles and determined that they can also fluctuate during a recording session. It was postulated that these changes in spontaneous firing rate and cardiac-related activity (CRA) of RVLM neurons were dependent on supratentorial inputs and related to the animal's alertness, vigilance, and attentiveness to its environment (4, 7, 9).

Studies have shown that much larger changes in body position are required to modulate the activity of RVLM neurons in conscious animals than in decerebrate animals (8). Inputs from the vestibular system participate in regulating sympathetic nervous system activity during changes in body position (10). In decerebrate felines, vestibular inputs elicited by small ($<10^\circ$) sinusoidal head rotations were sufficient to alter the activity of sympathetic efferent fibers in peripheral nerves as well as the firing rate of RVLM neurons (8, 11). However, in conscious animals the firing rates of RVLM neurons were unaffected by 10° sinusoidal body rotations (8, 9), although the activity of a third of the neurons was modulated by static 40° head-up tilts, with an increase in activity in ∼50% of units, and a decrease in the other 50% (9). These changes in unit activity were not correlated with changes in heart rate, suggesting that they were not due to engagement of the baroreceptor reflex. Gating of vestibular inputs to RVLM neurons such that these neurons only respond to large-amplitude static tilts has physiologic relevance, as head-up tilts $<40^\circ$ in amplitude do not appreciably affect the distribution of blood in the body requiring a compensatory change in sympathetic nervous system activity (12). This is unlike other vestibular-elicited responses, such as vestibulo-ocular reflexes, which are engaged during changes in head position $<1^\circ$ in magnitude (13).

Baroreceptor inputs are relayed to RVLM neurons through a pathway that includes neurons in nucleus tractus solitarius (NTS), which receive direct inputs from baroreceptor afferents (1–3). NTS neurons relay baroreceptor signals to the RVLM through connections in the medullary reticular formation (1–3). In felines, neurons in the dorsolateral medullary reticular formation, a region termed the lateral tegmental field (LTF), also play a key role in relaying baroreceptor signals to the RVLM (14–17). There is also evidence that both NTS and LTF neurons transmit vestibular signals to RVLM neurons. NTS (18–20) and LTF (21) receive direct projections from the vestibular nuclei. Projections from the vestibular nuclei to NTS are glutamatergic (20), but the neurotransmitters used by projections from the vestibular nuclei to LTF in felines are unknown. Experiments in decerebrate animals showed that NTS (22) and LTF (23) neurons respond to small-amplitude sinusoidal rotations of the animal's body, including low-frequency rotations that primarily activate otolith organs. To our knowledge, the activity of NTS neurons with baroreceptor inputs has not been recorded in conscious animals. Although one prior study considered the responses of LTF neurons to vestibular stimuli in conscious animals, the focus of this work was neurons that lacked CRA that presumably were part of the "vomiting center," which also is located in the dorsolateral medullary reticular formation (24).

The present study examined CRA and responses to 10° sinusoidal rotations and 40° static tilts of NTS and LTF neurons in conscious felines. The major goal was to ascertain whether NTS and LTF neurons are likely components of the vestibulo-sympathetic pathway in conscious animals, with responses to vestibular stimuli similar to those of RVLM neurons presumed to transmit these signals to sympathetic preganglionic neurons in the spinal cord (9). In addition, comparing the responses to whole-body tilts of NTS and LTF neurons with those of RLVM neurons provides insights into the role of neurons at each stage of the vestibulo-sympathetic reflex pathway in transforming signals from the inner ear. As noted above, changes in sympathetic nervous system activity are elicited only during large-amplitude changes in body position that can result in decreased venous return to the heart and diminished cardiac output (4, 12). A gating of signals thus occurs in the vestibulo-sympathetic circuitry to suppress responses to vestibular inputs elicited during small-amplitude movements. It is informative to compare how NTS and LTF neurons respond to small- and large-amplitude rotations in conscious animals, to determine if they are components of this gating mechanism.

A secondary goal of these experiments was to establish whether anticipation of a passive movement elicits changes in NTS and LTF neuronal activity. It is well-established that feedforward cardiovascular responses are elicited prior to exercise and some other active movements (25–27). A study that monitored changes in heart rate and cerebral blood flow in conscious felines before and during 60° head-up tilts preceded by a light cue demonstrated that no preparatory cardiovascular responses occur before such imposed changes in body position (28). The conclusion of this study was that preparatory cardiovascular responses occur before active movements, but not passive (imposed) movements requiring increases in sympathetic nervous system activity. This conclusion was supported by a study showing that no changes in RVLM neuronal activity occurred in conscious animals following a light cue and before the onset of head-up tilts (9). However, it is possible that changes in neuronal activity are present upstream in the vestibulo-sympathetic reflex pathway, but suppressed prior to being relayed to the RVLM. Thus, by determining whether the activity of LTF and NTS neurons changes preceding cued

head-up tilts, the present study provided an additional test of the hypothesis that feedforward cardiovascular responses occur only before active movements, but are absent prior to expected passive changes in body position (28).

A preliminary report of these findings has been published on the bioRxiv preprint server (29).

METHODS AND MATERIALS

All experimental procedures on animals followed the National Research Council's *Guide for the Care and Use of Laboratory Animals* (30) and were approved by the University of Pittsburgh's Institutional Animal Care and Use Committee. Experiments were performed on five female antibody profile defined and specific pathogen free (APD/SPF) domestic shorthair cats obtained from Marshall BioResources (North Rose, New York, USA). Animals were 4–6 months of age when acquired from the vendor. Juvenile female animals were obtained for these studies, following our prior experience that they are more amenable than males to be acclimated for the 2 h restraint period required for data collection. Moreover, the much higher growth rate in the first year for male cats makes it difficult to maintain chronically implanted recording devices. Animals were provided commercial cat food and water *ad libitum* and were housed under 12 h light/dark cycles. **Table 1** provides information about the animals and the parameters of the study.

This study employed procedures similar to those used in our prior experiments (7–9, 28, 31), which entailed acclimating animals for restraint on a computer-controlled tilt table, implanting instrumentation for recording the electrocardiogram (ECG) and single unit neuronal activity from the brainstem, and subsequently collecting data over a period of 112–399 days. Following data collection, animals were euthanized, and unit locations were histologically reconstructed.

Surgical Procedures

To avoid changes in hormone levels that could affect physiological responses, animals were spayed by a veterinarian prior to the beginning of the study. After they were spayed, the animals were conditioned for body restraint in an animal holder mounted on a computer-controlled tilt table. The period of gradual acclimatization for restraint lasted about 2 months per animal but varied based on the animal's behavior. At the beginning of acclimatization, animals were initially restrained for only a few minutes per session, but as training continued, the period of restraint was slowly increased to 2 h.

After an animal was acclimated to 2 h of body restraint, a recovery surgery was performed in a dedicated operating suite using aseptic techniques. The recovery surgery entailed a craniectomy, attachment of a head fixation plate and recording chamber to the skull, and implantation of wire bundles beneath the thoracic skin to record the ECG. These procedures were described in detail in prior manuscripts (7–9, 28, 31). During surgeries, animals were initially anesthetized by an intramuscular injection of ketamine (20 mg/kg) and acepromazine (0.2 mg/kg), and anesthesia was maintained using 1–2% isoflurane vaporized in O_2 provided through an endotracheal tube. Vital signs (heart rate, respiration rate, and blood oxygen saturation) were measured and recorded in the animal's anesthesia record every 15 min. Ringer lactate solution was provided intravenously and a heating lamp and pad were used to maintain body temperature near 38°C. Following the surgery, an antibiotic (amoxicillin, 50 mg/kg, orally twice per day) was provided for 10 days, and a transdermal fentanyl patch (25 μg/h) delivered analgesia for 72 h.

TABLE 1 | Information about the animals used in the study, the length of data collection, and the number of units included in data analysis.

Animal	Weight at surgery (kg)	Total period of data collection (days)	LTF Units ≥ 5 Trials		NTS Units ≥ 5 Trials	
			CRA	No CRA	CRA	No CRA
1	3.4	266	5	1	0	0
2	3.4	211	8	8	3	3
3	4.2	399	9	2	17	1
4	4.7	213	6	2	1	0
5	4.2	112	4	0	0	0
Total Number of Units Included in Analysis			32	13	21	4

Recording Procedures

After 2 weeks of recovery from surgery, animals were acclimated for a month to head restraint by inserting a screw into the head-mounted fixation plate, and 40° whole-body tilts in the pitch plane provided by a servo-controlled hydraulic tilt table (Neurokinetics, Pittsburgh, PA USA), which was operated using a Micro1401 mk 2 data collection system and Spike-2 version 7 software (Cambridge Electronic Design, Cambridge, UK). During experiments, the recording room was darkened, and black curtains were placed around the tilt table to mask any visual cues about the animal's position in space. An array of 10 LED lights generating a light intensity of 300 lumens was positioned 28 cm in front of the animal's face to provide a visual prompt prior to tilts. The light array was controlled by the Cambridge Electronic Design hardware and software, and illuminated for 2 s, from 8 to 10 s prior to the onset of tilts (see **Figure 1**). The light cue was presumably highly salient since the area surrounding the animal was darkened. The light cue was provided during every trial during the acclimation period, so animals had experienced several hundred tilts paired with a light cue prior to the onset of recordings. Animals were continuously monitored during recording sessions for indicators of distress, and to assure that they remained awake with eyes open.

Brainstem neuronal recordings were initiated once the animals were acclimated for restraint on the tilt table. A hydraulic microdrive (model 650, David Kopf Instruments, Tujunga, CA USA) and x-y positioner, both attached to the recording chamber, allowed for epoxy-insulated tungsten microelectrodes (5 MΩ, Frederick Haer, Bowdoin, ME USA) to be inserted at defined coordinates into the brainstem. Recordings were performed

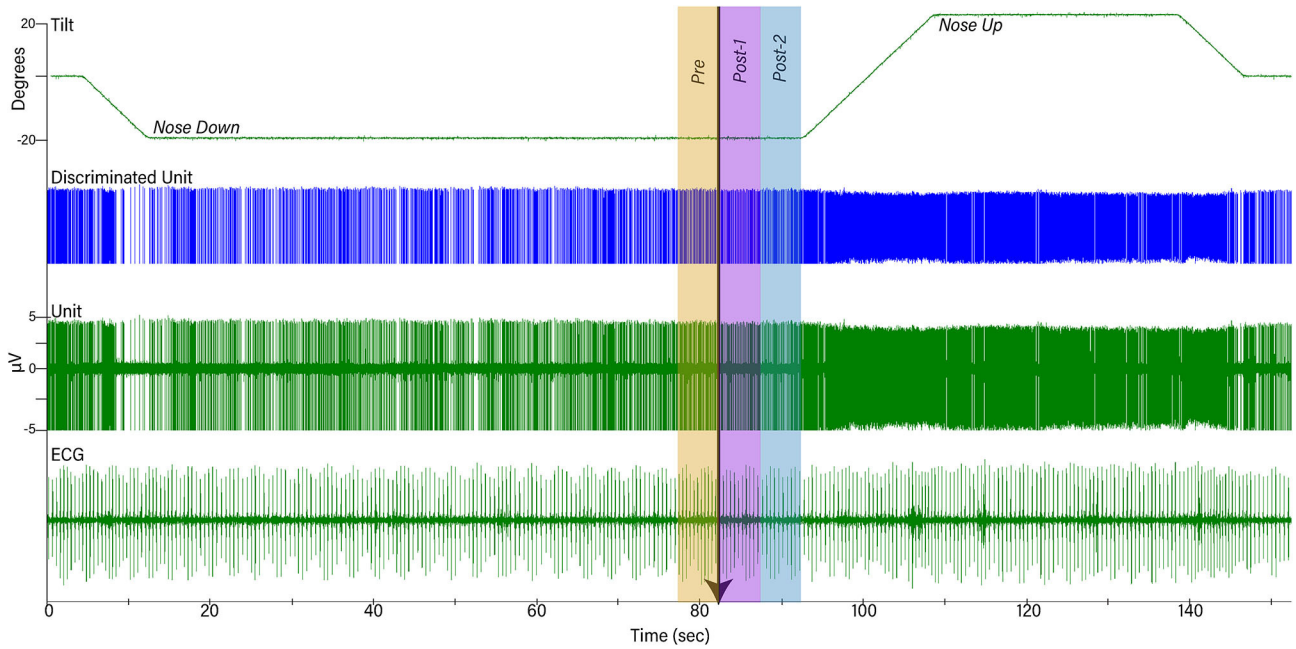

FIGURE 1 | Example of data collected during one trial. The top trace shows table position, the second shows discriminated activity for one unit, the third shows raw unit activity recorded by a microelectrode, and the bottom trace is a recording of the electrocardiogram (ECG). Initially, animals were positioned 20° nose-down for a variable amount of time. A light cue was presented (onset indicated by arrow) that lasted for 2 s. Ten seconds after the light cue was initiated, animals were tilted 40° head-up (20° nose-down to 20° nose-up) and remained in that position for 30 s prior to returning to the prone position. To determine if the light cue had any effect on a unit's activity, firing rate during the period 5 s before light onset (Pre-) was compared to that during the period 5–10 s prior to tilt onset (Post-2).

over a 122–399 day period (see **Table 1**) and targeted to LTF and NTS neurons located 0–5 mm rostral to the obex. Units were localized using stereotaxic coordinates and physiological landmarks including the dorsal and ventral respiratory groups (which were evident as clusters of neurons with respiratory-related activity).

Activity recorded from brainstem neurons was amplified by a factor of 10,000 and filtered with a band pass of 300–10,000 Hz using an AM Systems (Sequim, WA USA) model 1800 microelectrode AC amplifier. The output of the amplifier was sampled at 25,000 Hz using the Micro1401 mk 2 data collection system and Spike-2 version 7 software. The ECG signal was amplified by a factor of 1,000 and filtered with a bandpass of 10–10,000 Hz using an AM Systems model 1700 differential AC amplifier and sampled at 2,500 Hz. Voltages from potentiometers mounted on the tilt table that signaled table position were sampled at 100 Hz. An example of data recordings is shown in **Figure 1**.

When a presumed NTS or LTF neuron was isolated, the animal was tilted 20° nose-down. The animal remained in this position for 1–4 min to allow baseline recordings to be collected to determine if the cell exhibited cardiac-related activity (CRA). Subsequently, the light cue was provided, and the animal was tilted 20° nose-up (such that the table movement was 40°). Since the period when the animal was tilted nose-down varied between trials, animals were not able to predict the occurrence of the light cue or the following nose-up tilt. After the animals were tilted nose-up, they remained in this position for 30 s prior to returning to their initial prone position (see **Figure 1**). Multiple trials (up to 13) were conducted if unit activity remained stable. For most units responses to 10° (peak-to-peak) 0.5 Hz sinusoidal rotations in the pitch plane were also recorded.

Data Analysis Procedures

Typically, only one or two units were present in the recording field during trials. The spike detection and sorting algorithm of the Spike-2 software was used to isolate the activity of each unit in the recording field, and to verify that spike shape remained consistent between trials. If there was any doubt that data were not continually recorded from the same unit, the data were discarded. Event markers generated by the Spike-2 software indicated the timing of action potentials generated by each sampled neuron, as well as the peak ECG R-waves. These event markers were used in our subsequent data analyses.

Detection of CRA

Experimental procedures similar to those used in our prior studies were used to determine if a unit exhibited CRA (7–9). Trigger pulses coinciding with the R-wave of the ECG were used for the creation of post R-wave interval histograms (10 ms bin width) of unit activity (Datapac software, Run Technologies; Mission Viejo CA USA). Interval histograms between successive R-waves were constructed simultaneously. Trigger pulses were also used to generate an average of the peak ECG R-wave. The averages and histograms were generated using data segments of varying length (28–211 s). When multiple trials were conducted

for each neuron, a separate analysis was performed for each trial. A ratio of peak-to-background counts was calculated for each histogram. To classify a neuron as having CRA, the ratio of peak-to-background counts in the histogram had to be greater than a value of 2.0 for the majority of analyses for each unit. **Figure 2** shows examples of two analyses for an NTS unit.

Response of Units to Light Cue and 40° Tilts

The following analyses were conducted using MATLAB software (Mathworks, Natick, MA USA). Unit firing rate and heart rate were determined for a 30 s period prior to the light cue, while the animal was tilted nose-down, as well as when the animal was positioned nose-up. Furthermore, unit firing rate and heart rate were also determined for the time period 5 s prior to the light cue and during the two consecutive 5 s time periods prior to the onset of the 40° nose-up tilt (see **Figure 1**). Since the duration of the light cue was 2 s, the light remained illuminated during the first 2 s of Post-1 time interval indicated in **Figure 1**.

Subsequent statistical analysis of the data compared heart rate and unit firing rates when animals were positioned nose-up and nose-down, as well as during the pre- and post-light cue periods prior to the onset of the tilt. As established in a prior study (9), to provide adequate statistical power these analyses were only conducted for units in which five or more 40° tilts were delivered. Statistical analyses and plotting of experimental results were performed using Prism 8 software (GraphPad software, San Diego, CA USA). Confidence intervals are indicated as mean ± one standard deviation.

Response to Sinusoidal Rotations

We additionally tested the responses of most neurons to 10° (peak-to-peak amplitude) sinusoidal tilts at 0.5 Hz to determine if they responded to small dynamic vestibular stimuli as well as large amplitude tilts. During sinusoidal rotations, neural activity was binned (500 bins/cycle) for ∼35 stimulus repetitions and fitted with a sine wave using a least-squares minimization technique described in other reports (8, 22, 24, 31, 32). Two criteria were used to determine if a unit's activity was significantly modulated by 10° sinusoidal rotations: a signal-to-noise ratio >0.5 and only one evident first harmonic. To ensure that a unit's response to the rotations was not a reflection of its rhythmic spontaneous firing rate at the stimulus frequency, the stimulus was periodically stopped and restarted to determine if peak firing rate remained aligned with the same phase of head movement. Units were discarded from analysis if they were determined to have rhythmic activity at the frequency of the stimulus, although such occurrences were rare.

Reconstruction of Unit Locations

Once data collection was completed in an animal, electrolytic lesions were made at designated coordinates by passing a 100 μA negative current for 60 s through a 0.5 MΩ tungsten electrode. Approximately 1 week following the lesions, animals were anesthetized by an intramuscular injection of ketamine (20 mg/kg) and acepromazine (0.2 mg/kg) followed by an intraperitoneal injection of pentobarbital sodium (40 mg/kg). Animals were then transcardially perfused with saline followed by 10% formalin. The brain was removed and placed in a solution of 10% formalin/30% sucrose for at least 2 weeks to allow for additional fixation. After the brain was post-fixed, it was sectioned transversely at 50 μm thickness using a freezing microtome. The sections were mounted in serial order on microscope slides and stained using thionine. Images of sections were captured using a spot camera and digital software (Spot Imaging, Sterling heights, MI USA) through a Nikon Eclipse E600 microscope. Photomontages of sections were created with Adobe Illustrator software (Adobe Inc., Mountain View, CA USA) and used to plot specific unit locations. The locations of individual units were reconstructed with respect to the position of the lesions, the relative coordinates of each unit and unit depths.

RESULTS

Activity was recorded from a total of 134 units with CRA whose locations were histologically confirmed to be in the LTF (97 neurons) and NTS (57 neurons). The locations of the units are shown in **Figure 3**. Additionally, unit activity was recorded from 51 units without CRA: 39 neurons in the LTF and 12 neurons in the NTS. Thus, 71% of the sampled LTF neurons and 83% of the sampled NTS neurons had CRA. Recordings from LTF neurons occurred in all experiments, whereas recordings of NTS activity were included in three experiments.

Figures 2A–D shows examples of CRA in two trials for an NTS unit; **Figure 2E** compares the peak and trough activity for LTF neurons with CRA, and **Figure 2F** provides the same comparison for NTS neurons. Each point in **Figures 2E,F** is an average of all of the trials conducted for a cell. For every unit examined with five or more trials, a two-tailed paired *t*-test showed that on average peak counts were significantly greater ($P < 0.05$) than trough counts. For units located in the LTF, *P*-values ranged from <0.0001 to 0.02, with most units having $P < 0.001$, and only 5 having *P*-values between 0.002 and 0.02. On average, peak counts were 2.2 ± 0.5 (SD) times greater than trough counts. Similarly, for NTS units with five or more stimulus trials, *P*-values ranged from <0.0001 to 0.01, with most units having $P < 0.0004$, and only 7 having *P*-values between 0.001 and 0.01. On average, peak counts were 2.2 ± 0.4 (SD) times greater than trough counts. Even though CRA was present across trials for units that demonstrated this activity, the ratio for peak to trough counts often varied between trials, as illustrated in **Figure 4** for eight units each in the LTF and NTS. For LTF units, the difference in peak-to-trough ratios for a particular unit (the largest ratio minus the smallest ratio across trials) ranged from 0.7 to 2.7; the median difference was 1.0. For NTS units, the difference in peak-to-trough ratios ranged from 0.3 to 2.9; the median difference was also 1.0. The variability in peak-to-trough ratios between runs was not significantly different for LTF and NTS neurons ($P = 0.84$, unpaired two-tailed t-test).

Responses to Changes in Head Position

Analyses of data focused on units for which multiple 40° tilts (≥5) were completed, so we could statistically ascertain whether firing rate differed in the nose-down and nose-up positions (9).

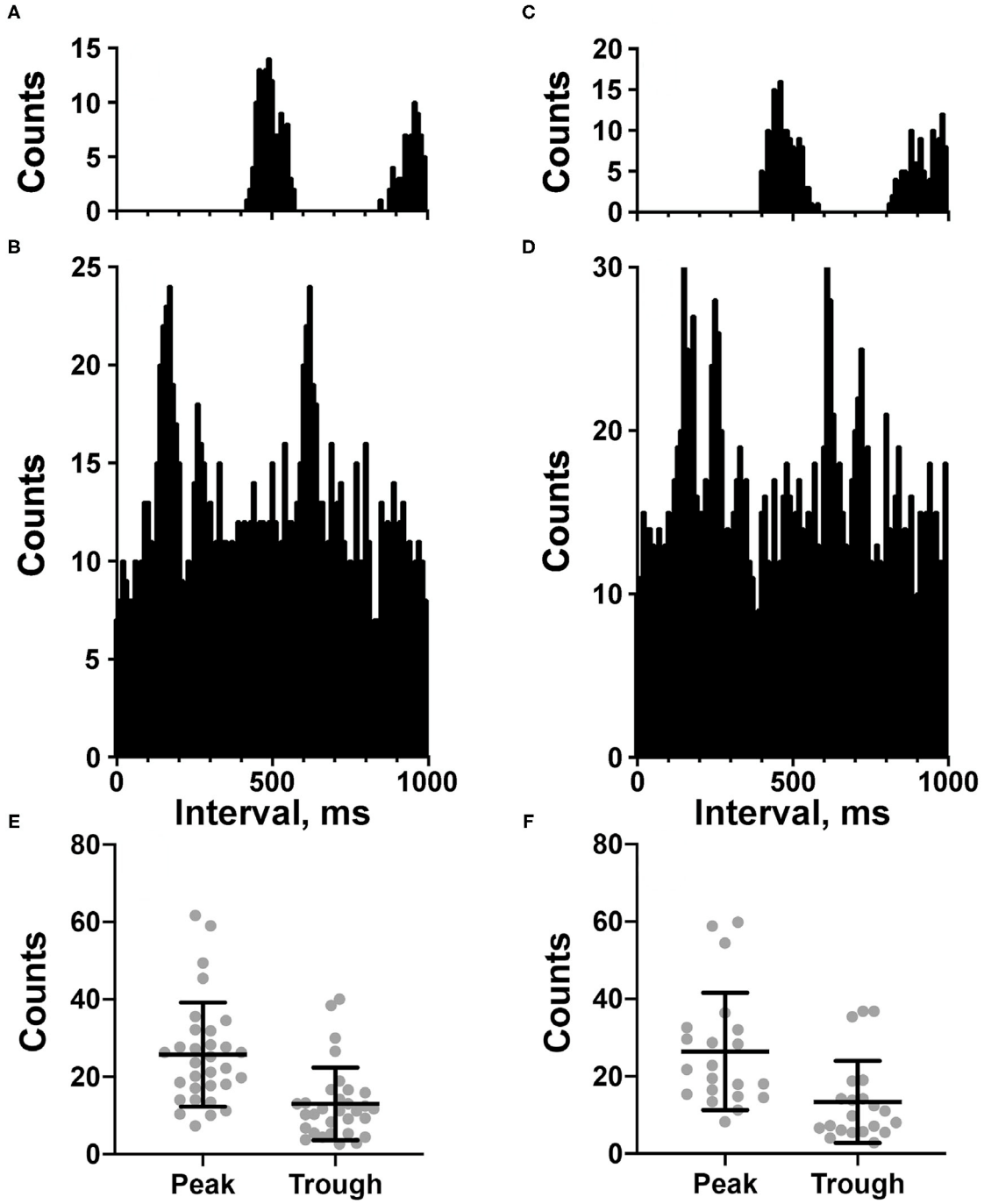

FIGURE 2 | (A–D) Cardiac-related activity (CRA) evident in two trials for an NTS neuron (**A,B** are for one trial and **C,D** are for the second trial). Histograms were triggered by event markers demarking ECG R-waves; bin width is 10 ms. **(A,C)** show intervals between R-waves, and **(B,D)** show intervals between the unit's action potentials. Unit activity peaked in periods between R-waves. **(E,F)** plot of counts during peak and trough periods for the LTF **(E)** and NTS **(F)** neurons classified as exhibiting CRA.

A total of 45 LTF units (46% of sampled neurons; 32 with CRA) and 25 NTS units (44% of sampled neurons; 21 with CRA) were included in this statistical analysis, as indicated in **Table 1**. For the 32 LTF units with CRA, the following number of tilts were performed: 5 for 7 units, 6 for 7 units, 7 for 8 units, 8 for 6 units, 9 for 2 units, 10 for 1 unit, and 11 for 1 unit. For the 21 NTS units with CRA, the following number of tilts were performed: 5 trials for 8 units, 6 trials for 3 units, 7 trials for 3 units, 8 trials for 1

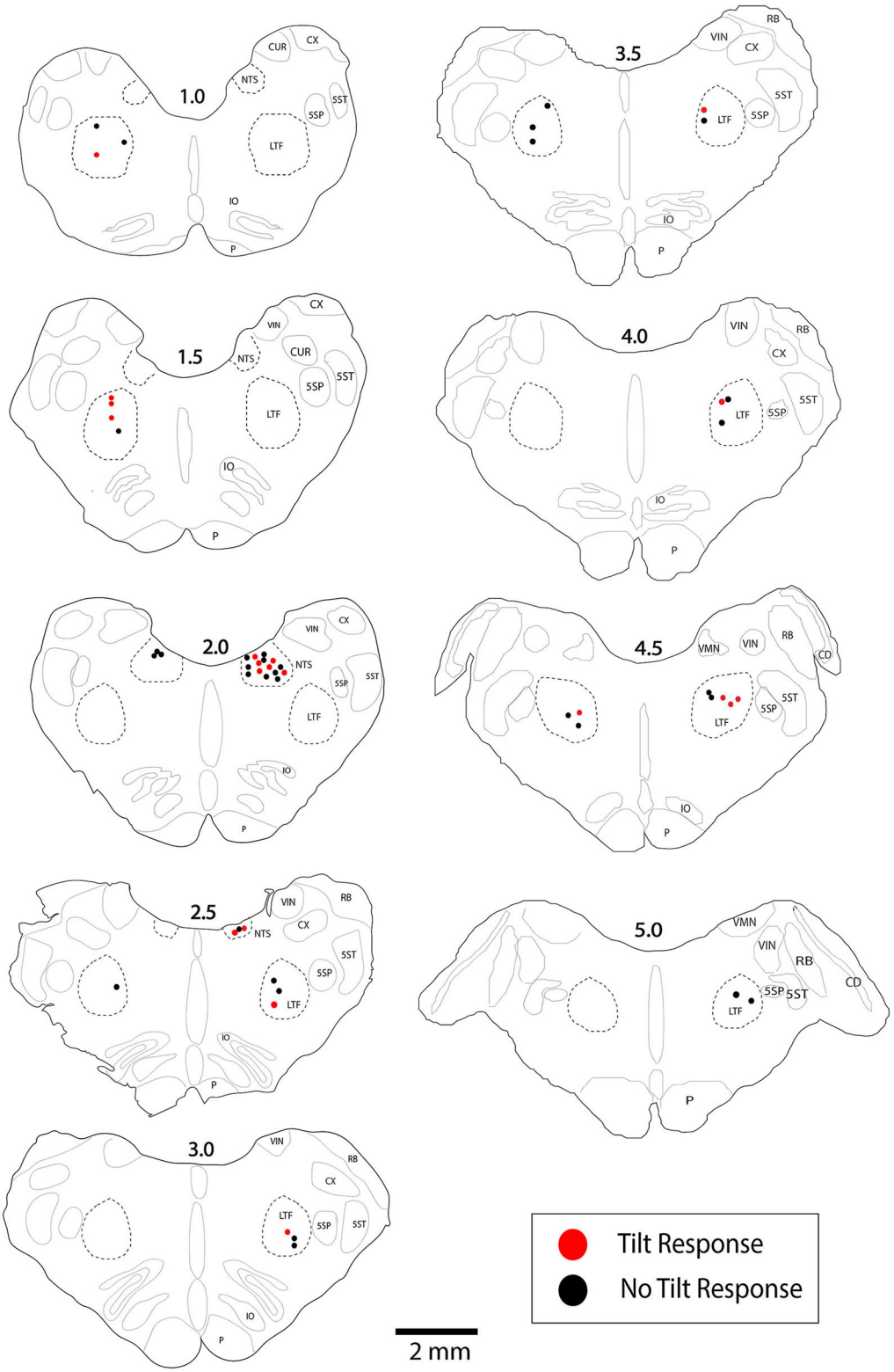

FIGURE 3 | Locations of LTF and NTS neurons with CRA whose responses to 40° tilts were recorded during five or more trials. Red symbols designate units with significant differences in unit activity in the nose-down and nose-up position. Black symbols designate units without significant responses to tilts. The numbers above each section indicate the distance rostral to the obex in mm. LTF, lateral tegmental field; NTS, nucleus tractus solitarius; 5SN, spinal trigeminal nucleus; 5ST, spinal trigeminal tract; CUR, cuneate nucleus, rostral; CX, external cuneate nucleus; IO, inferior olivary nucleus; P, pyramid; VIN, inferior vestibular nucleus; RB, restiform body; VMN, medial vestibular nucleus; CD, dorsal cochlear nucleus.

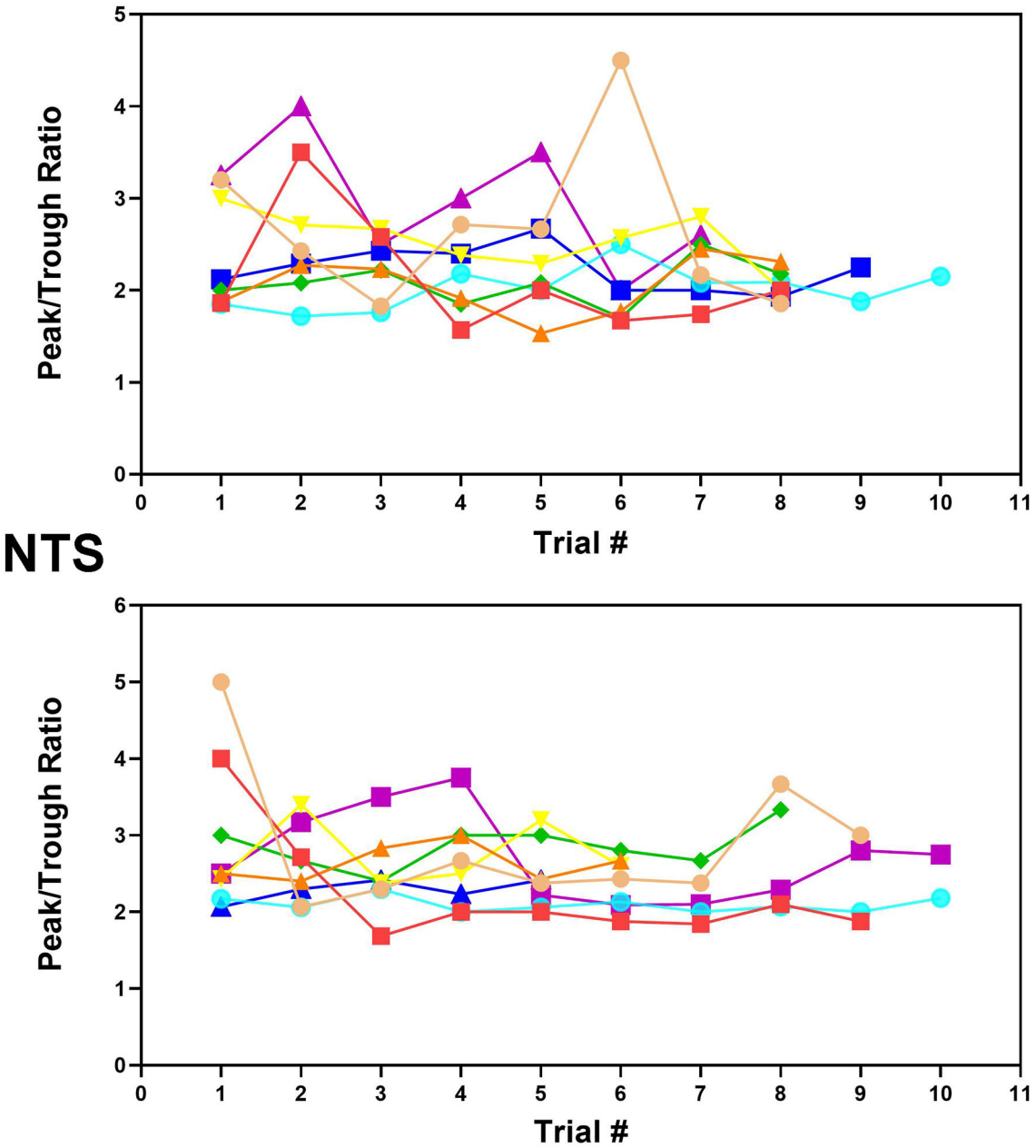

FIGURE 4 | Peak-to-trough ratio of activity related to the cardiac cycle for 8 LTF and 8 NTS units where multiple trials were conducted. Data for each unit is depicted by different shapes and colors. For most units, the peak-to-trough ratio varied throughout the course of recording although all units exhibited CRA during every trial.

unit, 9 trials for 1 unit, 10 trials for 3 units, 11 trials for 1 unit, and 13 trials for 1 unit. The locations of the LTF and NTS units with CRA are indicated in **Figure 3**.

Responses to 40° Static Tilts

The activity of units when animals were positioned 20° nose-down was compared using a two-tailed paired *t*-test to that when animals were positioned 20° nose-up. **Figure 1** illustrates the experimental paradigm, whereas **Figure 5** illustrates the change in activity of an NTS neuron during 10 tilt trials; the activity of the unit when the animal was positioned nose-down was significantly lower than when the animal was nose-up ($P < 0.0001$). Of the 32 LTF units with CRA, the activity of 12 (38%) was significantly different ($P < 0.05$) between the nose-down

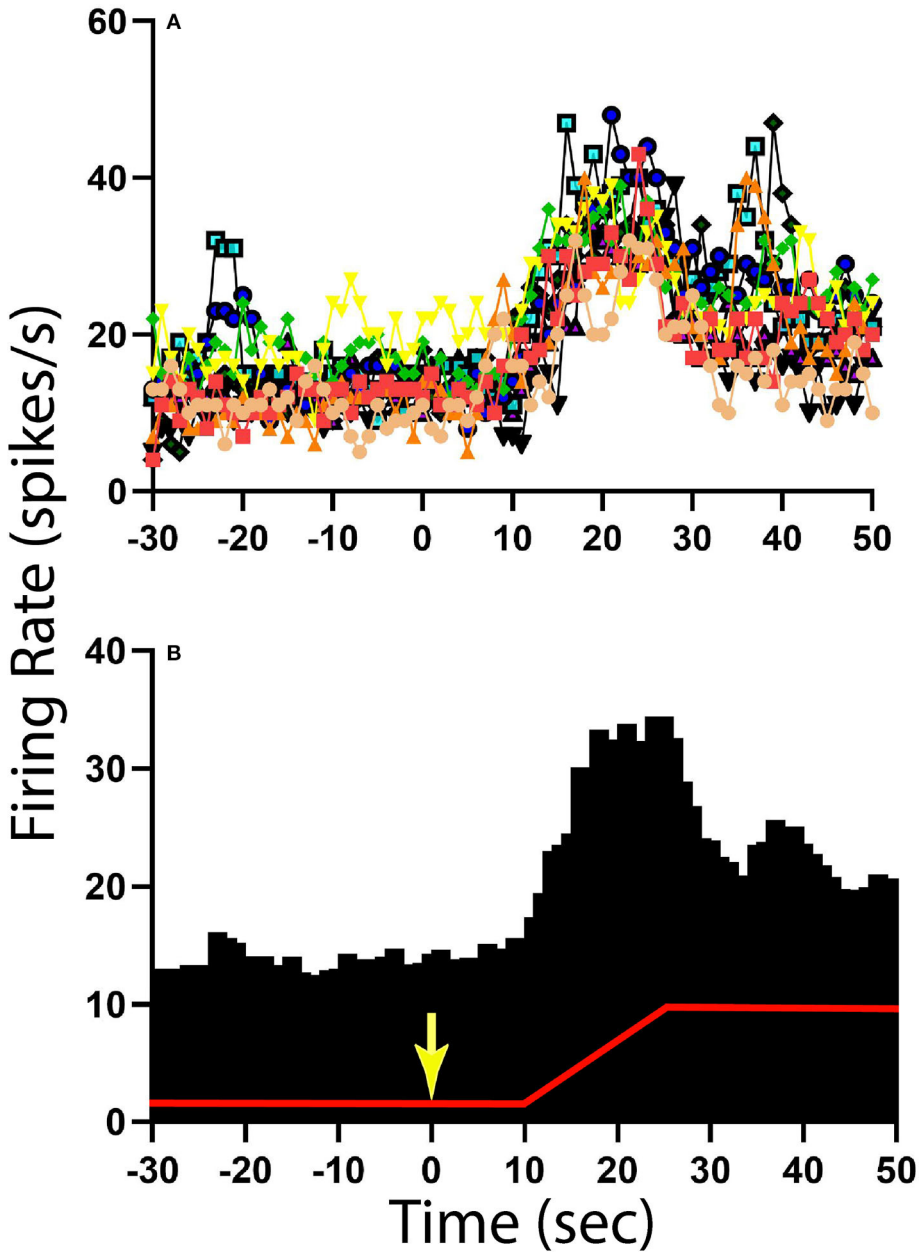

FIGURE 5 | Change in activity for one NTS unit with CRA during 40° head-up tilt. **(A)** Unit activity during 1 s bins for 10 individual trials; each trial is demarked by lines of different colors as well as different symbols. **(B)** Histogram of averaged activity during 1 s bins for all trials. The red line designates table position; the transition from 20° nose-down to the 20° nose-up position (40° change in animal position) occurred 10 s after the light cue, which is demarked by a yellow arrow.

and nose-up positions. Similarly, the activity of 8 of 21 NTS units with CRA (38%) was significantly different when animals were positioned nose-down and nose-up. **Figure 6** shows the average percent change in firing rate during nose-up rotations for the neurons with significant responses to the change in body position. The firing of the majority of LTF (7/12) and NTS (5/8) neurons was higher when the animals were in the nose-up position. The mean absolute change in firing rate during 40° nose-up tilt was 51 ± 25% for LTF neurons and 51 ± 23% for NTS neurons. These changes in activity for NTS and LTF neurons were not significantly different ($P = 0.94$, unpaired two-tailed t-test). **Figure 7** shows the activity during every trial for the LTF and NTS neurons that responded to tilts; P-values over each panel show the significance of the responses. In most cases, the changes in unit activity were similar between trials.

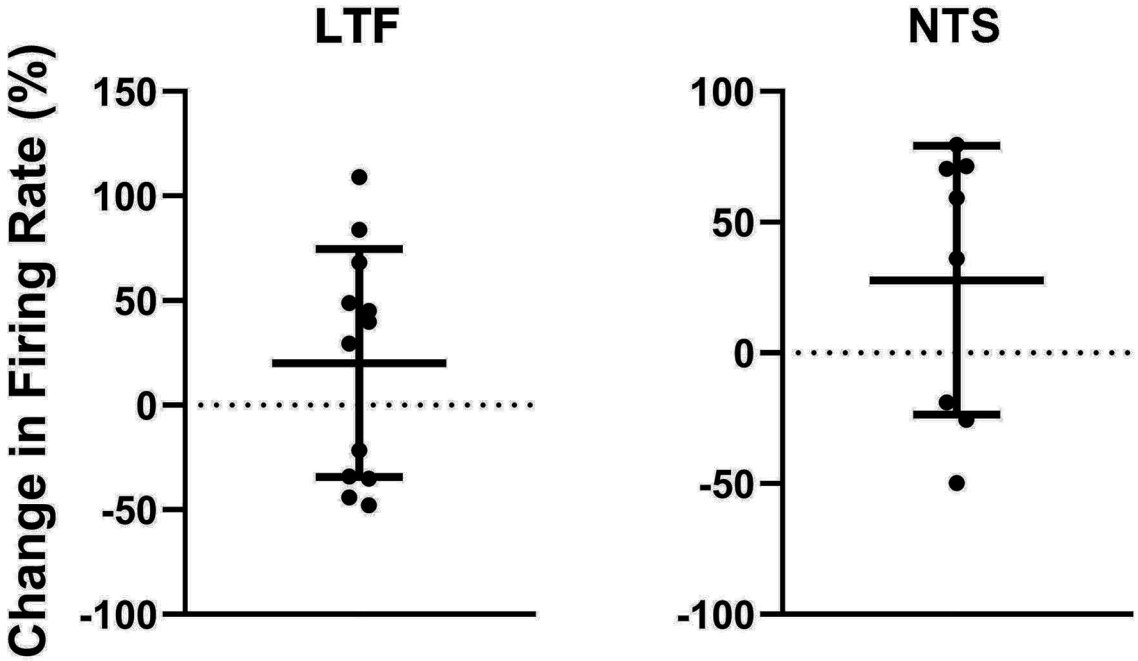

FIGURE 6 | Percent change in firing rate when the animal was tilted nose-up (firing rate in nose-up position ÷ firing rate in the nose-down position) for the 12 units in the LTF and 8 units in the NTS with CRA whose activity was significantly modulated during 40° head-up tilts. Error bars indicate mean ± one standard deviation.

LTF and NTS units with CRA whose firing rates were significantly altered by 40° head-up tilt were intermixed with neurons whose firing rates were unaffected by the tilts, as indicated in **Figure 3**. LTF neurons that responded to tilts were located on average 2.2 ± 1.3 mm rostral to the obex and 3.0 ± 1.0 mm lateral to the midline, while unresponsive cells were located 2.5 ± 1.2 mm rostral to the obex and 2.6 ± 0.9 mm lateral to the midline. A two-way ANOVA analysis showed that distances from the obex ($P = 0.74$) and midline ($P = 0.60$) were not significantly different for LTF neurons whose activity was significantly modulated or unaffected by the 40° nose-up tilts. NTS neurons that responded to tilts were located on average 1.9 ± 0.56 mm rostral to the obex and 2.7 ± 0.48 mm lateral to the midline, while unresponsive units were located 2.1 ± 0.47 mm rostral to the obex and 2.5 ± 0.5 mm lateral to the midline. A two-way ANOVA analysis revealed that distances from the obex ($P = 0.37$) and midline ($P = 0.26$) were not significantly different for NTS units that responded to or were unaffected by the 40° nose-up tilts.

We also considered whether the firing rates of LTF units lacking CRA were significantly modulated during 40° changes in body position. Out of the 13 LTF cells lacking CRA with five or more tilt trials, seven (54%) responded significantly to 40° head-up tilts. *P*-values ranged from 0.0004 to 0.02, with five responses having $P < 0.01$. Activity decreased in four units and increased in the other three during head-up tilts. The average absolute change in firing rate for the seven units that responded significantly to 40° head-up tilts was 26 ± 21%. A two-sided Fisher's exact test failed to reveal any significant difference in the proportion of LTF units with and without CRA that responded to tilts ($P = 0.31$). A similar analysis was not conducted for NTS neurons, as the firing rate of only four neurons lacking CRA was recorded during five or more tilts. One of these neurons responded significantly to head-up rotations.

Heart rate was also measured during 40° head-up tilts. For the 53 units with CRA (32 LTF and 21 NTS cells) tested using 5 or more trials, heart rate decreased in 68% and increased in 32% of the trials. However, these changes in heart rate were statistically significant for only 13 of the 53 units (25%). In 12 of these 13 cases, heart rate was lower (by an average of 5.1 ± 1.4%) when animals were positioned head-up. Heart rate changed significantly ($P < 0.05$) during rotations for only 2/12 (17%) LTF units with CRA that responded to 40° tilts and for 5/20 (25%) of the units with CRA whose activity was not significantly modulated by 40° tilts. In 6/7 (85%) of these cases, heart rate decreased during head-up tilts, and the magnitude of the heart rate changes was small: 3.5 ± 0.10% for units that responded to tilts and 3.4 ± 5.9% for those without significant responses to the rotations. Significant changes in heart rate occurred during rotations for 3/8 (38%) of the neurons in the NTS that responded to 40° head-up tilts and 3/13 (23%) that failed to respond these movements. Heart rate decreased in all of these cases during head-up tilt. On average, heart rate decreased by 5.4 ± 0.41% for trials in which the firing rates of NTS neurons were modulated by 40° head-up tilts and decreased by 6.0 ± 1.2% for trials in which no significant changes in firing rate occurred during the rotations. The changes in heart rate during tilts that altered or failed to alter the firing rate of cells in the

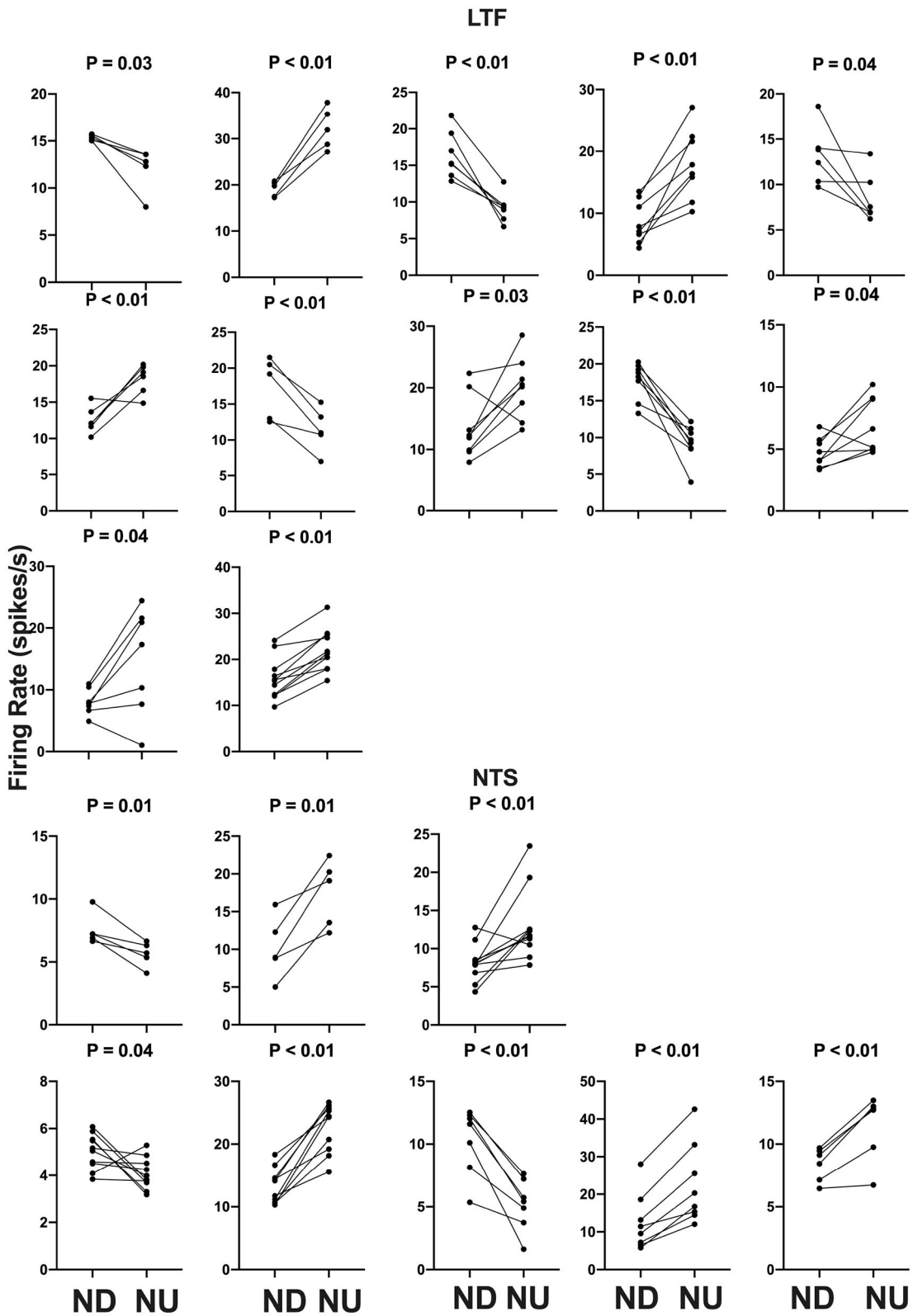

FIGURE 7 | Firing rate during each trial for the 12 LTF and 8 NTS units with CRA whose activity was significantly modulated by 40° head-up tilt. Each panel depicts the firing rate for a single unit when the animal was positioned 20° nose-down (ND) and then subsequently positioned 20° nose-up (NU). *P*-values indicating the significance of the difference in firing rate in the ND and NU positions (paired *t*-test) are provided above each panel. The greatest significance level indicated is $P < 0.01$.

NTS were not significantly different ($P = 0.32$), as indicated by a two-tailed t-test.

Responses to 10° Sinusoidal Tilts

Responses were also recorded during 10° sinusoidal rotations in the pitch plane at 0.5 Hz for the 12 LTF units and 8 NTS units that responded to static head-up tilts. Only two of the LTF units (17%) and one unit in the NTS (13%) had significant responses to these rotations, in accordance with established criteria (8, 22, 24, 31, 32). The responses of two LTF units to 10° sinusoidal rotations are illustrated in **Figure 8**. All 3 units that responded significantly to 10° sinusoidal rotations also had large (>30%) changes in activity during 40° head-up tilts.

Responses to Light Cue Preceding Static Tilts

Throughout the course of experimentation, a light cue was provided 10 s prior to the onset of each 40° head-up tilt, and we

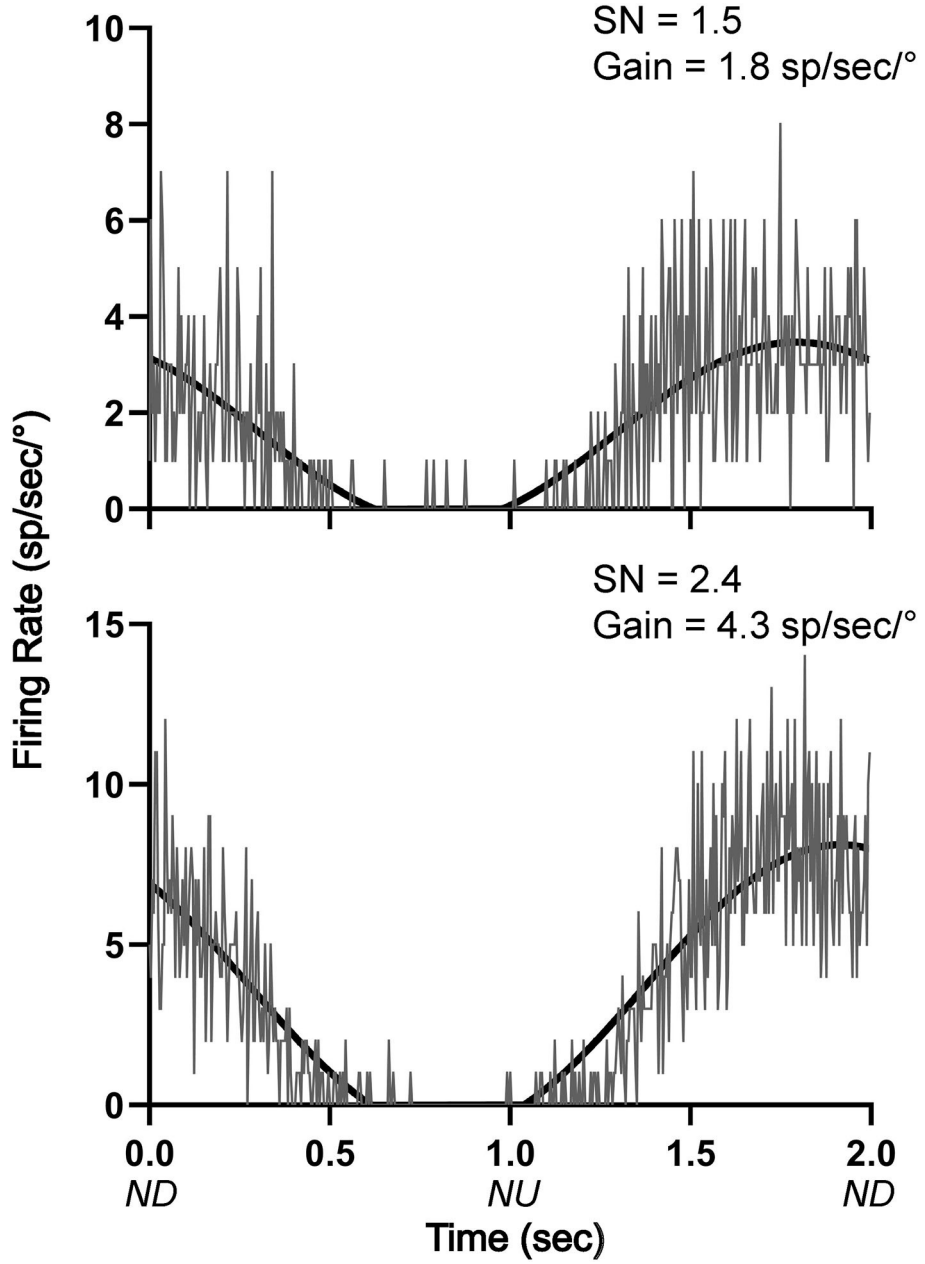

FIGURE 8 | Averaged responses (~30 trials) of two LTF units with CRA to 10° sinusoidal rotations in the pitch plane at 0.5 Hz. Bin width was 4 ms (500 bins/trace). A sine wave fitted to responses is shown by black lines. The signal-to-noise (SN) ratio and gain for each unit's response is indicated. ND, nose-down; NU, nose-up.

determined whether the activity of LTF or NTS units changed after this cue and before the onset of tilts (see **Figure 1**). As indicated in **Figure 9**, two-tailed paired *t*-tests revealed that only 3/32 LTF (9%) units with CRA, and just one that responded to head-up tilt, exhibited significant ($P < 0.05$) changes in activity in the 5 s time period prior to tilt onset (Post-2 period indicated in **Figure 1**) compared to the 5 s time period prior the light cue (Pre-period indicated in **Figure 1**). Only 1/21 NTS units with CRA, and none that responded to head-up tilts, had a significant increase in firing rate during the Post-2 period. A linear regression analysis failed to show a strong correlation between the significance of responses to the light cue and head-up tilts for LTF ($P = 0.11$, $R^2 = 0.23$) or NTS ($P = 0.03$, $R^2 = 0.21$) neurons.

DISCUSSION

These experiments included the first recordings in conscious animals from NTS and LTF neurons with changes in firing rate correlated with the cardiac cycle, which presumably participate in regulating cardiovascular responses mediated by the sympathetic nervous system (4). They showed that the activity of an appreciable fraction (38%) of both NTS and LTF neurons with CRA was significantly modulated by 40° static head-up tilts, with most (60%) having higher firing rates in the head-up position. The firing rates of NTS and LTF neurons with CRA changed on average ∼50% during the 40° head-up tilts.

Such responses are similar to those of RVLM neurons during 40° static head-up tilts: 31% responded to these rotations, with an average change in firing rate of 34% (9). Approximately half of the RVLM neurons that responded to 40° head-up tilts had higher firing rates in the head-up position, whereas firing rates decreased in the other half. There was not a significant difference in the magnitude of responses to head-up tilts for NTS, LTF, and RVLM neurons ($p = 0.1$, one-way ANOVA). Since RVLM neurons receive direct and/or multisynaptic inputs from NTS (1–3) and LTF (14–17), and the vestibular nuclei project to both regions (18–21), these data are consistent with the hypothesis that LTF and NTS neurons are components of the vestibulo-sympathetic reflex pathway.

Although the firing rate of over a third of NTS and LTF neurons with CRA was modulated by static head-up tilts, few of these neurons responded to 10° sinusoidal rotations of the body in the pitch plane. Studies in decerebrate animals have shown that an appreciable fraction of NTS neurons with baroreceptor inputs (54%) (22) and LTF neurons (∼60%) (23) responded to sinusoidal body rotations <10° in magnitude. Thus, as for RVLM neurons (8), LTF and NTS neurons with CRA only responded to large-amplitude body rotations that could produce fluid shifts requiring compensatory changes in sympathetic nervous system activity. In contrast, neurons in caudal regions of the vestibular nuclei that provide inputs to LTF and NTS responded robustly to small-amplitude body rotations in conscious felines (31, 33). Considering that the caudal aspect of the vestibular nuclei has direct projections to NTS and LTF (18–21), it is unclear how gating of labyrinthine signals occurs in vestibulo-sympathetic responses, such that sympathetic nerve activity only changes during large-amplitude body rotations. It is feasible that NTS and LTF neurons also receive convergent inputs from other regions of the nervous system that modify their responses to vestibular stimuli. It has been postulated that the caudal cerebellar uvula modulates vestibulo-sympathetic responses (10), and the present data raise the prospect that a pathway originating in the cerebellum or elsewhere in the nervous system alters the responsiveness of LTF and NTS neurons to vestibular stimuli. This hypothesis

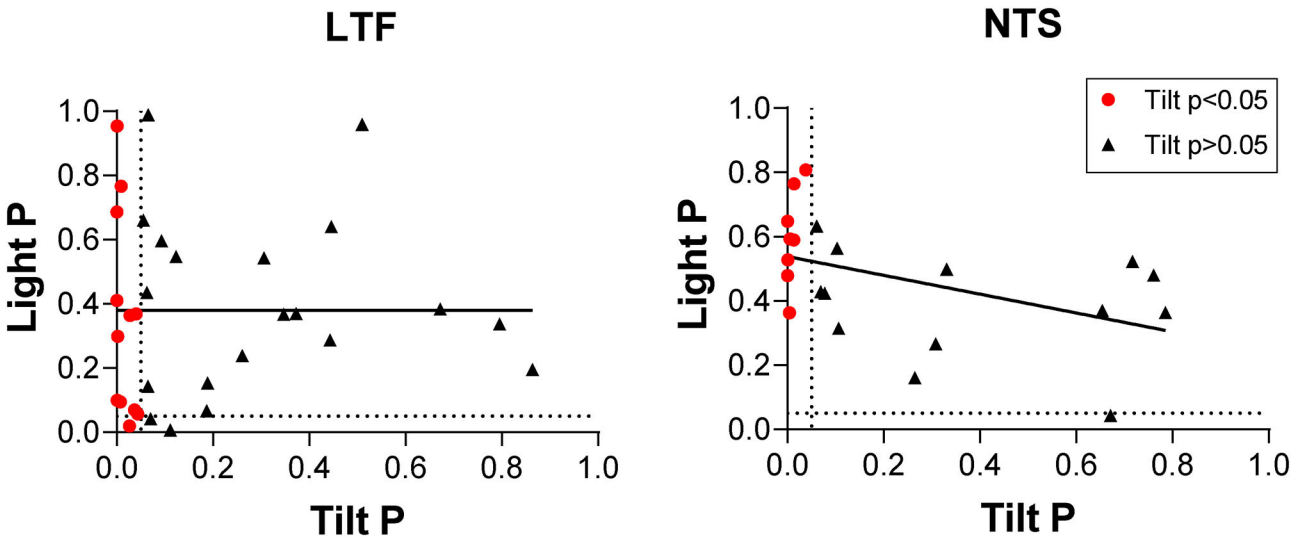

FIGURE 9 | Comparison of *P*-values (two-tailed *t*-test) for responses to head-up tilt (Tilt P) and responses to the light cue preceding tilts (Light P, pre-tilt vs. post-2 period indicated in **Figure 1**). Data for neurons with significant responses ($P < 0.05$) to head-up tilts are indicated by red symbols. Lines show the best-fit of the data with a linear regression analysis.

remains to be validated experimentally. However, a caveat is that sinusoidal rotations of the head activate both semicircular canal and otolith organ afferents, whereas static tilts only elicit otolith organ inputs (13). Although it is evident that LTF and NTS neurons respond differently to small-amplitude sinusoidal rotations in conscious and decerebrate animals, it is feasible that prolonged 10° static tilts would alter the activity of some LTF and NTS neurons.

We also evaluated whether the responses of NTS and LTF neurons to large-amplitude static tilts could be due to activation of the baroreceptor reflex. Heart rate changes related to tilts were small and significant during trials for only a small proportion of neurons with CRA whose neuronal activity changed appreciably during the rotations. In addition, significant heart rate changes were noted for approximately equal proportions of cells whose firing rates were and were not modulated by head-up rotations. These data suggest that the primary signals altering the firing rates of NTS and LTF neurons during whole-body tilts were not from baroreceptors.

The magnitude of CRA of LTF and NTS neurons, gauged by the ratio of peak to background counts time-locked to the cardiac cycle, varied between trials. A similar analysis for RVLM data (9) showed that the variability in peak-to-trough ratios ranged from 2.8 to 4.3; the median difference was 3.4 (mean of 3.5 ± 0.6). A one-way ANOVA combined with Dunnett's *post-hoc* test showed that the variability in the peak-to-trough ratios was significantly larger for RVLM neurons than either NTS or LTF neurons ($P < 0.0001$). This variability in peak-to-trough ratios did not appear to be related to unit spontaneous firing rate, which was not significantly different ($p = 0.15$, one-way ANOVA) for LTF (14 ± 6 spikes/s), NTS (11 ± 6 spikes/s), and RVLM (16 ± 11 spikes/s) neurons. The difference in CRA for RVLM

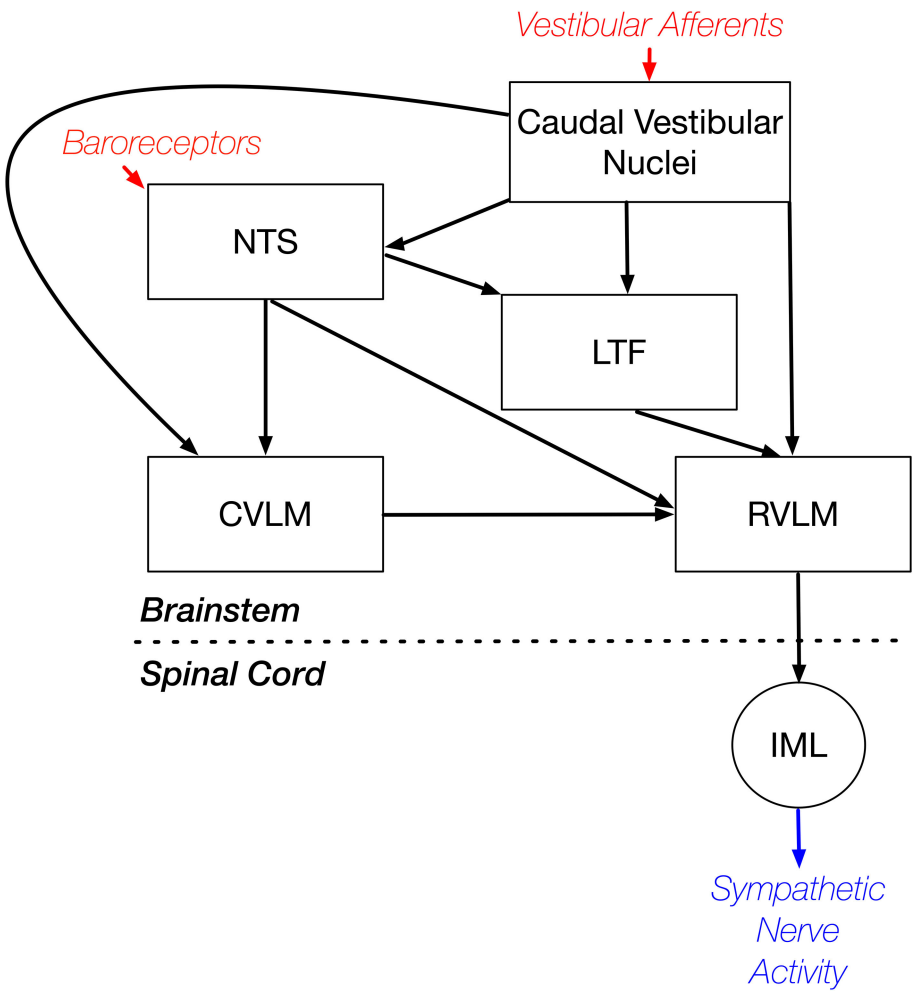

FIGURE 10 | Brainstem regions that relay vestibular signals to the RVLM. This neural circuit diagram is based on the findings of both anatomical (18–21, 39–42) and electrophysiologic (21, 43) studies that mapped connections in the vestibulo-sympathetic pathway. Red text and arrows indicate afferent inputs, and blue text and arrows denote efferent (output) pathways from the central nervous system. CVLM, caudal ventrolateral medulla; IML, sympathetic intermediolateral cell column; LTF, lateral tegmental field; NTS, nucleus tractus solitarius; RVLM, rostral ventrolateral medulla.

and NTS/LTF neurons may be a reflection of the complexity of inputs to the RVLM, which include projections from a variety of brainstem and supratentorial structures (4). These data suggest that factors such as alertness and vigilance have less of an impact on the excitability of LTF and NTS neurons than RVLM neurons, although this prospect is yet to be examined experimentally.

A light cue preceded 40° head-up tilts in these experiments, but there was no evidence that the activity of LTF or NTS units changed after the light cue and prior to the whole-body rotations. A previous experiment provided similar results for RVLM neurons (9). An earlier study showed that heart rate and cerebral blood flow was unaffected by a light cue delivered before 60° head-up tilts in conscious felines (28). Collectively, these data provide strong evidence that feedforward (preparatory) cardiovascular responses are absent prior to imposed postural changes that can result in a change in blood distribution in the body. This is in contrast to exercise and some other active movements (or imagination of active movements) in which cardiovascular responses occur prior to movement onset (25–27). There is considerable evidence that motor cortex has multisynaptic influences on sympathetic nervous system activity (34–36), as do subcortical areas involved in motor control (27). One possibility is that feedforward cardiovascular responses prior to movement are elicited through connections of brain motor areas with RVLM neurons, such that anticipation of imposed movements that do not entail motor responses fail to trigger changes in heart rate or peripheral blood flow. Additional experiments are needed to examine this hypothesis.

LTF and NTS neurons with and without CRA had similar responses during whole-body rotations in these studies. Studies in decerebrate and anesthetized animals have shown that neurons in these regions with respiratory-related activity and inputs from gastrointestinal receptors, as well as those with baroreceptor inputs, responded to vestibular stimuli (19, 22, 23). Head-up body rotations require changes in the activity of respiratory muscles to compensate for gravitational loading on these muscles (37), and both LTF and NTS neurons have been proposed as components of brainstem circuity that produces motion sickness (38). It is thus not surprising that NTS and LTF neurons lacking CRA responded to vestibular stimuli. However, the design of these experiments did not permit a determination of the physiologic role of neurons lacking CRA.

In summary, these experiments included the first recordings in conscious animals from NTS and LTF neurons with CRA that presumably participate in regulating cardiovascular responses mediated through the sympathetic nervous system. The studies showed that the responses of these neurons to whole-body rotations that activate the vestibular system were similar to those documented for RVLM neurons (9). In combination with other findings, these data support the conclusion that LTF and NTS neurons are components of the brainstem pathway that mediates vestibulo-sympathetic responses. However, variability in CRA from trial to trial was smaller for NTS and LTF neurons than for RVLM neurons. This observation suggests that RVLM neurons may receive stronger inputs from supratentorial regions than those in NTS and LTF, such that their excitability is modified more powerfully in accordance with an animal's vigilance and alertness. A caveat is that brainstem regions in addition to LTF and NTS, such as the caudal ventrolateral medulla (CVLM), convey both vestibular and baroreceptor signals to the RVLM, as indicated in **Figure 10**. This neural circuit diagram is based on the findings of both anatomical (18–21, 39–42) and electrophysiologic (21, 43) studies that mapped connections in the vestibulo-sympathetic pathway. Projections from the caudal aspect of the vestibular nuclei to the CVLM contain imidazole-4-acetic acid-ribotide, a putative neurotransmitter prevalent in brainstem regions that are involved in blood pressure control (39), whereas projections from the vestibular nuclei to NTS are glutamatergic (20). These observations raise the potential that responses of CVLM neurons to vestibular and baroreceptor stimuli could differ from those of NTS or LTF neurons, but this is not presently known as recordings from CVLM neurons have not yet been conducted in conscious animals.

DATA AVAILABILITY STATEMENT

The raw data supporting the conclusions of this article will be made available by the authors, without undue reservation.

ETHICS STATEMENT

The animal study was reviewed and approved by University of Pittsburgh Institutional Animal Care and Use Committee.

AUTHOR CONTRIBUTIONS

JB, ND, JS, AM, DM, PA, CM, and BY conducted the experiments. JB, ND, JS, AM, DM, PA, CM, SB, and BY analyzed the data, generated figures, revised the manuscript, and approved the final version. JB and BY wrote the original manuscript draft. All authors contributed to the article and approved the submitted version.

FUNDING

This study was supported by NIH grants R01-DC013788 and R01-DC018229. AM received support from NIH grant K08-DC013571 and DM received support from NIH grant F32-DC015157.

ACKNOWLEDGMENTS

The authors thank Rutha Chivate, Asmita Joshi, Emmanuel Kambouroglos, Robert Khorami, John Lausch, Christian Molfetto, Bridget Perry, Sophie Tayade, Anisha Venkatesh, and Samuel Wittman for their assistance with data collection and analysis. A preliminary report of these findings has been published on the bioRxiv preprint server (29).

REFERENCES

1. Spyer KM. Annual review prize lecture - central nervous mechanisms contributing to cardiovascular control. *J Physiol.* (1994) 474:1–19. doi: 10.1113/jphysiol.1994.sp019997
2. Guyenet PG, Koshiya N, Huangfu D, Baraban SC, Stornetta RL, Li YW. Role of medulla oblongata in generation of sympathetic and vagal outflows. In: Holstege Bandler GR, CB Saper, editors. *Emotional Motor System*. Amsterdam: Elsevier (1996). p. 127–44.
3. Dampney RA. Functional organization of central pathways regulating the cardiovascular system. *Physiol Rev.* (1994) 74:323–64. doi: 10.1152/physrev.1994.74.2.323
4. Barman SM, Yates BJ. Deciphering the neural control of sympathetic nerve activity: status report and directions for future research. *Front Neurosci.* (2017) 11:730. doi: 10.3389/fnins.2017.00730
5. Reis DJ, Ruggiero DA, Morrison SF. The C1 area of the rostral ventrolateral medulla oblongata a critical brainstem region for control of resting and reflex integration of arterial pressure. *Am J Hypertens.* (1989) 2:363S−74. doi: 10.1093/ajh/2.12.363S
6. Stornetta RL. Neurochemistry of bulbospinal presympathetic neurons of the medulla oblongata. *J Chem Neuroanat.* (2009) 38:222–30. doi: 10.1016/j.jchemneu.2009.07.005
7. Barman SM, Sugiyama Y, Suzuki T, Cotter LA, DeStefino VJ, Reighard DA, et al. Rhythmic activity of neurons in the rostral ventrolateral medulla of conscious cats: effect of removal of vestibular inputs. *Am J Physiol Regul Integr Comp Physiol.* (2011) 301:R937–46. doi: 10.1152/ajpregu.00265.2011
8. Destefino VJ, Reighard DA, Sugiyama Y, Suzuki T, Cotter LA, Larson MG, et al. Responses of neurons in the rostral ventrolateral medulla to whole body rotations: comparisons in decerebrate and conscious cats. *J Appl Physiol.* (2011) 110:1699–707. doi: 10.1152/japplphysiol.00180.2011
9. Miller DM, Joshi A, Kambouroglos ET, Engstrom IC, Bielanin JP, Wittman SR, et al. Responses of neurons in the rostral ventrolateral medulla of conscious cats to anticipated and passive movements. *Am J Physiol Regul Integr Comp Physiol.* (2020) 318:R481–92. doi: 10.1152/ajpregu.00205.2019
10. Yates BJ, Bolton PS, Macefield VG. Vestibulo-sympathetic responses. *Compr Physiol.* (2014) 4:851–87. doi: 10.1002/cphy.c130041
11. Yates BJ, Goto T, Bolton PS. Responses of neurons in the rostral ventrolateral medulla of the cat to natural vestibular stimulation. *Brain Res.* (1993) 601:255–64. doi: 10.1016/0006-8993(93)91718-8
12. Wilson TD, Cotter LA, Draper JA, Misra SP, Rice CD, Cass SP, et al. Vestibular inputs elicit patterned changes in limb blood flow in conscious cats. *J Physiol.* (2006) 575:671–84. doi: 10.1113/jphysiol.2006.112904
13. Goldberg JM, Wilson VJ, Cullen KE, Angelaki DE, Broussard DM, Büttner-Ennever JA, et al. *The Vestibular System: A Sixth Sense*. New York, NY: Oxford University Press (2012).
14. Gebber GL, Barman SM. Lateral tegmental field neurons of cat medulla: a potential source of basal sympathetic nerve discharge. *J Neurophysiol.* (1985) 54:1498–512. doi: 10.1152/jn.1985.54.6.1498
15. Orer HS, Gebber GL, Phillips SW, Barman SM. Role of the medullary lateral tegmental field in reflex-mediated sympathoexcitation in cats. *Am J Physiol Regul Integr Comp Physiol.* (2004) 286:R451–64. doi: 10.1152/ajpregu.00569.2003
16. Orer HS, Barman SM, Gebber GL, Sykes SM. Medullary lateral tegmental field: an important synaptic relay in the baroreceptor reflex pathway of the cat. *Am J Physiol.* (1999) 277:R1462–75. doi: 10.1152/ajpregu.1999.277.5.R1462
17. Barman SM, Gebber GL, Orer HS. Medullary lateral tegmental field: an important source of basal sympathetic nerve discharge in the cat. *Am J Physiol Regul Integr Comp Physiol.* (2000) 278:R995–1004. doi: 10.1152/ajpregu.2000.278.4.R995
18. Balaban CD, Beryozkin G. Vestibular nucleus projections to nucleus tractus solitarius and the dorsal motor nucleus of the vagus nerve: potential substrates for vestibulo-autonomic interactions. *Exp Brain Res.* (1994) 98:200–12. doi: 10.1007/BF00228409
19. Yates BJ, Grelot L, Kerman IA, Balaban CD, Jakus J, Miller AD. Organization of vestibular inputs to nucleus tractus solitarius and adjacent structures in cat brain stem. *Am J Physiol Regul Integr Comp Physiol.* (1994) 267:R974–83. doi: 10.1152/ajpregu.1994.267.4.R974
20. Gagliuso AH, Chapman EK, Martinelli GP, Holstein GR. Vestibular neurons with direct projections to the solitary nucleus in the rat. *J Neurophysiol.* (2019) 122:512–24. doi: 10.1152/jn.00082.2019
21. Yates BJ, Balaban CD, Miller AD, Endo K, Yamaguchi Y. Vestibular inputs to the lateral tegmental field of the cat: potential role in autonomic control. *Brain Res.* (1995) 689:197–206. doi: 10.1016/0006-8993(95)00569-C
22. Sugiyama Y, Suzuki T, DeStefino VJ, Yates BJ. Integrative responses of neurons in nucleus tractus solitarius to visceral afferent stimulation and vestibular stimulation in vertical planes. *Am J Physiol Regul Integr Comp Physiol.* (2011) 301:R1380–90. doi: 10.1152/ajpregu.00361.2011
23. Moy JD, Miller DJ, Catanzaro MF, Boyle BM, Ogburn SW, Cotter LA, et al. Responses of neurons in the caudal medullary lateral tegmental field to visceral inputs and vestibular stimulation in vertical planes. *Am J Physiol Regul Integr Comp Physiol.* (2012) 303:R929–40. doi: 10.1152/ajpregu.00356.2012
24. McCall AA, Moy JD, DeMayo WM, Puterbaugh SR, Miller DJ, Catanzaro MF, et al. Processing of vestibular inputs by the medullary lateral tegmental field of conscious cats: implications for generation of motion sickness. *Exp Brain Res.* (2013) 225:349–59. doi: 10.1007/s00221-012-3376-1
25. Fadel PJ, Raven PB. Human investigations into the arterial and cardiopulmonary baroreflexes during exercise. *Exp Physiol.* (2012) 97:39–50. doi: 10.1113/expphysiol.2011.057554
26. Gandevia SC, Killian K, McKenzie DK, Crawford M, Allen GM, Gorman RB, et al. Respiratory sensations, cardiovascular control, kinaesthesia and transcranial stimulation during paralysis in humans. *J Physiol.* (1993) 470:85–107. doi: 10.1113/jphysiol.1993.sp019849
27. Waldrop TG, Eldridge FL, Iwamoto GA, Mitchell JH. Central neural control of respiration and circulation during exercise. In: Rowell LB, Shepherd JT, editors. *Handbook of Physiology, Section 12, Exercise: Regulation and Integration of Multiple Systems*. New York, NY: Oxford University Press (1996). p. 334–80.
28. Patel NM, Baker EAG, Wittman SR, Engstrom IC, Bourdages GH, McCall AA, et al. Cardiovascular adjustments during anticipated postural changes. *Physiol Rep.* (2018) 6:e13554. doi: 10.14814/phy2.13554
29. Bielanin JP, Douglas NO, Shulgach JO, McCall AA, Miller DM, Amin PR, et al. Responses of neurons in the medullary lateral tegmental field and nucleus tractus solitarius to vestibular stimuli in conscious felines. *bioRxiv [Preprint].* (2020). doi: 10.1101/2020.10.23.352542
30. National Research Council. *Guide for the Care and Use of Laboratory Animals*. Washington, DC: National Academy Press (2011).
31. McCall AA, Miller DM, DeMayo WM, Bourdages GH, Yates BJ. Vestibular nucleus neurons respond to hindlimb movement in the conscious cat. *J Neurophysiol.* (2016) 116:1785–94. doi: 10.1152/jn.00414.2016
32. Arshian MS, Hobson CE, Catanzaro MF, Miller DJ, Puterbaugh SR, Cotter LA, et al. Vestibular nucleus neurons respond to hindlimb movement in the decerebrate cat. *J. Neurophysiol.* (2014) 111:2423–32. doi: 10.1152/jn.00855.2013
33. Miller DM, Cotter LA, Gandhi NJ, Schor RH, Cass SP, Huff NO, et al. Responses of caudal vestibular nucleus neurons of conscious cats to rotations in vertical planes, before and after a bilateral vestibular neurectomy. *Exp Brain Res.* (2008) 188:175–86. doi: 10.1007/s00221-008-1359-z
34. Dum RP, Levinthal DJ, Strick PL. Motor, cognitive, and affective areas of the cerebral cortex influence the adrenal medulla. *Proc Natl Acad Sci USA*. (2016) 113:9922–7. doi: 10.1073/pnas.1605044113
35. Dum RP, Levinthal DJ, Strick PL. The mind-body problem: circuits that link the cerebral cortex to the adrenal medulla. *Proc Natl Acad Sci USA*. (2019) 116:26321–28. doi: 10.1073/pnas.1902297116
36. Clancy JA, Johnson R, Raw R, Deuchars SA, Deuchars J. Anodal transcranial direct current stimulation (tDCS) over the motor cortex increases sympathetic nerve activity. *Brain Stimul.* (2014) 7:97–104. doi: 10.1016/j.brs.2013.08.005
37. Cotter LA, Arendt HE, Jasko JG, Sprando C, Cass SP, Yates BJ. Effects of postural changes and vestibular lesions on diaphragm and rectus abdominis activity in awake cats. *J Appl Physiol.* (2001) 91:137–44. doi: 10.1152/jappl.2001.91.1.137
38. Yates BJ, Catanzaro MF, Miller DJ, McCall AA. Integration of vestibular and emetic gastrointestinal signals that produce nausea and vomiting: potential

contributions to motion sickness. *Exp Brain Res.* (2014) 232:2455–69. doi: 10.1007/s00221-014-3937-6
39. Holstein GR, Friedrich VL Jr, Martinelli GP. Imidazoleacetic acid-ribotide in vestibulo-sympathetic pathway neurons. *Exp Brain Res.* (2016) 234:2747–60. doi: 10.1007/s00221-016-4725-2
40. Holstein GR, Friedrich VL Jr, Martinelli GP. Projection neurons of the vestibulo-sympathetic reflex pathway. *J Comp Neurol.* (2014) 522:2053–74. doi: 10.1002/cne.23517
41. Holstein GR, Friedrich VL Jr, Kang T, Kukielka E, Martinelli GP. Direct projections from the caudal vestibular nuclei to the ventrolateral medulla in the rat. *Neuroscience.* (2011) 175:104–17. doi: 10.1016/j.neuroscience.2010.12.011
42. Stocker SD, Steinbacher BC, Balaban CD, Yates BJ. Connections of the caudal ventrolateral medullary reticular formation in the cat brainstem. *Exp Brain Res.* (1997) 116:270–82. doi: 10.1007/PL00005755
43. Steinbacher BC, Yates BJ. Processing of vestibular and other inputs by the caudal ventrolateral medullary reticular formation. *Am J Physiol Regul Integr Comp Physiol.* (1996) 271:R1070–7. doi: 10.1152/ajpregu.1996.271.4.R1070

Conflict of Interest: The authors declare that the research was conducted in the absence of any commercial or financial relationships that could be construed as a potential conflict of interest.

frontiers in Neurology

REVIEW
published: 12 January 2021
doi: 10.3389/fneur.2020.624243

The Scientific Contributions of Bernard Cohen (1929–2019)

Jun Maruta [1,2]*

[1] Department of Neurology, Icahn School of Medicine at Mount Sinai, New York, NY, United States, [2] Department of Rehabilitation and Human Performance, Icahn School of Medicine at Mount Sinai, New York, NY, United States

Throughout Bernard Cohen's active career at Mount Sinai that lasted over a half century, he was involved in research on vestibular control of the oculomotor, body postural, and autonomic systems in animals and humans, contributing to our understanding of such maladies as motion sickness, mal de débarquement syndrome, and orthostatic syncope. This review is an attempt to trace and connect Cohen's varied research interests and his approaches to them. His influence was vast. His scientific contributions will continue to drive research directions for many years to come.

Keywords: cerebellum, eye movement, spatial orientation, velocity storage, vestibuloocular reflex

OPEN ACCESS

Edited by:
Michael Strupp, Ludwig Maximilian University of Munich, Germany

Reviewed by:
Michael Fetter, Stiftung Rehabilitation Heidelberg, Germany
Mathieu Beraneck, Université Paris Descartes, France

***Correspondence:**
Jun Maruta
jun.maruta@mssm.edu

Specialty section:
This article was submitted to Neuro-Otology, a section of the journal Frontiers in Neurology

Received: *30 October 2020*
Accepted: *11 December 2020*
Published: *12 January 2021*

Citation:
Maruta J (2021) The Scientific Contributions of Bernard Cohen (1929–2019). Front. Neurol. 11:624243. doi: 10.3389/fneur.2020.624243

INTRODUCTION

After education and training through Middlebury College, New York University School of Medicine, internship, residencies in neurology, and psychiatry, 2 years in the U.S. Army, and a 2-year experimental fellowship at Columbia University under Dominick Purpura, Bernard Cohen arrived at Mount Sinai Hospital in 1962 for good. Throughout his active career at Mount Sinai, he was involved in research on vestibular control of the oculomotor, body postural, and autonomic systems in animals and humans (**Figure 1**), and was continuously supported by grants from the NIH, NASA, the NSF, and New York City as a principal investigator. Most notably, the NIH grant entitled "The Oculomotor System and Body Postural Mechanisms" (NB00294, NS00294, EY11812), initially spearheaded by Morris B. Bender before the arrival of Cohen at Mount Sinai, ran for 50 years through 2009, an NIH record. Despite losing his central vision in both eyes circa 2012, Cohen pursued research in a full-time capacity until his retirement at the age of 88 years in 2017, thereafter he continued to be engaged in writing, mentoring, and organizing conferences. Cohen fell ill just days before the international conference born out of the Frontiers in Neurology Research Topic, "Vestibular Contributions to Health and Disease" (3), for which he was the main driving force of organization. Following a month long hospitalization, he passed away peacefully on November 27, 2019, at the age of 90 years.

FOUNDATION

Although only 2 years senior to Cohen, Purpura was already an established neurophysiologist by the time they crossed paths in 1960, running his own laboratory at Columbia University and having published some 40 papers by then. For 2 years with Purpura, Cohen recorded activities of thalamic and extrathalamic pathways in cats and honed his electrophysiological skills (4–6).

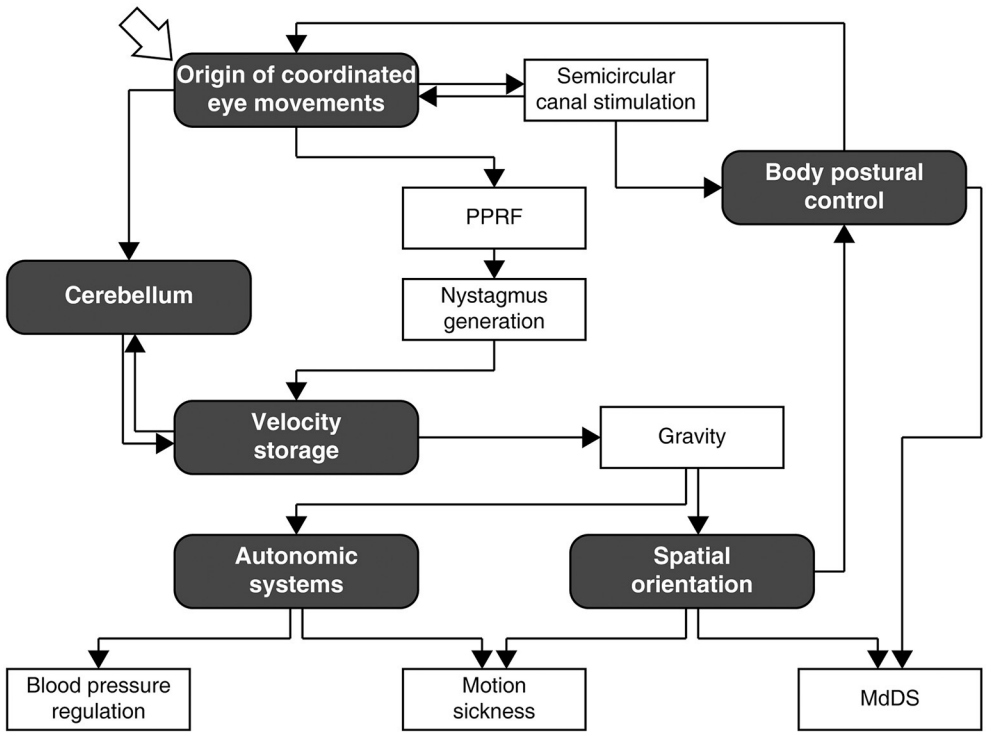

FIGURE 1 | A rough navigation guide for Bernard Cohen's research pursuit as interpreted by the author. Many branches and links are omitted for simplicity of exposition. Note that the diagram does not depict neural processes involved in the mechanisms that Cohen studied, which are reviewed in depth and comprehensively elsewhere (1, 2). PPRF, paramedian pontine reticular formation; MdDS, mal de débarquement syndrome.

OCULOMOTOR CONTROL

At Mount Sinai, Cohen began by identifying the eye, head, and body movements activated by the semicircular canals with Jun-Ichi Suzuki (7–9). Bender wanted Suzuki, who had just arrived from Tokyo with Fulbright support, to electrically stimulate the labyrinths. With Suzuki and Cohen respectively taking lead in surgery and electrophysiology, and aided by then-newly-available electronic technologies, the experiments were completed in 2 years (10). They were the first to demonstrate couplings of electrical stimulation of individual vestibular nerve branches to specific motor consequences. Extending from earlier pioneering studies by Lorente de Nó (11) and Szentágothai (12), Cohen and Suzuki's experiments revealed the machinery by which movement is controlled by the sum of three orthogonal vectors represented in the geometry of the semicircular canals, and their results opened a whole field of new research ranging from basic experimental, theoretical, to applied clinical (13–17).

This effort was followed by identification of the paramedian pontine reticular formation (PPRF) as the horizontal saccade premotor center, particularly in collaboration with Atushi Komatsuzaki and Volker Henn. Over the prior three decades, Bender and his colleagues had meticulously tabulated the results of stimulation and lesioning of essentially every cubic millimeter in a total volume of some 2,500 mm^3 in the brainstem of macaque monkeys to identify the origins of bilaterally coordinated activation of ocular motor nuclei (18). Following this path, Cohen and Komatsuzaki, with Bender, succeeded in more precisely associating PPRF lesions with distinctive conjugate horizontal gaze palsies (19). Cohen continued to accumulate evidence that PPRF is responsible for production of the premotor commands for ipsilateral horizontal saccades, be they for conjugate gaze shifts or fast phases of nystagmus (20–22). Cohen and Henn then went on to uncover many of the building blocks of horizontal saccade generation with single unit recording in PPRF (23, 24). These findings vastly expanded the understanding of the structure of ocular premotor commands by isolating a distinct eye movement element and further elucidating its underlying mechanisms, much akin to a discovery and dissection of a chemical element.

Cohen and Komatsuzaki also showed that conjugate eye movements produced by stimulation of PPRF occurred at a constant velocity, with the amplitude and speed linearly dependent on the frequency of stimulation pulses delivered up to that moment (22). This finding significantly advanced not only oculomotor research but also the field of biomechanics by providing evidence for neural implementation of a mathematical integration predicted from control system theories (25).

VELOCITY STORAGE

Cohen's next major contribution was with Theodore Raphan in quantitatively characterizing optokinetic nystagmus (OKN) and optokinetic after-nystagmus (OKAN) and formulating a mathematical model that emulated their characteristics featuring a leaky integrator (26). As noted by ter Braak as far back as in 1936 (27), OKAN, i.e., the persistence of nystagmus in darkness following a visual motion stimulus, indicates storage of motion-related signals and sustained output from this storage. Collewijn recognized the usefulness of such a storage mechanism in characterizing the slow build-up of OKN in the rabbit and conceptualized it also as a leaky integrator (28), but Cohen and Raphan put the integrator forth as the focus of the visual-vestibular interaction (29, 30), as also anticipated by ter Braak (27). Cohen's interest in this area was a natural extension of his earlier effort on saccade generation because understanding how nystagmus is shaped required ideation of a shared central processor of visual and vestibular inputs (2, 27). It had been generally assumed that there existed a brainstem mechanism that extended the time over which the vestibulo-ocular reflex (VOR) could compensate for constant-velocity head movement after the fall of the eighth nerve activity, but the conceived mechanism, shared between vestibular and visual functions, would provide a ground that could efficiently attenuate the after-response to prolonged rotation even when the vision was blocked at the stop of rotation (27, 29, 30). Cohen and Raphan termed this mechanism the velocity storage integrator.

A major impetus for this formulation was derived from fresh evidence by Waespe and Henn of vestibular nuclear activity that correlated with the strengths of nystagmus of the VOR, OKN, and OKAN in alert monkeys (31, 32) as well as from earlier results of labyrinthectomy in monkeys and rabbits, which degraded OKN and abolished OKAN (33, 34). Not surprisingly, David Robinson of the Johns Hopkins University also took note of these observations and simultaneously proposed an alternate model, which behaved equivalently to the Cohen-Raphan model but utilized a positive feedback loop in the implementation (35). While Robinson proposed his model as a demonstration of the utility of a model-based approach in understanding visual-vestibular interaction, Cohen, Raphan, and Matsuo elucidated nuances of velocity storage by testing their model against a well-defined experimental dataset (26, 29, 30). Both Cohen and Raphan, and Robinson postulated that velocity storage contributes to the sensation of self-motion (vection) (36).

Cohen and Raphan continued to characterize velocity storage as a mechanism that would facilitate ocular and postural compensation to turning motion—registration of not only the start and end of rotation but also whether one is continuing to rotate. They observed activation of velocity storage as, for example, prolonged nystagmus during the VOR to a constant velocity rotation in darkness, OKAN, and continuous unidirectional nystagmus during rotation about a tilted axis (off-vertical axis rotation, OVAR) or pitching/rolling about an earth-horizontal axis while rotating about an earth-vertical axis (pitching/rolling while rotating, PWR/RWR). Of note, the characterization of velocity storage expression to date still nearly exclusively relies on changes over time in the direction and magnitude of eye rotational velocity during slow phases of nystagmus. Two possible exceptions are subjective reporting of vection in human experiments (37, 38) and activity levels in specific classes of neurons in the vestibular nucleus in animal experiments (31, 39, 40).

Signature characteristics of velocity storage include: 1) stored rotational velocity can be discharged ("dumped") by visual fixation or a tilt, an indication that one is no longer turning (26, 29, 30, 41, 42); 2) the ability to store velocity is permanently abolished by labyrinthectomy or vestibular nerve section (33, 43), or by cutting the commissural fibers between the bilateral vestibular nuclei (44); 3) in contrast to 2), inactivation of the semicircular canal function by plugging the duct and interrupting the flow of the endolymph, thus keeping the vestibular nerve intact, spares the velocity storage function (43); 5) the storage mechanism can be reversibly and dose-dependently inactivated by the $GABA_B$ receptor agonist baclofen (45); 5) repeated vestibular stimulation can weaken, i.e., habituate, velocity storage without affecting the gain of VOR compensation during step velocity rotation, and once habituated, the state is retained for months or possibly longer (46, 47); and 6) the gain of VOR compensation can be changed up or down apparently without affecting the velocity storage capacity and is more malleable than habituation (47).

Note that tilt dumping of velocity storage occurs only in the absence of head rotation—more specifically, in the absence of head rotation about the axis with which the stored velocity is associated. In contrast, tilting the head while in rotation changes the alignment of the semicircular canals with the plane of rotation, which instead *activates* the velocity storage mechanism and, in combination with otolith input, permits reconstruction of signals related to rotation as demonstrated with PWR/RWR (41, 48–50). In further contrast, tilting the axis of rotation relative to gravity, that is OVAR (51, 52), also activates velocity storage, not through the semicircular canals but through continuous reorientation of the otoliths relative to gravity (43, 53). Incidentally, tilting the head while rotating is historically referred to as a Coriolis/cross-coupling stimulus (54), but Coriolis acceleration is not considered a significant contributor to velocity storage activation (48). On the other hand, sinusoidal translation in the plane of rotation, due to the combination of Coriolis and centripetal accelerations, tilts the gravito-inertial acceleration relative to the head without activating the semicircular canals, such that the stimulus generates a sweeping movement of linear acceleration around the head as in OVAR and similarly activates velocity storage (55).

Cohen and Raphan over time realized that velocity storage, when the head is tilted, undergoes dynamic transformation so that the axis of the output eye movement tends toward the spatial vertical as referenced by gravity (56–59). That is, the velocity storage integrator, a mechanism thought to facilitate ocular and postural compensation to rotation by representing the state of self-motion, is also equipped with orienting properties to act as a "neural gyroscope" (57, 60). This discovery led to an understanding of the three-dimensional functional configuration of velocity storage (61, 62) as well as how this configuration

can contribute to the sense of relationship between self and the environment, balance, and the production of motion sickness (63, 64). The postulate that three-dimensional properties of velocity storage might be coded by vestibular-only neurons in the medial and superior vestibular nuclei was later substantiated (40).

SPATIAL ORIENTATION AND BODY POSTURAL CONTROL

The study of velocity storage led Cohen to deeply contemplate the role of the vestibular system in spatial orientation (60, 65). The term spatial orientation describes the ability to relate the position and movement of the body and body parts to spatial cues, including sensing, establishing, and maintaining connections to space (66). Simply put, spatial orientation indicates readiness for spatial interactions. Results from other laboratories indicated that, in addition to visual or vestibular input, velocity storage could be activated by somatosensory input, such as with an extended arm passively following a rotating cylindrical wall in darkness (67) or walking on a circular treadmill (68). It thus became clear that velocity storage was a focal point of not just visual-vestibular but wider multimodal sensory interaction and played an essential role in spatial orientation by providing a working memory-like function for self-motion. Earlier, Cohen with Suzuki had established the specific nature of the reflex head and postural movements produced by semicircular canal stimulation across species as a compensatory mechanism for sudden angular displacements (9), but as Cohen began to recognize the orientation property of velocity storage, he again became interested in the vestibular control of body posture and locomotion.

The seemingly mundane act of holding a stable gaze during locomotion in fact involves precise coordination of movements of the torso, limbs, head, and eyes. To achieve this feat, information about movements of these various body parts must be coded in the brain using appropriate coordinate frames. It was from this perspective that Cohen studied various strategies used by animals and humans to generate compensatory head and eye movements during circular and linear locomotion, including both angular and linear vestibulocollic reflexes and velocity storage (69–71). Furthermore, from the studies of the VOR, it had become evident to Cohen that both compensatory and orienting eye movements could be generated by the reflex arc in relation to either angular or linear acceleration (1, 65, 72, 73). As put forward by Cohen and Raphan, while compensatory eye movements support maintenance of a fixed gaze direction or gaze point in space, orienting eye movements tend to align the eye vertical with the spatial reference vector of the gravito-inertial acceleration, with a stipulation that the outcome of the VOR depends on the temporal frequency of the head movement. It was then found that corresponding compensatory and orienting head and body movements were also generated to stabilize gaze during walking, with slower orienting mechanisms controlling the dynamics of compensatory movements (74). Thus, compensatory and orienting responses should be recognized as part of generalized vestibular functions.

This line of research was also greatly relevant to space exploration, which may take place in the environment where gravity, a fundamental parameter that defines one's relationship to the environment, is not detectable. In this context, Cohen et al. focused on characterizing potentially maladaptive changes in spatial orientation and perception due to exposure to microgravity as well as whether artificial gravity produced with centrifugation could provide an effective countermeasure against these changes (75–80).

AUTONOMIC SYSTEMS

Despite the depths of knowledge in both vestibular and autonomic systems, still relatively little is known about vestibular-autonomic/cardiovascular reflexes. Cohen believed that there were a wide variety of opportunities to fill this gap. By applying OVAR to human subjects, Cohen et al. first established that signals that produce constriction of blood vessels in the legs can come from the vestibular system, namely the otolith organs, at a latency much shorter than baroreflex (81), a significant finding in the context where baroreflex is considered rapid as compared to chemoreceptor- or endocrine-mediated blood pressure regulation. They then established that trans-mastoidal electrical stimulation, presumably by activating the otoliths, can effectively activate sympathetic pathways with a similar short latency (82). Still, how blood pressure and heart rate might be affected by such galvanic vestibular stimulation was not known. When Cohen et al. applied galvanic vestibular stimulation to anesthetized rats, instead of an anticipated increase, a sudden decrease in blood pressure and heart rate, i.e., a vasovagal response, was elicited (83). As the diagnosis of vasovagal syncope is supported by a tilt-table test, which activates vestibular and body tilt senses, they hypothesized that the otoliths could provide significant input to the generation of syncope. Clearly, insights on otolith-mediated regulation of blood pressure were available to Cohen from space research as well. Cohen et al. had earlier suggested that otolith stimulation with centrifugation could be a countermeasure for post-flight orthostatic intolerance commonly seen among astronauts returning from space (80). Cohen forged ahead with studies of mechanisms of vasovagal response, which also demonstrated the usefulness of the small-animal model that he and his colleagues developed in the rat (84–88).

VESTIBULAR-CEREBELLAR INTERACTION

Early on, on the heels of his work with Suzuki on semicircular canal stimulation, Cohen, in the tradition of Bender, sought to determine patterns of eye movement represented in the cerebellum by correlating ocular responses to systematic stimulation of wide regions of the cerebellum (89). This work showed that the patterns of cerebellar-evoked eye movements resembled those produced by semicircular canal stimulation, that there were topographic separations for different eye movement planes, and that eye movements could be combined when two points were stimulated simultaneously. The work also suggested

the possibility that, had the head not been fixed, postural movements might have been produced in place of eye movements at many points of stimulation, as well as paved the way for the idea that the brain may facilitate sensorimotor transformations for compensatory ocular and postural reflexes by using a common coordinate frame consistent with the arrangement of the semicircular canals (90), a point revisited by many authors (1, 91–96).

The cerebellar flocculus and nodulus are collectively known as the vestibulo-cerebellum for their close interactions with the vestibular system. Between the PPRF and velocity storage works, Cohen, with Takemori, showed that the flocculus aided rapid visual adjustment of the VOR (97), making a significant contribution to the field energized by Ito's hypothesis that placed the flocculus at the center of cerebellar motor control in the context of the VOR performance optimization (98).

With the formulation of velocity storage, the cerebellar control of the vestibular system fast became an essential consideration. To this effect, Cohen, with Waespe and Raphan, showed that the flocculus and the nodulus (together with the adjacent ventral uvula) have distinctive roles in vestibular control by demonstrating independent and model-predictable effects of floccular and nodular lesions on visual-vestibular interactions during the VOR, OKN/OKAN, and OVAR-generated nystagmus (42, 47, 99, 100)—in brief, the flocculus mediates the visual pathway with which the gain of the compensatory VOR is controlled, while the nodulus controls velocity storage. Cohen et al. further studied the nodulus to show that velocity storage dumping can be mimicked by electrical stimulation in the nodulus (101) and that the spatial orientation properties of velocity storage may be supported in relation to the parasagittal organization of the nodulus (102).

The thusly obtained knowledge had great implications in the approaches and clinical applications developed by Cohen and Mingjia Dai to motion sickness and mal de débarquement syndrome (MdDS). They postulated motion sickness as originating from a sensory conflict detected in the velocity storage mechanism, it being a focal point of multimodal sensory interaction and spatial orientation through its interactions with the nodulus and uvula (103–107). They then determined that, while velocity storage may be useful in other contexts, susceptibility to motion sickness could be reduced by *weakening* the velocity storage capacity in a targeted manner—reversibly by a pharmacological means with baclofen (108) or for a long-term effect by inducing a change in the VOR (109).

MdDS is still an under-recognized chronic balance disorder, characterized by persistent perception of oscillating self-motion, typically after coming off a cruise (110, 111). The condition, with additional likely secondary cognitive and affective symptoms, is debilitating. There is, as yet, not a fully effective treatment, but the approach developed recently at Mount Sinai has resulted in long-term improvement of symptoms in the majority of the treated patients (112, 113). The treatment was developed on the postulates that MdDS was a consequence of maladapted orientation properties of velocity storage (114) and that proper orientation properties could be restored through VOR re-adaptation. The success of the treatment was in many ways the culmination of Cohen's career. Interestingly, despite substantial evidence from Cohen's work that a change in the nodulus may have a significant behavioral consequence, the challenge remains to establish an experimental paradigm to explore plasticity in the nodulus amenable to cellular-level explanation.

CONCLUSION

Cohen's scientific style was marked by enthusiasm. Besides engaging in diverse works related to and extending from the endeavors outlined above (115–118), he was ready to jump in whenever a scientific opportunity presented (119–123). At a tribute symposium held at Mount Sinai in April 2018 following Cohen's retirement from his long-held fulltime position as Morris B. Bender Professor of Neurology, Albert Fuchs of Washington University succinctly stated, "He was bitten by a science bug as a young man and never recovered from it." He enjoyed good scientific battles like a proud prizefighter and inspired many with his spirit. Even after retirement, he continued to be deeply immersed in understanding neural mechanisms of vestibulosympathetic reflex, motion sickness, and MdDS. His scientific contributions will continue to drive research directions for many years to come.

AUTHOR CONTRIBUTIONS

The author confirms being the sole contributor of this work and has approved it for publication.

ACKNOWLEDGMENTS

The author thanks Drs. Robert Baker, Robert A. Hensbroek, Theodore Raphan, and Sergei B. Yakushin for their comments on an early version of the manuscript.

REFERENCES

1. Cohen B, Raphan T. The physiology of the vestibuloocular reflex (VOR). In: Highstein SM, Fay RR, Popper AM, editors. *The Vestibular System. Springer Handbook of Auditory Research, vol 19*. New York: Springer. (2004). p. 235–85. doi: 10.1007/0-387-21567-0_6
2. Raphan T. Vestibular, locomotor, and vestibulo-autonomic research: 50 years of collaboration with Bernard Cohen. *J Neurophysiol.* (2020) 123:329–45. doi: 10.1152/jn.00485.2019
3. Cohen B, Lewis R, Lopez-Escamez JA. (eds.) *Vestibular Contributions to Health and Disease*. Lausanne: Frontiers Media (2018). doi: 10.3389/978-2-88945-520-1
4. Cohen B, Housepian EM, Purpura DP. Intrathalamic regulation of activity in a cerebellocortical projection pathway. *Exp Neurol.* (1962) 6:492–506. doi: 10.1016/0014-4886(62)90074-2
5. Purpura DP, Cohen B, Marini G. Generalized neocortical responses and corticospinal neuron activity. *Science.* (1961) 134:729–30. doi: 10.1126/science.134.3481.729

6. Purpura DP, Cohen B. Intracellular recording from thalamic neurons during recruiting responses. *J Neurophysiol.* (1962) 25:621–35. doi: 10.1152/jn.1962.25.5.621
7. Suzuki JI, Cohen B, Bender MB. Compensatory eye movements induced by vertical semicircular canal stimulation. *Exp Neurol.* (1964) 9:137–60. doi: 10.1016/0014-4886(64)90013-5
8. Cohen B, Suzuki J, Bender MB. Eye movements from semicircular canal nerve stimulation in the cat. *Ann Otol Rhin Laryngol.* (1964) 73:153–69. doi: 10.1177/000348946407300116
9. Suzuki JI, Cohen B. Head, eye, body and limb movements from semicircular canal nerves. *Exp Neurol.* (1964) 10:393–405. doi: 10.1016/0014-4886(64)90031-7
10. Suzuki JI. What is left behind in the valley? In: Kaga K, editor. *The International Conference on the Visual and/versus Vestibular System; The Satellite Symposium to the IVth International Symposium on the Head/Neck System.* Tokyo (1999). p. 33.
11. Lorente de No R. The regulation of eye positions and movements induced by the labyrinth: Chapter, V Rotation reflexes on the eye muscles. *Laryngoscope.* (1932) 42:298–312. doi: 10.1288/00005537-193204000-00005
12. Szentágothai J. The elementary vestibulo-ocular reflex arc. *J Neurophysiol.* (1950) 13:395–407. doi: 10.1152/jn.1950.13.6.395
13. Simpson JI, Graf W. Eye-muscle geometry and compensatory eye movements in lateral-eyed and frontal-eyed animals. *Ann N Y Acad Sci.* (1981) 374:20–30. doi: 10.1111/j.1749-6632.1981.tb30856.x
14. Robinson DA. The use of matrices in analyzing the three-dimensional behavior of the vestibulo-ocular reflex. *Biol Cybern.* (1982) 46:53–66. doi: 10.1007/bf00335351
15. Highstein SM, Holstein GR. The anatomy of the vestibular nuclei. *Prog Brain Res.* (2006) 151:157–203. doi: 10.1016/S0079-6123(05)51006-9
16. Della Santina CC, Migliaccio AA, Patel AH. A multichannel semicircular canal neural prosthesis using electrical stimulation to restore 3-d vestibular sensation. *IEEE Trans Biomed Eng.* (2007) 54:1016–30. doi: 10.1109/TBME.2007.894629
17. Dlugaiczyk J, Gensberger KD, Straka H. Galvanic vestibular stimulation: from basic concepts to clinical applications. *J Neurophysiol.* (2019) 121:2237–55. doi: 10.1152/jn.00035.2019
18. Bender MB, Shanzer S. Oculomotor pathways defined by electric stimulation lesions in the brainstem of monkey. In Bender MB, editor. *The Oculomotor System*. New York: Harper and Row. (1964). p. 81–140.
19. Cohen B, Komatsuzaki A, Bender MB. Electrooculographic syndrome in monkeys after pontine reticular formation lesions. *Arch Neurol.* (1968) 18:78–92. doi: 10.1001/archneur.1968.00470310092008
20. Cohen B, Feldman M. Relationship of electrical activity in pontine reticular formation and lateral geniculate body to rapid eye movements. *J Neurophysiol.* (1968) 31:806–17. doi: 10.1152/jn.1968.31.6.806
21. Cohen B. Vestibulo-ocular relations. In: Bach-y-Rita P, Collins CC, editoes. *The Control of Eye Movements*. New York/London: Academic Press. (1971). p. 105–48.
22. Cohen B, Komatsuzaki A. Eye movements induced by stimulation of the pontine reticular formation: evidence for integration in oculomotor pathways. *Exp Neurol.* (1972) 36:101–17. doi: 10.1016/0014-4886(72)90139-2
23. Cohen B, Henn V. Unit activity in the pontine reticular formation associated with eye movements. *Brain Res.* (1972) 46:403–10. doi: 10.1016/0006-8993(72)90030-3
24. Henn V, Cohen B. Coding of information about rapid eye movements in the pontine reticular formation of alert monkeys. *Brain Res.* (1976) 108:307–25. doi: 10.1016/0006-8993(76)90188-8
25. Robinson DA. Integrating with neurons. *Annu Rev Neurosci.* (1989) 12:33–45. doi: 10.1146/annurev.ne.12.030189.000341
26. Cohen B, Matsuo V, Raphan T. Quantitative analysis of the velocity characteristics of optokinetic nystagmus and optokinetic after-nystagmus. *J Physiol.* (1977) 270:321–44. doi: 10.1113/jphysiol.1977.sp011955
27. ter Braak JWG. Untersuchungen über optokinetischen Nystagmus. Arch Neerl Physiol. 21:309-376 (translated to English. Investigation on optokinetic nystagmus. In: Collewijn, H. *The Oculomotor System of the Rabbit and Its Plasticity. Studies in Brain Function, Vol 5*. Berlin; Heidelberg; New York, NY: Springer-Verlag. (1936) p. 179-237).
28. Collewijn H. An analog model of the rabbit's optokinetic system. *Brain Res.* (1972) 36:71–88. doi: 10.1016/0006-8993(72)90767-6
29. Raphan T, Cohen B, Matsuo V. A velocity-storage mechanism responsible for optokinetic nystagmus (OKN), optokinetic after-nystagmus (OKAN) and vestibular nystagmus. In: Baker R. Berthoz A, editors. *Control of Gaze by Brain Stem Neurons*. Amsterdam/New York: Elsevier/North Holland Biomedical Press. (1977). p. 37–47.
30. Raphan T, Matsuo V, Cohen B. Velocity storage in the vestibulo-ocular reflex arc (VOR). *Exp Brain Res.* (1979) 35:229–48. doi: 10.1007/BF00236613
31. Waespe W, Henn V. Neuronal activity in the vestibular nuclei of the alert monkey during vestibular and optokinetic stimulation. *Exp Brain Res.* (1977) 27:523–38. doi: 10.1007/BF00239041
32. Waespe W, Henn V. Vestibular nuclei activity during optokinetic after-nystagmus (OKAN) in the alert monkey. *Exp Brain Res.* (1977) 30:323–30. doi: 10.1007/BF00237259
33. Cohen B, Uemura T, Takemori S. Effects of labyrinthectomy on optokinetic nystagmus (OKN) and optokinetic after-nystagmus (OKAN). *Equilib Res.* (1973) 3:88–93.
34. Collewijn H. Impairment of optokinetic (after-)nystagmus by labyrinthectomy in the rabbit. *Exp Neurol.* (1976) 52:146–56. doi: 10.1016/0014-4886(76)90207-7
35. Robinson D. Vestibular and optokinetic symbiosis: an example of explaining by modeling. In: Baker R, Berthoz A, editors. *Control of Gaze by Brain Stem Neurons*. Amsterdam/New York: Elsevier/North Holland Biomedical Press. (1977). p. 49–58.
36. Dichgans J, Brandt T. Visual-vestibular interaction: effects on self-motion perception postural control. In: Held R, Leibowitz HW, Teuber HL, editors. *Perception. Handbook of Sensory Physiology Vol. 8*. Berlin; Heidelberg: Springer-Verlag (1978). p. 755–804. doi: 10.1007/978-3-642-46354-9
37. Bertolini G, Ramat S, Laurens J, Bockisch CJ, Marti S, Straumann D, et al. Velocity storage contribution to vestibular self-motion perception in healthy human subjects. *J Neurophysiol.* (2011) 105:209–23. doi: 10.1152/jn.00154.2010
38. Bertolini G, Ramat S, Bockisch CJ, Marti S, Straumann D, Palla A. Is vestibular self-motion perception controlled by the velocity storage? Insights from patients with chronic degeneration of the vestibulo-cerebellum. *PLoS ONE.* (2012) 7:e36763. doi: 10.1371/journal.pone.0036763
39. Reisine H, Raphan T. Neural basis for eye velocity generation in the vestibular nuclei of alert monkeys during off-vertical axis rotation. *Exp Brain Res.* (1992) 92:209–26. doi: 10.1007/BF00227966
40. Yakushin SB, Raphan T, Cohen B. Coding of velocity storage in the vestibular nuclei. *Front Neurol.* (2017) 8:386. doi: 10.3389/fneur.2017.00386
41. Raphan T, Cohen B, Henn V. Effects of gravity on rotatory nystagmus in monkeys. *Ann N Y Acad Sci.* (1981) 374:44–55. doi: 10.1111/j.1749-6632.1981.tb30859.x
42. Waespe W, Cohen B, Raphan T. Dynamic modification of the vestibulo-ocular reflex by the nodulus and uvula. *Science.* (1985) 228:199–202. doi: 10.1126/science.3871968
43. Cohen B, Suzuki JI, Raphan T. Role of the otolith organs in generation of horizontal nystagmus: effects of selective labyrinthine lesions. *Brain Res.* (1983) 276:159–64. doi: 10.1016/0006-8993(83)90558-9
44. Katz E, de Jong JM, Buettner-Ennever J, Cohen B. Effects of midline medullary lesions on velocity storage and the vestibulo-ocular reflex. *Exp Brain Res.* (1991) 87:505–20. doi: 10.1007/BF00227076
45. Cohen B, Helwig D, Raphan T. Baclofen and velocity storage: a model of the effects of the drug on the vestibulo-ocular reflex in the rhesus monkey. *J Physiol.* (1987) 393:703–25. doi: 10.1113/jphysiol.1987.sp016849
46. Jäger J, Henn V. Habituation of the vestibulo-ocular reflex (VOR) in the monkey during sinusoidal rotation in the dark. *Exp Brain Res.* (1981) 41:108–14. doi: 10.1007/BF00236599
47. Cohen H, Cohen B, Raphan T, Waespe W. Habituation and adaptation of the vestibuloocular reflex: a model of differential control by the vestibulocerebellum. *Exp Brain Res.* (1992) 90:526–38. doi: 10.1007/BF00230935

48. Raphan T, Cohen B, Suzuki J, Henn V. Nystagmus generated by sinusoidal pitch while rotating. *Brain Res.* (1983) 276:165–72. doi: 10.1016/0006-8993(83)90559-0
49. Raphan T, Dai M, Maruta J, Waespe W, Henn V, Suzuki JI, et al. Canal and otolith afferent activity underlying eye velocity responses to pitching while rotating. *Ann N Y Acad Sci.* (1999) 871:181–94. doi: 10.1111/j.1749-6632.1999.tb09184.x
50. Hess BJ, Angelaki DE. Angular velocity detection by head movements orthogonal to the plane of rotation. *Exp Brain Res.* (1993) 95:77–83. doi: 10.1007/BF00229656
51. Guedry FEJr. Orientation of the rotation-axis relative to gravity: its influence on nystagmus and the sensation of rotation. *Acta Otolaryngol.* (1965) 60:30–48. doi: 10.3109/00016486509126986
52. Benson AJ, Bodin MA. Interaction of linear and angular accelerations on vestibular receptors in man. *Aerosp Med.* (1966) 37:144–54.
53. Correia MJ, Money KE. The effect of blockage of all six semicircular canal ducts on nystagmus produced by dynamic linear acceleration in the cat. *Acta Otolaryngol.* (1970) 69:7–16. doi: 10.3109/00016487009123331
54. Guedry FE Jr, Benson AJ. Coriolis cross-coupling effects: disorienting and nauseogenic or not? *Aviat Space Environ Med.* (1978) 49:29–35.
55. Maruta J, Simpson JI, Raphan T, Cohen B. Orienting eye movements and nystagmus produced by translation while rotating (TWR). *Exp Brain Res.* (2005) 163:273–83. doi: 10.1007/s00221-004-2178-5
56. Raphan T, Cohen B. Multidimensional organization of the vestibulo-ocular reflex (VOR). In Keller EL, Zee DS editors. *Adaptive Processes in Visual and Oculomotor Systems.* Oxford: Pergamon Press. (1986). p. 285-92.
57. Raphan T, Cohen B. Organizational principles of velocity storage in three dimensions: the effect of gravity on cross-coupling of optokinetic after-nystagmus. *Ann N Y Acad Sci.* (1988) 545:74–92. doi: 10.1111/j.1749-6632.1988.tb19556.x
58. Schiff D, Cohen B, Raphan T. Nystagmus induced by stimulation of the nucleus of the optic tract in the monkey. *Exp Brain Res.* (1988) 70:1–14. doi: 10.1007/BF00271841
59. Wearne S, Raphan T, Cohen B. Contribution of vestibular commissural pathways to spatial orientation of the angular vestibuloocular reflex. *J Neurophysiol.* (1997) 78:1193–7. doi: 10.1152/jn.1997.78.2.1193
60. Raphan T, Dai M, Cohen B. Spatial orientation of the vestibular system. *Ann N Y Acad Sci*. (1992) 656:140–57. doi: 10.1111/j.1749-6632.1992.tb25205.x
61. Dai MJ, Raphan T, Cohen B. Spatial orientation of the vestibular system: dependence of optokinetic after-nystagmus on gravity. *J Neurophysiol.* (1991) 66:1422–39. doi: 10.1152/jn.1991.66.4.1422
62. Raphan T, Sturm D. Modeling the spatiotemporal organization of velocity storage in the vestibuloocular reflex by optokinetic studies. *J Neurophysiol.* (1991) 66:1410–21. doi: 10.1152/jn.1991.66.4.1410
63. Cohen B, Wearne S, Dai M, Raphan T. Spatial orientation of the angular vestibulo-ocular reflex. *J Vestib Res.* (1999) 9:163–72.
64. Cohen B, Dai M, Raphan T. The critical role of velocity storage in production of motion sickness. *Ann N Y Acad Sci.* (2003) 1004:359–76. doi: 10.1196/annals.1303.034
65. Raphan T, Cohen B. How does the vestibulo-ocular reflex work? In: Baloh R, Halmagyi GM, editors. *Disorders of the Vestibular System.* New York: Oxford University Press. (1996). p. 20–47.
66. Schöne H. *Spatial Orientation*. Princeton, NJ: Princeton University Press. (1984).
67. Brandt T, Büchele W, Arnold F. Arthrokinetic nystagmus and ego-motion sensation. *Exp Brain Res.* (1977) 30:331–8. doi: 10.1007/BF00237260
68. Bles W, de Jong JM, de Wit G. Somatosensory compensation for loss of labyrinthine function. *Acta Otolaryngol.* (1984) 97:213–21. doi: 10.3109/00016488409130982
69. Solomon D, Cohen B. Stabilization of gaze during circular locomotion in light. I Compensatory head and eye nystagmus in the running monkey. *J Neurophysiol.* (1992) 67:1146–57. doi: 10.1152/jn.1992.67.5.1146
70. Hirasaki E, Moore ST, Raphan T, Cohen B. Effects of walking velocity on vertical head and body movements during locomotion. *Exp Brain Res.* (1999) 127:117–30. doi: 10.1007/s002210050781
71. Solomon D, Cohen B. Stabilization of gaze during circular locomotion in darkness. II Contribution of velocity storage to compensatory eye and head nystagmus in the running monkey. *J Neurophysiol.* (1992) 67:1158–70. doi: 10.1152/jn.1992.67.5.1158
72. Raphan T, Cohen B. The vestibulo-ocular reflex in three dimensions. *Exp Brain Res.* (2002) 145:1–27. doi: 10.1007/s00221-002-1067-z
73. Cohen B, Maruta J, Raphan T. Orientation of the eyes to gravitoinertial acceleration. *Ann N Y Acad Sci.* (2001) 942:241–58. doi: 10.1111/j.1749-6632.2001.tb03750.x
74. Imai T, Moore ST, Raphan T, Cohen B. Interaction of the body, head, and eyes during walking and turning. *Exp Brain Res.* (2001) 136:1–18. doi: 10.1007/s002210000533
75. Dai M, Raphan T, Kozlovskaya I, Cohen B. Vestibular adaptation to space in monkeys. *Otolaryngol Head Neck Surg.* (1998) 119:65–77. doi: 10.1016/S0194-5998(98)70175-5
76. Highstein SM, Cohen B. Neurolab mission. *Curr Opin Neurobiol.* (1999) 1999:495–9. doi: 10.1016/s0959-4388(99)80074-9
77. Clément G, Moore ST, Raphan T, Cohen B. Perception of tilt (somatogravic illusion) in response to sustained linear acceleration during space flight. *Exp Brain Res.* (2001) 138:410–8. doi: 10.1007/s002210100706
78. Moore ST, Clément G, Raphan T, Cohen B. Ocular counterrolling induced by centrifugation during orbital space flight. *Exp Brain Res.* (2001) 137:323–35. doi: 10.1007/s002210000669
79. Moore ST, Cohen B, Raphan T, Berthoz A, Clément G. Spatial orientation of optokinetic nystagmus and ocular pursuit during orbital space flight. *Exp Brain Res*. (2005) 160:38–59. doi: 10.1007/s00221-004-1984-0
80. Moore ST, Diedrich A, Biaggioni I, Kaufmann H, Raphan T, Cohen B. Artificial gravity: a possible countermeasure for post-flight orthostatic intolerance. *Acta Astronaut.* (2005) 56:867–76. doi: 10.1016/j.actaastro.2005.01.012
81. Kaufmann H, Biaggioni I, Voustianiouk A, Diedrich A, Costa F, Clarke R, et al. Vestibular control of sympathetic activity. An otolith-sympathetic reflex in humans. *Exp Brain Res.* (2002) 143:463–9. doi: 10.1007/s00221-002-1002-3
82. Voustianiouk A, Kaufmann H, Diedrich A, Raphan T, Biaggioni I, Macdougall H, et al. Electrical activation of the human vestibulo-sympathetic reflex. *Exp Brain Res.* (2006) 171:251–61. doi: 10.1007/s00221-005-0266-9
83. Cohen B, Martinelli GP, Ogorodnikov D, Xiang Y, Raphan T, Holstein GR, et al. Sinusoidal galvanic vestibular stimulation (sGVS) induces a vasovagal response in the rat. *Exp Brain Res*. (2011) 210:45–55. doi: 10.1007/s00221-011-2604-4
84. Holstein GR, Friedrich VL Jr, Martinelli GP, Ogorodnikov D, Yakushin SB, Cohen B. Fos expression in neurons of the rat vestibulo-autonomic pathway activated by sinusoidal galvanic vestibular stimulation. *Front Neurol.* (2012) 3:4. doi: 10.3389/fneur.2012.00004
85. Cohen B, Martinelli GP, Raphan T, Schaffner A, Xiang Y, Holstein GR, et al. The vasovagal response of the rat: its relation to the vestibulosympathetic reflex and to Mayer waves. *FASEB J.* (2013) 27:2564–72. doi: 10.1096/fj.12-226381
86. Cohen B, Martinelli GP, Xiang Y, Raphan T, Yakushin SB. Vestibular activation habituates the vasovagal response in the rat. *Front Neurol.* (2017) 8:83. doi: 10.3389/fneur.2017.00083
87. Yakushin SB, Martinelli GP, Raphan T, Xiang Y, Holstein GR, Cohen B. Vasovagal oscillations and vasovagal responses produced by the vestibulo-sympathetic reflex in the rat. *Front Neurol.* (2014) 5:37. doi: 10.3389/fneur.2014.00037
88. Raphan T, Cohen B, Xiang Y, Yakushin SB. A Model of blood pressure, heart rate, and vaso-vagal responses produced by vestibulo-sympathetic activation. *Front Neurosci.* (2016) 10:96. doi: 10.3389/fnins.2016.00096
89. Cohen B, Goto K, Shanzer S, Weiss AH. Eye movements induced by electric stimulation of the cerebellum in the alert cat. *Exp Neurol.* (1965) 13:145–62. doi: 10.1016/0014-4886(65)90105-6
90. Graf W, Simpson JI, Leonard CS. Spatial organization of visual messages of the rabbit's cerebellar flocculus. II Complex and simple spike responses of Purkinje cells. *J Neurophysiol.* (1988) 60:2091–121. doi: 10.1152/jn.1988.60.6.2091
91. Graf W, Wilson VJ. Afferents and efferents of the vestibular nuclei: the necessity of context-specific interpretation. *Prog Brain Res.* (1989) 80:149–57. doi: 10.1016/s0079-6123(08)62208-6

92. Masino T, Knudsen EI. Horizontal and vertical components of head movement are controlled by distinct neural circuits in the barn owl. *Nature.* (1990) 345:434–7. doi: 10.1038/345434a0
93. Hess BJ, Dieringer N. Spatial organization of linear vestibuloocular reflexes of the rat: responses during horizontal and vertical linear acceleration. *J Neurophysiol.* (1991) 66:1805–18. doi: 10.1152/jn.1991.66.6.1805
94. Wylie DR, Bischof WF, Frost BJ. Common reference frame for neural coding of translational and rotational optic flow. *Nature.* (1998) 392:278–82. doi: 10.1038/32648
95. Angelaki DE, Yakusheva TA, Green AM, Dickman JD, Blazquez PM. Computation of egomotion in the macaque cerebellar vermis. *Cerebellum.* (2010) 9:174–82. doi: 10.1007/s12311-009-0147-z
96. Branoner F, Straka H. Semicircular canal influences on the developmental tuning of the translational vestibulo-ocular reflex. *Front Neurol.* (2018) 9:404. doi: 10.3389/fneur.2018.00404
97. Takemori S, Cohen B. Loss of visual suppression of vestibular nystagmus after flocculus lesions. *Brain Res.* (1974) 72:213–24. doi: 10.1016/0006-8993(74)90860-9
98. Ito M. Neural design of the cerebellar motor control system. *Brain Res.* (1972) 40:81–4. doi: 10.1016/0006-8993(72)90110-2
99. Waespe W, Cohen B, Raphan T. Role of the flocculus and paraflocculus in optokinetic nystagmus and visual-vestibular interactions: effects of lesions. *Exp Brain Res.* (1983) 50:9–33. doi: 10.1007/BF00238229
100. Waespe W, Cohen B. Flocculectomy and unit activity in the vestibular nuclei during visual-vestibular interactions. *Exp Brain Res.* (1983) 51:23–35. doi: 10.1007/BF00236799
101. Solomon D, Cohen B. Stimulation of the nodulus and uvula discharges velocity storage in the vestibulo-ocular reflex. *Exp Brain Res.* (1994) 102:57–68. doi: 10.1007/BF00232438
102. Wearne S, Raphan T, Cohen B. Control of spatial orientation of the angular vestibuloocular reflex by the nodulus and uvula. *J Neurophysiol.* (1998) 79:2690–715. doi: 10.1152/jn.1998.79.5.2690
103. Dai M, Kunin M, Raphan T, Cohen B. The relation of motion sickness to the spatial-temporal properties of velocity storage. *Exp Brain Res.* (2003) 151:173–89. doi: 10.1007/s00221-003-1479-4
104. Dai M, Raphan T, Cohen B. Labyrinthine lesions and motion sickness susceptibility. *Exp Brain Res.* (2007) 178:477–87. doi: 10.1007/s00221-006-0759-1
105. Dai M, Sofroniou S, Kunin M, Raphan T, Cohen B. Motion sickness induced by off-vertical axis rotation (OVAR). *Exp Brain Res.* (2010) 204:207–22. doi: 10.1007/s00221-010-2305-4
106. Cohen B, Dai M, Ogorodnikov D, Laurens J, Raphan T, Müller P, et al. Motion sickness on tilting trains. *FASEB J.* (2011) 25:3765–74. doi: 10.1096/fj.11-184887
107. Cohen B, Dai M, Yakushin SB, Cho C. The neural basis of motion sickness. *J Neurophysiol.* (2019) 121:973–82. doi: 10.1152/jn.00674.2018
108. Cohen B, Dai M, Yakushin SB, Raphan T. Baclofen, motion sickness susceptibility and the neural basis for velocity storage. *Prog Brain Res.* (2008) 171:543–53. doi: 10.1016/S0079-6123(08)00677-8
109. Dai M, Raphan T, Cohen B. Prolonged reduction of motion sickness sensitivity by visual-vestibular interaction. *Exp Brain Res.* (2011) 210:503–13. doi: 10.1007/s00221-011-2548-8
110. Brown JJ, Baloh RW. Persistent mal de debarquement syndrome: a motion-induced subjective disorder of balance. *Am J Otolaryngol.* (1987) 8:219–22. doi: 10.1016/s0196-0709(87)80007-8
111. Cha YH. Mal de debarquement. *Semin Neurol.* (2009) 29:520–7. doi: 10.1055/s-0029-1241038
112. Dai M, Cohen B, Smouha E, Cho C. Readaptation of the vestibulo-ocular reflex relieves the mal de debarquement syndrome. *Front Neurol.* (2014) 5:124. doi: 10.3389/fneur.2014.00124
113. Dai M, Cohen B, Cho C, Shin S, Yakushin SB. Treatment of the mal de debarquement syndrome: a 1-year follow-up. *Front Neurol.* (2017) 8:175. doi: 10.3389/fneur.2017.00175
114. Dai M, Raphan T, Cohen B. Adaptation of the angular vestibulo-ocular reflex to head movements in rotating frames of reference. *Exp Brain Res.* (2009) 195:553–67. doi: 10.1007/s00221-009-1825-2
115. Cohen B, Büttner-Ennever JA. Projections from the superior colliculus to a region of the central mesencephalic reticular formation (cMRF) associated with horizontal saccadic eye movements. *Exp Brain Res.* (1984) 57:167–76. doi: 10.1007/BF00231143
116. Waitzman DM, Silakov VL, Cohen B. Central mesencephalic reticular formation (cMRF) neurons discharging before and during eye movements. *J Neurophysiol.* (1996) 75:1546–72. doi: 10.1152/jn.1996.75.4.1546
117. Holstein GR, Martinelli GP, Cohen B. L-baclofen-sensitive GABAB binding sites in the medial vestibular nucleus localized by immunocytochemistry. *Brain Res.* (1992) 581:175–80. doi: 10.1016/0006-8993(92)90361-c
118. Holstein GR, Martinelli GP, Cohen B. The ultrastructure of GABA-immunoreactive vestibular commissural neurons related to velocity storage in the monkey. *Neuroscience.* (1999) 93:171–81. doi: 10.1016/s0306-4522(99)00141-4
119. de Jong PT, de Jong JM, Cohen B, Jongkees LB. Ataxia and nystagmus induced by injection of local anesthetics in the neck. *Ann Neurol.* (1977) 1:240–6. doi: 10.1002/ana.410010307
120. Bala SP, Cohen B, Morris AG, Atkin A, Gittelman R, Kates W. Saccades of hyperactive and normal boys during ocular pursuit. *Dev Med Child Neurol.* (1981) 23:323–36.
121. Cohen G, Pasik P, Cohen B, Leist A, Mytilineou C, Yahr MD. Pargyline and deprenyl prevent the neurotoxicity of 1-methyl-4-phenyl-1,2,3,6-tetrahydropyridine (MPTP) in monkeys. *Eur J Pharmacol.* (1984) 106:209–10. doi: 10.1016/0014-2999(84)90700-3
122. Büttner-Ennever JA, Horn AK, Henn V, Cohen B. Projections from the superior colliculus motor map to omnipause neurons in monkey. *J Comp Neurol.* (1999) 413:55–67. doi: 10.1002/(sici)1096-9861(19991011)413:1<55::aid-cne3>3.0.co;2-k
123. Rucker JC, Buettner-Ennever JA, Straumann D, Cohen B. Case studies in neuroscience: instability of the visual near triad in traumatic brain injury-evidence for a putative convergence integrator. *J Neurophysiol.* (2019) 122:1254–63. doi: 10.1152/jn.00861.2018

Conflict of Interest: The author declares that the research was conducted in the absence of any commercial or financial relationships that could be construed as a potential conflict of interest.

frontiers in Neurology

REVIEW
published: 09 February 2021
doi: 10.3389/fneur.2021.635305

Measuring Vestibular Contributions to Age-Related Balance Impairment: A Review

Andrew R. Wagner[1,2]*, *Olaoluwa Akinsola*[3], *Ajit M. W. Chaudhari*[1,3], *Kimberly E. Bigelow*[4] *and Daniel M. Merfeld*[1,2,5]*

[1] School of Health and Rehabilitation Science, The Ohio State University, Columbus, OH, United States, [2] Department of Otolaryngology—Head and Neck Surgery, The Ohio State University, Columbus, OH, United States, [3] Department of Mechanical and Aerospace Engineering, The Ohio State University, Columbus, OH, United States, [4] Department of Mechanical and Aerospace Engineering, University of Dayton, Dayton, OH, United States, [5] Department of Biomedical Engineering, The Ohio State University, Columbus, OH, United States

OPEN ACCESS

Edited by:
Michael Strupp,
Ludwig Maximilian University of Munich, Germany

Reviewed by:
Klaus Jahn,
Schoen Clinic Bad Aibling—Department of Neurology, Germany
Christoph Helmchen,
Luebeck University of Applied Sciences, Germany
Alexander A. Tarnutzer,
University of Zurich, Switzerland

***Correspondence:**
Andrew R. Wagner
wagner.1386@osu.edu
Daniel M. Merfeld
merfeld.6@osu.edu

Specialty section:
This article was submitted to Neuro-Otology, a section of the journal Frontiers in Neurology

Received: 30 November 2020
Accepted: 18 January 2021
Published: 09 February 2021

Citation:
Wagner AR, Akinsola O, Chaudhari AMW, Bigelow KE and Merfeld DM (2021) Measuring Vestibular Contributions to Age-Related Balance Impairment: A Review. Front. Neurol. 12:635305. doi: 10.3389/fneur.2021.635305

Aging is associated with progressive declines in both the vestibular and human balance systems. While vestibular lesions certainly contribute to imbalance, the specific contributions of age-related vestibular declines to age-related balance impairment is poorly understood. This gap in knowledge results from the absence of a standardized method for measuring age-related changes to the vestibular balance pathways. The purpose of this manuscript is to provide an overview of the existing body of literature as it pertains to the methods currently used to infer vestibular contributions to age-related imbalance.

Keywords: vestibular, balance, aging, perceptual threshold, falls

INTRODUCTION

In the United States, 28–49% of older adults (≥65 years old) fall each year (1, 2). Falls are the most common cause of accidental death in older adults (1), and in non-fatal cases, the costs to manage fall-related sequelae are poised to exceed 55 billion dollars in 2020 (3, 4). Despite a great deal of research in the area of fall prevention (5, 6), falls, and fall-related deaths continue to rise (1) and the growing age of the United States population (4) is likely to perpetuate this trend. Although a fall can result from a variety of environmental or physiological causes (7–9), a principal contributor to falls among older adults is an age-related decline in balance (8–12). In this paper, we define the "human balance system" as the sensorimotor system that permits us to stand upright (and walk/run) even though the passive biomechanics are unstable, being comprised of interconnected inverted pendulums that are each unstable. Balance reflects "…the ability to maintain equilibrium in a gravitational field by keeping or returning the center of body mass over its base of support" (13) and is the critical component for successful (a) quiet stance, (b) compensatory postural reactions, and (c) anticipatory postural responses. It follows, then, that imbalance (i.e., the lack of balance) be defined as the inability to maintain equilibrium during quiet stance and to anticipate or respond appropriately to postural perturbations. Imbalance can be influenced by a myriad of age-associated declines in sensorimotor function, including somatosensation (14–16), vestibular function (17), vision (18), cognition (19), and strength (20, 21). Therefore, balance tests are often used to indirectly quantify these different sensorimotor contributors with different balance tests quantifying different balance elements. To develop targeted, personalized interventions to combat this epidemic of falls, it is crucial that we develop methods that isolate the primary contributors to an older adult's imbalance and fall risk.

Although deficits in any one of the aforementioned physiologic systems could likely contribute to imbalance, this review aims only to summarize studies that attempt to quantify contributions of the vestibular system to age-related balance impairment. The rationale for this decision is as follows: (1) Recent estimates suggest that falls due to vestibular impairment represent between the 3rd and the 10th leading cause of death amongst older adults (22), (2) 35% of adults over the age of 40 show evidence of vestibular dysfunction (23) and amongst adults that report unsteadiness, one third also report symptoms of dizziness (24), (3) increased noise within the vestibular system (assayed by roll tilt perceptual thresholds) has been shown to mediate 46% of age-related balance impairment in asymptomatic adults above age 40 (17), and (4) vestibular function has been shown to be modifiable with rehabilitation (25–32). Thus, we embark on this effort because despite the overabundance of evidence supporting both age-related declines in vestibular function (22, 23, 33–36) and a significant contribution of the vestibular system to postural control (37, 38), an understanding of the specific contributions of the vestibular system to age-related balance declines is lacking; recent proceedings from a National Institutes of Health workshop identified this as a critical gap in our understanding of fall prevention (39).

In an effort to address this critical knowledge gap, this manuscript aims to review the methods currently used to quantify vestibular contributions to age-related balance dysfunction including (I) measures of the peripheral vestibular end organs (i.e., otoliths and semicircular canals) that correlate with balance, (II) external stimulation of the descending vestibular pathways, (III) objective balance assessments, and (IV) measures of perceived vertical. We also highlight a recent line of research relating vestibular perceptual thresholds to age-related balance declines (V). We note that several areas of vestibular function (e.g., spatial cognition, navigation, and autonomic function) likely relevant to falls, but not directly relevant to balance, were intentionally omitted from this review given our focus on vestibular contributions to age-related imbalance. An indirect goal of this review is to motivate researchers and clinicians to develop novel methods for quantifying specific contributions of the aging vestibular system to balance impairment.

Tests of the Peripheral Vestibular Labyrinth

Semicircular Canals

Caloric irrigation is a gold standard for diagnosing a unilateral impairment in the horizontal semicircular canal and superior vestibular nerve (40), yet few studies have investigated its ability to predict balance impairment in healthy (i.e., without vestibular pathology) older adults. Jacobson et al. (41) compared the results of caloric irrigation to performance on a Modified Romberg Balance Test (MRBT) in a group of 45 asymptomatic adults over the age of 40—the age at which balance and vestibular function are thought to begin to decline (22, 23). Of the 20 subjects found to have an impaired caloric response, only 11 showed evidence of imbalance and of the 25 subjects found to have a normal caloric response, nine subjects demonstrated concurrent balance impairment (41). Similarly, in a sample of adults with balance impairment, Whitney et al. (42) identified an abnormal caloric response in only 13% (4/13) of recurrent fallers, while 44% (23/52) of subjects without a positive fall history demonstrated an abnormal caloric response. Collectively these results suggest that impairments in the low frequency vestibulo-ocular reflex (VOR) may not reflect impairment in the descending balance pathways.

Rotational chair testing measures bilateral horizontal canal function by quantifying the phase and gain of the mid to high frequency yaw VOR (43). Peterka and Black (35) found that although balance clearly declined with age, the incidence of abnormal VOR gain ($\pm$3 SD from the mean), was similar between adults with and without evidence of balance dysfunction (36). In a sample of healthy older adults, Baloh et al. (34) showed an age dependent decline in the VOR over a 5-year period despite stable balance performance. When these same participants were reassessed after an 8–10-year period, a multivariate regression model showed that although the VOR continued to decline with age, MRI evidence of white matter hyperintensities, visual acuity, and auditory function were the only variables significantly associated with changes on the Tinetti Gait and Balance (TGB) scale (a clinical measure of balance performance) (44). A subsequent study by Kerber et al. (45) did however identify a significant correlation between changes in the gain and phase of the low-frequency (0.05 Hz) VOR and TGB scores after a 9-year period. While this correlation remained after correcting for age ($p < 0.001$), the authors suggest that this relationship likely represents a common age-related central pathology, potentially white matter hyperintensities, that affect both balance and the VOR, rather than a causal relationship between age-related VOR declines and balance impairment (44–46). The aphysiologic vestibular stimulus (i.e., lacking head motion) during caloric irrigation (41) and the restricted frequency range of the vestibular stimuli during both caloric irrigation (0.006 Hz) and rotational chair testing [0.01–1.0 Hz (43)], relative to typical human motion [$\sim$0.8–3.2 Hz (47, 48)], pose possible explanations for the limited association between these standard assessments of canal function and balance impairment among older adults.

The video head impulse test (vHIT) instead measures canal function through the delivery of passive head rotations (i.e., impulses) that reach accelerations [$\sim$3,000°/s/s (49)] and frequencies [$\sim$6 Hz (50)] consistent with naturalistic human motion (48, 51). Over the past decade vHIT has been used to lateralize peripheral vestibular lesions (52–54) and to differentiate peripheral from central causes of an acute vestibular syndrome (55–57). However, the use of vHIT in healthy (i.e., without occult vestibular pathology) older adults has received little attention by comparison. Anson et al. (15) showed that a yaw vHIT VOR gain of <0.80 bilaterally (eye velocity < 80% of head velocity) was associated with greater amounts of postural sway in the eyes closed, compliant standing (i.e., foam) condition of the MRBT. Anson and colleagues subsequently showed that for every 0.1 decrease in VOR gain, the likelihood of failing (i.e., falling prior to 40 s) this same test increased by 8% (58). Compared to the low frequency range of calorics and rotational chair testing, the high frequency content (1–6 Hz) of impulsive

testing provides a stimulus to the vestibular system that is more representative of the demands of typical human locomotion [0.8–3.2 Hz (51)], providing a potential explanation for its superior association with balance impairments among older adults (50). Yet, in a group of 183 healthy older adults, Xie et al. (59) showed that yaw vHIT VOR gain was not associated with one's gait speed, narrow base of support balance, or the ability to rise from a chair. Thus, high frequency horizontal canal function, assayed using vHIT, may be most relevant for maintaining quiet stance in situations where visual and proprioceptive feedback are made less reliable (e.g., standing in a hallway at night on a thick rug while feeling for a light switch).

Whereas vHIT provides an objective measure of VOR gain, a bedside version of the HIT (bHIT) provides a less sensitive (53), but still clinically useful indicator of normal vs. abnormal (overt refixation saccade = abnormal function) horizontal canal function (60). Agrawal et al. (61) showed that after controlling for age, older adults with a positive bHIT walked 0.23 m/s slower, had 0.44 additional falls in the past year, and were 5 times more likely to have fallen in the previous 5 years. Davalos-Bichara and Agrawal (62) went on to show that 100% of older adults ($n = 15$) with an abnormal bilateral bHIT were unable to sustain balance in condition 4 of the MRBT [similar to the results of Anson et al. (15) when using vHIT] (62). Also since bHIT is dependent upon observation of an overt re-fixation saccade, rather than a continuous measure of VOR gain, these correlations may be representative of a more severe loss of horizontal canal function. However, despite the diagnostic utility of VOR assessments, the VOR is rarely used during daily life without an accompanying input from the visual system; thus, measures of dynamic visual acuity have been developed as complementary measures of the "real world" function of the VOR, and by extension, the horizontal canals.

The Dynamic Visual Acuity Test (DVAT) (63) is a common method for measuring the functional (or real world) status of the VOR. The DVAT requires a subject to interpret the orientation of a letter whilst the head is rotated about an earth vertical axis at a constant velocity of 120–180°/s (64). DVAT has been shown to degrade with age (63, 65) and with peripheral vestibular loss (28, 29, 63), yet few studies have investigated the relationship between DVAT and imbalance among older adults without a known vestibular diagnosis. Hall et al. (25) observed that by performing exercises which target improvements in dynamic visual acuity (i.e., gaze stabilization exercises) both fall risk and dynamic balance were improved in a sample of older adults with non-specific, presumably age-related, dizziness. Using a similar test that measured visual acuity while walking on a treadmill, Lord and colleagues however found no relationship between dynamic visual acuity and measures of balance, falls, or gait among older adults (14, 66–69).

The Gaze Stabilization Test (GST) is a methodologically distinct, yet conceptually similar test of dynamic visual acuity that measures the maximum speed at which a subject can rotate their head while retaining the ability to perceive the correct orientation of a stable (i.e., fixed size) visual target (70). In a group of 86 healthy older adults, Ward et al. (71) showed that after correcting for age, deficits on the GST (performed in yaw) were associated with poorer performance on a series of eyes closed balance tasks. Honaker et al. (72) similarly showed that in a sample of older adults the GST was significantly correlated with the Dynamic Gait Index (DGI), a measure of dynamic, ambulatory balance ($r = 0.65$, $p = 0.00009$). Honaker et al. (72) also showed that the GST (using a cutoff velocity of 100.5°/s) was able to identify participants with a positive fall history and participants who were deemed to be at a heightened risk for falls based upon their DGI scores (Sensitivity: 0.80 and 0.79, Specificity: 0.87 and 0.81, respectively). Whitney et al. (73) however showed no relationship between the GST and scores on either the DGI or the timed up and go (TUG) in a control group consisting of 20 healthy older adults.

Otolith Organs

Cervical vestibular evoked myogenic potentials (cVEMPs) use an auditory tone burst to probe the portion of the descending vestibulospinal pathway between the saccule and the motor neurons in the cervical spinal cord (74, 75). McCaslin et al. (76) showed that increased cVEMP asymmetry was associated with greater postural sway on the sensory organization test (SOT); however, this finding was made in young adults (<65 years of age) with symptoms suggestive of vestibular pathology, limiting extension to the healthy aging population. In a sample of healthy (i.e., asymptomatic) older adults, Layman et al. (77) showed a significant relationship between gait speed, an indirect measure of postural stability (78), and the latency of cVEMPs. In the only study to our knowledge to compare balance and cVEMPs in healthy older adults, Anson et al. (15) showed that a bilateral absence of cVEMP responses was associated with a mild decrease in total sway area. The interpretation of this finding is unclear since the observed effect was opposite to what would be expected (i.e., increased sway area) if abnormal cVEMPs were indeed representative of the influence of otolith dysfunction on age-related imbalance; such findings may represent a guarded postural control strategy. The effect of cVEMP loss on postural sway was also substantially smaller than that of proprioception and was only significant when sway was measured during quiet stance on a firm surface with the eyes open (15), a condition where vestibular function is least likely to be required.

The proximal location of the measured myogenic response (the sternocleidomastoid) limits the interpretation of cVEMP abnormalities as evidence of age-related decline in the distal vestibulospinal pathways that mediate balance; this provides one potential explanation for the limited correlation observed between balance and cVEMPs. To address this limitation, Rudisill and Hain (79) investigated a novel variant of cVEMPs, the aptly named "leg-VEMP," to probe the integrity of the more distal vestibulospinal pathways by recording EMG responses from the medial gastrocnemius. The primary limitation to measuring vestibular evoked myogenic potentials distally in a muscle that controls upright stance is the increased distance between the saccule and the targeted motor neurons. The added distance results in a lower amplitude and more variable EMG signal which limits any meaningful interpretation (79). Use of an intermediary muscle group, proximal to the MG but distal to the SCM (i.e., triceps brachii) (80, 81) has

been found to produce a more robust response but yields little added benefit compared to traditional cVEMPs when the goal is to investigate the influence of saccular dysfunction on postural control.

Electrical Stimulation of the Descending Vestibular Pathways

One limitation of cVEMPs is that auditory stimuli provide a rather weak stimulus to the vestibular labyrinth, with the intensity being limited by a risk of noise-induced damage to the middle ear. Galvanic vestibular stimulation (GVS) uses a direct electrical current applied to the skin overlying the mastoid processes to stimulate the vestibular afferents [predominantly irregular (82, 83)] that innervate both the otolith organs and semicircular canals (82, 84). In healthy adults, GVS causes a stereotyped response including postural sway toward the anode (i.e., away from the cathode) (85–87), ocular torsion (88–90), head and/or body tilt (91), an illusory sense of rotation (92, 93) or tilt (88), and an increase in EMG activity specifically in the muscles actively engaged in a postural task (e.g., soleus during upright stance) (94–96) [see (97, 98) for comprehensive reviews on GVS]. Studies that use GVS to probe descending vestibular control of balance typically measure either lower extremity EMG responses or the magnitude of GVS-induced postural sway (97). While well-characterized in healthy young adults (94) and subjects with vestibular pathology (85, 86), relatively few studies have investigated the responses to GVS in healthy older adults.

Welgampola and Colebatch (99) found a selective age-related change in the short latency GVS induced EMG responses in the soleus, such that the short latency responses in older adults were more delayed, more asymmetric, and lower in amplitude when compared to young adults. Dalton et al. (100) similarly found evidence of a selective decrease in the amplitude of short latency EMG signals in the soleus and medial gastrocnemius of older adults. Dalton et al. (100) also found a compensatory increase in tibialis anterior EMG responses to GVS, leading the authors to suggest a potential vestibular initiated compensation for age-related balance declines. Deshpande et al. (101) studied the influence of a combined stimulus including both GVS and a vibratory stimulus applied unilaterally to the dorsal aspect of the neck. They found that when walking with vision occluded, the young adult and older adult groups showed a similar increase in trunk velocity in the frontal plane. However, compared to young adults, the amount of lateral path deviation caused by the stimulus was attenuated in the older adult group, but this was only in regard to the response to the vibratory stimulus, not GVS (101). Tax et al. (86) however found that older adults showed a decrease in GVS induced postural sway during quiet stance. Yet, when compared to patients with bilateral vestibular hypofunction (86, 100), the reduction in GVS induced sway was minimal, potentially reflecting a more subtle decline in the descending vestibular pathways in older adults relative to patients with bilateral vestibular loss. Additional studies are needed determine if postural and EMG responses to GVS are predictive of balance impairment and fall risk in older adults.

Balance Assessments

Measuring Sensory Contributions to Balance

The Romberg (RBT) and Sharpened Romberg (SRBT) balance tests determine an individual's ability to stand with a narrow base of support (RBT, feet together; SRBT, heel to toe) when vision is removed. Performance is determined by the subject's ability to maintain balance for a predetermined time interval (typically between 15 and 60 s) and is graded as success (able to remain upright) or failure (unable to remain upright). The insensitivity of the RBT to vestibular dysfunction prompted Fregly and Graybiel (102) to investigate the SRBT (and heel to toe walking) as a method to screen for vestibular disorders. Fregly and Graybiel (102) showed that individuals with the lowest caloric responses showed the greatest deficits in both the SRBT and heel to toe walking when the eyes were closed. However, more recently, in an older adult population, Longridge et al. (103) showed that the SRBT was unable to separate healthy older adults from those with known vestibulopathy, with most subjects falling regardless of the presence of vestibular pathology; such differences from the original findings of Fregly and Graybiel (102) are likely explained by an age-associated floor effect of the SRBT due to the high degree of challenge. Such limitations provide support for the use of more comprehensive tests when attempting to detect vestibular contributions to imbalance.

One of the most frequently used methods is computerized dynamic posturography (CDP), and more specifically the sensory organization test (SOT) (36, 104–106). The SOT uses a sophisticated motion platform to quantify changes in a patient's postural sway (i.e., movement of the center of pressure, CoP) when the fidelity of visual and/or somatosensory cues is altered (105, 106). Pairing movement of either the visual surround and/or the surface with the participant's postural sway (i.e., sway referencing) diminishes one's ability to use proprioceptive and/or visual feedback for postural control. Therefore, the magnitude of postural sway is dependent upon the individual's ability to suppress any conflicting visual and/or proprioceptive cues and weight the remaining veridical cues (107). The vestibular system is the only unperturbed sensory modality controlling upright stance in conditions five and six of the SOT (SOT-5, SOT-6; **Table 1**), where proprioception is unreliable, and vision is either unreliable (SOT-6) or removed (SOT-5). As a result, patients with an acute vestibular lesion demonstrate marked instability in these conditions (111–115) and performance on SOT-5 and SOT-6 (relative unperturbed quiet stance, SOT-1) has been adopted as a surrogate measure of vestibulospinal function.

Evidence supporting use of SOT to detect *age-related* vestibular declines is not as straight forward. The output of the SOT, postural sway, is a complex sensorimotor response that requires the integration and weighting of multiple sensory cues and a sensorimotor transformation that ultimately produces a response using the distal musculature (116). Older adults experience an increase in reaction times (117), a decline in lower extremity strength (20), and reduced distal somatosensation (14, 16, 118); each of which can potentially influence balance (118). As a result, postural sway in SOT-5 and SOT-6 cannot with certainty be attributed

TABLE 1 | Table consists of conditions for the SOT, including parameters for head-shake variations established by both Mishra et al. (108) and Honaker et al. (109), respectively.

Condition	Vision	Platform	Unperturbed sensory systems	Head shake variation
SOT-1	Eyes Open + Stationary Surround	Stationary	Visual; Somatosensory; Vestibular	
SOT-2	Eyes CLOSED	Stationary	Somatosensory; Vestibular	60°/s (108) 120°/s (109)
SOT-3	Eyes Open + Sway Referenced	Stationary	Somatosensory; Vestibular	
SOT-4	Eyes Open + Stationary Surround	Sway-Referenced	Visual; Vestibular	
SOT-5	Eyes Closed + Stationary Surround	Sway-Referenced	Vestibular	15°/s (109) 60°/s (108)
SOT-6	Eyes Open + Sway Referenced	Sway-Referenced	Vestibular	

Graphical depictions for each condition can be found at (108–110).

solely to an age-related decline in vestibular function. This is highlighted by impaired performance in SOT-5 and SOT-6 (i.e., the "vestibular conditions"), in both healthy adults (119, 120) and in patients with various central nervous system pathologies (121), two populations without vestibular impairment.

Consistent with this notion, studies using SOT-5 and SOT-6 to probe vestibular contributions to age-related imbalance have produced conflicting results over the past 30 years (122). Woollacott et al. (123) showed that older adults were more likely to fall during SOT-5 rather than SOT-6, prompting the authors to propose a pattern of imbalance consistent with dysfunction in the vestibular periphery. Similarly, Ledin et al. (124) showed that sway was significantly increased in SOT 5, but not SOT-6, when comparing participants 70–75 years of age to participants 60–69 years of age. However, several authors have since identified a different pattern of imbalance among older adults, consistent with an age-related deficiency in the ability to resolve sensory conflict (46, 119, 122, 125–128), rather than a loss of peripheral vestibular inputs. Whipple et al. (122) and Wolfson et al. (126) each showed that when compared to young adults, older adults showed a larger increase in sway and a greater prevalence of falls, in conditions with inaccurate (SOT-6), rather than absent (SOT-5), visual feedback. Peterka and Black (36), observed that older adults fell most often when experiencing conflicting visual and proprioceptive cues (SOT-6), and when a fall did not occur, sway was increased in SOT-6 relative to SOT-5. Interestingly, the older adults in Peterka and Black's study that were able to remain upright for SOT-5 showed similar amounts of sway to the young adult control group (125). More recently, Pedalini et al. (127) showed that while older adults with symptoms of vestibular impairment performed worse on SOT-4–6 than asymptomatic older adults, asymptomatic adults also performed significantly worse than young adults in each of these same conditions. Thus, instability in SOT conditions 4–6 may be sensitive to aging, independent of vestibular decline. These findings lend support to the general conclusion that the instability observed in the vestibular conditions of the SOT may be indicative of an age-related inability to suppress conflicting sensory cues (107), suggesting a breakdown in the central integration (36, 122, 126) or reweighting of multiple sensory cues, both vestibular and extra-vestibular, rather than direct evidence of impaired descending vestibular function.

Furthermore, even in subjects with a known vestibular lesion, the sensitivity of the SOT to vestibular loss has been shown to be only around 50% (109, 121, 129). In an effort to improve sensitivity, Mishra et al. (108) studied the effect of adding active yaw head rotations to SOT-2 and SOT-5 (**Table 1**). Yet, the aptly named head shake SOT (HS-SOT) was found to offer little benefit over the traditional SOT secondary to a ceiling effect in HS-SOT-2 and a floor effect in HS-SOT-5 (108). Park et al. (130) tested the HS-SOT in a sample of 102 healthy older adults. The ratio between SOT-5 and HS-SOT-5 was found to be 54% higher in older adults compared to young adults; the authors concluded that the increase in sway with the addition of the head shake stimulus was indicative of impaired vestibular function in the older adult group (130). However, as stated in the original study by Mishra et al. (108), the HS-SOT-5 is exceptionally challenging, such that subjects with a known history of vestibular hypofunction could not be differentiated from healthy adults due to universally poor performance. Thus, the increased instability in HS-SOT-5 compared to SOT-5 seen by Park et al. (130) may simply reflect the added challenge, rather than the presence of vestibular impairment. Honaker et al. (131) has since addressed this floor effect by decreasing the rate of head rotation in SOT-5 (**Table 1**), improving upon the sensitivity (70%) of HS-SOT for unilateral vestibular loss (109); future studies should consider investigating this paradigm in an older adult population.

The clinical test of sensory interaction and balance (CTSIB) is a simplified version of the SOT, developed specifically for use in a clinical setting (13, 132). Subjects perform tasks analogous to the six conditions of the SOT, with the exception that sway referenced supports are replaced by foam and sway referenced visual surrounds are replaced by an opaque globe, meant to distort but not remove visual inputs (132). CTSIB conditions are scored based on the amount of time one can maintain upright stance, up to a maximum of 30 s, in each condition (132). Cohen et al. (133) investigated the use of the CTSIB in patients with vestibular disorders compared to older adults. Cohen et al. (133) showed that conditions 4 and 6, but not condition 5, of the CTSIB were more affected by vestibular dysfunction than by healthy

aging, suggesting a potential role for conditions 4 (globe plus firm surface) and 6 (globe plus foam surface) as a screening tool for vestibular dysfunction in older adults. Many clinicians and researchers have however opted for the use of a further simplified test, the modified CTSIB (mCTSIB), which consists only of static stance on both firm and foam surfaces, with the eyes open or closed (134, 135).

Condition 4 of the mCTSIB (i.e., condition 5 of the CTSIB) requires the participant to stand with the eyes closed, atop a foam pad meant to degrade somatosensory feedback from the distal lower extremity, similar to the sway referenced conditions of the SOT. Hong et al. (136) showed that although the full mCTSIB was a poor predictor of performance on the SOT, condition 4 of the mCTSIB correlated with SOT-5, demonstrating validity of this relatively simple test as an appropriate method for degrading somatosensory feedback. Since closing the eyes also removes visual input, leaving the vestibular system as the only undisturbed contributor to upright stance, an inability to maintain balance in condition 4 of the mCTSIB has been proposed as an indicator of impaired vestibulospinal function. An analogous test [a modified Romberg Balance Test (MRBT)], was recently used in a nationally representative sample of older adults, the National Health and Nutrition Evaluation Survey (NHANES), as a screening tool to estimate vestibular impairment (23). Agrawal et al. (23) reported that 34.5% of adults over the age of 40 and more than half of adults over age 60 failed condition 4 of the MRBT (i.e., could not stand 20 s on foam with eyes closed) with failure being associated with over a 6-fold increase in the odds of having experienced a fall in the previous year (23). The authors suggested that such findings represent the burden of vestibular dysfunction among older Americans (23). This suggestion has however been subsequently challenged. As described above, Jacobson et al. (41) found weak correlations between vestibular function tests and failure on the MRBT in a sample of adults over the age of 40, drawing the conclusion that the MRBT may be inappropriate as a screening tool for vestibular impairment in older adults. However, poor agreement between posturography and vestibular function tests need not discredit the applicability of such assessments, as one should expect dissimilar findings when using tests which probe different vestibular function contributions.

Static Posturography and Computational Approaches

As an alternative to the SOT assessment and the simpler RBT, sRBT, and mCTSIB assessments, a potential middle ground exists using digitized posturography tools, such as force plates, pressure sensors, and inertial measurement units, to track movement of the CoP during quiet stance. Such an approach improves upon the sensitivity of the time to failure scoring of traditional clinical balance tests (137) and takes less time to administer than the complete set of conditions performed in the SOT. Baloh et al. (138) used force plates to measure the velocity of postural sway in conditions analogous to the mCTSIB. Baloh found that older adults with a history of imbalance demonstrated an increase in sway velocity, regardless of the presence of vestibular hypofunction, when standing on foam with the eyes closed (138). Therefore, a critical consideration to making posturography during quiet stance valuable as a vestibular assessment is whether computational approaches can extract characteristics of the CoP motion that discriminate between those with vestibular hypofunction and those with normal vestibular function.

Recently, Gilfriche et al. (139) analyzed CoP data using a modified version of detrended fluctuation analysis (140), Frequency Specific Fractal Analysis (FsFA), which converts time scales (N) to frequency spectra (Fc) (Fc = Sample Frequency/N) (141). Gilfriche found that performing a fatiguing lower body exercise influenced the scaling exponent that described CoP fluctuations at higher frequencies (2–20 Hz), a frequency range thought to be dominated by somatosensory control, with no change in the lower frequency scaling exponent (<0.5 Hz), a frequency range suggested by Gilfriche to reflect visuo-vestibular control (139). Yet, such assumptions are in opposition to the preferential sensitivity of the vestibular afferents to high, rather than low, frequency stimuli (141). Consistent with this opposing view, using empirical mode decomposition, Yeh et al. (142) showed that young adults with vestibular disorders could be differentiated from healthy older adults by a characteristic increase in power within the high frequency range of the CoP time series. Thus, while these computationally driven analyses of quiet stance appear to be sensitive to both physiologic changes (i.e., somatosensory loss) and the effects of aging, the capacity to use these methods to detect alterations in postural sway that result specifically from age-related vestibular decline is still largely unknown. Future analysis of CoP complexity may benefit from 1) analyzing the dynamics of postural sway using SOT-5, condition 4 of the mCTSIB/MRBT (see above), or pseudorandom perturbations (see below), rather than unperturbed quiet stance and 2) by determining the association between the CoP frequency spectra and objective measures of sensory precision (e.g., perceptual thresholds).

Pseudorandom Perturbations

Peterka (37) developed a closed loop model of postural control to describe sagittal plane control of the center of mass when presented with ambiguous or unreliable sensory cues. In the model, postural sway results from an active corrective torque at the ankle proportional to the relative weighting of visual, proprioceptive, and vestibular cues (37). To empirically test the validity of this closed loop model, subjects were exposed to continuous rotations of the support platform or visual surround using a pseudorandom sequence of summed sinusoids while in upright stance. The perturbations were delivered under various sensory conditions (**Table 2**), including a sway-referenced platform or visual surround (as is done in the SOT). The use of external perturbations allows for the calculation of transfer functions that quantify the response of the postural control system as a function of the frequency spectra and amplitude of the imposed platform perturbation (37, 143). Peterka compared the gain and phase (i.e., the magnitude and timing of sway relative to the platform, respectively) of postural sway derived from these transfer functions to compare the behavior of healthy young adults to those with compensated bilateral vestibular loss (37). Peterka showed that when only vestibular and proprioceptive cues were available (i.e., with eyes closed) patients with compensated unilateral (UVL) or bilateral

vestibular loss (BVL) adopted a distinct pattern of sway in response to anteroposterior tilts of the platform (37, 144). At large amplitudes of tilt, it becomes advantageous to realign the body with gravitational vertical, rather than the platform; these participants however showed a monotonic increase in postural sway at increasing angles of platform tilt, reflecting a tendency to continue to align the center of mass with the support surface (37, 144). In the context of the closed loop model of postural control, this pattern can be interpreted as a persistent reliance upon proprioceptive feedback or a deficiency in the reweighting of the absent (BVL) or impaired (UVL) vestibular cues; this is highlighted by the comparison to healthy adults who instead readily reweight the intact vestibular cue, aligning the body with gravitational vertical rather than the platform during larger amplitude perturbations (37, 144).

The aforementioned studies (37, 144) included only patients who were more than a year removed from their injury and therefore were believed to be well-compensated (145); this highlights the sensitivity of this method to subtle vestibular declines, such as occur with aging (34). Cenciarini et al. (146) used pseudorandom platform tilts in a sample of healthy older adult subjects and showed that, relative to young adults, older adults showed a compensatory increase in stiffness and damping parameters, interpreted by the authors as evidence that older adults adopt a unique compensatory strategy to maintain balance (146). Unfortunately investigating the weighting of vestibular and proprioceptive cues was not a goal of their experiment. Wiesmeir et al. (147) showed that unlike patients with vestibular loss, healthy older adults showed a retained capacity to increase the use of vestibular cues at higher amplitudes of platform tilt. Yet, they also found that relative to young adults, older adults displayed a consistently increased weighting of proprioceptive cues. Since the group of older adults were asymptomatic and had normal VOR function on rotational testing, the observed age-related changes in sensory reweighting mechanisms may be related to subclinical declines in vestibular pathways distinct from those mediating the VOR. Yet, the relevant vestibular structure (i.e., otolith, canal, or central) underlying the ability to orient one's self with gravitational vertical during dynamic pseudorandom perturbations remains unknown.

Standardized Measures of Functional Mobility

The Fukuda (i.e., Unterburger) Stepping Test is a classic bedside test designed to assess descending vestibulospinal control by measuring the degree of rotation that occurs while stepping in place with the eyes closed (148). Studies showing poor sensitivity and specificity of the Fukuda Stepping Test for vestibular dysfunction (131, 149) have led many to adopt use of more comprehensive functional assessments. Several standardized tests incorporate elements meant explicitly to perturb the vestibular system (e.g., rotating the head and/or body) to determine a vestibular cause to postural instability. The timed up and go (TUG), DGI, and functional gait assessment (FGA) measure dynamic ambulatory balance and are capable of predicting fall risk among older adults (150–152) and patients with vestibular loss (153, 154). The DGI and FGA require subjects to ambulate while rotating their head in either pitch or yaw (151, 155), whereas the TUG requires subjects to walk a distance and then turn the body 180 degrees while walking (154). Although individuals with vestibular impairment struggle with the aforementioned tasks (154, 156, 157), it is worth emphasizing that the vestibular system is not the sole respondent to the imposed stimuli. Chang and Schubert (158) showed that DGI scores improved independent of VOR gain improvement in a sample of patients recovering from unilateral vestibular deafferentation surgery. Actively rotating the head involves vestibular, cervical proprioceptive, motor efferent, and visual cues; a compensatory change to any of these extra-vestibular systems could therefore improve balance performance independent of vestibular loss or recovery. Thus, imbalance provoked by movement of the head, while certainly a symptom of suboptimal vestibular function, cannot definitively indicate vestibular loss. Cohen et al. (134) did however find that the addition of yaw and pitch head movements improved the sensitivity of eyes closed heel to toe walking and the mCTSIB to vestibular pathology (e.g., Meniere's disease, BPPV) in older adults aged 40–79; whether this finding is generalizable specifically to sub-clinical vestibular declines, rather than the identification of vestibular pathology, remains to be seen.

Overall, functional outcome measures allow clinicians to efficiently predict fall risk and are often used to guide rehabilitative efforts (152, 155, 159). The capacity to mimic real world balance perturbations (e.g., stepping over an object) likely explains their predictive abilities. However, this functional emphasis conversely prevents such tests from isolating the culpable system causing the balance disturbance and this is particularly true in the evaluation of the older adult patient, as imbalance on clinical balance tests can be caused by a number of extra-vestibular age-related changes in sensorimotor function (e.g., kinesthesia, strength) (160).

Perception of Subjective Vertical

Subjective Visual Vertical

Tests of subjective visual vertical (SVV) quantify the relative contributions of otolith (predominantly utricle), visual, and somatosensory cues by estimating an individual's perception of gravitational vertical [See (161) for a review]. While methods vary, SVV generally requires an individual to orient an illuminated bar with what they perceive to be true vertical; testing can take place either in the dark (i.e., no veridical visual cues) or in the presence of a moving (dynamic SVV) or inaccurate (rod-and-frame SVV) visual cue. Tobis et al. (162) found that older adult fallers showed a significant bias in SVV in the direction of a tilted frame that surrounded the vertical bar (i.e., rod-and-frame SVV), suggesting an increased weighting of visual, relative to otolith cues, presumably as a compensation for vestibular declines (161). Lord and Webster (163) showed that when compared to healthy older adults, older adults with a positive fall history displayed greater errors (deviation from true vertical) in both static (fixed background) and dynamic (rotating background) SVV tasks. Barr et al. (164) showed that when in the presence of a rotating visual surround, a deviation in SVV of at least 6.5° was associated with greater fall risk and a significant decrease in postural sway when standing with

TABLE 2 | Conditions of the protocol developd by Peterka (37) using pseudorandom perturbations to model postural sway.

Condition	Vision	Platform	Sensory information		
			Vision	Proprioception	Vestibular
1	PRTS stimulus	Fixed	Accurate	Veridical	Veridical
2	PRTS stimulus	Sway-referenced	Accurate	Inaccurate	Veridical
3	Fixed	PRTS stimulus	Veridical	Accurate	Veridical
4	Eyes closed	PRTS stimulus	Absent	Accurate	Veridical
5	Sway-referenced	PRTS stimulus	Inaccurate	Accurate	Veridical
6	PRTS stimulus	PRTS stimulus	Accurate	Accurate	Veridical

Recreated from Peterka (37). PRTS, pseudorandom ternary sequence.

the eyes open or closed, and when standing in the presence of a moving visual field; such patterns suggest the adoption of a maladaptive stiffening of one's postural control strategy. Together, these results suggest that changes in the weighting of otolith relative to visual cues may predict altered postural control strategies and fall risk in older adults.

The presence of a stereotyped bias in SVV toward the side of an acute unilateral vestibular lesion suggests that the otolith organs are at least one of the principle contributors to one's estimate of subjective vertical (165). Yet, SVV is restored within weeks to months after a vestibular lesion (166, 167). This suggests that an individual with persistent vestibular loss can restore SVV by appropriately weighting residual vestibuar cues with intact visual, somatosensory (168) and/or somatic graviceptive (e.g., vascular receptors signaling a shift in blood volume within the trunk) cues (169). Also, it appears that a maladaptive reweighting of verticality cues, rather than isolated vestibular loss, may explain the correlations observed between SVV, fall risk, and postural sway in older adults, as such relationships are observed when SVV is measured in the presence of a spurious visual reference (i.e., tilted frame or rotating background) (162–164).

Subjective Postural Vertical

SPV is typically measured by having an individual report when they perceive their body to be aligned with gravitational vertical. SPV can be quantified both by the accuracy (deviation relative to upright) and precision (variability around the perception of upright) of their estimate of vertical (161). Barbieri et al. (170) showed that SPV gradually tilts backward with age, with nearly a doubling of backward inclination in healthy adults over 50 ($-1.15^{\circ} \pm 1.40$) when compared to adults 18–49 years of age ($-0.45^{\circ} \pm 0.97$, $p < 0.01$). Manckoundia et al. (171) found that this age-associated posterior displacement of the SPV was highly correlated ($r = 0.95$, $p < 0.000001$) with the extent of backward instability during a series of balance and mobility tasks (e.g., sitting, standing with and without vision and transitioning between sitting and standing). This deviation of SPV among older adults has been posited as a potential explanation for an asymmetrical pattern of postural instability experienced by older adults referred to as "backward disequilibrium" (170–172). Menant et al. (173) showed that both the precision and accuracy of SPV in the mediolateral direction was also significantly correlated with lateral sway ($r = 0.20$ and 0.16, respectively) measured during stance in a foam, eyes closed condition. This relationship persisted after correcting for age, gender, and other general indicators of mobility (i.e., the physiological profile assessment); considering the large sample size ($N = 195$), this finding provides convincing evidence that perceived vertical may be a potentially useful indicator of age-related balance dysfunction.

Yet, Bisdorf et al. (165) showed that neither chronic nor acute vestibular lesions were sufficient to induce a bias in SPV. Anastopolous similarly showed that SPV remained veridical following an acute vestibular lesion, despite a consistent tilt of SVV toward the side of the vestibular lesion (174). Ito and Gresty (175) showed that even in individuals with a total surgical loss of vestibular function (due to surgery to correct Neurofibromatosis Type II), the accuracy of SPV remained similar to healthy adults. These studies suggest that unlike SVV, otolith dysfunction has minimal impact on the accuracy (i.e., bias) of SPV. Instead, the increased variability of SPV in patients with bilateral vestibular loss and acute unilateral lesions suggests that graviceptive otolith cues may instead be more relevant for reducing the variability in one's estimate of postural vertical (161, 165). A clear bias in SPV has however been observed in individuals with somatosensory loss affecting the trunk (176, 177). Thus, the association between imbalance and the observed age-related shift in SPV, may be indicative of the impact of age-related somatosensory declines or alterations in the central integration of somatic graviceptive, somatosensory, and vestibular cues.

Vestibular Noise

Vestibular Perceptual Thresholds

Neural noise (referred to herein as "noise") is the random fluctuation in neural activity that occurs within each sensory system (178, 179). While low levels of external noise can enhance sensory signals [i.e., stochastic resonance (180)], excess internal noise impairs the communication between neurons, and has been posited as a potential cause of age-related cognitive decline (178, 181, 182). Neurophysiologic studies have provided evidence for age-related increases in neural noise, showing a relationship between electroencephalogram (EEG) $1/f$ power spectral density and both language and visual working memory in older adults (182). Behavioral studies have similarly shown that background sensory noise impairs the perception of visual

images in older adults (178). Psychophysical assessments of self-motion perception ("vestibular perceptual thresholds") provide evidence that neural noise may also affect the aging vestibular system (22, 183, 184).

Consistent with classic signal detection theory (185), a *vestibular threshold* represents the minimum stimulus value at which a subject can accurately (at a pre-defined accuracy level) perceive the direction of passive self-motion while using predominantly vestibular cues (186). In other words, a perceptual threshold is the magnitude of a vestibular stimulus required to overcome the level of internal noise within an individual's vestibular system, thereby allowing the self-motion signal to be reliably perceived by the subject (e.g., "I moved right"); *thus, vestibular thresholds are an assay of vestibular noise* (186). Although methods may vary, one-interval direction recognition tasks (e.g., "did I move right or left?") are the most common psychophysical technique for quantifying vestibular perceptual thresholds (186). By quantifying vestibular noise during self-motion, vestibular thresholds can independently assess each vestibular modality (tilt, rotation, and translation). While a comprehensive review of vestibular perceptual testing is beyond the scope of this review, we refer the interested reader to several reviews on the topics of signal detection theory and vestibular perceptual thresholds (185–189).

Vestibular Thresholds and Age-Related Imbalance

Vestibular thresholds have been shown to increase after age 40 in all planes of motion including supero-inferior translations, interaural translations, roll tilt, and yaw rotation (22). Despite thresholds being moderately correlated with one another, only low frequency (0.2 Hz or 5 s per motion) roll tilt perceptual thresholds show a significant association with *age-related* imbalance (190). Elevated roll tilt thresholds were found to be associated with an increase in the likelihood of failing (i.e., falling prior to the end of the 30 s trial) the "eyes closed, standing on a compliant surface" test condition of the MRBT in a sample of healthy adults over the age of 40 (190); this statistically significant relationship remained even after accounting for age. In a subsequent mediation analysis of these data, Beylergil et al. (17) showed that roll-tilt thresholds significantly mediated the relationship between age and balance impairment. Despite the multitude of factors that contribute to age-related balance impairment (e.g., vision, cognition, kinesthesia), this analysis showed that age-related increases in roll tilt thresholds accounted for nearly half (46%) of the relationship between age and balance impairment (17). We posit three possible explanations for this admittedly surprising finding, (1) roll tilt perceptual thresholds may represent a physiologically relevant vestibular cue (190) due to the inherent need for human beings to respond to changes in head position relative to gravity (i.e., tilt) in order to remain upright, (2) roll tilt perceptual thresholds may reflect a more global measure of central vestibular function, as the precision of roll tilt perception is dependent upon the ability of the aging brain to perform (191–197) complex neural computations to resolve ambiguous gravitoinertial cues from the otolith organs, and (3) canal and otolith cues are integrated during most, if not all, naturalistic human motions (198), and thus impaired roll tilt perception may specifically reflect imperfections associated with canal-otolith integration. Yet, similar to vHIT, such comparisons have been restricted to balance performance in quiet stance on a foam pad with the eyes closed, and thus one must be cautious with the extrapolation of these findings to alternative aspects of human balance.

Noise, Aging, and Velocity Storage

Recent empirical and modeling efforts have further implicated noise as an explanation for age-related changes in the temporal characteristics of the VOR (199) and in age-related changes in postural control (200). During a sustained, constant velocity yaw rotation about an earth vertical axis, activity in the peripheral vestibular afferents degrades quickly, with a time constant of around 4–6 s (141, 201, 202). However, compensatory nystagmus and the subjective perception of rotation persist up to 30 s (34, 43, 203); this propagation of behavioral vestibular activity is accomplished through a mechanism called velocity storage [see (204) for a review on this topic but also see (205, 206) for differing perspectives]. A reduced time constant (i.e., faster decay of nystagmus) has been identified in subjects with unilateral and bilateral vestibular loss (207), in those with central vestibular dysfunction (208), and in asymptomatic older adults (34, 35, 203, 209).

Karmali proposed an explanation for the observed effect of aging on the vestibular time constant (Tc) using a Bayesian framework (199, 210–212). Extending the Tc beyond the time constant of peripheral vestibular afferents requires the repeated integration of canal signals (213) which amplifies the accompanying noise (199). Thus, while prolonging the Tc results in a more accurate estimate of rotation, it comes at the cost of an accumulation of noise (i.e., reducing precision) (212). Using a Bayesian optimal Kalman filter model, Karmali et al. (199) showed that the age-related shortening of the Tc may be proportional to published data describing the rate of age-related decline in the vestibular hair cells (214). Karmali suggested that in order to compensate for this decline in the vestibular signal to noise ratio, the CNS may dynamically shorten the Tc to achieve an optimal balance between accuracy and precision (199, 212).

While vestibular noise, assayed by roll tilt perceptual thresholds, has been found to be associated with age-related balance impairment, similar work comparing the Tc to measures of balance is sparse. In the only study to our knowledge to empirically compare the Tc and balance, Jacobson et al. (215) showed that a lower Tc, even in the presence of normal VOR gain, was associated with greater postural instability among otherwise healthy older adults. It is worth noting that concomitant ischemic pontine lesions were also identified in ∼80% of the older adults with a balance impairment and shortened Tc, suggesting that velocity storage may be reflective of central vestibular dysfunction in older adults (215). Additional work is needed to determine if the Tc represents the contribution of central vestibular pathways to age-related balance declines.

DISCUSSION

Measures of low frequency horizontal canal function (i.e., caloric irrigation and rotational chair testing) appear to provide minimal

benefit when attempting to identify a vestibular cause to age-related imbalance. Alternative measures of canal function that include the integration of visual cues (i.e., GST) or a high frequency stimulus (i.e., vHIT), have instead demonstrated a capacity to predict postural instability and fall risk in older adults (71, 216). Given that correlations remained even after correcting for age, these findings indicate that vHIT and GST may be suitable measures to quantify specific contributions of the horizontal canal to age-related imbalance. However, one must consider several limitations when relying on assessments of the VOR to quantify the influence of impaired canal function on age-related imbalance.

Measures of the VOR are not solely measures of canal function, but instead reflect the integrity of the motor limb of the reflex (e.g., oculomotor plant) and can be influenced by extra-vestibular oculomotor strategies (e.g., compensatory saccades) (64, 217, 218). This point is highlighted by the typical course of recovery following unilateral vestibular loss (UVD). Dynamic visual acuity improves independent of any restoration in peripheral vestibular function (26, 27, 145, 219) secondary to the recruitment of compensatory saccades (220), the unmasking of cervical proprioceptive inputs (221–224) and the integration of motor efferent signals (64, 217, 218). Also, while the horizontal canals feed into both the ascending and descending vestibular pathways, VOR pathways are anatomically distinct from the vestibulospinal pathways (222, 223), diverging at the level of second order neurons in the vestibular nuclei [VOR via position vestibular pause (PVP) and vestibulospinal via vestibular only (VO) neurons, respectively; see (225) for a review on this topic]. Thus, the association between VOR measures and imbalance may be representative of imbalance that results from unstable gaze (the function of the VOR), rather than as an indication that such measures directly assay the pathway connecting the horizontal canals to the descending vestibular pathways. Nevertheless, VOR assessments irrefutably remain vital to lateralize vestibular loss (226, 227).

Since balance assessments, namely the SOT, directly measure balance performance, in principle, they are likely considered better suited to identify imbalance that results from vestibular impairment. The vestibular conditions of the SOT (i.e., SOT-5 and 6) have however shown limited sensitivity (109, 121, 129) and specificity (119–121) when used as a diagnostic site of lesion test. This is likely a result of the inability to differentiate a patient with restored vestibular function from a patient who has successfully re-weighted extra-vestibular cues and the analytical consideration of the "vestibular sense" as a single sense, when, in fact, it includes at least 3 sensory modalities (rotation, translation, tilt) (228, 229). These issues are accentuated when examining older adults due to (1) the inability to separate dysfunction of the descending vestibular pathways from alternative age-associated sensorimotor declines, (2) the relative insensitivity to subtle changes in vestibular function, and (3) the fact that all vestibular modalities, that may decline at different rates with aging, are lumped into a single entity. This is not meant to dissuade clinicians and researchers from using the SOT when vestibular decline is suspected, but rather to suggest that it be used as a vestibular screening tool and/or be paired with more direct assays of vestibular function. Asai et al. (230) showed that sensitivity of the SOT was improved when considered in conjunction with positive findings on a standard vestibular test battery. Cohen et al., recently showed that combining SOT-5 with a clinical balance test [e.g., the functional mobility test (FMT), Timed Up and Go (TUG), or Dynamic Gait Index (DGI)] improved sensitivity to vestibular impairment in a group of young adults (231).

Some of these limitations of the SOT may be addressable by treating postural sway as the output of a closed loop system, rather than directly as evidence of instability. In the SOT, as is true in nearly all balance tests, increased movement of the CoP is interpreted as evidence of instability. However, considering the magnitude of postural sway in isolation does not in of itself indicate instability, and may instead represent exploratory behavior (232) or could be the result of a compensatory re-weighting of sensory cues (37). By measuring sway evoked by continuous pseudorandom perturbations, one can compute transfer functions which determine if the center of mass orients relative to the stimulus (i.e., tilting platform), suggesting persistent weighting of proprioceptive cues, or with gravitational vertical, suggesting an amplitude dependent reweighting of vestibular cues (37, 233); this approach provides a quantitative explanation for the observed postural sway (37). Thus, in experimental conditions that alter the reliability of sensory cues (i.e., eyes closed or sway referencing) such an approach may offer improvements on the SOT by determining the postural control strategy being used to respond to the externally imposed perturbations and the relative weights assigned to each sensory channel. Pseudorandom stimuli also have the advantage of providing a less predictable perturbation to the vestibular system, an approach previously shown to be more discriminatory for identifying vestibular pathology (217).

Yet, an inherent limitation to the use of any complex sensorimotor task, including the SOT or pseudorandom perturbations, is that the output (i.e., sway as measured using CoP or CoM) is the only quantifiable indicator of performance. As a result, if one is attempting to determine if vestibular *sensory* function is the cause of a patient's imbalance or falls, this can only be *indirectly* inferred from the pattern of *motor* outputs. Similar to compensatory adjustments of the VOR by the oculomotor limb of the VOR, the results of posturographic assessments must be considered in light of potential downstream alterations in the motor limb of the vestibulospinal reflexes. In an oversimplified example, consider for a moment the optimal output of the vestibulospinal reflex in response to a perturbation, such as a sudden translation of the head. If the vestibular afferents, due to an age-related loss of hair cells (214), trigger a motor response that compensates for only 80% of the perturbation, the descending motor system could (in theory) simply boost its gain to 120% and the net output of postural sway will mirror a system with normal vestibular function. Redundancies and compensatory mechanisms, while beneficial to maintain mobility and prevent falls, can make isolating the cause of balance disturbance a daunting task;

such limitations motivate attempts to directly stimulate the vestibular labyrinth.

Beyond head motion, GVS may provide the most direct method for measuring the descending vestibular reflexes. The interpretation of GVS is however bounded by the dependence of the motor outputs on the context of the experimental task (234). Width of the base of support (91, 235), upper extremity support (96), availability of vision (96, 235, 236), reliability of proprioceptive feedback (234, 235), and testing posture (sitting vs. standing) (91, 96) have each been shown to modulate the magnitude of GVS induced EMG and/or postural responses, and thus can result in attenuated or enhanced responses to GVS, *independent of the integrity of the descending vestibular pathways*. The use of GVS paradigms in older adults can therefore only be interpreted relative to the reliability of extra-vestibular sensory cues [somatosensory (236, 237) and visual (234)] which are known to also decline with age (14, 118, 238, 239). Comparing responses to GVS in healthy older adults to older adults with vestibular decline, using tightly controlled experimental conditions that control for age-related visual and somatosensory loss, could however yield an interesting avenue for future research.

The limitations of existing assessments have motivated our recent study of vestibular perceptual thresholds as an assay of vestibular noise (17, 22, 190). As mentioned above, research out of our lab identified a significant association between 0.2 Hz roll tilt perceptual thresholds and age-related imbalance, yet, we emphasize that we are not suggesting that an inability to perceive roll-tilt is the cause of age-related balance impairment. We instead put forward the hypothesis that age-related changes in roll tilt vestibular thresholds reflect central vestibular noise that affects both perception and balance and thus may provide a method to quantify contributions of the central vestibular system to age-related balance impairment. The significant mediating effect of roll tilt thresholds and balance may therefore implicate central vestibular noise as a principle contributor to age-related imbalance. Considering that the participants studied were without symptoms of vestibular impairment, the observed age-related increase in vestibular thresholds also highlights the potential impact of sub-threshold (i.e., below the threshold for triggering symptoms) vestibular noise on age-related imbalance.

Although speculative, one potential explanation for this association is an age-related increase in noise within a specialized class of neurons within the vestibular nuclei [vestibular-only (VO) neurons] that act as relays for both vestibulospinal control and self-motion perception [see (240) for a review]. As justification for this hypothesis, the VOR and self-motion perceptual pathways relay through different neurons in the VN, and as such show qualitatively dissimilar behavior (193, 194). As an alternative explanation, since the perception of tilt is dependent upon one's ability to use vertical canal cues to disambiguate changes in net gravitoinertial force sensed by the otoliths (195), roll tilt thresholds may instead more generally represent a measure of age-related changes in central canal-otolith integration. Wiesmeir showed that postural responses to pseudorandom tilts of the support surface differed significantly between young and older adults within the frequency range (0.15–0.40 Hz) (147) where canal and otolith cues have been shown to be optimally integrated when rotating about an earth horizontal axis (241). Similar performance between age groups at 0.05 Hz suggests that at frequencies below the threshold for vertical SCC activation, where otolith cues predominate, the gain of postural sway is instead unaffected by age (241). Such findings lend support to our hypothesis that an age-associated increase in central vestibular noise, manifesting as a breakdown in central canal-otolith integration, may serve as a principle contributor to age-related balance declines.

While such explanations are plausible, as of now empirical proof is lacking, thus it does remain possible that roll tilt perceptual thresholds and balance are simply parallel yet independent consequences of aging. However as previously stated by Karmali et al. (190), this alternative is unlikely given that one would expect that if a common central nervous system pathology caused the correlation between roll tilt thresholds and balance, that most, if not all, vestibular thresholds, not just 0.2 Hz roll tilt, would display this same predictive relationship. Nevertheless, correlation does not equal causation, therefore additional studies are needed to (1) determine if the relationship between vestibular noise and age-related balance impairment is indeed causal, (2) to confirm or refute these findings in an independent sample of older adults, and (3) determine the mechanism explaining the association. Determining if alternative measures of vestibular noise, such as the vestibular time constant (199, 212) or measures of VOR variability (242), display similar associations with age-related balance impairment may provide further insights.

Summary

A standardized method for determining the specific contributions of the vestibular system to age-related balance impairment has yet to be developed. Although traditional measures of vestibular function allow one to infer the integrity

TABLE 3 | Summary of main findings.

- The video head impulse test and measures of dynamic visual acuity correlate with imbalance in older adults; tests of the low frequency VOR (i.e., caloric irrigation and rotational chair testing) do not.
- Clinical and instrumented balance tests capture age-related changes in balance performance but are limited in their capacity to isolate specific vestibular contributors (canal versus otolith versus central processing, etc.) to balance dysfunction.
- Postural responses to galvanic vestibular stimulation are attenuated in older adults yet the relevance of this finding to age-related imbalance is unclear.
- Biased perceptions of subjective postural vertical and subjective visual vertical correlate with imbalance in older adults suggesting that age-related changes in multisensory integration may contribute to age-related imbalance.
- Increased vestibular noise, quantified by roll tilt vestibular thresholds, is a significant predictor of sub-clinical balance impairment in asymptomatic older adults; this finding suggests that roll tilt vestibular thresholds may reflect a shared source of central vestibular rnoise affecting both the balance and perceptual pathways of older adults.

of the peripheral or central vestibular structures, the extent by which they capture the specific subclinical age-related changes that affect the vestibular balance pathways appears limited (**Table 3**). Standardized balance assessments are sensitive to acute vestibular lesions and predict fall risk, yet, fail to account for the multi-modal nature of the vestibular system. One hypothesis arising from recent basic research (17, 22, 23, 190) is that roll tilt vestibular thresholds reflect central vestibular noise that affects both perception and balance and thus may provide a method to quantify contributions of the central vestibular system to age-related balance impairment. Identifying a method to detect vestibular contributions to age-related postural instability would support efforts to screen for vestibular mediated fall risk and could potentially permit earlier implementation of targeted rehabilitative interventions.

AUTHOR CONTRIBUTIONS

AW and DM conceptualized the manuscript. AW created the initial draft of the manuscript. OA, AC, KB, and DM contributed to the writing and editing of the manuscript. All authors contributed to the article and approved the submitted version.

FUNDING

DM was funded by NIH/NIDCD R01-DC014924. DM, AC, and KB were funded by DoD Congressionally Directed Medical Research Program (CDMRP) grant W81XWH1920003. AC was funded by NIH/NIA R42-AG062065. AW was funded in part by a Promotion of Doctoral Studies (PODS) I Scholarship from the Foundation for Physical Therapy Research.

REFERENCES

1. Burns E, Kakara R. Deaths from falls among persons aged ≥65 years - United States, 2007-2016. *MMWR Morb Mortal Wkly Rep*. (2018) 67:509–14. doi: 10.15585/mmwr.mm6718a1
2. Bergen G, Stevens MR, Burns ER. Falls and fall injuries among adults aged ≥65 years - United States, 2014. *MMWR Morb Mortal Wkly Rep*. (2016) 65:993–8. doi: 10.15585/mmwr.mm6537a2
3. Florence CS, Bergen G, Atherly A, Burns E, Stevens J, Drake C. Medical costs of fatal and nonfatal falls in older adults: medical costs of falls. *J Am Geriatr Soc*. (2018) 66:693–8. doi: 10.1111/jgs.15304
4. Houry D, Florence C, Baldwin G, Stevens J, McClure R. The CDC injury center's response to the growing public health problem of falls among older adults. *Am J Lifestyle Med*. (2016) 10:74–7. doi: 10.1177/1559827615600137
5. Guirguis-Blake JM, Michael YL, Perdue LA, Coppola EL, Beil TL. Interventions to prevent falls in older adults: updated evidence report and systematic review for the US Preventive Services Task Force. *JAMA*. (2018) 319:1705. doi: 10.1001/jama.2017.21962
6. Gillespie LD, Robertson MC, Gillespie WJ, Sherrington C, Gates S, Clemson LM, et al. Interventions for preventing falls in older people living in the community. *Cochrane Database Syst Rev*. (2012) 9:CD007146. doi: 10.1002/14651858.CD007146.pub3
7. Blake AJ, Morgan K, Bendall MJ, Dallosso H, Ebrahim SBJ, Arie THD, et al. FALLS BY ELDERLY PEOPLE AT HOME: PREVALENCE AND ASSOCIATED FACTORS. *Age Ageing*. (1988) 17:365–72. doi: 10.1093/ageing/17.6.365
8. Tinetti ME, Speechley M, Ginter SF. Risk factors for falls among elderly persons living in the community. *N Engl J Med*. (1988) 319:1701–7. doi: 10.1056/NEJM198812293192604
9. Nevitt MC. Risk factors for recurrent nonsyncopal falls: a prospective study. *JAMA*. (1989) 261:2663. doi: 10.1001/jama.1989.03420180087036
10. Bergland A. Risk factors for serious fall related injury in elderly women living at home. *Inj Prev*. (2004) 10:308–13. doi: 10.1136/ip.2003.004721
11. Bergland A, Jarnlo G-B, Laake K. Predictors of falls in the elderly by location. *Aging Clin Exp Res*. (2003) 15:43–50. doi: 10.1007/BF03324479
12. Muir SW, Berg K, Chesworth B, Klar N, Speechley M. Quantifying the magnitude of risk for balance impairment on falls in community-dwelling older adults: a systematic review and meta-analysis. *J Clin Epidemiol*. (2010) 63:389–406. doi: 10.1016/j.jclinepi.2009.06.010
13. Horak FB. Clinical measurement of postural control in adults. *Phys Ther*. (1987) 67:1881–5. doi: 10.1093/ptj/67.12.1881
14. Lord SR, Clark RD, Webster IW. Postural stability and associated physiological factors in a population of aged persons. *J Gerontol*. (1991) 46:M69–M76. doi: 10.1093/geronj/46.3.M69
15. Anson E, Bigelow RT, Swenor B, Deshpande N, Studenski S, Jeka JJ, et al. Loss of peripheral sensory function explains much of the increase in postural sway in healthy older adults. *Front Aging Neurosci*. (2017) 9:202. doi: 10.3389/fnagi.2017.00202
16. Deshpande N, Simonsick E, Metter EJ, Ko S, Ferrucci L, Studenski S. Ankle proprioceptive acuity is associated with objective as well as self-report measures of balance, mobility, and physical function. *AGE*. (2016) 38:53. doi: 10.1007/s11357-016-9918-x
17. Beylergil SB, Karmali F, Wang W, Bermúdez Rey MC, Merfeld DM. Vestibular roll tilt thresholds partially mediate age-related effects on balance. In: John Leigh R, Ramat S, Shaikh A, editors. *Progress in Brain Research* (Amsterdam: Elsevier). p. 249-67.
18. Hong T, Mitchell P, Burlutsky G, Samarawickrama C, Wang JJ. Visual impairment and the incidence of falls and fractures among older people: longitudinal findings from the blue mountains eye study. *Investig Opthalmol Vis Sci*. (2014) 55:7589. doi: 10.1167/iovs.14-14262
19. Semenov YR, Bigelow RT, Xue Q-L, Lac S du, Agrawal Y. Association between vestibular and cognitive function in U.S. adults: data from the national health and nutrition examination survey. *J Gerontol A Biol Sci Med Sci*. (2016) 71:243–50. doi: 10.1093/gerona/glv069
20. Carter ND, Khan KM, Mallinson A, Janssen PA, Heinonen A, Petit MA, McKay HA, Fall-Free BC Research Group. Knee extension strength is a significant determinant of static and dynamic balance as well as quality of life in older community-dwelling women with osteoporosis. *Gerontology*. (2002) 48:360–8. doi: 10.1159/000065504
21. Muehlbauer T, Gollhofer A, Granacher U. Associations between measures of balance and lower-extremity muscle strength/power in healthy individuals across the lifespan: a systematic review and meta-analysis. *Sports Med Auckl NZ*. (2015) 45:1671–92. doi: 10.1007/s40279-015-0390-z
22. Bermúdez Rey MC, Clark TK, Wang W, Leeder T, Bian Y, Merfeld DM. Vestibular perceptual thresholds increase above the age of 40. *Front Neurol*. (2016) 7:162. doi: 10.3389/fneur.2016.00162
23. Agrawal Y, Carey JP, Della Santina CC, Schubert MC, Minor LB. Disorders of balance and vestibular function in US adults: data from the National Health and Nutrition Examination Survey, 2001-2004. *Arch Intern Med*. (2009) 169:938. doi: 10.1001/archinternmed.2009.66
24. Lin HW, Bhattacharyya N. Balance disorders in the elderly: epidemiology and functional impact. *Laryngoscope*. (2012) 122:1858–61. doi: 10.1002/lary.23376
25. Hall CD, Heusel-Gillig L, Tusa RJ, Herdman SJ. Efficacy of gaze stability exercises in older adults with dizziness. *J Neurol Phys Ther*. (2010) 34:64–9. doi: 10.1097/NPT.0b013e3181dde6d8
26. Scherer M, Migliaccio AA, Schubert MC. Effect of vestibular rehabilitation on passive dynamic visual acuity. *J Vestib Res*. (2008) 18:147–57.
27. Schubert MC, Della Santina CC, Shelhamer M. Incremental angular vestibulo-ocular reflex adaptation to active head rotation. *Exp Brain Res*. (2008) 191:435–46. doi: 10.1007/s00221-008-1537-z

28. Herdman SJ, Schubert MC, Das VE, Tusa RJ. Recovery of dynamic visual acuity in unilateral vestibular hypofunction. *Arch Otolaryngol Neck Surg.* (2003) 129:819. doi: 10.1001/archotol.129.8.819
29. Herdman SJ, Hall CD, Schubert MC, Das VE, Tusa RJ. Recovery of dynamic visual acuity in bilateral vestibular hypofunction. *Arch Otolaryngol Head Neck Surg.* (2007) 133:383–9. doi: 10.1001/archotol.133.4.383
30. Hillier SL, Hollohan V. Vestibular rehabilitation for unilateral peripheral vestibular dysfunction. *Cochrane Database Syst Rev.* (2007) 4:CD005397. doi: 10.1002/14651858.CD005397.pub2
31. McDonnell MN, Hillier SL. Vestibular rehabilitation for unilateral peripheral vestibular dysfunction. *Cochrane Database Syst Rev.* (2015) 1:CD005397. doi: 10.1002/14651858.CD005397.pub4
32. Hillier SL, McDonnell M. Vestibular rehabilitation for unilateral peripheral vestibular dysfunction. *Cochrane Database Syst Rev.* (2011) 2:CD005397. doi: 10.1002/14651858.CD005397.pub3
33. Pothula VB, Chew F, Lesser THJ, Sharma AK. Falls and vestibular impairment. *Clin Otolaryngol Allied Sci.* (2004) 29:179–82. doi: 10.1111/j.0307-7772.2004.00785.x
34. Baloh RW, Enrietto J, Jacobson KM, Lin A. Age-related changes in vestibular function: a longitudinal study. *Ann N Y Acad Sci.* (2001) 942:210–9. doi: 10.1111/j.1749-6632.2001.tb03747.x
35. Peterka R, Black FO. Age-related changes in human vestibulo-ocular reflexes: sinusoidal rotation and caloric tests. *J Vestib Res.* (1990) 1:49–59.
36. Peterka R, Black FO. Age-related changes in human posture control: sensory organization tests. *J Vestib Res.* (1990) 1:73–85.
37. Peterka RJ. Sensorimotor integration in human postural control. *J Neurophysiol.* (2002) 88:1097–118. doi: 10.1152/jn.2002.88.3.1097
38. Horak FB. Postural compensation for vestibular loss. *Ann N Y Acad Sci.* (2009) 1164:76–81. doi: 10.1111/j.1749-6632.2008.03708.x
39. Agrawal Y, Merfeld DM, Horak FB, Redfern MS, Manor B, Westlake KP, et al. Aging, vestibular function, and balance: proceedings of a National Institute on Aging/National Institute on Deafness and Other Communication Disorders Workshop. *J Gerontol Ser A.* (2020) 75:2471–80. doi: 10.1093/gerona/glaa097
40. Shepard NT, Jacobson GP. The caloric irrigation test. In: Furman J, Lempert T, editors. *Handbook of Clinical Neurology* (Amsterdam: Elsevier). p. 119–31.
41. Jacobson GP, McCaslin DL, Piker EG, Gruenwald J, Grantham S, Tegel L. Insensitivity of the "Romberg test of standing balance on firm and compliant support surfaces" to the results of caloric and VEMP tests. *Ear Hear.* (2011) 32:e1–5. doi: 10.1097/AUD.0b013e31822802bb
42. Whitney SL, Marchetti GF, Schade AI. The relationship between falls history and computerized dynamic posturography in persons with balance and vestibular disorders. *Arch Phys Med Rehabil.* (2006) 87:402–7. doi: 10.1016/j.apmr.2005.11.002
43. Furman JM. Rotational testing. In: Furman J, Lempert T, editors. *Handbook of Clinical Neurology* (Amsterdam: Elsevier). p. 177–86.
44. Baloh RW, Ying SH, Jacobson KM. A longitudinal study of gait and balance dysfunction in normal older people. *Arch Neurol.* (2003) 60:835–9. doi: 10.1001/archneur.60.6.835
45. Kerber KA, Ishiyama GP, Baloh RW. A longitudinal study of oculomotor function in normal older people. *Neurobiol Aging.* (2006) 27:1346–53. doi: 10.1016/j.neurobiolaging.2005.07.009
46. Kerber KA, Enrietto JA, Jacobson KM, Baloh RW. Disequilibrium in older people: a prospective study. *Neurology.* (1998) 51:574–80. doi: 10.1212/WNL.51.2.574
47. Grossman GE, Leigh RJ, Bruce EN, Huebner WP, Lanska DJ. Performance of the human vestibuloocular reflex during locomotion. *J Neurophysiol.* (1989) 62:264–72. doi: 10.1152/jn.1989.62.1.264
48. Carriot J, Jamali M, Chacron MJ, Cullen KE. Statistics of the vestibular input experienced during natural self-motion: implications for neural processing. *J Neurosci.* (2014) 34:8347–57. doi: 10.1523/JNEUROSCI.0692-14.2014
49. Halmagyi GM, Curthoys IS. A clinical sign of canal paresis. *Arch Neurol.* (1988) 45:737–9. doi: 10.1001/archneur.1988.00520310043015
50. McCaslin DL, Jacobson GP, Bennett ML, Gruenwald JM, Green AP. Predictive properties of the video head impulse test: measures of caloric symmetry and self-report dizziness handicap. *Ear Hear.* (2014) 35:e185–e91. doi: 10.1097/AUD.0000000000000047
51. Grossman GE, Leigh RJ, Abel LA, Lanska DJ, Thurston SE. Frequency and velocity of rotational head perturbations during locomotion. *Exp Brain Res.* (1988) 70:470–6. doi: 10.1007/BF00247595
52. MacDougall HG, Weber KP, McGarvie LA, Halmagyi GM, Curthoys IS. The video head impulse test: diagnostic accuracy in peripheral vestibulopathy. *Neurology.* (2009) 73:1134–41. doi: 10.1212/WNL.0b013e3181bacf85
53. Yip CW, Glaser M, Frenzel C, Bayer O, Strupp M. Comparison of the bedside head-impulse test with the video head-impulse test in a clinical practice setting: a prospective study of 500 outpatients. *Front Neurol.* (2016) 7:58. doi: 10.3389/fneur.2016.00058
54. Lee J-Y, Kwon E, Kim H-J, Choi J-Y, Oh HJ, Koo J-W, et al. Dissociated results between caloric and video head impulse tests in dizziness: prevalence, pattern, lesion location, and etiology. *J Clin Neurol.* (2020) 16:277. doi: 10.3988/jcn.2020.16.2.277
55. Newman-Toker DE, Curthoys IS, Halmagyi GM. Diagnosing stroke in acute vertigo: the HINTS family of eye movement tests and the future of the "Eye ECG." *Semin Neurol.* (2015) 35:506–21. doi: 10.1055/s-0035-1564298
56. Mantokoudis G, Saber Tehrani AS, Wozniak A, Eibenberger K, Kattah JC, Guede CI, et al. VOR gain by head impulse video-oculography differentiates acute vestibular neuritis from stroke. *Otol Neurotol.* (2015) 36:457–65. doi: 10.1097/MAO.0000000000000638
57. Newman-Toker DE, Saber Tehrani AS, Mantokoudis G, Pula JH, Guede CI, Kerber KA, et al. Quantitative video-oculography to help diagnose stroke in acute vertigo and dizziness: toward an ECG for the eyes. *Stroke.* (2013) 44:1158–61. doi: 10.1161/STROKEAHA.111.000033
58. Anson E, Pineault K, Bair W, Studenski S, Agrawal Y. Reduced vestibular function is associated with longer, slower steps in healthy adults during normal speed walking. *Gait Posture.* (2019) 68:340–5. doi: 10.1016/j.gaitpost.2018.12.016
59. Xie Y, Anson ER, Simonsick EM, Studenski SA, Agrawal Y. Compensatory saccades are associated with physical performance in older adults: data from the baltimore longitudinal study of aging. *Otol Neurotol.* (2017) 38:373–8. doi: 10.1097/MAO.0000000000001301
60. Herdman SJ. *Vestibular Rehabilitation, 4th edn*. Philadelphia, PA: F.A. Davis Company (2014).
61. Agrawal Y, Davalos-Bichara M, Zuniga MG, Carey JP. Head impulse test abnormalities and influence on gait speed and falls in older individuals. *Otol Neurotol.* (2013) 34:1729–35. doi: 10.1097/MAO.0b013e318295313c
62. Davalos-Bichara M, Agrawal Y. Normative results of healthy older adults on standard clinical vestibular tests. *Otol Neurotol.* (2014) 35:297–300. doi: 10.1097/MAO.0b013e3182a09ca8
63. Herdman SJ, Tusa RJ, Blatt P, Suzuki A, Venuto PJ, Roberts D. Computerized dynamic visual acuity test in the assessment of vestibular deficits. *Am J Otol.* (1998) 19:790–6.
64. Herdman SJ, Schubert MC, Tusa RJ. Role of central preprogramming in dynamic visual acuity with vestibular loss. *Arch Otolaryngol Neck Surg.* (2001) 127:1205. doi: 10.1001/archotol.127.10.1205
65. Verbecque E, Van Criekinge T, Vanloot D, Coeckelbergh T, Van de Heyning P, Hallemans A, et al. Dynamic Visual Acuity test while walking or running on treadmill: reliability and normative data. *Gait Posture.* (2018) 65:137–42. doi: 10.1016/j.gaitpost.2018.07.166
66. Lord SR, Lloyd DG, Li SK. Sensori-motor function, gait patterns and falls in community-dwelling women. *Age Ageing.* (1996) 25:292–9. doi: 10.1093/ageing/25.4.292
67. Lord S, Castell S. Effect of exercise on balance, strength and reaction time in older people. *Aust J Physiother.* (1994) 40:83–8. doi: 10.1016/S0004-9514(14)60454-2
68. Lord SR, Ward JA. Age-associated differences in sensori-motor function and balance in community dwelling women. *Age Ageing.* (1994) 23:452–60. doi: 10.1093/ageing/23.6.452
69. Lord S, Sturnieks D. The physiology of falling: assessment and prevention strategies for older people. *J Sci Med Sport.* (2005) 8:35–42. doi: 10.1016/S1440-2440(05)80022-2
70. Goebel JA, Tungsiripat N, Sinks B, Carmody J. Gaze stabilization test: a new clinical test of unilateral vestibular dysfunction. *Otol Neurotol Off Publ Am Otol Soc Am Neurotol Soc Eur Acad Otol Neurotol.* (2007) 28:68–73. doi: 10.1097/01.mao.0000244351.42201.a7

71. Ward BK, Mohammed MT, Brach JS, Studenski SA, Whitney SL, Furman JM. Physical performance and a test of gaze stabilization in older adults. *Otol Neurotol.* (2010) 31:168–72. doi: 10.1097/MAO.0b013e3181c4c3e2
72. Honaker JA, Lee C, Shepard NT. Clinical use of the gaze stabilization test for screening falling risk in community-dwelling older adults. *Otol Neurotol Off Publ Am Otol Soc Am Neurotol Soc Eur Acad Otol Neurotol.* (2013) 34:729–35. doi: 10.1097/MAO.0b013e31827d8a5f
73. Whitney SL, Marchetti GF, Pritcher M, Furman JM. Gaze stabilization and gait performance in vestibular dysfunction. *Gait Posture.* (2009) 29:194–8. doi: 10.1016/j.gaitpost.2008.08.002
74. Hunter JB, Patel NS, O'Connell BP, Carlson ML, Shepard NT, McCaslin DL, et al. Cervical and ocular VEMP testing in diagnosing superior semicircular canal dehiscence. *Otolaryngol Neck Surg.* (2017) 156:917–23. doi: 10.1177/0194599817690720
75. Colebatch JG, Rosengren SM, Welgampola MS. Vestibular-evoked myogenic potentials. In: Furman J, Lempert T, editors. *Handbook of Clinical Neurology* (Amsterdam: Elsevier). p. 133–55.
76. McCaslin DL, Jacobson GP, Grantham SL, Piker EG, Verghese S. The influence of unilateral saccular impairment on functional balance performance and self-report dizziness. *J Am Acad Audiol.* (2011) 22:542–9; quiz 560–1. doi: 10.3766/jaaa.22.8.6
77. Layman AJ, Li C, Simonsick E, Ferrucci L, Carey JP, Agrawal Y. Association between saccular function and gait speed: data from the baltimore longitudinal study of aging. *Otol Neurotol.* (2015) 36:260–6. doi: 10.1097/MAO.0000000000000544
78. Xie YJ, Liu EY, Anson ER, Agrawal Y. Age-Related imbalance is associated with slower walking speed: an analysis from the National Health and Nutrition Examination Survey. *J Geriatr Phys Ther.* (2017) 40:183–9. doi: 10.1519/JPT.0000000000000093
79. Rudisill HE, Hain TC. Lower extremity myogenic potentials evoked by acoustic stimuli in healthy adults. *Otol Neurotol Off Publ Am Otol Soc Am Neurotol Soc Eur Acad Otol Neurotol.* (2008) 29:688–92. doi: 10.1097/MAO.0b013e3181730377
80. Cherchi M, Bellinaso NP, Card K, Covington A, Krumpe A, Pfeifer MS, et al. Sound evoked triceps myogenic potentials. *Otol Neurotol.* (2009) 30:545–50. doi: 10.1097/MAO.0b013e31819d89eb
81. Brooke RE, Herbert NC, Thyer NJ. Repeatability of sound-evoked triceps myogenic potentials. *Int J Audiol.* (2014) 53:880–6. doi: 10.3109/14992027.2014.938780
82. Kim J, Curthoys IS. Responses of primary vestibular neurons to galvanic vestibular stimulation (GVS) in the anaesthetised guinea pig. *Brain Res Bull.* (2004) 64:265–71. doi: 10.1016/j.brainresbull.2004.07.008
83. Goldberg JM, Smith CE, Fernandez C. Relation between discharge regularity and responses to externally applied galvanic currents in vestibular nerve afferents of the squirrel monkey. *J Neurophysiol.* (1984) 51:1236–56. doi: 10.1152/jn.1984.51.6.1236
84. Curthoys IS, MacDougall HG. What galvanic vestibular stimulation actually activates. *Front Neurol.* (2012) 3:117. doi: 10.3389/fneur.2012.00117
85. Welgampola MS, Ramsay E, Gleeson MJ, Day BL. Asymmetry of balance responses to monaural galvanic vestibular stimulation in subjects with vestibular schwannoma. *Clin Neurophysiol.* (2013) 124:1835–9. doi: 10.1016/j.clinph.2013.03.015
86. Tax CMW, Bom AP, Taylor RL, Todd N, Cho K-KJ, Fitzpatrick RC, et al. The galvanic whole-body sway response in health and disease. *Clin Neurophysiol.* (2013) 124:2036–45. doi: 10.1016/j.clinph.2012.12.041
87. Cauquil AS, Bousquet P, Salon M-CC, Dupui P, Bessou P. Monaural and binaural galvanic vestibular stimulation in human dynamic balance function. *Gait Posture.* (1997) 6:210–7. doi: 10.1016/S0966-6362(97)00011-8
88. Watson SR, Brizuela AE, Curthoys IS, Colebatch JG, MacDougall HG, Halmagyi GM. Maintained ocular torsion produced by bilateral and unilateral galvanic (DC) vestibular stimulation in humans. *Exp Brain Res.* (1998) 122:453–8. doi: 10.1007/s002210050533
89. MacDougall HG, Brizuela AE, Burgess AM, Curthoys IS, Halmagyi GM. Patient and normal three-dimensional eye-movement responses to maintained (DC) surface galvanic vestibular stimulation. *Otol Neurotol.* (2005) 26:500–11. doi: 10.1097/01.mao.0000169766.08421.ef
90. MacDougall HG, Brizuela AE, Burgess AM, Curthoys IS. Between-subject variability and within-subject reliability of the human eye-movement response to bilateral galvanic (DC) vestibular stimulation. *Exp Brain Res.* (2002) 144:69–78. doi: 10.1007/s00221-002-1038-4
91. Day BL, Séverac Cauquil A, Bartolomei L, Pastor MA, Lyon IN. Human body-segment tilts induced by galvanic stimulation: a vestibularly driven balance protection mechanism. *J Physiol.* (1997) 500:661–72. doi: 10.1113/jphysiol.1997.sp022051
92. Fitzpatrick RC, Marsden J, Lord SR, Day BL. Galvanic vestibular stimulation evokes sensations of body rotation. *NeuroReport.* (2002) 13:2379–83. doi: 10.1097/00001756-200212200-00001
93. Peters RM, Blouin J-S, Dalton BH, Inglis JT. Older adults demonstrate superior vestibular perception for virtual rotations. *Exp Gerontol.* (2016) 82:50–7. doi: 10.1016/j.exger.2016.05.014
94. Fitzpatrick RC, Day BL. Probing the human vestibular system with galvanic stimulation. *J Appl Physiol.* (2004) 96:2301–16. doi: 10.1152/japplphysiol.00008.2004
95. Watson SRD, Colebatch JG. Vestibular-evoked electromyographic responses in soleus: a comparison between click and galvanic stimulation. *Exp Brain Res.* (1998) 119:504–10. doi: 10.1007/s002210050366
96. Britton TC, Day BL, Brown P, Rothwell JC, Thompson PD, Marsden CD. Postural electromyographic responses in the arm and leg following galvanic vestibular stimulation in man. *Exp Brain Res.* (1993) 94:143–51. doi: 10.1007/BF00230477
97. Dlugaiczyk J, Gensberger KD, Straka H. Galvanic vestibular stimulation: from basic concepts to clinical applications. *J Neurophysiol.* (2019) 121:2237–55. doi: 10.1152/jn.00035.2019
98. Curthoys IS. A critical review of the neurophysiological evidence underlying clinical vestibular testing using sound, vibration and galvanic stimuli. *Clin Neurophysiol.* (2010) 121:132–44. doi: 10.1016/j.clinph.2009.09.027
99. Welgampola M, Colebatch J. Selective effects of ageing on vestibular-dependent lower limb responses following galvanic stimulation. *Clin Neurophysiol.* (2002) 113:528–34. doi: 10.1016/S1388-2457(02)00020-2
100. Dalton BH, Blouin J-S, Allen MD, Rice CL, Inglis JT. The altered vestibular-evoked myogenic and whole-body postural responses in old men during standing. *Exp Gerontol.* (2014) 60:120–8. doi: 10.1016/j.exger.2014.09.020
101. Deshpande N, Patla AE. Postural responses and spatial orientation to neck proprioceptive and vestibular inputs during locomotion in young and older adults. *Exp Brain Res.* (2005) 167:468–74. doi: 10.1007/s00221-005-0182-z
102. Fregly AR, Graybiel A. Labyrinthine defects as shown by ataxia and caloric tests. *Acta Otolaryngol (Stockh).* (1970) 69:216–22. doi: 10.3109/00016487009123356
103. Longridge NS, Mallinson AI. Clinical romberg testing does not detect vestibular disease. *Otol Neurotol.* (2010) 31:803–6. doi: 10.1097/MAO.0b013e3181e3deb2
104. Nashner LM. A model describing vestibular detection of body sway motion. *Acta Otolaryngol (Stockh).* (1971) 72:429–36. doi: 10.3109/00016487109122504
105. Nashner LM, Black FO, Wall C. Adaptation to altered support and visual conditions during stance: patients with vestibular deficits. *J Neurosci Off J Soc Neurosci.* (1982) 2:536–44. doi: 10.1523/JNEUROSCI.02-05-00536.1982
106. Nashner LM, Peters JF. Dynamic posturography in the diagnosis and management of dizziness and balance disorders. *Neurol Clin.* (1990) 8:331–49. doi: 10.1016/S0733-8619(18)30359-1
107. Horak FB, Nashner LM, Diener HC. Postural strategies associated with somatosensory and vestibular loss. *Exp Brain Res.* (1990) 82:167–77. doi: 10.1007/BF00230848
108. Mishra A, Davis S, Speers R, Shepard NT. Head shake computerized dynamic posturography in peripheral vestibular lesions. *Am J Audiol.* (2009) 18:53–9. doi: 10.1044/1059-0889(2009/06-0024)
109. Honaker JA, Janky KL, Patterson JN, Shepard NT. Modified head shake sensory organization test: Sensitivity and specificity. *Gait Posture.* (2016) 49:67–72. doi: 10.1016/j.gaitpost.2016.06.024
110. Broglio SP, Sosnoff JJ, Rosengren KS, McShane K. A comparison of balance performance: computerized dynamic posturography and a random motion platform. *Arch Phys Med Rehabil.* (2009) 90:145–50. doi: 10.1016/j.apmr.2008.06.025

111. Cass SP, Kartush JM, Graham MD. Clinical assessment of postural stability following vestibular nerve section. *Laryngoscope.* (1991) 101:1056–9. doi: 10.1288/00005537-199110000-00005
112. Cass SP, Kartush JM, Graham MD. Patterns of vestibular function following vestibular nerve section. *Laryngoscope.* (1992) 102:388–94. doi: 10.1288/00005537-199204000-00004
113. Black FO, Shupert CL, Peterka RJ, Nashner LM. Effects of unilateral loss of vestibular function on the vestibulo-ocular reflex and postural control. *Ann Otol Rhinol Laryngol.* (1989) 98:884–9. doi: 10.1177/000348948909801109
114. Fetter M, Diener HC, Dichgans J. Recovery of postural control after an acute unilateral vestibular lesion in humans. *J Vestib Res Equilib Orientat.* (1990) 1:373–83.
115. Barin K, Seitz CM, Welling DB. Effect of head orientation on the diagnostic sensitivity of posturography in patients with compensated unilateral lesions. *Otolaryngol Head Neck Surg Off J Am Acad Otolaryngol-Head Neck Surg.* (1992) 106:355–62. doi: 10.1177/019459989210600407
116. Forbes PA, Chen A, Blouin J-S. Sensorimotor control of standing balance. *Handb Clin Neurol.* (2018) 159:61–83. doi: 10.1016/B978-0-444-63916-5.00004-5
117. Johari K, den Ouden D-B, Behroozmand R. Effects of aging on temporal predictive mechanisms of speech and hand motor reaction time. *Aging Clin Exp Res.* (2018) 30:1195–202. doi: 10.1007/s40520-018-0902-4
118. Ko S-U, Simonsick E, Deshpande N, Ferrucci L. Sex-specific age associations of ankle proprioception test performance in older adults: results from the Baltimore Longitudinal Study of Aging. *Age Ageing.* (2015) 44:485–90. doi: 10.1093/ageing/afv005
119. Hamid MA, Hughes GB, Kinney SE. Specificity and sensitivity of dynamic posturography. A retrospective analysis. *Acta Oto-Laryngol Suppl.* (1991) 481:596–600. doi: 10.3109/00016489109131480
120. Ford-Smith CD, Wyman JF, Elswick RK, Fernandez T, Newton RA. Test-retest reliability of the sensory organization test in noninstitutionalized older adults. *Arch Phys Med Rehabil.* (1995) 76:77–81. doi: 10.1016/S0003-9993(95)80047-6
121. Voorhees RL. Dynamic posturography findings in central nervous system disorders. *Otolaryngol Neck Surg.* (1990) 103:96–101. doi: 10.1177/019459890103000114
122. Whipple R, Wolfson L, Derby C, Singh D, Tobin J. Altered sensory function and balance in older persons. *J Gerontol.* (1993) 48:71–6. doi: 10.1093/geronj/48.Special_Issue.71
123. Woollacott MH, Shumway-Cook A, Nashner LM. Aging and posture control: changes in sensory organization and muscular coordination. *Int J Aging Hum Dev.* (1986) 23:97–114. doi: 10.2190/VXN3-N3RT-54JB-X16X
124. Ledin T, Kronhed AC, Möller C, Möller M, Odkvist LM, Olsson B. Effects of balance training in elderly evaluated by clinical tests and dynamic posturography. *J Vestib Res Equilib Orientat.* (1990) 1:129–38.
125. Peterka RJ. Postural control model interpretation of stabilogram diffusion analysis. *Biol Cybern.* (2000) 82:335–43. doi: 10.1007/s004220050587
126. Wolfson L, Whipple R, Derby CA, Amerman P, Murphy T, Tobin JN, et al. A dynamic posturography study of balance in healthy elderly. *Neurology.* (1992) 42:2069–75. doi: 10.1212/WNL.42.11.2069
127. Pedalini MEB, Cruz OLM, Bittar RSM, Lorenzi MC, Grasel SS. Sensory organization test in elderly patients with and without vestibular dysfunction. *Acta Otolaryngol (Stockh).* (2009) 129:962–5. doi: 10.1080/00016480802468930
128. Horak FB, Shupert CL, Mirka A. Components of postural dyscontrol in the elderly: a review. *Neurobiol Aging.* (1989) 10:727–38. doi: 10.1016/0197-4580(89)90010-9
129. Di Fabio RP. Sensitivity and specificity of platform posturography for identifying patients with vestibular dysfunction. *Phys Ther.* (1995) 75:290–305. doi: 10.1093/ptj/75.4.290
130. Park MK, Lim H-W, Cho JG, Choi C-J, Hwang SJ, Chae SW. A head shake sensory organization test to improve the sensitivity of the sensory organization test in the elderly. *Otol Neurotol Off Publ Am Otol Soc Am Neurotol Soc Eur Acad Otol Neurotol.* (2012) 33:67–71. doi: 10.1097/MAO.0b013e318238f75f
131. Honaker JA, Boismier TE, Shepard NP, Shepard NT. Fukuda stepping test: sensitivity and specificity. *J Am Acad Audiol.* (2009) 20:311–4; quiz 335. doi: 10.3766/jaaa.20.5.4
132. Shumway-Cook A, Horak FB. Assessing the influence of sensory interaction of balance. Suggestion from the field. *Phys Ther.* (1986) 66:1548–50. doi: 10.1093/ptj/66.10.1548
133. Cohen H, Blatchly CA, Gombash LL. A study of the clinical test of sensory interaction and balance. *Phys Ther.* (1993) 73:346–51. doi: 10.1093/ptj/73.6.346
134. Cohen HS, Mulavara AP, Stitz J, Sangi-Haghpeykar H, Williams SP, Peters BT, et al. Screening for vestibular disorders using the modified clinical test of sensory interaction and balance and tandem walking with eyes closed. *Otol Neurotol Off Publ Am Otol Soc Am Neurotol Soc Eur Acad Otol Neurotol.* (2019) 40:658–65. doi: 10.1097/MAO.0000000000002173
135. Park MK, Kim K-M, Jung J, Lee N, Hwang SJ, Chae SW. Evaluation of uncompensated unilateral vestibulopathy using the modified clinical test for sensory interaction and balance. *Otol Neurotol Off Publ Am Otol Soc Am Neurotol Soc Eur Acad Otol Neurotol.* (2013) 34:292–6. doi: 10.1097/MAO.0b013e31827c9dae
136. Hong SK, Park JH, Kwon SY, Kim J-S, Koo J-W. Clinical efficacy of the Romberg test using a foam pad to identify balance problems: a comparative study with the sensory organization test. *Eur Arch Otorhinolaryngol.* (2015) 272:2741–7. doi: 10.1007/s00405-014-3273-2
137. Edginton Bigelow K, Berme N. Development of a protocol for improving the clinical utility of posturography as a fall-risk screening tool. *J Gerontol A Biol Sci Med Sci.* (2011) 66A:228–33. doi: 10.1093/gerona/glq202
138. Baloh RW, Jacobson KM, Enrietto JA, Corona S, Honrubia V. Balance disorders in older persons: quantification with posturography. *Otolaryngol Neck Surg.* (1998) 119:89–92. doi: 10.1016/S0194-5998(98)70177-9
139. Gilfriche P, Deschodt-Arsac V, Blons E, Arsac LM. Frequency-specific fractal analysis of postural control accounts for control strategies. *Front Physiol.* (2018) 9:293. doi: 10.3389/fphys.2018.00293
140. Hausdorff JM, Mitchell SL, Firtion R, Peng CK, Cudkowicz ME, Wei JY, et al. Altered fractal dynamics of gait: reduced stride-interval correlations with aging and Huntington's disease. *J Appl Physiol Bethesda Md (1985).* (1997) 82:262–9. doi: 10.1152/jappl.1997.82.1.262
141. Fernandez C, Goldberg JM. Physiology of peripheral neurons innervating semicircular canals of the squirrel monkey. *II. Response to sinusoidal stimulation and dynamics of peripheral vestibular system. J Neurophysiol.* (1971) 34:661–75. doi: 10.1152/jn.1971.34.4.661
142. Yeh J-R, Hsu L-C, Lin C, Chang F-L, Lo M-T. Nonlinear analysis of sensory organization test for subjects with unilateral vestibular dysfunction. *PLoS One.* (2014) 9:e91230. doi: 10.1371/journal.pone.0091230
143. Cenciarini M, Peterka RJ. Stimulus-dependent changes in the vestibular contribution to human postural control. *J Neurophysiol.* (2006) 95:2733–50. doi: 10.1152/jn.00856.2004
144. Peterka RJ, Statler KD, Wrisley DM, Horak FB. Postural compensation for unilateral vestibular loss. *Front Neurol.* (2011) 2:57. doi: 10.3389/fneur.2011.00057
145. Mantokoudis G, Schubert MC, Saber Tehrani AS, Wong AL, Agrawal Y. Early adaptation and compensation of clinical vestibular responses after unilateral vestibular deafferentation surgery. *Otol Neurotol.* (2014) 35:148–54. doi: 10.1097/MAO.0b013e3182956196
146. Cenciarini M, Loughlin PJ, Sparto PJ, Redfern MS. Medial-lateral postural control in older adults exhibits increased stiffness and damping. In: *2009 Annual International Conference of the IEEE Engineering in Medicine and Biology Society* (Minneapolis, MN: IEEE). p. 7006–7009.
147. Wiesmeier IK, Dalin D, Maurer C. Elderly use proprioception rather than visual and vestibular cues for postural motor control. *Front Aging Neurosci.* (2015) 7:97. doi: 10.3389/fnagi.2015.00097
148. Fukuda T. The stepping test: two phases of the labyrinthine reflex. *Acta Otolaryngol (Stockh).* (1959) 50:95–108. doi: 10.3109/00016485909129172
149. Honaker JA, Shepard NT. Performance of fukuda stepping test as a function of the severity of caloric weakness in chronic dizzy patients. *J Am Acad Audiol.* (2012) 23:616–22. doi: 10.3766/jaaa.23.8.6
150. Shumway-Cook A, Gruber W, Baldwin M, Liao S. The effect of multidimensional exercises on balance, mobility, and fall risk in community-dwelling older adults. *Phys Ther.* (1997) 77:46–57. doi: 10.1093/ptj/77.1.46
151. Wrisley DM, Kumar NA. Functional gait assessment: concurrent, discriminative, and predictive validity in community-dwelling

older adults. *Phys Ther.* (2010) 90:761–73. doi: 10.2522/ptj.20090069
152. Lusardi MM, Fritz S, Middleton A, Allison L, Wingood M, Phillips E, et al. Determining risk of falls in community dwelling older adults: a systematic review and meta-analysis using posttest probability. *J Geriatr Phys Ther.* (2017) 40:1–36. doi: 10.1519/JPT.0000000000000099
153. Whitney SL, Hudak MT, Marchetti GF. The dynamic gait index relates to self-reported fall history in individuals with vestibular dysfunction. *J Vestib Res Equilib Orientat.* (2000) 10:99–105.
154. Whitney SL, Marchetti GF, Schade A, Wrisley DM. The sensitivity and specificity of the Timed "Up & Go" and the Dynamic Gait Index for self-reported falls in persons with vestibular disorders. *J Vestib Res Equilib Orientat.* (2004) 14:397–409.
155. Beninato M, Fernandes A, Plummer LS. Minimal clinically important difference of the functional gait assessment in older adults. *Phys Ther.* (2014) 94:1594–603. doi: 10.2522/ptj.20130596
156. Gill-Body KM, Beninato M, Krebs DE. Relationship among balance impairments, functional performance, and disability in people with peripheral vestibular hypofunction. *Phys Ther.* (2000) 80:748–58. doi: 10.1093/ptj/80.8.748
157. Wrisley DM, Walker ML, Echternach JL, Strasnick B. Reliability of the dynamic gait index in people with vestibular disorders. *Arch Phys Med Rehabil.* (2003) 84:1528–33. doi: 10.1016/S0003-9993(03)00274-0
158. Chang T-P, Schubert MC. Association of the Video head impulse test with improvement of dynamic balance and fall risk in patients with dizziness. *JAMA Otolaryngol Neck Surg.* (2018) 144:696. doi: 10.1001/jamaoto.2018.0650
159. Panzer VP, Wakefield DB, Hall CB, Wolfson LI. Mobility assessment: sensitivity and specificity of measurement sets in older adults. *Arch Phys Med Rehabil.* (2011) 92:905–12. doi: 10.1016/j.apmr.2011.01.004
160. Pisciottano MVC, Pinto SS, Szejnfeld VL, Castro CHM. The relationship between lean mass, muscle strength and physical ability in independent healthy elderly women from the community. *J Nutr Health Aging.* (2014) 18:554–8. doi: 10.1007/s12603-013-0414-z
161. Dakin CJ, Rosenberg A. Gravity estimation and verticality perception. In: Day BL, Lord SR, editors. *Handbook of Clinical Neurology* (Amsterdam: Elsevier). p. 43–59.
162. Tobis JS, Reinsch S, Swanson JM, Byrd M, Scharf T. Visual perception dominance of fallers among community-dwelling older adults. *J Am Geriatr Soc.* (1985) 33:330–3. doi: 10.1111/j.1532-5415.1985.tb07132.x
163. Lord SR, Webster IW. Visual field dependence in elderly fallers and non-fallers. *Int J Aging Hum Dev.* (1990) 31:267–77. doi: 10.2190/38MH-2EF1-E36Q-75T2
164. Barr C, McLoughlin JV, van den Berg MEL, Sturnieks DL, Crotty M, Lord SR. Visual field dependence is associated with reduced postural sway, dizziness and falls in older people attending a falls clinic. *J Nutr Health Aging.* (2016) 20:671–5. doi: 10.1007/s12603-015-0681-y
165. Bisdorff AR, Wolsley CJ, Anastasopoulos D, Bronstein AM, Gresty MA. The perception of body verticality (subjective postural vertical) in peripheral and central vestibular disorders. *Brain J Neurol.* (1996) 119 (Pt 5):1523–34. doi: 10.1093/brain/119.5.1523
166. Böhmer A, Mast F. Assessing otolith function by the subjective visual vertical. *Ann N Y Acad Sci.* (1999) 871:221–31. doi: 10.1111/j.1749-6632.1999.tb09187.x
167. Böhmer A. The subjective visual vertical as a clinical parameter for acute and chronic vestibular (otolith) disorders. *Acta Otolaryngol (Stockh).* (1999) 119:126–7. doi: 10.1080/00016489950181495
168. Yardley L. Contribution of somatosensory information to perception of the visual vertical with body tilt and rotating visual field. *Percept Psychophys.* (1990) 48:131–4. doi: 10.3758/BF03207079
169. Mittelstaedt H. Somatic graviception. *Biol Psychol.* (1996) 42:53–74. doi: 10.1016/0301-0511(95)05146-5
170. Barbieri G, Gissot A-S, Pérennou D. Ageing of the postural vertical. *AGE.* (2010) 32:51–60. doi: 10.1007/s11357-009-9112-5
171. Manckoundia P, Mourey F, Pfitzenmeyer P, Hoecke JV, Pérennou D. Is backward disequilibrium in the elderly caused by an abnormal perception of verticality? A pilot study. *Clin Neurophysiol.* (2007) 118:786–93. doi: 10.1016/j.clinph.2006.11.274
172. Scheets PL, Sahrmann SA, Norton BJ, Stith JS, Crowner BE. What is backward disequilibrium and how do i treat it? A complex patient case study. *J Neurol Phys Ther JNPT.* (2015) 39:119–26. doi: 10.1097/NPT.0000000000000084
173. Menant JC, St George RJ, Fitzpatrick RC, Lord SR. Perception of the postural vertical and falls in older people. *Gerontology.* (2012) 58:497–503. doi: 10.1159/000339295
174. Anastasopoulos D, Haslwanter T, Bronstein A, Fetter M, Dichgans J. Dissociation between the perception of body verticality and the visual vertical in acute peripheral vestibular disorder in humans. *Neurosci Lett.* (1997) 233:151–3. doi: 10.1016/S0304-3940(97)00639-3
175. Ito Y, Gresty MA. Shift of subjective reference and visual orientation during slow pitch tilt for the seated human subject. *Brain Res Bull.* (1996) 40:417–21. doi: 10.1016/0361-9230(96)00136-0
176. Anastasopoulos D, Bronstein A, Haslwanter T, Fetter M, Dichgans J. The role of somatosensory input for the perception of verticality. *Ann N Y Acad Sci.* (1999) 871:379–83. doi: 10.1111/j.1749-6632.1999.tb09199.x
177. Mazibrada G, Tariq S, Pérennou D, Gresty M, Greenwood R, Bronstein AM. The peripheral nervous system and the perception of verticality. *Gait Posture.* (2008) 27:202–8. doi: 10.1016/j.gaitpost.2007.03.006
178. Cremer R, Zeef EJ. What kind of noise increases with age? *J Gerontol.* (1987) 42:515–8. doi: 10.1093/geronj/42.5.515
179. Faisal AA, Selen LPJ, Wolpert DM. Noise in the nervous system. *Nat Rev Neurosci.* (2008) 9:292–303. doi: 10.1038/nrn2258
180. White O, Babič J, Trenado C, Johannsen L, Goswami N. The promise of stochastic resonance in falls prevention. *Front Physiol.* (2019) 9:1865. doi: 10.3389/fphys.2018.01865
181. Welford AT. THE MEASUREMENT OF SENSORY-MOTOR PERFORMANCE : SURVEY AND REAPPRAISAL OF TWELVE YEARS' PROGRESS. *Ergonomics.* (1960) 3:189–230. doi: 10.1080/00140136008930484
182. Voytek B, Kramer MA, Case J, Lepage KQ, Tempesta ZR, Knight RT, et al. Age-related changes in 1/f neural electrophysiological noise. *J Neurosci.* (2015) 35:13257–65. doi: 10.1523/JNEUROSCI.2332-14.2015
183. Roditi RE, Crane BT. Directional asymmetries and age effects in human self-motion perception. *J Assoc Res Otolaryngol JARO.* (2012) 13:381–401. doi: 10.1007/s10162-012-0318-3
184. Crane BT. Perception of combined translation and rotation in the horizontal plane in humans. *J Neurophysiol.* (2016) 116:1275–85. doi: 10.1152/jn.00322.2016
185. Green DM, Swets JA. *Signal Detection Theory and Psychophysics*. Oxford, England: John Wiley (1966).
186. Merfeld DM. Signal detection theory and vestibular thresholds: I. Basic theory and practical considerations. *Exp Brain Res.* (2011) 210:389–405. doi: 10.1007/s00221-011-2557-7
187. Lim K, Merfeld DM. Signal detection theory and vestibular perception: II. Fitting perceptual thresholds as a function of frequency. *Exp Brain Res.* (2012) 222:303–20. doi: 10.1007/s00221-012-3217-2
188. Chaudhuri SE, Merfeld DM. Signal detection theory and vestibular perception: III. Estimating unbiased fit parameters for psychometric functions. *Exp Brain Res.* (2013) 225:133–46. doi: 10.1007/s00221-012-3354-7
189. Macmillan NA, Creelman CD. *Detection Theory: A User's Guide, 2nd edn*. Mahwah, NJ: Lawrence Erlbaum Associates (2005).
190. Karmali F, Bermúdez Rey MC, Clark TK, Wang W, Merfeld DM. Multivariate analyses of balance test performance, vestibular thresholds, and age. *Front Neurol.* (2017) 8:578. doi: 10.3389/fneur.2017.00578
191. Angelaki DE, McHenry MQ, Dickman JD, Newlands SD, Hess BJ. Computation of inertial motion: neural strategies to resolve ambiguous otolith information. *J Neurosci Off J Soc Neurosci.* (1999) 19:316–327. doi: 10.1523/JNEUROSCI.19-01-00316.1999
192. Laurens J, Meng H, Angelaki DE. Neural representation of orientation relative to gravity in the Macaque Cerebellum. *Neuron.* (2013) 80:1508–18. doi: 10.1016/j.neuron.2013.09.029
193. Merfeld DM, Park S, Gianna-Poulin C, Black FO, Wood S. Vestibular perception and action employ qualitatively different mechanisms. I. Frequency Response of VOR and Perceptual Responses During Translation and Tilt. *J Neurophysiol.* (2005) 94:186–98. doi: 10.1152/jn.00904.2004

194. Merfeld DM, Park S, Gianna-Poulin C, Black FO, Wood S. Vestibular perception and action employ qualitatively different mechanisms. *II*. VOR and Perceptual responses during combined Tilt&Translation. *J Neurophysiol.* (2005) 94:199–205. doi: 10.1152/jn.00905.2004
195. Angelaki DE, Yakusheva TA. How vestibular neurons solve the tilt/translation ambiguity: comparison of brainstem, cerebellum, and thalamus. *Ann N Y Acad Sci.* (2009) 1164:19–28. doi: 10.1111/j.1749-6632.2009.03939.x
196. Angelaki DE, Shaikh AG, Green AM, Dickman JD. Neurons compute internal models of the physical laws of motion. *Nature.* (2004) 430:560–4. doi: 10.1038/nature02754
197. Green AM, Angelaki DE. An integrative neural network for detecting inertial motion and head orientation. *J Neurophysiol.* (2004) 92:905–25. doi: 10.1152/jn.01234.2003
198. Carriot J, Jamali M, Brooks JX, Cullen KE. Integration of canal and otolith inputs by central vestibular neurons is subadditive for both active and passive self-motion: implication for perception. *J Neurosci.* (2015) 35:3555–65. doi: 10.1523/JNEUROSCI.3540-14.2015
199. Karmali F, Whitman GT, Lewis RF. Bayesian optimal adaptation explains age-related human sensorimotor changes. *J Neurophysiol.* (2018) 119:509–20. doi: 10.1152/jn.00710.2017
200. Maurer C, Peterka RJ. A new interpretation of spontaneous sway measures based on a simple model of human postural control. *J Neurophysiol.* (2005) 93:189–200. doi: 10.1152/jn.00221.2004
201. Dai M, Klein A, Cohen B, Raphan T. Model-based study of the human cupular time constant. *J Vestib Res Equilib Orientat.* (1999) 9:293–301.
202. Goldberg JM, Fernandez C. Physiology of peripheral neurons innervating semicircular canals of the squirrel monkey. I. Resting discharge and response to constant angular accelerations. *J Neurophysiol.* (1971) 34:635–60. doi: 10.1152/jn.1971.34.4.635
203. Baloh RobertW, Demer JosephL. Optokinetic-vestibular interaction in patients with increased gain of the vestibulo-ocular reflex. *Exp Brain Res.* (1993) 97: doi: 10.1007/BF00228703
204. Raphan T. Vestibular, locomotor, and vestibulo-autonomic research: 50 years of collaboration with Bernard Cohen. *J Neurophysiol.* (2020) 123:329–45. doi: 10.1152/jn.00485.2019
205. Merfeld DM, Young LR, Oman CM, Shelhamer MJ. A multidimensional model of the effect of gravity on the spatial orientation of the monkey. *J Vestib Res Equilib Orientat.* (1993) 3:141–61.
206. Robinson DA. Vestibular and optokinetic symbiosis: an example of explaining by modelling. In: *Control Gaze Brainstem Interneurons.* (1977). Available online at: https://ci.nii.ac.jp/naid/10008955613/en/
207. Jenkins HA, Honrubia V, Baloh RH. Evaluation of multiple-frequency rotatory testing in patients with peripheral labyrinthine weakness. *Am J Otolaryngol.* (1982) 3:182–8. doi: 10.1016/S0196-0709(82)80052-5
208. King S, Priesol AJ, Davidi SE, Merfeld DM, Ehtemam F, Lewis RF. Self-motion perception is sensitized in vestibular migraine: pathophysiologic and clinical implications. *Sci Rep.* (2019) 9:14323. doi: 10.1038/s41598-019-50803-y
209. Dimitri PS, Wall C, Oas JG, Rauch SD. Application of multivariate statistics to vestibular testing: discriminating between Menière's disease and migraine associated dizziness. *J Vestib Res Equilib Orientat.* (2001) 11:53–65.
210. Berniker M, Kording K. Bayesian approaches to sensory integration for motor control: Bayesian approaches to sensory integration for motor control. *Wiley Interdiscip Rev Cogn Sci.* (2011) 2:419–28. doi: 10.1002/wcs.125
211. Laurens J, Droulez J. Bayesian processing of vestibular information. *Biol Cybern.* (2007) 96:389–404. doi: 10.1007/s00422-006-0133-1
212. Karmali F. The velocity storage time constant: balancing between accuracy and precision. In: John Leigh R, Ramat S, Shaikh A, editors. *Progress in Brain Research* (Amsterdam: Elsevier). p. 269–76.
213. Raphan T, Matsuo V, Cohen B. Velocity storage in the vestibulo-ocular reflex arc (VOR). *Exp Brain Res.* (1979) 35:229–48. doi: 10.1007/BF00236613
214. Rauch SD, Velazquez-Villaseñor L, Dimitri PS, Merchant SN. Decreasing hair cell counts in aging humans. *Ann N Y Acad Sci.* (2006) 942:220–7. doi: 10.1111/j.1749-6632.2001.tb03748.x
215. Jacobson GP, McCaslin DL, Patel S, Barin K, Ramadan NM. Functional and anatomical correlates of impaired velocity storage. *J Am Acad Audiol.* (2004) 15:324–33. doi: 10.3766/jaaa.15.4.6
216. Anson E, Bigelow RT, Studenski S, Deshpande N, Agrawal Y. Failure on the foam eyes closed test of standing balance associated with reduced semicircular canal function in healthy older adults. *Ear Hear.* (2019) 40:340–4. doi: 10.1097/AUD.0000000000000619
217. Della Santina CC, Cremer PD, Carey JP, Minor LB. Comparison of head thrust test with head autorotation test reveals that the vestibulo-ocular reflex is enhanced during voluntary head movements. *Arch Otolaryngol Neck Surg.* (2002) 128:1044. doi: 10.1001/archotol.128.9.1044
218. Dichgans J, Bizzi E, Morasso P, Tagliasco V. Mechanisms underlying recovery of eye-head coordination following bilateral labyrinthectomy in monkeys. *Exp Brain Res.* (1973) 18:548–62. doi: 10.1007/BF00234137
219. Schubert MC, Hall CD, Das V, Tusa RJ, Herdman SJ. Oculomotor strategies and their effect on reducing gaze position error. *Otol Neurotol.* (2010) 31:228–31. doi: 10.1097/MAO.0b013e3181c2dbae
220. Schubert MC, Migliaccio AA, Clendaniel RA, Allak A, Carey JP. Mechanism of dynamic visual acuity recovery with vestibular rehabilitation. *Arch Phys Med Rehabil.* (2008) 89:500–7. doi: 10.1016/j.apmr.2007.11.010
221. Sadeghi SG, Minor LB, Cullen KE. Neural correlates of motor learning in the vestibulo-ocular reflex: dynamic regulation of multimodal integration in the macaque vestibular system. *J Neurosci Off J Soc Neurosci.* (2010) 30:10158–68. doi: 10.1523/JNEUROSCI.1368-10.2010
222. Sadeghi SG, Minor LB, Cullen KE. Multimodal integration after unilateral labyrinthine lesion: single vestibular nuclei neuron responses and implications for postural compensation. *J Neurophysiol.* (2011) 105:661–73. doi: 10.1152/jn.00788.2010
223. Sadeghi SG, Minor LB, Cullen KE. Neural correlates of sensory substitution in vestibular pathways following complete vestibular loss. *J Neurosci Off J Soc Neurosci.* (2012) 32:14685–95. doi: 10.1523/JNEUROSCI.2493-12.2012
224. Schubert MC, Das V, Tusa RJ, Herdman SJ. Cervico-ocular reflex in normal subjects and patients with unilateral vestibular hypofunction. *Otol Neurotol Off Publ Am Otol Soc Am Neurotol Soc Eur Acad Otol Neurotol.* (2004) 25:65–71. doi: 10.1097/00129492-200401000-00013
225. Cullen KE. "Physiology of central pathways," In: Furman J, Lempert T, editors. *Handbook of Clinical Neurology* (Amsterdam: Elsevier). p. 17–40. doi: 10.1016/B978-0-444-63437-5.00002-9
226. Halmagyi GM, Curthoys IS, Cremer PD, Henderson CJ, Todd MJ, Staples MJ, et al. The human horizontal vestibulo-ocular reflex in response to high-acceleration stimulation before and after unilateral vestibular neurectomy. *Exp Brain Res.* (1990) 81:479–90. doi: 10.1007/BF02423496
227. Halmagyi GM, Chen L, MacDougall HG, Weber KP, McGarvie LA, Curthoys IS. The video head impulse test. *Front Neurol.* (2017) 8:258. doi: 10.3389/fneur.2017.00258
228. Wolfe JM, Kluender KR, Dennis LM, Bartoshuk LM, Herz RS, Lederman SJ, et al. *Sensation & Perception, 4th edn*. Sunderland, MA: Sinauer Associates, Inc., Publishers (2015).
229. Angelaki DE, Cullen KE. Vestibular System: The Many Facets of a Multimodal Sense. *Annu Rev Neurosci.* (2008) 31:125–50. doi: 10.1146/annurev.neuro.31.060407.125555
230. Asai M, Watanabe Y, Ohashi N, Mizukoshi K. Evaluation of vestibular function by dynamic posturography and other equilibrium examinations. *Acta Oto-Laryngol Suppl.* (1993) 504:120–4. doi: 10.3109/00016489309128136
231. Cohen HS, Kimball KT. Usefulness of some current balance tests for identifying individuals with disequilibrium due to vestibular impairments. *J Vestib Res Equilib Orientat.* (2008) 18:295–303.
232. Zhou J, Habtemariam D, Iloputaife I, Lipsitz LA, Manor B. The complexity of standing postural sway associates with future falls in community-dwelling older adults: the MOBILIZE Boston Study. *Sci Rep.* (2017) 7:2924. doi: 10.1038/s41598-017-03422-4
233. Peterka RJ. Sensory integration for human balance control. In: Day BL, Lord SR, editors. *Handbook of Clinical Neurology* (Amsterdam: Elsevier). p. 27–42.
234. Fitzpatrick R, Burke D, Gandevia SC. Task-dependent reflex responses and movement illusions evoked by galvanic vestibular stimulation in standing humans. *J Physiol.* (1994) 478:363–72. doi: 10.1113/jphysiol.1994.sp020257
235. Welgampola M, Colebatch J. Vestibulospinal reflexes: quantitative effects of sensory feedback and postural task. *Exp Brain Res.* (2001) 139:345–53. doi: 10.1007/s002210100754

236. Day BL. Vestibular-evoked postural responses in the absence of somatosensory information. *Brain.* (2002) 125:2081–8. doi: 10.1093/brain/awf212
237. Horak FB, Hlavacka F. Somatosensory loss increases vestibulospinal sensitivity. *J Neurophysiol.* (2001) 86:575–85. doi: 10.1152/jn.2001.86.2.575
238. Klein R, Klein BEK, Lee KE, Cruickshanks KJ, Gangnon RE. Changes in visual acuity in a population over a 15-year period: the Beaver Dam Eye Study. *Am J Ophthalmol.* (2006) 142:539–49.e2. doi: 10.1016/j.ajo.2006.06.015
239. Hong T, Mitchell P, Rochtchina E, Fong CS, Chia E-M, Wang JJ. Long-term changes in visual acuity in an older population over a 15-year period. *Ophthalmology.* (2013) 120:2091–9. doi: 10.1016/j.ophtha.2013.03.032
240. Cullen KE. Vestibular processing during natural self-motion: implications for perception and action. *Nat Rev Neurosci.* (2019) 20:346–63. doi: 10.1038/s41583-019-0153-1
241. Lim K, Karmali F, Nicoucar K, Merfeld DM. Perceptual precision of passive body tilt is consistent with statistically optimal cue integration. *J Neurophysiol.* (2017) 117:2037–52. doi: 10.1152/jn.00073.2016
242. Nouri S, Karmali F. Variability in the Vestibulo-ocular reflex and vestibular perception. *Neuroscience.* (2018) 393:350–65. doi: 10.1016/j.neuroscience.2018.08.025

Conflict of Interest: The authors declare that the research was conducted in the absence of any commercial or financial relationships that could be construed as a potential conflict of interest.

frontiers in Neurology

ORIGINAL RESEARCH
published: 09 February 2021
doi: 10.3389/fneur.2021.633356

Pre-habilitation Before Vestibular Schwannoma Surgery—Impact of Intratympanal Gentamicin Application on the Vestibulo-Ocular Reflex

Alexander A. Tarnutzer[1,2,3,4]*, *Christopher J. Bockisch*[1,4,5,6], *Elena Buffone*[1], *Alexander M. Huber*[5], *Vincent G. Wettstein*[5,7] and *Konrad P. Weber*[1,2,4,6]

[1] Department of Neurology, University Hospital Zurich, Zurich, Switzerland, [2] Faculty of Medicine, University of Zurich, Zurich, Switzerland, [3] Neurology, Cantonal Hospital of Baden, Baden, Switzerland, [4] Clinical Neuroscience Center, Zurich, Switzerland, [5] Department of Otorhinolaryngology, University Hospital Zurich, Zurich, Switzerland, [6] Department of Ophthalmology, University Hospital Zurich, Zurich, Switzerland, [7] Rautipraxis AG, Zurich, Switzerland

OPEN ACCESS

Edited by:
Michael Strupp,
Ludwig Maximilian University of Munich, Germany

Reviewed by:
Nicolas Perez-Fernandez, University Clinic of Navarra, Spain
Michael C. Schubert, Johns Hopkins University, United States
Swee Tin Aw, The University of Sydney, Australia

***Correspondence:**
Alexander A. Tarnutzer
alexander.tarnutzer@access.uzh.ch

Specialty section:
This article was submitted to Neuro-Otology, a section of the journal Frontiers in Neurology

Received: 25 November 2020
Accepted: 05 January 2021
Published: 09 February 2021

Citation:
Tarnutzer AA, Bockisch CJ, Buffone E, Huber AM, Wettstein VG and Weber KP (2021) Pre-habilitation Before Vestibular Schwannoma Surgery—Impact of Intratympanal Gentamicin Application on the Vestibulo-Ocular Reflex. Front. Neurol. 12:633356. doi: 10.3389/fneur.2021.633356

Background: Patients with vestibular schwannoma that show residual peripheral-vestibular function before surgery may experience sudden and substantial vestibular loss of function after surgical resection. To alleviate the sudden loss of peripheral-vestibular function after vestibular-schwannoma (VS) resection, pre-surgical intratympanic gentamicin application was proposed.

Objective: We hypothesized that this approach allows for a controlled reduction of peripheral-vestibular function before surgery but that resulting peripheral-vestibular deficits may be canal-specific with anterior-canal sparing as observed previously in systemic gentamicin application.

Methods: Thirty-four patients (age-range = 27–70 y) with unilateral VS (size = 2–50 mm) were included in this retrospective single-center trial. The angular vestibulo-ocular reflex (aVOR) was quantified before and after (29.7 ± 18.7 d, mean ± 1SD) a single or two sequential intratympanic gentamicin applications by use of video-head-impulse testing. Both aVOR gains, cumulative saccadic amplitudes, and overall aVOR function were retrieved. Statistical analysis was done using a generalized linear model.

Results: At baseline, loss of function of the horizontal (20/34) and posterior (21/34) canal was significantly ($p < 0.001$) more frequent than that of the anterior canal (5/34). After gentamicin application, loss of function of the horizontal (32/34) or posterior (31/34) canal remained significantly ($p \leq 0.003$) more frequent than that of the anterior canal (18/34). For all ipsilesional canals, significant aVOR-gain reductions and cumulative-saccadic-amplitude increases were noted after gentamicin. For the horizontal canal, loss of function was significantly larger (increase in cumulative-saccadic-amplitude: 1.6 ± 2.0 vs. 0.8 ± 1.2, $p = 0.007$) or showed a trend to larger changes (decrease in aVOR-gain: 0.24 ± 0.22 vs. 0.13 ± 0.29, $p = 0.069$) than for the anterior canal.

Conclusions: Intratympanic gentamicin application resulted in a substantial reduction in peripheral-vestibular function in all three ipsilesional canals. Relative sparing of anterior-canal function noted at baseline was preserved after gentamicin treatment. Thus, pre-surgical intratympanic gentamicin is a suitable preparatory procedure for reducing the drop in peripheral-vestibular function after VS-resection. The reasons for relative sparing of the anterior canal remain unclear.

Keywords: video-head-impulse testing, aminoglycosides, vestibulotoxicity, tumor size, anterior-canal sparing

INTRODUCTION

Treatment options for patients with growing vestibular schwannoma (VS) or with local compressive effects include radiosurgery and microsurgical resection (1–4). As a potential side effect of treatment, those patients with residual peripheral-vestibular function may experience sudden and substantial vestibular loss of function (5). To reduce such side effects due to dissection of the vestibular nerve, drug-induced ablation of ipsilateral peripheral-vestibular function by use of vestibulotoxic substances has been proposed as a pre-surgical treatment (6–9). Specifically, there is a level-3 recommendation from the Congress of Neurological Surgeons on pre-operative gentamicin ablation intratympanically to induce a controlled partial loss of semicircular canal (SCC) function and to improve post-operative mobility (10). Thus, after surgical VS resection, the delta in loss of function is presumably smaller than in untreated patients and their clinical symptoms after surgery will be smaller (11). This may have a positive impact on rehabilitation and recovery (12), including coping with vertigo and (multi)sensory input (9, 13–15). Furthermore, the gentamicin-induced pre-surgical loss of vestibular function will occur while the patient is in his/her natural state of health and mobility, which may facilitate recovery compared to his/her condition immediately after surgery.

Aminoglycosides are known for causing vestibular loss of function when applied intravenously (16–19), albeit hearing may deteriorate also (20). Recovery is usually limited, and underlying pathomechanisms of aminoglycoside-induced vestibulotoxicity are still unclear (21). Previously, relative sparing of the anterior canal(s) after aminoglycoside treatment has been reported (22). Whether this is true also for patients who received intratympanic aminoglycosides as part of pre-surgical treatment is not known. As intratympanic gentamicin application is an established, efficient treatment for Menière's disease (MD) (23, 24), this approach may serve as a model to study the vulnerability of the SCCs to pre-defined doses of gentamicin. Thus, we hypothesized that relative sparing of anterior-canal function will be present also in patients who received intratympanic gentamicin before VS resection. Alternatively, with a comparable reduction in SCC function for all three canals, this would speak against a selective vulnerability of specific SSCs to intratympanic aminoglycosides.

To test this hypothesis, we quantified SCC function before and after intratympanic gentamicin application in VS patients and compared the loss of function in individual canals. We predicted a significantly smaller loss of function in the ipsilesional anterior canal compared to the posterior and horizontal canal.

MATERIALS AND METHODS

The local ethics committee (Cantonal Ethics Committee Zurich) approved the experimental protocol. The protocol was in accordance with the ethical standards of the 2013 Declaration of Helsinki for research involving human beings. All subjects that had been treated after January 1st 2016 had previously provided written general consent for the use of health-related data and samples for research purposes, whereas those treated earlier could be included based on the approval of the study protocol by the local Ethics committee (study protocol 2018-00224). We retrospectively screened the Hospital's electronic files for patients who have received a diagnosis of unilateral VS and treatment with gentamicin prior to surgical resection between May 2013 and September 2017. Ten patients from the current study were previously published (25).

Intratympanic Gentamicin Treatment

All patients received a treatment with intratympanic gentamicin (solution = 80 mg/2 ml) ipsilaterally to the VS applied by an ENT specialist at least 6 weeks before surgery. vHIT was obtained at baseline and 2–6 weeks after gentamicin treatment. If loss of function was found to be insufficient, a second gentamicin dose was administered. Dosage of gentamicin ranged between 0.25 and 1 ml, depending on the volume of the tympanic cavity. Pure tone audiometry (PTA) was obtained in all patients at baseline and after treatment.

vHIT-Recording Procedure

All patients received quantitative vestibular testing before and after intratympanic gentamicin application. We required 20 valid head impulses for each canal (26), with SCCs tested in pairs according to the planes of stimulation (horizontal canals, RALP plane for right anterior and left posterior canal, LARP plane for left anterior and right posterior canal). For video-oculography, we used commercially available vHIT goggles (Otometrics, Taastrup, Denmark) with an infrared camera recording the right eye. Horizontal and vertical eye position was measured (frequency = 250 Hz), and angular head velocity was determined by three orthogonal mini-gyroscopes. For further analysis, eye-velocity values were calculated.

Patient Identification and Data Analysis

We reanalyzed angular VOR (aVOR) gains in all patients using Otosuite 4.0 (Otometrics, Taastrup, Denmark) and ran custom-written MATLAB (R2017b, The MathWorks, Natick, MA, USA)

routines for the quantification of overt corrective saccades, calculating cumulative saccadic amplitudes (CSA) per trial (22). For this study, we read out the standard aVOR gain calculations from the Otometrics vHIT goggles. Their algorithm calculates gain as the ratio of the area under the desaccaded eye-velocity curve to the area under the head-velocity curve, corresponding to a desaccaded position gain (27). Thus, the gain of the aVOR was calculated as the ratio of cumulative slow-phase eye velocity over cumulative head velocity from the onset of the head impulse to the moment when head velocity crossed zero again (27). As the amplitude of covert saccades on top of the (residual) aVOR response is ill-defined and hard to calculate reliably, we chose to only include overt saccades for our analysis (17, 28). Saccades were defined as "overt," if their onset occurred after head velocity crossed zero after the head impulse. Vestibular hypofunction was defined as a reduction in aVOR gain and/or the occurrence of compensatory saccades. For a diagnosis of unilateral-vestibular loss (UVL), hypofunction of at least one canal on one side was required.

For gains, cutoff values of 0.8 (horizontal canals) and 0.7 (vertical canals) have been proposed by the manufacturer (Otometrics) to distinguish normal from reduced aVOR function. Previously proposed cutoff values suggested that the CSA > 0.7–0.8°/trial indicates loss of function of the canal tested (22, 29). Here we adhered to the cutoff value (0.73°/trial) proposed by our group (22), as the same statistical approach was used.

On MR imaging (obtained in all patients), the maximal diameter of the tumor was determined. Two experienced neuro-ontologists (KPW, AAT) independently reviewed all vHIT traces. Traces were evaluated for reduced aVOR gain, increased CSA, or a combination of both (22). Inter-rater agreement for individual canal function (normal vs. pathological) was 0.83 (Cohen's kappa) (30). Discordant ratings were resolved by discussion among the reviewers.

Individual patterns of SCC hypofunction were assessed. MATLAB and SPSS 24 (IBM, Armonk, NY, USA) were used for statistical analyses. Fisher's exact-test with Bonferroni correction for multiple tests was applied to determine significant differences in the occurrence of specific conditions. The level of significance for all statistical tests was 0.05. We applied a generalized linear model (GLM, SPSS 24) to analyze the effects of the gentamicin treatment on the extent of peripheral-vestibular impairment. Fisher's least significant difference (LSD) method was used to correct for multiple tests when performing pairwise comparisons.

Principal component analysis (PCA) was applied for comparisons between two dependent variables (31). The coefficient of determination (R^2) was used to assess the goodness of fit. A correlation between two variables was considered significant whenever the 95% confidence interval (95% CI) of the slope did not include zero.

Standardized evaluation of hearing function on PTA was performed according to the CPT-AMA guidelines (32), assessing hearing at four different frequencies (500 Hz/1 kHz/2 kHz/4 kHz). Significant hearing loss was defined as a CPT value >20% on the affected side.

TABLE 1 | Epidemiology—key facts.

Gender (*n*)		**%**
Females	10	29
Males	24	71
Age (mean ± 1SD) (years)		
Females	52.1±11.9	
Males	50.5±8.4	
Affected side (*n*)		
Right	14	41
Left*	20	59
VS size (mm)		
1–10	5	15
11–20	12	35
21–30	14	41
31–40	2	6
>40	1	3
Range	2–50	
Mean ± 1SD	21.4 ± 9.3	
Gentamicin treatment sessions (*n*)		
One session	26	76
Two sessions	8	24
Gentamicin treatment dose (mean ± 1SD) (ml)		
First session	0.50 ± 0.20†	
Second session	0.55 ± 0.14‡	
Timing of vHIT testing relative to gentamicin treatment (days)		
Delay gentamicin treatment—baseline vHIT (mean ± 1SD)	20.2 ± 21.1	
Delay FU vHIT testing—gentamicin treatment (mean ± 1SD)	29.7 ± 18.7	
Delay FU vHIT testing—2nd gentamicin treatment (mean ± 1SD)	26.9 ± 16.6	
Delay gentamicin treatment—surgery (mean ± 1SD)	57 ± 44	

FU, follow-up.

**Results from patients with left-sided unilateral vestibular disease were mirrored for further analysis, so that the affected side is always on the right in the paper.*

†Missing values from 3 patients.

‡Missing values from 2 patients.

RESULTS

Between May 2013 and September 2017, 41 patients with unilateral VS received intratympanic gentamicin injections prior to VS resection at the University Hospital Zurich. From those subjects, seven were excluded due to missing/denied general consent (n=2) or due to missing post-gentamicin vHIT (n = 5). From the remaining 34 patients (aged = 27–70 years, 10 females), 26 received a single intratympanic gentamicin treatment, whereas eight patients received two doses. VS size varied between 2 and 50 mm (**Table 1**).

In **Figure 1**, vHIT results and MR imaging from two subjects are shown, illustrating different patterns before and after gentamicin treatment. While the first subject (#14, panels AB) demonstrated normal SCC function ipsilesionally and relative

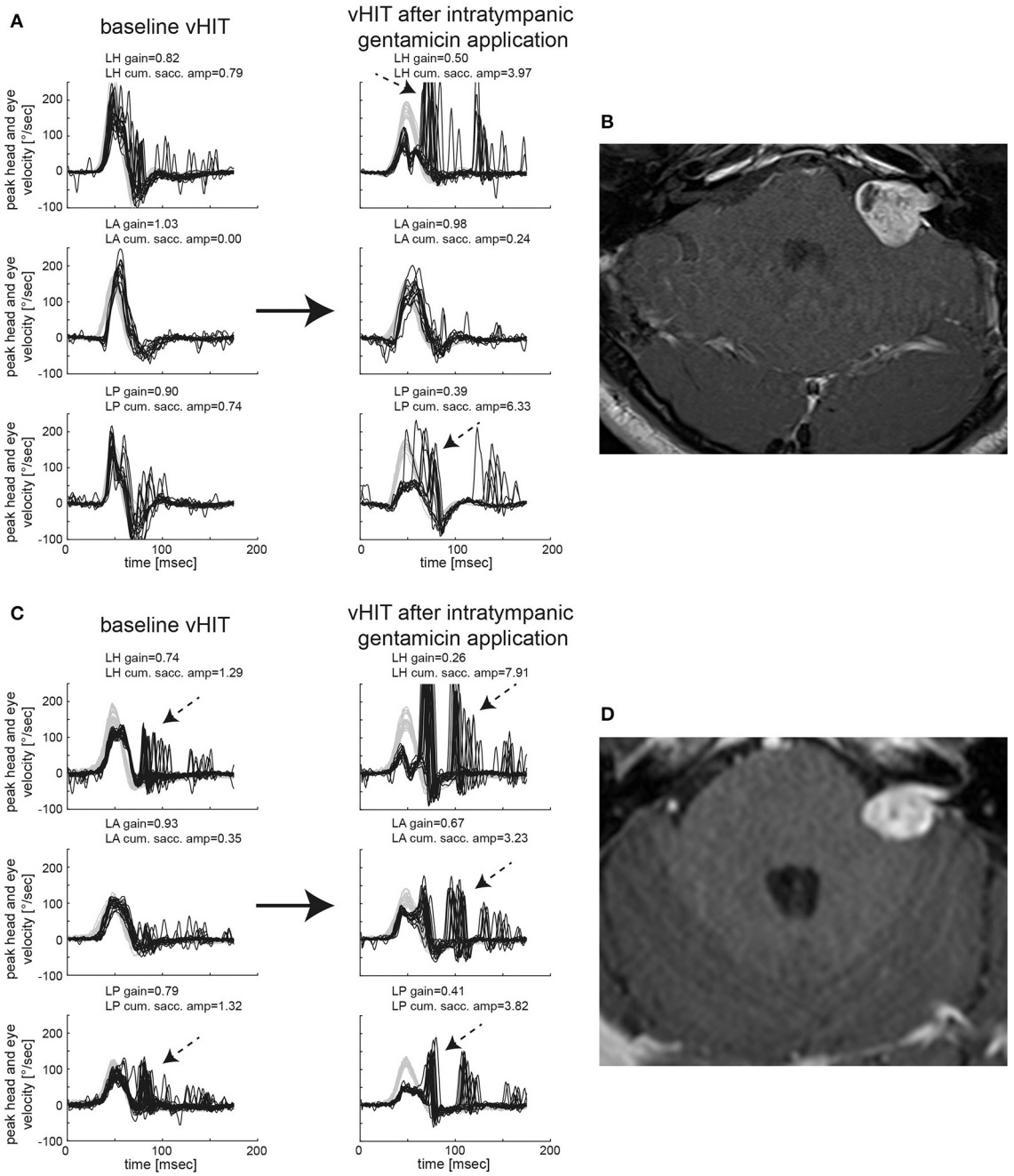

FIGURE 1 | Video-head-impulse testing before and after intratympanic gentamicin application is shown for two representative patients with unilateral VS. In **(A)** [patient #14, left-sided VS, max. diameter 20 mm as shown on axial T1-weighted contrast-enhanced MRI in **(B)**], baseline testing showed an overall normal aVOR response for all six SCCs with only very few saccades for the ipsilesional horizontal and posterior canal (only ipsilesional traces shown). One month after intratympanic gentamicin application (0.3 ml), vHIT demonstrates a significantly reduced aVOR gain for the left horizontal and left posterior SCC with accompanying overt catch-up saccades, whereas the left anterior canal remained functionally intact. In addition, low-amplitude, compensatory saccades are observed in the right horizontal and posterior SCC. In **(C)** [patient #32, left-sided VS, max. diameter 19 mm as shown on axial T1-weighted contrast-enhanced MRI in **(D)**], baseline testing indicated partial loss of function of the ipsilesional horizontal (with mild reduction in gain and overt catch-up saccades) and posterior (with normal gain but significant overt catch-up saccades) SCC, whereas anterior-canal function remained intact. Sixteen days after left-sided intratympanic gentamicin application (0.7 ml), gains of the ipsilesional horizontal and posterior canal had dropped sharply with covert and overt catch-up saccades having grown in amplitude as shown on vHIT. In addition, the ipsilesional (left) anterior SCC now demonstrated a partial loss of function with a mild decrease in gain and significant covert and overt catch-up saccades. However, in comparison to the left horizontal and posterior canal, the impairment in aVOR was clearly smaller for the left anterior canal, suggesting gentamicin-related anterior-canal sparing.

sparing of anterior-canal function after gentamicin treatment, the second subject (#32, panels CD) presented with impaired horizontal/posterior canal function before treatment and loss of function of all three SCCs after gentamicin treatment. Residual gains, however, were highest for the anterior SCC, pointing to relative sparing of anterior-canal function.

Video-Head-Impulse Testing in Vestibular Schwannoma–Baseline Testing

At baseline, an ipsilesionally impaired aVOR was noted by the two reviewers in at least one SCC in 24/34 VS patients (71%), whereas SCC function remained intact in 10 patients (29%). Different distribution patterns of ipsilesional SCC function at baseline were observed (**Figure 2A**), with impaired horizontal/posterior canal function (38%), preserved peripheral-vestibular function in all three SCCs (29%), impaired SCC function in all three SCCs (12%), and impaired posterior-canal function (12%) being most frequent. The fraction of loss of function for the different ipsilesional SCCs is illustrated in **Figure 2B**. In comparison to impairment of the anterior SCC, loss of function of the horizontal (5 vs. 20; $p < 0.001$, Fisher's exact-test, Bonferroni corrected) or posterior (5 vs. 21; $p < 0.001$) SCC was significantly more frequent.

Statistical analysis (GLM) of vHIT gains at baseline and after gentamicin treatment showed a significant main effect for the condition (df = 1, chi-square = 29.322, $p < 0.001$) and individual ipsilesional SCCs (df = 2, chi-square = 134.373, $p < 0.001$). Furthermore, a significant interaction between these two parameters was noted (df = 5, chi-square = 19.261, $p = 0.002$). Likewise, statistical analysis of CSA demonstrated a significant main effect for the condition (df = 1, chi-square = 53.974, $p < 0.001$) and the SCCs (df = 2, chi-square = 284.151, $p < 0.001$). Again, a significant interaction was noted (df = 5, chi-square = 44.926, $p < 0.001$).

Performing pairwise comparisons, ipsilesional mean gains (±1SD) at baseline (panel A) were significantly ($p < 0.001$) smaller than on the healthy side for the horizontal and posterior canal, but not for the anterior canal ($p = 0.670$) (**Figure 3** and **Table 2**). Likewise, CSA at baseline (panel C) were significantly larger on the affected side than on the healthy side for the horizontal canal ($p < 0.001$) and showed a trend toward significance for the posterior canal ($p = 0.052$), whereas this was not the case for the anterior canal ($p = 0.607$).

In a next step, we asked whether VS size had an impact on the extent of peripheral-vestibular loss of function. Using PCA, individual vHIT gains at baseline from all three ipsilesional SCCs were compared with the VS diameter (**Figure 3E**), showing a significant inverse correlation [$R^2 = 0.45$, slope = −0.03 (95%-CI = −0.03 to −0.02)].

Video-Head-Impulse Testing After Intratympanic Gentamicin Injection

After gentamicin treatment, overall SCC function was impaired ipsilesionally in at least one SCC in all 34 patients (**Figure 2A**). Most often, impairment of all three SCCs was observed (53%), followed by loss of function restricted to the horizontal and posterior canal (35%) or the horizontal canal (9%).

The fraction of deficient canals grew after gentamicin treatment (**Figure 2B**). In comparison to impairment of the anterior SCC, loss of function of the horizontal (18 vs. 32; $p < 0.001$) or posterior (18 vs. 31; $p = 0.003$) SCC remained significantly more frequent after gentamicin treatment.

Performing pairwise comparisons, ipsilesional mean gains after gentamicin treatment (**Figure 3B** and **Table 2**) were significantly ($p \leq 0.002$) smaller than on the contralesional side for all three SCCs. Likewise, CSA (**Figure 3D**) were significantly ($p < 0.001$) larger on the affected side than on the healthy side for all three SCCs.

Changes in aVOR Gains and CSA After Gentamicin Treatment

On the affected side, aVOR gains were significantly ($p \leq 0.006$) reduced and CSA were significantly ($p < 0.001$) increased for all three SCCs after gentamicin treatment. In contrast, no significant ($p > 0.05$) changes in vHIT gains and CSA after gentamicin treatment were noted contralesionally.

When comparing the delta (Δ) in aVOR gain for all SCCs, a significant main effect was noted (df = 5, chi-square = 25.860, $p < 0.001$) (**Figure 2C**). Pairwise comparisons demonstrated a trend toward a larger ipsilesional decrease in aVOR gain for the horizontal canal compared to the anterior canal after gentamicin treatment (0.24 ± 0.22 vs. 0.13 ± 0.29, $p = 0.069$), whereas no significant differences in ipsilesional ΔaVOR gain were noted when comparing the horizontal and posterior canal (0.24 ± 0.22 vs. 0.19 ± 0.29, $p = 0.353$) and the posterior and anterior canal (0.19 ± 0.29 vs. 0.13 ± 0.29, $p = 0.373$). When comparing the ΔCSA for all SCCs, a significant main effect was noted as well (df = 5, chi-square = 56.469, $p < 0.001$) (**Figure 2D**). The increase in CSA after gentamicin treatment was significantly larger for the horizontal canal than for the anterior canal (1.6 ± 2.0 vs. 0.8 ± 1.2, $p = 0.007$) and showed a trend toward a significantly larger increase for the posterior canal compared to the anterior canal (1.3 ± 1.6 vs. 0.8 ± 1.2, $p = 0.067$). No significant differences in ΔCSA were noted when comparing the horizontal and posterior ipsilesional canal ($p = 0.398$).

ΔaVOR gain (all ipsilesional SCCs pooled) after a first dose of gentamicin was compared with the aVOR gain at baseline, demonstrating a significant correlation [$R^2 = 0.76$, slope = 1.17 (95%-CI = 1.01–1.35)] (**Figure 3F**). Likewise, ΔCSA after a first dose of gentamicin was inversely correlated with the CSA at baseline [$R^2 = 0.55$, slope = −1.43 (95%-CI = −1.86 to −1.12)] (**Figure 3G**). In contrast, there was no correlation between the first gentamicin dose and the ΔaVOR-gain [$R^2 = 0.07$, slope = −1.45 (95%-CI = −2.08 to 1.43)] or the ΔCSA [$R^2 = 0.08$, slope = −8.66 (95%-CI = −12.13 to 8.30)].

Hearing-Impairment at Baseline and After Gentamicin Treatment

Pure tone audiometry at baseline demonstrated significant hearing loss in 31/34 patients (91%) at 0.5 Hz (mean = 43 dB HL, range = 5–120), 1 Hz (mean = 58 dB HL, range = 10–120), 2 Hz

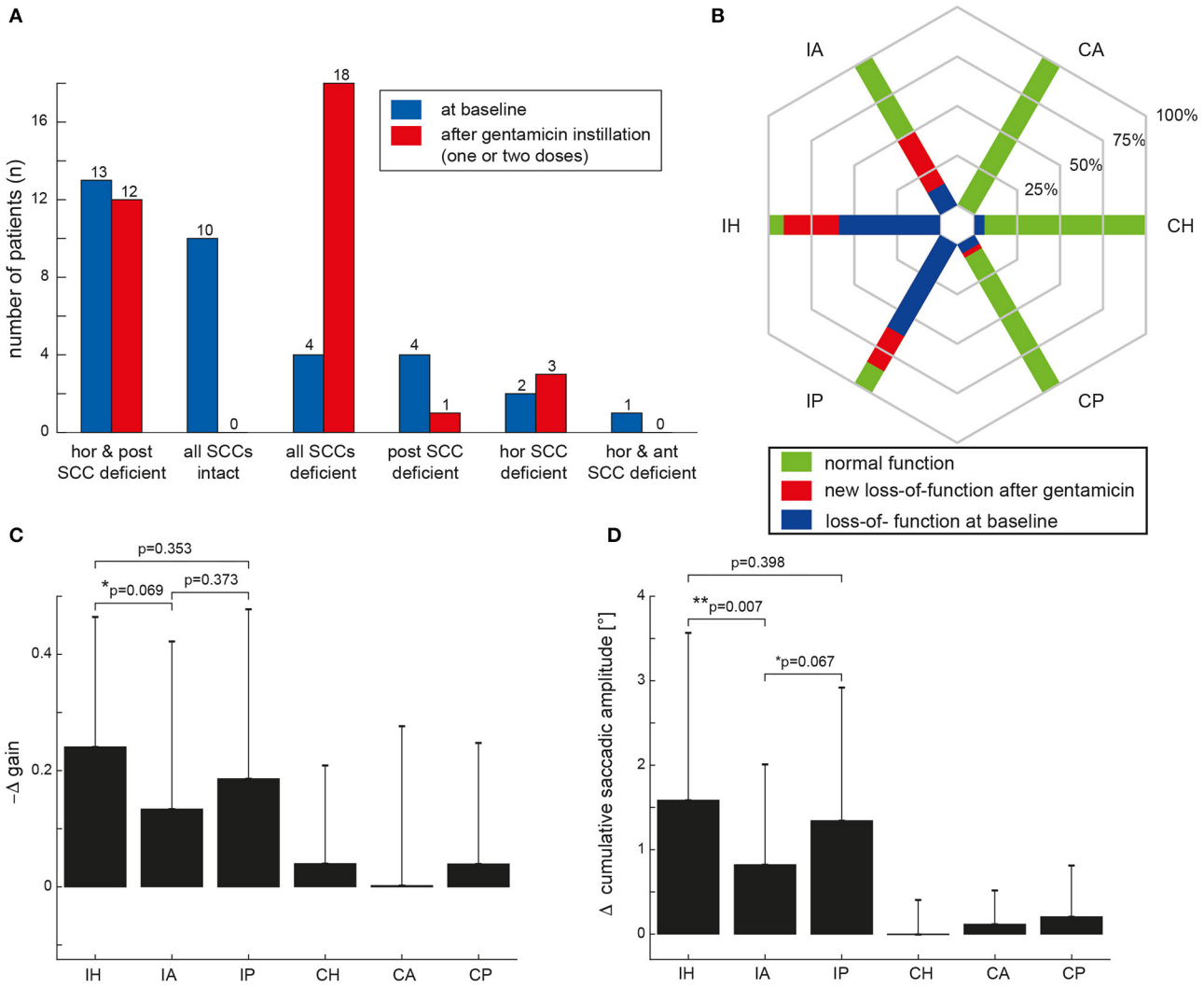

FIGURE 2 | (A) Distribution of ipsilesional impairment in semicircular canal (SCC) function based on the two reviewers' ratings both at baseline (in blue) and after intratympanic gentamicin treatment (one or two treatments, individually different) (in red). In **(B)**, the percentage of patients with normal function before and after gentamicin instillation (green areas) and with hypofunction based on the reviewers' overall ratings for the different SCCs [horizontal (H), anterior (A) and posterior (P)] are illustrated in a hexplot, differentiating between the ipsilesional (I) and the contralesional (C) side in the plot. Loss of function at baseline (indicated by the blue bars) is distinguished from new SCC hypofunction after intratympanic gentamicin application (indicated by the red bars); thus, the overall fraction of SCC impairment after gentamicin treatment is reflected by the red plus the blue fraction. In **(C,D)**, the mean (±1 SD) changes (Δ) in aVOR gain **(C)** and CSA **(D)** after intratympanic gentamicin application compared to baseline measurements (i.e., by subtracting the aVOR gain/the CSA at baseline from the aVOR gain/CSA after gentamicin instillation) are illustrated for all six SCCs. Note that aVOR-gain reductions after gentamicin instillation will result in a negative Δ gain [as indicated along the y-axis in **(C)**]. Results of the statistical analysis (GLM) are shown for the ipsilesional (I) side only as there were no significant changes ($p > 0.05$) on the contralesional (C) side. Differences with a trend to significance were indicated by "*," whereas significant (i.e., $p < 0.05$) differences were marked with a "**."

(mean = 68 dB HL, range = 5–120), and 4 Hz (mean = 73 dB HL, range = 25–120), with an average CPT-AMA hearing loss (±1SD) of 64 ± 27%. After gentamicin treatment (one or two injections), ipsilesional hearing was impaired in 32/34 patients (94%) at 0.5 Hz (mean = 50 dB HL, range = 10–120), 1 Hz (mean = 68 dB HL, range = 10–120), 2 Hz (mean = 82 dB HL, range = 25–120), and 4 Hz (mean = 86 dB HL, range = 40–120), with an increased average CPT-AMA hearing loss of 73 ± 24%. Note that no PTA was available after the first gentamicin treatment in 5 out 8 patients who received two gentamicin injections.

DISCUSSION

Vestibular pre-habilitation by use of intratympanic gentamicin prior to VS resection allows for a stepwise reduction in peripheral-vestibular function. In our study, all 34 patients showed significant reductions in aVOR gain and increases in CSA for all three SCCs compared to baseline. Changes were most profound for the horizontal SCC, and the number of patients showing normal function remained significantly larger for the anterior SCC compared to the

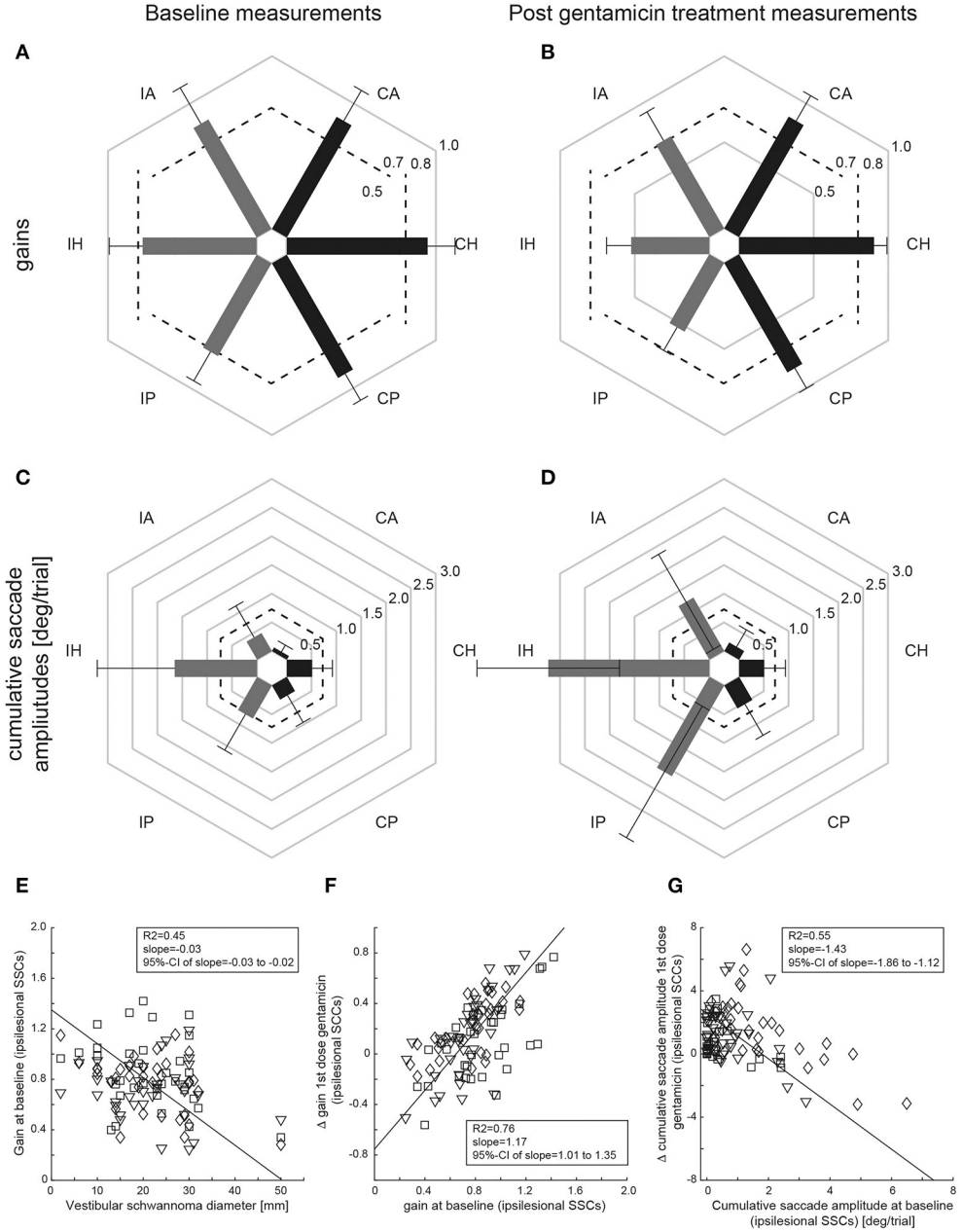

FIGURE 3 | Mean (±1SD) gains **(A,C)** and CSA **(B,D)** of all patients ($n = 34$) are shown separately for baseline (left column) and after gentamicin treatment (right column), with values from the affected [ipsilesional (I)] side and the unaffected [contralesional (C)] side indicated by gray and dark bars, respectively. Gain values (from 0 to 1) and CSA (°/trial, from 0 to 3) are provided along the different hexagons. Cutoff values for reduced gains (<0.8 for the horizontal canals, <0.7 for the vertical canals) and for abnormally increased cumulative saccade amplitudes (>0.73°/trial) are indicated by dashed lines. In **(E–G)**, correlation analyses using principal component analysis (PCA) are shown both for the size of the VS and for the aVOR gain of the individual SSCs on the affected side at baseline **(E)**, the difference (Δ) in aVOR gain (gain after 1st dose of gentamicin subtracted from gain at baseline) vs. baseline gain **(F)** and for the difference (Δ) in CSA (CSA at baseline subtracted from CSA after 1st dose of gentamicin) vs. baseline cumulative saccade amplitude **(G)**. The diamonds (horizontal canals), squares (anterior canals), and inverted triangles (posterior canals) refer to single-subject and single SCC measurements; the solid black line represents the fit of the PCA, with details shown in the inlets [including the 95% confidence interval (CI) of the slope]. Note that individual results from the three ipsilesional SCCs are combined for the PCS.

horizontal and posterior canal. Thus, the data confirms our hypothesis of preferential damage to selected SCCs due to intratympanic gentamicin application with relative sparing of the anterior canal in VS patients. Surprisingly, we also noted relative sparing of ipsilesional anterior-canal function at baseline.

TABLE 2 | Ipsilesional aVOR-gains and CSA—statistical analysis.

	Baseline aVOR gains			Post gentamicin aVOR gains			Baseline vs. post-gentamicin aVOR gains
	Ipsilesional	**Contralesional**	**Statistical analysis ipsilesional vs. contralesional**	**Ipsilesional**	**Contralesional**	**Statistical analysis ipsilesional vs. contralesional**	**Statistical analysis ipsilesional SCCs**
Horizontal SCC	0.76 ± 0.22	0.94 ± 0.19	$p < 0.001$	0.52 ± 0.16	0.91 ± 0.09	$p < 0.001$	0.76 ± 0.22 vs. 0.52 ± 0.16, $p < 0.001$
Anterior SCC	0.85 ± 0.28	0.87 ± 0.24	$p = 0.670$	0.71 ± 0.22	0.87 ± 0.19	$p = 0.002$	0.85 ± 0.28 vs. 0.71 ± 0.22, $p = 0.006$
Posterior SCC	0.72 ± 0.23	0.89 ± 0.21	$p < 0.001$	0.53 ± 0.18	0.85 ± 0.16	$p < 0.001$	0.72 ± 0.23 vs. 0.53 ± 0.18, $p < 0.001$
	Baseline CSA [°/trial]			**Post gentamicin CSA [°/trial]**			**Baseline vs. post-gentamicin CSA [°/trial]**
	Ipsilesional	**Contralesional**	**Statistical analysis ipsilesional vs. contralesional**	**Ipsilesional**	**Contralesional**	**Statistical analysis ipsilesional vs. contralesional**	**Statistical analysis ipsilesional SCCs**
Horizontal SCC	1.66 ± 1.56	0.51 ± 0.41	$p < 0.001$	3.24 ± 1.43	0.50 ± 0.43	$p < 0.001$	1.66 ± 1.56 vs. 3.24 ± 1.43, $p < 0.001$
Anterior SCC	0.42 ± 0.73	0.08 ± 0.16	$p = 0.607$	1.24 ± 1.10	0.20 ± 0.39	$p < 0.001$	0.42 ± 0.73 vs. 1.24 ± 1.10, $p < 0.001$
Posterior SCC	0.77 ± 0.83	0.32 ± 0.63	$p = 0.052$	2.11 ± 1.53	0.53 ± 0.73	$p < 0.001$	0.77 ± 0.83 vs. 2.11 ± 1.53, $p < 0.001$

aVOR, angular vestibulo-ocular reflex; CSA, cumulative saccadic amplitude; SCC, semicircular canal.

The Impact of Intratympanic Gentamicin on Peripheral-Vestibular Function in VS

The application of intratympanic gentamicin resulted in a substantial reduction in peripheral-vestibular function as assessed both by an overall rater-dependent score and by aVOR gains and CSA. Hearing loss was already substantial at baseline in most patients, remaining almost stable after gentamicin treatment. This supports the concept of pre-habilitation and emphasizes the effectiveness of gentamicin as a predominantly vestibulotoxic substance. Noteworthily, relative sparing of anterior-canal function was preserved after gentamicin application, speaking against the hypothesis that this vestibulotoxic substance eliminates any residual vestibular function in an unselective manner. In contrast, our data suggests that the anterior SCC is less susceptible to gentamicin toxicity. We have previously observed a similar effect in patients with bilateral-vestibular loss (22) due to systemic aminoglycoside treatment, and our current data confirms this characteristic pattern of anterior-canal sparing. Whereas, the manner of application (intravenous vs. intratympanic) seems to have little effect on the pattern, the underlying cause for relative sparing of anterior-canal function after aminoglycoside treatment remains unclear.

Currently, the pathophysiological mechanisms for anterior-canal sparing after aminoglycoside exposure remain unresolved. Potential explanations for anterior canal sparing [as previously discussed by (22)] after gentamicin instillation include an accumulation of gentamicin in the most basal parts of the vestibular organ, following the pull of gravity. Thus, the posterior and horizontal canal—being located below the anterior canal—would be exposed to higher doses of gentamicin. Alternatively, either the anterior SCC could be less vulnerable to gentamicin or it recovers more quickly after gentamicin-induced damage. Theoretically, anterior canal sparing in vHIT could be a measurement bias. This, however, seems unlikely for several reasons. First, sparing was restricted to certain disorders as reported 2016 by our group (22). Second, the vertical SCCs are always tested in pairs according to their planes of stimulation and head impulses of similar velocities were applied for all vertical SCCs. Third, as previously reported anecdotally, patients reported oscillopsia for upward head movements only, but not for downward head movements, matching their vHIT pattern of spared anterior SCCs (22).

Observed decreases in peripheral-vestibular function after intratympanic gentamicin ranged between 16% (anterior canal), 26% (posterior canal), and 32% (horizontal canal) as assessed by the aVOR and between 95% (horizontal canal), 174% (posterior canal), and 195% (anterior canal) reflected by increased CSA. In comparison, for the anterior canal the reduction in aVOR gain was smaller (showing a statistical trend) and the increase in CSA was significantly larger compared to the horizontal SCC. The effect size of gentamicin application depended on the initial aVOR gain, being larger in those patients with relatively preserved aVOR function. Thus, with aVOR function relatively

spared at baseline, anterior-canal function may experience a steeper decrease than horizontal-canal function, which already at baseline was more profoundly impaired. Nonetheless, aVOR-gain changes were larger for the horizontal canal than for the anterior canal, underlining the relative sparing of anterior-canal function.

Previous studies assessed aVOR reduction after intratympanic gentamicin treatment in VS by bedside head-impulse testing (13, 14, 33) and caloric irrigation (6, 7, 13, 14, 20, 33, 34). None of the published studies reported aVOR gains and/or CSA of all six SCCs assessed by vHIT.

From the perspective of pre-habilitation, residual anterior-canal function despite gentamicin treatment may make VS patients more prone to symptoms related to sudden loss of anterior-canal function after VS resection—i.e., predominantly vertical spinning vertigo. Also, a first dosage of gentamicin was ineffective in 8/34 patients, requiring a second dose. This emphasizes the need to monitor the effect of intratympanic gentamicin application by vHIT of all six SCCs.

Effect of Gentamicin Instillation on the aVOR in Menière's Disease

To further elaborate on the impact of intratympanic gentamicin treatment, we compared our results to published treatment studies on MD. Previously, others compared aVOR gains before and after gentamicin instillation in 32 patients with unilateral MD, reporting an average of 40% decrease in aVOR gain for all three canals (35). The observed drop in aVOR gain of 0.24–0.35 was similar for all three SCCs, showing no anterior-canal sparing. However, in this study only aVOR-gain values were assessed and no overall rating of the vHIT response was provided. This is distinct from our approach, possibly explaining the discrepant findings. In another study, average gains after treatment in 31 patients with unilateral definite MD were 0.61, 0.69, and 0.47, respectively, for the anterior, horizontal, and posterior SCC (36). Corresponding rates of reduction of vestibular function were 48, 26, and 36%, respectively. Using magnetic search coils to assess aVOR gains before/after gentamicin instillation in patients with MD, others reported average (±1SD) aVOR gains after intratympanic gentamicin of 0.40 ± 0.12, 0.35 ± 0.14, and 0.31 ± 0.14, for the horizontal, anterior, and posterior ipsilesional SCC (37). In another study from the same group, 18 patients with unilateral MD were followed up after a single or multiple gentamicin instillations after 12 months, again using magnetic search coils. Resulting aVOR gains after intratympanic gentamicin were 0.53 ± 0.27 (Δgain $= 0.32 \pm 0.35$), 0.47 ± 0.16 (Δgain $= 0.31 \pm 0.24$), and 0.43 ± 0.21 (Δgain $= 0.32 \pm 0.27$) for the horizontal, anterior, and posterior ipsilesional SCC (38). Thus, in these studies on the effect of gentamicin on the different SCCs in MD, no relative sparing of anterior-canal function was observed, contrasting our VS data. Potential explanations are differences in the analysis (we considered increased CSA as indicative for peripheral-vestibular loss also) and the recording system (vHIT vs. magnetic search coils).

In another study focusing on horizontal aVOR gains before and after gentamicin instillation in 20 patients with unilateral MD, both a delayed effect of gentamicin instillation with maximal aVOR gain reduction observed after 1 month and partial recovery after 3 months post-instillation were observed (39). Thus, timing after gentamicin instillation seems to be important; specifically, too early post-instillation vHIT assessment may underestimate the effect of gentamicin instillation, and in case of delayed (i.e., after more than 2 months) surgical removal of the VS the benefit of the pre-habilitation treatment may be reduced.

Anterior-Canal Sparing in VS at Baseline

In our study, baseline vHIT measurements demonstrated significantly more often ipsilesional sparing of anterior-canal function than horizontal or posterior canal function. For the anterior canal, ipsilesional aVOR gains were not significantly reduced and ipsilesional CSA were not significantly increased compared to the healthy side. In a recent study from our laboratory on the characterization of unilateral peripheral-vestibular deficits in a mixed cohort [using vHIT and ocular/cervical vestibular-evoked myogenic potentials (VEMPs)], the VS subgroup ($n = 55$) presented with anterior-canal sparing as well (25).

Noteworthily, horizontal head impulses are usually applied with higher peak head velocities than vertical head impulses and thus, may be more sensitive in detecting SCC loss of function. Whereas, in relation to horizontal canal function, this may explain relative sparing of anterior-canal function, this is not the case when comparing vertical head impulses (i.e., anterior vs. posterior canal function).

Previously, such anterior-canal sparing has been reported by others using the same vHIT goggles (40, 41). Specifically, the fraction of VS patients ($n = 41$) with loss of function of the ipsilesional anterior SCC was significantly lower than that of the horizontal (9 vs. 28, $p < 0.001$, Bonferroni-corrected for multiple tests) and the posterior (9 vs. 20, $p = 0.040$) SCC in one study (41). Likewise, in another study, rates of impairment of the ipsilesional horizontal, anterior, and posterior SCC were 34/55 (62%), 20/55 (36%), and 31/55 (57%), with significantly lower rates for the anterior canal than for the horizontal ($p = 0.002$, McNemar-test) and posterior ($p = 0.031$) SCC (40).

The reason for this anterior-canal sparing in untreated VS patients remains unclear. With the mechanism of damage being tumor growth and compression, one may speculate that those nerve fibers originating from the anterior SCC are either less prone to compression or are better protected, e.g., by a more remote location to the origin of the tumor growth.

Correlation of Tumor Size and Vestibular Loss

In our study with VS of varying size (range = 2–50 mm), we found that the size of the VS had a significant impact on the extent of peripheral-vestibular loss of function. Specifically, ipsilesional vHIT gains at baseline showed a significant inverse correlation with the VS diameter. Previously, others have reported similar findings (40). Specifically, using an audio-vestibular test battery (vHIT, PTA, ocular/cervical VEMPs), damage to at least one vestibular sensor was less frequent in those patients with a VS diameter of ≤ 14 *mm* compared to those with a VS diameter >14 mm (39 vs. 100%). Likewise, a significant association

between tumor size and horizontal-SCC function (assessed by vHIT or caloric irrigation) was reported by several groups (42–44). Noteworthily, others have failed to show such a relationship (41, 45). This discrepancy may be related to the patient sample size, the parameters chosen for comparison, and the statistical analyses performed.

Limitations

Our study has several limitations. This includes the individually varying doses of gentamicin applied intratympanically and also the lack of a control group receiving placebo instead. Furthermore, we did not assess the impact of gentamicin instillation on utricular and saccular function and did not assess the symptom severity after VS resection. Thus, based on the study design applied here (focusing on aVOR properties before and after gentamicin instillation), we cannot make any conclusions about the impact of vestibular pre-habilitation using intratympanic gentamicin application on recovery after VS resection. To answer this clinically important question, further research and specifically designed studies will be needed, comparing the outcome after VS resection in different treatment groups (pre-habilitation vs. standard treatment only).

CONCLUSIONS

Intratympanic gentamicin application resulted in a substantial reduction of peripheral-vestibular function in all three SCCs. Relative sparing of anterior-canal function noted at baseline was preserved after gentamicin treatment, with a significantly larger decrease in peripheral-vestibular function in the horizontal SCC compared to the anterior SCC (as reflected by changes in CSA). This has two major implications. First, our data confirms that pre-surgical intratympanic gentamicin was successful in reducing residual peripheral-vestibular function before surgery, thus further supporting the concept of vestibular pre-habilitation. Second, relative sparing of anterior-canal function in VS patients at baseline and after gentamicin application suggests that the vulnerability of the distinct SCCs to both local damage of nerve fibers due to tumor growth and to vestibulotoxic substances varies. The reasons for such relative sparing of the anterior SCC remain to be determined.

DATA AVAILABILITY STATEMENT

The raw data supporting the conclusions of this article will be made available by the authors, without undue reservation.

ETHICS STATEMENT

The studies involving human participants were reviewed and approved by Cantonal Ethics Committee Zurich. The patients/participants provided their written informed consent to participate in this study.

AUTHOR CONTRIBUTIONS

AT conception and design of the experiments, analysis and interpretation of data, drafting and revision of the article critically for important intellectual content. CB analysis and interpretation of data and revision of the article critically for important intellectual content. EB data collection and revision of the article critically for important intellectual content. AH, VW, and KW conception and design of the experiments, interpretation of data, revision of the article critically for important intellectual content. All authors have approved the final version of the manuscript, all persons designated as authors qualify for authorship, and all those who qualify for authorship are listed.

REFERENCES

1. Wolbers JG, Dallenga AH, Mendez Romero A, Van Linge A. What intervention is best practice for vestibular schwannomas? A systematic review of controlled studies. *BMJ Open.* (2013) 3:e001345. doi: 10.1136/bmjopen-2012-001345
2. Carlson ML, Link MJ, Wanna GB, Driscoll CL. Management of sporadic vestibular schwannoma. *Otolaryngol Clin North Am.* (2015) 48:407–22. doi: 10.1016/j.otc.2015.02.003
3. Hadjipanayis CG, Carlson ML, Link MJ, Rayan TA, Parish J, Atkins T, et al. Congress of neurological surgeons systematic review and evidence-based guidelines on surgical resection for the treatment of patients with vestibular schwannomas. *Neurosurgery.* (2018) 82:E40–3. doi: 10.1093/neuros/nyx512
4. Goldbrunner R, Weller M, Regis J, Lund-Johansen M, Stavrinou P, Reuss D, et al. EANO guideline on the diagnosis and treatment of vestibular schwannoma. *Neuro Oncol.* (2020) 22:31–45. doi: 10.1093/neuonc/noz153
5. Broomfield SJ, Mandavia AK, Nicholson JS, Mahmoud O, King AT, Rutherford SA, et al. Long-term quality of life following vestibular schwannoma excision via the translabyrinthine approach. *Otol Neurotol.* (2017) 38:1165–73. doi: 10.1097/MAO.0000000000001507
6. Magnusson M, Kahlon B, Karlberg M, Lindberg S, Siesjo P. Preoperative vestibular ablation with gentamicin and vestibular 'prehab' enhance postoperative recovery after surgery for pontine angle tumours–first report. *Acta Otolaryngol.* (2007) 127:1236–40. doi: 10.1080/00016480701663433
7. Magnusson M, Kahlon B, Karlberg M, Lindberg S, Siesjo P, Tjernstrom F. Vestibular "PREHAB". *Ann NY Acad Sci.* (2009) 1164:257–62. doi: 10.1111/j.1749-6632.2009.03778.x
8. Tjernstrom F, Fransson PA, Kahlon B, Karlberg M, Lindberg S, Siesjo P, et al. Vestibular PREHAB and gentamicin before schwannoma surgery may improve long-term postural function. *J Neurol Neurosurg Psychiatry.* (2009) 80:1254–60. doi: 10.1136/jnnp.2008.170878
9. Tjernstrom F, Fransson PA, Kahlon B, Karlberg M, Lindberg S, Siesjo P, et al. PREHAB vs. REHAB—presurgical treatment in vestibular schwannoma surgery enhances recovery of postural control better than postoperative rehabilitation: Retrospective case series. *J Vestib Res.* (2018) 27:313–25. doi: 10.3233/VES-170626
10. Van Gompel JJ, Agazzi S, Carlson ML, Adewumi DA, Hadjipanayis CG, Uhm JH, et al. Congress of neurological surgeons systematic review and evidence-based guidelines on emerging therapies for the treatment of patients with vestibular schwannomas. *Neurosurgery.* (2018) 82:E52–4. doi: 10.1093/neuros/nyx516
11. Amiraraghi N, Gaggini M, Crowther JA, Locke R, Taylor W, Kontorinis G. Benefits of pre-labyrinthectomy intratympanic gentamicin: contralateral vestibular responses. *J Laryngol Otol.* (2019) 133:668–73. doi: 10.1017/S0022215119001002
12. Deveze A, Bernard-Demanze L, Xavier F, Lavieille JP, Elziere M. Vestibular compensation and vestibular rehabilitation. *Curr Concepts New Trends Neurophysiol Clin.* (2014) 44:49–57. doi: 10.1016/j.neucli.2013.10.138

13. Cada Z, Balatkova Z, Chovanec M, Cakrt O, Hruba S, Jerabek J, et al. Vertigo perception and quality of life in patients after surgical treatment of vestibular schwannoma with pretreatment prehabituation by chemical vestibular ablation. *Biomed Res Int.* (2016) 2016:6767216. doi: 10.1155/2016/6767216
14. Balatkova Z, Cada Z, Hruba S, Komarc M, Cerny R. Assessment of visual sensation, psychiatric profile and quality of life following vestibular schwannoma surgery in patients prehabituated by chemical vestibular ablation. *Biomed Pap Med Fac Univ Palacky Olomouc Czech Repub.* (2019) 164:444–53. doi: 10.5507/bp.2019.056
15. Tjernstrom F, Fransson PA, Kahlon B, Karlberg M, Lindberg S, Siesjo P, et al. Different visual weighting due to fast or slow vestibular deafferentation: before and after schwannoma surgery. *Neural Plast.* (2019) 2019:4826238. doi: 10.1155/2019/4826238
16. Forge A, Schacht J. Aminoglycoside antibiotics. *Audiol Neurootol.* (2000) 5:3–22. doi: 10.1159/000013861
17. Weber KP, Aw ST, Todd MJ, Mcgarvie LA, Curthoys IS, Halmagyi GM. Horizontal head impulse test detects gentamicin vestibulotoxicity. *Neurology.* (2009) 72:1417–24. doi: 10.1212/WNL.0b013e3181a18652
18. Ahmed RM, Hannigan IP, Macdougall HG, Chan RC, Halmagyi GM. Gentamicin ototoxicity: a 23-year selected case series of 103 patients. *Med J Aust.* (2012) 196:701–4. doi: 10.5694/mja11.10850
19. Smyth D, Mossman S, Weatherall M, Jolliffe E, Joshi P, Taylor J, et al. Gentamicin vestibulotoxicity with modern systemic dosing regimens: a prospective study using video-oculography. *Acta Otolaryngol.* (2019) 139:759–68. doi: 10.1080/00016489.2019.1637935
20. Tjernstrom F, Fransson PA, Kahlon B, Karlberg M, Lindberg S, Siesjo P, et al. Hearing and vestibular function after preoperative intratympanic gentamicin therapy for vestibular schwanomma as part of vestibular prehab. *Ear Hear.* (2016) 37:744–50. doi: 10.1097/AUD.0000000000000340
21. Aw ST, Todd MJ, Aw GE, Weber KP, Halmagyi GM. Gentamicin vestibulotoxicity impairs human electrically evoked vestibulo-ocular reflex. *Neurology.* (2008) 71:1776–82. doi: 10.1212/01.wnl.0000335971.43443.d9
22. Tarnutzer AA, Bockisch CJ, Buffone E, Weiler S, Bachmann LM, Weber KP. Disease-specific sparing of the anterior semicircular canals in bilateral vestibulopathy. *Clin Neurophysiol.* (2016) 127:2791–801. doi: 10.1016/j.clinph.2016.05.005
23. Pullens B, Van Benthem PP. Intratympanic gentamicin for Meniere's disease or syndrome. *Cochrane Database Syst Rev.* (2011) 3:CD008234. doi: 10.1002/14651858.CD008234.pub2
24. Watson GJ, Nelson C, Irving RM. Is low-dose intratympanic gentamicin an effective treatment for Meniere's disease: the Birmingham experience. *J Laryngol Otol.* (2015) 129:970–3. doi: 10.1017/S0022215115002200
25. Tarnutzer AA, Bockisch CJ, Buffone E, Weber KP. Vestibular mapping in patients with unilateral peripheral-vestibular deficits. *Neurology.* (2020) 95:e2988–3001. doi: 10.1212/WNL.0000000000010812
26. Macdougall HG, Mcgarvie LA, Halmagyi GM, Curthoys IS, Weber KP. Application of the video head impulse test to detect vertical semicircular canal dysfunction. *Otol Neurotol.* (2013) 34:974–9. doi: 10.1097/MAO.0b013e31828d676d
27. Macdougall HG, Mcgarvie LA, Halmagyi GM, Curthoys IS, Weber KP. The video head impulse test (vHIT) detects vertical semicircular canal dysfunction. *PLoS ONE.* (2013) 8:e61488. doi: 10.1371/journal.pone.0061488
28. Weber KP, Aw ST, Todd MJ, Mcgarvie LA, Curthoys IS, Halmagyi GM. Head impulse test in unilateral vestibular loss: vestibulo-ocular reflex and catch-up saccades. *Neurology.* (2008) 70:454–63. doi: 10.1212/01.wnl.0000299117.48935.2e
29. Macdougall HG, Mcgarvie LA, Halmagyi GM, Rogers SJ, Manzari L, Burgess AM, et al. A new saccadic indicator of peripheral vestibular function based on the video head impulse test. *Neurology.* (2016) 87:410–8. doi: 10.1212/WNL.0000000000002827
30. Cohen J. A coefficient for agreement for nominal scales. *Educ Psychol Meas.* (1960) 20:37–46. doi: 10.1177/001316446002000104
31. Ward BK, Bockisch CJ, Caramia N, Bertolini G, Tarnutzer AA. Gravity dependence of the effect of optokinetic stimulation on the subjective visual vertical. *J Neurophysiol.* (2017) 117:1948–58. doi: 10.1152/jn.00303.2016
32. Council on Physical Therapy AMA. Tentative standard procedures for evaluating the percentage of useful hearing loss in medicolegal cases. *JAMA.* (1942) 119:1108–9.
33. Giannuzzi AL, Merkus P, Falcioni M. The use of intratympanic gentamicin in patients with vestibular schwannoma and disabling vertigo. *Otol Neurotol.* (2013) 34:1096–8. doi: 10.1097/MAO.0b013e3182804c41
34. Yang J, Jia H, Li G, Huang M, Zhu W, Wang Z, et al. Intratympanic gentamicin for small vestibular schwannomas with intractable vertigo. *Otol Neurotol.* (2018) 39:e699–703. doi: 10.1097/MAO.0000000000001899
35. Buki B, Junger H. Intratympanal gentamicin in Meniere's disease: effects on individual semicircular canals. *Auris Nasus Larynx.* (2018) 45:39–44. doi: 10.1016/j.anl.2017.02.008
36. Marques P, Manrique-Huarte R, Perez-Fernandez N. Single intratympanic gentamicin injection in Meniere's disease: VOR change and prognostic usefulness. *Laryngoscope.* (2015) 125:1915–20. doi: 10.1002/lary.25156
37. Carey JP, Minor LB, Peng GC, Della Santina CC, Cremer PD, Haslwanter T. Changes in the three-dimensional angular vestibulo-ocular reflex following intratympanic gentamicin for Meniere's disease. *J Assoc Res Otolaryngol.* (2002) 3:430–43. doi: 10.1007/s101620010053
38. Lin FR, Migliaccio AA, Haslwanter T, Minor LB, Carey JP. Angular vestibulo-ocular reflex gains correlate with vertigo control after intratympanic gentamicin treatment for Meniere's disease. *Ann Otol Rhinol Laryngol.* (2005) 114:777–85. doi: 10.1177/000348940511401007
39. Martin-Sanz E, Diaz JY, Esteban-Sanchez J, Sanz-Fernandez R, Perez-Fernandez N. Delayed effect and gain restoration after intratympanic gentamicin for Meniere's disease. *Otol Neurotol.* (2019) 40:79–87. doi: 10.1097/MAO.0000000000001973
40. Taylor RL, Kong J, Flanagan S, Pogson J, Croxson G, Pohl D, et al. Prevalence of vestibular dysfunction in patients with vestibular schwannoma using video head-impulses and vestibular-evoked potentials. *J Neurol.* (2015) 262:1228–37. doi: 10.1007/s00415-015-7697-4
41. Constanzo F, Teixeira BCA, Sens P, Ramina R. Video head impulse test in vestibular schwannoma: relevance of size and cystic component on vestibular impairment. *Otol Neurotol.* (2019) 40:511–6. doi: 10.1097/MAO.0000000000002158
42. Batuecas-Caletrio A, Santa Cruz-Ruiz S, Munoz-Herrera A, Perez-Fernandez N. The map of dizziness in vestibular schwannoma. *Laryngoscope.* (2015) 125:2784–9. doi: 10.1002/lary.25402
43. Tranter-Entwistle I, Dawes P, Darlington CL, Smith PF, Cutfield N. Video head impulse in comparison to caloric testing in unilateral vestibular schwannoma. *Acta Otolaryngol.* (2016) 136:1110–4. doi: 10.1080/00016489.2016.1185540
44. Brown CS, Peskoe SB, Risoli T, Jr., Garrison DB, Kaylie DM. Associations of video head impulse test and caloric testing among patients with vestibular schwannoma. *Otolaryngol Head Neck Surg.* (2019) 161:324–9. doi: 10.1177/0194599819837244
45. Fujiwara K, Morita S, Fukuda A, Akamatsu H, Yanagi H, Hoshino K, et al. Analysis of semicircular canal function as evaluated by video Head Impulse Test in patients with vestibular schwannoma. *J Vestib Res.* (2020) 30:101–8. doi: 10.3233/VES-200695

Conflict of Interest: KW was supported by the Swiss National Science Foundation (320030_166346) and the Uniscientia Stiftung, Vaduz, Liechtenstein. He acts as an unpaid consultant and has received funding for travel from Otometrics.

The remaining authors declare that the research was conducted in the absence of any commercial or financial relationships that could be construed as a potential conflict of interest.

frontiers in Neurology

REVIEW
published: 04 March 2021
doi: 10.3389/fneur.2021.636224

Neuroimaging Markers of Mal de Débarquement Syndrome

Yoon Hee Cha[1]*, *Lei Ding*[2,3] *and Han Yuan*[2,3]

[1] Department of Neurology, University of Minnesota, Minneapolis, MN, United States, [2] Stephenson School of Biomedical Engineering, University of Oklahoma, Norman, OK, United States, [3] Institute for Biomedical Engineering, Science, and Technology, University of Oklahoma, Norman, OK, United States

Mal de débarquement syndrome (MdDS) is a motion-induced disorder of oscillating vertigo that persists after the motion has ceased. The neuroimaging characteristics of the MdDS brain state have been investigated with studies on brain metabolism, structure, functional connectivity, and measurements of synchronicity. Baseline metabolism and resting-state functional connectivity studies indicate that a limbic focus in the left entorhinal cortex and amygdala may be important in the pathology of MdDS, as these structures are hypermetabolic in MdDS and exhibit increased functional connectivity to posterior sensory processing areas and reduced connectivity to the frontal and temporal cortices. Both structures are tunable with periodic stimulation, with neurons in the entorhinal cortex required for spatial navigation, acting as a critical efferent pathway to the hippocampus, and sending and receiving projections from much of the neocortex. Voxel-based morphometry measurements have revealed volume differences between MdDS and healthy controls in hubs of multiple resting-state networks including the default mode, salience, and executive control networks. In particular, volume in the bilateral anterior cingulate cortices decreases and volume in the bilateral inferior frontal gyri/anterior insulas increases with longer duration of illness. Paired with noninvasive neuromodulation interventions, functional neuroimaging with functional magnetic resonance imaging (fMRI), electroencephalography (EEG), and simultaneous fMRI-EEG have shown changes in resting-state functional connectivity that correlate with symptom modulation, particularly in the posterior default mode network. Reduced parieto-occipital connectivity with the entorhinal cortex and reduced long-range fronto-parieto-occipital connectivity correlate with symptom improvement. Though there is a general theme of desynchronization correlating with reduced MdDS symptoms, the prediction of optimal stimulation parameters for noninvasive brain stimulation in individuals with MdDS remains a challenge due to the large parameter space. However, the pairing of functional neuroimaging and noninvasive brain stimulation can serve as a probe into the biological underpinnings of MdDS and iteratively lead to optimal parameter space identification.

Keywords: mal de débarquement syndrome, persistent oscillating vertigo, functional MRI, voxel-based morphometry, positron emission tomography, independent component phase coherence, noninvasive brain stimulation

OPEN ACCESS

Edited by:
Michael Strupp, Ludwig Maximilian University of Munich, Germany

Reviewed by:
Eek-Sung Lee, Soon Chun Hyang University Bucheon Hospital, South Korea
Vincenzo Marcelli, Local Health Authority Naples 1 Center, Italy

***Correspondence:**
Yoon Hee Cha
ycha@umn.edu
orcid.org/0000-0003-3804-0879

Specialty section:
This article was submitted to Neuro-Otology, a section of the journal Frontiers in Neurology

Received: *01 December 2020*
Accepted: *22 January 2021*
Published: *04 March 2021*

Citation:
Cha YH, Ding L and Yuan H (2021) Neuroimaging Markers of Mal de Débarquement Syndrome. Front. Neurol. 12:636224. doi: 10.3389/fneur.2021.636224

INTRODUCTION

Mal de débarquement syndrome (MdDS) is a disorder of persistent oscillating vertigo that follows entrainment to passive motion such as during water, air, or land travel (1). Symptoms are described as a "rocking," "bobbing," or "swaying" perception that is nulled by exposure to passive motion such as driving/riding in a car or returning to the triggering stimulus. The nonspinning vertigo of MdDS is not based on any underlying peripheral vestibular dysfunction (2). It was hypothesized and then shown in neuroimaging studies using positron emission tomography (PET), structural magnetic resonance imaging (MRI), functional MRI (fMRI), electroencephalography (EEG), and simultaneous fMRI-EEG that there are central nervous system correlates of MdDS that are involved in the persistence of the disorder (3). These imaging correlates can be captured as baseline metrics and as dynamic changes following symptom modification with noninvasive brain stimulation. These studies indicate that functional connectivity measured by fMRI or EEG can be used as markers of MdDS and serve as guides for neuromodulation-based interventions.

Positron Emission Tomography

The earliest neuroimaging study and the only PET study that evaluated glucose metabolism during ongoing MdDS symptoms was reported by Cha et al. (4) in 2012. In this study, 20 individuals with MdDS (mean age 43.4 years, range 27–66 years) with a median symptom duration of 17.5 months (range 3–240 months) underwent $^{18}F^{18}$-FDG PET and were compared with 20 age-, sex-, and handedness-matched healthy controls. These participants underwent structural and resting-state fMRI on the same day immediately before the PET scan. After age and gray matter volume were corrected, as well as concurrent measures of anxiety and depression, a single cluster of hypermetabolism ($z >$ 3.3) at Montreal Neurological Institute (MNI) coordinates (−14, −8, −22) mapping to the junction between the left entorhinal cortex and amygdala was revealed (**Figure 1A**). Compared with the singular area of hypermetabolism in MdDS, there was a larger volume of cortex that exhibited hypometabolism. These areas were largely in the prefrontal and temporal cortices ipsilateral to the area of hypermetabolism (**Figure 1B**).

The potential role of the entorhinal cortex in MdDS pathophysiology discovered in this study relates to its function as a hub in a widespread brain network involved in memory, navigation, and mapping of self-location (5, 6). It provides the main efferent input into the hippocampus and is highly interconnected with the neocortex (5, 7, 8). Medial entorhinal cortex neurons fire in a hexagonally tuned manner sensitive to gaze direction, direction of heading, and speed (9–12). Graded persistent activity that is tunable to the periodicity of the stimulus is noted in both the entorhinal cortex and amygdala neurons, which is of particular relevance to MdDS since the main triggers of MdDS are characterized by oscillating motion inputs, and the entorhinal cortex is at least partially under vestibular influence (13–16). The functional consequences of reduced metabolism in the prefrontal and temporal areas are less clear, as all these areas are heteromodal, but both the left superior frontal gyrus and the left middle frontal gyrus just anterior to the precentral gyrus (as specifically found in this study) have been shown to activate during tasks of introspection and deactivate during sensorimotor processing (17).

While it may be premature to assign the functional relevance of the left-sided bias of the differential metabolic activity in this study to the semiology of MdDS, both the entorhinal cortex and the hippocampus to which it projects do exhibit some lateralization of function. Both the left and right entorhinal cortices activate during object recognition and spatial processing tasks, with the left side biased toward object recognition and the

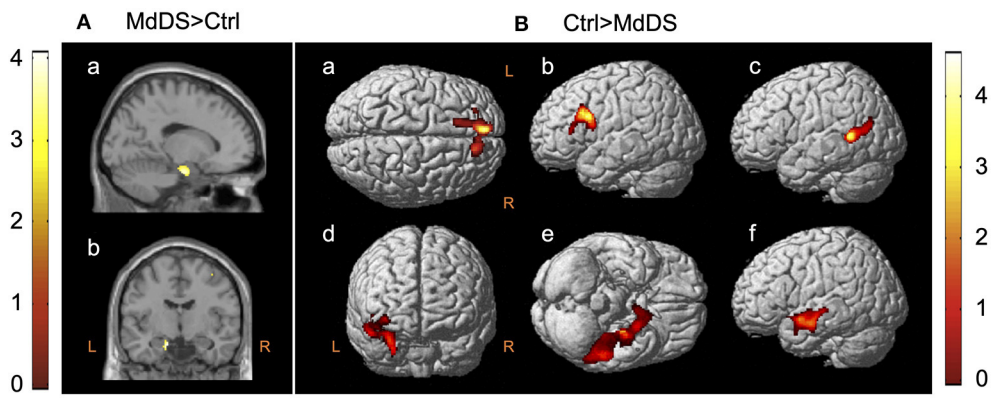

FIGURE 1 | ^{18}F-FDG PET contrasts between mal de débarquement syndrome (MdDS) and controls (Ctrl) with differences of $z > 3.3$. Clusters are shown at $z > 2.57$ for the MdDS > Ctrl contrast and at $z > 1.96$ for the Ctrl > MdDS contrast for better visualization. Coordinates of peak significance are indicated in parentheses. In SPM, negative *X*-values are on the left and positive on the right. **(A)** MdDS > Ctrl: left entorhinal cortex/amygdala [Montreal Neurological Institute (MNI): −14, −8, −22], (a) sagittal view and (b) coronal view. **(B)** Ctrl > MdDS: (a) left superior medial gyrus (MNI: −8, 52, 36), (b) left middle frontal gyrus (MNI: −32, 18, 30), (c) left middle temporal gyrus (MNI: −50, −52, 8), (d) right insula/amygdala (MNI: 30, −2, −26 and 40, 2, −8), (e) left inferior temporal gyrus (MNI: −52, −38, −24), and (f) left superior temporal gyrus (MNI: −52, 0, −14). Figure adapted from Cha YH et al., *PLOS One* 2012 (4).

right side biased toward spatial processing (18). This is consistent with electrical recordings with subdural and depth electrodes in people doing virtual reality tasks in which low theta (1–3 Hz) power increases in the left hippocampus during semantic memory tasks but in the right hippocampus during spatial navigation tasks (19). Navigation studies in humans playing virtual reality games during fMRI acquisition indicate that the left hippocampus activates when the participant uses "egocentric," self-orientation cues whereas the right hippocampus activates when they use "allocentric," environmental cues as navigation strategies (20). These studies indicate that the left entorhinal cortex–hippocampus bias toward semantic processing may be used to navigate based on self-reference (e.g., the person goes to *their* "left, then right, then left"), whereas the right entorhinal cortex–hippocampus bias toward spatial processing may be used to navigate based on an awareness of an environmental map (e.g., the person navigates in relation to where they are in a map). As a hypothesis, a shift to a semantic memory-based egocentric strategy for navigation may be more useful when external sensory stimuli cannot be processed reliably.

One concern related to the discovery of a limbic focus of altered activity in MdDS is the potential confound of concurrent depression and anxiety. In order to determine whether these metabolism findings could be related to concurrent anxiety or depression, the anxiety and depression subscores of the Hospital Anxiety and Depression Scale (HADS) were used as nuisance regressors and were additionally used in multiple regression analyses to determine which brain regions correlated most strongly with these scores (21). Depression scores correlated with increased metabolism in the pregenual anterior cingulate cortex (pgACC), while anxiety scores correlated with increased metabolism in the dorsal midbrain and anterior temporal lobes. These regions did not show any overlap with regions that showed differential metabolism between MdDS and healthy controls but had been previously identified as brain regions related to mood and anxiety disorders (22–24). Interestingly, though activation of the amygdala is typical in fMRI studies on mood and anxiety disorders, metabolic abnormalities are not found in limbic areas in these disorders but rather in the prefrontal, pregenual, and basal ganglia (25–27). Only one study in depression found an increased amygdala metabolism localized to the right side (28).

A second PET study of relevance to MdDS compared baseline cerebral metabolic differences in fishermen who were prone to land sickness vs. those who were not (29). In this study of 28 fishermen, 15 were susceptible to developing transient symptoms of land sickness for 2–6 h after coming off of fishing expeditions, while 13 were not. All peripheral vestibular testing metrics including video-oculography, video head impulse test (vHIT), cervical vestibular evoked myogenic potentials (cVEMPs), and ocular VEMPS (oVEMPs) were normal in the two groups. Though there was a trend toward younger age in the group that tended to develop land sickness vs. those who did not (mean 50.9 vs. 56.7 years), there was no difference in terms of years of experience or time at sea between the two groups. However, there were two notable differences between individuals who tended to develop land sickness and those who did not: land sickness-prone individuals performed better on a visuospatial short-term memory test called the Corsi block test, and they were much less likely to suffer from motion sickness on other modes of transportation. These individuals, who were evenly split between men and women, were imaged during the nonsymptomatic period.

In the individuals who were prone to developing land sickness, there was hypometabolism in the right cerebellar inferior semilunar lobule (HVIIA), uvula, nodulus, and tonsil with relative hypermetabolism in the bilateral prefrontal and occipital cortices, specifically in the left superior occipital, superior, and inferior parietal lobules (SPL and IPL), and bilateral superior frontal gyri including the dorsolateral prefrontal cortex (DLPFC). The foci that survived a statistical threshold of $z > 3.3$ were the right superior frontal gyrus and the left SPL. Structural imaging was reported as normal, but areas of difference in metabolism were not corrected for differences in gray matter volume.

Reduced vestibulocerebellar metabolism in land sickness-prone individuals was postulated to relate to suppression of visual–vestibular inputs during continuous vestibular activation during wave-motion exposure, while higher metabolism in the occipital cortices in these individuals was postulated to relate to greater visual dependence with perhaps a heightened ability to suppress low-frequency vestibular signals that can trigger motion sickness. Similarly, higher prefrontal activity was postulated to be involved in the regulation of mood and anxiety. Along with the increases in metabolism in the SPL, this higher prefrontal activity may contribute to enhanced visual orientation and visuospatial attention required to suppress motion sickness but could potentially lead to more land sickness.

Given the inclusion of different sexes and symptom states, it is not possible to directly compare the results of these two PET studies. Land sickness is well-recognized as a common phenomenon affecting over 70% of otherwise healthy individuals and is not considered to be pathologic (30–32). Consistent with prior studies on land sickness, the PET study on land sickness-prone fishermen found a roughly equal distribution of men and women in the groups prone to land sickness and those who were not (33, 34). This is in contrast to studies on persistent MdDS that show an overwhelming predominance of women (3, 33). However, both studies contribute to an understanding of how brain metabolism signatures can represent both current symptoms and serve as markers of vulnerability to post-motion oscillating vertigo.

RESTING-STATE FUNCTIONAL MAGNETIC RESONANCE IMAGING

Low-frequency spontaneous oscillations in cortical activity can be measured through blood oxygen level-dependent (BOLD) signals to reveal functionally connected regions (35, 36). Functional connectivity may be quantified by measurement of correlated activity between regions of interests or through independent component analysis to reveal intrinsic differences in connectivity between populations. Measurement of the synchronicity of very low-frequency BOLD fluctuations has revealed that the brain is organized into a number of functionally

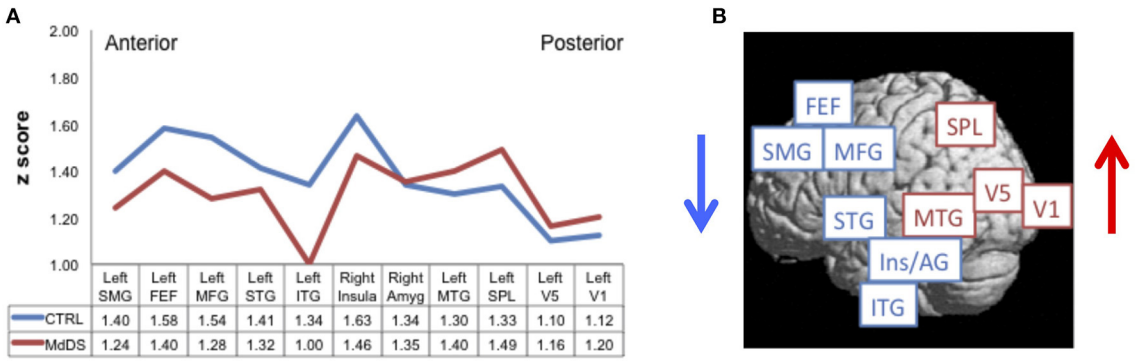

	Left SMG	Left FEF	Left MFG	Left STG	Left ITG	Right Insula	Right Amyg	Left MTG	Left SPL	Left V5	Left V1
CTRL	1.40	1.58	1.54	1.41	1.34	1.63	1.34	1.30	1.33	1.10	1.12
MdDS	1.24	1.40	1.28	1.32	1.00	1.46	1.35	1.40	1.49	1.16	1.20

FIGURE 2 | Resting-state functional connectivity reflected by Pearson correlation coefficients converted to *z*-scores **(A)** between the left entorhinal cortex/amygdala seed of hypermetabolism [entorhinal cortex/amygdala (EC/AG)] and regions of hypometabolism [left superior medial gyrus (SMG), left middle frontal gyrus (MFG), left superior temporal gyrus (STG), left inferior temporal gyrus (ITG), right insula (Insula), right amygdala (Amyg), and left middle temporal gyrus (MTG)], functionally defined frontal eye fields (FEF), motion-sensitive area V5 (V5), primary visual cortex V1 (V1), and anatomically defined superior parietal lobule (SPL). Connectivity for MdDS is shown in red; Controls (Ctrl) in blue. Connectivity differences of anterior to posterior nodes between MdDS and Ctrl participants are shown pictorially in **(B)**. Figure adapted from Cha YH et al., *PLOS One* 2012 (4).

distinct but spatially distributed networks across the cerebrum and cerebellum (37, 38). Temporally correlated activity within these distributed regions defines a resting-state network with over a dozen networks that have been consistently identified across studies. While some networks are related to specific tasks such as auditory, visual, language, and sensorimotor, there are others that are localized to particular regions such as the basal ganglia, posterior insula, and precuneus (39). Three networks that are considered to be "amodal" include the default mode network (DMN), the salience network (SN), and the executive control network (ECN) (aka central executive network) (39). These networks are involved in the general tasks of shifting attention and processing of self-referential or externally driven mental activity and function across task-specific networks. Imaging studies indicate a role for each of these networks in MdDS pathophysiology. Of note, MdDS is significantly more common in women, but connectivity within these major amodal intrinsic brain networks does not appear to be the reason, as they are robustly detectable in men and women to a similar degree (40).

The DMN is activated during self-referential information processing and is composed of key nodes in the medial prefrontal cortex (mPFC), posterior cingulate cortex (PCC), precuneus, intraparietal sulcus (IPS), and hippocampal formation (HF+), which includes the entorhinal cortex (41, 42). The DMN connection to the hippocampus proper flows through the entorhinal cortex (43). These hubs play critical roles in memory retrieval, navigation, internal mental monitoring, and taking on the perspective of others (39, 42). Dysfunction within the DMN has been noted in a growing number of brain disorders including autism, Alzheimer's disease, depression, and schizophrenia (42, 44).

The SN has major hubs in the anterior insula and the anterior cingulate cortex (ACC) and serves to shift attention to behaviorally relevant stimuli whether internal or external (45). The ECN is anchored in the DLPFC, ventrolateral prefrontal cortex (VLPFC), and supramarginal gyrus and is involved in working memory and directed attention (39).

Resting-state fMRI data acquired in 20 individuals with MdDS and 20 healthy controls were used to calculate the degree of functional connectivity between the entorhinal cortex/amygdala area of hypermetabolism and specific areas of the neocortex (4). Pearson's correlation coefficients were calculated between the entorhinal cortex/amygdala seed and primary visual cortex V1, motion-sensitive area V5 (localized with a visual motion task), SPL, the frontal eye fields (FEF) (localized with a saccade task), and all the regions that were hypometabolic in MdDS individuals compared with controls.

Comparisons between individuals with MdDS and healthy controls using this seed-based analysis revealed two distinct patterns of connectivity differences. First, individuals with MdDS showed decreased connectivity between the entorhinal cortex/amygdala seed and the left superior medial gyrus, left middle frontal gyrus, left superior and middle temporal gyri, FEF, and right insula, while showing increased connectivity with areas V1, V5, SPL, middle temporal gyrus, and right amygdala (**Figure 2A**). The general pattern was of increased connectivity with parieto-occipital visual–vestibular areas but reduced connectivity with prefrontal and temporal areas (**Figure 2B**). Second, functional connectivity was reduced between all homologous brain regions queried except for areas V1 and V5 in which the interhemispheric connectivity between MdDS and controls participants was the same. One interpretation was that this pattern represents enhanced visuo-spatial information transduction to a core hub of spatial information processing, which is under less regulatory control. Activation of the entorhinal cortex and amygdala neurons inhibits prefrontal neurons and vice versa, which are components of a network that can act in a reverberating manner (46–48). A mutually inhibitory process could lead to a "winner take all"

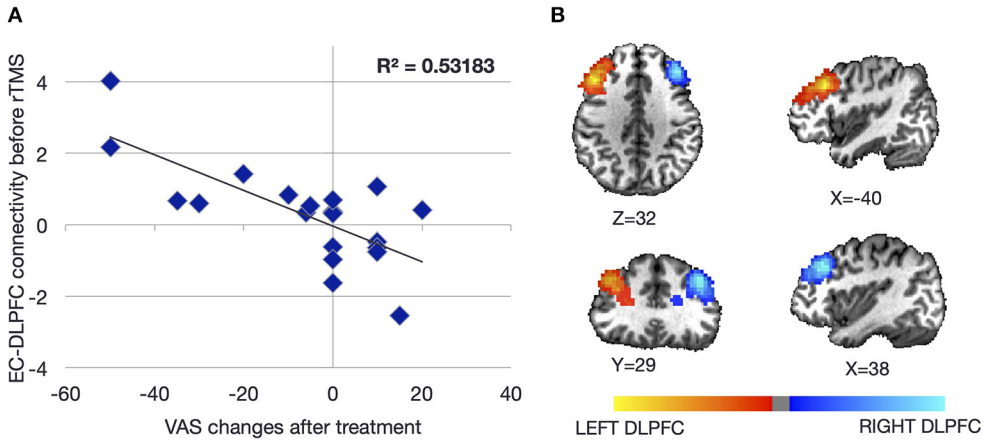

FIGURE 3 | Baseline resting-state functional connectivity between the left and right dorsolateral prefrontal cortices (DLPFCs) and the ipsilateral entorhinal cortex as a function of symptom severity change after repetitive transcranial magnetic stimulation (rTMS) to the DLPFC. Individuals with higher baseline connectivity between the DLPFC and ipsilateral entorhinal cortex responded better to rTMS **(A)**. The location of each DLPFC was determined from individualized neuronavigation targets aiming for the anterior portion of the middle of the middle frontal gyrus **(B)**. Coordinates of the entorhinal cortex were determined from individual structural scans. Figure adapted from Yuan et al., *Brain Connectivity* 2017 (49).

situation and be subject to toggling from one control system to another. These connectivity differences do not indicate whether the effects are primary or secondary or which hub of the network is critical for persistence of symptoms, however.

Change in functional connectivity measured by fMRI between the entorhinal cortex/amygdala and the whole brain as a function of response to transcranial magnetic stimulation (TMS) was assessed in 20 right-handed women who underwent five sessions of prefrontal repetitive TMS (rTMS) [mean age 52.9 (range of 28–68 years), median symptom duration of 30 months (range of 8–96 months)] (49). Symptom severity was measured on a 100-point visual analog scale with symptom change measured as a categorical variable of "positive," "neutral," or "negative," depending on whether symptoms improved, stayed the same, or worsened, respectively. Decreasing scores represented decrease in symptoms. The specific treatment entailed 1,200 pulses over the right DLPFC at 110% of the motor threshold (MT), followed by 2,000 pulses over the left DLPFC at 110% MT. Pearson's correlation coefficients were calculated between seeds in the left and right entorhinal cortices (defined in individual brains) (**Figure 3A**) and the specific locations in the DLPFC (**Figure 3B**) that were stimulated with neuronavigation (Localite®) guidance. The goal was to determine resting-state functional connectivity change as a function of symptom change as well as baseline measures of connectivity that correlated with treatment response.

Of the 20 individuals, six reported improvement, eight reported no significant change, and six reported worsening using a cutoff of 10 points on the visual analog scale (**Figure 4A**). Notably, the degree of improvement was much greater than the degree of worsening such that the response of the "neutral" group was similar to that of the "negative" group. In a conjunction analysis that required symptom and connectivity changes to the entorhinal cortex to correlate in a bidirectional manner, i.e., decrease with improvement and increase with worsening or vice versa, three brain regions were identified. Decrease in resting-state functional connectivity between the left entorhinal cortex and right IPL, left precuneus, and right entorhinal cortex correlated with symptom improvement, while increases in connectivity correlated with no change or symptom worsening (49). Corresponding to the closer scoring change between the neutral group and the negative response (worsening) group compared with the positive response (improvement) group, the connectivity changes were similar between the neutral and negative response groups. High baseline connectivity between the entorhinal cortex and the ipsilateral DLPFC correlated with response to rTMS in a continuous manner, perhaps indicating that a higher dynamic range of potential modulation is critical for treatment response (**Figure 3A**).

This study was one of the first to show that symptom improvement in MdDS corresponds to a general decrease in functional connectivity between posterior sensory processing regions and the entorhinal cortex. The higher baseline connectivity between posterior parietal and occipital cortex with the entorhinal cortex in individuals with MdDS compared with healthy controls may have been reversed in treatment responders (4). These data suggest that one goal of therapy may be to reduce parieto-occipital to limbic connectivity.

STRUCTURAL MAGNETIC RESONANCE IMAGING

Structural brain characteristics of MdDS were assessed with voxel-based morphometry (VBM). VBM is an imaging tool used to make voxel-by-voxel comparisons between segmented brain tissues (52). These methods can reveal subtle differences in regional brain volume that cannot be detected with clinical imaging. Whereas a typical T1 structural image acquired for

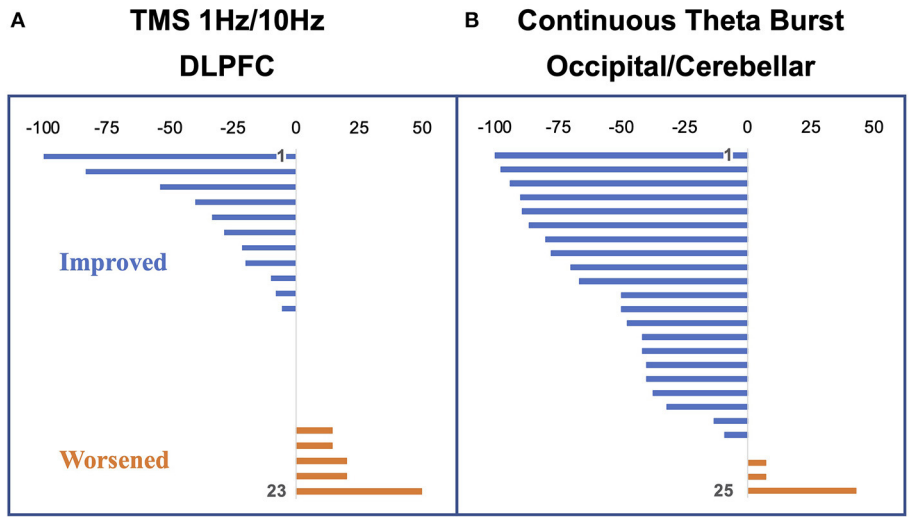

FIGURE 4 | Percent change in vertigo intensity measured as a visual analog scale change from pre to post stimulation. Negative deflections represent a decrease in symptoms; positive deflections, an increase in symptoms. **(A)** Participants in the dorsolateral prefrontal cortex (DLPFC) repetitive transcranial magnetic stimulation (rTMS) study (24 at baseline with one dropout). **(B)** Participants in the occipital/cerebellar theta burst study (26 participants with one dropout). Figure adapted from Cha YH et al., *Brain Stimulation* 2016 (50). and Cha YH et al., *Otology Neurotology* 2019 (51).

clinical purposes may include 36 slices for the whole brain, a T1 structural image used for VBM analysis may use 180+ slices. This allows the brain volume to be segmented into gray matter, white matter, and fluid volumes at a resolution of 1 mm^3. VBM analysis was performed on 28 individuals with MdDS compared with 18 healthy age- and sex-matched controls (53). Individuals with MdDS had a mean age of 43.0 ± 10.2 years and median duration of illness of 24 months (range 3–240 months). Without the outlier of 240 months, the mean duration was 35.7 ± 28.7 months.

In head-to-head whole brain contrasts, MdDS participants exhibited increased volumes in the following areas: the left IPL, right ventral occipital lobe (V3v), and right temporal lobe in the cerebrum and in bilateral hemispheric lobules VIIIb and IX, left Crus I, VIIa/VIIb, and VIIIa in the cerebellum ($t > 3.0$, $p < 0.005_{uncorr}$). Decreased volumes relative to controls were noted in the following areas: the bilateral middle orbital gyri, left pgACC, left middle temporal gyrus, left calcarine gyrus, and right inferior frontal gyrus (IFG) in the cerebrum and the left cerebellar lobule VIIa Crus II in the cerebellum. These analyses were done with nuisance covariates of age, and the anxiety and depression subscores of the HADS. Specific interrogation of motion-sensitive area V5/MT and the parieto-insular vestibular cortex (PIVC) were assessed because both regions receive vestibular projections and show volume changes after peripheral vestibular injury (54, 55). No volume differences were found between MdDS participants and controls in direct contrasts within these regions, however.

Multiple regression analysis for duration of illness showed two prominent cerebral areas with duration sensitive volume changes at a false discovery rate < 0.05. The pgACC volume decreased with duration with a correlation coefficient of −0.633 ($p < 0.05_{corr}$). Both IFG/anterior insular (AI) regions increased in volume with duration, with left and right correlation coefficients of +0.440 and +0.427, respectively ($p < 0.05_{corr}$) (**Figure 5**). Other cerebral areas that showed positive correlation with duration at a lower significance ($t > 3.0$, $p < 0.005_{uncorr}$) included the bilateral postcentral gyri, left superior occipital gyrus (V3a), right Heschl's gyrus, right cuneus, left middle occipital gyrus (V5/MT), left amygdala, left SPL, left lingual gyrus (V3v/V4v), bilateral calcarine gyri, left middle and inferior temporal gyri, and right temporal pole. In the cerebellum, the bilateral anterior cerebellum (lobules I–IV), left hemispheric lobule IX, and vermian lobule IX (uvula) increased in volume with duration. Cerebral volume decreases with duration included the bilateral middle ACC and the left middle frontal gyrus (area of the DLPFC). The right cerebellar lobule VIIIa/b was the only cerebellar region to decrease in volume with duration of illness (**Figure 5**). As a caveat, the volume changes in this study were measured in a cross-sectional rather than longitudinal manner. Therefore, whether they would show the same changes within an individual is not determined.

The most significant volume-related markers of MdDS were correlations of decreased pgACC volume and increased IFG/AI volumes with duration of illness. The pgACC is functionally connected to the limbic system, specifically reducing amygdala activity and activating in tasks related to emotional conflict regulation, fear extinction, and planning of responses to threats (56–59). The lower volume in this region as a function of longer duration of illness may reflect less limbic regulatory control as either a cause or a result of prolonged symptoms. The IFG/AI is a major hub of the SN (along with the dorsal ACC, amygdala, ventral striatum, and ventral tegmental area/substantia nigra), a network that is activated when assessing functionally relevant stimuli (60). Duration-related volume changes in the threat

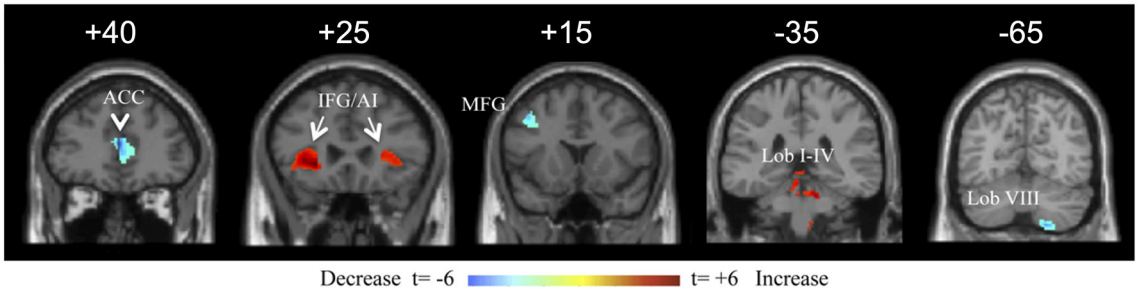

FIGURE 5 | Coronal view of a selection of brain regions with volume changes as a function of duration of illness of mal de débarquement syndrome (MdDS). Blue indicates volume decrease with duration of illness; red indicates volume increase with duration of illness. Coordinates of peak significance are indicated in parentheses. In SPM, negative *X*-values are on the left and positive on the right. ACC, anterior cingulate cortex [Montreal Neurological Institute (MNI): ±2, 40, 13). IFG/AI: inferior frontal gyrus/anterior insula (MNI: −26, 30, −3 and 27, 24, 4). MFG: middle frontal gyrus (MNI: −42, 15, 43). Lob I–IV: cerebellar lobules I–IV (MNI: −6, −38, −17 and 8, −50, −27). Lob VIII: cerebellar lobule VIII (18, −66, −55). Images are shown at the Y coordinate indicated above each image. Figure adapted from Cha YH and Chakrapani S, *PLOS One* 2015 (53).

regulation system and the SN could relate to decreased ability to appraise potential environmental threats along with increased demand on filtering sensory stimuli. Dysfunction within these networks could contribute to prolonged symptoms and increased morbidity. Reduced performance of the SN's function in toggling between the DMN and ECN could lead to an inability to efficiently activate working memory networks or lead to heightened interoceptive awareness (60, 61). This could potentially contribute to the problem of cognitive dysfunction ("brain fog") frequently reported by individuals with MdDS in which it is difficult for them to focus on task-relevant stimuli (2, 33).

A role for the cerebellum in MdDS may be related as much to its connectivity with resting-state networks as it does to specific pathways within the vestibular system. Bilateral cerebellar lobules VIII/IX showed increased volume compared with controls. Lobule VIII is functionally connected to the premotor cortex and is thus relevant for the planning of motor movements (38, 62). The right cerebellar lobule VIII, which was the only cerebellar region to show a negative correlation with duration of illness, is functionally connected to every portion of the precuneus, a hub of the DMN that plays a critical role in memory, attention, and visuospatial processing (63, 64). Cerebellar lobule IX (uvula) is functionally connected to the DMN but also receives ipsilateral primary vestibular afferents and bilateral secondary vestibular afferents in a complex with lobule X (nodulus) (65). There has been no peripheral vestibular injury noted in MdDS to date, but a hypothesis that MdDS pathophysiology could be related to a prolonged vestibulo-ocular reflex time constant that can be readapted using optokinetic stripes could be related to posterior cerebellar volume changes (66). Therefore, multiple potential hubs of the DMN and a hub for vestibular processing may be affected in MdDS.

ELECTROENCEPHALOGRAPHY

A case was reported of a marker of transient MdDS using an EEG-based source localization method called standardized low-resolution brain electromagnetic tomography (sLORETA) (67). sLORETA is a method for localizing electrical activity within the brain by the use of surface electrodes on the scalp (68). A 20-year-old man who experienced a swaying sensation and dizziness after a boat trip and bus ride was evaluated during the symptomatic period 3 days after the onset and after resolution of his symptoms 10 days later. It was reported that compared with resolution, the patient's brain in the symptomatic period exhibited a decrease in alpha (8–12 Hz) power in the left precentral gyrus and an increase in beta-2 power (19–21 Hz) in the right para-hippocampal region. With the caveat that sLORETA has poor localization in deep brain regions, this report highlights the potential role of structures involved in spatial navigation in MdDS symptomatology.

In the same studies that evaluated rTMS over DLPFC, functional connectivity with high density EEG was recorded before and after the intervention. Measurement of this connectivity was reflected through independent component phase coherence (ICPC), a calculation of synchronicity at individual frequency bands (delta, theta, low alpha, high alpha, beta, and gamma) on an independent component level rather than an individual channel level (69). ICPC calculations on 128-channel EEG data collected pre and post rTMS have shown distinct differences in synchronizations across independent component regions and frequencies (69, 70). In general, reduction in ICPC in the delta, high alpha, beta, and gamma bands were noted with symptom improvement, whereas increase in ICPC was noted in the low alpha band (**Figure 6A**). Most desynchronizations were either long-range frontal-parieto-occipital or parieto-occipital with some connectivity crossing hemispheres.

Similar to fMRI analyses, baseline high ICPC values correlated with greater treatment response; high ICPC values across all frequency bands portended better treatment response (**Figure 6B**). This may, again, correlate with a higher dynamic range of potential desynchronization being possible in individuals with higher baseline connectivity. The magnitude of treatment response was related to the magnitude of the number

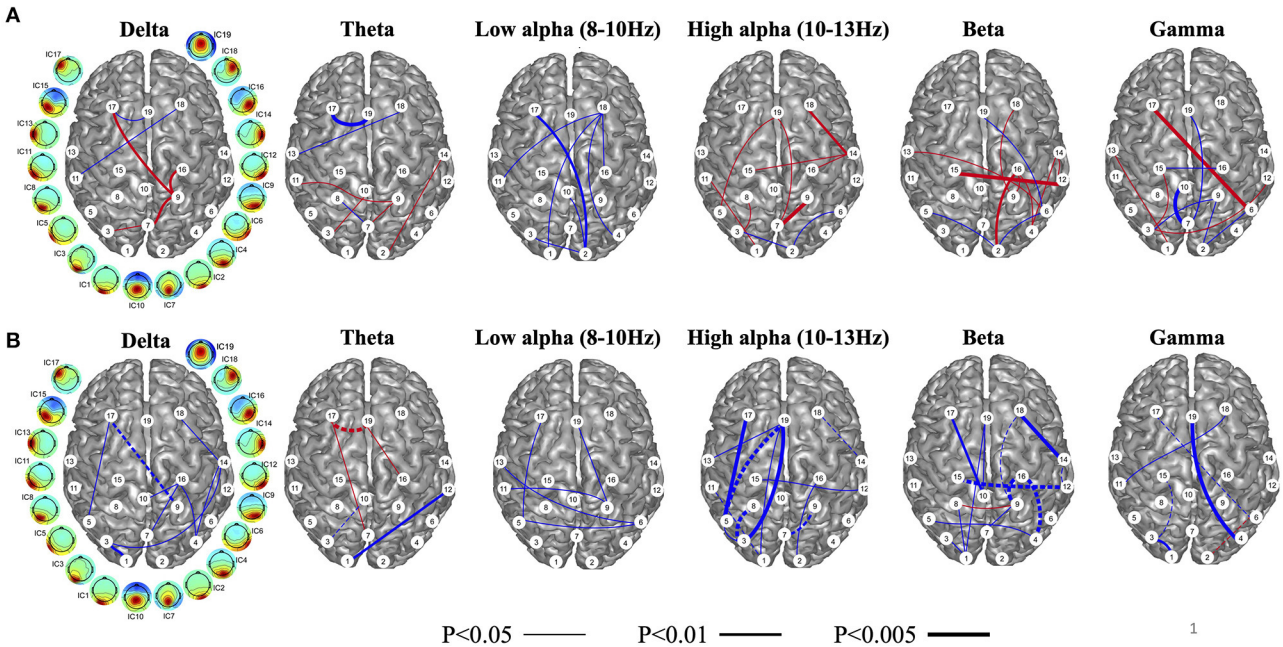

FIGURE 6 | Independent component phase coherence (ICPC) changes reflected as increases (blue) and decreases (red) of ICPC as a function of treatment response to repetitive transcranial magnetic stimulation (rTMS) over the dorsolateral prefrontal cortex (DLPFC) **(A)**. As a function of treatment response, connectivity in the high alpha, beta, and gamma, and delta bands decrease, while connectivity in the low alpha band increases with treatment response. Changes in the theta frequency are mixed. Baseline connectivity as a function of treatment response (blue represents high, and red represents low) in **(B)**. Baseline connectivity is high across all frequency bands in treatment responders. Lines connecting independent components are weighted for higher statistical significance. Dashed lines indicate connectivity that both changes and predicts treatment response. Figure adapted from Cha YH et al., *Brain Connectivity* 2018 (70).

of ICPC pairs that desynchronized, i.e., more desynchronized ICPC pairs correlated with greater symptom reduction, suggesting that the general goal of treatment may be to induce more desynchronization and particularly at the high alpha and beta frequencies.

In addition to the above ICPC studies that have revealed biomarker information at the EEG sensor level, investigations of EEG source level computations have been able to reproduce resting-state networks that spatially correspond to the standard template of brain networks (71–73). Our data revealed that EEG source network changes in the left medial frontal gyrus and primary visual cortex positively correlate with symptom changes, whereas EEG source network changes in the right middle temporal gyrus negatively correlate with symptom changes (72, 73). Furthermore, baseline EEG connectivity values in the primary visual cortex were found to predict symptom changes induced by rTMS, with particularly high baseline connectivity predictive of reduction of symptoms. In the visual cortex, functional connectivity decreased after rTMS in five out of six positive responders, notable since the visual cortex had previously been shown to exhibit higher baseline connectivity with the entorhinal cortex in MdDS (4). To date, EEG source imaging findings have corroborated symptom-related dynamic changes in fMRI, converging on the theory that the therapeutic mechanism of rTMS is to normalize pathological connectivity in MdDS.

SIMULTANEOUS FUNCTIONAL MAGNETIC RESONANCE IMAGING–ELECTROENCEPHALOGRAPHY

Simultaneously acquired fMRI-EEG data on individuals with MdDS have provided cross-modal validation of biomarkers found separately, showing that brain network-level changes associated with clinical effects are consistent across modalities of different temporal resolutions (49, 69, 70, 72–74). Our data showed that after rTMS at DLPFC, EEG synchronization changes in medial frontal gyrus were associated with fMRI-measured connectivity changes involving deeper cortical structures, particularly in a network that includes the entorhinal cortex and right IPL, indicating that the modulatory effect of rTMS is at least partially related to reducing the connectivity within the DMN (49, 73). Such a mechanism appears to be consistent with findings suggested in other disorders treated by rTMS over DLPFC, such as major depression (75, 76).

Our multimodal imaging data of EEG and fMRI have shown that improvement in symptom severity was correlated with a reduction in connectivity involving multiples nodes of the DMN, including the entorhinal cortex, precuneus, IPLs, and medial frontal gyrus. Specifically, in the positive responders to rTMS, a significant reduction of symptoms was associated with a reduction in connectivity in the medial frontal gyrus—a key

node of the DMN. In the DLPFC stimulation protocol, we have shown that the stimulation did not lead to increased connectivity between the stimulation site and entorhinal cortex itself, however, as we had hypothesized based on lower prefrontal-to-limbic connectivity in MdDS (4, 49). Rather, our data showed that stimulation at DLPFC played a modulatory role, resulting in decreases of connectivity between posterior DMN and the entorhinal cortex (49). Such a phenomenon of decreased connectivity in DMN nodes associated with symptom reduction has been observed in a later study utilizing continuous theta burst stimulation (cTBS) over the occipital cortex and cerebellar vermis and interrogating connectivity with EEG (51, 77). While the DLPFC rTMS protocol yielded 3 out 23 participants experiencing $\geq$50% symptom reduction, the cTBS over occipital cortex and cerebellar vermis protocol yielded 12 out of 25 participants with $\geq$50% symptom reduction (50, 51) (**Figure 4B**). This improved efficacy may be related to more direct engagement of fronto-parieto-occipital connectivity (both through the occipital cortex target and through functional connectivity through the vermis), greater treatment numbers, and more direct entrainment effects (42, 78–80).

Combined EEG-fMRI studies have suggested a strategy of using multimodal data to guide rTMS in MdDS. These investigations have indicated that connectivity within the DMN, measured by fMRI as well as EEG, can be an imaging-based symptom biomarker. Treatments guided by the modulation of this biomarker may be informative in trials of brain stimulation, potentially not limited to rTMS. More importantly, although fMRI reveals symptom-related connectivity, an EEG-based targeting strategy would be compatible with simultaneous rTMS and may provide instantaneous feedback in trial sessions of stimulation protocols. Biomarkers from the two modalities can be integrated to guide rTMS targets. For example, the high spatial resolution of fMRI can be used to capture a disease-modifying network involving deep cortical or subcortical structures, whereas connectivity involving superficial nodes of these networks can be identified with EEG, which has high temporal resolution, potentially through a matching procedure with the fMRI-measured network as described in our approaches. New stimulation protocols could therefore be designed to promote network modulation in desired directions.

CONCLUSION

MdDS represents a model of the human brain's entrainment to motion that results in a persistent sense of oscillating vertigo. The anatomical substrates for this perception have been interrogated with multiple neuroimaging modalities in order to evaluate metabolism, functional connectivity, brain volume, and synchronicity. A developing model for MdDS hypothesizes that at least one hub of the neural network that contributes to persistence of symptoms includes the left entorhinal cortex and amygdala. Through their reciprocal inhibitory action on the prefrontal cortex, these structures may wield outsized effects on both task-specific and amodal resting-state networks. Symptoms that are common in MdDS such as cognitive difficulty and feeling of sensory overload might be attributed to inefficiencies in toggling between resting states, e.g., DMN and ECN, and in dysfunction in neural substrates that filter irrelevant sensory stimuli, e.g., SN. A general neuroimaging feature of improved symptoms appears to be desynchronization of medium- and long-range connections, particularly between the parieto-occipital cortex and limbic areas as well as between frontal and parieto-occipital cortices. As further probing of these connections occurs through modulating symptoms with noninvasive brain stimulation, a more detailed understanding of the core neural components that drive persistence MdDS should emerge.

AUTHOR CONTRIBUTIONS

YC, LD, and HY were all involved in the manuscript preparation, figure generation, and review process. All authors contributed to the article and approved the submitted version.

FUNDING

This work was funded by the Mal de Debarquement Balance Disorders Foundation, MnDRIVE Scholars Program, and the National Science Foundation RII Track-2 FEC 1539068.

REFERENCES

1. Cha YH, Baloh RW, Cho C, Magnusson M, Song J-J, Strupp M, et al. Mal de debarquement syndrome diagnostic criteria: consensus document of the classification committee of the Barany Society. *J Vestib Res.* (2020) 30:285–93. doi: 10.3233/VES-200714
2. Cha YH, Brodsky J, Ishiyama G, Sabatti C, Baloh RW. Clinical features and associated syndromes of mal de debarquement. *J Neurol.* (2008) 255:1038–44. doi: 10.1007/s00415-008-0837-3
3. Cha YH. Mal de debarquement syndrome: new insights. *Ann N Y Acad Sci.* (2015) 1343:63–8. doi: 10.1111/nyas.12701
4. Cha YH, Chakrapani S, Craig A, Baloh RW. Metabolic and functional connectivity changes in mal de debarquement syndrome. *PLoS One.* (2012) 7:e49560. doi: 10.1371/journal.pone.0049560
5. Insausti R. Comparative anatomy of the entorhinal cortex and hippocampus in mammals. *Hippocampus.* (1993) 3:19–26. doi: 10.1002/hipo.1993.4500030705
6. Hafting T, Fyhn M, Molden S, Moser MB, Moser EI. Microstructure of a spatial map in the entorhinal cortex. *Nature.* (2005) 436:801–6. doi: 10.1038/nature03721
7. Takeyama H, Matsumoto R, Usami K, Nakae T, Kobayashi K, Shimotake A, et al. Human entorhinal cortex electrical stimulation evoked short-latency potentials in the broad neocortical regions: evidence from cortico-cortical evoked potential recordings. *Brain Behav.* (2019) 9:e01366. doi: 10.1002/brb3.1366
8. Hahn TT, McFarland JM, Berberich S, Sakmann B, Mehta MR. Spontaneous persistent activity in entorhinal cortex modulates cortico-hippocampal interaction *in vivo*. *Nat Neurosci.* (2012) 15:1531–8. doi: 10.1038/nn.3236

9. Hoydal OA, Skytoen ER, Andersson SO, Moser MB, Moser EI. Object-vector coding in the medial entorhinal cortex. *Nature.* (2019) 568:400–4. doi: 10.1038/s41586-019-1077-7
10. Kropff E, Carmichael JE, Moser MB, Moser EI. Speed cells in the medial entorhinal cortex. *Nature.* (2015) 523:419–24. doi: 10.1038/nature14622
11. Doeller CF, Barry C, Burgess N. Evidence for grid cells in a human memory network. *Nature.* (2010) 463:657–61. doi: 10.1038/nature08704
12. Nau M, Navarro Schroder T, Bellmund JLS, Doeller CF. Hexadirectional coding of visual space in human entorhinal cortex. *Nat Neurosci.* (2018) 21:188–90. doi: 10.1038/s41593-017-0050-8
13. Fransen E, Tahvildari B, Egorov AV, Hasselmo ME, Alonso AA. Mechanism of graded persistent cellular activity of entorhinal cortex layer v neurons. *Neuron.* (2006) 49:735–46. doi: 10.1016/j.neuron.2006.01.036
14. Egorov AV, Hamam BN, Fransen E, Hasselmo ME, Alonso AA. Graded persistent activity in entorhinal cortex neurons. *Nature.* (2002) 420:173–8. doi: 10.1038/nature01171
15. Egorov AV, Unsicker K, von Bohlen und Halbach O. Muscarinic control of graded persistent activity in lateral amygdala neurons. *Eur J Neurosci.* (2006) 24:3183–94. doi: 10.1111/j.1460-9568.2006.05200.x
16. Jacob PY, Poucet B, Liberge M, Save E, Sargolini F. Vestibular control of entorhinal cortex activity in spatial navigation. *Front Integr Neurosci.* (2014) 8:38. doi: 10.3389/fnint.2014.00038
17. Goldberg, II, Harel M, Malach R. When the brain loses its self: prefrontal inactivation during sensorimotor processing. *Neuron.* (2006) 50:329–39. doi: 10.1016/j.neuron.2006.03.015
18. Bellgowan PS, Buffalo EA, Bodurka J, Martin A. Lateralized spatial and object memory encoding in entorhinal and perirhinal cortices. *Learn Mem.* (2009) 16:433–8. doi: 10.1101/lm.1357309
19. Miller J, Watrous AJ, Tsitsiklis M, Lee SA, Sheth SA, Schevon CA, et al. Lateralized hippocampal oscillations underlie distinct aspects of human spatial memory and navigation. *Nat Commun.* (2018) 9:2423. doi: 10.1038/s41467-018-04847-9
20. Igloi K, Doeller CF, Berthoz A, Rondi-Reig L, Burgess N. Lateralized human hippocampal activity predicts navigation based on sequence or place memory. *Proc Natl Acad Sci U S A.* (2010) 107:14466–71. doi: 10.1073/pnas.1004243107
21. Zigmond AS, Snaith RP. The hospital anxiety and depression scale. *Acta Psychiatr Scand.* (1983) 67:361–70. doi: 10.1111/j.1600-0447.1983.tb09716.x
22. Holthoff VA, Beuthien-Baumann B, Zundorf G, Triemer A, Ludecke S, Winiecki P, et al. Changes in brain metabolism associated with remission in unipolar major depression. *Acta Psychiatr Scand.* (2004) 110:184–94. doi: 10.1111/j.1600-0447.2004.00351.x
23. Baeken C, Wu GR, De Raedt R. Dorsomedial frontal cortical metabolic differences of comorbid generalized anxiety disorder in refractory major depression: A [(18)F] FDG PET brain imaging study. *J Affect Disord.* (2018) 227:550–3. doi: 10.1016/j.jad.2017.11.066
24. Drevets WC, Price JL, Simpson JR Jr, Todd RD, Reich T, Vannier M, et al. Subgenual prefrontal cortex abnormalities in mood disorders. *Nature.* (1997) 386:824–7. doi: 10.1038/386824a0
25. Maron E, Nutt D. Biological markers of generalized anxiety disorder. *Dialogues Clin Neurosci.* (2017) 19:147–58. doi: 10.31887/DCNS.2017.19.2/dnutt
26. Wu JC, Buchsbaum MS, Hershey TG, Hazlett E, Sicotte N, Johnson JC. PET in generalized anxiety disorder. *Biol Psychiatry.* (1991) 29:1181–99. doi: 10.1016/0006-3223(91)90326-H
27. Videbech P. PET measurements of brain glucose metabolism and blood flow in major depressive disorder: a critical review. *Acta Psychiatr Scand.* (2000) 101:11–20. doi: 10.1034/j.1600-0447.2000.101001011.x
28. Abercrombie HC, Schaefer SM, Larson CL, Oakes TR, Lindgren KA, Holden JE, et al. Metabolic rate in the right amygdala predicts negative affect in depressed patients. *Neuroreport.* (1998) 9:3301–7. doi: 10.1097/00001756-199810050-00028
29. Jeon SH, Park YH, Oh SY, Kang JJ, Han YH, Jeong HJ, et al. Neural correlates of transient mal de debarquement syndrome: activation of prefrontal and deactivation of cerebellar networks correlate with neuropsychological assessment. *Front Neurol.* (2020) 11:585. doi: 10.3389/fneur.2020.00585
30. Cohen H. Mild mal de debarquement after sailing. *Ann N Y Acad Sci.* (1996) 781:598–600. doi: 10.1111/j.1749-6632.1996.tb15734.x
31. Gordon CR, Shupak A, Nachum Z. Mal de debarquement. *Arch Otolaryngol Head Neck Surg.* (2000) 126:805–6.
32. Gordon CR, Spitzer O, Doweck I, Melamed Y, Shupak A. Clinical features of mal de debarquement: adaptation and habituation to sea conditions. *J Vestib Res.* (1995) 5:363–9.
33. Cha YH, Cui YY, Baloh RW. Comprehensive clinical profile of mal de debarquement syndrome. *Front Neurol.* (2018) 9:261. doi: 10.3389/fneur.2018.00261
34. Hain TC, Cherchi M. Mal de debarquement syndrome. *Handb Clin Neurol.* (2016) 137:391–5. doi: 10.1016/B978-0-444-63437-5.00028-5
35. Biswal B, Yetkin FZ, Haughton VM, Hyde JS. Functional connectivity in the motor cortex of resting human brain using echo-planar MRI. *Magn Reson Med.* (1995) 34:537–41. doi: 10.1002/mrm.1910340409
36. Friston KJ, Jezzard P, Turner R. Analysis of functional MRI time-series. *Human Brain Mapping.* (1994) 1:153–71. doi: 10.1002/hbm.460010207
37. Yeo BT, Krienen FM, Sepulcre J, Sabuncu MR, Lashkari D, Hollinshead M, et al. The organization of the human cerebral cortex estimated by intrinsic functional connectivity. *J Neurophysiol.* (2011) 106:1125–65. doi: 10.1152/jn.00338.2011
38. Buckner RL, Krienen FM, Castellanos A, Diaz JC, Yeo BT. The organization of the human cerebellum estimated by intrinsic functional connectivity. *J Neurophysiol.* (2011) 106:2322–45. doi: 10.1152/jn.00339.2011
39. Menon V. *Large-Scale Functional Brain Organization.* In: Toga AW, editor. *Brain Mapping: An Encyclopedic Reference, Vol. 2*, Academic Press; Elsevier (2015) p. 449–59.
40. Weissman-Fogel I, Moayedi M, Taylor KS, Pope G, Davis KD. Cognitive and default-mode resting state networks: do male and female brains "rest" differently? *Hum Brain Mapp.* (2010) 31:1713–26. doi: 10.1002/hbm.20968
41. Greicius MD, Krasnow B, Reiss AL, Menon V. Functional connectivity in the resting brain: a network analysis of the default mode hypothesis. *Proc Natl Acad Sci U S A.* (2003) 100:253–8. doi: 10.1073/pnas.0135058100
42. Buckner RL, Andrews-Hanna JR, Schacter DL. The brain's default network: anatomy, function, and relevance to disease. *Ann N Y Acad Sci.* (2008) 1124:1–38. doi: 10.1196/annals.1440.011
43. Ward AM, Schultz AP, Huijbers W, Van Dijk KR, Hedden T, Sperling RA. The parahippocampal gyrus links the default-mode cortical network with the medial temporal lobe memory system. *Hum Brain Mapp.* (2014) 35:1061–73. doi: 10.1002/hbm.22234
44. Grimm S, Boesiger P, Beck J, Schuepbach D, Bermpohl F, Walter M, et al. Altered negative BOLD responses in the default-mode network during emotion processing in depressed subjects. *Neuropsychopharmacology.* (2009) 34:932–43. doi: 10.1038/npp.2008.81
45. Seeley WW, Menon V, Schatzberg AF, Keller J, Glover GH, Kenna H, et al. Dissociable intrinsic connectivity networks for salience processing and executive control. *J Neurosci.* (2007) 27:2349–56. doi: 10.1523/JNEUROSCI.5587-06.2007
46. Valenti O, Grace AA. Entorhinal cortex inhibits medial prefrontal cortex and modulates the activity states of electrophysiologically characterized pyramidal neurons *in vivo*. *Cereb Cortex.* (2009) 19:658–74. doi: 10.1093/cercor/bhn114
47. Quirk GJ, Likhtik E, Pelletier JG, Pare D. Stimulation of medial prefrontal cortex decreases the responsiveness of central amygdala output neurons. *J Neurosci.* (2003) 23:8800–7. doi: 10.1523/JNEUROSCI.23-25-08800.2003
48. Iijima T, Witter MP, Ichikawa M, Tominaga T, Kajiwara R, Matsumoto G. Entorhinal-hippocampal interactions revealed by real-time imaging. *Science.* (1996) 272:1176–9. doi: 10.1126/science.272.5265.1176
49. Yuan H, Shou G, Gleghorn D, Ding L, Cha YH. Resting state functional connectivity signature of treatment effects of repetitive transcranial magnetic stimulation in mal de debarquement syndrome. *Brain Connect.* (2017) 7:617–26. doi: 10.1089/brain.2017.0514
50. Cha YH, Urbano D, Pariseau N. Randomized single blind sham controlled trial of adjunctive home-based tDCS after rTMS for mal de debarquement syndrome: safety, efficacy, and participant satisfaction assessment. *Brain Stimul.* (2016) 9:537–44. doi: 10.1016/j.brs.2016.03.016
51. Cha YH, Gleghorn D, Doudican B. Occipital and cerebellar theta burst stimulation for mal de debarquement syndrome. *Otol Neurotol.* (2019) 40:e928–e37. doi: 10.1097/MAO.0000000000002341
52. Ashburner J, Friston KJ. Voxel-based morphometry–the methods. *Neuroimage.* (2000) 11(6 Pt 1):805–21. doi: 10.1006/nimg.2000.0582

53. Cha YH, Chakrapani S. Voxel based morphometry alterations in mal de debarquement syndrome. *PLoS One.* (2015) 10:e0135021. doi: 10.1371/journal.pone.0135021
54. zu Eulenburg P, Stoeter P, Dieterich M. Voxel-based morphometry depicts central compensation after vestibular neuritis. *Ann Neurol.* (2010) 68:241–9. doi: 10.1002/ana.22063
55. Helmchen C, Klinkenstein JC, Kruger A, Gliemroth J, Mohr C, Sander T. Structural brain changes following peripheral vestibulo-cochlear lesion may indicate multisensory compensation. *J Neurol Neurosurg Psychiatry.* (2011) 82:309–16. doi: 10.1136/jnnp.2010.204925
56. Etkin A, Egner T, Kalisch R. Emotional processing in anterior cingulate and medial prefrontal cortex. *Trends Cogn Sci.* (2011) 15:85–93. doi: 10.1016/j.tics.2010.11.004
57. Mobbs D, Marchant JL, Hassabis D, Seymour B, Tan G, Gray M, et al. From threat to fear: the neural organization of defensive fear systems in humans. *J Neurosci.* (2009) 29:12236–43. doi: 10.1523/JNEUROSCI.2378-09.2009
58. Egner T, Etkin A, Gale S, Hirsch J. Dissociable neural systems resolve conflict from emotional versus nonemotional distracters. *Cereb Cortex.* (2008) 18:1475–84. doi: 10.1093/cercor/bhm179
59. Etkin A, Egner T, Peraza DM, Kandel ER, Hirsch J. Resolving emotional conflict: a role for the rostral anterior cingulate cortex in modulating activity in the amygdala. *Neuron.* (2006) 51:871–82. doi: 10.1016/j.neuron.2006.07.029
60. Menon V. Salience Network. In: Toga AW, editor. *Brain Mapping: An Encyclopedic Reference, Vol. 2*, Academic Press; Elsevier (2015). p. 597–611.
61. Sridharan D, Levitin DJ, Menon V. A critical role for the right fronto-insular cortex in switching between central-executive and default-mode networks. *Proc Natl Acad Sci U S A.* (2008) 105:12569–74. doi: 10.1073/pnas.0800005105
62. Habas C, Kamdar N, Nguyen D, Prater K, Beckmann CF, Menon V, et al. Distinct cerebellar contributions to intrinsic connectivity networks. *J Neurosci.* (2009) 29:8586–94. doi: 10.1523/JNEUROSCI.1868-09.2009
63. Zhang S, Li CS. Functional connectivity mapping of the human precuneus by resting state fMRI. *Neuroimage.* (2012) 59:3548–62. doi: 10.1016/j.neuroimage.2011.11.023
64. Utevsky AV, Smith DV, Huettel SA. Precuneus is a functional core of the default-mode network. *J Neurosci.* (2014) 34:932–40. doi: 10.1523/JNEUROSCI.4227-13.2014
65. Barmack NH. Central vestibular system: vestibular nuclei and posterior cerebellum. *Brain Res Bull.* (2003) 60:511–41. doi: 10.1016/S0361-9230(03)00055-8
66. Dai M, Cohen B, Smouha E, Cho C. Readaptation of the vestibulo-ocular reflex relieves the mal de debarquement syndrome. *Front Neurol.* (2014) 5:124. doi: 10.3389/fneur.2014.00124
67. Jeong SH, Jung KY, Kim JM, Kim JS. Medial temporal activation in mal de debarquement syndrome revealed by standardized low-resolution brain electromagnetic tomography. *J Clin Neurol.* (2012) 8:238–40. doi: 10.3988/jcn.2012.8.3.238
68. Pascual-Marqui RD. Standardized low-resolution brain electromagnetic tomography (sLORETA): technical details. *Methods Find Exp Clin Pharmacol.* (2002) 24(Suppl D):5–12.
69. Ding L, Shou G, Yuan H, Urbano D, Cha YH. Lasting modulation effects of rTMS on neural activity and connectivityas revealed by resting-state EEG. *IEEE Trans Biomed Eng.* (2014) 61:2070–80. doi: 10.1109/TBME.2014.2313575
70. Cha YH, Shou G, Gleghorn D, Doudican BC, Yuan H, Ding L. Electrophysiological signatures of intrinsic functional connectivity related to rTMS treatment for mal de debarquement syndrome. *Brain Topogr.* (2018) 31:1047–58. doi: 10.1007/s10548-018-0671-6
71. Yuan H, Ding L, Zhu M, Zotev V, Phillips R, Bodurka J. Reconstructing large-scale brain resting-state networks from high-resolution EEG: spatial and temporal comparisons with fMRI. *Brain Connect.* (2016) 6:122–35. doi: 10.1089/brain.2014.0336
72. Li C, Yuan H, Shou G, Cha YH, Sunderam S, Besio W, et al. Cortical statistical correlation tomography of EEG resting state networks. *Front Neurosci.* (2018) 12:365. doi: 10.3389/fnins.2018.00365
73. Chen Y, Cha YH, Li C, Shou G, Gleghorn D, Ding L, et al. Multimodal imaging of repetitive transcranial magnetic stimulation effect on brain network: a combined electroencephalogram and functional magnetic resonance imaging study. *Brain Connect.* (2019) 9:311–21. doi: 10.1089/brain.2018.0647
74. Wirsich J, Giraud AL, Sadaghiani S. Concurrent EEG- and fMRI-derived functional connectomes exhibit linked dynamics. *Neuroimage.* (2020) 219:116998. doi: 10.1016/j.neuroimage.2020.116998
75. Fox MD, Buckner RL, Liu H, Chakravarty MM, Lozano AM, Pascual-Leone A. Resting-state networks link invasive and noninvasive brain stimulation across diverse psychiatric and neurological diseases. *Proc Natl Acad Sci U S A.* (2014) 111:E4367–75. doi: 10.1073/pnas.1405003111
76. Drysdale AT, Grosenick L, Downar J, Dunlop K, Mansouri F, Meng Y, et al. Resting-state connectivity biomarkers define neurophysiological subtypes of depression. *Nat Med.* (2017) 23:28–38. doi: 10.1038/nm.4246
77. Chen Y, Urbano D, Doudican B, Ding L, Cha YH, Yuan H. Modulation of brain networks by repetitive theta burst stimulation in mal de debarquement syndrome. In: *41st Annual International Conference of the IEEE Engineering in Medicine and Biology Society*. Berlin (2019).
78. Halko MA, Farzan F, Eldaief MC, Schmahmann JD, Pascual-Leone A. Intermittent theta-burst stimulation of the lateral cerebellum increases functional connectivity of the default network. *J Neurosci.* (2014) 34:12049–56. doi: 10.1523/JNEUROSCI.1776-14.2014
79. Huang YZ, Edwards MJ, Rounis E, Bhatia KP, Rothwell JC. Theta burst stimulation of the human motor cortex. *Neuron.* (2005) 45:201–6. doi: 10.1016/j.neuron.2004.12.033
80. Cardenas-Morales L, Nowak DA, Kammer T, Wolf RC, Schonfeldt-Lecuona C. Mechanisms and applications of theta-burst rTMS on the human motor cortex. *Brain Topogr.* (2010) 22:294–306. doi: 10.1007/s10548-009-0084-7

Conflict of Interest: The authors declare that the research was conducted in the absence of any commercial or financial relationships that could be construed as a potential conflict of interest.

frontiers in Neurology

REVIEW
published: 09 March 2021
doi: 10.3389/fneur.2021.635259

Adaptive Balance in Posterior Cerebellum

Neal H. Barmack[1]* *and Vito Enrico Pettorossi*[2]

[1] *Department of Physiology & Pharmacology, Oregon Health & Science University, Portland, OR, United States,* [2] *Section of Human Physiology and Biochemistry, Department of Experimental Medicine, University of Perugia, Perugia, Italy*

Vestibular and optokinetic space is represented in three-dimensions in vermal lobules IX-X (uvula, nodulus) and hemisphere lobule X (flocculus) of the cerebellum. Vermal lobules IX-X encodes gravity and head movement using the utricular otolith and the two vertical semicircular canals. Hemispheric lobule X encodes self-motion using optokinetic feedback about the three axes of the semicircular canals. Vestibular and visual adaptation of this circuitry is needed to maintain balance during perturbations of self-induced motion. Vestibular and optokinetic (self-motion detection) stimulation is encoded by cerebellar climbing and mossy fibers. These two afferent pathways excite the discharge of Purkinje cells directly. Climbing fibers preferentially decrease the discharge of Purkinje cells by exciting stellate cell inhibitory interneurons. We describe instances adaptive balance at a behavioral level in which prolonged vestibular or optokinetic stimulation evokes reflexive eye movements that persist when the stimulation that initially evoked them stops. Adaptation to prolonged optokinetic stimulation also can be detected at cellular and subcellular levels. The transcription and expression of a neuropeptide, corticotropin releasing factor (CRF), is influenced by optokinetically-evoked olivary discharge and may contribute to optokinetic adaptation. The transcription and expression of microRNAs in floccular Purkinje cells evoked by long-term optokinetic stimulation may provide one of the subcellular mechanisms by which the membrane insertion of the GABAA receptors is regulated. The neurosteroids, estradiol (E2) and dihydrotestosterone (DHT), influence adaptation of vestibular nuclear neurons to electrically-induced potentiation and depression. In each section of this review, we discuss how adaptive changes in the vestibular and optokinetic subsystems of lobule X, inferior olivary nuclei and vestibular nuclei may contribute to the control of balance.

Keywords: vestibular, inferior olive, Purkinje cell, microRNA, semicircular canal, otolith, corticotropin releasing factor, cerebellum

OPEN ACCESS

Edited by:
Michael Strupp, Ludwig Maximilian University of Munich, Germany

Reviewed by:
Dan M. Merfeld, The Ohio State University, United States
Hans Straka, Ludwig Maximilian University of Munich, Germany
Yoon-Hee Cha, University of Minnesota Twin Cities, United States

***Correspondence:**
Neal H. Barmack
barmackn@ohsu.edu

Specialty section:
This article was submitted to Neuro-Otology, a section of the journal Frontiers in Neurology

Received: *30 November 2020*
Accepted: *16 February 2021*
Published: *09 March 2021*

Citation:
Barmack NH and Pettorossi VE (2021) Adaptive Balance in Posterior Cerebellum. Front. Neurol. 12:635259. doi: 10.3389/fneur.2021.635259

INTRODUCTION

Vestibular and optokinetic space is represented in three-dimensions in vermal lobules IX-X (uvula, nodulus) and hemispheric lobule X (flocculus) of the cerebellum. The coordinates of these spaces correspond physically to the planar orientation of the three semicircular canals and to the planes of action of the three pairs of extraocular muscles (1–5). Although reflexive and centrally-initiated movements can be made without a fully functional cerebellum, its circuitry maintains a central representation of head position in space and is capable of adapting to modifications in vestibular and optokinetic stimulation.

In this review we describe the anatomy, physiology and certain molecular features of the vestibular and optokinetic afferent pathways to cerebellar Purkinje neurons. These pathways include information processing at the levels of the medial accessory optic system, vestibular nuclei, nuclei of the inferior olive and cellular features of the cerebellar cortical interneurons. At each step along the way we consider evidence that each nuclear structure may contribute to the adaptive balance of the vestibular system.

Vestibular Primary Afferent Fibers Project to Ipsilateral Vestibular Nuclei and Vermal Lobules IX-X

Vestibular primary afferents sprout a thinner collateral branch as the primary afferent passes through the superior and lateral vestibular nuclei and terminates on granule cells in the ipsilateral vermal lobules IXd-X (**Figures 1A,C,D**). The main branch terminates in each of the five vestibular nuclei. These include the descending, lateral, medial and superior nuclei and the parasolitary nucleus (Psol) (10–14) (**Figure 1B**). The thinner collateral branch of the vestibular nerve branches again within the cerebellar cortex and distributes its terminals both sagittally and medio-laterally within vermal lobules IXd-X. Vestibular mossy fibers account for ∼90% of the total mossy fiber projection to vermal lobules IXd-X (8, 15–23). The mossy fiber branching pattern is illustrated best by the spatial patterning of mossy fiber terminals (MFTs) that originate from the lateral reticular nucleus (LRN) after labeling with biotin dextran amine (BDA) (9) (**Figure 1E**). A single mossy fiber branch forms ∼40 MFTs that contact one of a granule cell's 3-6 dendrites of as many as ∼15 granule cells. These synapses include a descending Golgi cell axon terminal (6, 24). In total, a single mossy fiber makes synaptic contact with ∼600 granule cells (25).

Each vestibular endorgan, the three semicircular canals, utricular and saccular otoliths, projects to a principal folium within vermal lobules IX-X. However, the projection of MFTs is not restricted to a single folium, but includes other folia within lobules IX-X and as well. MFTs from, say the left posterior semicircular canal (LPC), project primarily to left vermal lobule X, but also, more sparsely to left vermal lobule IXd. The left saccule projects to the left vermal lobule IX, but more sparsely to the left vermal lobule X (23). This pattern of distributed projections of vestibular primary afferents could account for the "patchy-mosaic" of granule cell receptive fields described for cutaneous cerebellar cortical areas that appear spatially discontinuous (26).

Parallel Fibers Distribute Vestibular Primary Afferent Signals Medio-Laterally Within Vermal Folia

Granule cell axons ascend through the Purkinje cell layer and bifurcate into parallel fibers that run through the planar dendritic trees of Purkinje cells in the molecular layer. The lengths of parallel fibers, ∼5 mm (rat) and ∼7 mm (cat), adds to the dispersion of mossy fiber signals and assures that fractions of the parallel fibers that traverse dendrites of each Purkinje cell in lobules IXd-X convey information that originates from each of the ipsilateral vestibular endorgans (27–29). While parallel fibers are numerous, their signals are weak. Fewer than 10% of parallel fibers evoke a detectable synaptic response in Purkinje cells. Based on these measurements, it is estimated that the synchronous discharge of ∼150 parallel fibers is necessary to evoke a Purkinje cell action potential (30).

A small number of granule cell axons ascend through the Purkinje cell layer and into the molecular layer and make synaptic contact with the overlying Purkinje cell dendritic tree prior to bifurcating into parallel fibers. These ascending axons could potentially counteract the medio-lateral parallel fiber dispersion of endorgan signals by preferentially making synapses on overlying Purkinje cells (31, 32). However, the density of synapses made by ascending granule cell axons on Purkinje cells is small ($\leq$ 50) relative to the total number of synapses made by parallel fibers, ∼200,000, as they pass through the Purkinje cell dendritic tree (27, 33). Furthermore, the amplitude of the EPSP evoked in Purkinje cells by selective activation of an ascending axon is no greater than that of the EPSP evoked by activation of a single conventional parallel fiber (30).

Vestibular Secondary Mossy Fiber Afferents Terminate Bilaterally in the Cerebellum

In contrast to the ipsilateral projections of vestibular primary afferents, vestibular secondary afferents have bilateral projections from the DVN, MVN and SVN to vermal lobules IX-X and hemispheric lobule X (34–38). Vestibular secondary afferent mossy fibers terminate in more than one lobule and spread medially and laterally as they enter the granule cell layers of lobules IX-X in a pattern that mimics MFTs from the lateral reticular nucleus (**Figure 1E**) (9). The widespread distribution of MFTs onto granule cells contrasts with the narrow sagittal array of climbing fiber projections to Purkinje cell dendrites in lobules IX-X (**Figure 1F**).

The projection pattern of secondary vestibular afferent mossy fibers is bilateral and not restricted to lobules IX-X. Secondary vestibular afferents from the DVN and MVN also project to lobule VIII, the anterior vermis and paraflocculus (38, 39). Most of these ascending projections are cholinergic (40–43).

Purkinje cells in left vermal lobule X receive vestibular primary afferent mossy fiber projections that originate from the left vestibular endorgans. These same Purkinje cells receive vestibular climbing fiber projections that convey vestibular signals from the right inferior olive and right vestibular endorgans. The separate peripheral origins of vestibular climbing and mossy fibers influences how their signals modulate the activity of Purkinje cells.

Vestibular Primary Afferents Project to GABAergic Neurons in the Parasolitary Nucleus

Psol is a cluster of small, cells compacted between the caudal MVN, DVN and solitary nucleus. They are uniformly GABAergic and project to the β-nucleus and dorsomedial cell column (DMCC) of the ipsilateral inferior olive (**Figures 2A,D**) (44, 45).

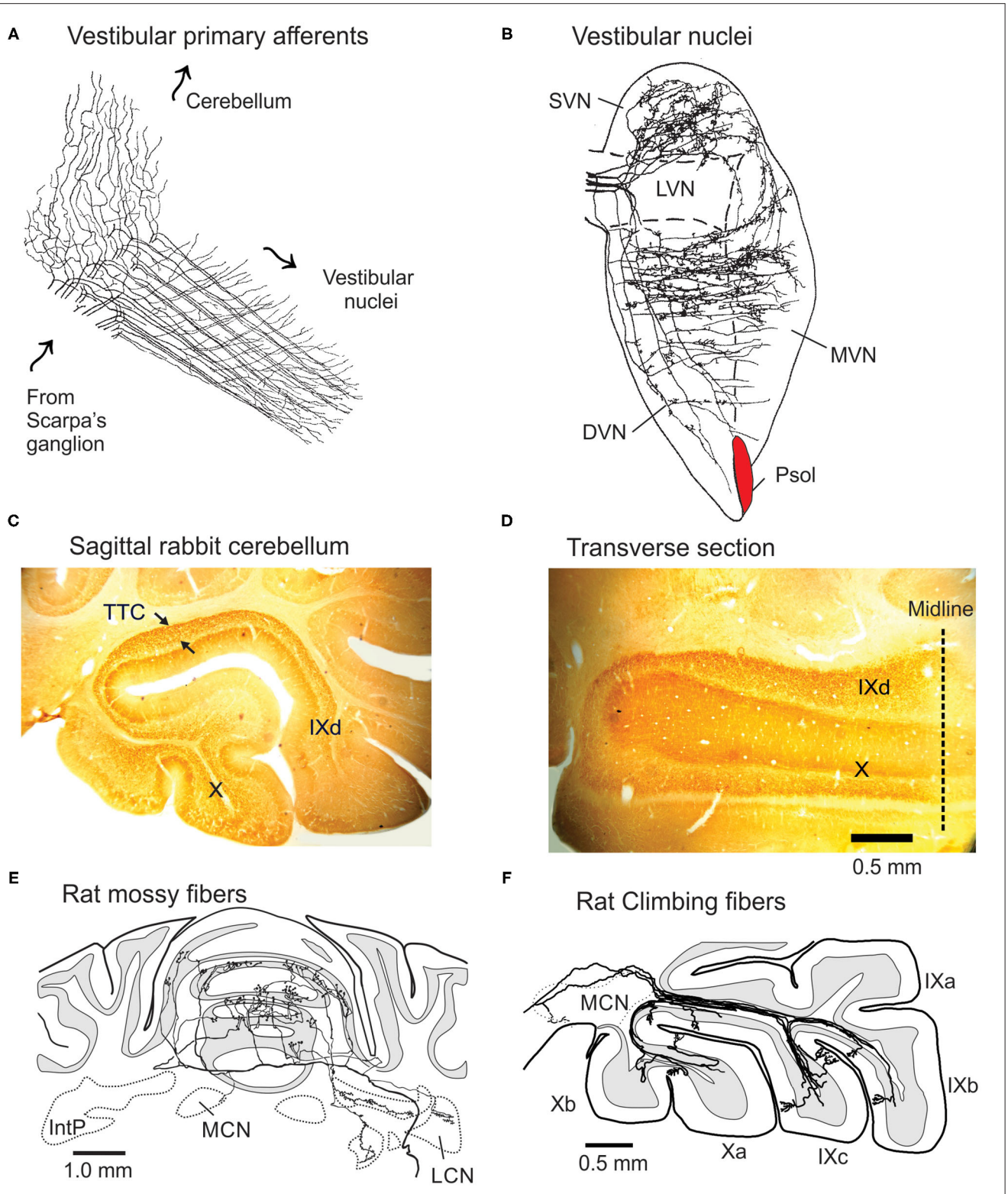

FIGURE 1 | Projections of vestibular primary afferents to cerebellum and vestibular nuclei. **(A)** Vestibular primary afferents from Scarpa's ganglion terminate in the vestibular nuclei after thin collateral branches separate and project to the granule cell layer of lobules IX-X as MFTs. Arrows indicate direction of signal propagation. Modified from Cajal (6). **(B)** Horizontal section through the vestibular complex illustrates the terminal fields of five horizontal semicircular canal afferents, intra-axonally labeled with HRP in rat. Modified from Sato and Sasaki (7). **(C)** The C fragment of tetanus toxin (TTC) injected into the left labyrinth of rabbit, orthogradely labels MFTs in lobules IX-X. Arrows show the profuse labeling in sagittal section. Note absence of labeling in other folia. **(D)** In horizontal section TTC-labeled mossy fibers stay

(Continued)

FIGURE 1 | within the bounds of left lobules IX-X. Modified from Barmack et al. (8). **(E)** Transverse section of the projection pattern of a BDA-labeled lateral reticular nucleus neuron of the rat. It projects bilaterally as a profusely branching mossy fiber to the anterior cerebellar vermis. **(F)** Sagittal view of several BDA-labeled climbing fibers that project in narrow sagittal bands to the contralateral lobules IX-X. DVN, LVN, MVN, and SVN, descending, lateral, medial, and superior vestibular nuclei; IntP, Interpositus nucleus; LCN and MCN, lateral and medial cerebellar nucleus; Psol, parasolitary nucleus. Modified from Wu et al. (9).

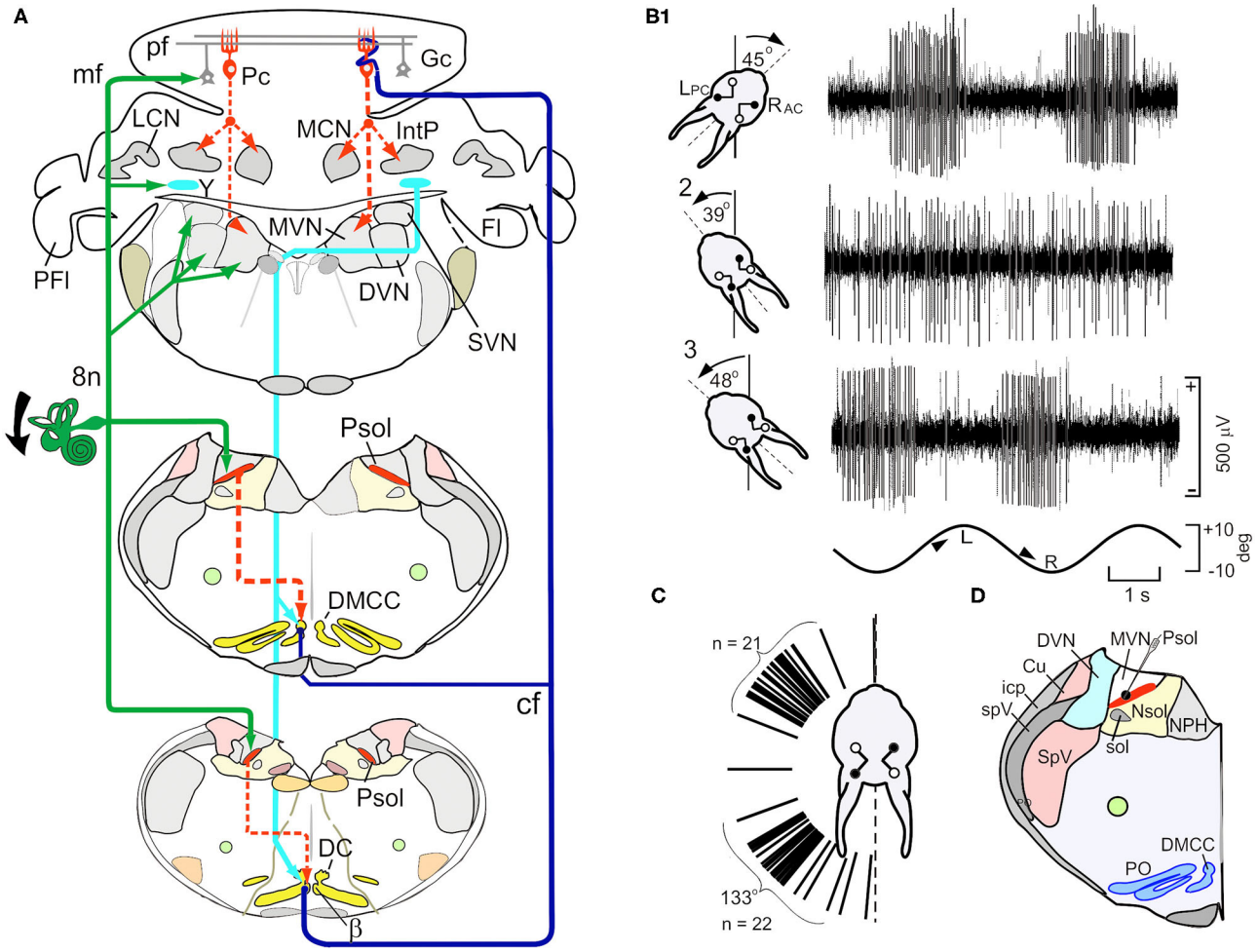

FIGURE 2 | Schematic paths of vestibular mossy and climbing fiber and activity of neurons in the parasolitary nucleus (Psol). **(A)** Schematic illustrates the vestibular mossy and climbing fiber projections to the brainstem and posterior cerebellar cortex. Vestibular primary afferent mossy fibers (mf) (green lines) project to the ipsilateral Psol, medial, descending, superior vestibular nuclei (MVN, DVN, and SVN), Y-group (Y) and cerebellar granule cells (Gc). GABAergic Psol neurons project to the ipsilateral β-nucleus (β) and dorsomedial cell column (DMCC) (dashed red lines). Neurons in the β and DMCC project as climbing fibers (cf) to contralateral lobules VIII-X (dark blue lines). Y-group neurons project to contralateral DC, β and DMCC (light blue lines). **(B1)** Vestibular stimulation about the longitudinal axis modulates the activity of a neuron in the left Psol. During leftward roll-tilt, discharge is modulated best when the left posterior semicircular canal is oriented 45 deg clockwise (CW). The sinusoidal rotation is indicated at the bottom of the panel. **(B2)** When the head of the rabbit is oriented 39 deg counter clockwise (CCW), neuronal discharge is not modulated, defining a null plane in which the axis of rotation of the LPC is orthogonal to the longitudinal axis. (A3) When the head of the rabbit is oriented 48 deg CCW with respect to the longitudinal axis (~9 deg past the null plane), modulation of neuronal activity again appears and is phase shifted by 180 deg with respect to the sinusoidal stimulus. **(C)** Optimal response planes for 47 Psol neurons cluster about the anatomical orientation of either the ipsilateral anterior or posterior semicircular canals. **(D)** The neuron illustrated in **(A)** is localized to Psol. Bg, Bergman astrocyte; Cu, cuneate nucleus; Fl, flocculus; Gc, granule cell; Go, Golgi cell; icp, inferior cerebellar peduncle; IntP, interpositus nucleus; LCN and MCN, lateral and medial cerebellar nucleus; Lu, Lugaro cell; $NG2^{+}$, glial cell; pf, parallel fiber; Pc, Purkinje cell; PFl, paraflocculus; Psol, parasolitary nucleus; 8n, vestibular nerve; MVN and DVN, medial and descending vestibular nuclei; NPH, nucleus prepositus hypoglossi; Nsol, nucleus solitarius; PO, principle olive; Psol, parasolitary nucleus; spV, spinal trigeminal tract; SpV, spinal trigeminal nucleus. Modified from Barmack and Yakhnitsa (14).

The activity of single Psol neurons is modulated by vestibular stimulation during rotation in a three-axis rate table. The modulated activity increases during ipsilateral roll-tilt and decreases during contralateral roll-tilt. By altering the angle of the head with respect to the axis of rotation it is possible to find the plane of rotation at which the modulated activity of a recorded

neuron is optimal (**Figures 2B,C**). Psol neurons are unresponsive to rotation about the vertical axis (13). Optimal response planes of Psol neurons are distributed throughout the hemifield, but align primarily with the anterior or posterior semicircular canals (**Figure 2C**).

Vestibular Primary and Secondary Afferents Project to the Dorsal Y-Group

Psol is one of two pre-olivary nuclei that provides vestibular inputs to the β-nucleus and DMCC. The other originates from the Dorsal Y-group. The ventral Y-group projects to the flocculus (46). Primary vestibular afferents and projections from vestibular nuclei terminate on Dorsal Y-group neurons which, in turn, project to the ipsilateral flocculus and nodulus, contralateral oculomotor complex and inferior olive (17, 47–51). Neurons from the Dorsal Y-group descend and cross the midline to terminate in the contralateral β-nucleus, DMCC and rostral DC. Dorsal Y-group neurons are immunolabeled by an antibody to aspartate and are excitatory (52).

Inferior Olivary Neurons Receive a GABAergic Projection From Psol Neurons

Two olivary nuclei, the β-nucleus and DMCC, receive descending inhibitory projections from the ipsilateral Psol (13, 45). Sinusoidal roll-tilt about the longitudinal axis modulates the discharge of neurons in the β-nucleus and DMCC. Roll-tilt onto the side contralateral to the recording site increases the discharge rate, and roll-tilt onto the ipsilateral side decreases it. This contralateral responsiveness of neurons in the β-nucleus and DMCC is consistent with the GABAergic projection from Psol. Like Psol neurons, β-nucleus and DMCC neurons have both static and dynamic sensitivity and are unresponsive to rotations about the vertical axis (**Figures 3A1,2,B**). The optimal response planes of neurons in the β-nucleus are topographically organized. β-nucleus neurons that align with the ipsilateral (right) anterior semicircular canal (RAC) are located caudally and neurons that align with the ipsilateral (right) posterior semicircular canal (RPC) are located rostrally (filled circles) (**Figure 3C**).

Like the β-nucleus, the DMCC receives descending GABAergic projections from Psol (**Figure 2A**). Neurons in the DMCC have optimal response planes distributed throughout the contralateral hemifield indicative of a more pervasive otolithic input (13, 53) (**Figures 3D1,2E,F**).

Climbing Fibers Are Aligned in Sagittal Zones in Vermal Lobules IX-X

Neurons in the β-nucleus and DMCC project contralaterally to Purkinje cells in vermal lobules IX-X in narrow sagittal zones (9, 54–61). As they enter the cerebellum climbing fibers branch sagittally to synapse upon ∼7 Purkinje cells (rat) within a multifolial sagittal zone (62). A single climbing fiber makes ∼500 synaptic contacts (rat) as it entwines Purkinje cell proximal dendrites (63).

Purkinje cells have two action potentials, termed Complex and Simple Spikes (CSs, SSs). CSs are multi-peaked action potentials and discharge at a rate of 0.1–5.0 imp/s. In contrast to the long duration and infrequent discharge of CSs, SSs are single peaked short duration action potentials (0.75-1.25 ms) that discharge at 20–60 imp/s (**Figure 4A**). Not surprisingly the activity of ∼90% of the Purkinje cells recorded in vermal lobules IX-X is modulated by sinusoidal roll-tilt (59, 64, 67) (**Figures 4A,B1,2**). Consistent with the crossed projection of climbing fibers, the discharge of CSs increases during *ipsilateral* side-down rotation rather than *contralateral* side-down rotation characteristic of cells in the inferior olive. Null and optimal planes disclose the origin within both labyrinths of the modulated signal (**Figures 4B1,2**). The discharge for populations of CSs and MFTs with respect to the sinusoidal vestibular stimulation are similar. Both CSs and MFTs discharge maximally during ipsilateral side-down roll-tilt. By contrast SSs discharge maximally during roll-tilt onto the contralateral side, 180 deg out of phase with climbing and mossy fiber inputs (**Figure 4C**). These data make problematic the idea that mossy fibers convey the signal that modulates the discharge of SSs since the population mossy fiber signal leads the discharge of SSs by ∼160 deg.

The response planes of vestibularly-driven CSs and SSs differ in Purkinje cells depending on the distance of Purkinje cells from the midline of vermal lobules IX-X. A sagittal strip of Purkinje cells, left of the midline, respond optimally during to ipsilateral roll-tilt when the head is maintained at an angle in which the axis of the L_{PC} and R_{AC} align with the longitudinal axis of rotation. In a second sagittal strip, lateral to the medial strip, Purkinje cells respond optimally during to ipsilateral roll-tilt in which the axis of the L_{AC} and R_{PC} align with the longitudinal axis of rotation. A two-dimensional representation of vermal lobules IX-X shows 146 Purkinje cells with optimal planes aligned with either the L_{PC} (green circles) or the L_{AC} (red squares) (**Figure 4D**). These two sagittal zones are ∼800 μm wide in the rabbit. Within either the medial or lateral the amplitude of modulation for both CSs and SSs is maximal at the center of the zone and decreases in either the medial or lateral direction (59). The borders of the two zones overlap. Postural responses are influenced by vestibular stimulation about three different axes. Vestibular stimulation about the rotational axis of the L_{AC} evokes a forward and lateral extension of the ipsilateral fore- and hind-paws. Vestibular stimulation about the rotational axis of the L_{PC} evokes a backward extension of the left paws. These two dimensions are insufficient to maintain balance in a three-dimensional space. Rotation about a third, vertical axis is detected by a horizontal optokinetic signal that originates from the contralateral dorsal cap of Kooy (DC) (68). The climbing fibers that originate from the DC respond optimally to posterior→anterior (P→A) stimulation of the ipsilateral eye (54, 64, 69, 70). In rabbits, an optokinetic parasagittal climbing fiber zone of Purkinje cells is interposed between the L_{PC} and L_{AC} zones on the ventral surface of left vermal lobule X. This horizontal optokinetic zone completes the third spatial dimension needed for three-dimensional balance (1, 54, 64) (**Figure 4D**).

In the mouse cerebellum, sagittal zones for optimal planes of SSs and CSs are consistent with the zones found in rabbit. In the mouse, these physiologically defined zones are ∼400 μm wide. The optimal planes of CSs and SSs can be quantified separately and displayed as a polar vector in which the amplitude of the

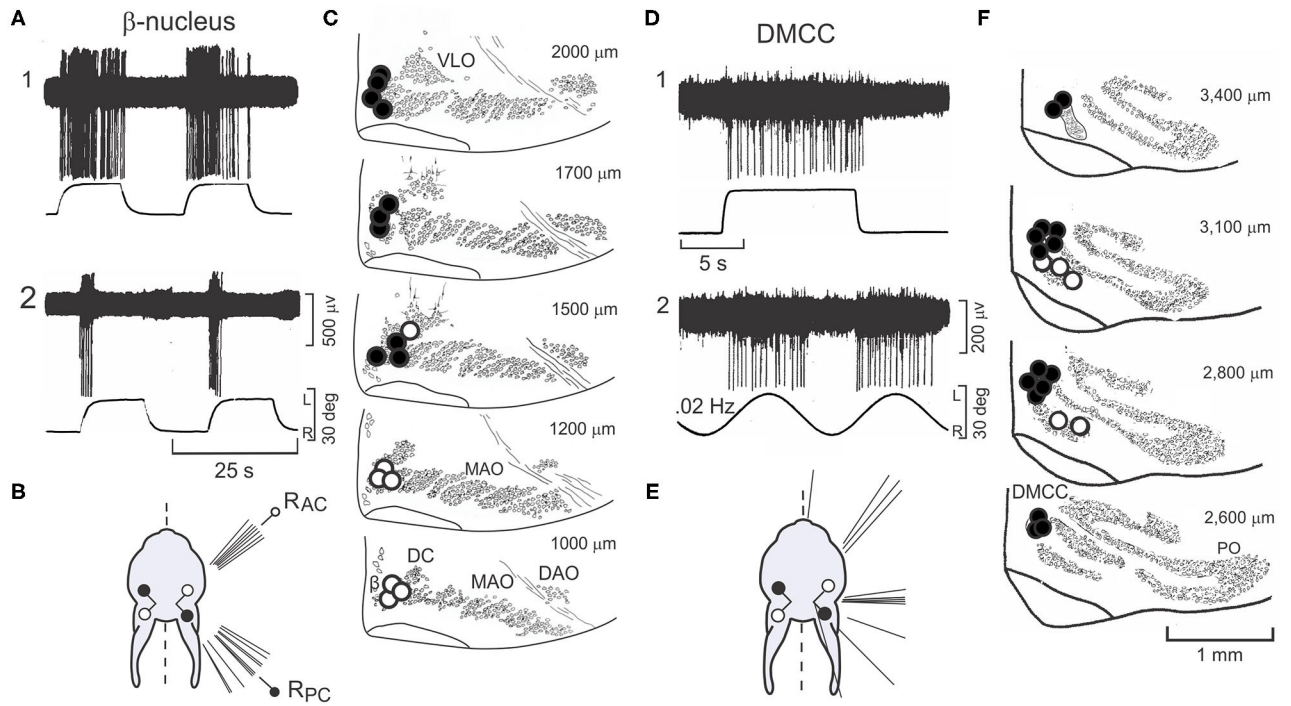

FIGURE 3 | Neurons in β-nucleus and Dorsomedial Cell Column respond to step-roll about the longitudinal axis. Contralateral roll-tilt increases discharge in neurons in the β-nucleus and dorsomedial cell column (DMCC) respond to. **(A)** The responses of two neurons recorded from the right β-nucleus to step-roll stimulation differ. The first responds to velocity and position during step-roll onto the left side. The second, responds primarily to velocity. **(B)** The figurine illustrates the distribution of optimal response planes for 15 neurons recorded from β-nucleus. While some respond to static head position, the optimal response planes of all the neurons aligned with the anatomical planes of either the RAC or RPC. **(C)** Neurons in the β-nucleus are mapped onto transverse sections of the olive. Optimal response planes that align with the RAC are located in the caudal β-nucleus (open circles). Neurons with optimal response planes that align with the RPC are found more rostrally (filled circles). The numbers to the right of each panel indicate distance from the caudal pole of the inferior olive. **(D)** Two neurons recorded from the right DMCC respond primarily to head position. **(E)** The figurine illustrates the distribution of optimal response planes for 19 neurons recorded from DMCC. **(F)** Neurons with optimal response planes that align with the vertical canals are distributed throughout the rostro-caudal extent of the DMCC. Numbers in the upper right corner indicate the distance of each transverse section from the caudal pole of the inferior olive. Modified from Barmack et al. (45). DAO, dorsal accessory olive; DC, dorsal cap; DMCC, dorsomedial cell column; MAO, medial accessory olive; PO, principal olive; RPC, right posterior semicircular canal; VLO, ventrolateral outgrowth.

vector corresponds to depth of modulation (**M**) and the phase angle (**ϕ**) corresponds to the phase of the response relative to the head position. For example, when $\phi = 0$ deg, the peak discharge of a Purkinje cell in the left nodulus is in phase with maximal tilt of the head onto the left side (**Figure 4E**). When $\phi = 180$ deg, the peak Purkinje cell discharge is in phase with peak rightward head tilt. Note that the population vector phase for CSs, $\phi = 56$ deg, leads head position. The population vector for SSs, $\phi = 222$ deg, lags CSs by 166 deg).

A Three-Axis Floccular Optokinetic Coordinate System Is Composed With Climbing Fiber Signals

Vermal lobule X comprises a hybrid three axis coordinate system that uses signals from the utricular otolith, vertical semicircular canals and a horizontal optokinetic pathway. Three distinct parasagittal climbing fiber zones demarcate the separate termination of these inputs. By contrast the hemispheres of lobule X comprise a three-axis system that uses optokinetic information conveyed by climbing fibers to track head position in three-dimensional visual space. The coordinates of this three-dimensional system roughly align with the orientation of semicircular canals and utricular otoliths also used by lobules IX-X.

Hemispheric lobule X receives a visual projection from the DC. The DC receives an optokinetic signal from the ipsilateral nucleus of the optic tract (NOT) and projects to the contralateral hemispheric and vermal lobule X (54, 68, 71–73). While more than 90% of the mossy fiber projections to vermal lobules IX-X are vestibular primary afferent collaterals, the mossy fiber projections to hemispheric lobule X are heterogeneous. The largest mossy fiber projections to the flocculus originate from the dorsomedial medullary reticular formation, paramedian reticular nucleus and the nuclei of the paramedian tracts as well as the raphe nuclei (74).

Neurons in the caudal DC respond to P→A horizontal optokinetic stimulation (HOKS) of the contralateral eye (**Figures 5A,B**). The peak sensitivity to HOKS is 1 deg/s. The velocity sensitivity of the optokinetic response is reduced by 3 dB

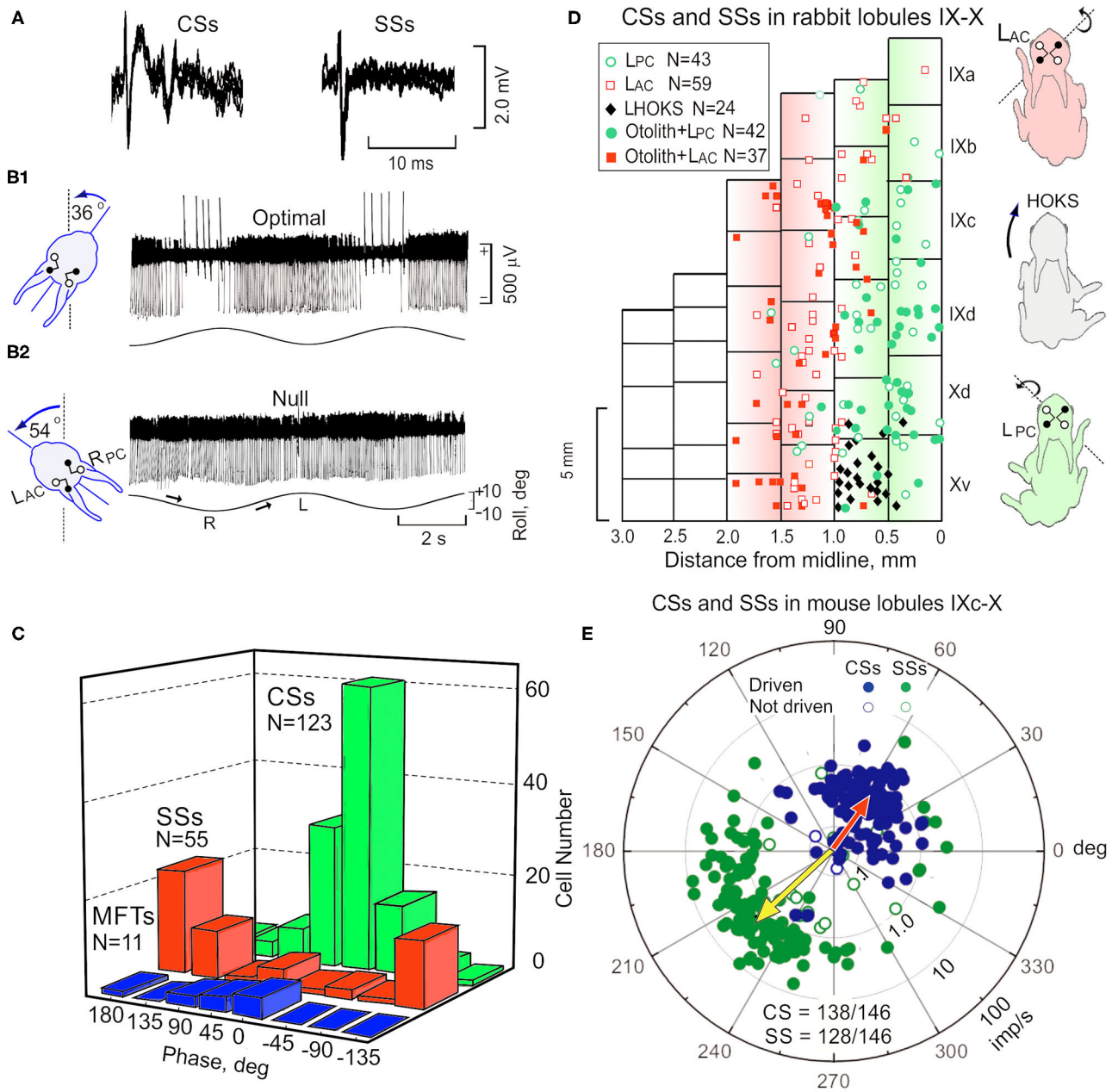

FIGURE 4 | Sinusoidal roll-tilt modulates the discharge of CSs, SSs and MFTs in lobules IX-X rabbit and mouse. **(A)** CSs are discriminated from SSs on the basis of their multi-peaked action potentials of longer duration. Five superimposed traces for each waveform are shown. **(B1)** Sinusoidal roll-tilt modulates the discharge of CSs and SSs. CSs have are positive-going and SSs have negative-going action potentials. With the head maintained at a CW angle of 36 deg (see figurine), the axes of LAC and R_{PC} are aligned with the longitudinal axis of rotation and optimal antiphasic modulation of CSs and SSs is achieved. **(B2)** When the head angle is maintained at a CCW angle of 54 deg, the axes of the L_{PC} and R_{AC} a null plane is reached at which modulated of both CSs and SSs is minimal. **(C)** Histograms compare the phase and numbers of recorded CSs (green), SSs (red), and MFTs (blue) during sinusoidal roll-tilt. **(D)** The anatomical location of 205 Purkinje cells in rabbit cerebellum are plotted on a two-dimensional representation of lobules IX-X. Cells with optimal planes that are co-planar with the L_{PC} are green. Cells with optimal plane co-planar with the L_{AC} are illustrated as red squares. Open symbols indicate cells in which the optimal plane is not tested for otolithic responses. Filled symbols indicate cells tested for static sensitivity and are positive. Black diamonds indicate cells that are not responsive to vestibular stimulation, but are modulated by HOKS of the ipsilateral eye in the P→A direction. Figurines illustrate postural responses induced by vestibular and optokinetic stimulation in different planes. Vestibular stimulation of LAC evokes a lateral and forward extension of the ipsilateral fore- and hind-paws. P→A HOKS of the left eye evokes a lateral extension of the contralateral paws. Vestibular stimulation of the LPc evokes a backward extension of the ipsilateral paws. **(E)** Polar plot for 146 Purkinje cells in mouse cerebellum illustrates vectors and phases of CSs (blue) and SSs (green). Population vector for CSs is red and for SSs is yellow. gl, granule cell layer; ml, molecular layer; Pl, Purkinje cell layer. Modified from Barmack and Yakhnitsa (60), Barmack and Shojaku (64), Barmack and Yakhnitsa (65), and Barmack and Yakhnitsa (66).

at 0.1 deg/s and 10.0 deg/s (75). Two other clusters of neurons in the DC convey information concerning OKS about the posterior axis (PA) and anterior axis (AA) (**Figures 5C–E**). These two axes lie along the azimuth and form angles of 135 deg (PA) and 45 deg (AA) with respect to the longitudinal axis (3, 69, 76). Each cluster in the DC projects to a sagittally arrayed zone in the contralateral flocculus (77, 78).

Vestibular and optokinetic climbing fiber systems in lobules IX-X have a similar organizational structure at the inferior olive and cerebellar cortex. Both systems are organized in three-dimensions. The vestibular system, anchored anatomically in the β-nucleus and DMCC, maintains a true gravitational vertical reference. However, it lacks input from the horizontal semicircular canals for detection of head rotation about the vertical axis. Instead, it relies on a small horizontal optokinetic input from the DC. The optokinetic system, anchored anatomically in the DC, detects self-motion about three axes, but lacks the non-visual dynamic and static sense of self-motion provided by the three semicircular canal ampullae and two otolith maculae.

The distribution of vestibular mossy fiber and vestibular climbing fiber signals assures that information from both labyrinths is represented bilaterally. Purkinje cells in left vermal lobule X (nodulus) receive vestibular primary afferent mossy fiber projections that arise from the left vestibular endorgans. These same Purkinje cells receive vestibular climbing fiber projections that convey vestibular signals from the contralateral inferior olive and right vestibular endorgans.

Floccular Optokinetic Zones Are Demarcated Anatomically and Physiologically

The flocculus, like the uvula-nodulus, has a topographic spatial map represented in its climbing fiber projection. The rabbit flocculus has five transfolial zones (1, 2, 3, 4, and C2) whose borders can be defined both anatomically and physiologically. Anatomically the zone borders in the floccular white matter can be visualized by a histochemical stain for acetylcholinesterase (AChE) (2, 57, 79–81). Climbing fibers from the caudal DC encode HOKS about the vertical axis (VA) to zones 2 and 4. Cells in rostral DC and ventrolateral outgrowth (VLO) detect OKS about the posterior axis (PA) and anterior axis (AA) and project to zones 1 and 3. These two axes lie along the azimuth and form angles of 135 deg (PA) and 45 deg (AA) with respect to the longitudinal axis. Climbing fibers from the rostral medial accessory olive (MAO) project to zone C2, but convey no optokinetic information (57, 69, 78, 82). Climbing fibers from the rostral DC in the rabbit encode optokinetic stimulation about the PA and AA and project to zones 1 and 3. Tracer and micro-stimulation studies suggest that these floccular zones have different projection patterns particularly to the vestibular complex (57, 81). Microstimulation of the white matter in the rabbit flocculus evokes eye movements consistent with the zone that is stimulated. Microstimulation of zones 2 and 4 evoke horizontal eye movements. Microstimulation of zones 1 and 3 evoke movements about the AA and PA axes (2). The function of the C_2 compartment may be linked to the control of head movement (83).

Immunohistochemical Zebrin II Parasagittal Zones and Physiological Climbing Fiber Zones in Lobule X

Physiologically defined parasagittal climbing fiber zones can be compared to the parasagittal zones described immunohistochemically using antibodies to Zebrin I and Zebrin II (84, 85) and to histochemical stains for acetylcholinesterase (86) and 5′-nucleotidase (87, 88). The expression of Zebrin II in vermal lobule X intensely labels Purkinje cells with only weakly labeled interlaced Zebrin negative bands (85, 89, 90). The prominent interlaced immunohistochemical zonation is more apparent in vermal lobule IX and the hemisphere of lobule X (flocculus).

Purkinje cells in in lobule X of the pigeon respond to one of the three axes of optokinetic stimulation (91), similar to the physiological pattern of optokinetic responses observed in rabbit (69) and mouse (92). Within a physiological optokinetic zone both zebrin II positive and zebrin II negative Purkinje cells exist. The amplitude of modulated discharge for Purkinje cells located in a zebrin II-positive zone exceeds that of Purkinje cells located in a zebrin II-negative zone. The cause of this difference is unresolved. However, it seems that zebrin II zones are not congruent with the optokinetic and vestibular sagittal zones in lobules IX-X.

The Antiphasic Discharge of CSs and SSs Depends Climbing Fibers

Presently, the origins of the synaptic signals that modulate the discharge of SSs is poorly understood. Often, it is argued that parallel fiber discharge modulates the activity SSs (93–102). If vestibular primary afferents→granule cells→parallel fibers→Purkinje cell were a straight-through pathway, then the discharge of vestibular primary afferents and the discharge of SSs ought to co-vary. However, during sinusoidal roll-tilt these two signals are antiphasic. SSs are also antiphasic with the discharge of CSs (**Figures 4B,C,E**) (64, 65). It is logically possible that vestibular nuclear neurons, a fraction of which project contralaterally, are the major synaptic driving force that modulates the activity of SSs, but at present there is no evidence that bears on this point. Perhaps the genesis of antiphasic discharge of CSs and SSs in lobules IX-X can be explained by known cerebellar circuitry.

An antiphasic interaction between CSs and SSs can be demonstrated directly by reversibly inactivating the inferior olive. Application of a cooling probe to the ventral brainstem of the rat reduces CS discharge and increases SS discharge (103, 104). The increased SS discharge reduces the spontaneous discharge rate of secondary vestibular neurons and cerebellar nuclear neurons. This cooling effect can be attributed to the decreased olivary activity. When the inferior olive is destroyed by a cocktail of 3-acetylpyridine and harmaline prior to cooling, the increased discharge of SSs evoked by cooling the inferior olive in intact rats does not occur (104–106).

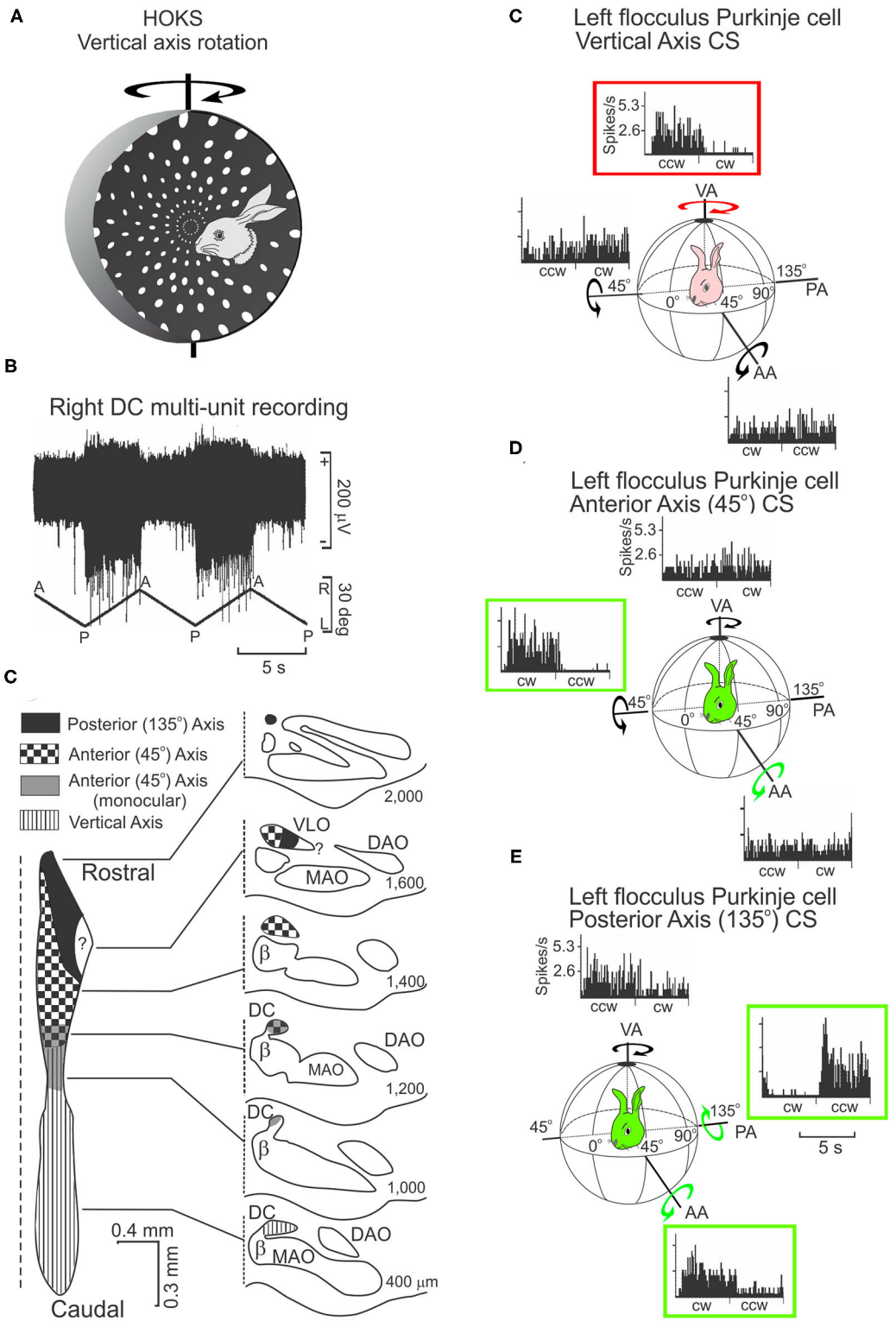

FIGURE 5 | HOKS evokes discharge of neurons in the dorsal cap (DC) and discharge of Purkinje neurons in the flocculus. **(A)** HOKS about the vertical axis (VA) modulates the activity of caudal DC neurons. **(B)** Activity of multiple neurons in the caudal, left DC increases during low velocity (1 deg/s) HOKS in the posterior→anterior (P→A) direction of the right eye. The neuronal activity is disfacilitated during A→P stimulation. **(C)** Inferior olive is divided into regions corresponding to activity modulated by optokinetic stimulation about one of three axes (AA, PA, VA). An unfolded longitudinal strip of DC neurons is illustrated to the

(Continued)

FIGURE 5 | left, transverse sections to the right. The numbers to the right of each transverse illustration show the distance of the section from the caudal pole of the inferior olive. **(C)** P→A HOKS of the ipsilateral eye about the VA, increases the frequency of CSs. The discharge frequency of CSs is not modulated by OKS about the AA or PA. **(D)** The discharge of CSs in a second Purkinje cell is modulated by OKS of the contralateral eye in the CW direction about the AA. **(E)** The discharge of a CSs in a third Purkinje cell is modulated by OKS in the CCW direction about the PA. All recordings are obtained from the left flocculus. bp, brachium pontis; fpl, primary floccular fissure; Fl, flocculus. Modified from Barmack and Hess (75) and Leonard et al. (76).

The antiphasic discharge of CSs and SSs following activation of climbing fibers does not depend on the occurrence of a CS in the same Purkinje cell. When climbing fibers are electrically stimulated in the inferior olive, the intensity of the electrical stimulus can be adjusted to be above or below a level needed to evoke a CS in a recorded Purkinje cell. Suprathreshold electrical stimulation evokes a CS and also suppresses the spontaneous discharge of SSs. However, a stimulus that is subthreshold for activating a CS in a recorded Purkinje cell may still cause suppression of its SSs (107). This finding has been replicated, substituting optical stimulation of channel rhodopsin-expressing climbing fibers instead of electrical stimulation. In this instance the spontaneous activity of a Purkinje cell whose climbing fiber is not activated, nevertheless decreases (108). This supports the idea that the suppression is caused by climbing fiber-evoked activation of inhibitory interneurons.

The effects of CSs on the discharge of SSs can be examined by altering the wiring of climbing and mossy fiber projections to the cerebellum. In the native pathway climbing fibers decussate in the ventral brainstem and then project to the contralteral cerebellum. It is possible to mutate this climbing fiber pathway so that the normal crossed contralateral projection is converted to an uncrossed ipsilateral projection. This is accomplished by insertion of the mutation (Ptf1a::cre;Robo3(lox/lox) in mice (109). The normally uncrossed mossy fiber projections remain undisturbed. Purkinje cell recordings from the flocculus of these mutant mice during optokinetic stimulation indicate that the favored P→A directional preference of normal mice is reversed in mutant mice. The CS discharge is now optimal for stimulation in the A→P direction because the uncrossed olivo-cerebellar projection in the mutant. More interesting is that the directional preference of optokinetically-evoked SSs is also reversed in the mutant. If the modulated discharge of SSs was caused by an intact mossy fiber→granule cell→parallel fiber projection, its polarity would not reverse.

Purkinje cells in lobules IX-X receive an excitatory climbing fiber signal from the contralateral β-nucleus and DMCC (**Figure 2B**). If the climbing fiber input were blocked by making a microlesion in the right β-nucleus, then Purkinje and stellate cells in the left lobules IX-X would retain only a vestibular primary afferent signal while right vermal lobules IX-X would retain both a climbing fiber signal and a vestibular primary signal. The antiphasic discharge of CSs and SSs is disrupted following a microlesion of the right β-nucleus. Such a microlesion leaves some cells in the β-nucleus and DMCC and their climbing fiber projections to Purkinje cells in the contralateral vermal lobules IX-X intact. The CSs and SSs in these Purkinje cells respond to sinusoidal roll-tilt with a normal antiphasic discharge (**Figure 6A1**). A second group of Purkinje cells retain spontaneously discharging CSs, but they are not driven by vestibular stimulation. The SSs in these Purkinje cells are unresponsive in spite of the fact that their vestibular primary afferent mossy fiber input is not compromised (**Figure 6A2**). A third group of Purkinje cells lack spontaneous and vestibularly-modulated CSs. In these Purkinje cells, 30/37 SSs cannot be modulated by vestibular roll-tilt (**Figure 6A3**) (110).

Vestibular primary afferent mossy fibers project exclusively to ipsilateral vermal lobules IX-X. Following a left unilateral labyrinthectomy (UL) Purkinje cells recorded from ipsilateral (left) vermal lobules IX-X retain a normal climbing fiber-evoked antiphasic response of CSs and SSs even though the left vestibular primary afferent mossy fiber signal is effectively removed (**Figure 6B1**). The climbing fiber pathway to the left vermal lobules IX-X remains intact since it originates from the contralateral (right) labyrinth. Conversely, the antiphasic responses of CSs and SSs in the right vermal lobule IX-X Purkinje cells ipsilateral to the *intact* labyrinth, are severely impaired (66) because the climbing fiber input to the left vermal lobules IX-X originates from the surgically destroyed (right) labyrinth (**Figure 6B2**). These recordings are made acutely within 3 h post-UL. Chronic recordings, are made at least 48 h post-UL reveal a strong recovery of CS-induced SS pauses in contralateral Purkinje cells (**Figure 6B3**). This can be attributed, in part, to the recovery in the activity of secondary neurons that project bilaterally to vermal lobule X (38, 111).

Cerebellar Interneurons and the Genesis of Climbing Fiber-Evoked Pauses

Climbing fiber evoked pauses in SS discharge can be viewed at three levels: [1] Spontaneous SS pauses are triggered for 5–10 ms due to the large climbing fiber-induced inactivation by a Ca2+ activated K+ conductance (112). A short-term SS inactivation may also be attributed, in part, to ephaptic coupling of Purkinje cells (113). This climbing fiber-evoked pause of SSs occurs even when GABAergic transmission by interneurons is blocked (114, 115). [2] Long-term depression (LTD), evoked by conjunctive activation of climbing fiber and parallel fiber synapse on a Purkinje cell dendrite has a duration of at least minutes (116–122). [3] A longer pause in SS discharge is induced by climbing fiber-evoked interneuronal inhibition. Three inhibitory interneurons are likely candidates to play this role; Golgi cells, stellate cells and basket cells. This pause is independent of the fast changes in Purkinje cell conductance and lasts 5-100 ms (123–126).

Golgi cells have large somata (10–20 μm) found at the base of the Purkinje cell layer. Their dendrites are oriented sagittally in the molecular layer and have a planar width of 180 μm, comparable to the planar width of Purkinje cells, 120 μm (65). Golgi cell axons branch extensively in the granule cell layer where

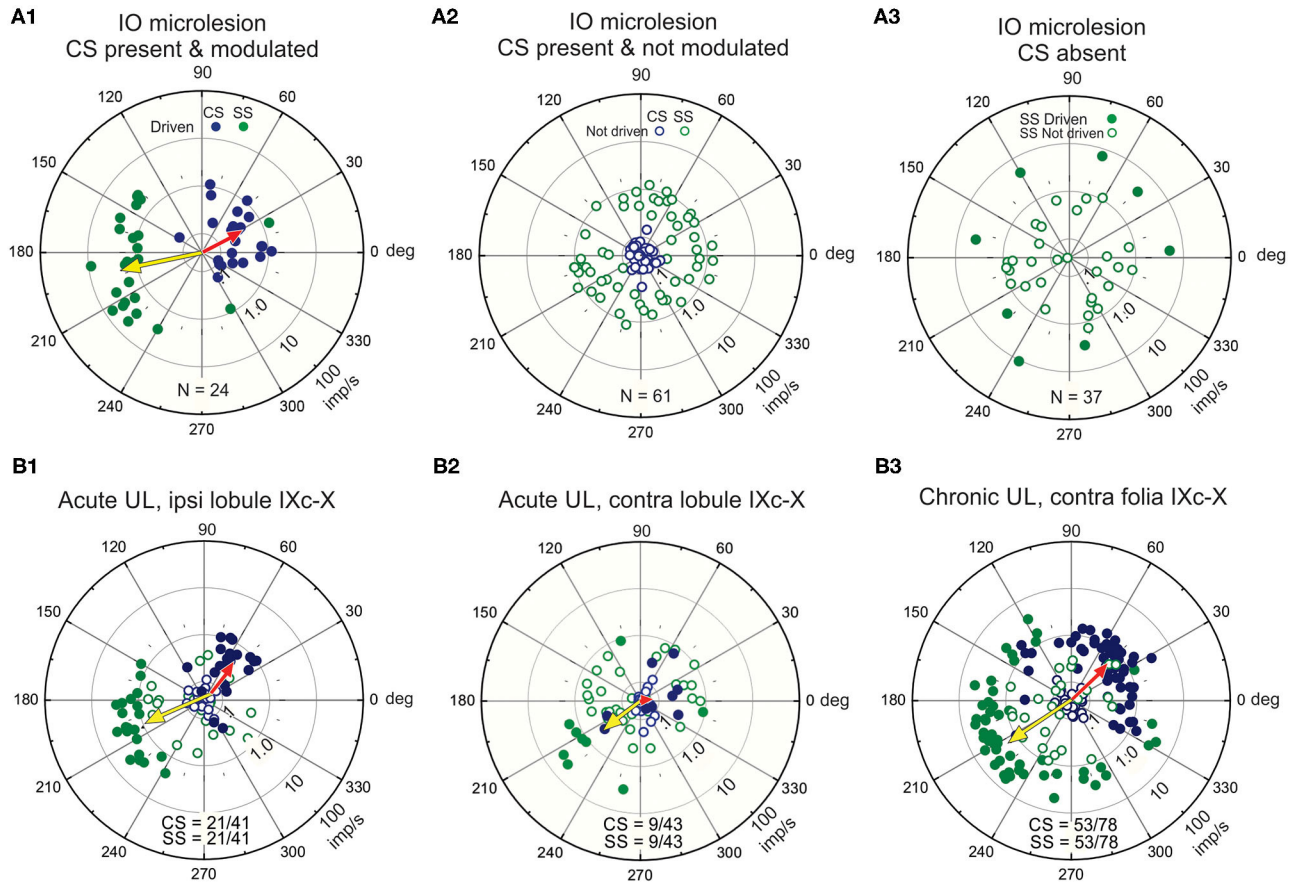

FIGURE 6 | Unilateral microlesions of the β-nucleus and unilateral labyrinthectomy (UL) alter the antiphasic discharge of CSs and SSs in vermal lobule IXc-X Purkinje neurons. **(A1–3)** Incomplete, unilateral microlesions are made in the right β-nucleus to examine how the discharge of SSs in lobules IX-X Purkinje cells are modulated by sinusoidal vestibular stimulation about the longitudinal axis with and without climbing fiber signals. **(A1)** Microlesions are incomplete. Some Purkinje cells with intact climbing fibers evince an antiphasic discharge of CSs and SSs. A polar plot of these responses and their population vectors is similar to that characterizes Purkinje cell discharge in mice with totally intact climbing fiber projections (see **Figure 4E**). **(A2)** Some Purkinje cells retain spontaneous CSs, but the discharge of these CSs is no longer modulated by vestibular stimulation. In these instances, SSs are also spontaneously active, but no longer driven by vestibular stimulation. **(A3)** In a third group of Purkinje cells, the microlesion destroys the climbing fiber projection. In this group, the discharge of 30/37 SSs is not modulated by vestibular stimulation. **(B1–3)** A UL deprives the ipsilateral vermal lobules IX-X of a vestibularly modulated primary afferent mossy fiber signal while leaving the contralateral primary afferent mossy fiber signal to the contralateral vermal lobules IX-X intact. **(B1)** The proportion of Purkinje cells ipsilateral to the UL in which CSs and SSs are antiphasically modulated vestibular stimulation is reduced by (21/41), but population vectors are comparable to those in normal mice. (B2) The proportion of Purkinje cells contralateral to the UL in which CSs and SSs are antiphasically modulated is reduced (9/43) even though their primary afferent mossy fiber input remains intact. The population vector for SSs is similar to that of normal mice, but the population vector for CSs is reduced to 0. **(B3)** Recordings, made at least 48 h post-UL show recovery of CS-induced SS pauses in contralateral Purkinje cells. Modified from Barmack and Yakhnitsa (66, 110).

they co-terminate with mossy fiber terminals on granule cell dendrites in a glomerular plexus (6, 24, 127, 128). Golgi cell axon terminals also contact unipolar brush cells (129). Climbing fibers make synaptic contact with Golgi cell dendrites in the molecular layer (130, 131). Consequently, Golgi cells are in a unique position to regulate the discharge of granule cells and thereby influence parallel fiber input to Purkinje cells and possibly account for the modulation of SSs. The activity of Golgi cells can be recorded *in vivo* and juxtacellularly labeled to confirm subsequently their identity. The activity Golgi cells in lobules IX-X is modulated sinusoidal vestibular stimulation. Interestingly, Golgi cells are not driven in phase with either CSs or parallel fibers. Rather during sinusoidal roll-tilt they respond during contralateral side-down rotation, in phase with the discharge of SSs and out of phase with the discharge of CSs ($\phi = 180$ deg), making it implausible that Golgi cells are responsible for the modulation of SSs during vestibular stimulation (65) (**Figure 7A**).

Stellate cell axons have lengths of ∼250 μm and since they are arrayed throughout the entire molecular layer, make multiple and repeated contact with the dendrites of Purkinje cells (132, 133). The mouse molecular layer contains at least 15 stellate cells/Purkinje cell. Climbing fibers make no direct synaptic contacts onto either basket or stellate cells (128, 134). Rather, the discharge of climbing fibers releases glutamate ("spillover") in sufficient concentration to excite stellate cell

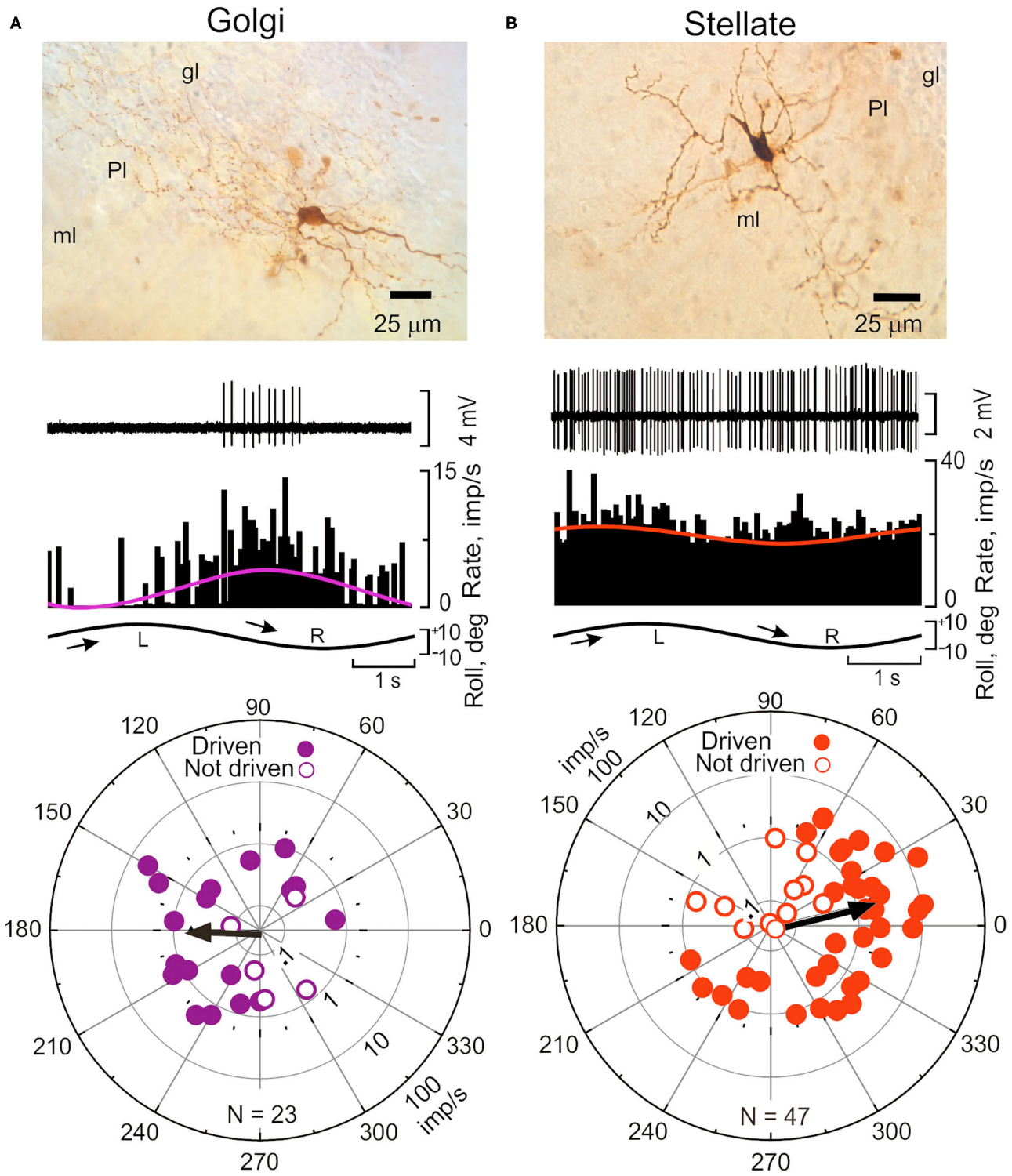

FIGURE 7 | Sinusoidal roll-tilt modulates the discharge of Golgi and Stellate interneurons in lobules IX-X. **(A)** Interneurons are identified with juxtacellular labeling neurobiotin (138). **(A)** Golgi cell in the granule cell layer (gl) of left vermal lobule IX responds to *contralateral* roll-tilt. The peristimulus histogram is fitted with a cosine function (purple). The population vector for 23 Golgi cells, $\phi = 184$ deg. **(B)** Stellate cell in left lobule X responds to *ipsilateral* roll-tilt. Peristimulus histogram is fitted with a cosine function (red). The population vector for 47 stellate cells, $\phi = 13$ deg. gl, granule cell layer; ml, molecular layer; Pl, Purkinje cell layer. Modified from Barmack and Yakhnitsa (65).

discharge (125, 126, 135–137). Stellate cell axon terminals release GABA onto $GABA_A\alpha_1$ receptors on Purkinje cell dendrites.

The discharge of stellate cells is well-modulated during sinusoidal roll-tilt with peak discharge frequency during ipsilateral side-down. The polarization vector for a population of 47 stellate cells ($\phi = 13$ deg) suggests that the antiphasic responses of CSs and SSs could be attribute to climbing fiber-evoked stellate cell inhibition of Purkinje neurons (**Figure 7B**) (65).

Stellate cell inhibition of Purkinje cells initiated by climbing fiber release of glutamate is not the only unconventional aspect of stellate cell synaptic influence on Purkinje cell excitability. If climbing fibers and parallel fibers are stimulated conjunctively in the cerebellar C3 zone of the cat, the stellate cell response to parallel fiber stimulation alone increases (139). Stellate cells express NMDA receptors. When stellate cells are stimulated in tissue slice preparations the stellate cells increase their discharge through a Ca2+ and CaMKII-dependent activation of voltage-gated Na+ channels (140). This signaling pathway lowers the gated action potential threshold by causing a hyperpolarizing shift in voltage gated Na+ channels. The increased discharge lasts for minutes.

Oscillatory Adaptation of Vestibular Circuitry Occurs During Prolonged Roll-Tilt Stimulation

The modulated pattern of discharge CSs in Purkinje cells during sinusoidal rotation about the longitudinal axis is usually invariant for tens of minutes (**Figure 4B1**). When vestibular stimulation stops, the pattern of CS discharge returns to a spontaneous level. However, the discharge of 5% CSs is not invariant (**Figures 8A–E**). In these Purkinje cells, the modulated discharge frequency of CSs decreases during repeated sinusoidal roll-tilt at 0.20 Hz (**Figure 8D**). After ∼345 s the vestibular stimulus fails to evoke a CS discharge (141). When sinusoidal stimulation is discontinued, the oscillatory pattern of CSs at 0.20 Hz re-appears (**Figure 8E**). Approximately 200–300 s after vestibular stimulation stops, this pattern disappears and is replaced with aperiodic spontaneous discharge. This pattern of oscillations, can be temporarily entrained to a different frequency of roll-tilt. An oscillation at 0.20 Hz can be entrained to 0.30 Hz. When the stimulation stops, the entrained oscillation at 0.30 Hz rapidly fades into 0.20 Hz and then back to aperiodic spontaneous activity. While it is tempting to speculate that this adaptive pattern originates in the inferior olive, the same adaptive pattern can be observed in the GABAergic neurons in the Psol (14). Possibly the oscillations originate at the Psol or at a more peripheral level. The medial vestibular nucleus has class of secondary neurons that express N-Methyl-D-Aspartate receptors (NMDA) (142). In tissue slice experiments the discharge of these neurons oscillates at frequencies of 0.1–0.3 hz with bath application of NMDA (143). The possibility of NMDA receptors in neurons in the MVN and Psol acting similarly to the NMDA receptors in stellate cells has not been explored. Possibly NMDA receptors provide a mechanism by which membrane oscillations induced by vestibular stimulation are controlled by neuromodulators.

The oscillatory discharge of Psol neurons and climbing fibers, while present in anesthetized preparations, have a behavioral analog in unanesthetized rabbits. Sinusoidal linear acceleration of a rabbit along the inter-aural axis for several hours evokes oscillatory vertical eye movements. These eye movements persist for 1–2 min when vestibular stimulation is stopped (144).

Activity of Floccular CSs Influences the Discharge of MVN Neurons

MVN neurons receive optokinetic as well as vestibular signals (145). By recording from MVN neurons before and after the dorsal cap is removed from the optokinetic circuitry the contribution of the DC through the flocculus to visually-modulated MVN activity can be determined (**Figure 9A**). In paired recordings, both DC and MVN neurons increase their rate of discharge during constant velocity (0.8 deg/sec) of the eye ipsilateral to the MVN and contralateral to the DC (146). At the onset of P→A stimulation the MVN neuron slowly increases its rate of discharge from ∼10 imp/s to a maximum of ∼60 imp/s over the 25 s interval (**Figure 9C**). When the optokinetic stimulus reverses direction, the activity of the MVN neuron slowly returns to a steady-state with a 10–15 s decay. When the site of the olivary recording is inactivated by an electrolytic microlesion made through the olivary recording electrode, the response profile of the MVN neuron is altered. The peak modulation is decreases and the slow build up and decay attenuates. The DC microlesion has no effect on MVN activity induced by rotation of the rabbit about the vertical axis (**Figure 9B**). Consistent with the known circuitry, the optokinetically evoked activity of neurons in the right DC project as climbing fibers to Purkinje cells in the left (contralateral) hemispheric lobule X. The increase in climbing fiber-evoked CSs reduces the discharge of SSs in Purkinje cells, thereby withdrawing Purkinje cell inhibition of the subjacent MVN neurons.

Hemispheric Lobule X Contributes Optokinetic Stabilization to Postural Control

In monkeys, post-rotatory vestibular nystagmus (PRN) is provoked by deceleration following constant velocity horizontal vestibular stimulation. PRN lasts for only a few seconds, but long enough to measure how the plane of PRN changes during pitch. Since monkeys have frontally placed eyes changes in pitch would be expected to alter the plane of PRN within the orbit to keep the plane in space constant. In normal monkeys, this is exactly what happens. In monkeys with bilateral lesions of the lobule X, PRN no longer is executed horizontally in space, but rather is executed horizontally within the orbit (147, 148).

In rabbits the same influence of the gravitational vector and eye movements can be examined by inducing a long-lasting optokinetic after-nystagmus by providing sustained exposure to HOKS. In rabbits, sustained HOKS (1–48 h) evokes an optokinetic after-nystagmus (OKAN II) that lasts for several hours (**Figures 10A–E**). The velocities of the slow phase of

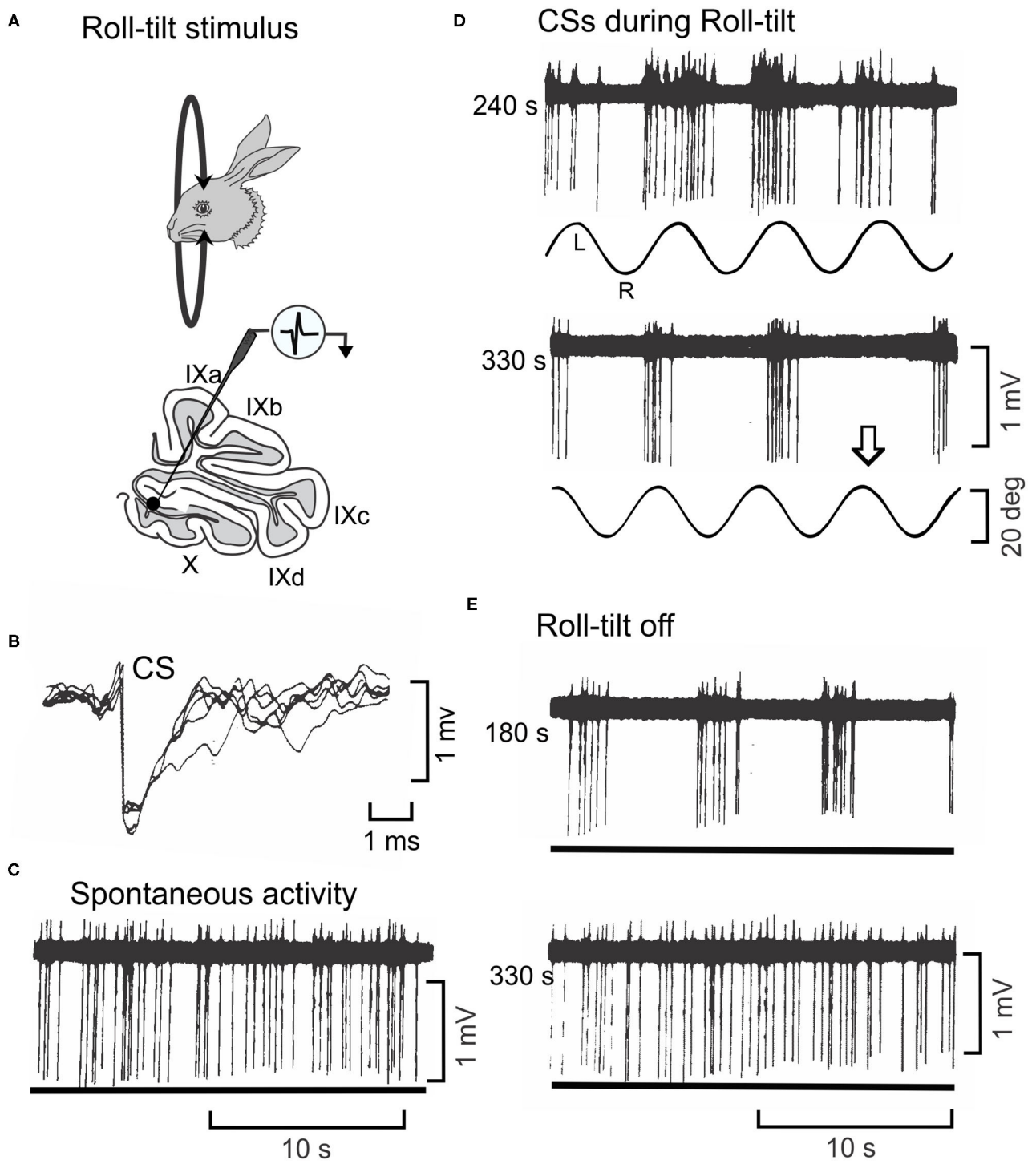

FIGURE 8 | Oscillatory discharge of a CS cell in lobule X of rabbit is entrained by sinusoidal roll-tilt. **(A)** Figurines depict a rabbit during roll-tilt and a microelectrode recording from a Purkinje cell in the left lobule X. **(B)** Five superimposed waveforms identify a CS in recorded Purkinje cell. **(C)** Spontaneous discharge of CSs occurs in absence of roll-tilt stimulation (lower trace). **(D)** Sinusoidal roll-tilt continues to modulate discharge of CSs 240 s after the stimulation begins. CS discharge increases during roll-tilt onto the left side. After 330 s of continuous roll-tilt, the modulation CS discharge decreases. Arrow indicates one cycle during which no CSs occur. **(E)** When the vestibular stimulus stops, the discharge of CSs oscillates at the previous stimulus frequency. This oscillatory discharge still occurs 180 s after the vestibular stimulus stops. It abates after 330 s. Modified from Barmack and Shojaku (141).

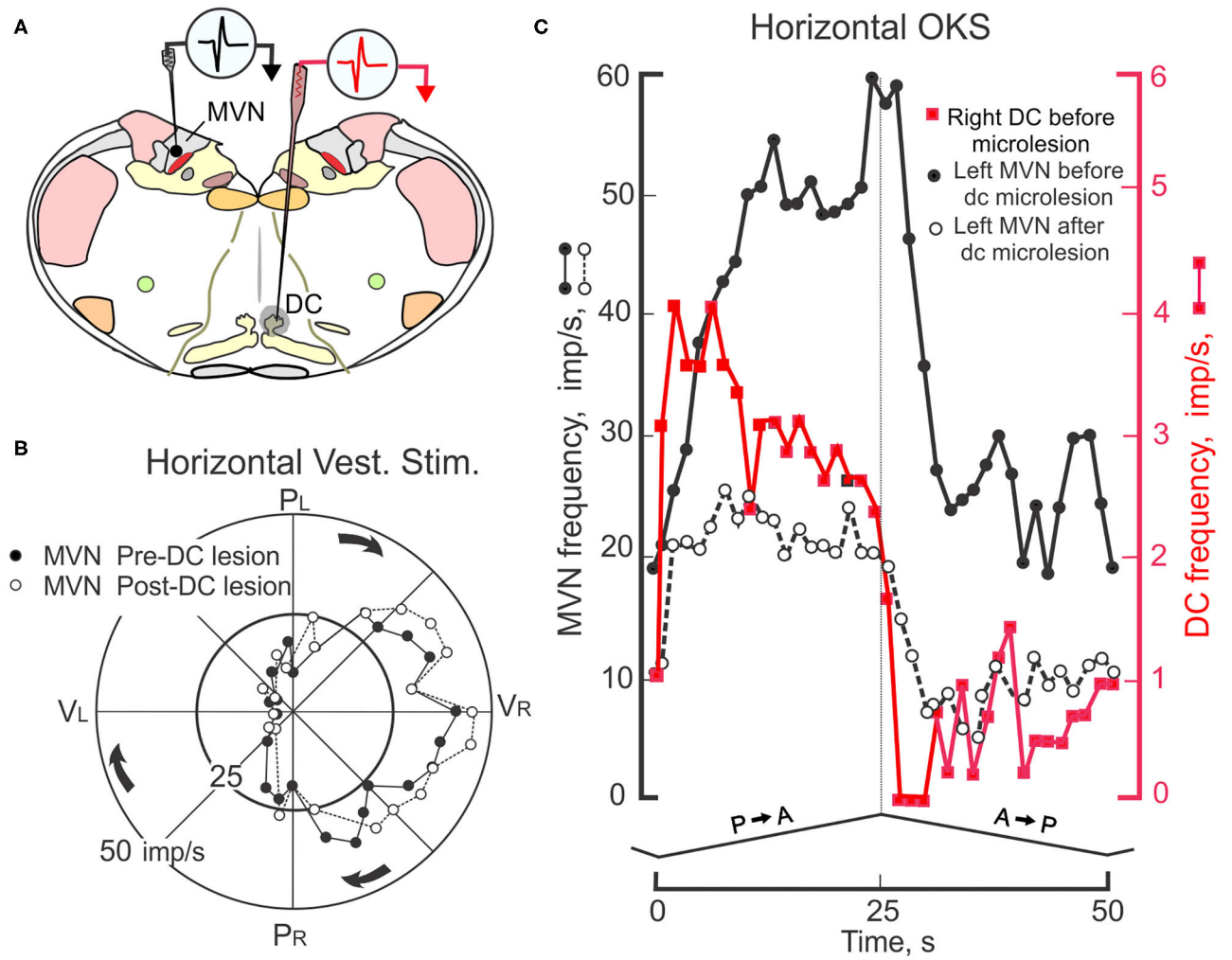

FIGURE 9 | Interaction of floccular and non-floccular optokinetic signals at the level of the medial vestibular nucleus (MVN). **(A)** Transverse brainstem section shows locations for two electrodes used to record simultaneously from two neurons; one he left MVN and the other in the right caudal DC. The activity of this pair of neurons is recorded during four cycles of horizontal sinusoidal vestibular stimulation and four cycles of monocular, triangular waveform, constant velocity HOKS of 1 deg/s delivered to the left eye. A microlesion (-50 μa, 30 s) is then made at the recording site in the caudal DC. The destroyed area is indicated by shading. Subsequently, the responses of the MVN neuron during horizontal vestibular and HOKS are recorded again. **(B)** Polar plot shows MVN responses evoked during sinusoidal horizontal vestibular stimulation (± 10 deg, 0.4 Hz) in the dark before (filled circles) and after (open circles) the electrolytic microlesion is placed in the right caudal DC. The gain and phase of the discharge of the MVN neuron are unmodified by the DC microlesion. **(C)** HOKS modulates the activity of the left MVN neuron (black filled circles) and the right DC neuron (red filled squares). After the microlesion of the right DC, the optokinetically-evoked discharge of the left MVN neuron is reduced (open circles). Modified from Barmack (146).

OKAN II vary between 30 and 50 deg/s and exceed the normal range of rabbit slow phase velocities, even exceeding the slow phase velocities induced by a unilateral labyrinthectomy (**Figure 10E**). During sustained binocular HOKS the gain of the horizontal optokinetic reflex (eye velocity/drum velocity) decreases gradually from ∼0.95 at the onset of stimulation to ∼0.50 after 36 h of HOKS (**Figure 10D**). One way of thinking about the genesis of OKAN II is that the animal adapts to a visual environment that moves slowly about the vertical axis. Retinal slip increases as the gain of the optokinetic reflex decreases. When the rabbit is removed from this environment and placed in the dark, eye movements are generated that attempt to restore the adapted stimulus condition without negative feedback. In many rabbits OKAN II would persist at the onset even in an illuminated background since the eyes are moving at velocities that exceed the detection range of direction-selective ganglion cells.

Because OKAN II persists for hours, it is relatively easy to measure the plane of OKAN II and how it is modified by changes when the head is pitched and rolled. In the lateral-eyed rabbit, roll-tilt should yield equivalent results to pitch in monkeys. During rotation about the longitudinal axis in normal rabbits OKAN II remains horizontal in space and compensates for the roll-tilt by moving vertically within the orbit (**Figure 11A**). OKAN II remains horizontal in space during pitch about the inter-aural axis in both normal and nodulectomized

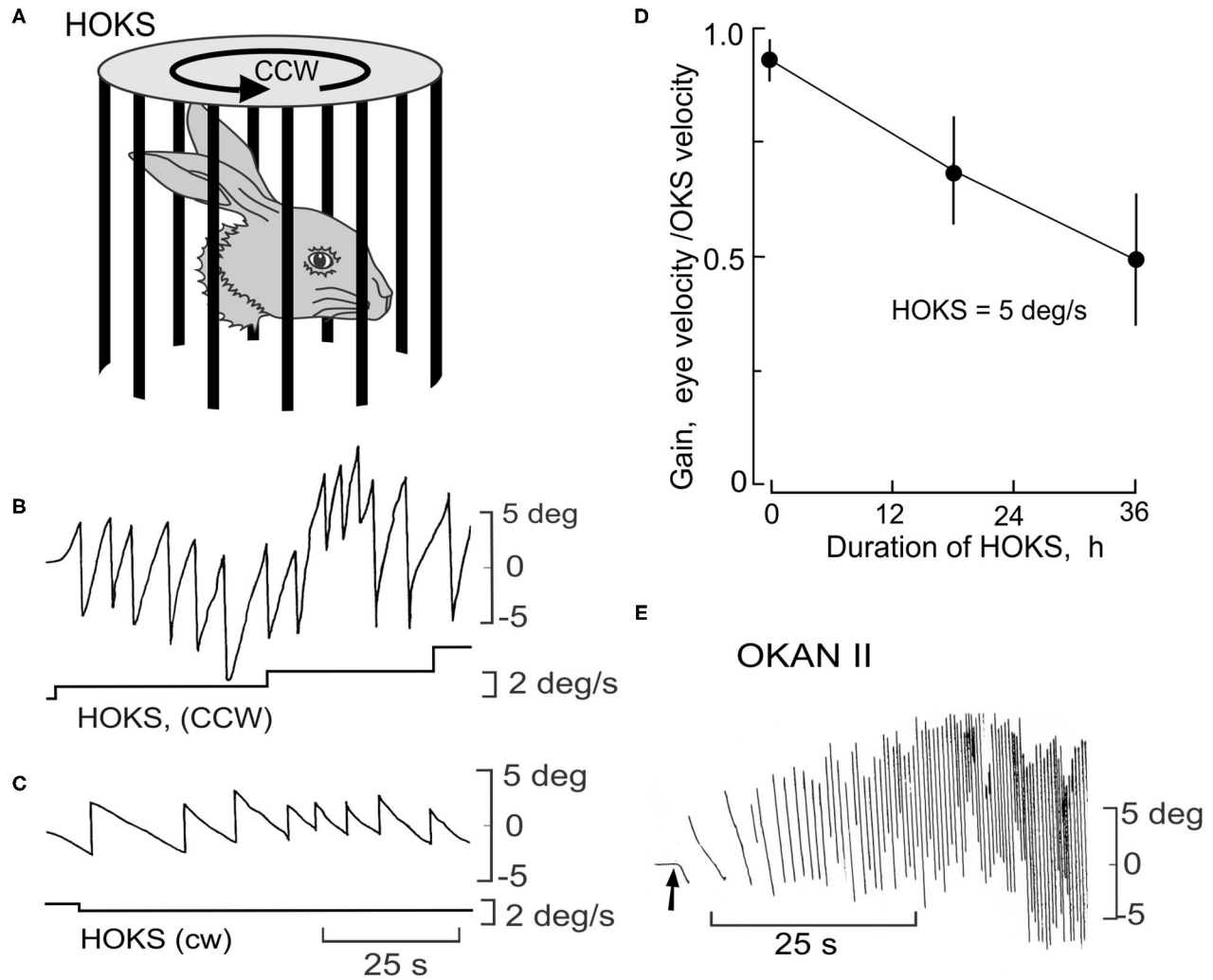

FIGURE 10 | Long-term HOKS induces a prolonged negative optokinetic after-nystagmus (OKAN II). **(A)** Rabbits are exposed to monocular HOKS by placing them in the center of a cylinder that rotates at an angular velocity that changes stepwise from 1 to 5 deg/s and stimulates the right eye in the P→A direction. Eye position is measured with a photoelectric technique (149). Patterned vision of the left eye is occluded. **(B)** P→A HOKS of the right eye at 5 deg/s evokes horizontal eye movements with a slow phase velocity of ∼4.5 deg/s. The bottom trace indicates HOKS velocity. **(C)** A→P HOKS of the right eye evokes an eye movement in the same direction, but with a lower velocity. **(D)** The gain of the eye movements evoked by binocular HOKS is measured in three rabbits at 0, 18, and 24 h after the onset of HOKS. The gain decreases with increasing duration of HOKS. **(E)** HOKS is maintained for 24 h. When it stops (arrow) and the rabbit is placed in the dark, the slow phase of the nystagmus reverses direction with respect to the now absent HOKS. OKAN II accelerates to a velocity of 30–50 deg/s and lasts for 12-24 h. Modified from Barmack and Nelson (150).

rabbits (**Figure 11B**). However, in nodulectomized rabbits this gravitational reference is lost (**Figure 11C**) (151).

Both PRN and OKAN II reflect an imbalance in pre-oculomotor circuitry. It is astounding to consider that during roll-tilt a gravitational vector can be interpreted by cerebellar and brainstem circuitry to perform the same horizontal eye movement in space by executing graded commands for the reciprocal activation of the horizontal and vertical rectus muscles.

During roll-tilt the lobules IX-X are necessary to maintain the plane of OKAN II constant with respect to gravity. This is consistent with the abundance of climbing fiber-encoded signals related to static roll and the absence of climbing fiber-encoded signals from the horizontal canals. Conversely, a nodulectomy has no effect on the gain of the HVOR and causes only a small decrease in the gain of the VVOR. Nor does a nodulectomy disrupt optokinetic suppression of either the HVOR or VVOR (151).

HOKS Evokes Transcription and Expression of Corticotropin Releasing Factor (CRF)

Sustained binocular HOKS evokes OKAN II that lasts 24 h or longer, depending on the parameters of stimulation (150).

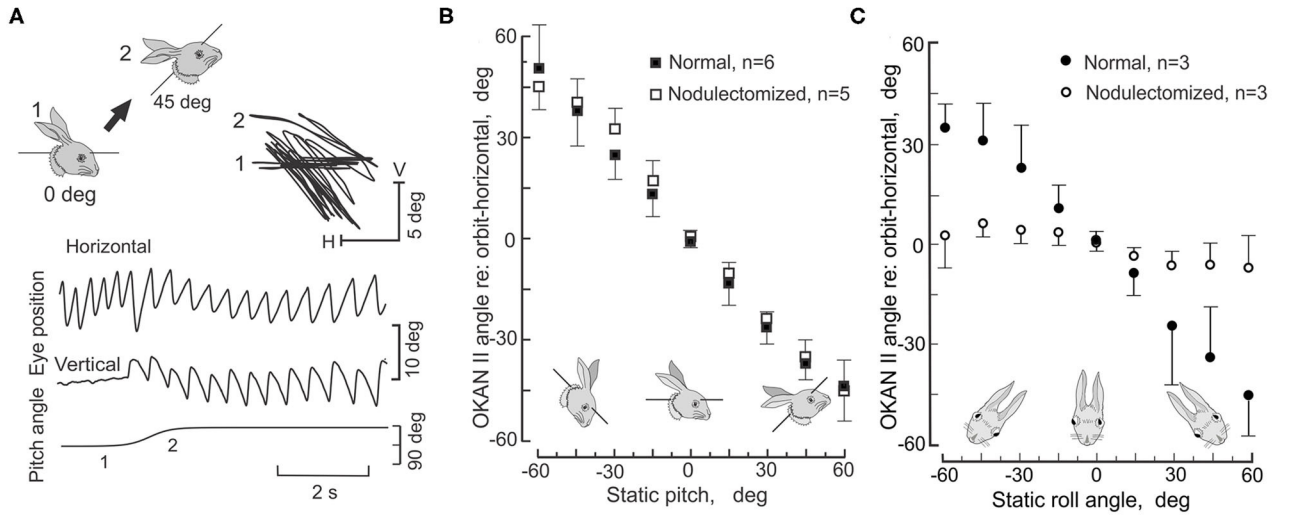

FIGURE 11 | Nodulectomy distorts plane of OKAN II during static roll, but not during static pitch. OKAN II is induced following 24–48 h of binocular HOKS at 5 deg/s. **(A)** During static pitch about the inter-aural axis in normal rabbits, OKAN II remains orthogonal to the gravitational vector (filled circles). This is shown by the sequential change in the vertical and horizontal eye movement records as the rabbit's head position is shifted about the interaural axis by 45 deg as indicated by the figurines. **(B)** OKAN II remains executed in spatial coordinates after a nodulectomy when the rabbit is pitched about the inter-aural axis. **(C)** During roll-tilt about the longitudinal axis, OKAN II adjusts vertically to maintain its horizontal plane in spatial coordinates. After a nodulectomy, OKAN II is no longer executed in spatial coordinates during roll-tilt about the longitudinal axis. Rather it is executed in orbital coordinates. Modified from Barmack et al. (151).

While the cerebellar flocculus has been the focus of experiments designed to test the role of the inferior olivary neurons in visual-vestibular adaptation, changes observed following sustained HOKS suggest that optokinetic adaptation is already present in optokinetic circuitry prior to its entry to the cerebellum (152, 153). Binocular HOKS in rabbits for 16–48 h increases the transcription and expression of corticotropin releasing factor (CRF) in neurons in the caudal DC contralateral to the eye receiving P→A optokinetic stimulation (**Figures 12A–D**). If the rabbit is anesthetized and euthanized immediately after HOKS is stopped, neurons in the DC contralateral to the eye that received P→A stimulation have elevated transcription of CRF (**Figure 12A**). Following 24 h of binocular HOKS an estimate of the hybridized grain densities in neurons in the two DCs yield an estimate of a 4-7X increase of CRF mRNA transcripts in neurons in the DC stimulated in the P→A direction relative to the transcripts in neurons in the contralateral DC. If binocular HOKS is given for 48 h and the rabbit is allowed to recover for 16–18 h in the light before it is anesthetized and euthanized, elevated expression of CRF is still found in neurons in the DC contralateral to the eye stimulated in the P→A direction, with a smaller increase in CRF expression in the DC contralateral to the eye stimulated in the AP direction (**Figure 12C**). If monocular, HOKS in the *null* (A→P) direction is given for 48 h and the animal is allowed to recover for 18 h in the dark, then elevated expression of CRF is found in the DC contralateral to the eye previously stimulated in the AP direction (**Figure 12D**) (154). HOKS is essential to evoke the change in CRF expression. If contour vision is obscured by translucent occluders then no change in CRF expression in DC neurons on either side of the brain is observed (**Figure 12B**). After HOKS stops these neurons may evince a rebound excitation when the disfacilitatory signal is removed. OKAN II persists in rabbits that recover in the dark. When rabbits recover in the light, OKAN II is suppressed by visual feedback. This effectively uncouples the retinal slip signal from the eye movement signal. A rebound in activity in the caudal DC previously stimulated in the A→P direction could occur if subsequently the caudal DC receives an OKAN II-associated eye movement signal in the form of reduced inhibition from the contralateral NPH. This explanation is consistent with the idea that floccular CSs encode not just retinal slip, but a mixture of retinal slip and eye movement signals (155).

Cerebellar Purkinje cells, particularly those in hemispheric lobule X and vermal lobules IX-X, express CRF binding sites (156–158). Only one of the two CRF receptor subtypes, CRF_1, is expressed in the cerebellum (159). CRF receptors belong to the VIP/calcitonin family of G protein-coupled receptors. They are positively coupled to adenylate cyclase. Direct application of CRF onto Purkinje neurons *in vitro* increases excitability attributed activation of a sodium current and a voltage-dependent potassium current (160). In cerebellar cultures, CRF modulates gene expression via a cAMP pathway (161). This pathway could be responsible for the long-term regulation of calcium-activated potassium conductance and thereby account for the decreased after-hyperpolarization observed in Purkinje cells *in vitro* after bath application of CRF (162).

CRF is localized in neurons that comprise the hypothalamo-pituitary-adrenal (HPA) axis, principally engaged in the

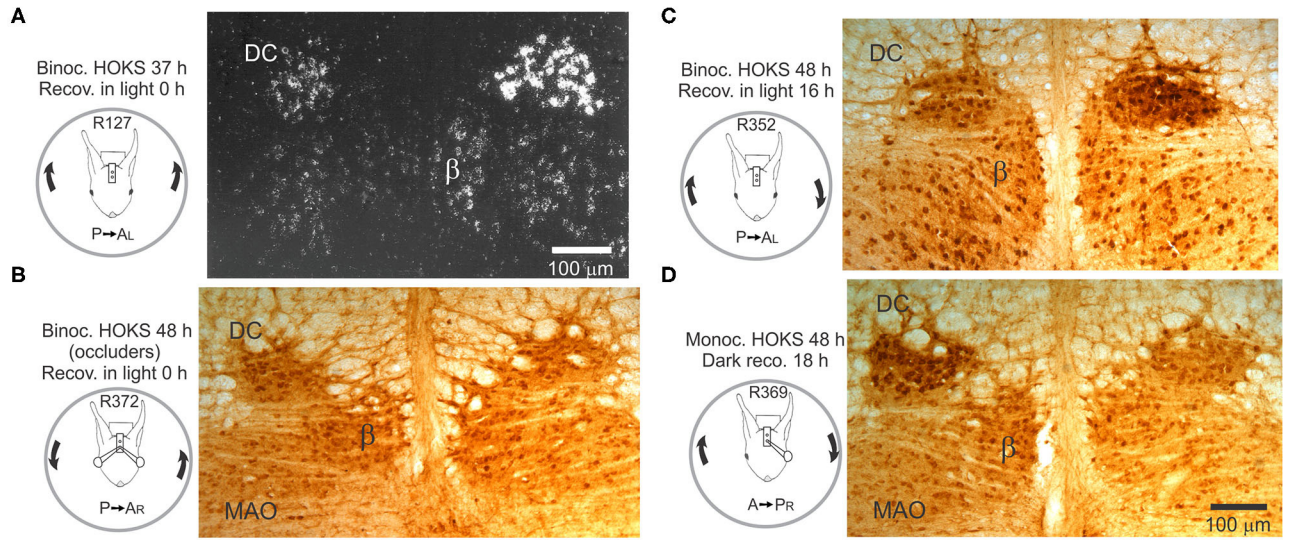

FIGURE 12 | Transcription and expression of corticotropin-releasing factor (CRF) is modified by HOKS. **(A)** Binocular P→A HOKS at 5 deg/s with respect to the right is given for 37 h. The rabbit is then anesthetized and euthanized. Emulsion-coated brainstem sections show increased CRF mRNA over individual neurons in caudal dorsal cap. **(B)** Binocular HOKS is given for 48 h during which vision of both eyes is blocked by ping-pong ball occluders. Brainstem sections are reacted with α-CRF antibody. Neither the left nor right caudal DC has elevated expression of CRF. **(C)** Binocular P→A HOKS is given for 48 h with respect to the right eye, after which the rabbit remains in the dark for 18 h. The right caudal DC has elevated CRF expression. The left caudal DC has a modest increase in CRF expression. **(D)** Monocular A→P HOKS with respect to the right eye is delivered for 48 h while the left eye is occluded. When HOKS stops the rabbit recovers in total darkness for 18 h. During the recovery period the left caudal DC develops increased expression of CRF; an apparent rebound following stimulation in the non-preferred direction. Modified from Barmack (146) and Barmack and Young (152).

neuroendocrine response to stress. Sex differences in the HPA axis are manifest in gonadal sex steroids and neuroactive metabolites. CRF expression may be one of the dynamic antecedents of motion sickness.

HOKS of CSs Evokes Epigenetic Changes in Transcription

Changes in synaptic efficacy observed during LTD last seconds to tens of minutes. The changes in such short-term plasticity involve the translocation of as many as 100 proteins (163). Longer-term changes in synaptic efficacy may also involve changes in gene transcription. Sustained neuronal activity could regulate a variety of transcription factors, each acting on a single gene. Alternatively, neuronal activity could regulate a few transcription factors, each acting on several genes. This second possibility could be realized through the regulation of microRNAs, short, 22 nucleotides, non-proton-coding, RNA that regulates expression of protein-coding mRNAs by repressing their translation or enhancing their degradation (164). Theoretically, a single microRNA may have nucleotide complementarity with as many as 30 different mRNAs, giving it a potential wide regulatory influence (165). Based upon microRNA complementarity, derived from genome databases, as many as one-third of human protein-coding genes may be influenced by microRNAs (166). Functionally, the transcription of most microRNAs is correlated with cellular development, apoptosis (164, 167–172) and microbial defense (164, 173, 174).

HOKS Evokes Increased Transcription of Several microRNAs

The mouse optokinetic pathway offers the opportunity of learning how repeated activation of a climbing fiber synapse changes transcription of microRNAs in floccular Purkinje cells. Specific microRNAs might suppress mRNAs involved in the expression of target proteins related to cellular adaptation. This is especially attractive because it uses circuitry that is well-described physiologically and known to be critical for adaptation at behavioral and cellular levels. It is also attractive because it allows for the measurement of the subcellular consequences of sustained activation of the most powerful synapse in the central nervous system.

Mice are restrained at the center of an optokinetic sphere rotated CCW at 6 deg/s, stimulating the right eye in the P→A direction and the left eye in the A→P direction. The optokinetic pathway from the right retina to the left DC and then to the right flocculus is indicated by a dashed red line (**Figures 13A,B**). Tissue samples from both the left and right flocculi are collected, RNA extracted and run on a microRNA microarray. The data set from the microarray are plotted in a Volcano plot that includes information about representation of microRNA transcripts, their copy number, frequency of occurrence, and difference in ratio of transcription of the right floccular sample/left floccular sample (**Figure 13C**). The microRNAs with the largest differential transcription in the left and right flocculi are identified (**Figure 13D**).

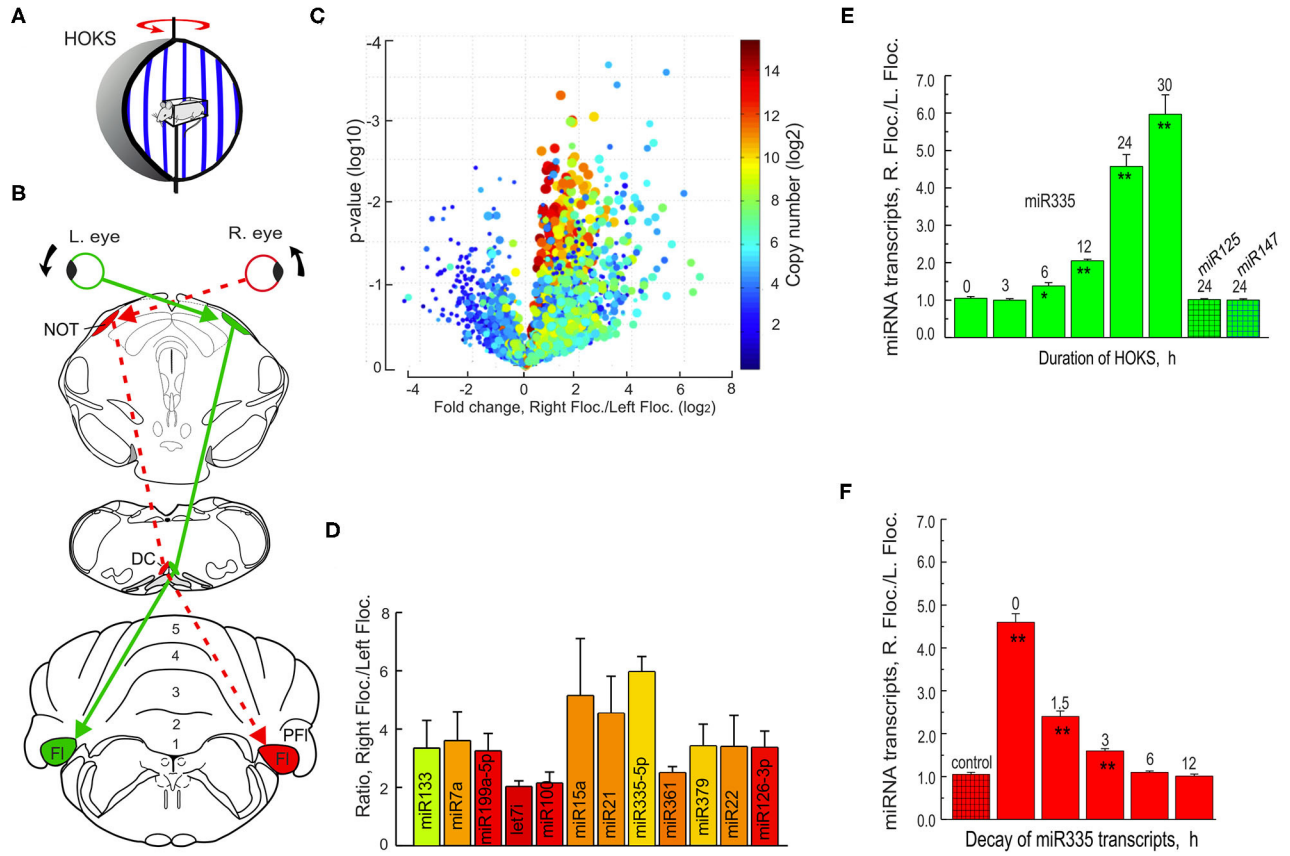

FIGURE 13 | Monocular HOKS increases microRNA transcription in the right flocculus. **(A)** Mice are restrained at the center of an optokinetic sphere. Rotation of the sphere provides P→A HOKS of the right eye at 6 deg/s. The left eye is occluded. **(B)** Functional optokinetic pathway from the right retina to the left DC and right flocculus are depicted. The dashed red lines indicate the excitatory pathway. **(C)** RNA samples from left and right flocculi from the optokinetically stimulated mice are analyzed with a microRNA microarray that includes 616 human and 361 mouse mature microRNAs and are illustrated in a Volcano plot. **(D)** Twelve microRNAs are detected by the microarray in which the ratio of the right flocculus/left flocculus is at least 3X > 1.0. **(E)** The time course of transcription of miR335 is measured following 0-30 h of monocular HOKS. The flocculi are dissected and prepared for RNA extraction. cDNAs are synthesized and amplified by PCR. U6 is co-amplified and used as a loading control. Each paired sample is run on a gel to determine the optical density of the amplified bands. The ratio of PCR band density (RF/LF) shows increased transcription in the right flocculus for miR335. Two control microRNA samples, miR125 or miR147, show no change in transcription. Each histogram bar represents the mean for three mice. **(F)** The decay of HOKS transcripts of miR335 is measured at different intervals following termination of 24 h of HOKS. Statistical significance is indicated by * for $p < 0.02$ and ** for $p < 0.001$. DC, dorsal cap; Fl, flocculus; NOT, nucleus of the optic tract; PFl, paraflocculus. Modified from Barmack et al. (175).

The single microRNA with the largest differential transcription, miR335, is then PCR-amplified and the ratio of the right/left flocculus measured after HOKS stimulation for different durations. Binocular HOKS for 6 h is the minimal duration of stimulation that induces a detectable increase in transcription of miR335 in the right/left flocculus ratio (RF/LF) (**Figure 13E**). With increasing duration of HOKS RF/LF increases up to 30 h of HOKS, the experimental limit. At 30 h of HOKS, miR335 RF/LF increased 6-fold relative to unstimulated controls. This optokinetically evoked transcriptional change does not occur in two other microRNAs, miR125, and miR147.

A potential role of microRNAs in any HOKS-induced neuronal adaptation is, in part, dependent on the duration of the RF/LF ratio of transcripts after the stimulus stops. The time course of microRNA decay regulates the duration of suppressive effect on its complementary mRNA target and ultimately on the decreased expression of a protein. By exposing mice to a fixed duration of monocular P→A HOKS (24 h) and then delaying anesthesia and euthanasia for fixed intervals, this question is addressed. HOKS-induced miR335 transcripts decay with a time-constant of ∼2.5 h (**Figure 13F**) (176).

Following HOKS, microRNAs can be measured with greater accuracy by collecting floccular samples from the zone within the flocculus that contains only Purkinje cells whose discharge is modulated by HOKS. This is possible because the topography of optokinetically responsive floccular Purkinje cells in the mouse has already been obtained (92) (**Figure 14A1**). The spindle-shaped single folium flocculus is ∼1.2 mm long and includes five separate regions classified by their sensitivity to optokinetic stimulation about three axes. Purkinje cells in the central region

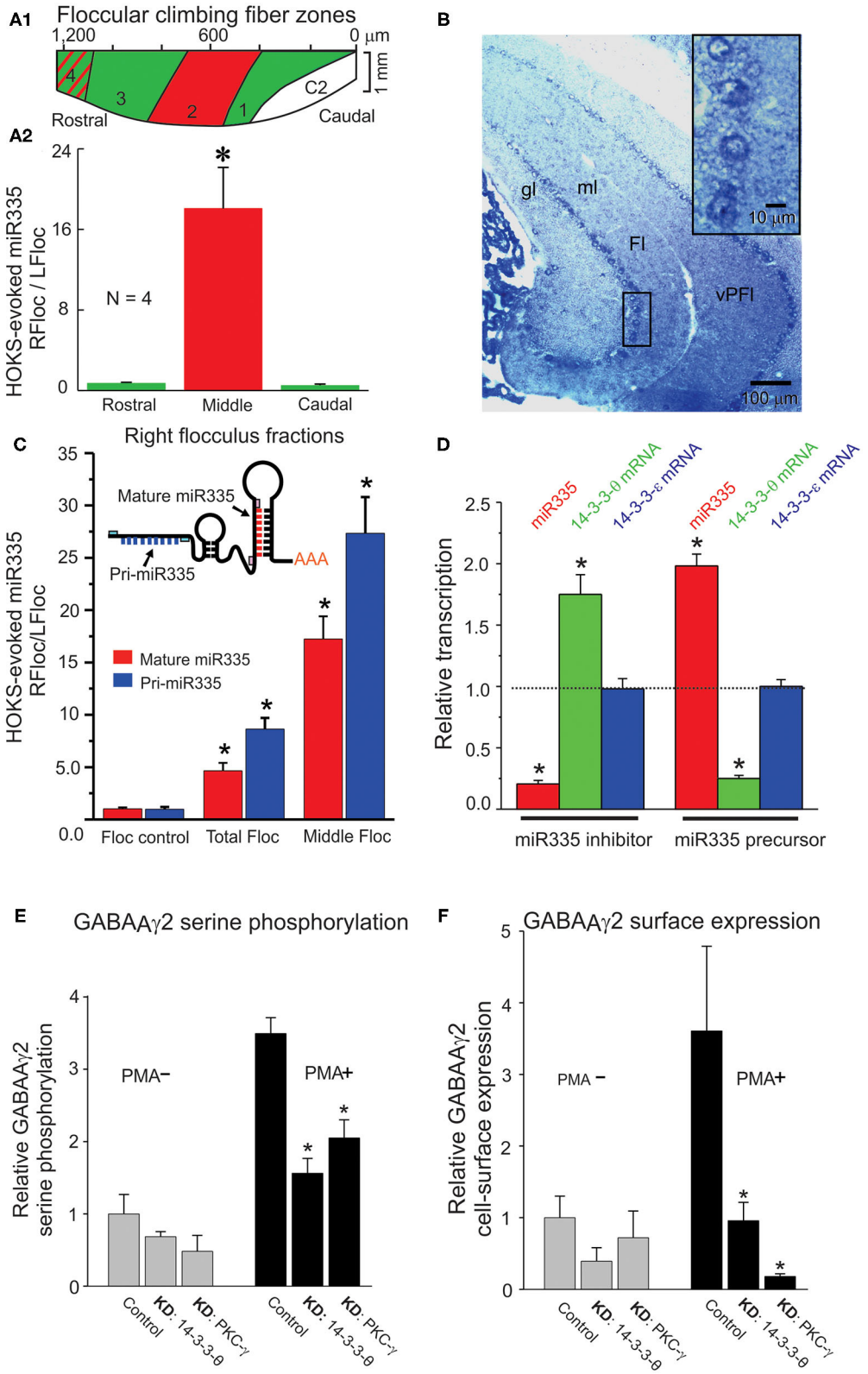

FIGURE 14 | HOKS-evokes transcription of miR335 in Purkinje cells and decreases cell surface expression $GABA_A\gamma_2$. Three mice receive monocular P→A HOKS of the right eye for 24 h. The right flocculus is divided rostro-caudally, *in situ*, into three fractions from which RNA is extracted separately to obtain a cell fraction (middle) rich in Purkinje cells that respond to HOKS. **(A1)** Planar map of five climbing fiber floccular zones. Purkinje cells in zones 1 and 3 (green) respond to vertical optokinetic

(Continued)

FIGURE 14 | stimulation (VOKS). Cells in zone 2 (red) respond to HOKS. Cells in zone 4 (green with red stripes) respond to VOKS and partially to HOKS. Cells in C2 respond to neither HOKS nor VOKS. **(A2)** PCR-amplified cDNAs of miR335 and U6 are shown for each fraction. The ratio of miR335 transcripts in each of the right floccular fractions is plotted relative to transcripts of the unstimulated left flocculus. **(B)** Hybridization histochemistry shows that miR335 is expressed in Purkinje cells. Transverse sections through the cerebellar flocculus and paraflocculus are hybridized to a digoxigenin-labeled oligonucleotide complementary to miR335 and immunolabeled with an antibody to digoxigenin. Four Purkinje cells, denoted by a boxed outline, are shown at higher magnification in upper right corner. The oligonucleotide probe immuno-labels cytoplasm surrounding unlabeled nuclei. **(C)** Both intranuclear pri-microRNA and mature microRNA transcripts are measured to examine whether changes in mature microRNA accurately reflect changes in transcription. qPCR is used to identify miR335 both pri-miR335 and mature miR335 using specific primer pairs as shown in the cartoon. Following 24 h of monocular P→A HOKS of the right eye both pri-miR335 and mature miR335 transcripts increase. **(D)** miR335 reduces transcripts of 14-3-3-θ *in vitro*. Treatment of N2a cells with the miR335 inhibitor decreases miR335 transcripts, increases 14-3-3-θ transcripts, and has no effect on 14-3-3-θ transcripts. Treatment with the miR335 precursor increases miR335 transcripts, decreases 14-3-3-θ transcripts, and has no effect on 14-3-3-θ transcripts. In N2a cells, two native proteins, 14-3-3-θ and PKC-γ are knocked down independently by siRNA treatment or miRNA transfection. The N2a cells are "stimulated" by treatment with 200 nM of phorbol 12-myristate-13-acetate (PMA), a PKC activator, or they are "not stimulated" with no PMA treatment. **(E)** PMA treatment increases serine phosphorylation of $GABA_A\gamma_2$ in N2a cells. Knockdown of 14-3-3-θ (KD: 14-3-3-θ or PKC-γ (KD: PKC-γ decreases serine phosphorylation only in cells treated with PMA. **(F)** Knockdown of 14-3-3-θ or PKC-γ decreases cell surface expression of $GABA_A\gamma_2$ in N2a cells "stimulated" by PMA. Cell-surface expression of $GABA_A\gamma_2$ is measured by selective biotinylation of membrane proteins. (ANOVA, $p < 0.001$ indicated by asterisk). Fl, flocculus; gl, granule cell layer; ml, molecular layer; vPFl, ventral paraflocculus. Modified from Schonewille et al. (92), Barmack et al. (176), Barmack et al. (175), and Qian et al. (177).

respond to HOKS. This central region is flanked by Purkinje cells that respond to stimulation about the anterior and posterior axes (92) (**Figure 14A2**). Using these improved floccular samples, the right "stimulated" miR335 transcripts increase 18X relative to the "unstimulated" left flocculus miR335 transcripts after 24 h of HOKS.

Increased miR335 transcripts in a cerebellar lysate is not proof that the increase can be localized to Purkinje cells. However, hybridization histochemistry localizes miR335 transcripts to Purkinje cells (**Figure 14B**). The inserted box shows at a higher magnification that the miR335 hybridization probe labels Purkinje cell cytoplasm, not the nucleus.

The increase and subsequent decay of microRNA transcripts in the flocculus after HOKS could indicate differences in miR335 transcription or changes in cytoplasmic post-transcriptional events or both. Nuclear transcription of microRNAs is preceded by transcription of larger pri-microRNAs. A variety of enzymatic post-transcriptional factors could contribute to the regulation of microRNAs. These factors might confound interpretations concerning increases or decreases in cytoplasmic microRNA transcripts and whether such changes can be attributed to transcription or to post-transcriptional cytoplasmic regulatory events. This question can be answered by measuring transcripts of pri-miR335 and mature miR335 in floccular mRNA samples extracted from "stimulated" and "non-stimulated" flocculi (**Figure 14C**). Following 24 h of HOKS, pri-miR335 transcripts from the middle zone of the stimulated (right) flocculus increase 28X relative to the transcripts in the unstimulated (left) flocculus. Mature miR335 transcripts increase by 18X.

The nucleotide sequence of miR335, analyzed with the use of two data bases offers a long list of clues as to the likely complementary mRNA targets. However, even under the most stringent conditions, these lists are unacceptably large. The microRNA Registry and EnsEMBL propose more than 149 mRNAs with sufficient complementarity to hybridize with miR335.

As an alternative, mRNA arrays can screen mRNAs whose transcripts decrease after 24h of HOKS. A total of 42 such mRNA transcripts are reduced in the right flocculus by P→A HOKS of the right eye for 24 h (176, 178). Using a more direct approach, miR335 inhibitors can be transfected directly into the posterior vermis to assess possible changes in mRNA transcripts. Combining results from these three methods: [1] miR335 is predicted to be complementary to many transcripts including transcripts of calbindin and 14-3-3-θ a regulatory protein that binds to functionally diverse signaling proteins (179, 180), [2] The transcripts of many proteins including calbindin and 14-3-3-θ decrease following 24 h of HOKS, and [3] Transcripts of calbindin and 14-3-3-θ increase after injection of miR335 inhibitors into cerebellar tissue (175).

Interactions of microRNA and mRNA Transcripts Are Examined in N2A Cells

The interaction of miR335 with its complementary targets could be achieved through interactions within the cerebellar cortex also induced by climbing fiber activity. Alternatively, interactions of miR335 with its target mRNAs can be examined directly *in vitro*. N2a cells serve as a model system for detecting interactions of miR335 with calbindin and 14-3-3-θ. These three components are expressed natively in N2a cells. The effects of transfecting N2a can with miR335 inhibitors or miR335 precursors on mRNA transcripts for miR335, 14-3-3-θ calbindin and 14-3-3-θ (control) can be measured directly using quantitative PCR. When N2a cells are transfected with a miR335 inhibitor, transcripts of miR335 decrease and transcripts of 14-3-3-θ increase. Transfection of N2a cells with a miR335 precursor increases transcripts of miR335 and decreases transcripts of 14-3-3-θ. The specificity of these effects is strengthened by the lack of changes in 14-3-3-θ transcripts, a control isoform (**Figure 14D**).

14-3-3-θ, PKC-γ, and $GABA_A\gamma_2$ Are Functionally Linked in Purkinje Cell $GABA_A$ Receptors

Increased transcription of miR335, evoked by climbing fiber excitation of Purkinje cells, decreases transcripts of 14-3-3-θ. In cerebellar lysates 14-3-3-θ interacts with PKC-γ, one of numerous constitutively-expressed isoforms of protein kinase C. PKC-γ phosphorylates several proteins expressed in the cerebellum. Immunoprecipitation of 14-3-3-θ co-immunoprecipitates PKC-γ. Immunoprecipitation of 14-3-3-θ also co-immunoprecipitates $GABA_A\gamma_2$, a subunit of the

pentameric $GABA_A$ receptor involved with its membrane assembly (177, 181–186). This role of these proteins in the assembly of $GABA_A$ receptors can be examined in N2a cells in which these proteins are native as is the $GABA_A$ receptor. To mimic synaptic activation of N2a cells they are "stimulated" by treatment with 200 nM of phorbol 12-myristate-13-acetate (PMA), a PKC activator. "Stimulated" cells can be compared with "unstimulated" control cells not treated with PMA. 14-3-3-θ and PKC-γ are "knocked down" by transfecting N2a cells with siRNAs or miRNAs designed specifically to knockdown either 14-3-3-θ or PKC-γ. The objective is to examine how 14-3-3-θ and PKC-γ contribute to the serine phosphorylation of $GABA_A\gamma_2$ in two groups of N2a cells, one treated with 200 nM of PMA and one untreated control. The outcome of this test is that knockdown of either 14-3-3-θ or PKC-γ reduces serine phosphorylation of $GABA_A\gamma_2$ only in N2a cells that also are activated by PMA (**Figure 14E**).

The possibility that knockdown of either 14-3-3-θ or PKC-γ reduces the cell surface expression of $GABA_A\gamma_2$ is examined with the use of an assay that preferentially biotinylates cell surface proteins (177). Again, one can compare the efficacy of the knockdowns in N2a cells that are treated with PMA in contrast to those that are untreated (**Figure 14F**). In PMA treated N2a cells knockdowns of either 14-3-3-θ or PKC-γ reduce cell surface expression of $GABA_A\gamma_2$.

If the same interactions of microRNA that occur in N2a cells also occur in Purkinje cells then a possible homeostatic mechanism is at least one of the consequences of sustained HOKS as follows: The gain of the horizontal optokinetic reflex slowly attenuates with sustained HOKS. Sustained HOKS increases transcription of miR335. Increased miR335 transcripts block expression of 14-3-3-θ and PKC-γ mRNAs thereby reducing the serine phosphorylation of $GABA_A\gamma_2$ and reducing its insertion into the post-synaptic membrane. Fewer $GABA_A$ receptors reduces inhibition of Purkinje cells and perhaps maintain a constant level of excitability during sustained stimulation.

Plasticity of Neurons in the Medial Vestibular Nucleus

Secondary vestibular neurons share with cerebellar Purkinje cells adaptive characteristics that may account for vestibular compensation and visuo-vestibular calibration (187–190). In secondary vestibular neurons this property depends on changes in the cellular excitability and synaptic responsiveness (191, 192). This adaptation can be investigated in brainstem slices in which high frequency tetanic stimulation of vestibular primary afferents evokes long-term potentiation (LTP) in secondary neurons of the medial vestibular nucleus (MVN). LTP is evoked through the activation of metabotropic glutamate type-1 NMDA receptors. On the other hand, low frequency stimulation evokes long-term depression (LTD) (193). The more relevant characteristic of the stimulation for stimulus-induced plastic changes in EPSP amplitude is the temporal organization of repetitive bursts, probably causing different intracellular levels of postsynaptic Ca2+. Short burst intervals (four trains, 1 s, 100 Hz) induce LTP, longer burst intervals induce LTD. Temporal stimulation sequencies may assure a persistent selectivity of the MVN neuron in response to input from semicircular canals, otolithic receptors and optokinetic signals or to cerebellar output. Moreover, the induction of vestibular LTP and LTD is influenced by sex neurosteroids, as occurs in several areas of the CNS (194). In the MVN 17 beta-Estradiol (E2) and 5α-dihydrotestosterone (DHT) rapidly and oppositely regulate synaptic transmission and plasticity by directly interacting with membrane estrogen and androgen receptors (ERs and ARs) (195–197). Estradiol mediates the LTP, while DHT mediates LTD (**Figures 15A–C**). A similar influence of estradiol is found in cerebellar Purkinje neurons (198, 199).

Both the occurrence and amplitude of LTP in the MVN of female rats is altered at different phases of the cycle (192, 200). Specifically, high frequency stimulation induces LTP in male rats within seconds (fast-developing LTP). However, this same stimulation elicits variable long-term synaptic effects in female rats; fast-developing LTP or slow-developing LTP or even LTD. LTP amplitude and frequency of occurrence depends on the neural E2 levels, fluctuating according to oestrous phases, with a high probability of inducing fast LTP in dioestrus phase (**Figure 15D**). A high E2 level decreases LTP by preventing the transformation of testosterone into E2 and facilitating its transformation into DHT (192).

Cerebellar Functions and Cellular Mechanisms

The zonal architecture of visual and vestibular climbing fiber projections to hemispheric and vermal lobules IX-X establishes a three-dimensional optokinetic and vestibular space. These sagittal zones are defined by their afferents and by their projections. The climbing fiber afferents appear to be the primary regulators of Purkinje cell SS discharge frequency. In vermal lobule X, vestibular primary afferent→granule cell→parallel fiber→Purkinje cell signals originate from the three ipsilateral semicircular canals and two otolith organs. These primary afferent signals are mixed with secondary afferent signals from the vestibular nuclei. This mixture of signals modulates the discharges of Purkinje cells in the medial sagittal zone by climbing fiber signals that originate from the contralateral anterior semicircular canal and utricle. More rostrally, in vermal lobules IXa,b, primary vestibular afferents are absent. In their absence, secondary vestibular afferents remain and perhaps additional mossy fiber afferents from neck and shoulder muscle proprioceptors are added to the mix. Climbing fiber projections that originate from the contralateral anterior semicircular canal and utricle persist. In both the caudal and rostral zones, the modulated polarity of CSs and SSs remains the same, although the depth of modulation may vary depending on the intensity of parallel fiber discharge. The outputs of sagittal climbing fiber zones are distributed along a longitudinal gradient to the cerebellar nuclei, vestibular nuclei and other brainstem nuclei. The functions of these sagittal zones encompass a more global view of the same basic signal tailored to different functional subnuclei all of which require an accurate reading of head orientation in space.

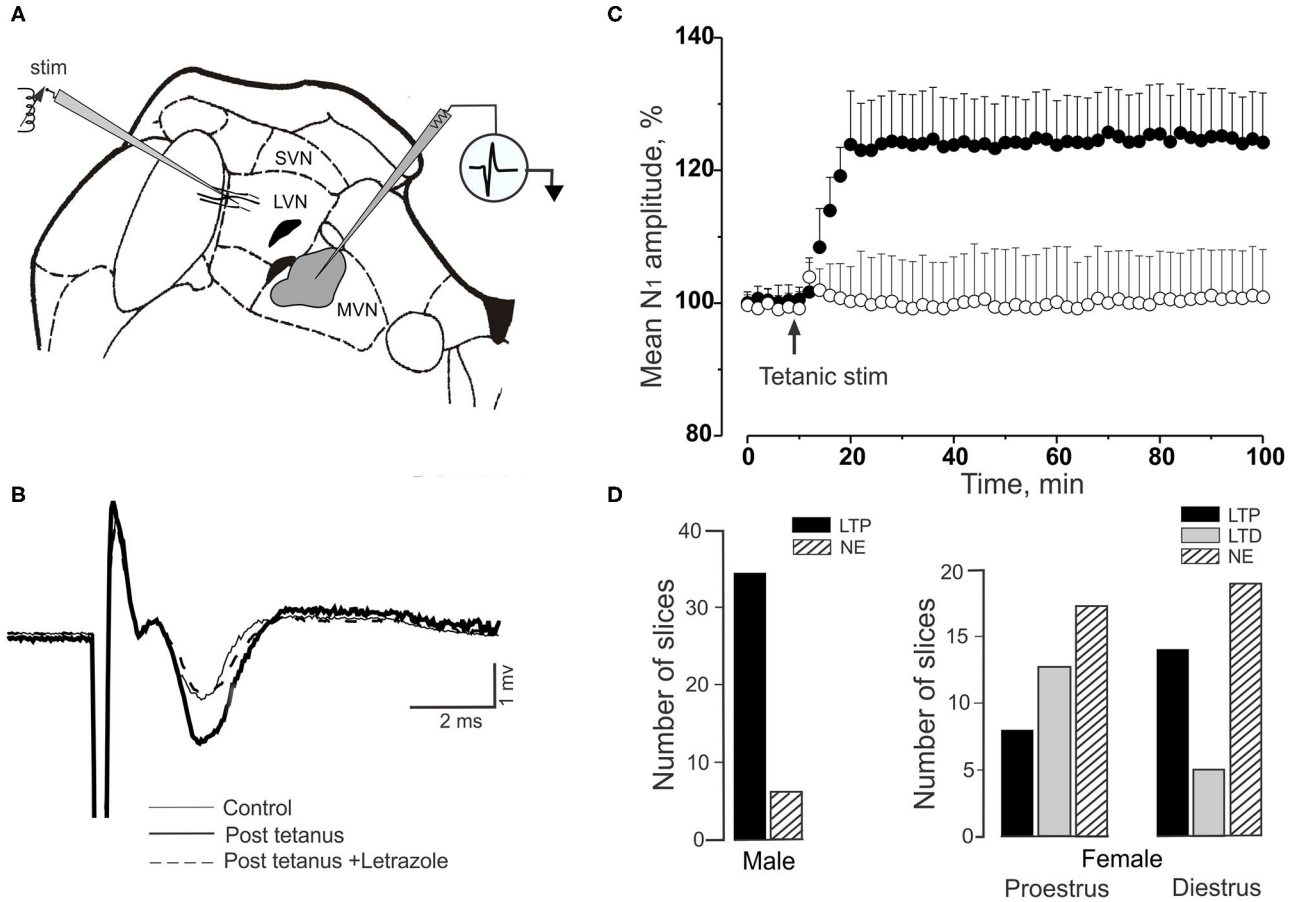

FIGURE 15 | Induction of long-term potentiation (LTP) in medial vestibular nucleus (MVN) neurons differs in brain slices of male and female rats. **(A)** Tetanic stimulation (Four trains, 1 s and 100 Hz, are applied to the vestibular afferents distal to their termination in the MVN. The zone of recording is demarcated by gray shading. **(B)** Field potentials from the MVN evoked by single shock stimulation to vestibular afferents in rat brain stem are illustrated. The thin trace is evoked prior to tetanic stimulation. The thicker trace is recorded after tetanic stimulation. The dashed trace is evoked after blockade of neurosteroid 17beta-Estradiol (E2) synthesis by Letrozole. **(C)** Time course of field potential amplitude in two male rats. In one slice LTP is induced by tetanic stimulation (filled circles). In the other LTP is prevented with bath-applied aromatase inhibitor, Letrozole (open circles). In both conditions the symbols indicate means and SDs of 8 responses to stimuli delivered every 15 s. **(D)** The histograms compare long-term effects induced by tetanic stimulation in male, proestrus and diestrus of female rats. Left histogram panel shows number of experiments with LTP in male brain slices (black bar) and the number of male brain slices in which tetanic stimulation fails to evoke LTP (NE, striped bar). Right panels show female brain slices tested during proestrus and diestrus. In the brain slices of females, LTP (black bars) is reduced in frequency, compared with LTP in male slices. In both proestrus and diestrus females LTD is induced (gray bars), while LTD is not induced in male slices. In proestrus, the incidence of LTP is lower than that in diestrus, suggesting that the level of the circulating E2 interferes with local neurosteroid E2 synthesis required for LTP induction. LVN, MVN, SVN, lateral, medial and superior vestibular nuclei. Modified from Grassi et al. (191).

Spontaneous increases or decreases in SS discharge can, on occasion, precede as well as follow the occurrence of CSs in the same Purkinje cell (64, 201–204). Under certain stimulus and recording conditions the modulation SS discharge occurs in the absence of modulation of CS discharge. In these instances, the SSs are often regarded as a consequence of a mossy fiber→granule cell→parallel fiber→Purkinje cell throughput that is independent of the climbing fiber pathway with the possible exception of undefined "novel" responses evoked by climbing fibers (201–204). Given the significance of sagittal zones in lobules IX-X it would seem useful to learn if zonal architecture also influences the responses of Purkinje cells in other cerebellar lobules. In lobules IX-X it has been helpful to deploy a variety of well-controlled vestibular and optokinetic stimuli to investigate the discharge characteristics of Purkinje cells. Perhaps a refinement of stimulus conditions would similarly be useful for investigating other cerebellar regions.

At a more molecular level, the potential role of NMDA receptors in homeostatic regulation of the discharge of MVN neurons (205) and cerebellar stellate cells (139, 140) offers the possibility of enhancing our understanding of cellular plasticity within a behavioral context.

Epigenetic factors also may contribute to dynamic regulation of climbing fiber discharge. Stimulus-evoked changes in microRNA transcription provides one of several ways to investigate epigenetic factors that may regulate the synaptic

efficacy of Purkinje cell discharge. Climbing fiber-evoked increases in microRNA transcription in Purkinje cells suggests that microRNAs contribute to the homeostatic regulation of proteins critical for Purkinje cell synaptic function. The trick will be to learn how the suppressive effects of microRNAs contribute to the regulation of proteins critical for maintaining and altering synaptic function.

AUTHOR'S NOTE

Cerebellar adaptation to vestibular and optokinetic depends on specialized circuitry that represents three dimensions in a space in which the coordinates correspond physically to the orientation of the semicircular canals and utricular otolith. This circuitry is localized to the hemispheric and vermal lobule X (flocculus and nodulus). The nodular coordinate system senses gravity and head movement around the axes of the vertical semicircular canals and utricular otolith. The flocculus senses low velocity optokinetic stimulation about three axes in the absence of a gravity vector. We review three aspects of vestibular and optokinetic adaptation in which the flocculus and nodulus play an important role. Cerebellar adaptation to sustained optokinetic or vestibular stimulation is revealed physiologically in the persistence of responses after initial stimulation has ceased. It is also shown behaviorally in the persistence of eye movements in the absence of the stimulation that first evoked them. We link these sensory adaptations to epigenetic signaling in Purkinje cells and to stimulus-evoked expression of sex-related peptides, corticotropin releasing factor and neurosteroid 17beta-Estradiol (E2). We suggest that these peptides may also explain, in part, the female predominance in the mal de debarquement disorder.

AUTHOR CONTRIBUTIONS

All authors listed have made a substantial, direct and intellectual contribution to the work, and approved it for publication.

FUNDING

This research was supported by NEI (EY18561) and by NIDCD (DC006668).

REFERENCES

1. Foster IZ, Hanes DA, Barmack NH, McCollum G. Spatial symmetries in vestibular projections to the uvula-nodulus. *Biol Cybern.* (2007) 96:439–53. doi: 10.1007/s00422-006-0136-y
2. Van der Steen J, Simpson JI, Tan J. Functional anatomic organization of three-dimensional eye movements in rabbit cerebellar flocculus. *J Neurophysiol.* (1994) 72:31–46. doi: 10.1152/jn.1994.72.1.31
3. Simpson JI, Graf W, Leonard C. The coordinate system of visual climbing fibers to the flocculus. In: Fuchs AF, Becker W, editors. *Developments in Neuroscience, Vol. 12. Progress in Oculomotor Research*. North Holland: Elsevier. (1981). p. 475–84.
4. Yakusheva T, Blazquez PM, Angelaki DE. Relationship between complex and simple spike activity in macaque caudal vermis during three-dimensional vestibular stimulation. *J Neurosci.* (2010) 30:8111–26. doi: 10.1523/JNEUROSCI.5779-09.2010
5. Billig I, Balaban CD. Zonal organization of the vestibulo-cerebellum in the control of horizontal extraocular muscles using pseudorabies virus: I. Flocculus/ventral paraflocculus. *Neuroscience.* (2004) 125:507–20. doi: 10.1016/j.neuroscience.2004.01.051
6. Cajal SR. *Histologie du Système Nerveux de L'homme et des Vertebrés*. Paris: Maloine (1911).
7. Sato F, Sasaki H. Morphological correlations between spontaneously discharging primary vestibular afferents vestibular nucleus neurons in the cat. *J Comp Neurol.* (1993) 333:554–6. doi: 10.1002/cne.903330408
8. Barmack NH, Baughman RW, Errico P, Shojaku H. Vestibular primary afferent projection to the cerebellum of the rabbit. *J Comp Neurol.* (1993) 327:521–34. doi: 10.1002/cne.903270405
9. Wu HS, Sugihara I, Shinoda Y. Projection patterns of single mossy fibers originating from the lateral reticular nucleus in the rat cerebellar cortex nuclei. *J Comp Neurol.* (1999) 411:97–118. doi: 10.1002/(SICI)1096-9861(19990816)411:1<97::AID-CNE8>3.0.CO;2-O
10. Brodal A, Pompeiano O. The vestibular nuclei in the cat. *J Anat.* (1957) 91:438–54.
11. Brodal A. Anatomy of the vestibuloreticular connections and possible "ascending" vestibular pathways from the reticular formation. In: Brodal A, Pompeiano O, editors. *Basic Aspects of Central Vestibular Mechanisms. Progress in brain research Vol. 37*. Amsterdam, NY: Elsevier Publ. Comp. (1972).
12. Brodal A. Anatomy of the vestibular nuclei and their connections. In: Kornhuber HH, editor. *Handbook of Sensory Physiology, Vestibular System, Morphology, Vol. 6*. Berlin: Springer Verlag. (1974). doi: 10.1007/978-3-642-65942-3_9
13. Barmack NH, Fredette BJ, Mugnaini E. Parasolitary nucleus: A source of GABAergic vestibular information to the inferior olive of rat rabbit. *J Comp Neurol.* (1998) 392:352–72. doi: 10.1002/(SICI)1096-9861(19980316)392:3<352::AID-CNE6>3.0.CO;2-0
14. Barmack NH, Yakhnitsa V. Vestibular signals in the parasolitary nucleus. *J Neurophysiol.* (2000) 83:3559–69. doi: 10.1152/jn.2000.83.6.3559
15. Korte G, Mugnaini E. The cerebellar projection of the vestibular nerve in the cat. *J Comp Neurol.* (1979) 184:265–78. doi: 10.1002/cne.901840204
16. Sato Y, Kanda K-I, Ikarashi K, Kawasaki T. Differential mossy fiber projections to the dorsal ventral uvula in the cat. *J Comp Neurol.* (1989) 279:149–64. doi: 10.1002/cne.902790113
17. Kevetter GA, Perachio A. Distribution of vestibular afferents that innervate the sacculus posterior canal in the gerbil. *J Comp Neurol.* (1986) 254:410–24. doi: 10.1002/cne.902540312
18. Gerrits NM, Epema AH, Van Linge A, Dalm E. The primary vestibulocerebellar projection in the rabbit: Absence of primary afferents in the flocculus. *Neurosci Lett.* (1989) 105:27–33. doi: 10.1016/0304-3940(89)90006-2
19. Akaogi K-I, Sato Y, Ikarashi K, Kawasaki T. Mossy fiber projections from the brain stem to the nodulus in the cat. An experimental study comparing the nodulus, the uvula and the flocculus. *Brain Res.* (1994) 638:12–20. doi: 10.1016/0006-8993(94)90627-0
20. Purcell IM, Perachio AA. Peripheral patterns of terminal innervation of vestibular primary afferent neurons projecting to the vestibulocerebellum in the gerbil. *J Comp Neurol.* (2001) 433:48–61. doi: 10.1002/cne.1124
21. Newlands SD, Purcell IM, Kevetter GA, Perachio AA. Central projections of the utricular nerve in the gerbil. *J Compar Neurol.* (2002) 452:11–23. doi: 10.1002/cne.10350
22. Newlands SD, Vrabec JT, Purcell IM, Stewart CM, Zimmerman BE, Perachio AA. Central projections of the saccular utricular nerves in macaques. *J Comp Neurol.* (2003) 466:31–47. doi: 10.1002/cne.10876
23. Maklad A, Fritzsch B. Partial segregation of posterior crista and saccular fibers to the nodulus and uvula of the cerebellum in mice, its development. *Dev Brain Res.* (2003) 140:223–36. doi: 10.1016/S0165-3806(02)00609-0
24. Fox CA, Hillman DE, Siegesmund KA, Dutta CR. The primate cerebellar cortex: A Golgi and electron microscopic study. In: Fox CA, Snider RS,

editors. *Progress in Brain Research, Vol.25: The Cerebellum*. New York, NY: Elsevier. (1967). p. 174–225. doi: 10.1016/S0079-6123(08)60965-6
25. Palkovits M, Magyar P, Szentagothai J. Quantitative histological analysis of the cerebellar cortex in the cat. IV. Mossy fiber-Purkinje cell numerical transfer. *Brain Res.* (1972) 45:15–29. doi: 10.1016/0006-8993(72)90213-2
26. Kassel J, Shambes GM, Welker W. Fractured cutaneous projections to the granule cell layer of the posterior cerebellar hemisphere of the domestic cat. *J Comp Neurol.* (1984) 225:458–68. doi: 10.1002/cne.902250311
27. Napper RM, Harvey RJ. Number of parallel fiber synapses on an individual Purkinje cell in the cerebellum of the rat. *J Comp Neurol.* (1988) 274:168–77. doi: 10.1002/cne.902740204
28. Brand S, Dahl AL, Mugnaini E. The length of parallel fibers in the cat cerebellar cortex. An experimental light and electron microscopic study. *Exp Brain Res.* (1976) 26:39–58. doi: 10.1007/BF00235248
29. Mugnaini E. The length of cerebellar parallel fibers in chicken rhesus monkey. *J Comp Neurol.* (1983) 220:7–15. doi: 10.1002/cne.902200103
30. Isope P, Barbour B. Properties of unitary granule cell–>Purkinje cell synapses in adult rat cerebellar slices. *J Neurosci.* (2002) 22:9668–78. doi: 10.1523/JNEUROSCI.22-22-09668.2002
31. Cohen D, Yarom Y. Patches of synchronized activity in the cerebellar cortex evoked by mossy-fiber stimulation: questioning the role of parallel fibers. *Proc Natl Acad Sci USA.* (1998) 95:15032–6. doi: 10.1073/pnas.95.25.15032
32. Gundappa-Sulur G, De Schutter E, Bower JM. Ascending granule cell axon: an important component of cerebellar cortical circuitry. *J Comp Neurol.* (1999) 408:580–96 doi: 10.1002/(SICI)1096-9861(19990614)408:4<580::AID-CNE11>3.0.CO;2-O
33. Harvey RJ, Napper RM. Quantitative studies on the mammalian cerebellum. *Prog Neurobiol.* (1991) 36:437–63. doi: 10.1016/0301-0082(91)90012-P
34. Brodal A, Torvik A. The origin of secondary vestibulo-cerebellar fibers in cats; an experimental anatomical study. *Arch Psychiatr Nervenkr Z Gesamte Neurol Psychiatr.* (1957) 195:550–67.
35. Yamamoto M. Topographical representation in rabbit cerebellar flocculus for various afferent inputs from the brainstem investigated by means of retrograde axonal transport of horseradish peroxidase. *Neurosci Lett.* (1979) 12:29–34. doi: 10.1016/0304-3940(79)91475-7
36. Kotchabhakdi N, Walberg F. Cerebellar afferent projections from the vestibular nuclei in the cat: an experimental study with the method of retrograde axonal transport of horseradish peroxidase. *Exp Brain Res.* (1978) 31:591–604. doi: 10.1007/BF00239814
37. Brodal A, Brodal P. Observations on the secondary vestibulocerebellar projections in the macaque monkey. *Exp Brain Res.* (1985) 58:62–74. doi: 10.1007/BF00238954
38. Thunnissen IE, Epema AH, Gerrits NM. Secondary vestibulocerebellar mossy fiber projection to the caudal vermis in the rabbit. *J Comp Neurol.* (1989) 290:262–77. doi: 10.1002/cne.902900207
39. Epema AH, Gerrits NM, Voogd J. Secondary vestibulocerebellar projections to the flocculus and uvulo-nodular lobule of the rabbit: A study using HRP and double fluorescent tracer techniques. *Exp Brain Res.* (1990) 80:72–82. doi: 10.1007/BF00228849
40. Barmack NH, Baughman RW, Eckenstein FP. Cholinergic innervation of the cerebellum of the rat by secondary vestibular afferents. In: Cohen B, Tomko DL, Guedry F, editors. *Sensing and Controlling Motion: Vestibular and Sensorimotor Function*. New York, NY: New York Academy of Sciences. (1992). p. 566–79. doi: 10.1111/j.1749-6632.1992.tb25236.x
41. Barmack NH, Baughman RW, Eckenstein FP. Cholinergic innervation of the cerebellum of rat, rabbit, cat monkey as revealed by choline acetyltransferase activity immunohistochemistry. *J Comp Neurol.* (1992) 317:233–49. doi: 10.1002/cne.903170303
42. Tago H, McGeer PL, McGeer EG, Akiyama H, Hersh LB. Distribution of choline acetyltransferase immunopositive structures in the rat brainstem. *Brain Res.* (1989) 495:271–97. doi: 10.1016/0006-8993(89)90221-7
43. Barmack NH, Baughman RW, Eckenstein FP, Shojaku H. Secondary vestibular cholinergic projection to the cerebellum of rabbit rat as revealed by choline acetyltransferase immunohistochemistry, retrograde orthograde tracers. *J Comp Neurol.* (1992) 317:250–70. doi: 10.1002/cne.903170304
44. Nelson BJ, Adams JC, Barmack NH, Mugnaini E. A comparative study of glutamate decarboxylase immunoreactive boutons in the mammalian inferior olive. *J Comp Neurol.* (1989) 286:514–39. doi: 10.1002/cne.902860409
45. Barmack NH, Fagerson M, Fredette BJ, Mugnaini E, Shojaku H. Activity of neurons in the beta nucleus of the inferior olive of the rabbit evoked by natural vestibular stimulation. *Exp Brain Res.* (1993) 94:203–15. doi: 10.1007/BF00230288
46. Langer T, Fuchs AF, Scudder CA, Chubb MC. Afferents to the flocculus of the cerebellum in the Rhesus macaque as revealed by retrograde transport of horseradish peroxidase. *J Comp Neurol.* (1985) 235:1–25. doi: 10.1002/cne.902350102
47. Blazquez P, Partsalis A, Gerrits NM, Highstein SM. Input of anterior and posterior semicircular canal interneurons encoding head-velocity to the dorsal Y group of the vestibular nuclei. *J Neurophysiol.* (2000) 83:2891–904. doi: 10.1152/jn.2000.83.5.2891
48. Sato Y, Kawasaki T. Target neurons of floccular caudal zone inhibition in Y-group nucleus of vestibular nuclear complex. *J Neurophysiol.* (1987) 57:460–80. doi: 10.1152/jn.1987.57.2.460
49. Wylie DR, DeZeeuw CI, DiGiorgi PL, Simpson JI. Projections of individual Purkinje-cells of identified zones in the ventral nodulus to the vestibular and cerebellar nuclei in the rabbit. *J Compar Neurol.* (1994) 349:448–63. doi: 10.1002/cne.903490309
50. Wentzel PR, Wylie DR, Ruigrok TJ, De Zeeuw CI. Olivary projecting neurons in the nucleus prepositus hypoglossi, group y and ventral dentate nucleus do not project to the oculomotor complex in the rabbit and the rat. *Neurosci Lett.* (1995) 190:45–8. doi: 10.1016/0304-3940(95)11496-J
51. Partsalis AM, Zhang Y, Highstein SM. Dorsal Y group in the squirrel monkey. I. Contribution of the cerebellar flocculus to neuronal responses in normal and adapted animals. *J Neurophysiol.* (1995) 73:632–50. doi: 10.1152/jn.1995.73.2.632
52. Kumoi K, Saito N, Tanaka C. Immunohistochemical localization of γ-aminobutyric acid- and aspartate-containing neurons in the guinea pig vestibular nuclei. *Brain Res.* (1987) 416:22–3. doi: 10.1016/0006-8993(87)91492-2
53. Kaufman GD, Anderson JH, Beitz AJ. Otolith-brain stem connectivity: Evidence for differential neural activation by vestibular hair cells based on quantification of FOS expression in unilateral labyrinthectomized rats. *J Neurophysiol.* (1993) 70:117–27. doi: 10.1152/jn.1993.70.1.117
54. Alley K, Baker R, Simpson JI. Afferents to the vestibulo-cerebellum and the origin of the visual climbing fibers in the rabbit. *Brain Res.* (1975) 98:582–9. doi: 10.1016/0006-8993(75)90375-3
55. Hoddevik GH, Brodal A. The olivocerebellar projection studied with the method of retrograde axonal transport of horseradish peroxidase. V. The projections to the flocculonodular lobe and the paraflocculus in the rabbit. *J Comp Neurol.* (1977) 176:269–80. doi: 10.1002/cne.901760208
56. Groenewegen HJ, Voogd J. The parasagittal zonation within the olivocerebellar projection I. Climbing fiber distribution in the vermis of cat cerebellum. *J Comp Neurol.* (1977) 174:417–88. doi: 10.1002/cne.901740304
57. Tan J, Gerrits NM, Nanhoe R, Simpson JI, Voogd J. Zonal organization of the climbing fiber projection to the flocculus nodulus of the rabbit: A combined axonal tracing acetylcholinesterase histochemical study. *J Comp Neurol.* (1995) 356:23–50. doi: 10.1002/cne.903560103
58. Voogd J, Gerrits NM, Ruigrok TJ. Organization of the vestibulocerebellum. *Ann N Y Acad Sci.* (1996) 781:553–79. doi: 10.1111/j.1749-6632.1996.tb15728.x
59. Fushiki H, Barmack NH. Topography reciprocal activity of cerebellar Purkinje cells in the uvula-nodulus modulated by vestibular stimulation. *J Neurophysiol.* (1997) 78:3083–94. doi: 10.1152/jn.1997.78.6.3083
60. Barmack NH, Yakhnitsa V. Cerebellar climbing fibers modulate simple spikes in cerebellar Purkinje cells. *J Neurosci.* (2003) 23:7904–16. doi: 10.1523/JNEUROSCI.23-21-07904.2003
61. Andersson G, Oscarsson O. Climbing fiber microzones in cerebellar vermis and their projection to different groups of cells in the lateral vestibular nucleus. *Exp Brain Res.* (1978) 32:565–79. doi: 10.1007/BF00239553
62. Schild RF. On the inferior olive of the albino rat. *J Comp Neurol.* (1970) 140:255–60. doi: 10.1002/cne.901400302
63. Palay SL, Chan-Palay V. *Cerebellar Cortex: Cytology and Organization*. Heidelberg: Springer-Verlag (1974). doi: 10.1007/978-3-642-65581-4

64. Barmack NH, Shojaku H. Vestibular visual signals evoked in the uvula-nodulus of the rabbit cerebellum by natural stimulation. *J Neurophysiol.* (1995) 74:2573–89. doi: 10.1152/jn.1995.74.6.2573
65. Barmack NH, Yakhnitsa V. Functions of interneurons in mouse cerebellum. *J Neurosci.* (2008) 28:1140–52. doi: 10.1523/JNEUROSCI.3942-07.2008
66. Barmack NH, Yakhnitsa V. Modulated discharge of Purkinje and stellate cells persists after unilateral loss of vestibular primary afferent mossy fibers in mice. *J Neurophysiol.* (2013) 110:2257–74. doi: 10.1152/jn.00352.2013
67. Yakhnitsa V, Barmack NH. Antiphasic Purkinje cell responses in mouse uvula-nodulus are sensitive to static roll-tilt and topographically organized. *Neuroscience.* (2006) 143:615–26. doi: 10.1016/j.neuroscience.2006.08.006
68. Kooy FH. The inferior olive in vertebrates. *Folia Neurobiol.* (1916) 10:205–369.
69. Graf W, Simpson JI, Leonard CS. Spatial organization of visual messages of the rabbit's cerebellar flocculus. IComplex I, and simple spike responses of Purkinje cells. *J Neurophysiol.* (1988) 60:2091–121. doi: 10.1152/jn.1988.60.6.2091
70. Takeda T, Maekawa K. Olivary branching projections to the flocculus, nodulus uvula in the rabbit. II. Retrograde double labeling study with fluorescent dyes. *Exp Brain Res.* (1989) 76:323–32. doi: 10.1007/BF00247892
71. Maekawa K, Simpson JI. Climbing fiber responses evoked in vestibulocerebellum of rabbit from visual system. *J Neurophysiol.* (1973) 36:649–66. doi: 10.1152/jn.1973.36.4.649
72. Simpson JI, Alley KE. Visual climbing fiber input to rabbit vestibulocerebellum: a source of direction-specific information. *Brain Res.* (1974) 82:302–8. doi: 10.1016/0006-8993(74)90610-6
73. Maekawa K, Takeda T. Electrophysiological identification of the climbing and mossy fiber pathways from the rabbit's retina to the contralateral cerebellar flocculus. *Brain Res.* (1976) 109:169–74. doi: 10.1016/0006-8993(76)90388-7
74. Büttner-Ennever JA, Horn AK. Pathways from cell groups of the paramedian tracts to the floccular region. *Ann N Y Acad Sci.* (1996) 781:532–40. doi: 10.1111/j.1749-6632.1996.tb15726.x
75. Barmack NH, Hess DT. Multiple-unit activity evoked in dorsal cap of inferior olive of the rabbit by visual stimulation. *J Neurophysiol.* (1980) 43:151–64. doi: 10.1152/jn.1980.43.1.151
76. Leonard CS, Simpson JI, Graf W. Spatial organization of visual messages of the rabbit's cerebellar flocculus. I. Typology of inferior olive neurons of the dorsal cap of Kooy. *J Neurophysiol.* (1988) 60:2073–90. doi: 10.1152/jn.1988.60.6.2073
77. Kusunoki M, Kano M, Kano M-S, Maekawa K. Nature of optokinetic response zonal organization of climbing fiber afferents in the vestibulocerebellum of the pigmented rabbit. I. The flocculus. *Exp Brain Res.* (1990) 80:225–37. doi: 10.1007/BF00228151
78. Kano M, Kano M-S, Kusunoki M, Maekawa K. Nature of optokinetic response zonal organization of climbing fiber afferents in the vestibulocerebellum of the pigmented rabbit. II. The nodulus. *Exp Brain Res.* (1990) 80:238–51. doi: 10.1007/BF00228152
79. De Zeeuw CI, Wylie DR, DiGiorgi PL, Simpson JI. Projections of individual Purkinje cells of identified zones in the flocculus to the vestibular cerebellar nuclei in the rabbit. *J Comp Neurol.* (1994) 349:428–47. doi: 10.1002/cne.903490308
80. Tan J, Simpson JI, Voogd J. Anatomical compartments in the white matter of the rabbit flocculus. *J Comp Neurol.* (1995) 356:1–22. doi: 10.1002/cne.903560102
81. Sato Y, Yamamoto F, Shojaku H, Kawasaki T. Neuronal pathway from floccular caudal zone contributing to vertical eye movements in cats - role of group y nucleus of vestibular nuclei. *Brain Res.* (1984) 294:375–80. doi: 10.1016/0006-8993(84)91054-0
82. De Zeeuw CI, Gerrits NM, Voogd J, Leonard CS, Simpson JI. The rostral dorsal cap ventrolateral outgrowth of the rabbit inferior olive receive a GABAergic input from dorsal group Y the ventral dentate nucleus. *J Comp Neurol.* (1994) 341:420–32. doi: 10.1002/cne.903410311
83. De Zeeuw CI, Koekkoek SK. Signal processing in the C2 module of the flocculus and its role in head movement control. *Prog Brain Res.* (1997) 114:299–320. doi: 10.1016/S0079-6123(08)63371-3
84. Hawkes R, Gravel C. The modular cerebellum. *Prog Neurobiol.* (1991) 36:309–27. doi: 10.1016/0301-0082(91)90004-K
85. Hawkes R, Leclerc N. Antigenic map of the rat cerebellar cortex: The distribution of parasagittal bands as revealed by monoclonal anti-Purkinje cell antibody mabQ113. *J Comp Neurol.* (1987) 256:29–41. doi: 10.1002/cne.902560104
86. Boegman RJ, Parent A, Hawkes R. Zonation in the rat cerebellar cortex: patches of high acetylcholinesterase activity in the granular layer are congruent with Purkinje cell compartments. *Brain Res.* (1988) 448:237–51. doi: 10.1016/0006-8993(88)91261-9
87. Scott TG. A unique pattern of localization within the cerebellum of the mouse. *J. Comp. Neurol.* (1964) 122:1–7. doi: 10.1002/cne.901220102
88. Eisenman LM, Hawkes R. 5′-nucleotidase and the MABQ113 antigen share a common distribution in the cerebellar cortex of the mouse. *Neurosci.* (1989) 31:231–5. doi: 10.1016/0306-4522(89)90045-6
89. Gravel C, Eisenman LM, Sasseville R, Hawkes R. Parasagittal organization of the rat cerebellar cortex: Direct correlation between antigenic Purkinje cell bands revealed by mabQ113 the organization of the olivocerebellar projection. *J Comp Neurol.* (1987) 265:294–310. doi: 10.1002/cne.902650211
90. Fujita H, Oh-Nishi A, Obayashi S, Sugihara I. Organization of the marmoset cerebellum in three-dimensional space: lobulation, aldolase C compartmentalization and axonal projection. *J Comp Neurol.* (2010) 518:1764–91. doi: 10.1002/cne.22301
91. Long RM, Pakan JMP, Graham DJ, Hurd PL, Gutierrez-Ibanez C, Wylie DR. Modulation of complex spike activity differs between zebrin-positive and -negative Purkinje cells in the pigeon cerebellum. *J Neurophysiol.* (2018) 120:250–62. doi: 10.1152/jn.00797.2017
92. Schonewille M, Luo C, Ruigrok TJ, Voogd J, Schmolesky MT, Rutteman M, et al. Zonal organization of the mouse flocculus: physiology, input, output. *J Comp Neurol.* (2006) 497:670–82. doi: 10.1002/cne.21036
93. Ghez C, Thach WT. The cerebellum. In: Kandel ER, Schwartz J, Jessel TM, editors. *Principles of Neuroscience*. New York, NY: Elsevier (2000). p. 832–52.
94. Apps R, Garwicz M. Anatomical and physiological foundations of cerebellar information processing. *Nat Rev Neurosci.* (2005) 6:297–311. doi: 10.1038/nrn1646
95. Bloedel JR, Bracha V. Cerebellar functions. In: Binder MD, Hirokawa N, Windhorst U, editors. *Encyclopedic Reference of Neuroscience*. Heidelberg: Springer Verlag. (2009). p. 667–71. doi: 10.1007/978-3-540-29678-2_917
96. Ebner TJ, Bloedel JR. Role of climbing fiber afferent input in determining responsiveness of Purkinje cells to mossy fiber inputs. *J Neurophysiol.* (1981) 45:962–71. doi: 10.1152/jn.1981.45.5.962
97. Armstrong DM, Edgley SA. Discharges of interpositus Purkinje cells of the cat cerebellum during locomotion under different conditions. *J Physiol.* (1988) 400:425–45. doi: 10.1113/jphysiol.1988.sp017130
98. Nagao S. Role of cerebellar flocculus in adaptive interaction between optokinetic eye movement response and vestibulo-ocular reflex in pigmented rabbits. *Exp Brain Res.* (1989) 77:541–51. doi: 10.1007/BF00249607
99. Kano M, Kano M-S, Maekawa K. Simple spike modulation of Purkinje cells in the cerebellar nodulus of the pigmented rabbit to optokinetic stimulation. *Neurosci Lett.* (1991) 128:101–4. doi: 10.1016/0304-3940(91)90769-P
100. Lisberger SG, Pavelko TA, Bronte-Stewart HM, Stone LS. Neural basis for motor learning in the vestibuloocular reflex of primates. II. Changes in the responses of horizontal gaze velocity Purkinje cells in the cerebellar flocculus and ventral paraflocculus. *J Neurophysiol.* (1994) 72:954–73. doi: 10.1152/jn.1994.72.2.954
101. Walter JT, Khodakhah K. The linear computational algorithm of cerebellar Purkinje cells. *J. Neurosci.* (2006) 26:12861–72. doi: 10.1523/JNEUROSCI.4507-05.2006
102. Thach WT. Discharge of Purkinje cerebellar nuclear neurons during rapidly alternating arm movements in the monkey. *J Neurophysiol.* (1968) 31:785–97. doi: 10.1152/jn.1968.31.5.785
103. Montarolo PG, Raschi F, Strata P. Are the climbing fibres essential for the Purkinje cell inhibitory action. *Exp Brain Res.* (1981) 42:215–8. doi: 10.1007/BF00236909
104. Benedetti F, Montarolo PF, Strata P, Tempia F. Inferior olive inactivation decreases the excitability of the intracerebellar lateral vestibular nuclei in the rat. *J Physiol.* (1983) 340:195–208. doi: 10.1113/jphysiol.1983.sp014758
105. De Montigny C, Lamarre Y. Rhythmic activity induced by harmaline in the olivocerebello-bulbar system of the cat. *Brain Res.* (1973) 53:81–95. doi: 10.1016/0006-8993(73)90768-3

106. Llinás R, Volkind RA. The olivo-cerebellar system: Functional properties as revealed by harmaline-induced tremor. *Exp Brain Res.* (1973) 18:69–87. doi: 10.1007/BF00236557
107. Bloedel JR, Roberts WJ. Action of climbing fibers in cerebellar cortex of the cat. *J Neurophysiol.* (1971) 34:17–31. doi: 10.1152/jn.1971.34.1.17
108. Mathews PJ, Lee KH, Peng Z, Houser CR, Otis TS. Effects of climbing fiber driven inhibition on Purkinje neuron spiking. *J Neurosci.* (2012) 32:17988–97. doi: 10.1523/JNEUROSCI.3916-12.2012
109. Badura A, Schonewille M, Voges K, Galliano E, Renier N, Gao Z, et al. Climbing fiber input shapes reciprocity of Purkinje cell firing. *Neuron.* (2013) 78:700–13. doi: 10.1016/j.neuron.2013.03.018
110. Barmack NH, Yakhnitsa V. Microlesions of the inferior olive reduce vestibular modulation of purkinje cell complex and simple spikes in mouse cerebellum. *J Neurosci.* (2011) 31:9824–35. doi: 10.1523/JNEUROSCI.1738-11.2011
111. Ris L, De Waele C, Serafin M, Vidal PP, Godaux E. Neuronal activity in the ipsilateral vestibular nucleus following unilateral labyrinthectomy in the alert guinea pig. *J Neurophysiol.* (1995) 74:2087–99. doi: 10.1152/jn.1995.74.5.2087
112. McKay BE, Engbers JD, Mehaffey WH, Gordon GR, Molineux ML, Bains JS, et al. Climbing fiber discharge regulates cerebellar functions by controlling the intrinsic characteristics of purkinje cell output. *J Neurophysiol.* (2007) 97:2590–604. doi: 10.1152/jn.00627.2006
113. Han KS, Chen CH, Khan MM, Guo C, Regehr WG. Climbing fiber synapses rapidly and transiently inhibit neighboring Purkinje cells via ephaptic coupling. *Nat Neurosci.* (2020) 23:1399–409. doi: 10.1038/s41593-020-0701-z
114. Johansson F, Jirenhed DA, Rasmussen A, Zucca R, Hesslow G. Memory trace timing mechanism localized to cerebellar Purkinje cells. *Proc Natl Acad Sci USA.* (2014) 111:14930–4. doi: 10.1073/pnas.1415371111
115. Wulff P, Schonewille M, Renzi M, Data L, Sassoe-Pognetto M, Data L, et al. Synaptic inhibition of Purkinje cells mediates consolidation of vestibulo-cerebellar motor learning. *Nat Neurosci.* (2009) 12:1042–9. doi: 10.1038/nn.2348
116. Ito M, Sakurai M, Tongroach P. Climbing fibre induced depression on both mossy fibre responsiveness glutamate sensitivity of cerebellar Purkinje cells. *J Physiol.* (1982) 324:113–34. doi: 10.1113/jphysiol.1982.sp014103
117. Ito M, Karachot L. Long-term desensitization of quisqualate-specific glutamate receptors in Purkinje cells investigated with wedge recording from rat cerebellar slices. *Neurosci Res.* (1989) 7:168–71. doi: 10.1016/0168-0102(89)90058-8
118. Sakurai M. Synaptic modification of parallel fibre-Purkinje cell transmission in in vitro guinea-pig cerebellar slices. *J Physiol.* (1987) 394:463–80. doi: 10.1113/jphysiol.1987.sp016881
119. Crépel F, Jaillard D. Pairing of pre- postsynaptic activities in cerebellar Purkinje cells induces long-term changes in synaptic efficacy *in vitro*. *J Physiol.* (1991) 432:123–41. doi: 10.1113/jphysiol.1991.sp018380
120. Narasimhan K, Linden DJ. Defining a minimal computational unit for cerebellar long-term depression. *Neuron.* (1996) 17:333–41. doi: 10.1016/S0896-6273(00)80164-6
121. Crepel F. Role of presynaptic kainate receptors at parallel fiber-Purkinje cell synapses in induction of cerebellar LTD: interplay with climbing fiber input. *J Neurophysiol.* (2009) 102:965–73. doi: 10.1152/jn.00269.2009
122. Ito M. Historical review of the significance of the cerebellum the role of Purkinje cells in motor learning. *Ann N Y Acad Sci.* (2002) 978:273–88. doi: 10.1111/j.1749-6632.2002.tb07574.x
123. Midtgaard J. Membrane properties synaptic responses of Golgi cells stellate cells in the turtle cerebellum *in vitro*. *J Physiol.* (1992) 457:329–54. doi: 10.1113/jphysiol.1992.sp019381
124. Dzubay JA, Jahr CE. The concentration of synaptically released glutamate outside of the climbing fiber-Purkinje cell synaptic cleft. *J Neurosci.* (1999) 19:5265–74. doi: 10.1523/JNEUROSCI.19-13-05265.1999
125. Carter AG, Regehr WG. Prolonged synaptic currents and glutamate spillover at the parallel fiber to stellate cell synapse. *J Neurosci.* (2000) 20:4423–34. doi: 10.1523/JNEUROSCI.20-12-04423.2000
126. Szapiro G, Barbour B. Multiple climbing fibers signal to molecular layer interneurons exclusively via glutamate spillover. *Nat Neurosci.* (2007) 10:735–42. doi: 10.1038/nn1907
127. Eccles JC, Llinás R, Sasaki K. The mossy fibre-granule cell relay of the cerebellum and its inhibitory control by Golgi cells. *Exp Brain Res.* (1966) 1:82–101. doi: 10.1007/BF00235211
128. Hámori J, Szentágothai J. Lack of evidence of synaptic contacts by climbing fibre collaterals to basket and stellate cells in developing rat cerebellar cortex. *Brain Res.* (1980) 186:454–7. doi: 10.1016/0006-8993(80)90990-7
129. Dugué GP, Dumoulin A, Triller A, Dieudonné S. Target-dependent use of coreleased inhibitory transmitters at central synapses. *J Neurosci.* (2005) 25:6490–8. doi: 10.1523/JNEUROSCI.1500-05.2005
130. Desclin JC. Early terminal degeneration of cerebellar climbing fibers after destruction of the inferior olive in the rat. Synaptic relationships in the molecular layer. *Anat Embryol.* (1976) 149:87–112. doi: 10.1007/BF00315087
131. Hámori J, Szentágothai J. Participation of Golgi neuron processes in the cerebellar glomeruli: an electron microscope study. *Exp Brain Res.* (1966) 2:35–48. doi: 10.1007/BF00234359
132. Eccles JC, Ito M, Szentágothai J. *The Cerebellum as a Neuronal Machine*. New York, NY: Springer-Verlag (1967). doi: 10.1007/978-3-662-13147-3
133. Chan-Palay V, Palay SL. The stellate cells of the rat's cerebellar cortex. *Z Anat Entwicklungsgesch.* (1972) 136:224–48. doi: 10.1007/BF00519180
134. Pouzat C, Hestrin S. Developmental regulation of basket/stellate cell–>Purkinje cell synapses in the cerebellum. *J Neurosci.* (1997) 17:9104–12. doi: 10.1523/JNEUROSCI.17-23-09104.1997
135. Wadiche JI, Jahr CE. Multivesicular release at climbing fiber-Purkinje cell synapses. *Neuron.* (2001) 32:301–13. doi: 10.1016/S0896-6273(01)00488-3
136. Nishiyama H, Linden DJ. Pure spillover transmission between neurons. *Nat Neurosci.* (2007) 10:675–7. doi: 10.1038/nn0607-675
137. Ekerot CF, Jörntell H. Parallel fibre receptive fields of Purkinje cells and interneurons are climbing fibre-specific. *Euro J Neurosci.* (2001) 13:1303–10. doi: 10.1046/j.0953-816x.2001.01499.x
138. Pinault D. A novel single-cell staining procedure performed *in vivo* under electrophysiological control: morpho-functional features of juxtacellularly labeled thalamic cells and other central neurons with biocytin or neurobiotin. *J Neurosci Methods.* (1996) 65:113–36. doi: 10.1016/0165-0270(95)00144-1
139. Jörntell H, Ekerot CF. Receptive field plasticity profoundly alters the cutaneous parallel fiber synaptic input to cerebellar interneurons *in vivo*. *J Neurosci.* (2003) 23:9620–31. doi: 10.1523/JNEUROSCI.23-29-09620.2003
140. Alexander RPD, Bowie D. Intrinsic plasticity of cerebellar stellate cells is mediated by NMDA receptor regulation of voltage-gated Na(+) channels. *J Physiol.* (2021) 599:647–65. doi: 10.1113/JP280627
141. Barmack NH, Shojaku H. Vestibularly induced slow oscillations in climbing fiber responses of Purkinje cells in the cerebellar nodulus of the rabbit. *Neurosci.* (1992) 50:1–5. doi: 10.1016/0306-4522(92)90376-D
142. De Waele C, Vibert N, Baudrimont M, Vidal PP. NMDA receptors contribute to the resting discharge of vestibular neurons in the normal and hemilabyrinthectomized guinea pig. *Exp Brain Res.* (1990) 81:125–33. doi: 10.1007/BF00230108
143. Serafin M, Khateb A, De Waele C, Vidal PP, Mühlethaler M. Medial vestibular nucleus in the guinea-pig: NMDA-induced oscillations. *Exp Brain Res.* (1992) 88:187–92. doi: 10.1007/BF02259140
144. Kleinschmidt HJ, Collewijn H. A search for habituation of vestibulo-ocular reactions to rotatory and linear sinusoidal accelerations in the rabbit. *Exp Neurol.* (1975) 47:257–67. doi: 10.1016/0014-4886(75)90255-1
145. Henn V, Young L, Finley C. Vestibular nucleus units in alert monkeys are also influenced by moving visual fields. *Brain Res.* (1974) 71:144–9. doi: 10.1016/0006-8993(74)90198-X
146. Barmack NH. Inferior olive and oculomotor system. *Prog Brain Res.* (2005) 151:269–91. doi: 10.1016/S0079-6123(05)51009-4
147. Angelaki DE, Hess BJM. Lesion of the nodulus ventral uvula abolish steady-state off- vertical axis otolith response. *J Neurophysiol.* (1995) 73:1716–20. doi: 10.1152/jn.1995.73.4.1716
148. Wearne S, Raphan T, Cohen B. Control of spatial orientation of the angular vestibuloocular reflex by the nodulus and uvula. *J Neurophysiol.* (1998) 79:2690–715. doi: 10.1152/jn.1998.79.5.2690
149. Erickson RG, Barmack NH. A comparison of the horizontal and vertical optokinetic reflexes of the rabbit. *Exp Brain Res.* (1980) 40:448–56. doi: 10.1007/BF00236153

150. Barmack NH, Nelson BJ. Influence of long-term optokinetic stimulation on eye movements of the rabbit. *Brain Res.* (1987) 437:111–20. doi: 10.1016/0006-8993(87)91532-0
151. Barmack NH, Errico P, Ferraresi A, Fushiki H, Pettorossi VE, Yakhnitsa V. Cerebellar nodulectomy impairs spatial memory of vestibular optokinetic stimulation in rabbits. *J Neurophysiol.* (2002) 87:962–75. doi: 10.1152/jn.00528.2001
152. Barmack NH, Young WS, III. Optokinetic stimulation increases corticotropin-releasing factor mRNA in inferior olivary neurons of rabbits. *J Neurosci.* (1990) 10:631–40. doi: 10.1523/JNEUROSCI.10-02-00631.1990
153. Errico P, Barmack NH. Origins of cerebellar mossy climbing fibers immunoreactive for corticotropin-releasing factor in the rabbit. *J Comp Neurol.* (1993) 336:307–23. doi: 10.1002/cne.903360211
154. Barmack NH, Errico P. Optokinetically-evoked expression of corticotropin-releasing factor in inferior olivary neurons of rabbits. *J Neurosci.* (1993) 13:4647–59. doi: 10.1523/JNEUROSCI.13-11-04647.1993
155. Frens MA, Mathoera AL, van der SJ. Floccular complex spike response to transparent retinal slip. *Neuron.* (2001) 30:795–801. doi: 10.1016/S0896-6273(01)00321-X
156. DeSouza EB. Corticotropin-releasing factor receptors in the rat central nervous system: Characterization regional distribution. *J Neurosci.* (1987) 7:88–100. doi: 10.1523/JNEUROSCI.07-01-00088.1987
157. Madtes PC, King JS. Distribution of corticotropin-releasing factor (CRF) binding sites in the opossum cerebellum. *Neuropeptides.* (1995) 28:51–8. doi: 10.1016/0143-4179(95)90074-8
158. Madtes PC, King JS. The temporal spatial development of corticotropin-releasing factor (CRF) binding sites CRF afferents in the opossum cerebellum. *J Chem Neuroanat.* (1996) 11:231–41. doi: 10.1016/S0891-0618(96)00164-0
159. Gilligan PJ, Robertson DW, Zaczek R. Corticotropin releasing factor (CRF) receptor modulators: Progress and opportunities for new therapeutic agents. *J Med Chem.* (2000) 43:1641–60. doi: 10.1021/jm990590f
160. Libster AM, Title B, Yarom Y. Corticotropin-releasing factor increases Purkinje neuron excitability by modulating sodium, potassium, Ih currents. *J Neurophysiol.* (2015) 114:3339–50. doi: 10.1152/jn.00745.2015
161. Barthel F, Loeffler JP. Characterization genetic analysis of functional corticotropin- releasing hormone receptors in primary cerebellar cultures. *J Neurochem.* (1993) 60:696–703. doi: 10.1111/j.1471-4159.1993.tb03203.x
162. Fox EA, Gruol DL. Corticotropin-releasing factor suppresses the afterhyperpolarization in cerebellar Purkinje neurons. *Neurosci Lett.* (1993) 149:103–7. doi: 10.1016/0304-3940(93)90358-R
163. Sanes JR, Lichtman JW. Can molecules explain long-term potentiation? *Nat Neurosci.* (1999) 2:597–604. doi: 10.1038/10154
164. Cullen BR. Transcription and processing of human microRNA precursors. *Mol Cell.* (2004) 16:861–5. doi: 10.1016/j.molcel.2004.12.002
165. Robins H, Press WH. Human microRNAs target a functionally distinct population of genes with AT-rich 3' UTRs. *Proc Natl Acad Sci USA.* (2005) 102:15557–62. doi: 10.1073/pnas.0507443102
166. Lewis BP, Burge CB, Bartel DP. Conserved seed pairing, often flanked by adenosines, indicates that thousands of human genes are microRNA targets. *Cell.* (2005) 120:15–20. doi: 10.1016/j.cell.2004.12.035
167. Ambros V. The functions of animal microRNAs. *Nature.* (2004) 431:350–5. doi: 10.1038/nature02871
168. Reinhart BJ, Slack FJ, Basson M, Pasquinelli AE, Bettinger JC, Rougvie AE, et al. The 21-nucleotide let-7 RNA regulates developmental timing in Caenorhabditis elegans. *Nature.* (2000) 403:901–6. doi: 10.1038/35002607
169. Harfe BD. MicroRNAs in vertebrate development. *Curr Opin Genet Dev.* (2005) 15:410–5. doi: 10.1016/j.gde.2005.06.012
170. Kosik KS. The neuronal microRNA system. *Nat Rev Neurosci.* (2006) 7:911–20. doi: 10.1038/nrn2037
171. Schratt GM, Tuebing F, Nigh EA, Kane CG, Sabatini ME, Kiebler M, et al. A brain-specific microRNA regulates dendritic spine development. *Nature.* (2006) 439:283–9. doi: 10.1038/nature04367
172. Bushati N, Cohen SM. microRNA functions. *Annu Rev Cell Dev Biol.* (2007) 23:175–205. doi: 10.1146/annurev.cellbio.23.090506.123406
173. Bartel DP. MicroRNAs: genomics, biogenesis, mechanism, and function. *Cell.* (2004) 116:281–97. doi: 10.1016/S0092-8674(04)00045-5
174. Zeng Y, Cai X, Cullen BR. Use of RNA polymerase II to transcribe artificial microRNAs. *Methods Enzymol.* (2005) 392:371–80. doi: 10.1016/S0076-6879(04)92022-8
175. Barmack NH, Qian Z, Yakhnitsa V. Long-term climbing fibre activity induces transcription of microRNAs in cerebellar Purkinje cells. *Philos Trans R Soc Lond B Biol Sci.* (2014) 369:20130508. doi: 10.1098/rstb.2013.0508
176. Barmack NH, Qian Z, Yakhnitsa V. Climbing fibers induce microRNA transcription in cerebellar Purkinje cells. *Neuroscience.* (2010) 171:655–65. doi: 10.1016/j.neuroscience.2010.09.039
177. Qian Z, Micorescu M, Yakhnitsa V, Barmack NH. Climbing fiber activity reduces 14-3-3-θ regulated $GABA_A$ receptor phosphorylation in cerebellar Purkinje cells. *Neurosci.* (2012) 201:34–45. doi: 10.1016/j.neuroscience.2011.11.021
178. Barmack NH, Qian Z. Activity-dependent expression of calbindin in rabbit floccular Purkinje cells modulated by optokinetic stimulation. *Neuroscience.* (2002) 113:235–50. doi: 10.1016/S0306-4522(02)00008-8
179. Aitken A. 14-3-3 and its possible role in co-ordinating multiple signalling pathways. *Trends Cell Biol.* (1996) 6:341–7. doi: 10.1016/0962-8924(96)10029-5
180. Berg D, Holzmann C, Riess O. 14-3-3 proteins in the nervous system. *Nat Rev Neurosci.* (2003) 4:752–62. doi: 10.1038/nrn1197
181. Moss SJ, Doherty CA, Huganir RL. Identification of the cAMP-dependent protein kinase protein kinase C phosphorylation sites within the major intracellular domains of the beta 1, gamma 2S, gamma 2L subunits of the gamma-aminobutyric acid type A receptor. *J Biol Chem.* (1992) 267:14470–6. doi: 10.1016/S0021-9258(19)49736-6
182. Krishek BJ, Xie X, Blackstone C, Huganir RL, Moss SJ, Smart TG. Regulation of GABAA receptor function by protein kinase C phosphorylation. *Neuron.* (1994) 12:1081–95. doi: 10.1016/0896-6273(94)90316-6
183. Brandon NJ, Delmas P, Kittler JT, McDonald BJ, Sieghart W, Brown DA, et al. GABAA receptor phosphorylation functional modulation in cortical neurons by a protein kinase C-dependent pathway. *J Biol Chem.* (2000) 275:38856–62. doi: 10.1074/jbc.M004910200
184. Meier J, Grantyn R. Preferential accumulation of GABAA receptor gamma 2L, not gamma 2S, cytoplasmic loops at rat spinal cord inhibitory synapses. *J Physiol.* (2004) 559:355–65. doi: 10.1113/jphysiol.2004.066233
185. Herring D, Huang R, Singh M, Dillon GH, Leidenheimer NJ. PKC modulation of GABAA receptor endocytosis and function is inhibited by mutation of a dileucine motif within the receptor beta 2 subunit. *Neuropharmacology.* (2005) 48:181–94. doi: 10.1016/j.neuropharm.2004.09.015
186. Terunuma M, Xu J, Vithlani M, Sieghart W, Kittler J, Pangalos M, et al. Deficits in phosphorylation of GABA(A) receptors by intimately associated protein kinase C activity underlie compromised synaptic inhibition during status epilepticus. *J Neurosci.* (2008) 28:376–84. doi: 10.1523/JNEUROSCI.4346-07.2008
187. Precht W, Shimazu H, Markham CH. A mechanism of central compensation of vestibular function following hemilabyrinthectomy. *J Neurophysiol.* (1966) 29:996–1010. doi: 10.1152/jn.1966.29.6.996
188. Johnston AR, Seckl JR, Dutia MB. Role of the flocculus in mediating vestibular nucleus neuron plasticity during vestibular compensation in the rat. *J Physiol.* (2002) 545:903–11. doi: 10.1113/jphysiol.2002.024281
189. Boyden ES, Katoh A, Raymond JL. Cerebellum-dependent learning: the role of multiple plasticity mechanisms. *Annu Rev Neurosci.* (2004) 27:581–609. doi: 10.1146/annurev.neuro.27.070203.144238
190. Lisberger SG, Miles FA. Role of primate medial vestibular nucleus in long-term adaptive plasticity of vestibuloocular reflex. *J Neurophysiol.* (1980) 43:1725–45. doi: 10.1152/jn.1980.43.6.1725
191. Grassi S, Frondaroli A, Dieni C, Scarduzio M, Pettorossi VE. Long-term potentiation in the rat medial vestibular nuclei depends on locally synthesized 17beta-estradiol. *J Neurosci.* (2009) 29:10779–83. doi: 10.1523/JNEUROSCI.1697-09.2009
192. Grassi S, Frondaroli A, Scarduzio M, Dieni CV, Brecchia G, Boiti C, et al. Influence of sex and estrous cycle on synaptic responses of the medial vestibular nuclei in rats: role of circulating 17beta-estradiol. *Brain Res Bull.* (2012) 87:319–27. doi: 10.1016/j.brainresbull.2011.11.008

193. Scarduzio M, Panichi R, Pettorossi VE, Grassi S. The repetition timing of high frequency afferent stimulation drives the bidirectional plasticity at central synapses in the rat medial vestibular nuclei. *Neuroscience.* (2012) 223:1–11. doi: 10.1016/j.neuroscience.2012.07.039
194. Tozzi A, Bellingacci L, Pettorossi VE. Rapid estrogenic and androgenic neurosteroids effects in the induction of long-term synaptic changes: implication for early memory formation. *Front Neurosci.* (2020) 14:572511. doi: 10.3389/fnins.2020.572511
195. Grassi S, Frondaroli A, Di Mauro M, Pettorossi VE. Influence of testosterone on synaptic transmission in the rat medial vestibular nuclei: estrogenic and androgenic effects. *Neuroscience.* (2010) 171:666–76. doi: 10.1016/j.neuroscience.2010.09.035
196. Grassi S, Scarduzio M, Panichi R, Dall'Aglio C, Boiti C, Pettorossi VE. Opposite long-term synaptic effects of 17beta-estradiol and 5alpha-dihydrotestosterone and localization of their receptors in the medial vestibular nucleus of rats. *Brain Res Bull.* (2013) 97:1–7. doi: 10.1016/j.brainresbull.2013.05.006
197. Scarduzio M, Panichi R, Pettorossi VE, Grassi S. Synaptic long-term potentiation and depression in the rat medial vestibular nuclei depend on neural activation of estrogenic and androgenic signals. *PLoS ONE.* (2013) 8:e80792. doi: 10.1371/journal.pone.0080792
198. Dieni CV, Sullivan JA, Faralli M, Contemori S, Biscarini A, Pettorossi VE, et al. 17 beta-estradiol synthesis modulates cerebellar dependent motor memory formation in adult male rats. *Neurobiol Learn Mem.* (2018) 155:276–86. doi: 10.1016/j.nlm.2018.08.011
199. Dieni CV, Ferraresi A, Sullivan JA, Grassi S, Pettorossi VE, Panichi R. Acute inhibition of estradiol synthesis impacts vestibulo-ocular reflex adaptation and cerebellar long-term potentiation in male rats. *Brain Struct Funct.* (2018) 223:837–50. doi: 10.1007/s00429-017-1514-z
200. Pettorossi VE, Frondaroli A, Grassi S. Cyclic estrogenic fluctuation influences synaptic transmission of the medial vestibular nuclei in female rats. *Acta Otolaryngol.* (2011) 131:434–9. doi: 10.3109/00016489.2010.536992
201. Bell CC, Grimm RJ. Discharge properties of Purkinje cells recorded on single double microelectrodes. *J Neurophysiol.* (1969) 32:1044–55. doi: 10.1152/jn.1969.32.6.1044
202. McDevitt CJ, Ebner TJ, Bloedel JR. The changes in Purkinje cell simple spike activity following spontaneous climbing fiber inputs. *Brain Res.* (1982) 237:484–91. doi: 10.1016/0006-8993(82)90460-7
203. Sato Y, Miura A, Fushiki H, Kawasaki T. Short-term modulation of cerebellar Purkinje cell activity after spontaneous climbing fiber input. *J Neurophysiol.* (1992) 68:2051–62. doi: 10.1152/jn.1992.68.6.2051
204. Sendhilnathan N, Semework M, Goldberg ME, Ipata AE. Neural correlates of reinforcement learning in mid-lateral cerebellum. *Neuron.* (2020) 106:188–98 e5. doi: 10.1016/j.neuron.2020.05.021
205. deWaele C, Sarafin M, Khateb A, Yabe Y, Vidal PP, Muhlethaler M. Medial vestibular nucleus in the guninea-pig: apamin-induced rhthmic burst firing - an *in vitro* and *in vivo* study. *Exp Brain Res.* (1993) 95:213–22. doi: 10.1007/BF00229780

Conflict of Interest: The authors declare that the research was conducted in the absence of any commercial or financial relationships that could be construed as a potential conflict of interest.

frontiers in Neurology

ORIGINAL RESEARCH
published: 10 March 2021
doi: 10.3389/fneur.2021.631409

Predicting Vasovagal Responses: A Model-Based and Machine Learning Approach

Theodore Raphan[1,2]* *and Sergei B. Yakushin*[3]

[1] Department of Computer and Information Science, Institute for Neural and Intelligent Systems, Brooklyn College of CUNY, Brooklyn, NY, United States, [2] Graduate Center of CUNY, New York, NY, United States, [3] Department of Neurology, Icahn School of Medicine at Mount Sinai Hospital, New York, NY, United States

Vasovagal syncope (**VVS**) or neurogenically induced fainting has resulted in falls, fractures, and death. Methods to deal with **VVS** are to use implanted pacemakers or beta blockers. These are often ineffective because the underlying changes in the cardiovascular system that lead to the syncope are incompletely understood and diagnosis of frequent occurrences of **VVS** is still based on history and a tilt test, in which subjects are passively tilted from a supine position to 20° from the spatial vertical (to a 70° position) on the tilt table and maintained in that orientation for 10–15 min. Recently, is has been shown that vasovagal responses (**VVRs**), which are characterized by transient drops in blood pressure (**BP**), heart rate (**HR**), and increased amplitude of low frequency oscillations in **BP** can be induced by sinusoidal galvanic vestibular stimulation (sGVS) and were similar to the low frequency oscillations that presaged **VVS** in humans. This transient drop in **BP** and **HR** of 25 mmHg and 25 beats per minute (bpm), respectively, were considered to be a **VVR**. Similar thresholds have been used to identify **VVR's** in human studies as well. However, this arbitrary threshold of identifying a **VVR** does not give a clear understanding of the identifying features of a VVR nor what triggers a **VVR**. In this study, we utilized our model of **VVR** generation together with a machine learning approach to learn a separating hyperplane between normal and **VVR** patterns. This methodology is proposed as a technique for more broadly identifying the features that trigger a **VVR.** If a similar feature identification could be associated with **VVRs** in humans, it potentially could be utilized to identify onset of a **VVS,** i.e, fainting, in real time.

Keywords: rat, vasovagal syncope, relaxation oscillator, baroreflex sensitivity, machine learning, modeling and simulation, vasovagal response

OPEN ACCESS

Edited by:
Richard Lewis,
Harvard University, United States

Reviewed by:
Bill J. Yates,
University of Pittsburgh, United States
Bryan Kevin Ward,
Johns Hopkins University,
United States

***Correspondence:**
Theodore Raphan
raphan@nsi.brooklyn.cuny.edu

Specialty section:
This article was submitted to Neuro-Otology, a section of the journal Frontiers in Neurology

Received: *20 November 2020*
Accepted: *12 February 2021*
Published: *10 March 2021*

Citation:
Raphan T and Yakushin SB (2021) Predicting Vasovagal Responses: A Model-Based and Machine Learning Approach. Front. Neurol. 12:631409. doi: 10.3389/fneur.2021.631409

INTRODUCTION

A neurogenically induced vasodilation and corresponding inappropriate bradycardia can lead to hypotension and transient loss of body tone and consciousness, that is, fainting. This condition has been termed neurogenic or vasovagal syncope (**VVS**) (1–4). Many nerves connect to the heart and blood vessels, which help control the beat frequency of the heart and the dilation and contraction of the blood vessels that control blood pressure (**BP**). Usually, these control signals are coordinated so that a decrease in **BP** is compensated by an increase in heart rate (**HR**) so that proper blood flow to the brain is maintained through sympathetic outflow (5). If the nerve signals are not coordinated, it could create a condition where the blood vessels dilate while the heart rate slows causing blood

to pool in the legs and not enough reaches the brain, resulting in syncope (5). Although **VVS** is not considered harmful because lying down causes a resumption of blood flow to the brain, it can result in falls, fractures, and in some cases death (1, 2). Thus, a correct diagnosis of frequent occurrences of **VVS** is critical for the management of this disease. Yet, diagnosis of **VVS** is usually based on history and a tilt test, in which subjects are passively tilted from a supine position to 20° from the spatial vertical (to a 70° position) on a tilt table and maintained in that orientation for 10–15 min. This maneuver usually brings on the symptoms of fainting and returning subjects to a reclining position makes them go away. Treatment of recurrent **VVS** using implanted pacemakers or beta blockers is often ineffective (6–10), because the underlying changes in the cardiovascular system that lead to the syncope are still incompletely understood (11, 12), although there has been an acknowledgment that the relative timing of **BP** and **HR** plays an important role in **VVS** generation (3, 4). The role of the vestibular system in generating the timing has only recently been explored and has suggested ways of habituating **VVS** as a treatment option (13).

The interest in better managing **VVS** has seen a concerted attempt to relate **VVS** to drops in blood pressure (**BP**) and heart rate (**HR**), which have been termed vasovagal responses (**VVR's**). There have been suggestions that **BP** oscillations during tilt testing are a predictive marker for **VVS** (14). In support of this idea, multiresolution analysis with wavelets demonstrated that there was increased power in low frequency modulations of BP that presage an episode of **VVS** in a human fainter (15). Recently, **VVRs** have been generated in anesthetized rats by repetitively activating the Vestibulo-Sympathetic Reflex (**VSR**), using sinusoidal galvanic vestibular stimulation (**sGVS**) or with 70° head-up tilts and ±70° oscillation in pitch (16–18). Although in anesthetized rats there is no concept of fainting, the **VVRs** are surprisingly similar to those in humans and we postulated that they would be a good animal model for **VVRs** in humans and their corresponding **VVS** responses (16).

In the studies on the rat, vasovagal oscillations were induced by sinusoidal galvanic vestibular stimulation (sGVS) with low frequency oscillations (16–18) in each of six rats. These low frequency modulations in **BP** and **HR** were referred to as vasovagal oscillations (18). In some instances, **sGVS** induced a substantial fall in BP and HR, that is, the transient **VVR**, which recovered over several minutes. We identified this transient component as a **VVR**, if there was a drop in BP and HR of 25 mmHg and 25 beats per minute (bpm), respectively. Similar thresholds have been used to identify **VVR's** in human studies as well (14, 15). These data have shown that **VVRs** may be an outcome of an aberrant type of vestibular stimulation of the vestibulosympathetic reflex and not a disease (17). The data also show that the rat may be a useful animal model for understanding how human **VVRs** may be generated and studied. However, this arbitrary threshold of identifying a **VVR** from **BP** drops does not give a clear understanding of the identifying features of a **VVR** nor what triggers a vasovagal response. The purpose of this study is to utilize our model of **VVR** generation (19) together with a machine learning approach to identify a separating hyperplane (20) between a normal and **VVR**, based on simultaneous **BP** and **HR** changes. This technique would more broadly identify the features that trigger **VVRs.** If a similar feature identification could be associated with **VVR**s in humans, it potentially could be utilized to identify **VVS** onset of fainting in real time.

METHODS

Experimental Methods

Adult, male Long-Evan rats (Harlan Laboratories, MA) weighing 300–400 g were used in these studies. All experiments were approved by the Institutional Care and Use Committee of the Mount Sinai School of Medicine. In this study, the data were taken from previous studies (16, 17, 21). We give a brief summary of the surgical and **sGVS** procedures.

Surgical Procedures

The implantation of a blood pressure measurement device and a head fixation mount were accomplished during the same aseptic surgical session. Throughout the surgery, rats were kept on a heating-pad controlled by the feedback of a rectal temperature probe. The surgery and testing were conducted under isoflurane anesthesia (4% induction, 2% maintenance).

Implantation of Bolts to Allow Painless Fixation of the Head During Experiments

Bolts were secured with dental acrylic cement, and two nuts were encased semisoft acrylic. A telemetric blood pressure sensor (DSI, St Paul, MN) was implanted in the abdominal aorta. These animals were utilized in a series of experiments performed over the next 2 months [see (16) for details].

Sinusoidal Galvanic Vestibular Stimulation for Inducing VVR

During testing, the heads of the rats were immobilized using the head mounts attached to a cylindrical holder for the animal's body. Sinusoidal currents generated by a computer-controlled stimulator (22) were delivered via two Ag/AgCl needle electrodes inserted into the skin over the mastoids, behind the external auditory meati. sGVS was given binaurally with currents of 1–4 mA and frequencies of 0.008 to 0.5 Hz. Current and frequencies were randomized, and 15–30 min were allowed to elapse between stimuli to reduce possible effects of habituation.

Tilt Protocol to Initiate VVR

The rats were statically tilted 70° and held in this position until they developed a vasovagal response. If a vasovagal response developed or if there was no response after several minutes, they were then brought back to the prone position.

Data Collection and Analysis

BP in response to sGVS was recorded continuously using customized A/D conversion hardware (Grass Technologies, West Warwick, RI) and Polyview software (Grass technologies) and stored at a rate of 1 KHz. BP data from the telemetric sensors were collected via a wand receiver (DSI, St Paul, MN) at 1 KHz with 12 bit resolution (Data Translation, Inc.) using our data collection program. The data were converted for analysis into

what we have referred to as Virtual Memory File (VMF) format. The data format is comprised of channels that represent stimuli and responses and can be representations of analog data, that are acquired via an A/D converter or event channels that associate an event with a time of occurrence. The VMF application software that we developed contains modules, which operate on the data and perform a wide range of transformations, such as a correlation analysis, power spectral analysis, timing of events, etc. The program also has visualization capabilities so that data can be displayed as time functions. The transformed data can also be displayed in the frequency domain or as one variable against another [See (23) for a more thorough description].

BP was utilized to obtain heart rate (**HR**) off-line. HR was identified from the peaks in BP. Stored pulses were converted to instantaneous frequency (beats·s^{-1}) and stored in a separate channel for further analysis. Mean square sinusoidal fits to the data were used to estimate variations of **BP** and **HR** to the sinusoidal oscillations.

RESULTS

Data Underpinnings of Modeling Vasovagal Responses

There were two characteristics of typical data that characterized a **VVR** during sGVS and tilts in anesthetized rats that were used to model the response (**Figure 1**). At a 2 s time scale, there were triangular type oscillations corresponding to the rapid transition (systole) and the slower transitions (diastole) (**Figure 1A**, inset). At a 1,000 s time scale, there was a coordinated drop in the in **BP** oscillations (**Figure 1A**) as well as in **HR (Figure 1B)** during sGVS (**Figure 1C**). Similar kinds of drops in **BP** (**Figure 1C**) and **HR (Figure 1E)** occurred during head up tilts of 70° (**Figure 1F**). The responses of **BP** and **HR** are similar to that observed during head up tilts when testing for fainting (15) and strategies for stopping **VVS** by leg-crossing and muscle tensing (24). The model therefore encompassed the systolic-diastolic oscillations and a central control structure to predict the drops in **BP** and **HR** over the longer time scale (19). The modeling approach in this paper considers what features of the model can be used to better identify the drops in **BP** and **HR** using the data and machine learning.

Modeling Approach

The basis of the model (**Figure 2**) that generates the triangular systolic-diastolic oscillations is a relaxation oscillator (19, 25). There is a signal Desired Blood Pressure ($\mathbf{BP_d}$), which acts as input that maintains the relaxation oscillations and is dependent on metabolic needs of the muscles and cells (26). This model not only simulates the basic diastolic and systolic behavior of **BP** as monitored by an intra-aortic sensor, but also predicts their variations in response to vestibular stimuli. The model also showed that alterations in $\mathbf{BP_d}$ changed the oscillation amplitude and its frequency, which compared favorably with data on systolic **BP**, pulse pressure, and Baroreflex Sensitivity **(BRS)** (19). It also predicts that as the **BP** drops, the period of the systolic-diastolic oscillations increases, and therefore **HR** drops (19). It is this relationship that is explored in this paper to elucidate the features that best describe a **VVR** and by extrapolation to predict a **VVS**.

Briefly, the relaxation oscillator model, which is of second order, has two states, $\mathbf{x_1}$ and $\mathbf{x_2}$, which are generated by delays

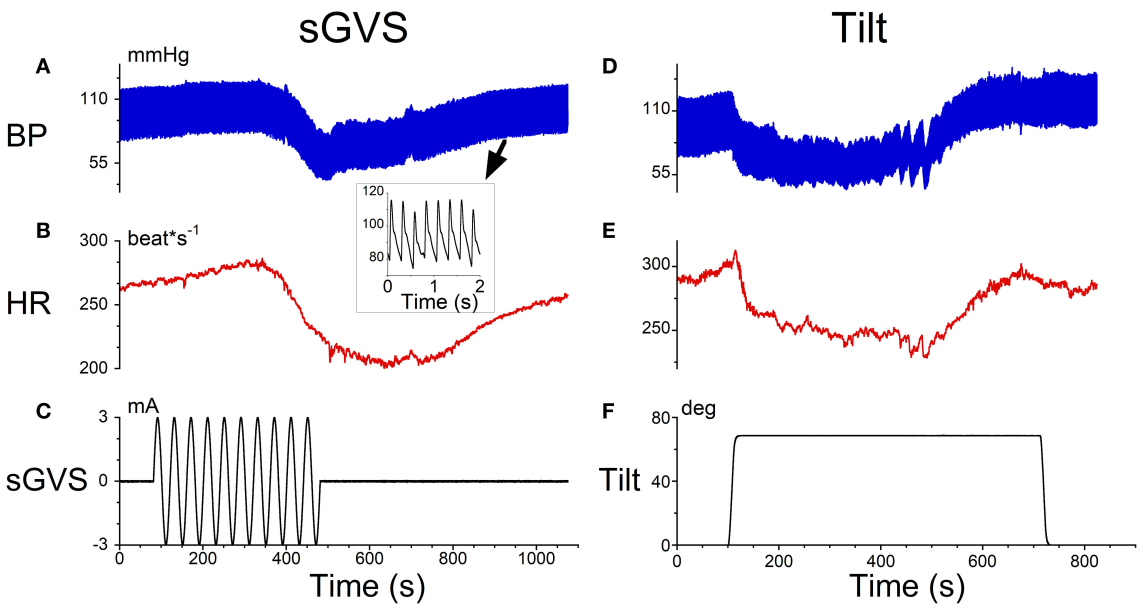

FIGURE 1 | Typical data that initiated a **VVR** in an anesthetized rat obtained from sGVS **(A–C)** and head up tilts of 70°. The inset in **(A)** shows a 2 s time scale. There were triangular type oscillations corresponding to the rapid transition (systole) and the slower transitions (diastole). **(A)** At a 1,000 s time scale, there was a coordinated drop in the in **BP** oscillations **(A)** as well as in **HR (B)** during sGVS **(C)**. Similar drops in **BP (D)** and **HR (E)** occurred during head up tilts of 70° **(F)**.

Δ_t with feedback elements that are discrete representations of leaky integrators (dashed rectangles) in continuous system models (27). The non-linear element ($\mathbf{f_1}$, **Figure 1**), was modeled as piecewise linear with threshold, **T,** and saturation, **S**. This nonlinear feedback is responsible for making the system oscillate, mimics the non-linear feedback present in the baroreflex (28, 29) and is a minimal structure for inducing relaxation oscillations (25). The realization of these integrators

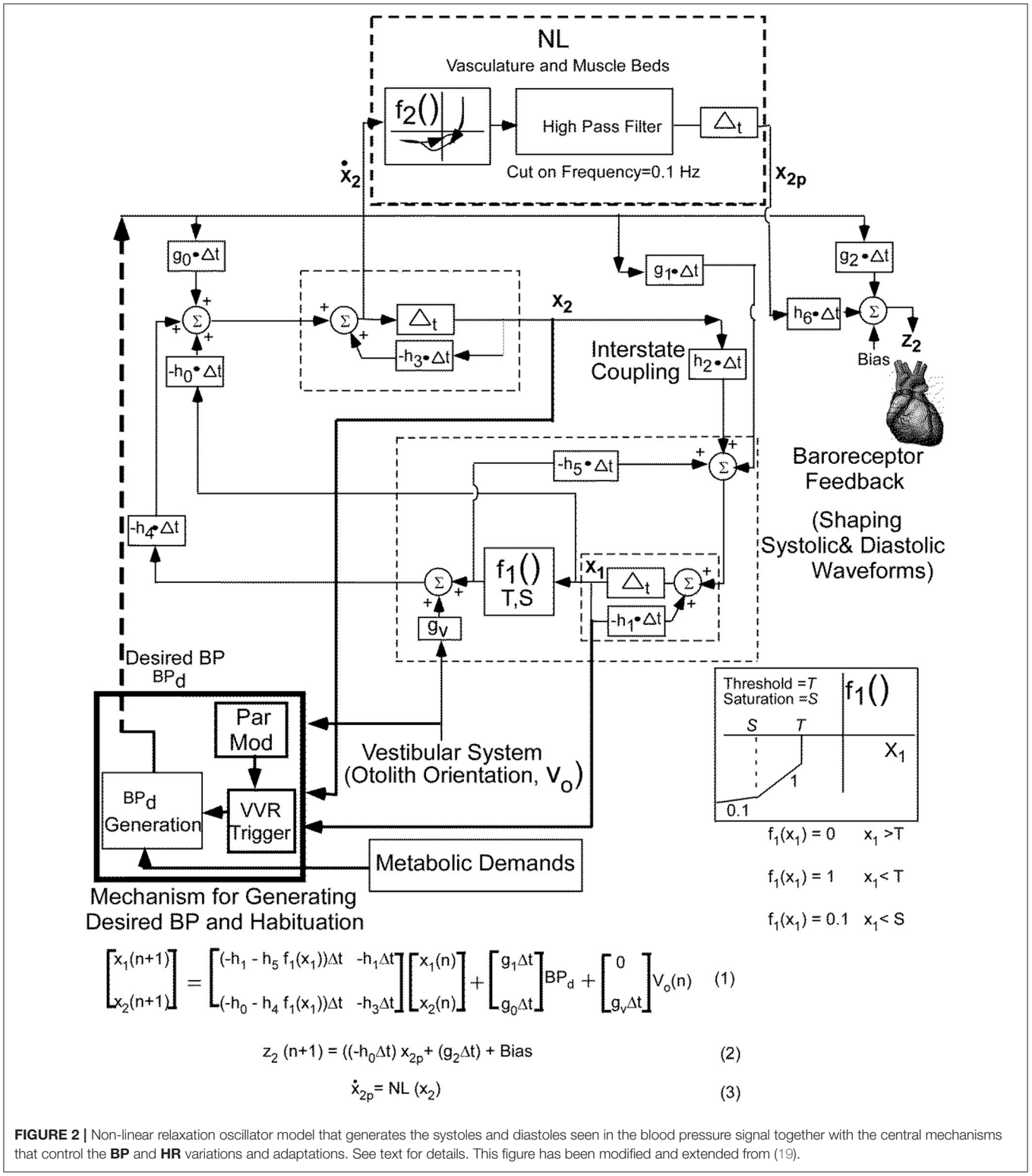

FIGURE 2 | Non-linear relaxation oscillator model that generates the systoles and diastoles seen in the blood pressure signal together with the central mechanisms that control the **BP** and **HR** variations and adaptations. See text for details. This figure has been modified and extended from (19).

by central circuits is not known, but may be accomplished through functional commissural connections between neurons in the rostral ventrolateral medulla (RVLM) and those in the nucleus tractus solitarius NTS) (30, 31). The vestibular system affects the oscillator in two ways: First, by adding an input in the feedback loop from the otolith orientation signal $\mathbf{V_0}$ through $\mathbf{g}_v$. Second it affects the parameter modification of the **VVR** trigger, which causes a drop in $\mathbf{Bp}_d$, initiating a **VVR (Figure 2)**.

In order to fit the data better on both systole-diastole transition and its derivative, a non-linear function (**NL**, $\mathbf{f_2}$) of the derivative of the integrator state ($\mathbf{x_2}$) was implemented as an enhancement of the model developed in Raphan et al. (19) **(Figure 2)**. The output of this non-linearity was processed by a high pass filter with a cut-in frequency of 0.1 Hz and then processed by an integrator, whose output has been labeled $\mathbf{x}_{2p}$. We postulate that this output combined with $\mathbf{BP}_d$ through parameters $\mathbf{h_6}$ and $\mathbf{g_2}$, which is offset by a bias (Bias) generates the signal $\mathbf{z_2}$ that controls **BP** and presumably the Volumetric Flow rate by constricting and dilating the muscle beds (32, 33). The purpose of the high pass filter was to prevent drifts at the output of the integrator due to any level component (**DC**) generated by the non-linearity, $\mathbf{f_2}$. The oscillator maintained the systolic to diastolic transitions and the non-linearity shaped and constrained the **BP** and its derivative, which fit the data. The equations below the model (**Figure 2)** were implemented in Matlab and used to simulate model predictions.

Model Predictions of Data and Defining the Features for Identifying a VVR

The simulations presented here are only those that have a direct bearing on the **VVR**. A more complete analysis of the model performance and the testing of the model against a wide range of data is given in (19). When activated by a constant $\mathbf{BP}_d$, the output of the model, $\mathbf{z_2}$, oscillated at a fixed frequency and the systolic and diastolic phases compared favorably with those from an anesthetized rat when there was no external vestibular stimulus (**Figure 3**, $\mathbf{BP}_d = 50$). When $\mathbf{BP}_d$ was dropped at $t =$ 5 s from 50 to 40 (**Figure 3**), due to the peak to peak amplitude of each simulated systole was reduced (**Figure 3**), and **BP** had the same properties as the experimental data (18, 19). Thus, the model had the flexibility to simulate experimental data not only in the normal state, but also during a **VVR.** Altering parameters, such as the threshold, or other parameters did not produce a **VVR** with these characteristics (19). Thus, a key prediction of the model is that it is a drop in $\mathbf{BP}_d$ that triggers a **VVR**.

From the above findings, we hypothesize that in non-susceptible animals, or in animals that are habituated, the internal signal, $\mathbf{BP}_d$**,** is prevented from dropping (13). We have also postulated that the $\mathbf{BP}_d$ signal originated in specific circuits that reconstruct this signal from states of the relaxation oscillator. We have further postulated that there is a specific trigger circuit that monitors the states and output variables of the relaxation oscillator in the brainstem as well as vestibular inputs to the baroreflex feedback, correlates these signals and determines whether to initiate a **VVR**. In order to determine the signals that activate this mechanism, we propose a new method for identifying **VVR**s, which utilizes a metric that combines features associated with both **BP** and **HR**.

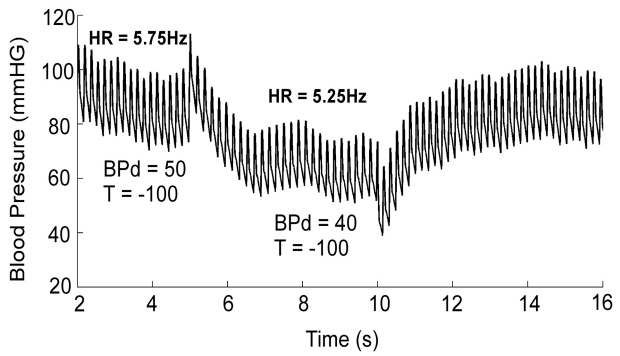

FIGURE 3 | Model simulation showing the effects of dropping $\mathbf{BP}_d$ from 50 to 40 mmHG. The threshold, **T**, in the feedback loop, responsible for the transition from diastole to systole was held constant at −100. $\mathbf{BP}_d$ is the only parameter that effectively mimics a **VVR** when it is dropped from its stable value. This figure was adapted from (19).

These features were derived as follows: we incorporated stochastic variations in threshold of the baroreflex feedback, **T**. When this was done, the model predicted what has commonly been referred to as baroreflex sensitivity (**BRS**) (**Figure 4**), which has been defined as the slope of the regression when R-R interval is plotted as a function of previous systolic pressure (34, 35). When the threshold, **T**, was varied randomly, the model output achieved varying systolic levels and intersystolic intervals (**Figure 4A**). This was the approximate behavior of the systolic levels and intersystolic intervals in the alert rat (**Figure 4B**). When the intersystolic interval was plotted as a function of Systolic Pressure **(BRS)**, the model predicted a positive correlation for the **BRS** for vestibular input $\mathbf{V_0} = 0$ in the model (**Figure 4C**, Shaded dotted line, slope = 0.31). This compared favorably with the data obtained in the alert rat (**Figure 4D**) as well as habituated anesthetized rats (13). It also predicted the **BRS** of anesthetized rats (**Figure 4C**, slope = 0). For a constant input $\mathbf{V_0} = 10$, the slope was increased to 0.6, which was the range of the baroreceptor in humans (34). The slopes could be altered by changes in sinusoidal vestibular input. (**Figure 4C**, slope −0.78), showing the wide range of baroreflex sensitivities that could be obtained from the model.

It has been noted that both **BP** and **HR** drops characterize a **VVR** (18, 36, 37). We have identified a signal $\mathbf{BP}_d$ that when it drops, both **BP** and the inverse of intersystolic interval drop. It is therefore of interest that baroreflex sensitivity is a parameter that is determined from a ratio of intersystolic interval and systolic **BP.** Thus, the **BRS** parameter has information about instantaneous **HR** and **BP**, rather than **BP** alone and could be the important trigger signal for **VVR** initiation. In this study, we therefore examined the temporal variations in **BRS** to determine

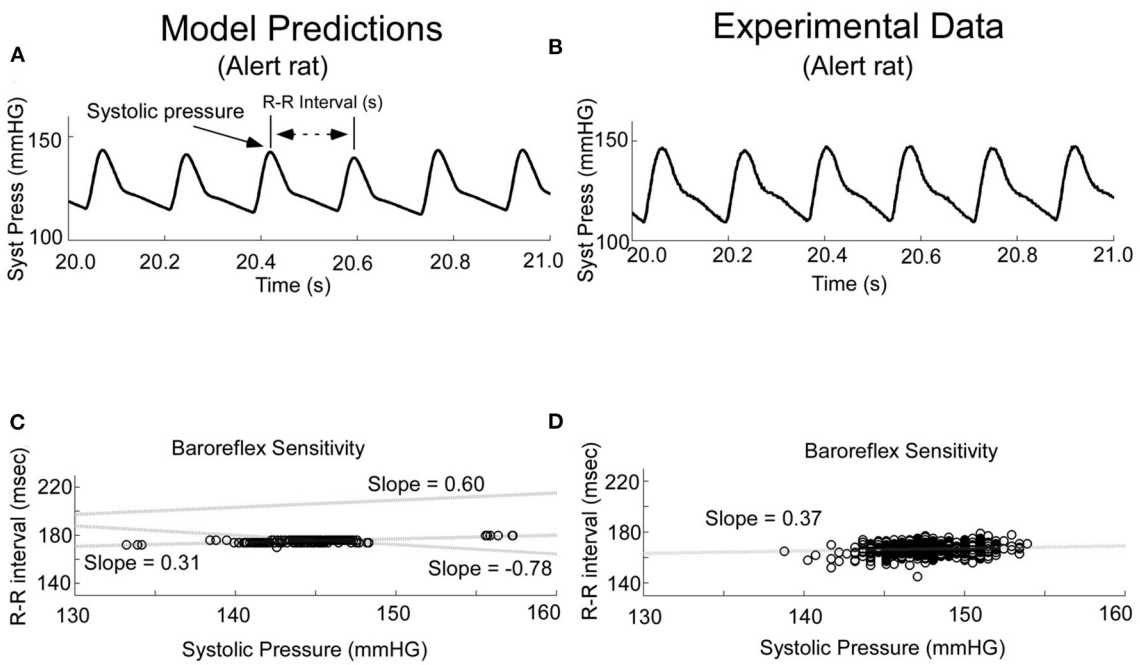

FIGURE 4 | Comparison of Model Predictions **(A**,**C)** and Experimental Data **(B**,**D)** of Baroreceptor Sensitivity (BRS). The model predicted the experimental data **(A**,**B)** and had the flexibility to predict the Baroreflex Sensitivity **(C**,**D)**. This figure was taken from (19).

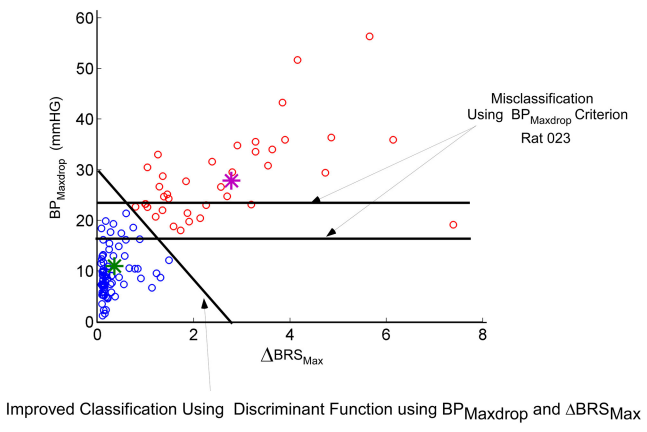

FIGURE 5 | Machine learning approach to finding a linear discriminant function that seperates a known **VVR** from normal. The blue circles are not **VVR**s while the others are **VVR**s. The features that are being plotted are the maximum drop in **BP** ($\mathbf{BP}_{Maxdrop}$) vs. maximum change in the new metric Δ**BRS** (See Text). Using a threshold on $\mathbf{BP}_{Maxdrop}$ alone (horizontal lines) misclassifies a significant greater **VVR**s than does the learned linear discriminant function, which utilizes a combination of $\mathbf{BP}_{Maxdrop}$ and Δ**BRS**.

the normal variation in anesthetized and alert states and the threshold that needs to be reached to generate a **VVR**.

We then considered an instantaneous Baroreflex Sensitivity function (Δ**BRS**) to determine whether this feature is a better prognosticator of **VVR**s and determine how the states of the model are related to Δ**BRS.** The computation of Δ**BRS** was implemented as a moving average window of instantaneous ratios of changes in intersystolic interval (related to **HR**) to changes in systolic **BP**. When a **VVR** occurred, the peak drop in systolic **BP**, **BPmaxdrop**, was plotted vs. the maximum of Δ**BRS** ($\Delta\mathbf{BRS}_{max}$). This plot had a considerable overlap in classifying a **VVR** according to a criterion based on maximal drops in **BP** alone (**Figure 5**). If the threshold for **BPmaxdrop** is chosen at 25 mmHG, then there are many **VVR**s that are missed (**Figure 4**, orange circles below 25 mmHG). If the threshold for classifying a **VVR** is 18 mmHG, many **non-VVRs** are classified as **VVR**s (**Figure 5**, blue circles). This shows that choosing a threshold for **BPMaxdrop** alone for identifying a **VVR** is an insufficient metric. A "**Machine Learning**" algorithm was used to find the discriminant function between what we termed **normal vs. VVR** (**Figure 5** Separating Linear function of orange from blue circles). First a small "test set" of what had been identified as **VVR**s using large values of **BPmaxdrop** was clasiified (**Figure 5**, purple star). The remaining data points were classified using the learned discriminant function based on the test set. There was improved identification and separation of a **VVR** from a **non-VVR (Figure 5)**. This shows that a linear combination of $\mathbf{BP}_{Maxdrop}$ and Δ**BRS** was a more appropriate metric.

Because Δ**BRS** is an important part of classifying a **VVR**, we then considered whether the time series Δ**BRS** (**Figure 6B**) or its derivative **(Figure 6D)** could be used **(Figure 6A)** to predict the

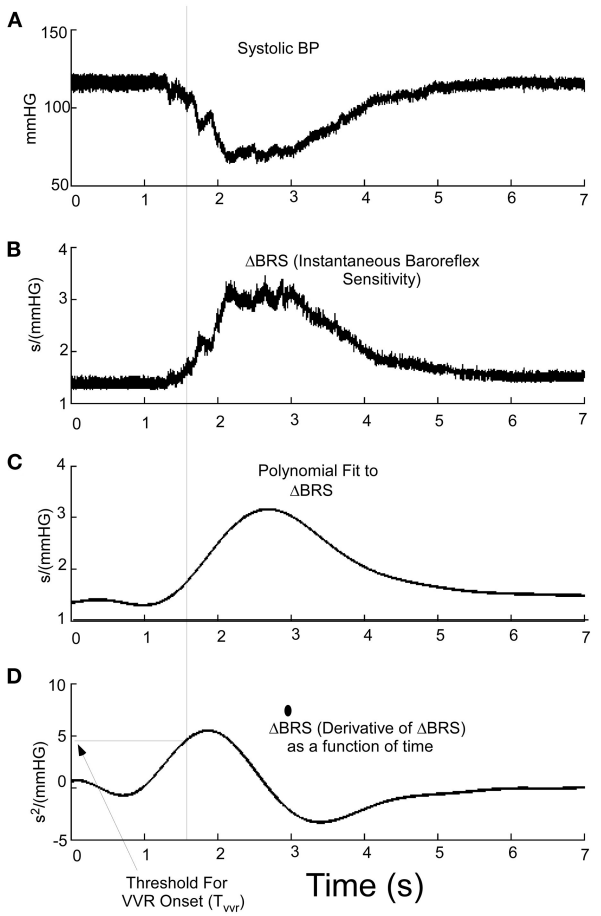

FIGURE 6 | (A) Systolic **BP** as a function of time during a **VVR**. **(B)** Using the instantaneous baroreflex sensitivity, Δ**BRS**, allows for the polynomial fitting **(C)** and determining the derivative where a threshold ($\mathbf{T}_{vvr}$) **(D)** aligns and is a predictor of the drop in systolic pressure at the beginning of a VVR.

triggering of a **VVR.** The polynomial fit to Δ**BRS (Figure 6C)** is an intermediate step in finding the derivative and suggests that the derivative of Δ**BRS r**eaches a threshold, **Tvvr** (**Figure 6D**), before there is a drop in systolic level of **BP (Figure 6, Dotted Vertical Line)**. This threshold metric, **Tvvr,** which is derived from the temporal characteristics of the derivative of Δ**BRS**, is consistent with the idea that Δ**BRS** is an important part of the discriminant function that separates a **VVR** from a non-**VVR.** Therefore, this newly defined Δ**BRS** function and its derivative are better predictors of a **VVR** and could be a metric that combines both **BP** and **HR** as determinants of an impending **VVR** and associated **VVS** in humans if a large data set were utilized.

DISCUSSION

This study has shown that this newly defined function, Δ**BRS,** and its derivative are predictive of a **VVR** and potentially could be important in predicting **VVS** in humans. This is consistent with the finding that a better discriminant for identifying a **VVR** is when $\mathbf{BP}_{max}$ is combined with $\Delta\mathbf{BRS}_{Max}$. This new metric takes into account a critical feature of **VVR**s in humans and rats as the simultaneous occurrence of both bradycardia and hypotension at the onset of the **VVR** (38). It is supported by the idea that it is the loss of baroreflex function that triggers a **VVS** (17, 36, 39). Consistent with this, there is also an immediate loss of the baroreflex-generated Muscle Sympathetic Nerve Activity (MSNA) at the onset of syncope (40–42). The pathophysiological mechanism and significance of the baroreflex disengagement in producing bradycardia and hypotension have been conjectured to be the basis for **VVS** (3, 4), but no specific mechanism has been identified that could produce these changes. As such, despite being relatively common (1, 12, 43), the origin and neural basis of **VVR**s, which are related to **VVS** are not known (2, 36, 38) and there are no physical signs of neurogenically mediated **VVR**. Therefore, identifying the features that could be correlated with triggering the a **VVR** that underlies **VVS**, could be important in predicting their onset and managing the condition.

The pressure and flow dynamics are not easily modeled from a biophysical perspective. We have therefore taken a system theoretic approach to this problem to model the neural control of the cardiovascular oscillations as an internal model that entrains the natural cardiovascular oscillations (19). This approach encompasses not only the physical volumetric flow rate and pressure dynamics, but also how the **BP** and **HR** system is controlled by sensory-motor neural mechanisms that constrain the shape of the systolic-diastolic oscillatory waves (19). It had been suggested that the systolic-diastolic oscillations in **BP** had characteristics of a relaxation oscillator (44, 45). Recently, we demonstrated how relaxation oscillations could be embedded in a control system that could regulate its performance. In this model, the shape of the systolic/diastolic waveform is not determined strictly by the heart, but by a neural network, which mimics the oscillation features of the heart, referred to as the internal model. The feedback mechanisms implement closed loop control and drive actuators through non-linear mechanisms that can rapidly control the constriction of the arteries and vascular beds (33), regulating volumetric **blood flow rate** and **BP** (19). This kind of control is referred to as Model Reference Adaptive Control (**MRAC**) (46–48). The output of the internal model is compared to a feedback signal from baro-receptors that code **BP**, generating an error signal whose control parameters are updated based on this error signal. The control parameters then converge to ideal values that cause the actual **BP** and **HR** to ∼match the response of the reference model. We have simulated the reference model behavior as a function of alteration of specific parameters and tested the predictions against data. This kind of control is different from eye movement control or leg control. These systems are stationary and need to be activated to have them move. The blood pressure and heart rate control requires the maintenance of oscillations by an already oscillating system. Therefore, it is reasonable that the control strategies would be different.

The model was implemented as a state determined second order relaxation oscillator, whose oscillation characteristics are governed essentially by a threshold and saturation mechanism

in the feedback loop and a driving signal that maintains the oscillations. The threshold non-linearity, which has been observed in the baroreflex feedback (28, 29, 49), puts the system into systolic or diastolic mode. The model was adapted from work done on modeling oculomotor oscillations during nystagmus (25) and repetitive motion of the legs during locomotion (50, 51) where there are also oscillating fast and slow components of the stepping. An important enhancement to the model above over that presented previously (19), is a component, which we have labeled Mechanism for Generating $\mathbf{BP_d}$ and habituation. We propose that this component generates $\mathbf{BP_d}$ to maintain the relaxation oscillations. We also postulate that it correlates the signals arising from the states of the relaxation oscillator that is responsible for activating the **VVR** trigger, which inhibits $\mathbf{BP_d}$ Generation and initiates a **VVR**. Finally, it is responsible for activating the **Par Mod** component during habituation that adapts the parameters of $\mathbf{BP_d}$ Generation, which raises the threshold for triggering a **VVR** as habituation is ongoing (13).

There is some evidence that mechanism for generating $\mathbf{BP_d}$ and the parameter modification for maintaining **BP** oscillations or initiating a **VVR** is performed in the uvula. Optogenetic inhibition of Purkinje cell activity in the uvula modulates **BP** when anesthetized rats are tilted (52). There are also afferent (53) and efferent (54) connections to autonomic nuclei in the rabbit. These findings together with the fact that neural activity in the caudal medial, lateral and descending VN (55–58) are critical for **VSR** (59, 60) may contain a mediator that modulates **BP** (61–63) is consistent with the model structure that is being proposed.

In conclusion, much of the efforts in identifying the onset of a **VVR** has been focused on **BP** (14, 15, 18). The **VVR**s in rats were associated with increased power in the low frequency band (0.025–0.05 Hz) with synchronous oscillations in **BP** and **HR**, which have been termed vasovagal Oscillations; higher frequencies of **sGVS** rarely induced a **VVR** (18). The approach in this study was to base our criteria for predicting a **VVR** on a model that (1) predicted the approximate triangular shape of systolic/diastolic oscillations. (2) identified parameters, which could modify the oscillations. (3) Encompassed a theory for how amplitudes and frequencies of these systolic/diastolic oscillations could be controlled by vestibular input (4). Better Identified the features that could be used to separate a **VVR** from the normal systolic/diastolic oscillations using a machine learning technique.

The method developed was based on small data set, yet proved valuable in finding a separation between the systolic-diastolic beats during **VVR** and normal beats. Finding discriminant functions using a "Big Data" set for each animal should give us a better understanding of how **BP** and **HR** are processed to generate a **VVR** and how it is reflected in our newly defined Δ**BRS** function and its derivative. If a similar feature identification could be associated with **VVR**s in humans, it potentially could be utilized to identify onset of fainting in real time.

DATA AVAILABILITY STATEMENT

The raw data supporting the conclusions of this article will be made available by the authors, without undue reservation.

ETHICS STATEMENT

The animal study was reviewed and approved by IACUC, Icahn School of Medicine at Mount Sinai Hospital.

AUTHOR CONTRIBUTIONS

TR contributed to the overall conceptual framework of this study. TR was responsible for developing the model, defining and testing the parameters that were used to identify **VVRs** and showing the plausibility of such an approach. TR also was responsible for the organization and writing of the manuscript. SY contributed by performing the experiments on the rats as well as contributing of the writing of the manuscript.

FUNDING

The authors gratefully acknowledge the support of the Jewish Communal fund donated by Mrs. Pheobe Cohen to support the research of TR. The work was also supported by grant NIH/NIDC DC 012573 (TR). SY was supported by NIH/NIDCD DC018390.

ACKNOWLEDGMENTS

We thank G. P. Martinelli for implanting the Blood pressure monitors. We would like to acknowledge the funding obtained by BC (deceased) that support the experimental work.

REFERENCES

1. Gendelman HE, Linzer M, Gabelman M, Smoller S, Scheuer J. Syncope in a general hospital patient population. Usefulness of the radionuclide brain scan, electroencephalogram, and 24-hour Holter monitor. *N Y State J Med.* (1983) 83:1161–5.
2. Moya A, Sutton R, Ammirati F, Blanc JJ, Brignole M, Dahm JB, et al. Guidelines for the diagnosis and management of syncope (version 2009). Task Force for the Diagnosis and Management of Syncope; European Society of Cardiology (ESC); European Heart Rhythm Association (EHRA); Heart Failure Association (HFA); Heart Rhythm Society (HRS). *Eur Heart J.* (2009) 30:2631–71. doi: 10.1093/eurheartj/ehp298
3. Saal DP, Thijs RD, van Zwet EW, Bootsma M, Brignole M, Benditt DG, et al. Temporal relationship of a systole to onset of transient loss of conciousness in tilt Induced reflex syncope. *JACC: Clinical Electrophysiol.* (2017) 3:1592–8. doi: 10.1016/j.jacep.2017.07.006
4. van Dijk JG, van Rossum IA, Thijs RD. Timing of circulatory and neurological events in syncope. *Front Cardiovasc Med.* (2020) 7:36. doi: 10.3389/fcvm.2020.00036
5. Wallin BG, Sundlof G. Sympathetic outflow to muscles during vasovagal syncope. *J Auton Nerv Syst.* (1982) 6: 287–91.
6. Calkins H. Pharmacological approaches to therapy for vasovagal syncope. *Am J Cardiol.* (1999) 84:20Q–5Q.

7. Sheldon R. Role of pacing in the treatment of vasovagal syncope. *Am J. Cardiol.* (1999) 84:26Q−32Q.
8. Sheldon R, Connolly S. Second Vasovagal Pacemaker Study (VPS II): rationale, design, results, and implications for practice and future clinical trials. *Card Electrophysiol Rev.* (2003) 7:411–5. doi: 10.1023/B:CEPR.0000023157.37745.76
9. Sheldon R, Rose S, Connolly S. Prevention of syncope trial (POST): a randomized clinical trial of beta blockers in the prevention of vasovagal syncope; rationale and study design. *Europace.* (2003) 5:71–5. doi: 10.1053/eupc.2002.0284
10. Kapoor JR. Predicting the effectiveness of beta-blocker therapy in vasovagal syncope. *J Am Coll Cardiol.* (2008) 51:2372. doi: 10.1016/j.jacc.2008.02.070
11. Sutton R, Bloomfeld DM. Indications, methodology, and classification of results of tilt-table testing. *Am J. Cardiol.* (1999) 84:10Q–9Q.
12. Grubb BP. Neurocardigenic syncope. *N Engl J Med.* (2005) 352:1004–10. doi: 10.1056/NEJMcp042601
13. Cohen B, Martinelli GP, Xiang Y, Raphan T, Yakushin SB. Vestibular activation habituates the vasovagal response in the rat. *Front Neurol.* (2017) 8:83. doi: 10.3389/fneur.2017.00083
14. Hausenloy DJ, Arhi C, Chandra N, Franzen-McManus A-C, Meyer A, Sutton R. Blood pressure oscillations during tilt testing as a predictive marker of vasovagal syncope. *Eurospace.* (2009) 11:1696–701. doi: 10.1093/eurospcae/eup338
15. Nowak JA, Ocon A, Taneja I, Medow MS, Steward JM. Multiresolution wavelet analysis of time dependent physiological response in syncopal youths. *Am J Physiol Heart Circ Physiol.* (2009) 296:H171–9. doi: 10.1152/ajpheart.00963.2008
16. Cohen B, Martinelli GP, Ogorodnikov D, Xiang Y, Raphan T, Holstein GR, et al. Sinusoidal galvanic vestibular stimulation (sGVS) induces a vasovagal response in the rat. *Exp Brain Res.* (2011) 210:45–55. doi: 10.1007/s00221-011-2604-4
17. Cohen B, Martinelli GP, Raphan T, Schaffner A, Xiang Y, Holstein GR, et al. The vaso-vagal response (VVR) of the rat: its relation to the vestibulo-sympathetic reflex (VSR) and to Mayer waves. *FASEB.* (2013) 27:2564–72. doi: 10.1096/fj.12-226381
18. Yakushin SB, Martinelli GP, Raphan T, Xiang Y, Holstein GR, Cohen B. Vasovagal oscillations and vasovagal responses produces by the vestibulo-sympathetic reflex in the rat. *Front Neurol.* (2014) 5:1–11. doi: 10.3389/fneur.2014.00037.ecollections 2014
19. Raphan T, Cohen B, Xiang Y, Yakushin SB. A model of blood pressure, heart rate, and vaso-vagal responses produced by vestibulo-sympathetic activation. *Front Neurosci.* (2016) 10:1–16. doi: 10.3389/fnins.2016.00096
20. Bishop CM. *Pattern Recognition and Machine Learning*. New York, NY: Springer Science +Business Media (2006). p. 738.
21. Yakushin SB, Martinelli GP, Raphan T, Cohen B. The response of the vestibulosympathetic reflex to linear acceleration in the rat. *J Neurophysiol.* (2016) 116: 2752–64. doi: 10.1152/jn.00217.2016
22. Kaufmann H, Biaggioni I, Voustianiouk A, Diedrich A, Costa F, Clarke R, et al. Vestibular control of sympathetic activity. An otolith-sympathetic reflex in humans. *Exp Brain Res.* (2002) 143:463–9. doi: 10.1007/s00221-002-1002-3
23. Rudowsky I, Kulyba O, Kunin M, Ogarodnikov D, Raphan T. A relational database application in support of integrated neuroscience research. *J Integr Neurosci.* (2004) 3:363–78. doi: 10.1142/S0219635204000609
24. Krediet CTP, van Dijk N, Linzer M, van Lieshout JJ, Wouter W. Management of vasovagal Syncope controlling or aborting faints by leg crossing and muscle tensing. *Circulation.* (2002) 106:1684–9. doi: 10.1161/01.CIR.0000030939.12646.8F
25. Raphan T. A parameter adaptive approach to oculomotor system modeling. In: *Engineering*. New York, NY: CUNY (1976). p. 204.
26. Berne RM, Levy MN. *Cardiovascular Physiology*. Philadelphia, PA: Mosby (2001).
27. Zadeh LA, Desoer CA. *Linear System Theory: The State Space Approach. Series in Systems Science*. New York, NY: McGraw Hill (1963). p. 628.
28. Chen HI, Kuo-Chu C. Assessment of threshold and saturation pressure in the baroreflex function curve: a new mathematical analysis. *Jpn J Physiol.* (1991) 41:861–77.
29. Chen S, Shi X. Re-parameterization of the logistic model in assessing changes in baroreceptor reflex. *Neurosci Med.* (2011) 2: 110–6. doi: 10.4236/nm.2011.22016
30. Blessing WW. *The Lower Brainstem and Bodily Homeostasis*. Oxford: Oxford University Press (1997).
31. Granata AR. Modulatory inputs on sympathetic neurons in the rostral ventrlateral medulla in the rat. *Cell Mol Neurobiol.* (2003) 23:665–80. doi: 10.1023/a:1025040600812
32. Barcroft H, Edholm OG, Mcmichael J, Sharpey-Schafer EP. Posthaemorrhagic fainting: study by cardiac output and forearm flow. *Lancet.* (1944):489–90.
33. Barcroft H, Edholm OG. On the vasodilation in human skeletal muscle during post-haemorrhagic fainting. *J Physiol.* (1945) 104.2:161–75.
34. Davos CH, Davies LC, Piepoli M. The effect of baroreceptor activity on cardiovascular regulation. *Hellenic J Cardiol.* (2002) 43:145–55.
35. La Rovere M, Pinna G, Raczak G. Baroreflex sensitivity: measurement and clinical implications. *Ann Noninv Electrocardiol.* (2008) 13:191–207. doi: 10.1111/j.1542-474X.2008.00219.x
36. Julu POO, Cooper VL, Hansen S, Hainsworth R. Cardiovascular regulation in the period preceding vasovagal syncope in concious humans. *J Physiol.* (2003) 549:299–311. doi: 10.1113/jphysiol.2002.036715
37. Kaufmann H, Hainsworth R. Why do we faint? *Muscle Nerve.* (2001) 24:981–3. doi: 10.1002/mus.1102
38. Lewis T. Vasovagal syncope and the carotid sinus mechanism. *Br Med J.* (1932) 3723: 873–6.
39. Thomson HL, Wright K, Frenneaux M. Baroreflex sensitivity in patients with vasovagal syncope. *Circulation.* (1997) 95:395–400.
40. Morillo CA, Eckberg DL, Ellenbogen KA, Beightol LA, Hoag JB, Tahvanainen KU, et al. Vagal and sympathetic mechanisms in patients with orthostatic vasovagal syncope. *Circulation.* (1997) 96:2509–13.
41. Morillo CA, Villar JC. Neurocardiology. Neurogenic syncope. *Baillieres Clin Neurol.* (1997) 6:357–80.
42. Mosqueda-Garcia R, Furlan R, Fernandez-Violante R, Desai T, Snell M, Jarai Z, et al. Sympathetic and baroreceptor reflex function in neurally mediated syncope evoked by tilt. *J Clin Invest.* (1997) 99: 2736–44.
43. Soteriades ES. Incidence and prognosis of syncope. *N Engl J Med.* (2002) 347:875–85. doi: 10.1056/NEJMoa012407
44. van Der Pol B. On relaxation-oscillations. The London, Edinburgh and Dublin. *Phil Mag Sci.* (1926) 2:978–92. doi: 10.1080/1478644260856127
45. Noble PJ, Noble D, A historical perspective on the development of models of rhythm in the heart. In: Tripathi ON, Ravens U, Sanguinetti MC, editors. *Heart Rate and Rhythm*. New York, NY: Springer Verlag (2011). p. 155–74.
46. Horrocks T. Investigations into model reference adaptive control systems. *Proc IEEE.* (1964) 3:1894–906.
47. Landau ID. *Adaptive Control: The Model Reference Approach*. New York NY: Marcel Dekker (1979).
48. White AJ. Analysis and design of model-reference adaptive control systems. *Proc IEEE.* (1966) 113:175–84.
49. Chen LY, Benditt DG. Perhaps past performance does predict future results after all: a key to evaluating treatment interventions in vasovagal syncope. *J Cardiovasc Electrophysiol.* (2010) 21:1381–3. doi: 10.1111/j.1540-8167.2010.01881.x
50. Osaki Y, Kunin M, Cohen B, Raphan T. Three-dimensional kinematics and dynamics of the foot during walking: a model of central control mechanisms. *Exp Brain Res.* (2007) 176:476–96. doi: 10.1007/s00221-006-0633-1
51. Osaki Y, Kunin M, Cohen B, Raphan T. Relative contribution of walking velocity and stepping frequency to the neural control of locomotion. *Exp Brain Res.* (2008) 185: 121–35. doi: 10.1007/s00221-007-1139-1
52. Tsubota T, Ohashi Y, Tamura K, Miyashita Y. Optogenetic inhibition of Purkinje cell activity reveals cerebellar control of blood pressure during postural alterations in anesthetized rats. *Neuroscience.* (2012) 210: 137–44. doi: 10.1016/j.neuroscience.2012.03.014
53. Bradley DJ, Ghelarducci B, La Noce A, Paton JFR, Spyer KM, Withington-Wray DJ. An electrophysiological and anatomical study of afferents reaching the cerebellar uvula in the rabbit. *Exp Physiol.* (1990) 75:163–77.
54. Paton JFR, La Noce A, Sykes RM, Sebastiani L, Bagnoli P, Ghelarducci B, et al. Efferent connections of lobule IX of the posterior cerebellar cortex in the rabbit—some functional considerations. *J Auton Nerv Syst.* (1991) 36:209–24.

55. Yates BJ, Grelot L, Kerman IA, Balaban CD, Jakus J, Miller AD. Organization of vestibular inputs to nucleus tractus solitarius and adjacent structures in cat brain stem. *Am J Physiol.* (1994) 267(4 Pt. 2): R974–83.
56. Doba N, Reis DJ. Changes in regional blood flow and cardiodynamics evoked by electrical stimulation of the fastigial nucleus in the cat and their similarity to orthstatic reflexes. *J Phusiol (Lond.).* (1972) 227: 729–47.
57. Pan PS, Zhang YS, Chen YZ. Role of the nucleus vestibularis medialis in vestibulo-sympathetic response in rats. *Acta Physiol Sin, Chinese.* (1991) 43:184–8.
58. Uchino Y, Kudo N, Tsuda K, Iwamura Y. Vestibular inhibition of sympathetic nerve activities. *Brain Res.* (1970) 22:195–206.
59. Yates BJ. Vestibular influences on the sympathetic nervous system. *Brain Res.* (1992) 17:51–9.
60. Yates BJ, Goto T, Kerman I, Bolton PS. Responses of caudal medullary raphe neurons to natural vestibular stimulation. *J Neurophysiol.* (1993) 70:938–46.
61. Bozdagi O, Wang XB, Martinelli GP, Prell G, Friedrich VL Jr., Huntley GW, et al. Imidazoleacetic acid-ribotide induces depression of synaptic responses in hippocampus through activation of imidazoline receptors. *J Neurophysiol.* (2011) 105:1266–75. doi: 10.1152/jn.00263.2010
62. Martinelli GP, Friedrich VL Jr., Prell GD, Holstein GR. Vestibular neurons in the rat contain imidazoleacetic acid-ribotide, a putative neurotransmitter involved in blood pressure regulation. *J Comp Neurol.* (2007) 501:568–81. doi: 10.1002/cne.21271
63. Prell GD, Martinelli GP, Holstein GR, Matulic-Adamic J, Watanabe KA, Chan SLF, et al. Imidazoleacetic acid-ribotide: an endogenous ligand that stimulates imidazol(in)e receptors. *Proc Natl Acad Sci.* (2004) 101:13677–82. doi: 10.1073/pnas.0404846101

Conflict of Interest: The authors declare that the research was conducted in the absence of any commercial or financial relationships that could be construed as a potential conflict of interest.

frontiers in Neurology

ORIGINAL RESEARCH
published: 29 April 2021
doi: 10.3389/fneur.2021.663173

The Impact of Coronavirus Disease 2019 Epidemic on Dizziness/Vertigo Outpatients in a Neurological Clinic in China

*Changqing Li[1], Dongsheng Guo[2], Xiangke Ma[3], Siwei Liu[1], Mingyong Liu[1] and Lichun Zhou[1]**

[1] Department of Neurology, Beijing Chaoyang Hospital, Capital Medical University, Beijing, China, [2] Department of Emergency, Beijing Chaoyang Hospital, Capital Medical University, Beijing, China, [3] Department of Neurosurgery, Beijing Chaoyang Hospital, Capital Medical University, Beijing, China

OPEN ACCESS

Edited by:
Michael Strupp,
Ludwig Maximilian University of Munich, Germany

Reviewed by:
Diego Kaski,
University College London, United Kingdom
Andreas Zwergal,
Ludwig Maximilian University of Munich, Germany
Ji Soo Kim,
Seoul National University, South Korea

***Correspondence:**
Lichun Zhou
zhlc8888@hotmail.com

Specialty section:
This article was submitted to Neuro-Otology, a section of the journal Frontiers in Neurology

Received: 02 February 2021
Accepted: 19 March 2021
Published: 29 April 2021

Citation:
Li C, Guo D, Ma X, Liu S, Liu M and Zhou L (2021) The Impact of Coronavirus Disease 2019 Epidemic on Dizziness/Vertigo Outpatients in a Neurological Clinic in China. Front. Neurol. 12:663173. doi: 10.3389/fneur.2021.663173

Objective: This study aims to investigate the impact of the coronavirus disease 2019 (COVID-19) epidemic on dizziness/vertigo outpatients in a neurological clinic in China.

Methods: Against the background of the COVID-19 epidemic, the data of patients who visited the neurological clinic of Beijing Chaoyang Hospital West Branch during the pandemic (February 1–May 30, 2020) and the corresponding period in 2019 (February 1–May 30, 2019) were analyzed, and patients with dizziness/vertigo from these two periods were compared to discover their demographic features and etiologic distribution according to their age and sex.

Result: The absolute number of neurological outpatients decreased from 14,670 in 2019 to 8,763 in 2020 (−40.3%), with a corresponding decline in dizziness/vertigo patients (2019: $n = 856$; 2020: $n = 1,436$, −40.4%). Dizziness/vertigo was more common in women than men in these two periods (2019: women = 63.6%; 2020: women = 63.1%, $p = 0.82$). The overall etiology distribution was different among all disorders between the two periods ($p < 0.001$). There was an increase in benign paroxysmal positional vertigo (BPPV) (2019 vs. 2020: 30.7 vs. 35%, $p < 0.05$) and psychogenic/persistent postural perceptual dizziness (PPPD) (2019 vs. 2020: 28.5 vs. 34.6%, $p < 0.05$) while a decrease in vascular vertigo during the epidemic (2019 vs. 2020: 13 vs. 9.6%, $p < 0.05$). During the epidemic, the top three causes of dizziness/vertigo were BPPV (35%), psychogenic/PPPD (34.6%), and vascular vertigo (9.6%). A female predominance was observed in BPPV (women = 67.7%, $p < 0.05$) and psychogenic/PPPD (women = 67.6%, $p < 0.05$). In addition, the etiology ratio of different age groups was significantly different ($p < 0.001$). The most common cause for young and young-old patients was BPPV, and the most common cause for middle-aged and old-old patients was psychogenic/PPPD.

Conclusion: The absolute number of outpatients with dizziness/vertigo during the COVID-19 pandemic was reduced during the early period of the COVID-19 outbreak.

BPPV and psychogenic/PPPD were more abundant, and vascular vertigo was less frequent. Based on those data, health-care management policy for dizziness/vertigo and mental disorder should be developed during the outbreak of COVID-19 and other infective diseases.

Keywords: COVID-19, dizziness/vertigo, BPPV, psychogenic/PPPD, China

INTRODUCTION

As a sudden acute respiratory infectious disease, coronavirus disease 2019 (COVID-19) imposed such a great impact on public health that people's focus in life underwent tremendous changes overnight. During the early phase of the COVID-19 outbreak, people spent less time outdoors, and tried to stay away from public places such as hospitals. Moreover, the urgent diversion of medical staff and hospital resources to COVID-19 emergencies inevitably severely compromised normal medical care. Dizziness/vertigo as a subjective and non-specific symptom is frequently complained by outpatients in the neurology department, with high incidence and recurrence rates. Does the COVID-19 epidemic affect the occurrence of dizziness/vertigo? This study compared the demographic characteristics and etiological distribution of dizziness/vertigo outpatients in a neurological clinic during the COVID-19 epidemic in 2020 and the same period in 2019 in order to assess the possible relationship between these changes and occurrence of COVID-19.

METHODS

Subjects

The data of all outpatients and dizziness/vertigo outpatients in the neurological clinic of the West Branch of Beijing Chaoyang Hospital were retrospectively and continuously collected, which included 856 dizziness/vertigo patients aged 19–90 during the epidemic period (from February 1 to May 30, 2020) and 1,436 dizziness/vertigo patients aged 18–92 during the same period in 2019 (from February 1 to May 30, 2019).

Information covers the characteristics of dizziness/vertigo attacks (including duration, provoking factors, frequency, accompanying symptoms, and comorbidities) and detailed medical records including the patient's vital signs, nervous system examination, neuro-otological examination, vestibular function tests [for example, electronystagmography, caloric vestibular test, pure-tone audiometry, and head impulse–nystagmus–test of skew (HINTS)] Hamilton anxiety and depression scale, magnetic resonance imaging of the head or internal auditory canal, magnetic resonance angiography or CT of the head, cervical spine X-ray or MRI, carotid ultrasound, subclavian artery ultrasound, cardiac ultrasound, routine blood tests, and blood biochemistry. Based on these, the patients' demographic characteristics and etiological distribution according to their age and sex were analyzed and summarized.

Diagnostic Criteria

The etiology of dizziness/vertigo was diagnosed according to the classification of International Classification of Vestibular Disorders (ICVD), including benign paroxysmal positional vertigo (BPPV) (1), psychiatric or persistent postural perceptual dizziness (psychogenic/PPPD) (2), vascular vertigo [caused by transient ischemic attack (TIA), acute cerebral infarction, cerebral hemorrhage, and cerebral small vascular disease] (3), vestibular migraine (VM) (4), vestibular neuritis (VN) (5), Mènière's disease (MD) (6), sudden sensorineural hearing loss (SSHL) accompanied by vertigo (7), systemic diseases (including hypertension, diabetes mellitus, postural hypotension, anemia, and cardiogenic diseases), and vestibular paroxysmia (VP) (8). Other causes include hereditary, metabolic, toxic, trauma-related, inflammatory, and demyelinating diseases. In addition, psychogenic dizziness and PPPD are not calculated separately because these two disorders are related to each other and often overlap (2).

Statistical Analysis

The *t*-test was used to analyze quantitative variables such as the age difference between the two periods, and the chi-squared test was used to compare dizziness/vertigo patients during the COVID-19 period and the same period in 2019 in terms of etiologic distribution according to their age and sex. All statistical analyses were conducted using R statistical language (version 3.6.3, https://www.r-project.org/), and $p < 0.05$ was considered significant.

RESULTS

Overall Comparison During the Two Periods

During the epidemic period, the absolute number of outpatients massively dropped ($n = 8{,}763$) compared with the same period in 2019 ($n = 14{,}670$, −40.3%), paralleling the decline in dizziness/vertigo patients (2019: $n = 856$; 2020: $n = 1{,}436$, −40.4%), while the relative dizziness/vertigo rate remained unchanged (9.7 vs. 9.7%, $p = 0.97$).

Comparison of Demographic Features and Etiologic Distribution According to Their Age and Sex During Two Periods

Our data showed a female predominance (2019: women = 63.6%; 2020: women = 63.1%, $p = 0.82$) in both periods. The average age of dizziness/vertigo patients was 56.78 ± 14.12 years during the epidemic period and 55.97 ± 15.05 years during the same

TABLE 1 | The etiologic distribution of 856 dizziness/vertigo patients during the COVID-19 epidemic.

Diagnosis	*n* (%)
BPPV	300 (35)
psychogenic/PPPD	296 (34.6)
Vascular vertigo	82 (9.6)
VM	33 (3.9)
VN	6 (0.7)
MD	8 (0.9)
SSHL accompanied by vertigo	9 (1.1)
Systemic disease	74 (8.6)
VP	5 (0.6)
Other causes	43 (5)

COVID-19, coronavirus disease 2019; BPPV, benign paroxysmal positional vertigo; VM, vestibular migraine; VN, vestibular neuritis; MD, Mènière's disease; SSHL, sudden sensorineural hearing loss; VP, vestibular paroxysmia.

period in 2019. There is no statistically significant difference in age ($p = 0.20$).

During the epidemic period, BPPV was the most common cause, accounting for 35%, followed by psychogenic/PPPD (34.6%), and vascular vertigo (9.6%). These three diseases comprised 79.2% of all disorders. Notably, BPPV and psychogenic/PPPD accounted for nearly half of all disorders (see **Table 1**).

The overall etiology distribution was different among all disorders between the two periods ($p < 0.001$). There was an increase in BPPV (2019 vs. 2020: 30.7 vs. 35%, $p < 0.05$) and psychogenic/PPPD (2019 vs. 2020: 28.5 vs. 34.6%, $p < 0.05$) while a decrease in vascular vertigo during the epidemic (2019 vs. 2020: 13 vs. 9.6%, $p < 0.05$). In addition, the distribution of VM, VN, MD, sudden deafness with dizziness, dizziness caused by systemic diseases, VP, and other causes did not show a significant difference in the two-period comparison ($p > 0.05$) (see **Figure 1**).

Sex Stratification of the Causes of Dizziness/Vertigo During Coronavirus Disease 2019

The sex ratio was significantly different among all disorders ($p < 0.001$). A female predominance was observed in BPPV (women = 67.7%, $p < 0.05$) and psychogenic/PPPD (women = 67.6%, $p < 0.05$). In contrast, the sex ratio of other causes did not show a significant difference ($p > 0.05$) (see **Figure 2**).

Age Stratification of the Causes of Dizziness/Vertigo During Coronavirus Disease 2019

Our data showed that among all the causes, the patients with vascular vertigo were the oldest (56.52 ± 14.21), while those with VM were the youngest (48.79 ± 12.70). All patients were divided into four groups according to their age, namely, young (18–44 years old), middle-aged (45–59 years old), young-old (60–75 years old), and old-old (over 75 years old) groups. The etiology of 856 patients was stratified by age, and it was found that the etiology ratio of different age groups was significantly different ($p < 0.001$). The most common cause of young was BPPV, the most common cause of middle-aged was psychogenic/PPPD, the most common cause of young-old was BPPV, and the most common cause of old-old was psychogenic/PPPD (see **Figure 3**).

DISCUSSION

To our knowledge, this is the first study to examine the change in dizziness/vertigo outpatients in a neurological clinic. Our data showed a profound decrease in the number of neurology clinic visitors during the peak of the COVID-19 pandemic, paralleling a corresponding decline in the absolute number of dizziness/vertigo patients. Similar changes can also be observed in other neurological diseases. Many reports indicated that the COVID-19 outbreak impacted stroke care significantly all over the world, including a significant drop in acute stroke care, TIA, intravenous thrombolysis, and intracerebral hemorrhages (9–11). Fear of COVID-19 infection when visiting the hospital reduced the frequency of patients seeking medical help during the pandemic, and most patients opted for remote medical platforms for consultation. Besides, after the lockdown of Wuhan, strict isolation measures were implemented in Beijing, and the availability of traffic was also severely restricted. Meanwhile, social isolation may also have reduced the chance of identifying dizziness/vertigo among relatives and friends.

BPPV and psychogenic/PPPD are common causes of dizziness, and the reason for their relative increase in the early period of the COVID-19 outbreak lies in people's psychological stress response to the epidemic, resulting in emotional abnormalities such as anxiety/depression, insomnia, and acute stress. Shi et al. found that in the initial stage of the epidemic, among the Chinese population, depression accounted for 27.9%, anxiety 31.6%, insomnia 29.2%, and acute stress 24.4% (12). Xiang et al. also showed that major public health events or disasters, such as severe acute respiratory syndrome, bird flu, and Wenchuan earthquake, lead to a significant increase in the incidence of emotional problems during and after the occurrence (13). Meanwhile, a previous research revealed that anxiety and depression are common among patients with BPPV, and mood disorders increase the risk of the incidence of BPPV regardless of any gender and age (14, 15). Furthermore, from both anatomical and functional points of view, widespread vestibular projections to networks are involved in emotional processing (16).

The relative decrease of vascular vertigo during the pandemic corresponded to the similar change in stroke vascular events. However, these data only include statistics of hospitalized and emergency patients (9–11). Our data referred to face-to-face outpatients with mild symptoms and patients with severe or acute illness who often visit the emergency department, resulting in fewer patients with vascular vertigo. In addition, vascular vertigo in this study was diagnosed with not only TIA and stroke but also small cerebral vascular disease. A growing number of studies have found that unexplained dizziness, especially in the elderly, is often attributed to small cerebral vascular disease (17, 18).

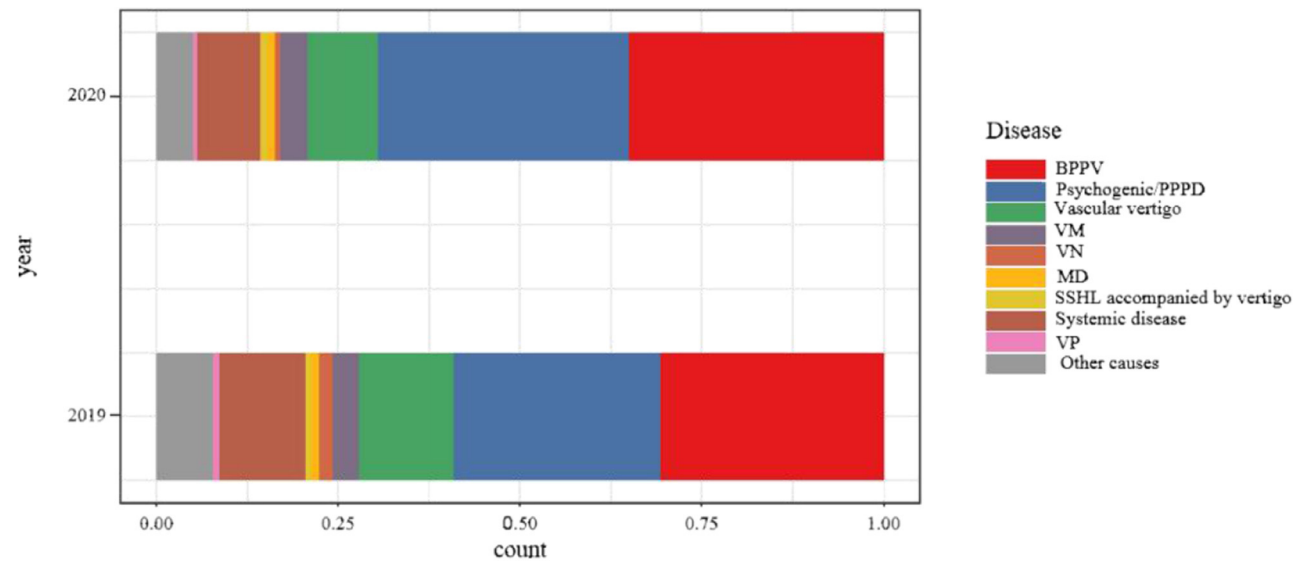

FIGURE 1 | Comparison of etiologic distribution of patients with dizziness/vertigo of the study period in 2019 and 2020.

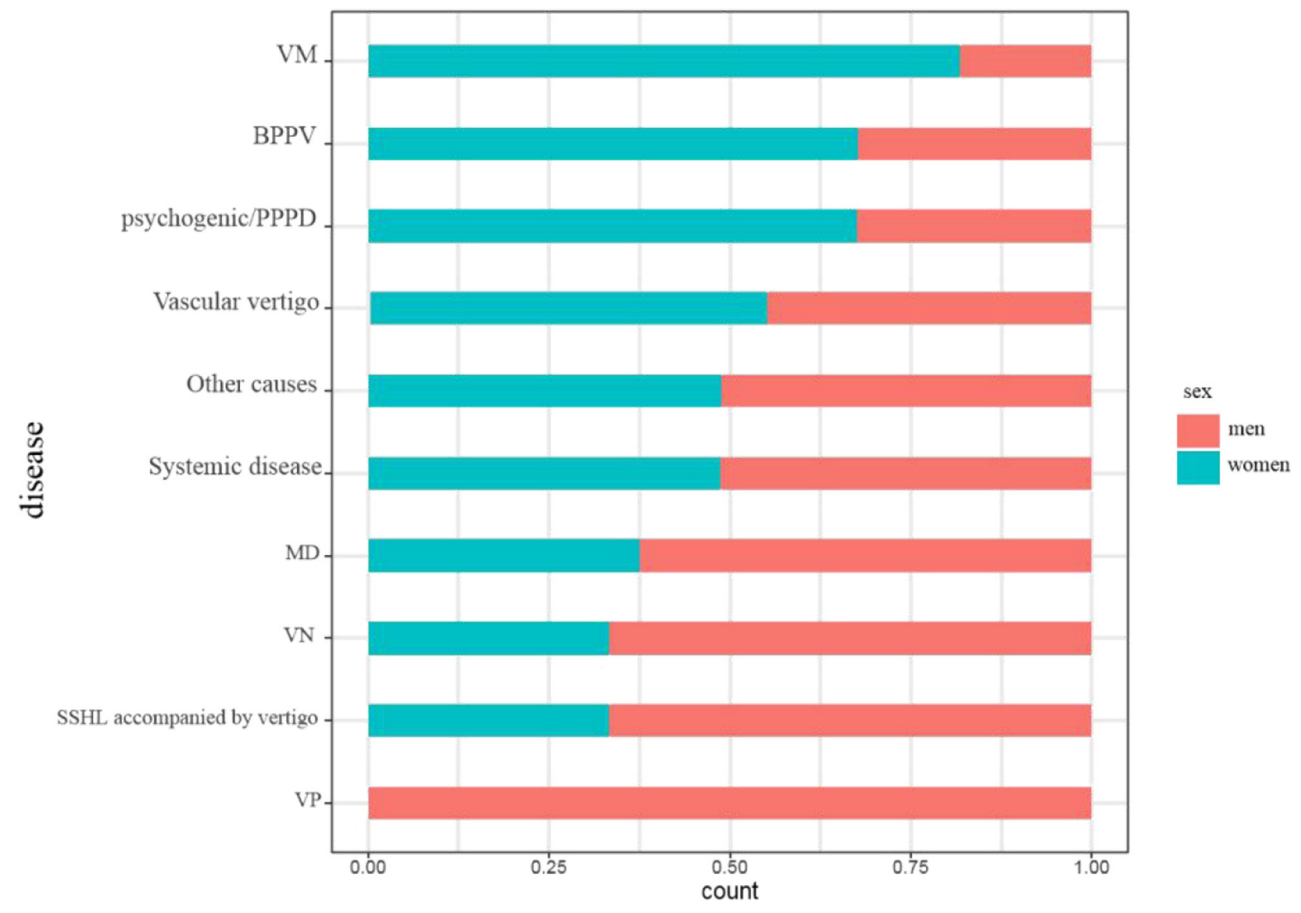

FIGURE 2 | The sex ratios of each cause during the coronavirus disease 2019 (COVID-19) epidemic.

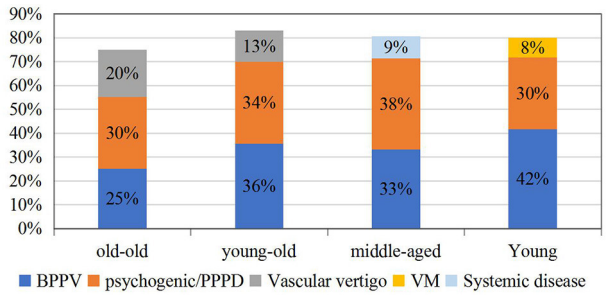

FIGURE 3 | The etiologic distribution of dizziness/vertigo by the age group during the coronavirus disease 2019 (COVID-19) epidemic.

In the case of vascular vertigo outpatients with confirmed or suspected stroke or TIA, epidemiological and fast-track COVID-19 screening was implemented. If intravenous thrombolysis is needed, the stroke team went into action to quickly initiate an optimal treatment plan and in-hospital consultation. Patients with confirmed or suspected COVID-19 infection should be isolated in the negative pressure carrier isolators and should undergo a special examination to determine risk–benefit ratio if intravenous thrombolysis and mechanical thrombectomy are initiated. Patients with non-COVID-19 infection must then be admitted to an isolated ward in the emergency department for intravenous thrombolysis. When mechanical thrombectomy is required, if the patient is diagnosed as confirmed or suspected COVID-19 infection by fast-track tests and the multidisciplinary team consultation, weighing the potential risks and benefits of treatment is essential, and patients with non-COVID-19 infection should follow routine surgical procedures and be admitted to the buffer ward after the operation, which was set up by the administrator of our hospital.

The low number of VN was remarkable in this study. At present, VN accounts for 0.5–9.0% in the vertigo clinic of the neurology department in China (19). Due to the lack of epidemiological data, insufficient understanding, and possible research selection bias, the incidence of this disorder may be underestimated. In addition, VN is characterized by rapid onset and long duration, so patients with VN are more likely to go to the emergency department for treatment, resulting in low incidence in the outpatient clinics.

Our data described a female preponderance among patients with dizziness/vertigo especially in BPPV and psychogenic/PPPD, which is in line with previous studies (20–22). The reason for the sex difference may be related to hormonal changes, differences in structure in the peripheral vestibular system, gender-based comorbidity, and so on (23, 24). Unfortunately, no sex difference was observed in vascular vertigo.

In addition to sex, age is also an important factor in the etiology of dizziness/vertigo. The causes of dizziness/vertigo at different ages had their characteristics. This study revealed that BPPV and psychogenic/PPPD were most prevalent in all disorders across all age groups during the COVID-19 epidemic, which is inconsistent with previous studies, especially in the old-old group (20, 25). The reason for this change might be the special stress caused by the epidemic. For the old-old, the social isolation during the epidemic posed a "serious public health problem" because it put them at greater risks of cardiovascular disease, autoimmune, neurocognitive, and mental health problems. Armitage et al. found that social isolation confronts the old-old with greater risks of depression and anxiety (26), so the incidence of BPPV and psychogenic/PPPD in the old-old group was also high.

It is well-known that the prevalence of BPPV increases with age (15, 20). Our data discovered that in the young (18–44 years old), BPPV (42%) was the most common, followed by PPPD. Recently, several studies have focused on the association of BPPV with the levels of 25(OH)D (27, 28), so its prevalence could be explained by lower 25(OH)D levels of both males and females aged <40 years in BPPV. Moreover, anxiety during the epidemic in the young increased the risk of BPPV (13).

This research has certain shortcomings. First of all, the data were a summary of neurological outpatients, so their characteristics may be different from those of general practice, otolaryngology, emergency, and other outpatients. Second, due to the lack of a sound general practitioner system in my country, a large number of patients with mental disorders related to dizziness visit the neurology department, which may be different from the results analyzed by foreign neurology and otolaryngology clinics. And lastly, although our center is a tertiary hospital in western Beijing, this study was a single-center study, which may be less representative.

CONCLUSION

In short, we found a profound decline in the absolute numbers of outpatients with dizziness/vertigo in the neurological clinic during the COVID-19 pandemic. The etiological distribution of dizziness/vertigo during this period was different from that of the corresponding period in 2019. BPPV and psychogenic/PPPD were more abundant, and vascular vertigo was less frequent. Given the high incidence of BPPV and psychogenic/PPPD in the neurological clinic, clinicians should pay attention to the identification of these two causes, as well as the emotional disorders as a triggering factor that are likely to be caused by the epidemic. Maybe it is necessary to develop measures to improve health management of dizziness/vertigo and enhance mental health management during the outbreak of COVID-19 and other infective diseases.

DATA AVAILABILITY STATEMENT

The raw data supporting the conclusions of this article will be made available by the authors, without undue reservation.

ETHICS STATEMENT

The studies involving human participants were reviewed and approved by Beijing Chaoyang Hospital. The

patients/participants provided their written informed consent to participate in this study.

AUTHOR CONTRIBUTIONS

LZ, ML, and CL conceived and designed the study. CL, DG, and SL performed the study. XM and CL analyzed the data. CL wrote the paper. All authors reviewed and revised the manuscript critically for important intellectual content. All authors read and approved the final manuscript.

ACKNOWLEDGMENTS

Thanks to Professor Xiaokun Qi (from the Sixth Medical Center of PLA General Hospital) for the guidance.

REFERENCES

1. von Brevern M, Bertholon P, Brandt T, Fife T, Imai T, Nuti D, et al. Benign paroxysmal positional vertigo: diagnostic criteria Consensus document of the Committee for the classification of vestibular disorders of the Bárány society. *Acta Otorrinolaringol Esp*. (2017) 68:349–60. doi: 10.1016/j.otorri.2017.02.007
2. Staab JP, Eckhardt-Henn A, Horii A, Jacob R, Strupp M, Brandt T, et al. Diagnostic criteria for persistent postural-perceptual dizziness (PPPD): Consensus document of the committee for the classification of vestibular disorders of the bárány society. *J Vestib Res.* (2017) 27:191–208. doi: 10.3233/VES-170622
3. Choi KD, Kim JS. Vascular vertigo: updates. *J Neurol.* (2019) 266:1835–43. doi: 10.1007/s00415-018-9040-3
4. Lempert T, Olesen J, Furman J, Waterston J, Seemungal B, Carey J, et al. Vestibular migraine: diagnostic criteria. *J Vestib Res.* (2012) 22:167–72. doi: 10.3233/VES-2012-0453
5. Strupp M, Magnusson M. Acute unilateral vestibulopathy. *Neurol Clin.* (2015) 33:669–85. doi: 10.1016/j.ncl.2015.04.012
6. Lopez-Escamez JA, Carey J, Chung WH, Goebel JA, Magnusson M, Mandalà M, et al. Diagnostic criteria for Menière's disease. *J Vestib Res.* (2015) 25:1–7. doi: 10.3233/VES-150549
7. Schreiber BE, Agrup C, Haskard DO, Luxon LM. Sudden sensorineural hearing loss. *Lancet.* (2010) 375:1203–11. doi: 10.1016/S0140-6736(09)62071-7
8. Strupp M, Lopez-Escamez JA, Kim JS, Straumann D, Jen JC, Carey J, et al. Vestibular paroxysmia: diagnostic criteria. *J Vestib Res.* (2016) 26:409–15. doi: 10.3233/VES-160589
9. Zhao J, Li H, Kung D, Fisher M, Shen Y, Liu R. Impact of the COVID-19 epidemic on stroke care and potential solutions. *Stroke.* (2020) 51:1996–2001. doi: 10.1161/STROKEAHA.120.030225
10. Sacco S, Ricci S, Ornello R, Eusebi P, Petraglia L, Toni D. Reduced admissions for cerebrovascular events during COVID-19 outbreak in Italy. *Stroke.* (2020) 51:3746–50. doi: 10.1161/STROKEAHA.120.031293
11. Nogueira R, Abdalkader M, Qureshi MM, Frankel MR, Mansour OY, Yamagami H, et al. EXPRESS: global Impact of the COVID-19 pandemic on stroke hospitalizations and mechanical thrombectomy volumes. *Int J Stroke.* (2021) 29;1747493021991652. doi: 10.1177/1747493021991652
12. Shi L, Lu ZA, Que JY, Huang XL, Liu L, Ran MS, et al. Prevalence of and risk factors associated with mental health symptoms among the general population in China during the coronavirus disease 2019 Pandemic. *JAMA Netw Open.* (2020) 3:e2014053. doi: 10.1001/jamanetworkopen.2020.14053
13. Xiang YT, Yang Y, Li W, Zhang L, Zhang Q, Cheung T, et al. Timely mental health care for the 2019 novel coronavirus outbreak is urgently needed. *Lancet Psychiatr.* (2020) 7:228–9. doi: 10.1016/S2215-0366(20)30046-8
14. Chen ZJ, Chang CH, Hu LY, Tu MS, Lu T, Chen PM, et al. Increased risk of benign paroxysmal positional vertigo in patients with anxiety disorders: a nationwide population-based retrospective cohort study. *BMC Psychiatr.* (2016) 16:238. doi: 10.1186/s12888-016-0950-2
15. Kim SK, Hong SM, Park IS, Lee HJ, Park B, Choi HG. Mood disorders are associated with increased risk of BPPV: a national sample cohort. *Laryngoscope.* (2021) 131:380–5. doi: 10.1002/lary.28638
16. Hitier M, Besnard S, Smith PF. Vestibular pathways involved in cognition. *Front Integr Neurosci.* (2014) 8:59. doi: 10.3389/fnint.2014.00059
17. Ahmad H, Cerchiai N, Mancuso M, Casani AP, Bronstein AM. Are white matter abnormalities associated with "unexplained dizziness"? *J Neurol Sci.* (2015) 358:428–31. doi: 10.1016/j.jns.2015.09.006
18. Kaski D, Rust HM, Ibitoye R, Arshad Q, Allum JHJ, Bronstein AM. Theoretical framework for "unexplained" dizziness in the elderly: The role of small vessel disease. *Prog Brain Res.* (2019) 248:225–40. doi: 10.1016/bs.pbr.2019.04.009
19. Chinese Medical Doctor Association Stroke and Vertigo Branch, Chinese Stroke Association. Multidisciplinary experts consensus on vestibular neuritis. *Chin J Geriatr.* (2021) 39:985–94. doi: 10.1097/CM9.0000000000000064
20. Kim HJ, Lee JO, Choi JY, Kim JS. Etiologic distribution of dizziness and vertigo in a referral-based dizziness clinic in South Korea. *J Neurol.* (2020) 267:2252–9. doi: 10.1007/s00415-020-09831-2
21. Chang J, Hwang SY, Park SK, Kim JH, Kim HJ, Chae SW, et al. Prevalence of dizziness and associated factors in south korea: a cross-sectional survey from 2010 to 2012. *J Epidemiol.* (2018) 28:176–84. doi: 10.2188/jea.JE20160113
22. Adamec I, Juren Meaški S, Krbot Skorić M, JaŽić K, Crnošija L, Milivojević I, et al. Persistent postural-perceptual dizziness: Clinical and neurophysiological study. *J Clin Neurosci.* (2020) 72:26–30. doi: 10.1016/j.jocn.2020.01.043
23. Ogun OA, Janky KL, Cohn ES, Büki B, Lundberg YW. Gender-based comorbidity in benign paroxysmal positional vertigo. *PLoS ONE.* (2014) 9:e105546. doi: 10.1371/journal.pone.0105546
24. Jeong SH. Benign paroxysmal positional vertigo risk factors unique to perimenopausal women. *Front Neurol.* (2020) 11:589605. doi: 10.3389/fneur.2020.589605
25. Pan Q, Zhang Y, Long T, He W, Zhang S, Fan Y, et al. Diagnosis of vertigo and dizziness syndromes in a neurological outpatient clinic. *Eur Neurol.* (2018) 79:287–94. doi: 10.1159/000489639
26. Armitage R, Nellums LB. COVID-19 and the consequences of isolating the elderly. *Lancet Public Health.* (2020) 5:e256. doi: 10.1016/S2468-2667(20)30061-X
27. Song P, Zhao X, Xu Y, Zhao Z, Wang L, Liu Y, et al. Correlation between benign paroxysmal positional vertigo and 25-hydroxyvitamin D. *Front Neurol.* (2020) 11:576. doi: 10.3389/fneur.2020.00576
28. Jeong SH, Kim JS, Kim HJ, Choi JY, Koo JW, Choi KD, et al. Prevention of benign paroxysmal positional vertigo with vitamin D supplementation: a randomized trial. *Neurology.* (2020) 95:e1117–25. doi: 10.1212/WNL.0000000000010343

Conflict of Interest: The authors declare that the research was conducted in the absence of any commercial or financial relationships that could be construed as a potential conflict of interest.

frontiers in Neurology

REVIEW
published: 14 May 2021
doi: 10.3389/fneur.2021.646640

The Importance of Being in Touch

*James R. Lackner**

Ashton Graybiel Spatial Orientation Laboratory, Brandeis University, Waltham, MA, United States

This paper describes a series of studies resulting from the finding that when free floating in weightless conditions with eyes closed, all sense of one's spatial orientation with respect to the aircraft can be lost. But, a touch of the hand to the enclosure restores the sense of spatial anchoring within the environment. This observation led to the exploration of how light touch of the hand can stabilize postural control on Earth even in individuals lacking vestibular function, and can override the effect of otherwise destabilizing tonic vibration reflexes in leg muscles. Such haptic stabilization appears to represent a long loop cortical reflex with contact cues at the hand phase leading EMG activity in leg muscles, which change the center of pressure at the feet to counteract body sway. Experiments on dynamic control of balance in a device programmed to exhibit inverted pendulum behavior about different axes and planes of rotation revealed that the direction of gravity not the direction of balance influences the perceived upright. Active control does not improve the accuracy of indicating the upright vs. passive exposure. In the absence of position dependent gravity shear forces on the otolith organs and body surface, drifting and loss of control soon result and subjects are unaware of their ongoing spatial position. There is a failure of dynamic path integration of the semicircular canal signals, such as occurs in weightless conditions.

Keywords: non-orientation, dynamic balance, position cues, path integration, vestibular loss, velocity storage, spatial orientation, vehicle control

OPEN ACCESS

Edited by:
Michael Strupp,
Ludwig Maximilian University of Munich, Germany

Reviewed by:
Marco Schieppati,
Istituti Clinici Scientifici Maugeri (ICS Maugeri), Italy
Diego Manzoni,
University of Pisa, Italy
John Allum,
University of Basel, Switzerland

***Correspondence:**
James R. Lackner
lackner@brandeis.edu

Specialty section:
This article was submitted to Neuro-Otology, a section of the journal Frontiers in Neurology

Received: *27 December 2020*
Accepted: *07 April 2021*
Published: *14 May 2021*

Citation:
Lackner JR (2021) The Importance of Being in Touch. Front. Neurol. 12:646640. doi: 10.3389/fneur.2021.646640

INTRODUCTION

The studies described below had an unexpected starting point. I was working with Ashton Graybiel to determine the etiological factors causing motion sickness in the weightless conditions of orbital space flight. We were looking at the provocativeness of different types of head movements in the weightless and high g force phases of parabolic flight maneuvers. During the weightless phases, I would often free float to observe that subjects were carrying out their head movements appropriately. One day when free floating without any contact with the aircraft, when I closed my eyes, within seconds my sense of orientation to the aircraft disappeared. I could sense the relative configuration of my body, and cognitively I knew my spatial position in relation to the fuselage of the aircraft; but, I no longer felt being in any orientation. I had lost the sense of spatial anchoring that we normally have on Earth to our spatial context. However, when I touched the wall of the aircraft with one hand, the sense of my spatial position within the aircraft was restored. On removing hand contact, within a second or two, I was again anchorless. I was not spatially disoriented, instead I was "non-oriented." We confirmed these observations with multiple subjects in later parabolic flight studies (1, 2).

I also found that when I walked on the deck of the aircraft during the high g phases of parabolic flight, it seemed unstable and my movements felt abnormal. I probed this instability by doing shallow deep knee bends during exposure to 1.8 g acceleration levels. I found that this elicited

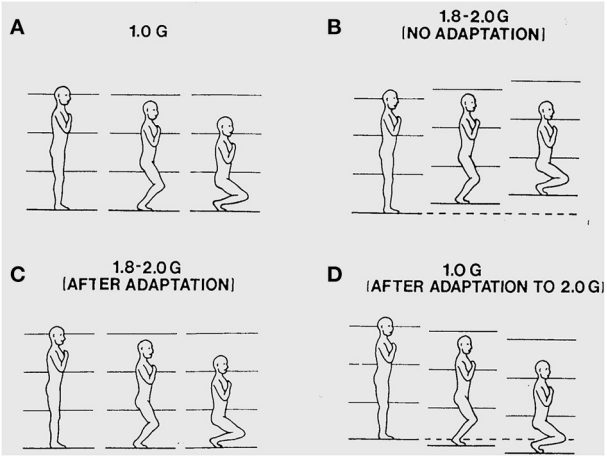

FIGURE 1 | (A) Illustration of a deep knee bend made in 1 g. The surface of support and the visual surroundings are felt and seen to remain stationary as the body is lowered. **(B)** During a deep knee bend made during initial exposure to 1.8 g, it feels as if the knees have flexed too rapidly and the aircraft is seen and felt to displace upwards under the feet causing too rapid flexion of the knees. **(C)** Following about 50 deep knee bends made over subsequent parabolas, the deep knee bends again feel normal and the aircraft is seen and felt to be stable again as the body is lowered. **(D)** Following adaptation to 1.8 g, the initial deep knee bends made during 1 g straight-and-level flight again seem abnormal with the body seeming to move downward too slowly because the aircraft seems to move downward slowing the flexing of the legs.

powerful visual and postural illusions. During the body lowering phase, it would seem as if my body had moved downward too rapidly in relation to the deck of the aircraft and that simultaneously the aircraft had moved vertically upward causing unexpectedly rapid bending of my knees. The apparent upward motion of the aircraft seemed greater when I closed my eyes. After I made repeated deep knee bends with eyes open during subsequent parabolas, adaptation occurred and the illusions abated. But, then, on return to 1 g conditions in straight and level flight, deep knee bends elicited illusions of opposite sign that then gradually abated with additional deep knee bends. Graybiel and I systematically replicated these observations experimentally. The results are illustrated in **Figure 1** and show the initial illusory movements before adaptation and the aftereffects experienced upon returning to 1 g conditions after having adapted to 1.8 g. These findings indicate that sensory-motor control and perception of our body movements are dynamically adjusted to the force background of Earth gravity (3).

In later parabolic flight studies, Paul DiZio and I found out that if we made finger contact with a nearby surface when making deep knee bends during exposure to 1.8 g, the illusory visual and postural motions normally elicited were suppressed. The illusions returned as soon as finger contact was broken (2). These two sets of findings were critical: 1) loss of a sense of orientation when free floating with eyes closed that is restored by hand contact, and 2) illusions of self-motion and aircraft motion elicited during deep knee bends in a 1.8 g force background that are eliminated by hand contact with an aircraft-fixed surface. They led us to explore whether light touch contact might stabilize balance during upright stance under normal 1 g conditions.

LIGHT TOUCH STABILIZATION OF POSTURAL CONTROL

In our first study, we measured body sway parameters for one-legged stance with and without visual cues, and with light touch or force touch of the index finger of the right hand with a laterally placed force plate. We limited light touch to a maximum of 1 N (<100 g) because biomechanical modeling of the subject's posture and arm configuration and applied finger tip forces showed this would be mechanically inadequate to attenuate body sway. No-touch conditions were included in addition to the light-touch and force-touch (ad lib as much force as the subject desired). The results showed that touch of the finger had a major effect (4). Subjects in their light-touch conditions were much more stable than in the no-touch conditions. Moreover, they spontaneously adopted an average contact force of ≈40 g. This value is interesting because Johansson and Westling earlier had shown that variations about this level lead to the largest modulation of firing activity in the tactile receptors in the fingertips of the thumb and index finger that are involved in the control of precision grip. During precision grip when a held object begins to slip, a long loop cortical reflex is elicited that adjusts grip forces within 125 ms (less than a voluntary reaction time) to stabilize the object (5, 6).

Force levels subjects adopted for light touch and ad lib force touch were ≈0.4 N (40 g) and 5–8 N, respectively. Light touch of the hand with vision stabilized the body somewhat more than with vision alone. The applied forces in the ad lib fingertip force condition were adequate to allow some mechanical stabilization according to our mathematical modeling but not to the extent actually observed. These observations together led us to hypothesize that light touch stabilization was the result of a long loop cortical reflex with the finger and the feet providing the contact surfaces of a pincer grip, with the feet serving as the "thumb" of the pincer (4). The results of this early study led us to explore the range of conditions under which non-supportive light touch of the hand can influence postural control. Only a sub-set of these studies can be described here. **Figure 2** illustrates the typical test configuration. Test subjects would stand on a force plate in a heel to toe sharpened Romberg stance. A stand with a force plate was positioned to the subject's right side so that contact could be made with the right index finger in trials involving finger contact. In light-touch trials, an alarm would be sounded were the subject to apply more than 100 g to the touch surface. Before experimental data were collected, subjects would press on the plate to see how much force was necessary to trigger the alarm. Measures included mean sway amplitude, mean sway velocity, and power spectral density plots of sway as well as mean finger applied forces. All conditions referred to below as being different are statistically different by at least $p < 0.01$. The studies described below include: EMG evidence for light touch stabilization representing a long loop cortical reflex, finger force levels adequate for stabilization, time course of stabilization

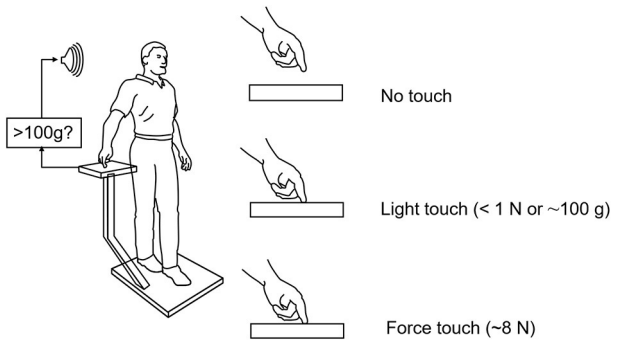

FIGURE 2 | Typical test situation for our light-touch stabilization of posture studies. The alarm sounds when the force on the finger touch plate exceeds 1 N (≈103 g). Subjects in practice never reach this force level in their experimental trials. The alarm is off during force touch trials.

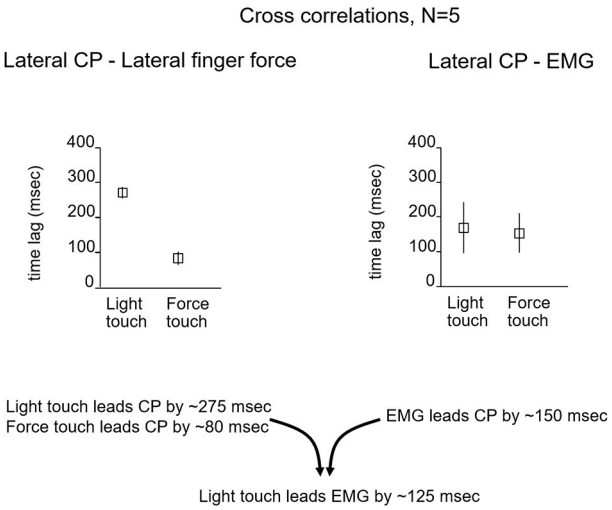

FIGURE 3 | The relationship between the lateral CP and fingertip force changes and EMG activity that leads to CP changes. For light-touch, force changes at the fingertip lead EMG activity by 125 ms and CP changes by ≈275 ms. The EMG reflects muscle activation that 150 ms later alters the CP to counteract body sway. With force touch, changes in applied finger force lead CP changes by ≈80 ms, indicating some mechanical stabilization by the finger force level.

following finger contact, resistance to perturbations, entrainment of sway to a moving contact surface, and stabilization of balance of individuals without functioning labyrinths.

Light Touch Stabilization of Posture Represents a Long Loop Cortical Reflex

To evaluate the possibility of a long-loop cortical reflex being involved, John Jeka and I looked at the relationship between force contact changes during light touch of the fingertip, the center of pressure (CP) under the two feet, and EMG activity in the peroneus longus muscles. The subjects ($N = 5$) were blindfolded and in a heel-to-toe (sharpened Romberg) stance. Force changes at the fingertip during light touch led by 125 ms the EMG activity in the peroneus muscles that 150 ms later produced changes in the CP to attenuate sway as shown in **Figure 3**. This pattern persisted throughout the balance task and was analogous to the long loop cortical reflexes modulating precision grip control that are elicited when an object held in a pincer grip begins to slip. The difference in force generation latency between precision grip adjustments and postural control is related to the longer latency to control the mass of the body vs. that of the fingers (7, 8). Force touch led CP changes by 80 ms indicating that the force touch was mechanically adequate to attenuate sway.

Finger Contact Thresholds for Touch Stabilization of Postural Sway

Our goal was to determine the lowest level of force contact with the right index finger that would provide postural stabilization. Subjects stood with eyes closed, heel-to-toe, on a force plate while holding their right hand over a laterally placed touch plate. Von Frey filaments that are used to test tactile sensitivity in the clinic (9) or a rigid metal filament 1 mm in diameter would be mounted vertically on the hand touch plate. The Von Frey filaments had buckling values of 10, 35, and 85 g. Conditions were run in which the subjects touched the Von Frey filaments with and without enough force to bend the filaments, made finger contact with a flat surface, or held their finger as steady as possible just above the touch plate. **Figure 4** illustrates the test results for no-touch condition, touching the 10 g filament, the rigid metal filament, and the flat surface, the latter two conditions were most effective in attenuating body sway and applied force levels hovered about 40 g. Holding the finger as steady as possible in imagined contact with a location just above the touch plate was the least stable condition. The Von Frey filaments all attenuated sway relative to the no-touch imagined contact condition. The non-bent filaments reduced sway more than the bent filaments of the same diameter. The bent filaments reduced sway magnitude such that sway never exceeded the range that would have led to a shift of the filament's contact point with the fingertip. Force levels of 10 g on our most slender Von Frey filament produced significant sway attenuation relative to the imagined contact condition. In all touch conditions, force changes at the finger led changes in CP by ≈300 ms (10).

Time Course of Postural Stabilization After Fingertip Contact

As our studies of haptic stabilization progressed we began thinking about potential haptic aids for enhancing the balance control of individuals at risk for falling. A key issue was how long would it take after touch contact was made for stabilization to begin. We tested blindfolded subjects in the heel-to-toe stance. They started a trial with their right index finger just above the laterally positioned touch force plate. Half-way through 25 s long trials they were cued to lower their finger to make contact. We found that the fingertip became fully settled on the plate to

apply a force of ≈0.4 N with a time constant of ≈4 s. Mean sway amplitude of the body upon finger contact decreased by 50% with a time constant of 1.6 s (**Figure 5**). Importantly, within 500 ms after initial finger contact, correlated changes in the CP began to lag fingertip force fluctuations by 275–300 ms, even though the finger was not yet stabilized in position (11).

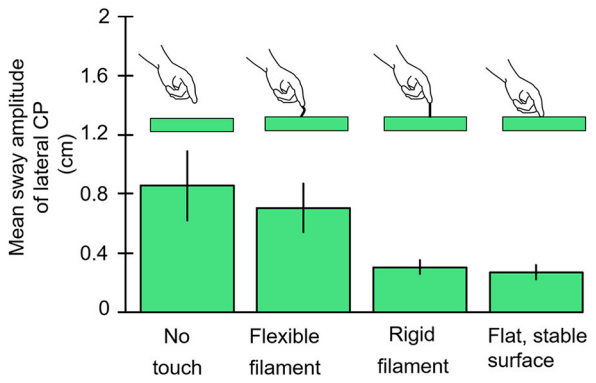

FIGURE 4 | The results are illustrated for the no-contact, von Frey Filament with 10 g bending resistance, rigid metal filament, and light-touch finger conditions. The von Frey filaments with larger bending constants are not shown but all attenuate sway more than the 10 g filament. The rigid filament and finger touch attenuate CP mean sway amplitude more than other conditions.

Tactile Suppression of Postural Destabilization Induced by Tonic Vibration Reflexes

We also wondered whether an haptic cue from the hand would enhance postural stability in the face of perturbations. Our approach was to make use of tonic vibration reflexes (TVRs). When a skeletal muscle's tendon is stimulated using a physiotherapy vibrator (circa 100–120 Hz), muscle spindle receptors are activated and elicit a reflexive contraction of the vibrated muscle (12, 13). Eklund (14) had induced backward sway and loss of balance in standing subjects by vibrating their Achilles tendons. We wondered whether light finger contact with a stationary surface could overcome the destabilizing effects of leg muscle vibration and also whether vibrating the biceps muscle of the right arm of subjects making light touch with their right index finger would destabilize them.

Figure 6 illustrates the test conditions and summarizes the experimental findings. The leg vibration conditions included: no-touch and no-vibration, touch and no-vibration, no-touch

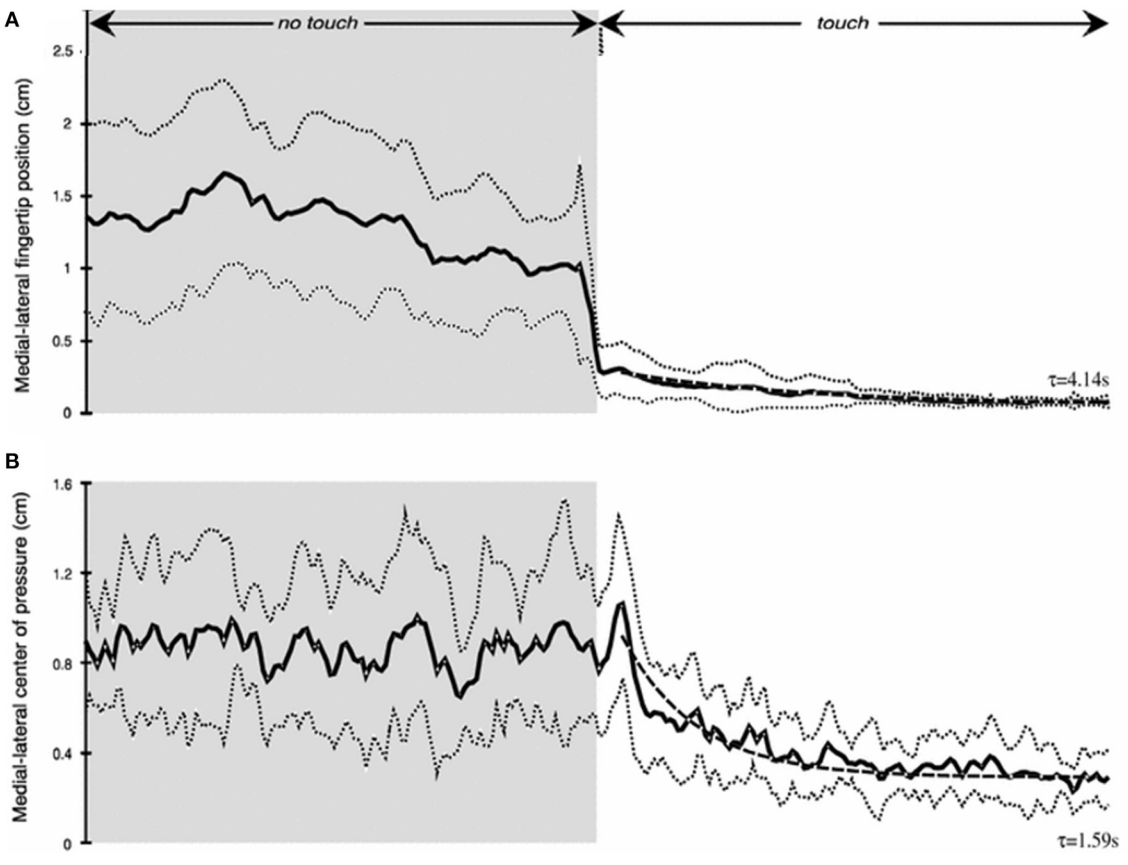

FIGURE 5 | Time course of haptic stimulation after finger contact is made ≈ 12 s into 25 s long trial. **(A)** shows medial-lateral finger position (cm) and **(B)** medial-lateral center of pressure (cm). Note rapid decrease in sway even prior to full finger stabilization.

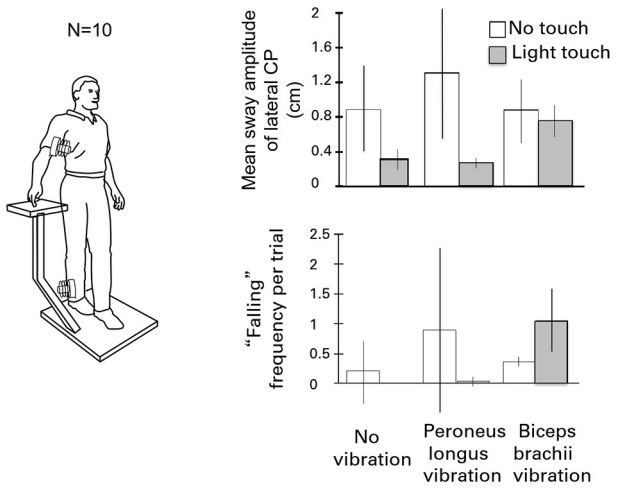

FIGURE 6 | The effects of eliciting tonic vibration reflexes in the peroneus longus muscle of the standing subject's right leg or in the biceps of the right arm are shown for the different touch conditions. Vibrating the peroneus longus destabilizes subjects and can evoke falling. Light touch fully eliminates the effect. By contrast, during light-touch, biceps vibration is destabilizing and can induce falling or protective stepping.

and vibration, touch and vibration. Subjects had their eyes closed during the trials. Vibration involved stimulation of the right peroneus brevis and longus muscles at 120 Hz to elicit tonic vibration reflexes. The results were striking. The touch and vibration and touch and no-vibration conditions were not significantly different for any sway measure and were vastly superior to the no-touch and no-vibration and no-touch and vibration conditions. Importantly, in the touch and vibration condition, many of the subjects reported that it felt as though the vibrator on their leg had not been turned on. By contrast, in the no-touch and vibration condition, subjects often had to take a protective step to avoid falling (15).

In the parallel set of conditions for the influence of vibration of the biceps of the right arm on postural stability, the no-touch with vibration and touch with vibration conditions did not differ in mean sway amplitude from the control condition of no touch and no vibration. In addition, the incidence of "falling" or making a protective step, was increased when the biceps of the arm of the touching finger was vibrated to cause reflexive contraction. The forearm motion elicited by biceps vibration led to postural shifts to null the finger's displacement, sometimes eliciting lateral falling and stepping.

Entrainment of Sway to a Moving Touch Surface

We had found that finger contact with a stationary surface was a powerful stabilizer of posture, but we wondered how contact with a moving surface would affect sway when the subjects did not know the surface could move. We had subjects, with eyes closed, stand in a sharpened Romberg stance and make finger contact with a laterally placed surface at <100 g force. In a control condition the surface was stationary, in five other conditions it oscillated laterally at 0.1, 0.2, 0.3, 0.4, or 0.5 Hz at an amplitude of ≈4 mm. As shown in **Figure 7**, spectral analyses of head and body sway in relation to touch surface displacement frequency showed a close coupling with amplitude peaks at the frequency of motion of the touch surface. Touch forces applied to the surface were always <100 g and were comparable across all six test conditions. Modeling the postural control system as a second-order linear dynamical system led us to conclude that the velocity of the signal at the fingertip was key to the sway coupling (16). Jeka et al. (17) have further explored this coupling in conditions where stimulus velocity was maintained constant across different frequencies and found coupling to both displacement and velocity.

Haptic Stabilization of Posture in Individuals Without Vestibular Function

We were especially interested in whether people with loss of vestibular function could be aided by haptic cues. We knew that such individuals typically can stand heel-to-toe with eyes closed for only a few seconds without having to take a protective step. To evaluate the role of haptic cues, we tested five labyrinthine loss subjects. They ranged in age from 52 to 70 years, mean 59 years. Several had bilateral vestibular loss from streptomycin poisoning, another from an autoimmune disease, and one from progressive neural degeneration of unidentified etiology. All had been evaluated at the Vestibular Testing Laboratory at the Massachusetts Eye and Ear Infirmary in Boston. They were selected from a large group of patients with vestibular loss because they fell at the lowest end of the vestibular loss category of performance on semicircular canal, otolith, vestibulo-ocular, dynamic posturography, and visual-vestibular interaction tests. Their gains on the sinusoidal vertical axis rotation test (0.05 Hz) ranged from 0.017 to 0.169, with an average of 0.057. Responses to caloric irrigation were absent, as were responses to the head thrust test. Five age and sex matched control subjects were recruited from members of the Brandeis University staff. Their performance on all tests of vestibular function and balance were within the normal range.

The subjects were tested in the sharpened Romberg stance under eyes open and eyes closed conditions for each of three fingertip conditions: no contact, light contact (<100 g) with a laterally place surface, and ad lib force level contact. Safety railings surrounded the test setup. The control subjects did not lose balance in any test condition. All of the labyrinthine loss subjects ($N = 5$) lost balance within 5 s in the eyes closed no-touch condition and had to grasp the safety railings or take a protective step. By contrast, as shown in **Figure 8**, when allowed light touch contact, they were more stable with eyes closed than the normal subjects were with eyes closed and no finger contact. With eyes open and no touch, the labyrinthine loss subjects typically had to touch the safety railings several times for support during the 25 s duration trials. However, with eyes closed and light touch, they were more stable than they were in the eyes open no-touch condition. Both groups of subjects were most stable with eyes open and light touch. The ad lib touch force condition usually conferred the greatest stability for both groups. In the light-touch conditions, for all subjects force changes at

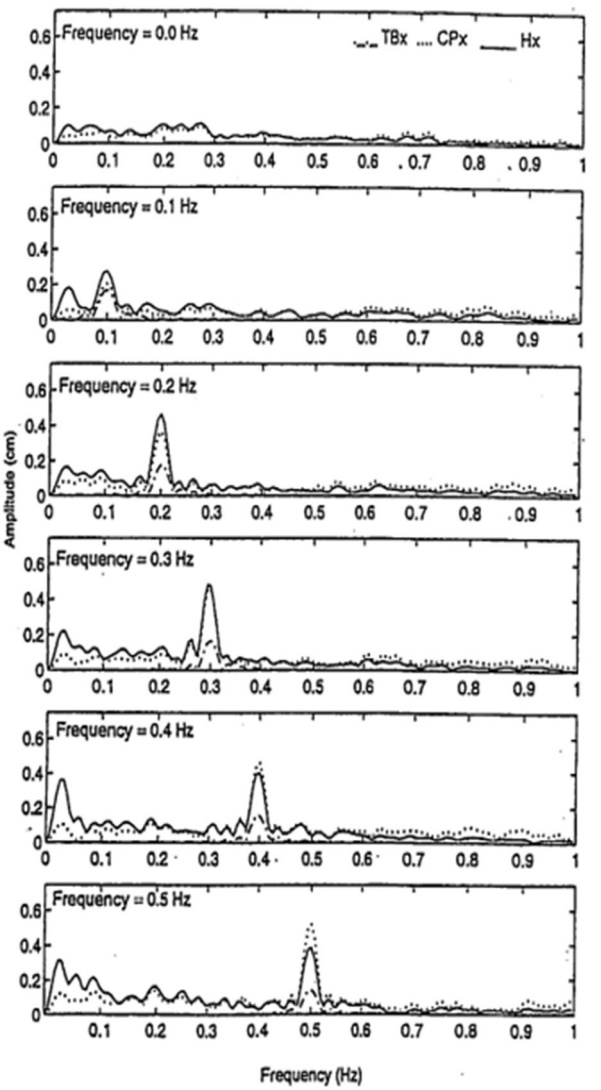

FIGURE 7 | Entrainment of body sway to cyclical lateral oscillations of the touch bar at frequencies of 0, 0.1, 0.2, 0.3, 0.4, and 0.5 Hz. TB_x = lateral motion (≈4 mm amplitude) of touch bar, CP_x = lateral motion of the center of pressure, and H_x = lateral head motion. Subjects ($n = 5$) show entrainment of head and center of pressure to the touch bar frequency of oscillation.

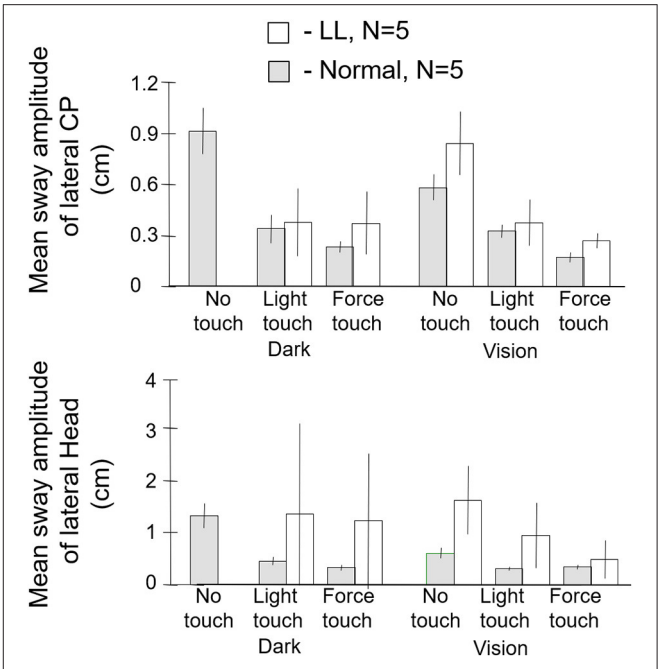

FIGURE 8 | Mean sway amplitude of center of pressure (CP), top panel, and of head, bottom panel of labyrinthine loss (LL), $N = 5$ and normal subjects, $N = 5$. There are no entries in the dark no-touch conditions for the LL subjects because they lose balance within several seconds. With light touch in the dark, the LL subjects have a significantly lower CP mean sway amplitude than the normal subjects in their no-touch vision condition.

the fingertip led changes in the CP by 250–300 ms (18). There is no entry in **Figure 8** for the labyrinthine loss subjects for the eyes closed, no-touch condition because they could not perform the task.

ALTERNATIVE INTERPRETATIONS

Our light touch studies elicited considerable interest as well as alternative interpretations. These included proposals that posture was stabilized to allow precise finger contact rather than the reverse (19). Other investigators provided evidence that passive touch was as effective as active touch in stabilizing posture (20, 21). We recently have completed work showing that when passive touch (100 g) is applied to the shoulder by a lever device attached to a force plate so that the instant of contact and change in contact force can be determined, within 500 ms, the force changes at the shoulder elicited by body sway lead by ≈300 ms changes in the CP to counteract the sway. Put differently, the cortical long loop reflex to stabilize sway is not confined to the finger but can be evoked by other parts of the body as well. When the passive probe is lifted from the shoulder, within 1 s postural sway increases despite attempts to be as stable as possible (Lackner et al., in preparation). Another earlier study manipulating stance configuration and the location of the touched surface showed that contact in the direction of body sway maximizes stabilization (22). Immobilizing the entire arm of the touching finger using a "Freedom Gunslinger" splint (AliMed, Dedham, MA) did not prevent contact of its finger with a stable surface from attenuating sway (23). Bove et al. (24) have shown that light touch suppresses the disorientation evoked by neck muscle vibration, just as it suppresses the effects of leg muscle vibration.

The touch stabilization paradigm has been extended by Wing and Johanssen in a number of very imaginative ways of potential use for rehabilitation and fall prevention. They have shown that interpersonal touch at very low force levels can be helpful in stabilizing older people's posture and gait (25–29). Sawers and Ting have shown how small inter-person forces can be used to

communicate goals and actions between individuals but also how they can be incorporated in the design of rehabilitation robots (30, 31).

CENTRAL CONTRIBUTIONS TO BALANCE CONTROL

The postural stabilization experienced by the labyrinthine loss subjects when provided light touch of the hand with a stable surface was an important finding for us, but it also presented a conundrum. In posture studies, the CP under the feet during quiet stance is often used as a proxy for the location of the body center of mass (CM), and the soles of the feet can be thought of as providing a map of the projection of the CM (32, 33). Normal subjects during quiet stance with eyes closed sway at velocities and magnitudes that can be near or just above vestibular detection thresholds. Why then are labyrinthine loss subjects unable to stand heel to toe for more than a few seconds when they close their eyes? Presumably, they have the same somatosensory cues from their feet about CM position as normal subjects do. We knew from our light-finger touch studies that they benefitted as much from sensory cues from the hand as normal subjects. Why then did not the soles of their feet convey similar benefit?

Karmali et al. have recently conducted the most comprehensive assessments of semicircular canal and otolith detection thresholds for all axes of rotation and translation yet carried out (34). Their apparatus was a 6 DOF motorized platform that subjects were seated on in the dark. They measured the smallest motion that subjects could reliably detect. They then correlated these thresholds with a variety of postural tests carried out on the same subjects. A key finding was that lateral translation thresholds were correlated with medial-lateral CP sway during passive stance; but, the other thresholds were not. They conclude that vestibular noise contributes to the magnitude of lateral postural sway because their threshold measurements also represent the magnitude of sensory noise. From this perspective, labyrinthine loss subjects would be expected to have larger postural sway.

Stoffregen and Riccio have made the important point that during upright stance on a horizontal surface the direction of balance coincides with the direction of gravity (35, 36). They posed the possibility that the perceived vertical corresponds with the direction of balance not that of gravity. To explore this idea they used a device programmed to behave like an inverted pendulum in roll. A subject would sit in it and use a joystick to set it to the "upright." This approach takes advantage of the fact that human passive stance is often modeled as a single link inverted pendulum (37), which is appropriate for their test situation. The novel feature of their device was that its direction of balance (DOB) could be offset from the direction of gravity (DOG). When the DOB is offset from that of the DOG, this means that when the device is at the DOG there is an acceleration driving it in the direction opposite the DOB. The DOB represents the position of dynamic equilibrium, rather than that of gravity as is normally the case in upright stance. In their studies, Stoffregen and Riccio had subjects set the device to the "upright" when its DOB corresponded with the DOG and when its DOB was displaced in the roll plane to the left or right of the DOG. With an offset DOB, in setting themselves to the upright their subjects maintained the average position of the device between the DOB and DOG. Consequently, it was concluded that the DOB influenced the perception of the upright and that it, rather than gravity, was key to the perceived upright (38).

We realized that a similar apparatus provided a means to separate peripheral mechanisms related to foot control in balance from central mechanisms, and could potentially provide insight into the conundrum we felt was posed by our labyrinthine loss subjects. "Peripheral" is meant here to include vestibulospinal reflexes and other leg muscle reflexes, as well as pressure distribution on the soles of the feet, the plantar map of the center of mass. This led us to develop a device that allowed us to look at more than one axis of rotation and plane of motion to assess central contributions to balance control. The advantages of our multiaxis rotation system (MARS) are that it can rotate about a pitch, roll, or yaw axis, singly or in combination, and that the plane of motion can be set to any desired angle in relation to the direction of gravity. Subjects seated in the MARS control it using a joystick. When subjects exceed $\pm 60^{\circ}$ from the instructed goal heading they are regarded as having "crashed" and the MARS is reset to its original start position and the trial continues. An important feature of the MARS is that its motion profile as generated by a subject actively controlling it can be recorded and then played back to the same or a different subject who sits in it and uses joystick trigger presses to indicate when he or she is at the instructed goal direction. **Figure 9** illustrates the MARS device configured for vertical roll plane balancing.

Direction of Balance vs. Direction of Gravity in Perception of the Upright

We first studied roll orientation to confirm the observations of Riccio et al. (38). In different trials, we asked blindfolded subjects to orient to the "upright," the DOB, or the DOG. In addition, we instructed subjects to press the joystick trigger whenever they were at or just passing through the intended goal. We found that when the DOB was offset from the DOG, settings to the upright were on average displaced past the DOG away from the DOB. However, trigger presses to indicate the perceived upright or the DOG closely coincided with the DOG. Settings to the DOB were on average about midway between the DOB and DOG, but trigger presses to indicate the DOB were closer to it. Thus, as shown in **Figure 10**, there was a discrepancy between the average orientation of the subject in the MARS to the goal orientations and the subject's trigger presses. To understand why this could be the case we looked at the relationship among joystick control inputs, the ongoing position of the MARS, and the joystick trigger presses in relation to the goal orientation. This analysis resolved the paradox. With an offset DOB, subjects trying to set the apparatus to the perceived upright were being exposed to a unidirectional acceleration that increased in magnitude as they got close to the DOG. To orient

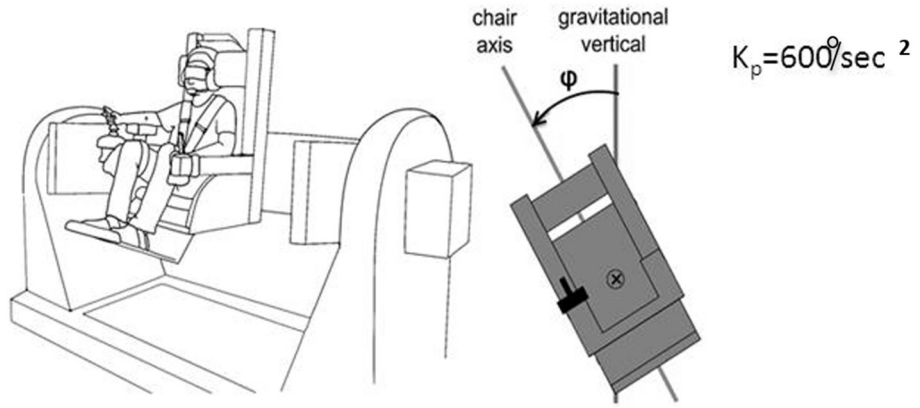

FIGURE 9 | Illustration of the MARS configured for vertical plane roll balancing. The axis of roll motion is indicated by the ⊗ symbol, the deviation from the gravitational vertical is angle φ. Kp = 600°/s^2 is the inverted pendulum constant.

to the DOG, subjects as they neared the DOG slowed the MARS motion and their trigger presses occurred when it was just at the DOG. They then eased off on the joystick and the MARS was again pushed away from the DOG in the direction opposite the DOB. In other words, the discrepancy relates to using a joystick to control the apparatus during exposure to an unidirectional acceleration that progressively increases near and beyond the DOG. To avoid going past the DOG in the direction of the DOB subjects try to reverse the device's direction just as they are nearing the DOG. Consequently, the average position of the device ends up being beyond the DOG and away from the DOB as a consequence of control rather than perceptual limitations (39). The direction of gravity, not that of balance, determines the perceived upright.

Perception of the Upright Is Not Enhanced by Active Control

We were also interested in whether active control influenced the ability of subjects to distinguish between the DOG and DOB when the DOB was offset from the DOG. To test this we recorded the motion of the MARS when subjects were actively controlling it and then played it back to subjects who rode in it "passively" and pressed the joystick trigger when they felt that they were at their goal orientation. The goal was to indicate the DOB, the DOG, or the "upright" depending on the active subject's task during the profile that was being played back to them. The findings were unequivocal: the trigger presses of the passive subjects for each goal condition were not significantly different from those of the active subjects. Together these results mean that subjects balancing in the apparatus or being passively transported in it identify the perceived upright with the DOG and can accurately indicate it (39).

Balancing With Diminished Gravity Dependent Positional Signals

We then asked what happens to balance performance when the roll plane is tilted backwards from the vertical so that the contribution of the otolith organs is progressively diminished. We realized that this provided an analog of weightless conditions in which the otolith organs do not provide signals about changing body orientation, but the semicircular canals will still be activated by angular accelerations. In this experiment, subjects were orienting to and indicating the DOB, which if the roll plane were vertical would correspond with the DOG. We tested a range of tilt-back roll plane angles and performance remained unchanged until about 55°, after which it rapidly diminished, until at 90° tilt back subjects showed cyclical or looping patterns of drifting and frequent crashes. At this body orientation the utricular planes are near parallel with the DOG and the saccular planes are near perpendicular to it. Consequently, they no longer provide

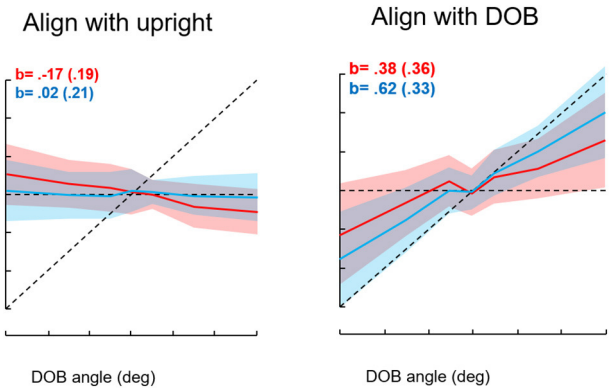

FIGURE 10 | Results for the conditions "align with the upright" and "align with the direction of balance." Seven directions of balance (DOB) were presented twice for each instruction type for 16 subjects. The DOBs were −30°, −15°, −5°, 0°, +5°, +15°, and +30°. Red entries represent achieved angles, blue represents indicated angles. The shading indicates standard deviations. The b entries represent slopes of MARS angles in degrees vs. DOB angles. The sign convention is minus entries represent rightward tilts of the subject and DOB, positive is leftward tilts. The intersection of the dotted horizontal and diagonal lines corresponds to 0°, the direction of gravity.

positional information about body location within the roll plane. This situation is an analog condition to that of labyrinthine-loss subjects who have to balance without otolith (and semi-circular canal) signals. Gravity dependent somatosensory cues about body position in roll are also minimized. In this circumstance, subjects exhibit drift, cyclical oscillations, and frequent crashes. They report not knowing which way they are moving and where they are in the roll plane. This is the case despite angular acceleration levels being well above measured semicircular canal thresholds (40). **Figures 11**, **12** illustrate vertical and horizontal roll plane performance, respectively.

Asymmetric Transfer of Training Between Vertical and Horizontal Roll Plane Balancing

The decrement in roll balance control with the body supine was concerning given its implications for performance in space flight conditions. To see whether practice in balancing with gravity-dependent cues could enhance performance when balancing without them, we gave one group of subjects repeated trials of balancing the MARS in the vertical roll plane where they had otolith and somatosensory cues about body position. We then tested them to see whether they would show transfer of learning to balancing in a supine roll plane the next day. We exposed another group of subjects to supine roll plane balancing on Day 1, where they only had transient semicircular canal and tactile cues to rely on, and then on Day 2 had them balance in the upright roll plane. We then compared the two groups performances for vertical and supine roll plane balancing. The results were unexpected. Subjects who were tested in the vertical roll plane on Day 2 (after supine roll plane balancing on Day 1) showed significantly better performance on five key measures compared to subjects who had vertical roll plane balancing on Day 1, including control of MARS position and standard deviation, fewer destabilizing joystick commands leading to crashes, less cumulative drifting, and reduced joystick deflection magnitude. Thus, the subjects who had already experienced supine roll plane balancing showed substantive transfer to vertical roll plane balancing. By contrast, subjects who underwent supine roll plane balancing on Day 2 following vertical roll plane balancing on Day 1 performed no better on any measure than the subjects who balanced in supine roll on Day 1. Prior experience with vertical roll plane balancing had provided no benefit whatsoever (41).

On examining the detailed pattern of the experimental results, we realized that subjects initially exposed to upright roll could rely on both gravitationally dependent otolith and somatosensory signals to determine their orientation. Consequently, when exposed on Day 2 to supine roll where such cues were absent, they were in the same situation as subjects exposed to supine roll on Day 1. They had to rely on semicircular canal signals to orient and try to avoid crashes. Subjects exposed on Day 2 to upright roll had learned on Day 1 to rely on semicircular canal signals associated with joystick movements to try and avoid crashing during supine roll. From debriefings it became clear that subjects tested in supine roll on Day 1 had learned joystick strategies to avoid crashes. The strategies did not improve their sense of body position but the joystick strategies coupled with the addition of otolith and somatosensory cues about ongoing position benefited them when exposed to upright roll on Day 2.

Training Strategies to Enhance Dynamic Balance Control in Supine Roll

We then asked whether we could train subjects to use strategies that would improve their ability to balance in the absence of position dependent gravity cues. Our approach was to expose subjects to vertical roll balancing with a DOB offset with respect to the DOG. Their goal was to orient to the DOB. They were repeatedly exposed to offset DOBs to the left or right of the DOG and, after each trial, were given verbal feedback about where the DOB had been and how well they had performed. We found that this approach helped them to learn strategies to home in on the DOB when they had ongoing otolith and somatosensory cues to their body orientation. After training in this fashion, when then exposed to supine roll balancing, all subjects showed performance improvements compared to their initial trials of exposure to supine roll prior to training. They had benefitted from the training but still had no firm sense of where the DOB was. They could not sense their actual position within the horizontal roll plane (42).

Predicting Ultimate Performance Levels

A key focus of ongoing work is to see whether our training paradigms to enhance balance control under conditions of reduced positional cues can be translated to operational aerospace conditions by relating joystick control movements to the subject's current ongoing position, direction, and velocity in relation to the DOB. By looking at these parameters and using machine learning computational modeling, we have found that it is possible with 80% accuracy within an initial block of five 100 s duration trials to classify subjects as "proficient," "average," or "non-proficient" in terms of their ultimate performance level at the completion of 10 blocks of 5 trials (43). This classification capability is important for assessing performance in dynamic conditions involving vehicular control in aviation, e.g., helicopters, and situations involving precise maneuvering control, e.g., spacecraft docking conditions. It raises the possibility of identifying early on individuals training to be pilots who would benefit from individualized training protocols.

Failure of Path Integration in Dynamic Balance Conditions Without Gravity Dependent Position Cues

A prominent feature of terrestrial life is path integration, keeping track of our ongoing position in relation to the environment. Path integration is often studied in the laboratory by exposing subjects seated upright in a rotating chair or robotic chair to angular displacements of various magnitudes and having them estimate their experienced displacements, using "look back" saccades or their feet to return the chair to its start positions. Typically such estimates are quite accurate and are thought to depend on integration of semicircular canal velocity signals to give a positional change (44–51). A key feature of our MARS device is that it can be programmed as an inverted pendulum about any axis. When we programmed it to exhibit inverted pendulum

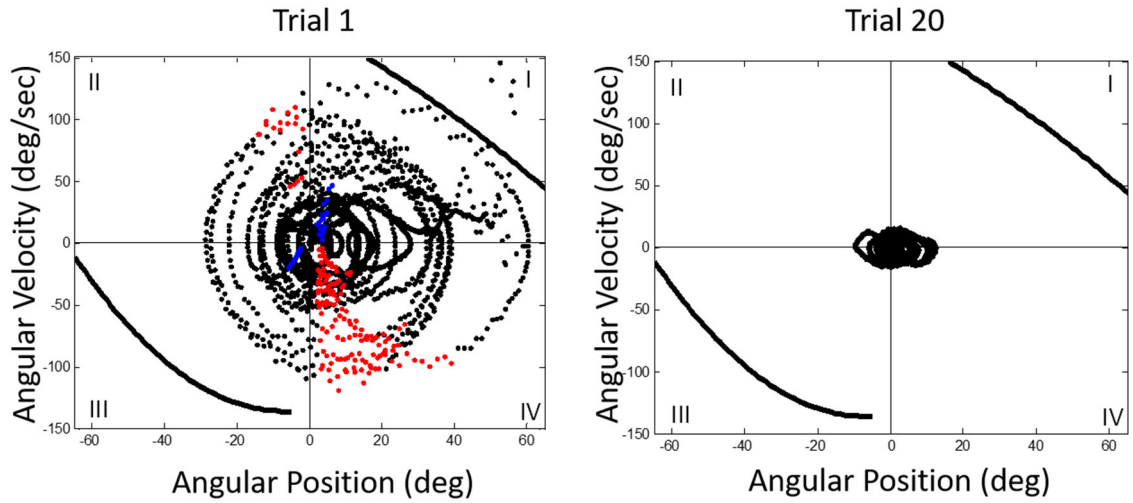

FIGURE 11 | Velocity-position phase plots for a typical subject in vertical roll plane balancing. Solid lines in quadrants 1 and 3 represent crash boundaries where joystick commands cannot prevent the MARS from exceeding + or −60 degrees. Dots outside these lines represent crashes. The MARS is reset to the start position after a crash and the trial then continues. Performance is near perfect after 20 trials. The red dots represent anticipatory joystick commands that slow the MARS down as it approaches the balance point. Blue dots represent destabilizing joystick commands that accelerate the MARS in the direction of a crash boundary.

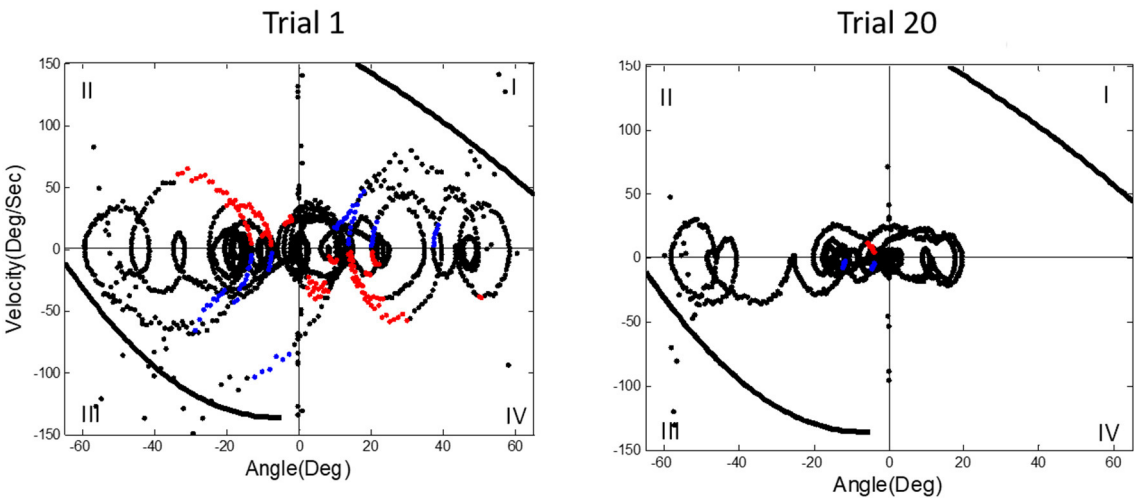

FIGURE 12 | Velocity-position phase plots for a typical subject in horizontal roll plane balancing show cyclical patterns of looping and drifting. The drifting and looping are reduced but not eliminated over repeated trials. Crashes are decreased but not eliminated as shown by dots outside crash boundaries.

behavior about a vertical yaw axis, we found that subjects trying to orient to the DOB showed cyclical drifting and were unable to sense the DOB. The velocity-position phase plot for a typical subject is shown in **Figure 13**. By contrast, when the axis of yaw rotation was horizontal, subjects were able to sense and orient to the DOB, as shown in **Figure 14**.

In upright yaw, there are no position dependent gravity shear forces on the otolith organs and body surface; by contrast, in horizontal yaw balancing strong position dependent otolith and somatosensory cues are present. Thus, these results are exactly parallel to those for horizontal and vertical roll plane balancing, respectively (52). In the absence of position dependent shear forces on their body, subjects have to rely on semicircular canal signals and performance breaks down. The canal signals apparently cannot be accurately sequentially integrated to give a fiducial representation of ongoing body position. These results

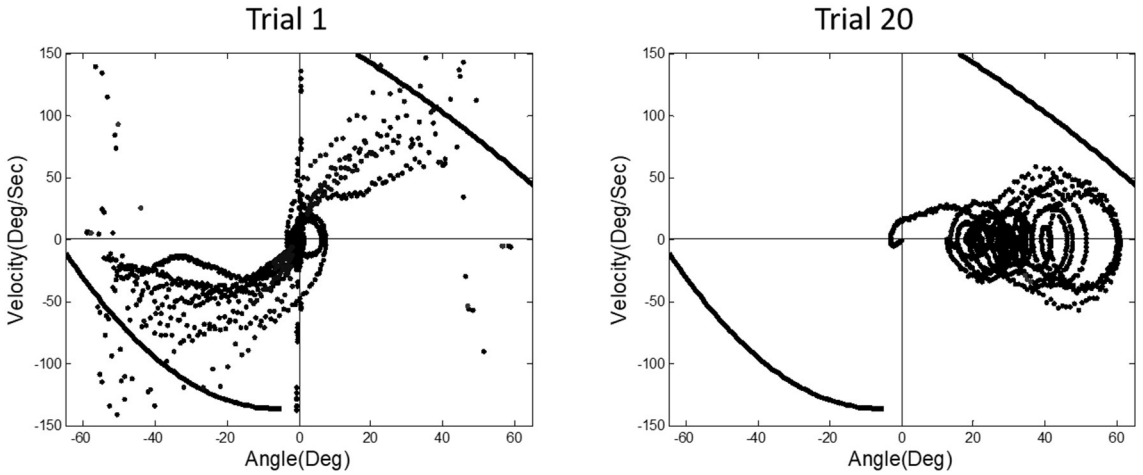

FIGURE 13 | Velocity-position phase plots for vertical yaw axis balancing. The drifting and looping and crashes characteristic of horizontal roll plane balancing (**Figure 12**) are apparent for the yaw axis, where there are also no gravity dependent positional cues available about ongoing yaw rotational position. Subjects, as in horizontal roll, report being unable to sense their ongoing position relative to the direction of balance.

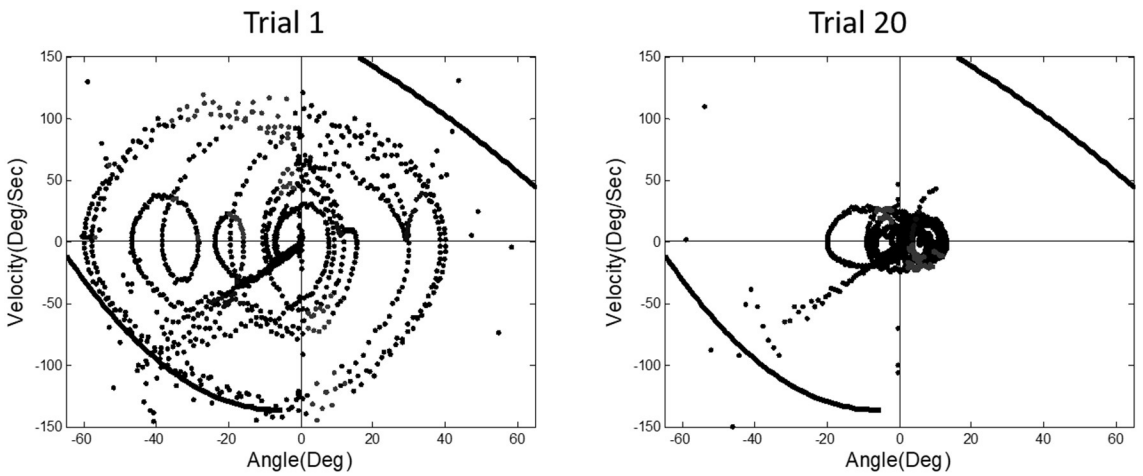

FIGURE 14 | Position-velocity phase plots for a typical subject performing horizontal yaw axis dynamic balancing. In this situation, gravity dependent positional shear forces are present and learning is obvious from Trial 1 to 20, just as in vertical roll plane balancing shown in **Figure 11**.

for yaw axis control were initially surprising given the work showing accurate path integration for single positional changes in upright yaw axis rotation.

Resolving the Conundrum of Why Static Postural Control Is so Degraded in Vestibular Loss Subjects

The MARS experiments suggest that a normal subject's ability during quiet stance to sway near vestibular threshold levels for detecting linear or angular acceleration relates to the otolith organs providing a fiducial signal of head position with respect to gravity. Coupled with pressure information about the CP from the feet and proprioceptive information about body configuration the control problem is greatly simplified because quiet stance can be modeled as a dual link inverted pendulum for both normal and labyrinthine loss subjects (53, 54), and for perturbed stance (55, 56). Consequently, when head orientation with respect to gravity is provided by the otolith organs, albeit a noisy signal (34), the center of pressure under the feet, approximately reflecting the body center of mass, can be regulated to control sway and prevent falling. Such cues

can be profoundly important as shown by Rademaker's classic observations in Das Stehen (57) as well as many recent studies showing how standing on foam to degrade foot cues increases body sway, e.g., Creath et al. (55); Horlings et al. (53); Karmali et al. (34).

The advantage of hand contact for the labyrinthine-loss subjects is that a fiducial static reference is available by finger contact and can be used to drive an automatic pincer grip long-loop reflex, with the finger and feet serving as the pincer elements. It is also important to realize that what we typically refer to as "vestibular thresholds" are actually multisensory thresholds. To stimulate the otoliths or semicircular canals, forces have to be applied to the surface of the body to displace it to stimulate the vestibular receptors. Such forces necessarily activate a range of somatosensory afferents. This is why, under passive tilt conditions, seated vestibular loss subjects can be as accurate as normal subjects in indicating when they are aligned with the gravitational vertical. In passive tilt, somatosensory cues about pressure distribution on the body surface are adequate for them to perform well despite their absence of otolith function (58).

The oculogravic illusion refers to the apparent upward displacement of a visual target when a subject is exposed to a centripetal force causing a change in magnitude of the resultant gravitoinertial force vector. A subject facing the center of rotation and fixating a visual target will see the target displace upward and simultaneously experience backwards self-tilt (59). Labyrinthine loss subjects exhibit oculogravic illusions with similar time course but diminished magnitude relative to normal controls (60). Importantly, when control subjects and labyrinthine loss subjects are allowed to stand and align themselves with the gravitoinertial resultant vector during rotation there is no significant difference in the magnitude of the oculogravic illusions they experience (61). By contrast, when normal and labyrinthine loss subjects, while submerged in water to the neck to attenuate body contact cues, are exposed to centrifugation to generate oculogravic illusions, the normal subjects exhibit little decrement in oculogravic illusion magnitude but it is abolished or diminished greatly in magnitude for the subjects without vestibular function (62).

These studies with labyrinthine loss subjects show the multiple factors that can be affecting performance under normal conditions and that can easily elude notice. They emphasize the importance of body contact with the environment and the wide range of information obtained thereby. Additional insights into how postural control can be simplified are embodied in a new non-parallel engaged leg model of postural control that explains and predicts body sway patterns in stationary and rotating environments, and in hyper-gravity conditions (56, 63–67). The model shows how foot based control can simplify adaptive maintenance of upright balance.

The Role of Velocity Storage During Dynamic Balance Control

In a classic paper, Cohen et al. systematically described the "velocity storage" of semicircular canal signals, with vestibular afternystagmus outlasting the peripheral time constant of the canals and of optokinetic afternystagmus outlasting optokinetic nystagmus (68). These observations are relevant to the inability

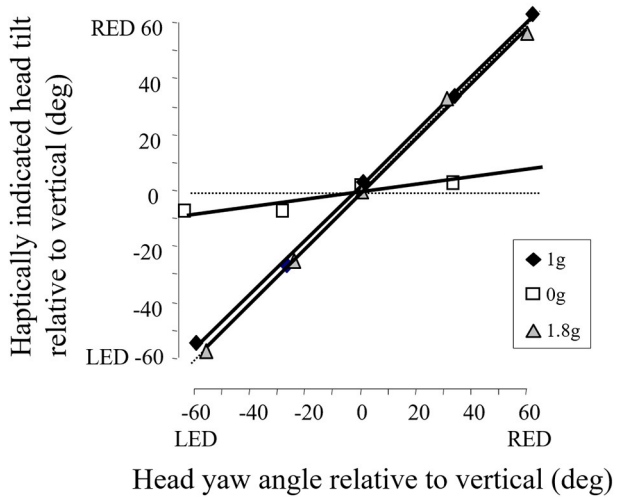

FIGURE 15 | Recumbent subjects ($N = 6$) indicated the amplitude of imposed passive yaw-axis rotations during the 0 and 1.8 g phases of parabolic flight maneuvers and in straight-and-level flight. Rotations were 30° or 60° in amplitude and lasted <1.5 s. Subjects used a gravity neutral pointer and tried to keep it aligned with their start position. In 0 g, rotations were greatly underestimated. Similar results were obtained for vertical yaw axis rotation in 0 g.

of subjects exposed to vertical yaw and to horizontal roll rotation in our MARS device to track their ongoing position. They point to what Cohen would identify as a "leaky" integrator. Velocity storage is also an important factor in motion sickness evocation (69, 70). In our early parabolic flight studies, we had found that velocity storage of semicircular canal and optokinetic signals is greatly attenuated in weightless conditions. The time constant of post-rotation afternystagmus is ≈15 s in 1 g straight-and-level flight and ≈9.5 s in the weightless phase of flight (71, 72). This finding helped explain why Coriolis cross-coupling stimulation caused by head movements out of the axis of rotation is so provocative and nauseogenic in 1 g but was so mild when studied in the Skylab M-131 experiments conducted in orbital flight (73).

We later found in the weightless phases of parabolic flight that when we exposed blindfolded subjects to angular displacements that were well above horizontal semicircular canal thresholds on Earth, they reported a slight tug on their body but underestimated or failed to detect their angular displacement (see **Figure 15**). The canal signals are not being accurately integrated in weightless conditions to give a sense of positional displacement (74). This finding is consistent with our observations that velocity storage is substantially attenuated in weightlessness. It is also consistent with the loss of a sense on one's ongoing position in the MARS supine roll and upright yaw dynamic balancing conditions, where the direction of balance cannot be sensed, only strategies to avoid crashing can be developed.

However, a puzzle remains: velocity storage is also attenuated in 1.8 g acceleration levels but head movements during rotation are greatly enhanced in provocativeness compared to 1 and

0 g acceleration levels (71, 72, 75, 76). Loading of the head by adding a mass to increase its weight can be provocative under 1 g conditions (77). Is this the causative factor for increased provocativeness of Coriolis cross-coupling in 1.8 g conditions (78)?

CONCLUDING REMARKS

When Bernie Cohen invited me to participate in the meeting for which this paper has been prepared, he reminded me of all the NASA working groups we had been on together and the wonderful times we had. He asked me to put in context how my early NASA work had influenced my later work on human sensory-motor adaptation to the terrestrial force environment. Little did I know when first studying the effects of head movements on susceptibility to motion sickness that a chance observation would lead to an insight that would become a theme of study in my future work. The realization when I closed my eyes while freefloating, that I had lost my sense of spatial anchoring meant that body contact with the environment was profoundly important for orientation. Hand contact later turned out to be important as well for calibrating auditory and visual localization, for updating motor control, and even for influencing the perceived dimensions of the body (79).

AUTHOR CONTRIBUTIONS

The author confirms being the sole contributor of this work and has approved it for publication.

FUNDING

Funding over the years has been provided by NASA, NSF, NIH, ONR, and AFOSR.

ACKNOWLEDGMENTS

Many individuals contributed to the work summarized here including: Ashton Graybiel, Paul DiZio, Joel Ventura, John Jeka, Simone Bortolami, Maureen Holden, Ely Rabin, Heather Panic, Sacha Panic, Alberto Pierobon, Janna Kaplan, Avijit Bakshi, Vivekanand Vimal. Heather and Sacha Panic programmed the MARS to be a marvelously flexible tool and conducted the initial experiments using it.

REFERENCES

1. Lackner JR, Graybiel A. Parabolic flight: loss of sense of orientaton. *Science.* (1979) 206:1105–8. doi: 10.1126/science.493998
2. Lackner JR, DiZio P. Aspects of body self-calibration. *Trends Cogn Sci.* (2000) 84:279–88. doi: 10.1016/S1364-6613(00)01493-5
3. Lackner JR, Graybiel A. Illusions of postural, visual, and substrate motion elicited by deep knee bends in the increased gravitoinertial force phase of parabolic flight. *Exp Brain Res.* (1981) 44:312–6. doi: 10.1007/BF00236568
4. Holden M, Ventura J, Lackner JR. Stabilization of posture by precision contact of the index finger. *J Vestib Res.* (1994) 4:285–301.
5. Johansson RS, Westling G. Signals in tactile afferents from the fingers eliciting adaptive motor responses during precision grip. *Exp Brain Res.* (1987) 66:141–54. doi: 10.1007/BF00236210
6. Westling G, Johansson RS. Responses in glaborous skin mechanoreceptors during precision grip in humans. *Exp Brain Res.* (1987) 66:128–40. doi: 10.1007/BF00236209
7. Jeka JJ, Lackner JR. Fingertip contact influences human postural control. *Exp Brain Res.* (1994) 100:495–502. doi: 10.1007/BF02738408
8. Jeka JJ, Lackner JR. The role of haptic cues from rough and slippery surfaces on human postural control. *Exp Brain Res.* (1995) 103:267–76. doi: 10.1007/BF00231713
9. Vallbo AB, Johansson RS. Properties of cutaneous mechanoreceptors in the human hand related to touch sensation. *Hum Neurobiol.* (1984) 3:3–14.
10. Lackner JR, Rabin E, DiZio P. Stabilization of posture by precision touch of the index finger with rigid and flexible filaments. *Exp Brain Res.* (2001) 139:454–64. doi: 10.1007/s002210100775
11. Rabin E, Dizio P, Lackner JR. Time course of haptic stabilization of posture. *Exp Brain Res.* (2006) 170:122–6. doi: 10.1007/s00221-006-0348-3
12. Hagbarth KE, Eklund G. Motor effects of vibratory stimuli in man. In: Granit R, editor. *Muscular Afferents Motor Control.* Stockholm: Almqvist and Wiksell (1966). p. 177–86.
13. Goodwin GM, McCloskey DI, Matthews PB. The contribution of muscle afferents to kinaesthesia shown by vibration induced illusions of movement and by the effects of paralysing joint afferents. *Brain.* (1972) 95:705–48. doi: 10.1093/brain/95.4.705
14. Eklund G. General features of vibration-induced effects on balance. *Uppsala J Med Sci.* (1972) 77:112–4. doi: 10.1517/03009734000000016
15. Lackner JR, Rabin E, DiZio P. Fingertip contact suppresses the destabilizing influence of leg muscle vibration. *J Neurophysiol.* (2000) 84:2217–24. doi: 10.1152/jn.2000.84.5.2217
16. Jeka JJ, Schoner G, Dijkstra T, Ribeiro P, Lackner JR. Coupling of fingertip somatosensory information to head and body sway. *Exp Brain Res.* (1997) 113:475–83. doi: 10.1007/PL00005600
17. Jeka J, Oie K, Schoner G, Dijkstra T, Henson E. Position and velocity coupling of postural sway to somatosensory drive. *J Neurophysiol.* (1998) 79:1661–74. doi: 10.1152/jn.1998.79.4.1661
18. Lackner JR, DiZio P, Jeka JJ, Horak F, Krebs D, Rabin E. Precision contact of the fingertip reduces postural sway of individuals with bilateral vestibular loss. *Exp Brain Res.* (1999) 126:459–66. doi: 10.1007/s002210050753
19. Riley MA, Stoffregen TA, Grocki MJ, Turvey MT. Postural stabilization for the control of touching. *Hum Mov Sci.* (1999) 18:795–817. doi: 10.1016/S0167-9457(99)00041-X
20. Rogers MW, Wardman DL, Lord SR, Fitzpatrick RC. Passive tactile sensory input improves stability during standing. *Exp Brain Res.* (2001) 136:514–22. doi: 10.1007/s002210000615
21. Krishnamoorthy V, Slijper H, Latash ML. Effects of different types of light touch on postural sway. *Exp Brain Res.* (2002) 147:71–9. doi: 10.1007/s00221-002-1206-6
22. Rabin E, Bortolami SB, DiZio P, Lackner JR. Haptic stabilization of posture: changes in arm proprioception and cutaneous feedback for different arm orientations. *J Neurophysiol.* (1999) 82:3541–9. doi: 10.1152/jn.1999.82.6.3541
23. Rabin E, DiZio P, Ventura J, Lackner JR. Influences of arm proprioception and degrees of freedom on postural control with light touch feedback. *J Neurophysiol.* (2008) 99:595–604. doi: 10.1152/jn.00504.2007
24. Bove M, Bonzano L, Trompetto C, Abbruzzese G, Schieppati M. The postural disorientation induced by neck muscle vibration subsides on lightly touching a stationary surface or aiming at it. *Neuroscience.* (2006) 143:1095–103. doi: 10.1016/j.neuroscience.2006.08.038
25. Clapp S, Wing AM. Light touch contribution to balance in normal bipedal stance. *Exp Brain Res.* (1999) 125:521–4. doi: 10.1007/s002210050711
26. Johannsen L, Guzman-Garcia A, Wing AM. Interpersonal light touch assists balance in the elderly. *J Mot Behav.* (2009) 41:397–9. doi: 10.3200/35-09-001
27. Wing AM, Johannsen L, Endo S. Light touch for balance: influence of a time-varying external driving signal. *Philos Trans R Soc Lond B Biol Sci.* (2011) 366:3133–41. doi: 10.1098/rstb.2011.0169

28. Johannsen L, Wing AM, Hatzitaki V. Contrasting effects of finger and shoulder interpersonal light touch on standing balance. *J Neurophysiol.* (2012) 107:216–25. doi: 10.1152/jn.00149.2011
29. Johannsen L, McKenzie E, Brown M, Redfern MS, Wing AM. Deliberately light interpersonal touch as an aid to balance control in neurologic conditions. *Rehabil Nurs.* (2017) 42:131–8. doi: 10.1002/rnj.197
30. Sawers A, Ting LH. Perspectives on human-human sensorimotor interactions for the design of rehabilitation robots. *J Neuroeng Rehabil.* (2014) 11:142. doi: 10.1186/1743-0003-11-142
31. Sawers A, Bhattacharjee T, McKay JL, Hackney ME, Kemp CC, Ting LH. Small forces that differ with prior motor experience can communicate movement goals during human-human physical interaction. *J Neuroeng Rehabil.* (2017) 14:8. doi: 10.1186/s12984-017-0217-2
32. Kavounoudias A, Roll R, Roll JP. The plantar sole is a 'dynamometric map' for human balance control. *Neuroreport.* (1998) 9:3247–52. doi: 10.1097/00001756-199810050-00021
33. Kavounoudias A, Roll R, Roll JP. Foot sole and ankle muscle inputs contribute jointly to human erect posture regulation. *J Physiol.* (2001) 532:869–78. doi: 10.1111/j.1469-7793.2001.0869e.x
34. Karmali F, Goodworth AD, Valko Y, Leeder T, Peterka RJ, Merfeld DM. The role of vestibular cues in postural sway. *J Neurophysiol.* (2021) 125:672–82. doi: 10.1152/jn.00168.2020
35. Stoffregen TA, Riccio GE. An ecological theory of orientation and the vestibular system. *Psychol Rev.* (1988) 95:3–14. doi: 10.1037/0033-295X.95.1.3
36. Riccio GE, Stoffregen TA. Gravitoinertial force versus the direction of balance in the perception and control of orientation. *Psychol Rev.* (1990) 97:135–7. doi: 10.1037/0033-295X.97.1.135
37. Winter DA. *(Anatomy* ABC, *Biomechanics, Control) of Balance During Standing and Walking*. Waterloo Biomechanics (1995).
38. Riccio GE, Martin EJ, Stoffregen TA. The role of balance dynamics in the active perception of orientation. *J Exp Psychol Hum Percept Perform.* (1992) 18:624–44. doi: 10.1037/0096-1523.18.3.624
39. Panic H, Panic AS, Dizio P, Lackner JR. Direction of balance and perception of upright are perceptually dissociable. *J Neurophysiol.* (2015) 113:3600–9. doi: 10.1152/jn.00737.2014
40. Panic AS, Panic H, Dizio P, Lackner JR. Gravitational and somatosensory influences on control and perception of roll balance. *Aerosp Med Hum Perform.* (2017) 88:993–9. doi: 10.3357/AMHP.4853.2017
41. Vimal VP, Dizio P, Lackner JR. Learning dynamic balancing in the roll plane with and without gravitational cues. *Exp Brain Res.* (2017) 235:3495–503. doi: 10.1007/s00221-017-5068-3
42. Vimal VP, Dizio P, Lackner JR. Learning and long-term retention of dynamic self-stabilization skills. *Exp Brain Res.* (2019) 237:2775–87. doi: 10.1007/s00221-019-05631-x
43. Vimal VP, Zheng H, Hong P, Fakharzadeh LN, Lackner JR, Dizio P. Characterizing individual differences in a dynamic stabilization task using machine learning. *Aerosp Med Hum Perform.* (2020) 91:479–88. doi: 10.3357/AMHP.5552.2020
44. Beritov IV. *Neural Mechanisms of Higher Vertebrate Behavior*. Boston, MA: Little-Brown (1965).
45. Bloomberg J, Jones GM, Segal B, McFarlane S, Soul J. Vestibular-contingent voluntary saccades based on cognitive estimate of remembered vestibular information. *Adv Otorhinolaryngol.* (1988) 41:71–5. doi: 10.1159/000416034
46. Bloomberg J, Jones GM, Segal B. Adaptive plasticity in the gaze stabilization synergy of slow and saccadic eye movement. *Exp Brain Res.* (1991) 84:35–46. doi: 10.1007/BF00231760
47. Metcalfe T, Gresty M. Self-controlled reorienting movements in response to rotational displacements in normal subjects and patients with labyrinthine disease. *Annals N Y Acad Sci.* (1992) 656:695–8. doi: 10.1111/j.1749-6632.1992.tb25246.x
48. Loomis JM, Klatzky RL, Golledge RG, Cicinelli JG, Pellegrino JW, Fry PA. Nonvisual navigation by blind and sighted: assessment of path integration ability. *J Exp Psychol.* (1993) 122:73–91. doi: 10.1037/0096-3445.122.1.73
49. Jürgens R, Boss T, Becker W. Estimation of self-turning in the dark: comparison between active and passive rotation. *Exp Brain Res.* (1999) 128:491–504. doi: 10.1007/s002210050872
50. Loomis JM, Klatsky RL, Golledge RG, Philbeck JW, Golledge RG. Human navigation by path integration. In: Golledge RG, editor. *Wayfinding Behavior: Cognitive Mapping and Other Spatial Processes*. Baltimore, MD: Johns Hopkins University Press (1999). p. 125–151.
51. Siegler I, Viaud-Delmon I, Israel I, Berthoz A. Self-motion perception during a sequence of whole-body rotations in darkness. *Exp Brain Res.* (2000) 134:66–73. doi: 10.1007/s002210000415
52. Vimal VP, Dizio P, Lackner JR. Learning dynamic control of body yaw orientation. *Exp Brain Res.* (2018) 236:1321–30. doi: 10.1007/s00221-018-5216-4
53. Horlings CG, Kung UM, Honegger F, Van Engelen BG, Van Alfen N, Bloem BR, et al. Vestibular and proprioceptive influences on trunk movements during quiet standing. *Neuroscience.* (2009) 161:904–14. doi: 10.1016/j.neuroscience.2009.04.005
54. Honegger F, van Spijker GJ, Allum JH. Coordination of the head with respect to the trunk and pelvis in the roll and pitch planes during quiet stance. *Neuroscience.* (2012) 213:62–71. doi: 10.1016/j.neuroscience.2012.04.017
55. Creath R, Kiemel T, Horak F, Peterka R, Jeka J. A unified view of quiet and perturbed stance: simultaneous co-existing excitable modes. *Neurosci Lett.* (2005) 377:75–80. doi: 10.1016/j.neulet.2004.11.071
56. Bakshi A, DiZio P, Lackner JR. Rapid adaptation of Coriolis force perturbations of voluntary body sway. *J Neurophysiol.* (2019) 121:2028–41. doi: 10.1152/jn.00606.2018
57. Rademaker GGJ. *The Physiology of Standing (Das Stehen)*. Minneapolis, MN: University of Minnesota Pres. (1980). p. 55514.
58. Clark B, Graybiel A. A perception of the postural vertical in normals and subjects with labyrinthine deficits. *J Exp Psychol.* (1963) 63:490–4. doi: 10.1037/h0045606
59. Graybiel A. Oculogravic illusion. *AMA Arch Ophthalmol.* (1952) 48:605–15. doi: 10.1001/archopht.1952.00920010616007
60. Graybiel A, Clark B. The validity of the oculogravic illusion as a specific indicator of otolith function. *Aerosp Med.* (1965) 36:1173–81.
61. Clark B, Graybiel A. Influence of contact cues on the perception of the oculogravic illusion. *Acta Otolaryngol.* (1968) 65:373–80. doi: 10.3109/00016486809120978
62. Graybiel A, Miller EF, Newsom B, Kennedy R. The effect of water immersion on perception of the oculogravic illusion in normal and labyrinthine defective subjects. *Acta Otolaryngol.* (1968) 65:599–610. doi: 10.3109/00016486809119294
63. Bakshi A, DiZio P, Lackner JR. Statistical analysis of quiet stance sway in 2-D. *Exp Brain Res.* (2014) 232:1095–108. doi: 10.1007/s00221-013-3815-7
64. Bakshi A, Ventura J, DiZio P, Lackner JR. Adaptation to Coriolis perturbations of voluntary body sway transfers to pre-programmed fall-recovery behavior. *J Neurophysiol.* (2014) 111:977–83. doi: 10.1152/jn.00927.2012
65. Bakshi A, DiZio P, Lackner JR. Adaptation to Coriolis force perturbations of postural sway requires an aymmetric two-leg model. *J Neurophysiol.* (2019) 121:2042–60. doi: 10.1152/jn.00607.2018
66. Bakshi A, DiZio P, Lackner JR. Multiple roles of active stiffness in upright balance and multi-directional sway. *J Neurophysiol.* (2020) 124:1995–2011. doi: 10.1152/jn.00612.2019
67. Bakshi A, DiZio P, Lackner JR. The effect of hypergravity on upright balance and voluntary sway. *J Neurophysiol.* (2020) 124:1986–994. doi: 10.1152/jn.00611.2019
68. Cohen B, Matsuo V, Raphan T. Quantitative analysis of the velocity characteristics of optokinetic nystagmus and optokinetic after-nystagmus. *J Physiol.* (1977) 270:321–44. doi: 10.1113/jphysiol.1977.sp011955
69. Yakushin SB, Raphan T, Cohen B. Coding of velocity storage in the vestibular nuclei. *Front Neurol.* (2017) 8:386. doi: 10.3389/fneur.2017.00386
70. Cohen B, Dai M, Yakushin SB, Cho C. The neural basis of motion sickness. *J Neurophysiol.* (2019) 121:973–82. doi: 10.1152/jn.00674.2018
71. DiZio P, Lackner JR, Evanoff JN. The influence of gravitoinertial force level on oculomotor and perceptual responses to Coriolis, cross-coupling stimulation. *Aviat Space Environ Med.* (1987) 58:A218–23.
72. DiZio P, Lackner JR, Evanoff JN. The influence of gravitoinertial force level on oculomotor and perceptual responses to sudden-stop stimulation. *Aviat Space Environ Med.* (1987) 58:A224–30.

73. Graybiel A, Miller, 2nd EF, Homick JL. Experiment M-131. Human vestibular function. In: Johnson RS, Dietlein LF, editors. *Biomedical Results From Skylab, NASA SP-377*. Washington, DC: US Govt Print Office (1977). p. 74–103.
74. Lackner JR, DiZio P. Angular displacement perception modulated by force background. *Exp Brain Res*. (2009) 195:335–43. doi: 10.1007/s00221-009-1785-6
75. Lackner JR, Graybiel A. The effective intensity of Coriolis, cross-coupling stimulation is gravitoinertial force dependent: implications for space motion sickness. *Aviat Space Environ Med*. (1986) 57:229–35.
76. DiZio P, Lackner JR. The effects of gravitoinertial force level and head movements on post-rotational nystagmus and illusory after-rotation. *Exp Brain Res*. (1988) 70:485–95. doi: 10.1007/BF00247597
77. Lackner JR, DiZio P. Altered sensory-motor control of the head as an etiological factor in space-motion sickness. *Percept Mot Skills*. (1989) 68:784–6. doi: 10.2466/pms.1989.68.3.784
78. Lackner JR, DiZio P. Velocity storage: its multiple roles. *J Neurophysiol*. (2020) 123:1206–15. doi: 10.1152/jn.00139.2019
79. Lackner JR, DiZio P. Dynamic sensory-motor adaptation to earth gravity. In: Wixted JT, editor. *Stevens' Handbook of Experimental Psychology Cognitive Neuroscience*. 4th ed. New York, NY: Wiley (2018). p. 887–906.

Conflict of Interest: The author declares that the research was conducted in the absence of any commercial or financial relationships that could be construed as a potential conflict of interest.

frontiers in Neurology

ORIGINAL RESEARCH
published: 28 May 2021
doi: 10.3389/fneur.2021.680044

Pulsed Infrared Stimulation of Vertical Semicircular Canals Evokes Cardiovascular Changes in the Rat

Darrian Rice[1], *Giorgio P. Martinelli*[2], *Weitao Jiang*[1], *Gay R. Holstein*[2,3] *and Suhrud M. Rajguru*[1,4]*

[1] Department of Biomedical Engineering, University of Miami, Miami, FL, United States, [2] Department of Neurology, Icahn School of Medicine at Mount Sinai, New York, NY, United States, [3] Department of Neuroscience, Icahn School of Medicine at Mount Sinai, New York, NY, United States, [4] Department of Otolaryngology, University of Miami, Miami, FL, United States

A variety of stimuli activating vestibular end organs, including sinusoidal galvanic vestibular stimulation, whole body rotation and tilt, and head flexion have been shown to evoke significant changes in blood pressure (BP) and heart rate (HR). While a role for the vertical semicircular canals in altering autonomic activity has been hypothesized, studies to-date attribute the evoked BP and HR responses to the otolith organs. The present study determined whether unilateral activation of the posterior (PC) or anterior (AC) semicircular canal is sufficient to elicit changes in BP and/or HR. The study employed frequency-modulated pulsed infrared radiation (IR: 1,863 nm) directed via optical fibers to PC or AC of adult male Long-Evans rats. BP and HR changes were detected using a small-animal single pressure telemetry device implanted in the femoral artery. Eye movements evoked during IR of the vestibular endorgans were used to confirm the stimulation site. We found that sinusoidal IR delivered to either PC or AC elicited a rapid decrease in BP and HR followed by a stimulation frequency-matched modulation. The magnitude of the initial decrements in HR and BP did not correlate with the energy of the suprathreshold stimulus. This response pattern was consistent across multiple trials within an experimental session, replicable, and in most animals showed no evidence of habituation or an additive effect. Frequency modulated electrical current delivered to the PC and IR stimulation of the AC, caused decrements in HR and BP that resembled those evoked by IR of the PC. Frequency domain heart rate variability assessment revealed that, in most subjects, IR stimulation increased the low frequency (LF) component and decreased the high frequency (HF) component, resulting in an increase in the LF/HF ratio. This ratio estimates the relative contributions of sympathetic nervous system (SNS) and parasympathetic nervous system (PNS) activities. An injection of atropine, a muscarinic cholinergic receptor antagonist, diminished the IR evoked changes in HR, while the non-selective beta blocker propranolol eliminated changes in both HR and BP. This study provides direct evidence that activation of a single vertical semicircular canal is sufficient to activate and modulate central pathways that control HR and BP.

Keywords: optical stimulation, vestibulo-sympathetic reflex, vestibular system, autonomic, heart rate, blood pressure, infrared stimulation

OPEN ACCESS

Edited by:
Michael Strupp, Ludwig Maximilian University of Munich, Germany

Reviewed by:
Hans Straka, Ludwig Maximilian University of Munich, Germany
Leo Ling, University of Washington, United States

***Correspondence:**
Suhrud M. Rajguru
s.rajguru@miami.edu

Specialty section:
This article was submitted to Neuro-Otology, a section of the journal Frontiers in Neurology

Received: *13 March 2021*
Accepted: *20 April 2021*
Published: *28 May 2021*

Citation:
Rice D, Martinelli GP, Jiang W, Holstein GR and Rajguru SM (2021) Pulsed Infrared Stimulation of Vertical Semicircular Canals Evokes Cardiovascular Changes in the Rat. Front. Neurol. 12:680044. doi: 10.3389/fneur.2021.680044

Prior studies have shown that vestibular inputs from otolith organs can modulate the autonomic pathway and contribute to the control of blood pressure and heart rate during movement. However, the role of the semicircular canals in this respect has not been completely clear. The present study elucidated the role for the vertical semicircular canals in altering autonomic activity using focused, pulsed infrared stimulation of posterior and anterior canals in the rat. Unilateral activation of either the posterior or anterior semicircular canal was sufficient to evoke profound changes in the heart rate and blood pressure, suggesting that canals also contribute to the vestibulo-autonomic pathway.

INTRODUCTION

The vestibular system is exquisitely sensitive to linear and angular accelerations of the head, informing the nervous system about head position and head movements in space. These two types of signals are detected by different sets of end organs, with the semicircular canals specialized to transduce angular accelerations and the otolith organs detecting linear forces such as gravity, tilt and translation. Vestibular information from both types of end organs is conveyed centrally to participate in well-characterized neural pathways involved in spatial orientation, gaze stabilization, balance, posture and cognition [for reviews, see Holstein (1), Vidal et al. (2)]. In addition, vestibular information is conveyed to regions of the central autonomic nervous system, thereby altering blood pressure (BP), heart rate (HR), and respiration in response to changes in head position and movement [for reviews, see Yates and Miller (3); Yates et al. (4); Yates and Miller (5)]. Since many of these functional pathways specifically target pre-sympathetic brainstem nuclei, they are often referred to as the vestibulo-sympathetic reflex pathways. However, vestibular input to cell groups associated with parasympathetic activity (6) argues for the more general description of the projections as vestibulo-autonomic (7).

The existence and overall functions of the vestibulo-autonomic pathways in humans and animals are now well-established [for reviews, see (Yates et al. (4); Barman and Yates (8)]. For cardiovascular control, the vestibular system provides a rapid and open-loop input to baroreflex pathways mediating changes in peripheral vasoconstriction to compensate for postural adjustments such as standing from a seated or horizontal position (9). Although the baroreflex is an extremely efficient mechanism for maintaining vasomotor homeostasis, it is a closed loop through a long latency negative feedback pathway. In fact, a change in BP following electrical stimulation of baroreceptor afferents requires ∼1 s (10). In addition, the baroreflex is entirely reactive, adjusting sympathetic nerve activity to BP perturbations that have already transpired (4).

Most studies of vestibulo-autonomic pathways and functions in humans and experimental animals have focused on the role of the otolith organs in supplying the initial head-related signal. In human subjects, cardiovascular responses evoked by front-back linear acceleration, head pitch, off-vertical-axis rotation and galvanic vestibular stimulation (GVS) (11–23) have typically been attributed to activation of utricular afferents. Similarly, nose-up pitch, head-down tilt, forward linear acceleration, and GVS (24–29) have been utilized in animal models to specifically address the ability of the otolith organs to activate the vestibulo-sympathetic reflex (VSR) and modulate BP. While a contribution from the vertical semicircular canals to vestibulo-autonomic pathways has been suggested previously (30), a specific role for these end organs in central mechanisms of cardiovascular control remains to be identified.

The present study investigated the contributions of the posterior and anterior semicircular canals (PC and AC, respectively) to the vestibulo-autonomic activity using focused, pulsed infrared radiation (IR). This stimulus is advantageous because it offers greater spatial and temporal selectivity than electrical activation (31–34). In the vestibular system, pulsed IR has been shown to rapidly alter the rate of transmitter release from inner ear hair cells and modulate the discharge rate of primary afferent fibers (34–36). In addition, our group recently reported that pulsed IR can be used to selectively activate the PC in anesthetized rats (37). In the present study, we measured eye movements, BP, HR, and heart rate variability (HRV) during unilateral pulsed IR stimulation of the PC or AC. The findings provide new evidence directly linking activation of the vertical semicircular canals to changes in HR and BP.

EXPERIMENTAL METHODS

Animal Preparation and Surgical Approach

All experiments were carried out in accordance with the National Institutes of Health Guide for the Care and Use of Laboratory Animals and the Institutional Animal Care and Use Committee (IACUC) of the University of Miami approved all procedures. In total, 30 adult male Long Evans rats (Charles River Laboratories) weighing 300–500 g were used in this study. Infrared stimulation of the PC was attempted in 23 animals including the pharmacological studies, PC electrical stimulation results were obtained from an additional three animals, and IR evoked responses to AC IR stimulation were obtained from four rats. The experimental approach and examples of the physiological data obtained during the experiments are illustrated in **Figure 1**.

Surgical Approach

For stimulation experiments, animals were initially anesthetized with intraperitoneal injections of ketamine (44 mg/kg) and xylazine (5 mg/kg). Anesthesia was maintained with supplemental doses of these agents, based on assessments of the animal's pinch reflex tested every 15 min throughout the experimental session. Vital signs were continuously monitored, and the core body temperature was maintained at 37°C by resting the animal on a heating pad (Deltaphase® Isothermal pads; Braintree Scientific) throughout the procedure. Body temperature was monitored using the telemetric system described below. Prior to stimulation, all rats were anesthetized (as above), fitted with head posts and secured on a custom-designed stereotaxic system (Kopf Instruments). To accomplish this, a 2 cm skin incision was made over the skull and the bony

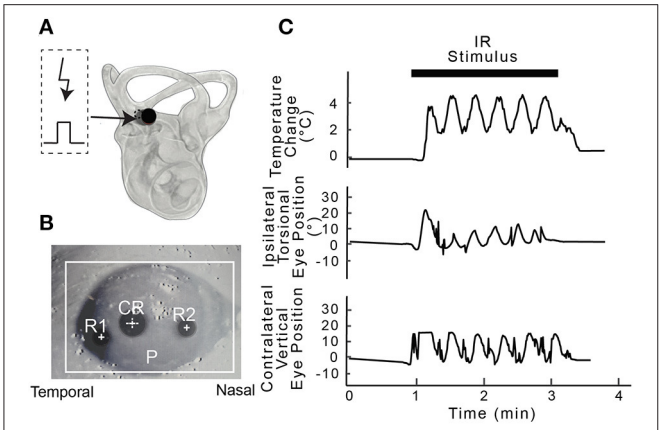

FIGURE 1 | Experimental setup. **(A)** Shows an example post-mortem microtomography image of the right inner ear of a rat with a 400 μm optical fiber (solid circle) used for IR stimulation targeting the PC ampulla. A micro thermistor (dotted circle) was inserted beside optical fiber and used to measure the change in temperature along the beam path during posterior canal stimulation. **(B)** Eye recording setup highlighting pupil (P), cornea reflection (CR) and rotational marks (R1 and R2) was used to calculate the magnitude of the movement during IR stimulation. **(C)** Simultaneous physiological recordings were carried out during each 2-min IR stimulation period. The panels show IR stimulation of the vestibular end organs at 0.5 Hz, the change in temperature along the beam path (°C), and frequency-matched ipsilateral torsional and contralateral vertical eye position change (°) from IR stimulation of the PC in one rat.

surface was exposed and cleaned. Two surgical screws were anchored into symmetrically-placed holes drilled in the parietal bones. A stainless-steel head post was fitted between the screws and secured in place by dental acrylic cement (Jet Repair). To access the vestibular end organs, a C-shaped incision was made behind the right pinna and blunt dissection was performed to remove the surrounding muscles and expose the bulla. The bulla was opened using a motorized surgical drill in order to visualize the round window and direct the laser stimulation toward the PC ampulla. To target the AC, the middle ear ossicles were carefully removed with forceps and the AC ampulla was identified using local anatomical landmarks (38).

The animals were placed on the stereotaxic frame and secured using the head post to maintain immobility during the stimulation experiment. Note that the bony labyrinth covering the crista ampullaris was not opened since IR directed at the canal crista through the thin bone was sufficient to evoke physiological responses. Confirmation that the end organs were accurately targeted by the IR stimulation was based on evoked eye movements and by post-mortem microtomography (37). For the microtomography, following the terminal experiment the inner ears were fixed in 4% paraformaldehyde in 0.1 M phosphate buffer with the optical fiber fixed in place using dental acrylic. The tomographic images taken of the samples (Skyscan 1176 Micro Photonic Inc.) were imported in Osirix Lite (Pixmeo) for 3-D reconstruction, low-pass filtered and the fiber orientation relative to the AC or PC crista was determined from the three-dimensional reconstructions (**Figure 1A**).

Infrared Stimulation

Pulsed IR stimulation (1,863 nm wavelength) was achieved with a Capella diode laser (Lockheed Martin Aculight Corp.) and frequency modulated by external function generators (Tektronix, mode CFG250, AFG320) where $f = f0\ \left((1-a)+a\sin\left(2\pi fst\right)\right)$; the baseline frequency was $f_0 = 250$ Hz, the modulation frequency was $f_s = 0.05$ Hz, and the dynamic range was a was fixed at 0.9. The laser was coupled to a 200 or 400 μm optical fiber (P200-5-VIS-NIR and P400-5-VIS-NIR, Ocean Optics) to target the vestibular neuroepithelium. IR with a wavelength of 1863 nm, frequency of 250 pulses per second (pps), and pulse duration of 200 μs, was delivered sinusoidally at 0.05 Hz to the right posterior or anterior ampullae for 2 min. The penetration depth used in the present study was ∼0.8 mm in water (39). Only the radiant energy was varied between 20 and 149 μJ/pulse for the 200 μm fiber and between 94 and 512 μJ/pulse for the 400 μm fiber to determine dose-dependent stimulation-evoked changes in BP and HR. The output radiant energies reported in the results were characterized from end-polished optical fibers in air (40). These energy values likely vary from those experienced *in vivo* at the target tissue depending upon the distance between the fiber tip and the target tissue, thickness of the bone, and/or the beam path. In one rat, local temperature at the crista during IR stimulation was recorded using a micro-thermocouple (Omega) placed in the path of the IR optical beam. The temperature was recorded at a sampling rate of 60 Hz for three 2-min stimulation periods (**Figure 1C**).

Electrical Stimulation

To further confirm the involvement of the vertical semicircular canals in the evoked BP and HR changes, electrical stimulation of the PC was performed in 3 rats. The surgical approach to the bulla and round window were as described above for the IR stimulation. In each rat, a standard bipolar needle electrode was placed at the site of the PC ampulla and a second electrode was placed at the upper rim of the round window. Monophasic pulses of 500 μs pulse duration, 250 pps, and 700 μA per pulse were generated by an isolated stimulator (ISO-STIM 01M, NPI) and sinusoidally modulated at 0.05 Hz, a frequency that was used in the IR experiments. The total duration for electrical stimulation was 2 min, consistent with the IR stimulation.

Eye Movements

Activation of the targeted end organ—PC or AC—during either infrared or electrical stimulation was confirmed using eye movements (37, 41) that were observed and recorded in some animals using a video-oculography system (ETL-200; ISCAN Inc., **Figure 1B** and lower traces in **Figure 1C**). The system located and tracked the center of the pupil and corneal reflections of both eyes. The linear positions of the pupil and corneal reflection were converted to angular rotation in the horizontal and vertical directions using previously detailed methods (37). Sinusoidally-modulated IR stimulation of the PC evoked frequency-matched torsion in the ipsilateral eye and a vertical downward movement in the contralateral eye whereas that of the AC evoked primarily upward movements ipsilaterally and upward extorsion contralaterally. In majority of the rats,

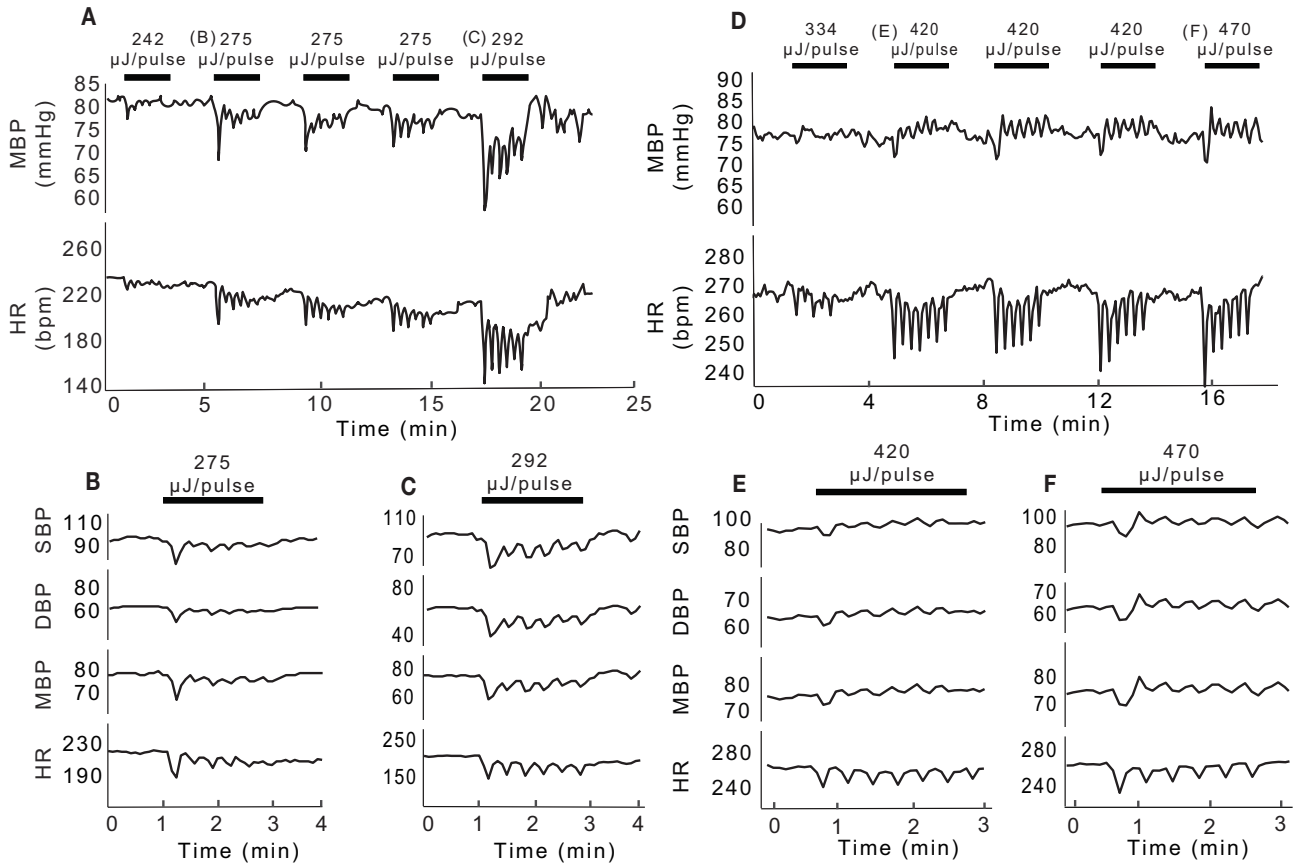

FIGURE 2 | Changes in BP and HR evoked by unilateral pulsed IR directed at PC. **(A)** Shows example mean BP (mmHg) and HR (bpm) responses recorded in one rat at different IR radiant exposures. Black bars indicate the 2-min IR stimulus intervals with the radiant energy at each interval noted above (242 to 292 µJ/pulse). The initial observable response (threshold) occurred at 242 µJ/pulse. **(B,C)** Show single events at 275 and 292 µJ/pulse, respectively and the corresponding changes in systolic (SBP), diastolic (DBP), and mean (MBP) pressures as well as changes in HR. **(D)** Shows responses recorded in another rat at different radiant exposures (292 to 470 µJ/pulse) with the observed threshold at 420 µJ/pulse. **(E,F)** Show single events at 420 and 470 µJ/pulse, respectively, and the corresponding changes in SBP, DBP, MBP, and HR.

eye movements continued to modulate for the duration of the experiment.

Sensor Implantation

During the stimulation experiments, HR, BP, and body temperature were measured with a small animal single pressure device (DSI Pressure Sensing Technologies, model HD-S10) implanted in the femoral artery prior to stimulation. Implantation surgeries were conducted at least 24 h before the IR experiments using aseptic technique. Animals were anesthetized with isoflurane (2–3%) using a portable anesthesia workstation (Eagle Eye Anesthesia). The telemetry device was implanted according to procedures reported previously (42). Briefly, the insertion area above the left groin was shaved and cleaned with a surgical antiseptic (Providone-iodine), and then a small incision was made to expose the femoral artery. An arteriotomy was performed and the transducer catheter was inserted into the vessel. The artery was tied off to secure the catheter and the body of the sensor was secured in a subcutaneous pouch. The incision was closed with a suture and surgical staples. Post-surgical pain was monitored and managed with buprenorphine (0.3 mg/ml). Animals recovered for a minimum of 24 h before they were used in stimulation experiments.

BP and HR Recordings

Physiological data were collected continuously using the implanted single pressure telemetric sensor and Ponemah software (DSI). Using this system, arterial pressures were recorded continuously and analyzed every 5 s to calculate parameters including: systolic BP, diastolic BP, mean BP, HR, and body temperature. BP and HR recordings were initiated prior to the stimulation in order to establish the baseline activity for each animal, and continued throughout the experiment. The start and end times for each 2-min IR stimulus were marked as trigger events in the recordings to facilitate the subsequent data analysis. Data exported from Ponemah as CSV files were analyzed with custom scripts written in MATLAB (Mathworks).

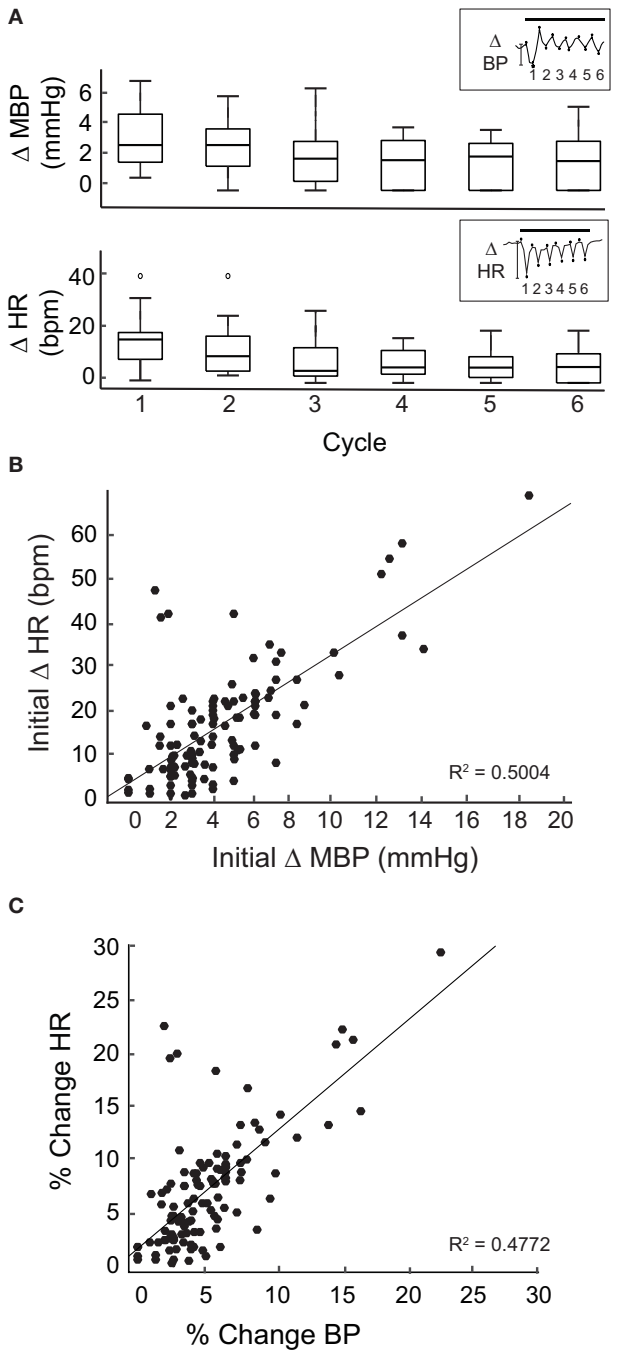

FIGURE 3 | Magnitude of change per cycle. **(A)** Shows a box plot of the changes in MBP (top) and HR (bottom) for each cycle (20 s) of the 2-min stimulation period at 470 μJ/pulse in 6 rats. Inset shows one example of a MBP (top) and HR (bottom) measurement during a stimulation event at 470 μJ/pulse divided into 6 cycles. The magnitude of change was measured peak-to-peak (*) for each cycle. Change in MPB and HR between cycles was not significant [repeated measures ANOVA: HR ($p = 0.3644$) and BP: ($p = 0.7952$)]. **(B)** The initial change in MPB (mmHg) from 113 events in 17 rats correlated moderately to the corresponding initial changes in HR (bpm) ($R^2 = 0.5004$, $p < 0.0005$). **(C)** Percent change was taken for both MBP (initial change MBP/MBP baseline) and HR (initial change HR/baseline HR) at 113 stimulation events across 17 rats. The percent changes in HR and MBP correlated moderately ($R^2 = 0.4772$, $p < 0.0005$).

Heart Rate Variability Analysis

The inter-beat intervals of arterial BP signals were analyzed using the Ponemah (DSI) software to calculate heart rate variability (HRV). Using Fast Fourier transforms to perform the spectral analysis, HRV was divided into components that operate in different frequency ranges (43, 44). The HRV frequency bands used in rat are: Very Low Frequency (VLF) [0.05–0.25 Hz], Low Frequency (LF) [0.25–1 Hz], and High Frequency (HF) [1–3 Hz]. Our HRV data are presented as the ratio between normalized LF and HF, which excludes the VLF data including the IR stimulation frequency 0.05 Hz. As noted above, HRV measures were initially obtained for the overall baseline BP recorded prior to any IR stimulation. Baseline HRV measures were then confirmed from the 2 min BP recordings obtained immediately preceding each IR stimulation trial. The changes recorded during each 2 min stimulation trial were compared to the HRV during the baseline (no stimulation) condition. The data compiled in Ponemah (DSI) were exported to CSV files and further analyzed and plotted in MATLAB (Mathworks, MA). The ratio of LF to HF power was also used to estimate the relative ratio of sympathetic to parasympathetic nervous system activity (43).

Pharmacological Blockers of Autonomic Function

In six experiments, we evaluated the contributions of sympathetic and parasympathetic activity to the vestibulo-autonomic responses evoked by IR. The muscarinic cholinergic receptor antagonist atropine (1 mg/kg) or the non-selective beta-adrenergic receptor blocker propranolol (1 mg/kg) were administered systemically via the tail vein in anesthetized rats. Baseline and IR-evoked changes in BP and HR were recorded prior to and following administration of the drug. Pulsed IR (0.05 Hz) stimulation of the PC was performed as above. IR evoked responses were compared (a) prior to drug injection, (b) after the BP and HR baselines stabilized following drug administration, and (c) 40–50 min following drug administration to determine whether the BP and HR responses recovered.

RESULTS

IR Stimulation of the PC Modulates HR and BP

Unilateral stimulation of the PC with pulsed IR of wavelength 1,863 nm induced changes in eye position that matched the stimulus frequency (0.05 Hz, in 17 rats). The torsional, vertical movement of the ipsilateral (right) eye and downward movement of the contralateral (left) eye that are characteristic of PC stimulation (37) were confirmed visually in all rats. **Figure 1C** shows an example of the evoked sinusoidal eye movements from one of the rats that also provided the HR and BP data. The eye movements were used to confirm positioning of the optical fiber to target the PC sensors.

In the experiments highlighted in **Figure 2**, IR was delivered via a 400 μm optical fiber and the radiant energy of the stimulation was varied. At each energy level, decreases in HR and

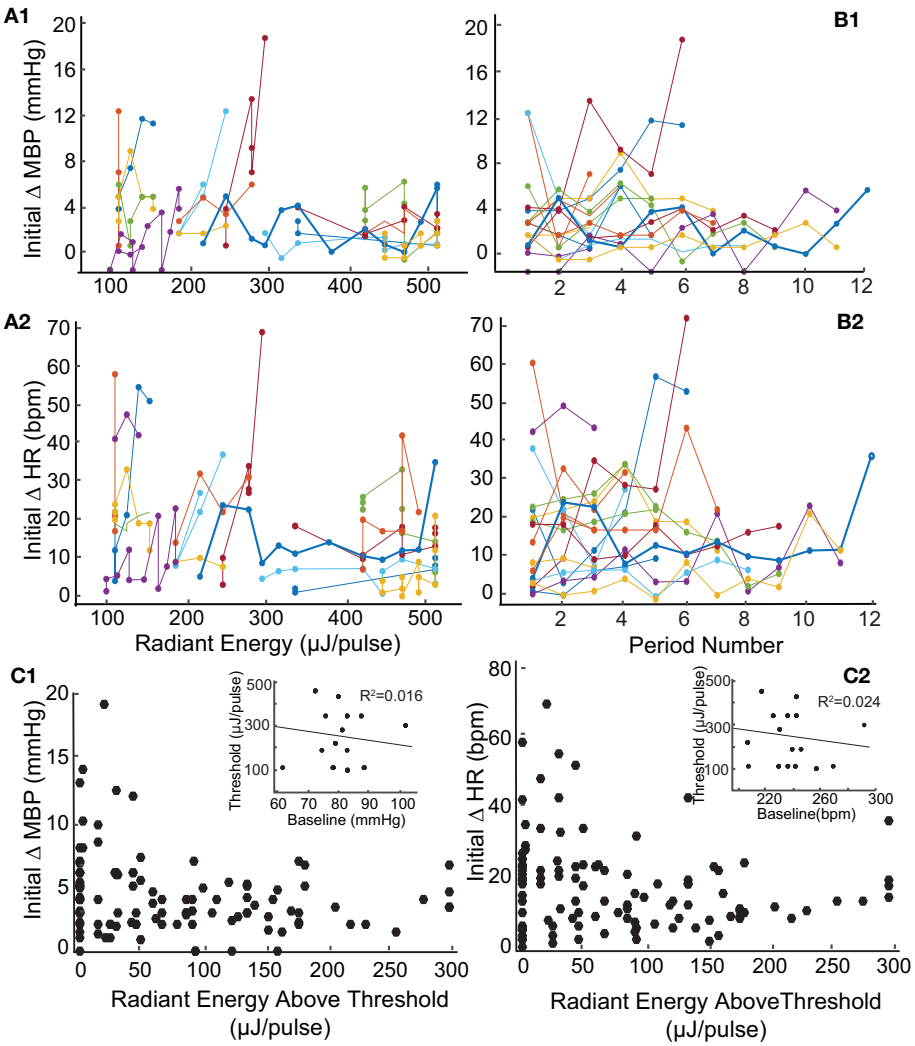

FIGURE 4 | Relationship between magnitude of change in blood pressure and heart rate and radiant energy or IR stimulation trials. **(A)** There is a no correlation between stimulation radiant energies (μJ/pulse) and the initial changes in **(A1)** MBP (mmHg) ($r = -0.331$) and **(A2)** HR (bpm) ($r = -0.269$). The results shown are from 113 IR stimulation events across 17 rats. **(B)** Shows the relationship between consecutive IR stimulation periods and the magnitude of change in **(B1)** MBP (mmHg) ($r = -0.0647$) and **(B2)** HR (bpm) ($r = -0.0725$) in 17 rats. The responses over multiple IR stimuli for individual rats are represented using different colors. **(C1,C2)** The initial changes in both parameters with stimuli radiant energy normalized to that at thresholds are shown. The insets show a weak correlation of threshold radiant energy required to evoke a response to baseline MBP or HR.

mean BP were observed at the onset of the sinusoidal stimulation (**Figure 2A**). As the IR stimulation proceeded over the 2-min periods (black bars, **Figure 2A**), the BP and HR modulated with the stimulus, and returned to baseline when the laser power was switched off. Multiple 2-min activation periods using the same stimulus conditions evoked similar responses during an experiment. For the example shown in **Figure 2A**, the threshold radiant energy required to elicit a change in BP or HR was 242 μJ/pulse. Subsequent stimuli at higher radiant energies, 275 and 292 μJ/pulse in this rat, resulted in characteristically similar, but larger BP and HR responses. Both physiological responses continued to modulate sinusoidally, matching the 0.05 Hz IR stimulation frequency. In this experiment, the initial decrease in BP ranged from 3.5 to 19 mmHg and initial decrease in HR ranged from 7.5 to 70 bpm, depending on the radiant energy of the pulses. HR and mean, systolic and diastolic BP changes in response to pulses of two different energy levels are shown on an expanded time scale in **Figures 2B,C.**

Figures 2D–F illustrate data from a second rat, in which the threshold IR radiant energy required to elicit a change in BP and HR was notably higher at 420 μJ/pulse (**Figure 2D**). In this animal, HR decreased at the onset of IR and remained below the baseline for the duration of IR stimuli. However, BP decreased transiently at the onset of IR stimulation and continued to modulate at low amplitude near the baseline. At the cessation of IR, both BP and HR returned to baseline and

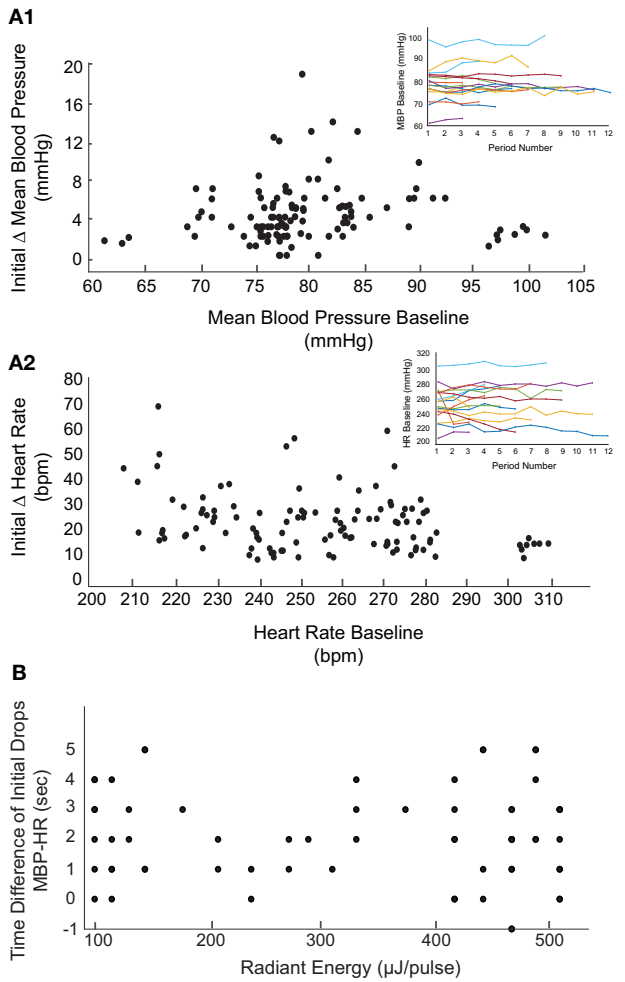

FIGURE 5 | Relationship between baseline and magnitude of changes in BP and HR. The initial decreases in MBP **(A1)** and HR **(A2)** in response to the 113 IR stimulation events (17 rats) are shown with respect to the averaged baseline MBP and HR prior to each stimulation. Overall, MBP and HR remained steady throughout the experiment (insets show the MBP and HR baselines over multiple IR periods for the 17 rats). **(B)** The relationship between latency of responses to IR at varying radiant energies (μJ/pulse) is shown. Latency of responses were calculated by taking the difference in time (seconds) of the initial decrease in MBP from initial decrease in HR.

remained stable until the next stimulus. The initial reduction in BP ranged from 4.06 to 7.24 mmHg and that of HR ranged from 23.65 to 34.13 bpm across the five stimuli shown in **Figure 2**. **Figures 2E,F** show the changes in HR and mean, systolic and diastolic BP for 2-min stimulation periods at the threshold of 420 μJ/pulse and at a higher radiant energy of 470 μJ/pulse, respectively. Consecutive stimulation cycles continued to evoke characteristically similar responses.

Overall, similar HR and BP responses were obtained from 17 rats in 113 IR stimulation trials of the PC. Across animals, the general profiles of the transient responses during IR were similar and IR stimulation evoked responses in each rat. However, the amplitude of the initial and subsequent decreases in BP and HR varied across animals and across stimulation trials. To determine whether the evoked changes decreased over the course of the stimulation period, we analyzed the peak-to-peak BP and HR responses over six intervals or cycles within the 2-min IR stimuli. The initial trough was taken as the first lowest value of HR or MBP when compared with an averaged baseline. Subsequent peaks/troughs were defined by the next highest/lowest values of MBP and HR when compared with the previous peak or trough. Responses from six rats in which IR stimulation was carried out for a cumulative total of 12 times at the same radiant energy (470 μJ/pulse) were pooled. The change in HR during the first stimulus cycle ranged from 1 to 43 bpm with a median of 17.47 bpm, while that for Cycle 6 ranged from 0 to 21 bpm with a median of 6.39 bpm (**Figure 3A**). The change in BP during the first cycle ranged from 1 to 7.24 mmHg with a median of 3 mmHg, and from 0 to 5.53 mmHg, median of 1.94 mmHg, for the sixth cycle. These cycle-to-cycle changes in BP and HR were not statistically significant (repeated measures ANOVA: HR, $p = 0.3644$ and BP, $p = 0.7952$).

Next, we focused on the initial declines in mean BP and HR at the onset of IR stimulation. When these magnitudes were calculated for each of the 113 IR stimuli delivered to the 17 rats, a moderate correlation was observed between magnitudes of the initial changes in mean BP and HR ($R^2 = 0.5004$, $p < 0.0005$, **Figure 3B**). To further investigate this, the percent changes in BP and HR were calculated by dividing the magnitude of change (initial decrease) in BP or HR for each IR stimulation period by the pre-stimulation baseline BP or HR for each rat. We found that these percent changes in BP and HR also correlated moderately ($R^2 = 0.4772$, $p < 0.0005$, **Figure 3C**) **Supplementary Figure 1** shows the relationship between percent change in BP and percent change in HR for each of the rats that received PC stimulation. These data show that, despite the variability in responses between individual animals, the overall correlation between changes in HR and changes in BP during IR stimulation is moderate.

Like the two examples shown in **Figure 2**, the levels of IR radiant energy that were required to elicit BP and HR changes varied across the 17 rats. To examine this further, we sought to determine whether the radiant energy per IR pulse (strength of the stimulus), the compilation of stimuli (multiple trials in the same rat), or baseline physiology of the rat affected BP or HR. Across the 113 IR stimuli applied to the 17 rats with PC stimulation, radiant energy varied between 72 and 512 μJ/pulse. **Figure 4** shows the magnitude of changes in BP (**Figure 4A1**) and HR (**Figure 4A2**) evoked by IR across different radiant energies per pulse in each of the 17 rats. The BP decreased between 1 and 19 mmHg with a median of 4 mmHg. However, these decrements in BP did not correlate with increasing radiant energy in a dose-dependent manner ($r = -0.331$). Similarly, HR diminished between 1 and 68 bpm with a median of 15 bpm, and also did not correlate with increasing radiant energy ($r = -0.269$). Each IR stimulation was 2 mi in duration and in most of the rats, the stimuli were repeated several times over 60–90 min. On average, 7 IR consecutive stimulation trials were applied per rat. To investigate potential adaptation or additive effects with repeated stimulation, the initial changes in BP and HR evoked at IR onset were compared across stimulation trials (**Figures 4B1,B2**).

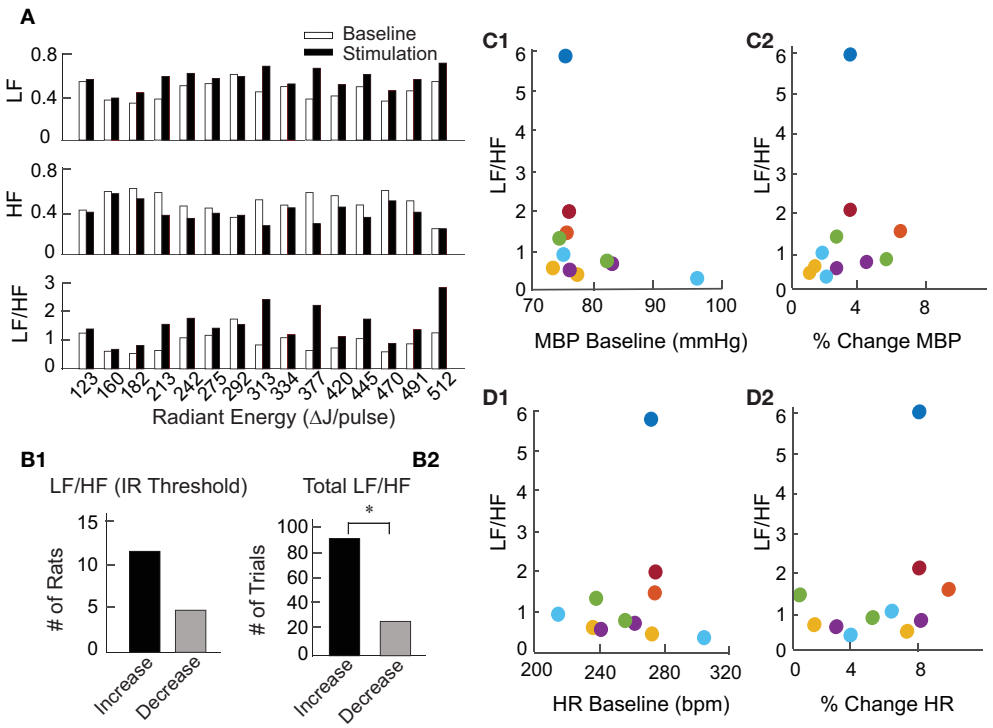

FIGURE 6 | Heart rate variability during pulsed IR targeting PC. **(A)** Shows an example of HRV changes in the LF, HF, and LF/HF components evoked by IR in one rat. Baseline responses, shown by white bars, were recorded for 2 min prior to initiation of IR. Responses to stimulation, shown by black bars, were recorded for 2 min during stimulation of the PC by IR. **(B1)** Shows the number of rats with an increase or decrease in LF/HF at each of the 17 rats' stimulation threshold. **(B2)** Shows the number of stimulation periods that resulted in either an increase or decrease in LF/HF over all periods (113) in 17 rats, (sign test, $p < 0.001$). **(C1,D1)** Show the relationship between HRV (LF/HR ratio) and baseline levels of MBP or HR for responses to IR stimulation of the PC at 470 μJ/pulse in 6 rats which are color coded. **(C2,D2)** Similarly show the relationship between HRV (LF/HF ratio) and percent change in MBP (initial change MBP/MBP baseline, or percent change in HR (initial change HR/baseline HR) for responses to IR stimulation of the PC at 470 μJ/pulse in the 6 rats.

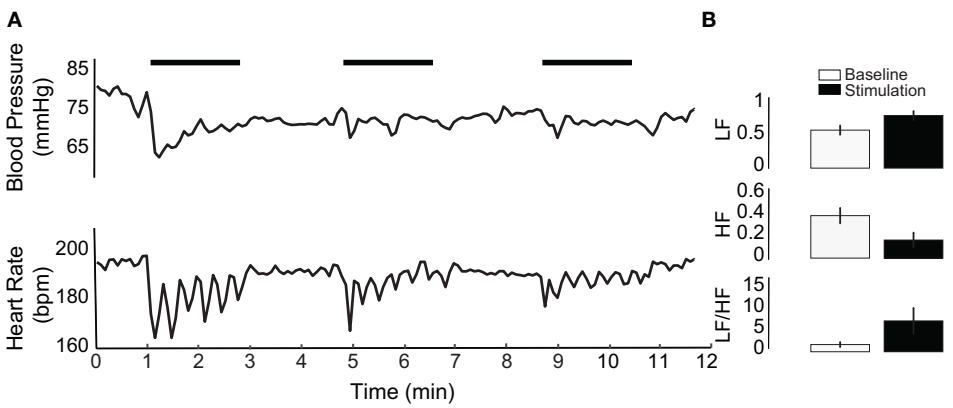

FIGURE 7 | Electrical stimulation of the PC. **(A)** An example of electrical stimulation in one of three stimulated rats. IR stimulation periods are indicated by horizontal black bars. **(B)** Shows HRV of the electrically stimulated rat in **(A)**, averaged over three stimulation periods. LF increases, HF decreases, and the LF/HF ratio increases with electrical stimulation of the PC.

Neither the BP decrease ($r = -0.0647$) nor the fall in HR ($r = -0.25$) correlated with the number of consecutive IR stimuli or with the radiant energy required to evoke the response above threshold. The threshold radiant energy required to elicit a change in BP or HR had a broad range, from 94 to 445 μJ/pulse (224 ± 118 μJ/pulse, mean ± SD, **Figures 4C1,C2**, insets).

The baseline BP (82.3 ± 8.6) and HR (244.9 ± 22.7) prior to stimulation varied significantly between the animals. The

baseline physiological responses can be affected by the duration of surgeries, effects of anesthesia (including multiple dosages), and inter-subject physiological variations. To determine whether the baseline physiology at the time of IR stimulation affected the evoked changes, the IR-evoked changes in mean BP and HR were compared to pre-stimulation baseline measurements. These results are summarized in **Figure 5**. The baseline measurements were obtained from averaged BP and HR recorded over a 2-min duration prior to each IR stimulation trial in each rat. The baseline MBP and HR in the 17 rats did not vary significantly over the duration of experiments (**Figure 5**, insets). Across the 113 trials in the 17 rats, the averaged baseline BP ranged from 61 to 102 mmHg (82.3 ± 8.6) while the BP changes during the first cycle of IR stimulation ranged from 1 to 19 mmHg. The largest changes in BP were observed in rats in which the baseline BP was within a physiological range of 72 to 90 mmHg. The baseline HR varied significantly, ranging from 208 to 311 bpm, while the HR decreases during the first cycle of IR stimulation ranged from 7 to 71 bpm.

To investigate the physiological changes underlying the reductions in BP and HR upon IR stimulation, heart rate variability (HRV) was analyzed for all animals. In the frequency domain, spectral analysis of the inter-beat interval was used to divide the variability into VLF (0.05–0.25 Hz), LF (0.25–1.0 Hz), and HF (1.0–3.0 Hz) components. The LF and HF components were normalized to remove VLF components for each stimulation event across the 17 rats, thereby eliminating the potential power contributions at the 0.05 Hz IR stimulation frequency. The LF/HF ratios were then calculated to assess HRV over the 2 min prior to stimulation (baseline) and for 2 min during stimulation at each radiant energy level. **Figure 6A** shows one example comparing the LF, HF, and LF/HF ratios at baseline and during IR-evoked responses. In this experiment, IR was delivered in 15 trials with increasing steps of radiant energy ranging from 123 to 512 μJ/pulse. In 11 of 17 animals, including this example (**Figure 6B1**), the LF components increased, HF components decreased, and the resulting LF/HF ratios increased during the IR-evoked responses. Of 113 IR trials, 90 resulted in an increase in the LF/HF ratio whereas only 23 resulted in a decrease (**Figure 6B2**). Additionally, we investigated the relationships between the frequency components (LF and HF) and pre-stimulation BP and HR baselines (**Figure 2**) as well as the relationships between the frequency components and baselines (**Figures 6C1,D1**) or percent changes (**Figures 6C2,D2**) in BP and HR in animals that were stimulated at a single radiant energy: 470 μJ/pulse. Neither component was significantly correlated with resting hemodynamic parameters or the IR induced total change in these parameters.

We also investigated the latency of PC- stimulation-induced cardiovascular responses across all 113 stimulation events (radiant energy varying from 105 to 512 μJ/pulse). The latency was calculated as the time required for the BP or HR to decrease to the lowest measured value following IR onset. The BP and HR latencies in 12 trials at a single radiant energy (470 μJ/pulse) demonstrate that the decrease in HR at this relatively high IR radiant energy occurred 1.42 ± 1.62 s prior to the reduction in MBP. At this radiant energy, the latency to the first drop in MBP was 16 ± 4.4 s whereas for HR was 14.4 ± 5.03. These findings are summarized in **Figure 5B** and reported as the time difference between the initial decrease in MBP and the initial decrease in HR. Time differences greater than zero indicate that the decrease in HR occurred prior to the decrement in MBP. Across the 117 trials, the reduction in HR occurred on average 2.05 ± 1.51 s prior to the decrease in BP. There was no correlation between these latencies and the radiant energy per pulse delivered during the IR stimulation.

HR and BP Responses to Electrical Stimulation of the PC

Our previous research has shown that IR of the vestibular neuroepithelium evokes diverse post-synaptic afferent spike trains with inhibition, excitation, and/or phase-locked responses (34, 36). The photothermally driven mechanism of IR stimulation in cells also leads to local temperature increases at higher radiant energies (36, 45) (**Figure 1A**). The IR stimulation used in the present study was also unilateral, and as such not a physiological stimulus condition. To assess the reliability of the evoked physiological responses, the PC was stimulated with frequency-modulated electrical currents in three naïve rats (no prior IR stimulation). Monophasic pulses of 500 μs phase duration and 700 μA per pulse were sinusoidally modulated at 0.05 Hz for three consecutive 2-min intervals matching the IR stimulation paradigm. The electrically-evoked BP and HR responses are shown in **Figure 7A** for one animal during three successive trials. Across these trials, the initial decrease in BP varied between 6.41 and 16.68 mmHg, and the reduction in HR varied between 7.3 and 33.63 bpm. Responses to 9 electrical stimulation trials in the three rats (three trials per rat) were obtained. Overall, the BP decrements ranged between 1.28 and 18.13 mmHg and those of HR varied between 3.84 and 72.78 bpm. In each of the three animals (example in **Figure 7B**), the HRV analysis was characteristically similar to that resulting from IR stimulation: the LF components increased and HF components decreased. All nine electrical stimulation trials resulted in an increase in the LF/HF ratio (**Figure 7B**), matching the majority of responses to IR stimulation of the PC.

IR Stimulation of the AC Modulates HR and BP

The IR parameters described above were used to stimulate the AC in 4 naïve rats (13 trials) while measuring changes in BP and HR. Stimulation of the AC was confirmed in each rat by the characteristic eye movements evoked in response to IR (37). **Figure 8A** shows an example of the reductions in HR and BP evoked by IR stimulation of the AC in two trials. Despite significant fluctuations in the BP response, an initial decrease in HR and sinusoidal modulation with pulsed IR were observed. We were unable to determine an initial decrement in BP using a radiant energy of 445 μJ/pulse, although an initial decrease in HR of 3.49 bpm occurred. Using higher stimulus energy (512 μJ/pulse), an initial reduction in BP from baseline levels of 0.81 mmHg was observed, together with a 8.17 bpm decline in

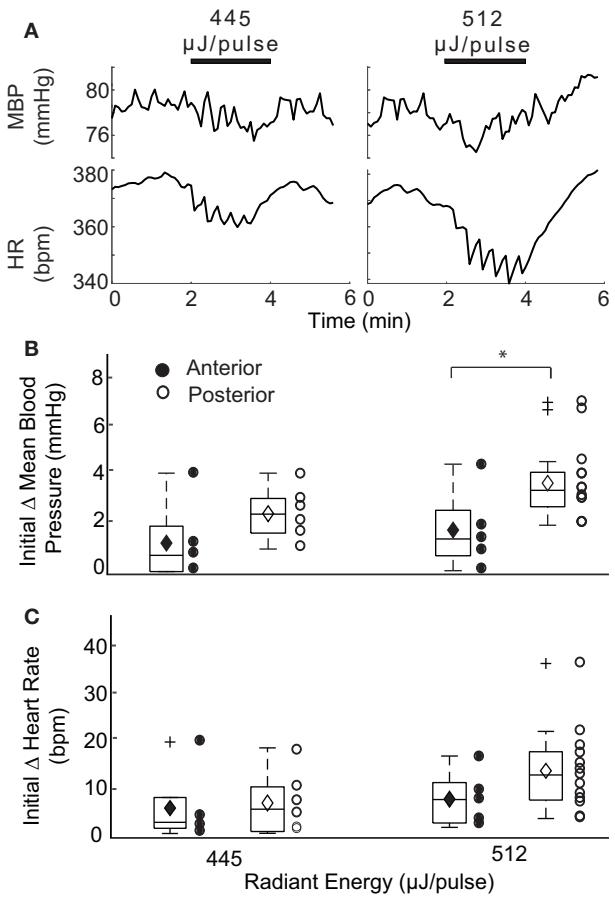

FIGURE 8 | Responses evoked with IR stimulation of the AC vs PC. **(A)** Shows two example responses recorded in one rat at different IR stimulation of the AC. Changes in mean BP and HR were recorded for cycles stimulated at 445 and 512 μJ/pulse. The initial decrease in BP at the higher radiant energy of 512 μJ/pulse was determined to be 0.81 mmHg. Initial decreases in HR were observed to be 3.49 and 8.17 bpm at respective radiant exposures. Box plots show comparison of the initial changes in MBP **(B)** and HR **(C)** between IR stimulation of AC (closed circle) and PC (open circle) at two different energy levels: 445 and 512 μJ/pulse. A significant difference in the responses evoked by IR stimulation of the two canals was observed in MBP and only at 512 μJ/pulse [P(T≤t) two tail = 0.047].

HR. Both BP and HR returned to baseline post-IR, and similar responses were observed in all 4 rats.

A comparison of the responses evoked by the two vertical semicircular canals is summarized in **Figures 8B,C** for mean BP and HR at two different radiant energies. Overall, IR stimulation of the AC evoked MBP changes ranging from 0.65 to 3.94 (median 1.11) at 445 μJ/pulse and 0.81 to 4.33 (median 1.56) at 512 μJ/pulse. AC evoked decrements in HR ranged from 1.22 to 19.82 (median 3.49) at 445 μJ/pulse and 2.82 to 16.54 (median 8.17) at 512 μJ/pulse. These responses modulated with the IR stimulation and were characteristically similar to those observed with PC stimulation. Significant differences between the AC- and PC-evoked responses were found only for the initial reduction in MBP at 512 μJ/pulse ($p = 0.047$, two-tail t-test). The AC-evoked responses were also analyzed to examine the relationships between magnitude of change and pre-stimulation baselines as well as the radiant energy and consecutive stimulation periods **Supplementary Figure 2**. The responses were similar to those observed during PC activation.

Effect of Autonomic Blockade on HR and BP Responses to IR Stimulation of the PC

The pharmacological blockade of vagal and sympathetic activities was achieved in naïve, additional rats by atropine (1 mg/kg) and propranolol (1 mg/kg) administration, respectively. The effects of these two drugs on BP and HR responses to unilateral pulsed IR stimulation of the PC were analyzed in separate experiments. The response after β-adrenergic receptor blockade with propranolol (1 mg/kg, iv) was used to estimate the sympathetic tone; the response after muscarinic cholinergic receptor blockade with methyl atropine (1 mg/kg, iv) was used to estimate the vagal tone (46). The initial changes induced by IR stimulation prior to the administration of atropine experiments was 2.54 ± 1.92 mmHg and 10.11 ± 6.52 bpm in the three rats tested (**Figures 9A1,B1**). Similarly, prior to the administration of propranolol, IR stimulation resulted in decreases of 3.46 ± 2.07 mmHg 15.40 ± 6.99 bpm (**Figures 9C1,D1**). Consistent with the effects of these drugs, we found a decrease in baseline HR by 21.83 ± 19.16 bpm following atropine administration and 88.99 bpm with propranolol (examples in **Figures 9B2,D2**). Recovery of HR was observed at ∼50 min post-administration of atropine in most rats (**Figure 9B3**). IR stimulation of PC did not evoke a change in HR with administration of either drug in all three rats (**Figures 9B2,D2**). The IR evoked responses recovered 40–50 min after administration of both drugs (**Figures 9B3,D3** and insets, for the example shown the HR recovered to 5.44 bpm post-atropine and 5.75 bpm post-proporanalol). In contrast, IR stimulation continued to evoke sinusoidal changes in BP after administration of atropine (**Figures 9A2,A3**, for the example shown the response was 5.49 mmHg), although these responses were eliminated following administration of propranolol (**Figure 9C2**). Responses from all three rats were characteristically similar.

DISCUSSION

In the present study, we used selective activation of either the PC or AC using pulsed IR to test a hypothesis that stimulation of a single vertical semicircular canal is sufficient to evoke a cardiovascular response. A subject-specific threshold level of radiant energy was necessary to elicit a cardiovascular response, above which there was a rapid decrease in HR and BP. Both measures then oscillated with the sinusoidal pulsed IR stimulation around the decreased plateau, returning to pre-stimulation baseline at the end of stimulation. The magnitude of the initial decrements in HR and BP did not correlate with the energy of the suprathreshold stimulus. This

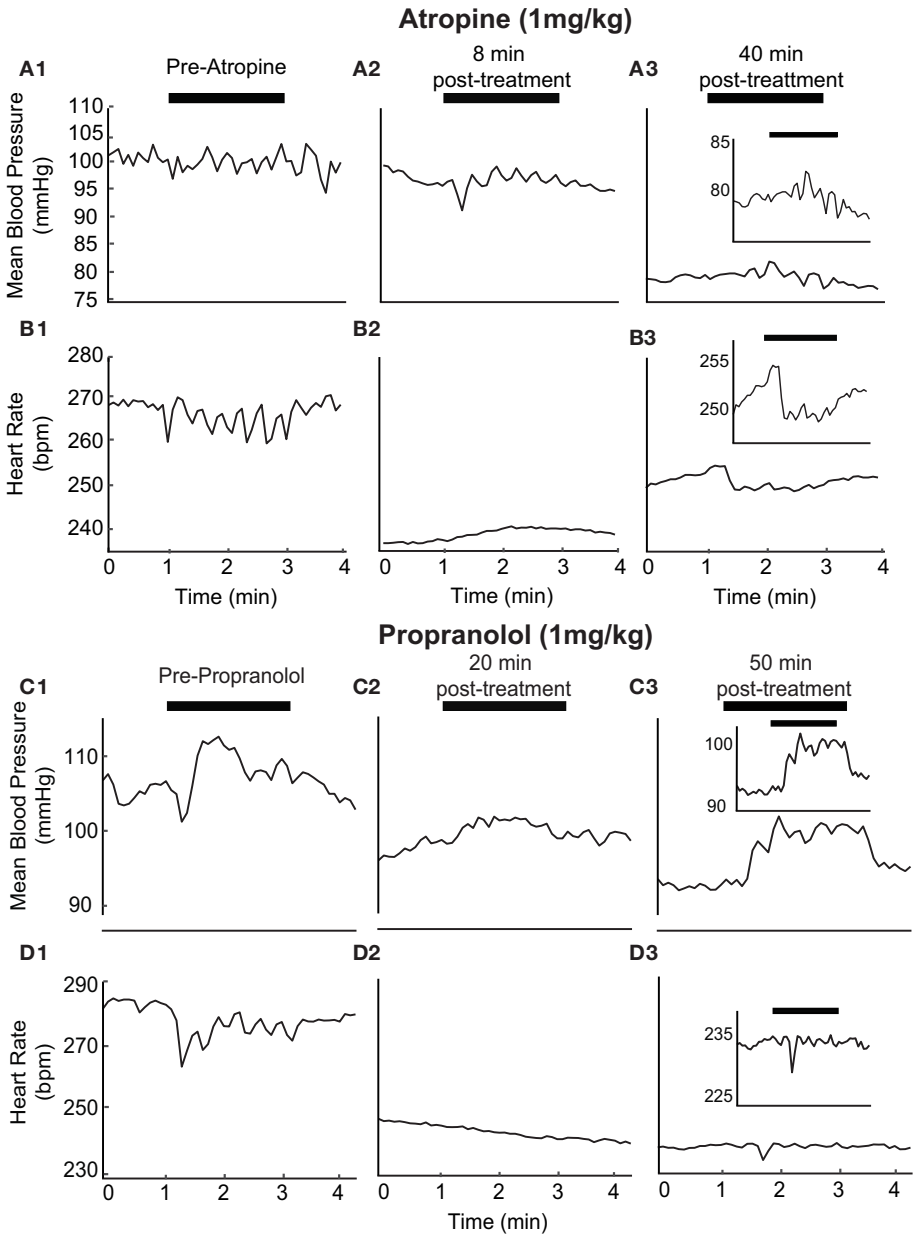

FIGURE 9 | Autonomic blockers affect changes in BP and HR with activation of PC: The pharmacological blockers Atropine (1 mg/kg) (**A1–3** and **B1–3**) and Propranolol (1 mg/kg) (**C1–3** and **D1–3**) were used to block autonomic activity prior to IR stimulation. We observed BP and HR in response to IR stimulation of the PC prior to the injection of either drug consistent with previous results **(A1, B1, C1, D1)**. Treatment with either blocker led to alterations in IR evoked responses (Atropine: **A2, A3, Be, B3**, and Proporanalol: **C2, C3, D2, D3**). A more detailed view of recovering BP and HR responses can be seen for atropine and propranolol (insets). HR baselines reduced from 270 to 235 bpm with atropine and 285 to 245 bpm with propranolol. HR responses to stimulation are suppressed following administration of either drug and begin to return to baseline levels 40–50 minutes following injection.

response pattern was consistent across multiple trials within an experimental session, replicable across subjects, and in most animals showed no evidence of habituation or an additive effect. Frequency modulated electrical current delivered to the PC caused decrements in HR and BP that resembled those evoked by IR stimulation of the PC and AC. Frequency domain HRV assessment revealed that, in most subjects, IR stimulation increased the low frequency component and decreased the high frequency component, resulting in an increase in the LF/HF ratio. Lastly, propranolol administration caused a substantial drop in baseline HR, and IR of the PC under these conditions did not evoke a change in HR or BP. In contrast, systemic atropine caused a small drop in baseline HR. IR of the PC during atropine treatment did not evoke a change in HR although stimulus-dependent sinusoidal modulations of BP were observed.

The brain requires stable cerebral perfusion in order to function normally and avoid syncope. One of the key physiological mechanisms mediating cardiovascular homeostasis is the baroreflex, a closed-loop negative feedback pathway deriving input from baroreceptors in the carotid body and aortic arch. When blood pressure increases, the associated distention of the arterial blood vessel walls is detected by these receptors, which convey excitatory signals via glossopharyngeal and vagal afferents to the caudal solitary nucleus (SolN) (47). SolN neurons relay the baroreflex-related input to GABAergic cells in the caudal ventrolateral medulla (CVLM), which project to pre-sympathetic cells of the adjacent rostral ventrolateral medulla (RVLM) (10, 48, 49). This inhibition reduces the level of activity in a series of barosensitive cell groups from RVLM, to preganglionic sympathetic neurons in the spinal cord, and ultimately the sympathetic trunk. Through this pathway, an increase in mean arterial pressure has been shown to result in a reduction in sympathetic nerve activity, relaxation of the vascular smooth muscle, and a reduction in arterial blood pressure due to baroreceptor unloading [for review, see Guyenet (50)].

Most of the vasculature receives innervation exclusively from sympathetic autonomic fibers, in a noradrenergic projection mediated by alpha adrenergic receptors. In contrast, HR is modulated by both sympathetic and parasympathetic fibers. The sympathetic fibers are noradrenergic, and their activation increases both contractility and relaxation rate of the heart muscles. The parasympathetic innervation originates from the dorsal motor vagal nucleus and nucleus ambiguus, and the cardiac ganglion cells receiving their input are cholinergic and activate muscarinic cholinergic receptors. In addition to its key role in mediating sympathetic outflow, SolN neurons can influence HR through projections to preganglionic parasympathetic cells in the nucleus ambiguus. Normally, the parasympathetic fibers restore cardiac homeostasis following sympathetic perturbation.

A large body of evidence from clinical observations and experimental studies in humans and animal models supports the notion that the vestibular system participates in the control of HR and BP during movement and postural adjustments (51). The redistribution of body fluids that occurs upon standing or rearing requires a rapid and proactive cardiovascular response in order to prevent blood from pooling in the legs and a subsequent decrease in cerebral perfusion (52). Since changes in head position and head motion activate the otolith organs and semicircular canals, the vestibular system is optimally situated to provide the requisite input to central cardiovascular circuits. This connection between the vestibular and autonomic systems allows for rapid modulation of HR and BP with changes in head position or body posture via vestibulo-autonomic pathways. Experimental studies in humans using various vestibular stimulation approaches have shown that activation of the vestibular labyrinth alters BP, blood flow, respiration and/or sympathetic nerve activity [for reviews, see Yates et al. (4); Hammam and Macefield (53); Yates and Miller (5)]. As highlighted in these reviews, considerable data exists showing that the vestibular inputs have complex effects on blood flow rates and pressure regulation to the head and hindlimbs and response patterning (54–56). Sinusoidally-modulated galvanic vestibular stimulation (sGVS) has been shown to evoke patterned sympathetic nerve activity in humans, specifically resulting in vasoconstriction of blood vessels in the legs (18, 20). This patterning of nerve activity resembles the sympathetic responses normally observed in humans during tilt and standing, and is thought to reflect an interaction between the baroreflex and the vestibular system (21). Moreover, head-up and head-down tilt delivered through off-vertical-axis rotation elicit up-and-down modulation of muscle sympathetic nerve activity that is in-phase with the oscillating stimulus (14). Since continuous off-vertical-axis rotation is thought to adapt the semicircular canals, this sympathetic modulation has been attributed to otolith end organ activation. There is little evidence until now from animal or human studies that stimulation of the vertical semicircular canals changes sympathetic nerve activity. However, studies on whole body oscillations in the yaw plane, which stimulate the horizontal semicircular canals, show a decrease in HR in humans (57). Warm and cool-water irrigation activate the horizontal canals and elicit caloric nystagmus, though its effects on sympathetic nerve activity and cardiovascular parameters in human subjects appear to be inconclusive (11, 58), for review, see Yates et al. (4).

There is a substantial literature demonstrating that sympathetic nerve activity changes during natural and electrical stimulation of the vestibular nerve in animals [for review, see Yates et al. (4)]. Following the initial seminal reports (24, 59), these studies generally indicate that head-up tilt and linear acceleration increase sympathetic nerve activity and raise BP (25, 29, 60), and that these increases are attenuated by bilateral peripheral vestibular damage (61). While the head-up tilts activate afferents from PC bilaterally, it is possible that our results when stimulating unilateral vertical canals reflect altered activity of vestibular nuclei neurons receiving convergent input from otolith and canals. A previous study has also shown that head-down tilt induced a rapid reduction in HR in normal subjects (62). Nose-down rotation causes a transient decrease in BP, which has also been attributed to vestibular input to autonomic pathways (28). Similar response was observed in patients with unilateral benign paroxysmal positional vertigo where the PC biomechanics is affected but only if the patients are tilted in the plane of the unaffected, contralateral PC (62). Future studies need to employ bilateral vertical canal stimulation to further characterize the observed responses. Furthermore, sGVS in rats can evoke drops in both BP and HR (29, 42, 63, 64). Most studies attribute the effects of sGVS, including those on autonomic activity, to otolith activation because of the low frequency characteristics of the stimuli and the perceptual, ocular, and postural responses that are elicited (18, 65). However, it has been suggested that the vertical canals may also be activated by the stimulus (4, 66, 67), raising the possibility that the vertical canals contribute to vestibulo-autonomic activity. In fact, both the otolith organs and semicircular canals can respond to tilt (17) and the vestibulo-ocular and -spinal reflexes can be evoked by combined otolith and canal input (60). We observed initial drops in HR with IR stimulation that were correlated with drops in BP and continued to modulate in-phase with the low frequency sinusoidal IR stimulation. These responses were replicable and stable over multiple trials, delivered over several

hours. The magnitude of responses did not vary significantly over this prolonged experimental period. We did observe that the threshold IR radiant energy or strength of stimulus required to evoke a change in BP or HR varied (between 94 and 512 μJ/pulse) across the animals and was likely a result of small differences in orientation of the optical fiber between experiments. Overall, these results demonstrate that activation of a single vertical canal is sufficient to alter BP and HR. In future studies, it will be important to test contributions of the horizontal semicircular canals as well as stimulation of combined vertical canal and utricular macula.

The morphological basis for this vestibulo-autonomic activity has been demonstrated previously using sGVS to activate neurons in the caudal vestibular nuclei (42), and from there to brainstem regions involved in the central regulation of BP (9, 68–70) and HR (6, 71), as well as respiration (5, 72). These studies suggest that the vestibular system provides a means for rapid detection and autonomic activation in response to a postural change, requiring only ∼100 ms to accomplish a change in BP following stimulation (10). This rapid change is followed by baroreflex activity, which re-establishes BP homeostasis 30–60 s after standing. Our results show that vertical semicircular canal activation induces a drop in both the HR and BP. This vaso-vagal-type response has also been reported following sGVS in rats (73), and can be attributed to the interaction between vestibulo-autonomic and baroreceptor reflexes. Supporting this interpretation, we observed that a measurable change in HR occurred prior to that of BP during IR stimulation. This observation highlights the non-linear nature of the relationship between HR and BP and suggests that the initial rapid cardiovascular response mediated by the vestibular system (14, 74, 75) is followed by baroreflex activity that has a substantially longer latency and as a result, may exacerbate or ameliorate the effects of the initial vestibulo-autonomic drive (76).

We used HRV analysis from the 17 rats (113 IR stimuli) receiving PC stimulation to further understand the effects of vertical canal stimulation on autonomic activity. HRV generally reflects the ability of the cardiovascular system to adapt to changing stimulus conditions and is used to assess fluctuations in autonomic innervation of the heart, as an alternative measure to average activity level. In general, healthy individuals have high HRV and reduced HRV is interpreted as an abnormal imbalance in the activity of the sympathetic and parasympathetic branches of the autonomic system (77). However, a decrease in HRV can reflect either withdrawal or excessively high activity in either of these branches. In the frequency domain, three components of HRV are distinguished: high, low and very low frequencies. The HF component can be viewed as predominantly an indicator of parasympathetic (vagal) activity. The LF component, however, reflects both the sympathetic and parasympathetic branches (78). The VLF component is typically a reflection of the stimulus. We found that IR stimulation caused an increase in the LF components with a corresponding decrease in HF components (**Figure 7**). This result is likely to reflect the interaction of short-latency vestibular effects on both sympathetic pathways through RVLM and on parasympathetic pathways through SolN, followed by cardiac and baroreflex efforts to re-establish homeostasis. In research using GVS, the HF component increased during stimulation and corresponded to increased mean arterial pressure in down-facing patients. The LF/HF ratio, a reflection of sympathetic nerve activity, increased with GVS in up-facing patients only (79). These results are consistent with studies using head-down neck rotation (80) and head-up off-vertical-axis rotation (14).

We further investigated the tonic sympathetic and vagal influences on the heart with selective pharmacological blockade of cardiac autonomic receptors. The ACh antagonist atropine was used to inhibit the effects of excessive vagal activation on the heart. The non-selective beta blocker propranolol works by blocking epinephrine and norepinephrine at β -adrenergic receptors. The response after β-adrenergic receptor blockade with propranolol was used to estimate the sympathetic tone; the response after muscarinic cholinergic receptor blockade with atropine was used to assess the vagal tone (46). Our results with IR following the pharmacological blocks suggest that the changes in HR evoked by IR are dependent on both sympathetic and parasympathetic activity but that BP responses are likely to be independent of parasympathetic activation.

Conclusion

The present study demonstrates that activation of the vertical semicircular canals evokes significant autonomic activity in the anesthetized rats. The resulting decreases in MBP and HR confirm that these end organs provide a means for rapid detection and autonomic activation in response to a postural change. A direct comparison to the stimulation of unilateral otolith organs or augmentation of the responses seen here by otolith organs remain a goal for future studies.

DATA AVAILABILITY STATEMENT

The raw data supporting the conclusions of this article will be made available by the authors, without undue reservation.

ETHICS STATEMENT

The animal study was reviewed and approved by Institutional Animal Care and Use Committee (IACUC) of the University of Miami.

AUTHOR CONTRIBUTIONS

DR, GM, GH, and SR conceptualized, designed the experiments, and prepared the manuscript. DR, GM, WJ, and SR carried out the experiments and collected the data. DR, GH, and SR analyzed the data and prepared all the figures. All authors approved the final manuscript.

FUNDING

This work was supported by NIH NIDCD 1R01DC008846 (GH) and 1R01DC013798 (SR), a pilot award from National Center for Advancing Translational Sciences of the National Institutes of Health under Award Number UL1TR002736, Miami Clinical

and Translational Science Institute, and the Wallace H. Coulter Center for Translational Research Neural Engineering SEED Grants (SR).

SUPPLEMENTARY MATERIAL

The Supplementary Material for this article can be found online at: https://www.frontiersin.org/articles/10.3389/fneur.2021.680044/full#supplementary-material

Supplementary Figure 1 | Percent change in BP and HR. Percent changes in MBP (initial change in MPB/baseline MPB) and HR (initial change in HR/baseline HR) for each stimulation period for individual animals with PC stimulation (17 total with IR and 3 with electrical stimulation, outlined using dotted rectangle). R^2-values are shown with each rat identification number.

Supplementary Figure 2 | Magnitude of IR evoked changes in AC. The magnitude of changes in MBP (top) and HR (bottom) for 13 stimulation periods across four rats during the initial cycle of AC stimulation with IR are shown. **(A,B)** Show the responses to IR applied at varying radiant energies (377–512 μJ/pulse) when compared to the averaged baseline MBP (mmHg) ($R^2 = 0.078$) and HR (bpm) ($R^2 = 0.083$). **(C,D)** Show weak correlation between stimulation radiant energies (μJ/pulse) and the initial changes in MBP (mmHg) ($R^2 = 0.030$) and HR (bpm) ($R^2 = 0.081$). **(E,F)** show the relationship between consecutive periods and the magnitude of change in **(B1)** MBP (mmHg) ($R^2 = 0.174$) and **(B2)** HR (bpm) ($R^2 = 0.118$). Period numbers signify the number of events a single rat has undergone.

REFERENCES

1. Holstein GR. The vestibular system. In: Mai JK and Paxinos G, editors. *The Human Nervous System*. 3rd Edition ed. Boston, MA: Academic Press (2012). p. 1239–69.
2. Vidal PP, Cullen K, Curthoys IS, Du Sac S, Holstein G, Idoux E, et al. Chapter 28 - the vestibular system. In: Paxinos G, editors. *The Rat Nervous System (Fourth Edition)*. Boston, MA: Elsevier Inc. (2015). p. 805–864. doi: 10.1016/B978-0-12-374245-2.00028-0
3. Yates BJ, Miller AD. Vestibulo-respiratory regulation. In: *Neural Control of Respiratory Muscles*. Boca Raton, FL: CRC Press (1996). p. 271–283.
4. Yates BJ, Bolton PS, Macefield VG. Vestibulo-sympathetic responses. *Compr Physiol.* (2014) 4:851–87. doi: 10.1002/cphy.c130041
5. Yates BJ, Miller AD. Vestibular respiratory regulation. In: Miller AD, Bianchi AL, Bishop BP, editors. *Neural Control of the Respiratory Muscles*. 1st Edition. Boca Raton, FL: CRC Press (2019).
6. Balaban CD, Beryozkin G. Vestibular nucleus projections to nucleus tractus solitarius and the dorsal motor nucleus of the vagus nerve: potential substrates for vestibulo-autonomic interactions. *Exp Brain Res.* (1994) 98:200–12. doi: 10.1007/BF00228409
7. Holstein GR. Morphophysiological organization of vestibulo-autonomic pathways. In: Fritzsch B, editors. *The Senses: A Comprehensive Reference,* 2nd Edition. Boston, MA: Elsevier (2020). p. 432–444.
8. Barman SM, Yates BJ. Deciphering the neural control of sympathetic nerve activity: status report and directions for future research. *Front Neurosci.* (2017) 11:730. doi: 10.3389/fnins.2017.00730
9. Holstein GR, Friedrich VL Jr, Martinelli GP. Glutamate and GABA in vestibulo-sympathetic pathway neurons. *Front Neuroanat.* (2016) 10:7. doi: 10.3389/fnana.2016.00007
10. Jeske I, Morrison SF, Cravo SL, Reis DJ. Identification of baroreceptor reflex interneurons in the caudal ventrolateral medulla. *Am J Physiol.* (1993) 264:R169–78. doi: 10.1152/ajpregu.1993.264.1.R169
11. Cui J, Mukai C, Iwase S, Sawasaki N, Kitazawa H, Mano T, et al. Response to vestibular stimulation of sympathetic outflow to muscle in humans. *J Auton Nerv Syst.* (1997) 66:154–62. doi: 10.1016/S0165-1838(97)00077-5
12. Ray CA, Hume KM, Steele SL. Sympathetic nerve activity during natural stimulation of horizontal semicircular canals in humans. *Am J Physiol.* (1998) 275:R1274–8. doi: 10.1152/ajpregu.1998.275.4.R1274
13. Cui J, Iwase S, Mano T, Kitazawa H. Responses of sympathetic outflow to skin during caloric stimulation in humans. *Am J Physiol.* (1999) 276:R738–44. doi: 10.1152/ajpregu.1999.276.3.R738
14. Kaufmann H, Biaggioni I, Voustianiouk A, Diedrich A, Costa F, Clarke R, et al. Vestibular control of sympathetic activity. An otolith-sympathetic reflex in humans. *Exp Brain Res.* (2002) 143:463–9. doi: 10.1007/s00221-002-1002-3
15. Kuipers NT, Sauder CL, Ray CA. Aging attenuates the vestibulorespiratory reflex in humans. *J Physiol.* (2003) 548:955–61. doi: 10.1113/jphysiol.2002.033357
16. Ray CA, Carter JR. Vestibular activation of sympathetic nerve activity. *Acta Physiol Scand.* (2003) 177:313–9. doi: 10.1046/j.1365-201X.2003.01084.x
17. Cathers I, Day BL, Fitzpatrick RC. Otolith and canal reflexes in human standing. *J Physiol.* (2005) 563:229–34. doi: 10.1113/jphysiol.2004.079525
18. Bent LR, Bolton PS, Macefield VG. Modulation of muscle sympathetic bursts by sinusoidal galvanic vestibular stimulation in human subjects. *Exp Brain Res.* (2006) 174:701–11. doi: 10.1007/s00221-006-0515-6
19. Sauder CL, Conboy EE, Chin-Sang SA, Ray CA. Otolithic activation on visceral circulation in humans: effect of aging. *Am J Physiol Renal Physiol.* (2008) 295:F1166–9. doi: 10.1152/ajprenal.90408.2008
20. Grewal T, James C, Macefield VG. Frequency-dependent modulation of muscle sympathetic nerve activity by sinusoidal galvanic vestibular stimulation in human subjects. *Exp Brain Res.* (2009) 197:379–86. doi: 10.1007/s00221-009-1926-y
21. James C, Stathis A, Macefield VG. Vestibular and pulse-related modulation of skin sympathetic nerve activity during sinusoidal galvanic vestibular stimulation in human subjects. *Exp Brain Res.* (2010) 202:291–8. doi: 10.1007/s00221-009-2131-8
22. Grewal T, Dawood T, Hammam E, Kwok K, Macefield VG. Low-frequency physiological activation of the vestibular utricle causes biphasic modulation of skin sympathetic nerve activity in humans. *Exp Brain Res.* (2012) 220:101–8. doi: 10.1007/s00221-012-3118-4
23. Hammam E, Kwok K, Macefield VG. Modulation of muscle sympathetic nerve activity by low-frequency physiological activation of the vestibular utricle in awake humans. *Exp Brain Res.* (2013) 230:137–42. doi: 10.1007/s00221-013-3637-7
24. Doba N, Reis DJ. Role of the cerebellum and the vestibular apparatus in regulation of orthostatic reflexes in the cat. *Circ Res.* (1974) 34:9–18. doi: 10.1161/01.RES.34.1.9
25. Woodring SF, Rossiter CD, Yates BJ. Pressor response elicited by nose-up vestibular stimulation in cats. *Exp Brain Res.* (1997) 113:165–8. doi: 10.1007/BF02454153
26. Jian BJ, Cotter LA, Emanuel BA, Cass SP, Yates BJ. Effects of bilateral vestibular lesions on orthostatic tolerance in awake cats. *J Appl Physiol (1985).* (1999) 86:1552–60. doi: 10.1152/jappl.1999.86.5.1552
27. Abe C, Tanaka K, Awazu C, Morita H. Strong galvanic vestibular stimulation obscures arterial pressure response to gravitational change in conscious rats. *J Appl Physiol.* (2008) 104:34–40. doi: 10.1152/japplphysiol.00454.2007
28. Nakamura Y, Matsuo S, Hosogai M, Kawai Y. Vestibular control of arterial blood pressure during head-down postural change in anesthetized rabbits. *Exp Brain Res.* (2009) 194:563–70. doi: 10.1007/s00221-009-1732-6
29. Abe C, Tanaka K, Awazu C, Morita H. Galvanic vestibular stimulation counteracts hypergravity-induced plastic alteration of vestibulo-cardiovascular reflex in rats. *J Appl Physiol.* (2009) 107:1089–94. doi: 10.1152/japplphysiol.00400.2009
30. Cui J, Iwase S, Mano T, Katayama N, Mori S. Muscle sympathetic outflow during horizontal linear acceleration in humans. *Am J Physiol Regul Integr Comp Physiol.* (2001) 281:R625–34. doi: 10.1152/ajpregu.2001.281.2.R625
31. Wells J, Kao C, Mariappan K, Albea J, Jansen ED, Konrad P, et al. Optical stimulation of neural tissue *in vivo*. *Opt Lett.* (2005) 30:504–6. doi: 10.1364/OL.30.000504
32. Izzo AD, Richter CP, Jansen ED, Walsh JT Jr. Laser stimulation of the auditory nerve. *Lasers Surg Med.* (2006) 38:745–53. doi: 10.1002/lsm.20358

33. Rajguru SM, Matic AI, Robinson AM, Fishman AJ, Moreno LE, Bradley A, et al. Optical cochlear implants: evaluation of surgical approach and laser parameters in cats. *Hear Res.* (2010) 269:102–11. doi: 10.1016/j.heares.2010.06.021
34. Rajguru SM, Richter CP, Matic AI, Holstein GR, Highstein SM, Dittami GM, et al. Infrared photostimulation of the crista ampullaris. *J Physiol.* (2011) 589:1283–94. doi: 10.1113/jphysiol.2010.198333
35. Liu Q, Frerck MJ, Holman HA, Jorgensen EM, Rabbitt RD. Exciting cell membranes with a blustering heat shock. *Biophys J.* (2014) 106:1570–7. doi: 10.1016/j.bpj.2014.03.008
36. Rabbitt RD, Brichta AM, Tabatabaee H, Boutros PJ, Ahn J, Della Santina CC, et al. Heat pulse excitability of vestibular hair cells and afferent neurons. *J Neurophysiol.* (2016) 116:825–43. doi: 10.1152/jn.00110.2016
37. Jiang W, Rajguru SM. Eye movements evoked by pulsed infrared radiation of the rat vestibular system. *Ann Biomed Eng.* (2018) 46:1406–18. doi: 10.1007/s10439-018-2059-x
38. Hitier M, Sato G, Zhang YF, Zheng Y, Besnard S, Smith PF, et al. Anatomy and surgical approach of rat's vestibular sensors and nerves. *J Neurosci Methods.* (2016) 270:1–8. doi: 10.1016/j.jneumeth.2016.05.013
39. Hale GM, Querry MR. Optical constants of water in the 200-nm to 200-microm wavelength region. *Appl Opt.* (1973) 12:555–63. doi: 10.1364/AO.12.000555
40. Moreno LE, Rajguru SM, Matic AI, Yerram N, Robinson AM, Hwang M, et al. Infrared neural stimulation: beam path in the guinea pig cochlea. *Hear Res.* (2011) 282:289–302. doi: 10.1016/j.heares.2011.06.006
41. Stahl JS, Van Alphen AM, De Zeeuw. C. I. A comparison of video and magnetic search coil recordings of mouse eye movements. *J Neurosci Methods.* (2000) 99:101–10. doi: 10.1016/S0165-0270(00)00218-1
42. Holstein GR, Friedrich VL Jr, Martinelli GP, Ogorodnikov D, Yakushin SB, et al. Fos expression in neurons of the rat vestibulo-autonomic pathway activated by sinusoidal galvanic vestibular stimulation. *Front Neurol.* (2012) 3:4. doi: 10.3389/fneur.2012.00004
43. Esc, Nscpe. Heart rate variability. Standards of measurement, physiological interpretation, clinical use. Task Force of the European Society of Cardiology and the North American Society of Pacing and Electrophysiology. *Eur Heart J.* (1996) 17:354–81. Available online at: https://www.semanticscholar.org/paper/Heart-rate-variability%3A-standards-of-measurement%2C-Camm-Malik/b58c40da4051134954fccf0ab765b314f58ff18b
44. Mccraty R SF. Heart rate variability: new perspectives on physiological mechanisms, assessment of self-regulatory capacity, health risk. *Glob Adv Health Med.* (2015) 4:46–61. doi: 10.7453/gahmj.2014.073
45. Barrett JN, Rincon S, Singh J, Matthewman C, Pasos J, Barrett EF, et al. Pulsed infrared releases Ca(2+) from the endoplasmic reticulum of cultured spiral ganglion neurons. *J Neurophysiol.* (2018) 120:509–24. doi: 10.1152/jn.00740.2017
46. Fazan R Jr, De Oliveira M, Oliveira JA, Salgado HC, Garcia-Cairasco N. Changes in autonomic control of the cardiovascular system in the Wistar audiogenic rat (WAR) strain. *Epilepsy Behav.* (2011) 22:666–70. doi: 10.1016/j.yebeh.2011.09.010
47. Spyer KM. Neural organisation and control of the baroreceptor reflex. *Rev Physiol Biochem Pharmacol.* (1981) 88:24–124. doi: 10.1007/BFb0034536
48. Blessing WW. Depressor neurons in rabbit caudal medulla act via GABA receptors in rostral medulla. *Am J Physiol.* (1988) 254:H686–92. doi: 10.1152/ajpheart.1988.254.4.H686
49. Natarajan M, Morrison SF. Sympathoexcitatory CVLM neurons mediate responses to caudal pressor area stimulation. *Am J Physiol Regul Integr Comp Physiol.* (2000) 279:R364–74. doi: 10.1152/ajpregu.2000.279.2.R364
50. Guyenet PG. The sympathetic control of blood pressure. *Nat Rev Neurosci.* (2006) 7:335–46. doi: 10.1038/nrn1902
51. Yates BJ. Vestibular influences on the autonomic nervous system. *Ann N Y Acad Sci.* (1996) 781:458–73. doi: 10.1111/j.1749-6632.1996.tb15720.x
52. Serrador JM, Schlegel TT, Black FO, Wood SJ. Vestibular effects on cerebral blood flow. *BMC Neurosci.* (2009) 10:119. doi: 10.1186/1471-2202-10-119
53. Hammam E, Macefield VG. Vestibular modulation of sympathetic nerve activity to muscle and skin in humans. *Front Neurol.* (2017) 8:334. doi: 10.3389/fneur.2017.00334
54. Wilson TD, Cotter LA, Draper JA, Misra SP, Rice CD, Cass SP, et al. Vestibular inputs elicit patterned changes in limb blood flow in conscious cats. *J Physiol.* (2006) 575:671–84. doi: 10.1113/jphysiol.2006.112904
55. Wilson TD, Cotter LA, Draper JA, Misra SP, Rice CD, Cass SP, et al. Effects of postural changes and removal of vestibular inputs on blood flow to the head of conscious felines. *J Appl Physiol (1985).* (2006) 100:1475–82. doi: 10.1152/japplphysiol.01585.2005
56. Yavorcik KJ, Reighard DA, Misra SP, Cotter LA, Cass SP, Wilson TD, et al. Effects of postural changes and removal of vestibular inputs on blood flow to and from the hindlimb of conscious felines. *Am J Physiol Regul Integr Comp Physiol.* (2009) 297:R1777–84. doi: 10.1152/ajpregu.00551.2009
57. Thurrell A, Jauregui-Renaud K, Gresty MA, Bronstein AM. Vestibular influence on the cardiorespiratory responses to whole-body oscillation after standing. *Exp Brain Res.* (2003) 150:325–31. doi: 10.1007/s00221-003-1422-8
58. Costa F, Lavin P, Robertson D, Biaggioni I. Effect of neurovestibular stimulation on autonomic regulation. *Clin Auton Res.* (1995) 5:289–93. doi: 10.1007/BF01818894
59. Tang PC, Gernandt BE. Autonomic responses to vestibular stimulation. *Exp Neurol.* (1969) 24:558–78. doi: 10.1016/0014-4886(69)90158-7
60. Yates BJ, Miller AD. Properties of sympathetic reflexes elicited by natural vestibular stimulation: implications for cardiovascular control. *J Neurophysiol.* (1994) 71:2087–92. doi: 10.1152/jn.1994.71.6.2087
61. Zhu H, Jordan JR, Hardy SP, Fulcher B, Childress C, Varner C, et al. Linear acceleration-evoked cardiovascular responses in awake rats. *J Appl Physiol (1985).* (2007) 103:646–54. doi: 10.1152/japplphysiol.00328.2007
62. Jauregui-Renaud K, Aw ST, Todd MJ, Mcgarvie LA, Halmagyi GM. Benign paroxysmal positional vertigo can interfere with the cardiac response to head-down tilt. *Otol Neurotol.* (2005) 26:484–8. doi: 10.1097/01.mao.0000169783.76964.f6
63. Fitzpatrick RC, Day BL. Probing the human vestibular system with galvanic stimulation. *J Appl Physiol (1985).* (2004) 96:2301–16. doi: 10.1152/japplphysiol.00008.2004
64. Cohen B, Martinelli GP, Ogorodnikov D, Xiang Y, Raphan T, Holstein GR, et al. Sinusoidal galvanic vestibular stimulation (sGVS) induces a vasovagal response in the rat. *Exp Brain Res.* (2011) 210:45–55. doi: 10.1007/s00221-011-2604-4
65. Watson SR, Brizuela AE, Curthoys IS, Colebatch JG, Macdougall HG, Halmagyi GM. Maintained ocular torsion produced by bilateral and unilateral galvanic (DC) vestibular stimulation in humans. *Exp Brain Res.* (1998) 122:453–8. doi: 10.1007/s002210050533
66. Curthoys IS, Macdougall HG. What galvanic vestibular stimulation actually activates. *Front Neurol.* (2012) 3:117. doi: 10.3389/fneur.2012.00117
67. Reynolds RF, Osler CJ. Galvanic vestibular stimulation produces sensations of rotation consistent with activation of semicircular canal afferents. *Front Neurol.* (2012) 3:104. doi: 10.3389/fneur.2012.00104
68. Holstein GR, Friedrich VL Jr, Kang T, Kukielka E, Martinelli GP. Direct projections from the caudal vestibular nuclei to the ventrolateral medulla in the rat. *Neuroscience.* (2011) 175:104–17. doi: 10.1016/j.neuroscience.2010.12.011
69. Kasumacic N, Glover JC, Perreault MC. Vestibular-mediated synaptic inputs and pathways to sympathetic preganglionic neurons in the neonatal mouse. *J Physiol.* (2012) 590:5809–26. doi: 10.1113/jphysiol.2012.234609
70. Holstein GR, Friedrich VL Jr, Martinelli GP. Projection neurons of the vestibulo-sympathetic reflex pathway. *J Comp Neurol.* (2014) 522:2053–74. doi: 10.1002/cne.23517
71. Gagliuso AH, Chapman EK, Martinelli GP, Holstein GR. Vestibular neurons with direct projections to the solitary nucleus in the rat. *J Neurophysiol.* (2019) 122:512–24. doi: 10.1152/jn.00082.2019
72. Mandel DA, Schreihofer AM. Central respiratory modulation of barosensitive neurones in rat caudal ventrolateral medulla. *J Physiol.* (2006) 572:881–96. doi: 10.1113/jphysiol.2005.103622
73. Cohen B, Martinelli GP, Raphan T, Schaffner A, Xiang Y, Holstein GR, et al. The vasovagal response of the rat: its relation to the vestibulosympathetic reflex and to Mayer waves. *FASEB J.* (2013) 27:2564–72. doi: 10.1096/fj.12-226381
74. Gulli G, Cooper VL, Claydon VE, Hainsworth R. Prolonged latency in the baroreflex mediated vascular resistance response

in subjects with postural related syncope. *Clin Auton Res.* (2005) 15:207–12. doi: 10.1007/s10286-005-0273-8

75. Voustianiouk A, Kaufmann H, Diedrich A, Raphan T, Biaggioni I, Macdougall H, et al. Electrical activation of the human vestibulo-sympathetic reflex. *Exp Brain Res.* (2006) 171:251–61. doi: 10.1007/s00221-005-0266-9
76. Gotoh TM, Fujiki N, Matsuda T, Gao S, Morita H. Roles of baroreflex and vestibulosympathetic reflex in controlling arterial blood pressure during gravitational stress in conscious rats. *Am J Physiol Regul Integr Comp Physiol.* (2004) 286:R25–30. doi: 10.1152/ajpregu.00458.2003
77. European Society of Cardiology and the North American Society of Pacing and Electrophysiology TF. Heart rate variability: standards of measurement, physiological interpretation and clinical use. *Circulation*. (1996) 93:1043–65. doi: 10.1161/01.CIR.93.5.1043
78. Zygmunt A, Stanczyk J. Methods of evaluation of autonomic nervous system function. *Arch Med Sci.* (2010) 6:11–8. doi: 10.5114/aoms.2010.13500
79. Tanaka K, Ito Y, Ikeda M, Katafuchi T. RR interval variability during galvanic vestibular stimulation correlates with arterial pressure upon head-up tilt. *Auton Neurosci.* (2014) 185:100–6. doi: 10.1016/j.autneu.2014.04.001
80. Shortt TL, Ray CA. Sympathetic and vascular responses to head-down neck flexion in humans. *Am J Physiol.* (1997) 272:H1780–4. doi: 10.1152/ajpheart.1997.272.4.H1780

Conflict of Interest: The authors declare that the research was conducted in the absence of any commercial or financial relationships that could be construed as a potential conflict of interest.

frontiers in Neurology

REVIEW
published: 04 June 2021
doi: 10.3389/fneur.2021.676723

Translations of Steinhausen's Publications Provide Insight Into Their Contributions to Peripheral Vestibular Neuroscience

Hans Straka[1], *Michael G. Paulin*[2] *and Larry F. Hoffman*[3]*

[1] Department Biology II, Ludwig-Maximilians-University Munich, Munich, Germany, [2] Department of Zoology, University of Otago, Dunedin, New Zealand, [3] Department of Head & Neck Surgery and the Brain Research Institute, David Geffen School of Medicine at University of California at Los Angeles, Los Angeles, CA, United States

The quantitative relationship between angular head movement and semicircular canal function is most often referenced to the well-known torsion-pendulum model that predicts cupular displacement from input head acceleration. The foundation of this model can be traced back to Steinhausen's series of papers between 1927 and 1933 whereby he endeavored to document observations of cupular displacements that would directly infer movement of the endolymph resulting from angular rotation. He also was the first to establish the direct relationship between cupular displacement and compensatory eye movements. While the chronology of these findings, with their successes and pitfalls, are documented in Steinhausen's work, it reflects a fascinating journey that has been inaccessible to the non-German speaking community. Therefore, the present compilation of translations, with accompanying introduction and discussion, was undertaken to allow a larger component of the vestibular scientific community to gain insight into peripheral labyrinthine mechanics provided by this historical account.

Keywords: cupula, endolymph, biomechanical model, crista, labyrinth, torsion-pendulum

OPEN ACCESS

Edited by:
Richard Lewis,
Harvard University, United States

Reviewed by:
Theodore Raphan,
Brooklyn College (CUNY), United States
Klaus Jahn,
Schoen Clinic Bad Aibling, Germany

***Correspondence:**
Larry F. Hoffman
lfh@g.ucla.edu

Specialty section:
This article was submitted to Neuro-Otology, a section of the journal Frontiers in Neurology

Received: *05 March 2021*
Accepted: *08 April 2021*
Published: *04 June 2021*

Citation:
Straka H, Paulin MG and Hoffman LF (2021) Translations of Steinhausen's Publications Provide Insight Into Their Contributions to Peripheral Vestibular Neuroscience. Front. Neurol. 12:676723. doi: 10.3389/fneur.2021.676723

INTRODUCTION

The early part of the twentieth century was a period of significant intellectual activity for vestibular physiology. It was known since the time of Valsalva (1) and Scarpa (2) that the labyrinth housed fluid-filled ducts that received branches of the *acoustic* nerve terminating in epithelia that were likely the origins of sensation, though the prevailing notion at the time was that they served auditory function. The presence of *hearing hairs* (*Hörhaare*) within the semicircular canal ampullae were suggested by Breuer as being important for signaling the direction and intensity of head movements (3). Confirmation that these projections from the surface of the crista were associated with hair cells was made by Retzius (4), whose exquisite drawings illustrated vestibular epithelia with "hairs" (stereocilia) that projected from the hair cells into the overlying cupula. The work of several investigators attempted to establish the direct correlate between semicircular canal function and head rotation-induced eye movements or postural reactions (3, 5–12), mostly following blockage of semicircular canals, selective lesions of the supplying peripheral branches of the VIIIth nerve, or eventually electric/galvanic activation of the sensory epithelia and corresponding nerve branches. This led to the meticulous dissections performed in the 1920s by McNally through which he and Tait deciphered the contributions of the different vestibular epithelia to balance and posture

(13–15). Shortly afterward the first electrophysiologic recordings from vestibular afferents were conducted which laid the foundation for our current understanding of head movement encoding by vestibular afferent neurons through trains of action potentials transmitted to the central nervous system (16, 17).

The association between rotation-induced eye movements and sensory activation originating within the fluid-filled semicircular canals fostered questions concerning the kinematic relationship between the fluid within the canals and the sensory structures within the ampullae. These questions captured the interests of Breuer (3), Crum Brown (7), and Mach (10), who independently theorized that while the semicircular canals would move with the head during rotation, the inertia of the fluid within the canals would result in a force exerted by the endolymph within the semicircular canals. This became known as the *Mach-Breuer-Brown* theory of semicircular canal function. Though the theory was associated with their three names, only Breuer and Crum Brown advocated that head movements induce an endolymph displacement (3, 7). In agreement with the hypothesis advanced by Goltz (9), Mach proposed that fluid movement did not occur but that the pressure induced by the head rotation was sensed by the epithelia within the semicircular canal ampullae (10, 18). Mach's position was later taken up and supported by Breuer [see (19)].

Steinhausen endeavored to test the theory of endolymph movement through experiments in which movements of the cupula overlying the *crista ampullares* could be directly observed by visual inspection. He posited that the cupula would be displaced if head rotations resulted in endolymph movement. His original observations were made on a euthanized pike (20) using an approach which was subsequently further refined to enable observations from a more carefully and rapidly "freshly-produced" preparation (21). Thus, the main goal of the '31 paper was the demonstration that head rotation causes a movement of the cupula, ostensibly refuting the concept advanced by Mach (10) that the inertia of endolymph resulting from angular head movements imparted pressure upon the cupula without endolymph displacement. To ultimately address a principal criticism of his work arguing that his results were impacted by the isolation procedure and *in vitro* nature of the preparation, particularly purported by Wittmaack (22), Steinhausen repeated his experiments in a live preparation (23). Moreover, a major goal of this third investigation was to establish the relationship between cupula movements and eye movements, thereby confirming the fact that cupula motion generates excitation within the semicircular canal cristae during endolymph flow. This behavioral outcome further supported Steinhausen's claim that relative endolymph flow and cupular displacement was the foundation of semicircular canal function, and not due to a pathologic condition resulting from anomalies of the experimental preparation. In the '33 report, Steinhausen also differentiated between "normal," short stimuli, which elicited tonic eye deviations and "abnormal" long-lasting rotations that caused a nystagmus. Collectively, the results from these experiments were quantified by a mathematical model of harmonic motion to describe cupular displacement in response to "step" stimuli (i.e., either at the onset or cessation of constant velocity rotations of different durations). This became the foundation of the analytical model of stimulus-evoked cupular displacement and referred to as the classic torsion-pendulum model (24, 25), driving investigations of peripheral vestibular physiology for decades to come [e.g., (26–28)].

The torsion-pendulum model provided a formal framework within which various attributes of semicircular canal physiology have been analyzed. It has been important not only for integrating the critical physical parameters of the semicircular canals and cupula that contribute to the encoding of rotational head movements, but also for identifying deviations from the model that reflect the contributions of non-mechanical characteristics of the coding cascade. Though Steinhausen's publications have been among the most oft-cited papers in the history of modern vestibular physiology, non-German readers have been deprived of a direct reading of this seminal work owing to the absence of a translation. This situation is remedied through this monograph. Translations of the 1927 (20), 1931 (21), and the "classical" 1933 Steinhausen (23) monographs are included, and are intended to provide practitioners of the field with the entire story of this classic experimental work. A summary follows the three translations in which Steinhausen's findings are briefly discussed in the context of contemporary knowledge of models of semicircular canal function. Our intention was not to provide a comprehensive review, but simply to provide some context regarding the importance of Steinhausen's findings to the conceptual questions of his day and their place in our understanding of semicircular canal function.

The original Steinhausen papers were translated from German into English by a native German speaker (HS) and subsequently edited by two native English speakers (MGP and LFH). The sentence-by-sentence translations reflect compromises between retention of the original style and sentiment of scientific publications from the early 1930s while making them linguistically accessible for present-day readers. This balance was challenging at times, particularly in view of the often long and tedious original German sentences and the very careful and often repetitious writing style of Steinhausen by which he attempted to be as precise as possible when referring to results and theories in the scientific literature. Nonetheless, all anecdotal advises and descriptions were maintained, but were occasionally supplemented by a note from the translator or editors. All original figures were reused and the labeling was translated and replaced to meet the quality requirements of contemporary publications. The error in the labeling in Figure 1 of Steinhausen's 1931 monograph (21), where the *ampulla* and the *barberry spine* in the original publication were reciprocally mislabeled, was maintained but explicitly noted in the translation.

On Visualization and Functional Inspection of the Cupula Terminalis in the Semicircular Canal Ampullae of the Labyrinth[1]

Wilhelm Steinhausen

Institut für Animalische Physiologie Theodor Stern-Haus, Frankfurt (Received June 1, 1927)

Over time, a number of theories about the excitation process in the vestibular organ have been put forward. A decision about which of these theories is the most correct could not be made until now, because the experimental foundations are not yet sufficiently known. A contribution to further knowledge of these experimental foundations will be given below.

HISTORICAL PREFACE

The finer anatomical structure of the nervous endorgans in the semicircular canals of the labyrinth has been the topic of many studies. As early as 1858, *M. Schultze*[2] described the hairs that rest on the crista ampullaris and protrude far into the semicircular canal lumen of rays and sharks, which as an "infinitely delicate, finely striated mass" form the cupula terminalis according to *Lang*.[3] *M. Schultze*[4] claims to have observed the cupula in isolation in the pike. As far as I could determine, a repetition of this observation including simultaneous functional testing has not yet been made.

The presence of hairs in the cupula terminalis was confirmed by all follow-up studies. Whether the agglutinative substance visible in the fixed preparation is an artificial product or not has become the subject of a lively dispute. *Hensen*[5] has strongly advocated the opinion that only the hairs exist in life and the agglutinative substance is produced by the fixation. This conclusion is based on his observations of young, transparent fish (Gobius amongst others) in which only the hairs are visible, but not the agglutinative substance. More recently, all investigations have been performed almost exclusively on fixed preparations.

Any experimental data on the elastic properties of the cupula and its function during labyrinth stimulation is so far missing. There are only theories about it. Apart from the old *Mach-Breuer*[6] theory of cupula movement, according to which the bending of the cupular hairs from their normal position by the endolymph flow should represent the physiological stimulus, a whole series of other theories have been put forward.[7] Recently, the main question is how to reconcile the mathematical[8] and experimental[9] results about the short duration of the endolymph flow during adequate stimulation with the observations of the potentially very long-lasting stimulation symptoms (nystagmus, etc.). Of recent theories, special mention should be made in this context: the attempts of *Rohrer*[10] to assume elastic after-vibrations of the cupula as the cause for the long post-duration symptoms and the theory of *Schmaltz*,[11] according to which the cupula remains stationary during adequate stimulation and only a diffusion gradient at the cupula boundary is propagated by the endolymph flow. The resulting disturbance of a concentration equilibrium supposedly is the cause of the excitation.

Thus, our knowledge about the anatomical and physiological properties of the cupula terminalis is not yet sufficient to form a reasonably accurate picture of its effectiveness during stimulation of the labyrinth.

---

[1] A preparation, produced according to the method indicated here was demonstrated in the meeting of the medical-biological evening at the University of Frankfurt a. M. on February 14, 1927. See Klin. Wochenschr. 6, 1164. 1927.
[2] *M. Schultze*, Arch. f. Anat. u. Physiol. 1858, P. 330–381.
[3] *Lang*, Zeitschr. f. wiss. Zool. 17. 1863.
[4] *M. Schultze*, a. a. O., P. 351ff.
[5] *V. Hensen*, Arch. f. Anat. u. Physiol., Anat. Abt., 1878, P. 466–489; 1881. P. 405–418.
[6] *Mach-Breuer* 1873/74. Cf. Nagel, Handbuch der Physiologie Bd. III, P. 778. 1905.
[7] Cf. e.g., Handbuch der normalen und pathologischen Physiologie 11, 797ff., 985ff. 1925.
[8] *W. Gaede*, Arch. f. Ohren-, Nasen- u. Kehlkopfheilk. 110, 6–14. 1923.
[9] *G. Rossi*, Arch. di fisiol. 13, 335–343. 1915. *Maier* und *Lion*, Pflügers Arch. f. d. ges. Physiol. 187, 47. 1921.
[10] *F. Rohrer*, Schweiz. med. Wochenschr. 1922, Nr. 27; cf. also *Rohrer* and *Masuda*, Handbuch der normalen und pathologischen Physiologie 11. 1925.
[11] G. Schmaltz, Pflügers Arch. f. d. ges. Physiol. 207, 127.

EXPERIMENTS ON VITAL STAINING OF THE CUPULA

All problems of the theories about the function of the semicircular canal organ could be resolved if it were possible to directly observe the cupula during labyrinth stimulation.

Of the various possibilities that would lead to a direct observation of the cupula terminalis, I first tried to use the method of vital staining of the cupula.

In frogs, one ampulla—usually the horizontal—was exposed.[12] Then the whole preparation was submerged in a methylene blue-Ringer solution. After a certain period of time, the duration of which was subject to exploration, the preparation was returned to a dye-free Ringer solution.

In several cases, it was possible to visualize the unstained cupula through the reappearing translucence of the ampullary walls and also to demonstrate deflections during the endolymph flow. The flow in the semicircular canal was generated by compressing the semicircular canal with a glass rod, which, bolted to an arm of a micromanipulator, was pushed onto the semicircular canal.[13] However, the staining succeeded only in so few cases that the method had to be abandoned in view of the difficulty of producing the preparation.[14]

DIRECT OBSERVATION ON SMALL TRANSPARENT ANIMALS

In the literature, occasional statements[15] can be found that in certain animals (Gobius species, perch, amphibians, larvae, etc.) the cupula or its hairs can be seen in the living animal from the outside without any dissection. I have not yet been able to study the respective species. In other small transparent and live fish, such as eel and grayling fry,[16] small freshwater fish, including ornamental fish, I have often clearly seen the hairs at their base on the crista, with occasional indications of longitudinal stripes inside the ampulla. However, the cupula as a whole was never visible to such an extent that physiological experiments (rotation on the turntable or other means of flow generation in the semicircular canals) could have been performed.

INCISION OF A WINDOW INTO THE AMPULLA

The method, which finally led to the intended success consisted of cutting a window into the wall of the ampulla, thus making the cupula accessible to direct observation.

METHODOLOGICAL DETAILS

The experiments were carried out on pikes, usually weighing 0.5–1 kg that arrived alive for the dissection. The right side of the skull was ablated and the brain was carefully removed. This provides a view from the inside onto the labyrinth, located freely in the cranial cavity, with a specific view of the utricle and the anterior vertical ampulla. The ampulla is exposed as far as possible. During this process, the ampulla as well as the entire labyrinth must not be touched. After this exposure, the cupula cannot be made visible by any means. I therefore believe that the claims made in the literature that it is possible to see the cupula inside the ampulla does not apply to freshly-produced preparations. Only when the cupula turns opaque due to phenomena related to the degeneration process it becomes visible from the outside with suitable illumination (strong transmitted light or lateral slit lamp illumination).

The opening of the ampulla requires a particular technique since the tissue of the ampulla is exceptionally flexible. Even with the micromanipulator, I have not been able to easily incise the ampullary wall, as it evades even the finest instruments. It is therefore necessary to harden the ampullary wall prior to the dissection, which can be easily accomplished without bringing more than the target piece of tissue in contact with the fixative.

As fixation solution, I used the following mixture reported by Nakamura[17]:

Müller's solution.....243
4% Formalin solution.....180
Acetic acid.....16
Distilled water.....540

The preparation, which is placed in 1.3x Ringer solution[18] is slightly lifted out of the solution such that the ampullary wall emerges just above the surface. A trace of the fixation solution is applied to the ampullary wall with a fine rod, thereby hardening the wall. After some time, the preparation is completely re-submersed in the Ringer solution. At this point, the dilution of the fixation solution becomes so strong that no detrimental effect is induced in the rest of the tissue. With some practice, it is then possible to incise a window into the ampulla by free hand[19] under the binocular loupe without damaging or even rupturing the cupula. As tools for cutting the window, I used tweezers, sharpened under the magnifying lens and splitters, made of

[12] With sufficient caution, this can also be done in the living animal.

[13] I reported on these experiments in a meeting of the med.-biol. evening at the University of Frankfurt on February 23, 1925, after I had first demonstrated the deflection of the cupula in our institute. Cf. Klin. Wochenschr. 4, 853. 1925.

[14] In retrospect, an explanation for the rather infrequent success of the staining experiments is tentatively explainable. The cupula may be potentially altered postmortem (coagulation?) to become stained by the used Methylene Blue-Ringer solution. If the solution exerts its effect on the cupula in a freshly-produced preparation, the cupula potentially becomes damaged and destroyed by the solution. I come to this conclusion because during the first attempts I was able to stain the cupula, however, later, when I had managed to work faster, I was not able to find the cupula at all, despite the most diligent efforts.

[15] *El. Fr. Schulze*, Arch. f. Anat. u. Physiol. 1862. Hensen, a. a. O. *G. Retzius*, Das Gehörorgan der Wirbeltiere Bd. II, P. 363.

[16] I am grateful to the authorities of the German Fisheries Association in Berlin and the Munich State Fish Hatcheries for providing me with fish stocks.

[17] *Y. Nakamura*, Beitrag zur Anatomie des Ohres 8, H. 1–3. 1914; cit. in *N. Satoh*, Der histologische Bau der Vogelschnecke. Basel 1917.

[18] 1.3x Frog Ringer solution was isotonic for the pikes that I examined.

[19] The use of the micromanipulator, as I have found, is not advantageous at this point. The surgery only takes much longer because of the inconvenient setting.

Gillette blades, soldered to holders and sharpened at the tip—again under the magnifying lens. For illumination, a specially designed slit lamp from the Leitz company[20] was at my disposal, with a 250-W high notch lamp replacing their illumination lamp. This type of illumination has considerable advantages for the dissection and was also used for the microphotography of the preparations.

Once the window has been cut into the ampullary wall, it is possible to see into the ampulla. Since transmitted light cannot be used, only lateral slit lamp illumination is possible. But even now the cupula is not immediately recognizable. The cupula is so transparent that its existence can only be inferred indirectly. In fact, with sufficient attention, debris can be detected, which accidentally has become trapped by the surface of the cupula, and which, in contrast to particles floating around freely in the fluid, occupy a relatively fixed position in space and thus render the outline of the cupula clearly visible. The fixed position in space is relative in the sense that fluid movements cause considerable movements of the cupula, which can be deduced from the motion of the adherent debris. Thereby, the cupula repeatedly returns to a defined resting position, which corresponds to the one that is theoretically to be expected. However, from this resting position the cupula can be very easily deflected. Particularly extensive movements can be observed by generating a flow within the semicircular canal through compression of the semicircular canal wall or by causing water movements when drops are made to fall onto the free surface of the fluid (cf. later).

However, endolymph flow, as corresponding to adequate stimulation, also causes noticeable cupula movements. If the ampullary window is covered with a fragment of a coverslip and the preparation, including microscope and illumination equipment, is placed on a turntable, then movements of the cupula are observed which, as far as can be deduced from subjective observations, correspond to those which should be expected according to the old *Mach-Breuer* theory.

Whether and to what extent cupular movements can occur, as assumed by *Rohrer* (cf. above) to explain the long duration of the nystagmus, cannot be reliably deduced from subjective observations. Also, to determine the natural oscillation frequency, the attenuation, etc. of the cupula, it appears necessary to supplement the subjective observations by an objective registration. Since a micro-cinematographic device was not at my disposal until now,[21] I only can report about photographic images acquired with a still camera for the time being.

The debris, randomly adhering to the cupula is not sufficiently distinguishable from the background to produce photograms suitable for reproduction, even when the lateral slit lamp illumination is optimally adjusted. The reproduction of a photogram of the cupula in this state shall therefore be refrained from. Better images are obtained by artificially enhancing the contrast, which was achieved by applying Chinese ink according to Prof. *Bethe's* suggestion.

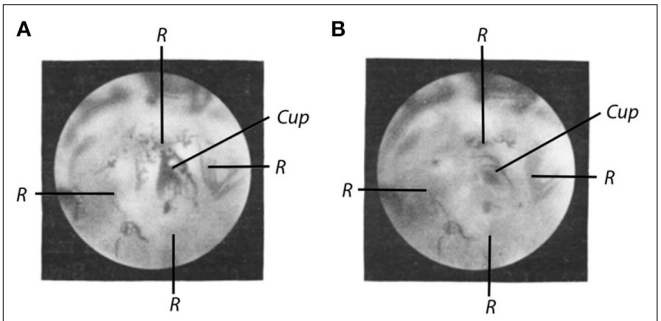

FIGURE 1 | (A) Ampulla of the anterior semicircular canal of the pike with incised window in which the cupula (*Cup*) can be seen. *R* = edges of the window. Freshly-produced preparation. The dark areas are Chinese ink particles. Lateral slit lamp illumination. Image captured on May 30, 1927 at 5.30. Beginning of the dissection at 2.10. Exposure time 9 min (to obtain the best possible depth effect, the exposure was set to 3 min, respectively, at 3 different depths). Objective Leitz 3. Ocular Leitz 1. Magnification 50x (Image number 30) **(B)**. Same preparation. Cupula in motion (cf. text). Captured at 5.00, otherwise as **(A)** (Image number 29).

Chinese ink powder was mixed with 1.3x Frog Ringer solution and a trace of this solution was applied to the cupula using a finely pulled pipette.

Figure 1A (Image number 30) shows a photogram of the cupula obtained according to the described method. **Figure 1B** (Image number 29) represents the same preparation, captured under the same conditions with the only difference that during the capture a fluid movement was generated by dropping isotonic solution onto the exposed surface of the fluid in which the preparation was placed.

The equipment used for this purpose can be seen in **Figure 2**. A microscope slide (*T*) is placed above the object (*O*) to prevent image distortion caused by the movement of water on the surface. *M* is the microscope, *Sp* the slit lamp.

From the comparison of the two images, it can be seen that the cupula obviously moves extensively during the water movement. Its contour, which is clearly visible in **Figure 1A**, forms an arc in **Figure 1B**, the length of which allows determining the extent of the cupula oscillation. An image of the cupula movement during rotations on the turntable could not be achieved so far due to technical reasons. After all, the cupula appears to be very mobile, which must be taken into account in theories about the function of the semicircular canal organ. Deeper insight into the trajectory of the movement and the physical properties of the cupula can, of course, only be provided by the cinematographic recording of the cupula movement.

The method described here can also be used to study the currently relevant question[22] on alterations of the cupula caused by the impact of heterotonic solutions and fixatives, as shown by several photograms obtained from fixed preparations.

[20] I would also like to take this opportunity to thank the Leitz company in Wetzlar for providing the lamp.

[21] But we hope to be able to make cinematographic recordings of the cupula movement at a later stage.

[22] Cf. *W. Kolmer*, Arch. f. Ohrenheilk. 116, 10–26. 1926 and *Wittmaack*, ibid p. 27–30.

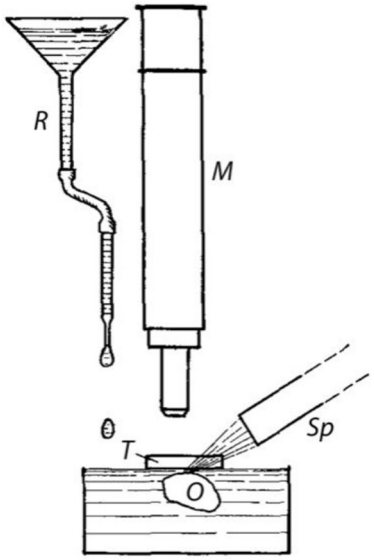

FIGURE 2 | Device for the generation of fluid flow. *O* = Object, i.e., preparation with opened ampulla; *T* = Slide as protection against image distortion (cf. text); *M* = microscope; *Sp* = slit lamp; *R* = reservoir and tube for applying drops onto the water surface.

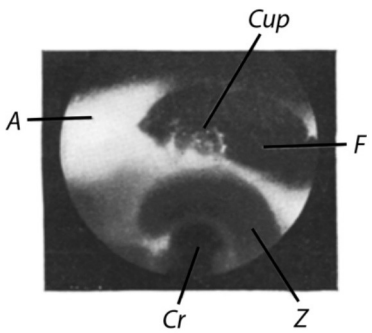

FIGURE 3 | Cupula of a pike. Fixed preparation. Pike with a weight of about 0.5 kg. Dissected on May 14, 1927. Image captured on May 18, 1927. Lateral slit lamp illumination. Exposure time: 4 min. *Cup* = cupula; *A* = ampulla; *F* = window; *Z* = zona lunata; *Cr* = crista (Image number 10).

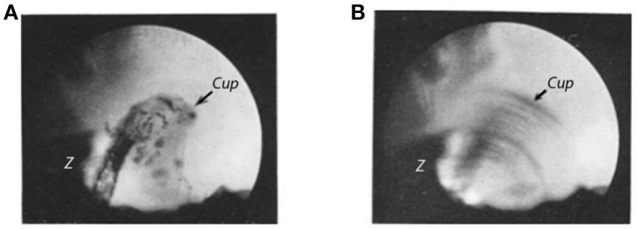

FIGURE 4 | (A) Cupula of a pike. Isolated ampulla of the horizontal semicircular canal. Fixed preparation. The ampullary wall is completely ablated except for vestiges of the zona lunata (*Z*). Pike with a weight of about 2.25 kg. Dissected on March 8, 1927, image captured on May 20, 1927. Illumination: transmitted light. Exposure time: 1 min. Objective: Leitz 3, Ocular: Leitz 8. Magnification 80x (Image number 16) **(B)**. Same preparation as in **(A)**. Cupula in motion [cf. text for **(B)**]. All other as in **(A)** (Image number 17).

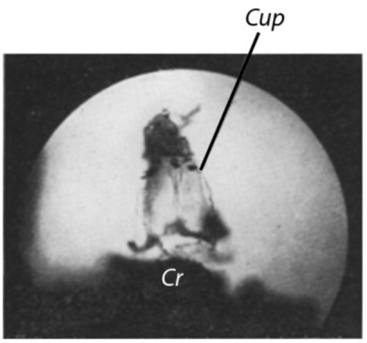

FIGURE 5 | Cupula of a pike. From the posterior vertical ampulla. Pike with a weight of 0.5 kg. Fixed preparation. Dissected on May 20, 1927, image captured on May 24, 1927. Transmitted light. Exposure time 1 min. Objective L3, Ocular L3. Magnification 80x (Image number 18).

Figure 3 shows an image of the fixed preparation. The crista and the epithelial layer of the zona lunata (*Z*), expanding above in a crescent shape, shine through the ampullary wall. There is no indication of the zona lunata and the crista in the unfixed preparation (cf. **Figure 1**). Above the zona lunata, the window (*F*) in the ampullary wall is visible, and through the window, the cupula (*Cup*) residing on the crista can be seen. Fixation causes the contour of the cupula to emerge in a clarity never seen in the unfixed preparation. Apparently, shrinkage has also been induced by the fixative.

Figure 4A shows an image of the cupula of a larger pike (about 2.25 kg). The ampulla has been removed and the ampullary wall has been ablated to a large extent. Part of the zona lunata is also removed, such that the cupula becomes visible almost down to its base at the crista. Since the cupula was freely accessible from both sides, it was possible in this case to capture images using transmitted light.

That the cupula can still be mobile despite fixation is shown in **Figure 4B**. The setting is exactly the same as in **Figure 4A**. The only difference is that a flow has been created by applying drops to the surface of the fluid in which the preparation was placed, as described in more detail in the text for **Figures 1B**, **2**. The cupula has become much more rigid due to fixation compared to the freshly-produced state, but at least it remains sufficiently mobile such that distinct movements occur in the described experimental setting, as well as during rotations on the turntable. For demonstration purposes, this mobility also of the fixed cupula is very convenient.

Finally, **Figure 5** depicts a cupula from the posterior vertical ampulla of a pike with a weight of 0.5 kg. The preparation shows the effect of fixation and a somewhat rough mechanical treatment. After all, it appears in better condition than some of

the cupula images obtained by conventional histological methods presented in publications on the histology of the labyrinth.

The last images (**Figure 4A** and following) were taken with transmitted light. Since even stronger light sources could have been used in this case, images could also have been captured at higher magnification and thus the histological details could have been more distinctly highlighted.

Since we were more concerned with the function than with the histology of the cupula, the histological questions were postponed for the time being. Also, further efforts are directed mainly toward expanding the method of functional testing of the cupula, described here, to other animals, including intact preparations, in order to extend it in such a way that the physical properties of the living cupula (oscillation period, attenuation, etc.) can be accurately determined.

SUMMARY

A method is provided that allows exposing the cupula within the ampulla of the semicircular canal and studying its physical properties in freshly-produced preparations. The method essentially consists of incising a window into the ampulla and observing the cupula through the window under slit lamp illumination.

When creating a flow in the endolymphatic space (falling drops onto the exposed surface of the fluid within which the preparation is placed, or by rotation on the turntable), the cupula is deflected.

A series of photomicrographs of the cupula under various experimental conditions serves to demonstrate the applicability of the method.

On the Evidence of the Movement of the Cupula in the Intact Semicircular Canal Ampulla of the Labyrinth During Natural Rotational and Caloric Stimulation

Wilhelm Steinhausen

Physiological Institute of the University Greifswald (Received April 25, 1931)

Some time ago, I described in this archive[1] a method that allows visualizing the cupula in the semicircular canal ampullae of the labyrinth.

The method consists essentially in the fact that a window is cut into the exposed membranous ampulla and the cupula is observed through this window (*Note by the translators: even though Steinhausen used the word "window," it is more likely a ruptured or pierced opening*). The shape and position of the cupula, which itself is completely transparent, can be deduced from the observation of the finest debris (ink or aluminum particles, or tissue debris, randomly floating in the preparation fluid, which adhere to the surface of the cupula).

As far as the physiological behavior of the cupula is concerned, the very large mechanical mobility of the cupula could be demonstrated, such that the original theory of the cupula function by *Mach-Breuer-Brown* was considered experimentally proven.

Wittmaack[2] expressed concerns about my experiments. Based on his theory of the turgescence of the cupula, *Wittmaack* believes that by unintentional injuries during my preparation method, the surface of the cupula was destroyed. Its turgescence was thereby decreased to such an amount that like a liquid-filled bladder, which slackens by piercing, it had collapsed as a result of the injury and had been transformed into a mass of fibers floating hither and thither. The great motility is thus only a consequence of the injury. Also, symptoms related to degradation, as *Wittmaack* stipulated, could have changed the structure of the cupula in the sense of softening the tissue.

Although I do not share the view of *Wittmaack*, it was nonetheless desirable to find a gentler and faster preparation method. Also, for another reason, which seemed to me even more important, I aimed at an improvement of the method: the motility of the cupula in my earlier experiments was examined under conditions that were not quite physiological. The ampulla had been opened through the window and the flow produced in the surrounding liquid (either by movement of the liquid surface or by rotation) and affecting the cupula were of quite unpredictable magnitude and perhaps much stronger than those that occur in the intact ampulla during adequate rotational and caloric stimulation. It was therefore still possible to assume that during the small movements that occur during physiological stimulation in the endolymph, the cupula remains immobile. Thus, for the physiological stimulation, the various hypotheses that have replaced the deflection hypothesis may still apply, that is, the pressure hypothesis of *Wittmaack* among others, or the hypothesis of the movement of a diffusion gradient after *Schmaltz* among others.

It was therefore strongly desired to find a method that allows the cupula to be observed in the *intact* ampulla during adequate rotational and caloric stimulation and to reveal its mechanical behavior. In the meantime, I have developed such a method. In the process, I have found that the cupula is indeed also deflected under physiological stimulus conditions. It shows the deflections that are predicted by the movement of the endolymph according to the *Mach-Breuer* theory.

METHOD

The experiments were preferentially carried out on the labyrinth of the pike, specifically on a freshly-produced preparation. The ampulla of the left anterior semicircular canal was exposed as described in the first publication (*Note by the translators: Steinhausen, 1927*). The preparation was then adjusted such that the semicircular canal was oriented vertically and the end of the semicircular canal ampulla (*Note by the translators: "end" refers to the region where the ampulla transitions into the semicircular canal*) emerged just slightly from the fluid (1.4-fold Ringer) in which the preparation is made. Thereafter a hole of about 0.1 mm in diameter was burnt into the wall of the semicircular canal using a pointed thermo cauterizer made of 0.1 mm thick platinum wire.

Care has to be taken that the semicircular canal does not extend too far out of the fluid, otherwise the wall will be slightly scorched by the heat of the thermo cauterizer. When adjusting to the correct height, the only effect at the contact with the thermo-cauterizer is a circular hole of about 0.1 mm in diameter.

[1] *W. Steinhausen*, Pflügers Arch. 217, 747–755 (1927). Vgl. Z. Zellforschg 7, 513–518 (1928). Fol. otolaryng. 17, 410–415 (1929).
[2] *K. Wittmaack*, Über den Tonus der Sinnesendzellen des Innenohres, III. Arch. Ohrenheilk. 120, 256–296, spez. 270 (1929).

Thereafter Ringer solution is added, so that the semicircular canal is completely submerged. Using a micromanipulator, a small funnel, with a diameter of about 0.1 mm at its lower end is placed above the hole, such that the end of the funnel reaches into the hole. Into the funnel, a trace of ink solution (some Chinese ink dissolved in 1.4x Ringer's solution) is added.

When applying the ink to the funnel, extreme care must be taken to ensure that fluid is not sucked out of the funnel by capillary phenomena. If one takes e.g., an ordinary glass rod to transfer the ink, and brings it to the funnel, fluid (*Note by the translators: endolymph from the semicircular canal*) will be sucked onto the glass rod. This leads to a strong flow within the semicircular canal and the ampulla and the cupula becomes detached. Such and similar incidents caused the loss of many preparations.

The ink solution is strongly cooled prior to the application. As a result of the cooling and its higher relative density compared to the endolymphatic fluid, it falls as a fine stream into the semicircular canal and the ampulla, attaches to the surface of the cupula and stains the cupula.

Appropriate positioning of the semicircular canal allows the most important parts for observation of the cupula to be stained. It is very important to avoid introducing too much ink into the ampulla; even more, one must prevent any debris from falling into the ampulla because even the smallest contaminant or the slightest agglomeration of ink particles can prevent movements of the cupula if these obstacles fall between the cupula and the ampullary wall.

As our experiments show, the cupula in a freshly-produced state has a size that causes it to almost touch the roof of the ampulla. There is only so little space between the cupula and the ampullary wall that a movement is just possible. The smallest particle of debris that gets stuck in this space fixes the cupula at the roof of the ampulla, making it consequently impossible to conduct physiological investigations on the movement of the cupula.

If the staining was successful, the hole in the ampullary wall is preferentially closed with a small spine, inserted into the hole. For closure, I use the most anterior tip of a barberry spine.

The described preparation method appears to me as the gentlest one possible, because the ampulla itself is not injured at all, rather a small hole is burnt into the end of the semicircular canal ampulla (*Note by the translators: "end" refers to the region where the ampulla transitions into the semicircular canal; see location of the barberry spine in* ***Figure 1***). One might think that this manipulation could create a strong flow in the endolymph of the semicircular canal, and consequently injure the cupula. The experiment shows that this is not the case. Because the warming occurs at the highest place of the semicircular canal, and there is thus no reason that a fluid flow is generated. Thereby, the cupula remains completely at rest. The burning of the hole is a matter of moments, it suffices to simply touch the wall of the semicircular canal with the thermo cauterizer. It is evident that this is considerably time-saving compared with the previous method of cutting a window.

In addition, closing the hole with the tip of a spine is such a simple and gentle method, that any sort of noteworthy deflection of the cupula or even injury cannot occur.

This only leaves symptoms related to degradation as cause for potential changes of the physical state of the cupula prior to the observation of its physical behavior. In order to delay the occurrence of symptoms related to degradation as long as possible, we have always kept the preparation in rather chilled preparation fluid (*Note by the translators: 1.4x Ringer*). The time required for the preparation procedure from sacrificing the animal to studying the cupula movement under the microscope

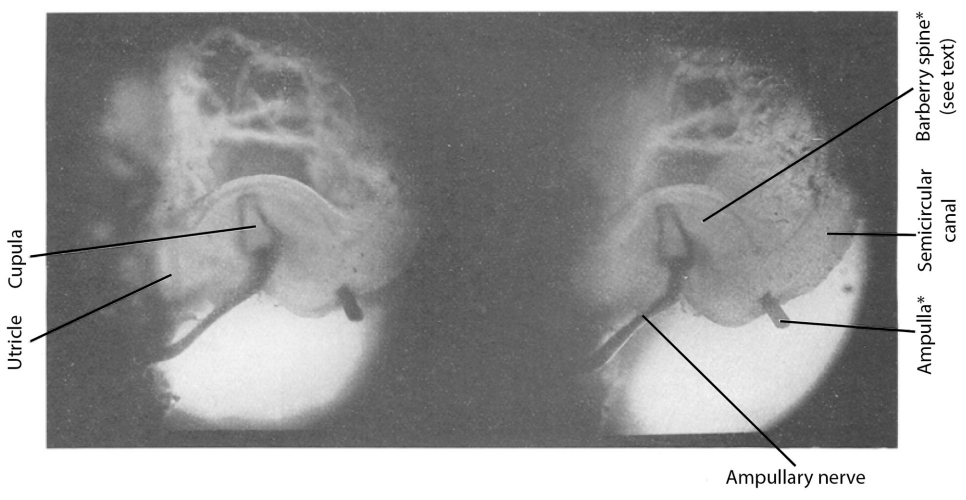

FIGURE 1 | Stereo image of an ink-stained cupula in the intact semicircular canal ampulla of a freshly-produced pike labyrinth *[Note by the translators: the two labels indicated by * (i.e., Ampulla* and Barberry spine*) were erroneously placed in the original paper and should be swapped].*

was about $1–1^{1/2}$ h. Explicit symptoms related to degradation under these conditions, however, occur only after many hours, sometimes only on the next day in such preparations. Therefore, I believe that the studies on the cupula movement can be considered to be made on a freshly-produced cupula.

After establishing the preparation method as indicated, it naturally is our next aim to investigate the cupula movement in living animals and I hope to be able to report on the respective outcome in the near future.

RESULTS

Shape of the Cupula and Its Size Relation to the Ampulla

Figure 1 shows a stereo image of the stained cupula. The cupula is stained from both sides for greater clarity.

Figure 2 shows a cupula at higher magnification. The magnification is about 30x.

As can be deduced from the figures, and as we have already concluded from our previous experiments, the hitherto existing assumptions—which could only rely on histological images of fixed preparations—about the size of the cupula in the freshly-produced state, are all more or less incorrect. The cupula is much larger than one has assumed until now, it almost touches the roof of the ampulla with its upper end. Also, its shape is much more complex than can deduced from the histological images.

In a forthcoming work, Mr. cand. med. *Fr. K. Wünn,* who kindly provided support during the preparation and the acquisition of photographic images of the cupula, will report on the shape of the cupula in the freshly-produced state and the influence on the shape by the fixative.

ROTATORY STIMULATION

The produced preparation was placed on a turntable with the semicircular canal positioned horizontally and was observed under the microscope (Busch objective AO and eyepiece 5–15-fold). The microscope was adjusted such that the optical axis passed through the axis of rotation. When the turntable was set in rotation, the expected cupula deflections were seen most clearly. A mistake, such as by parallax errors, was completely excluded. However, in order to be able to exclude all objections, cinematographic recordings were made.

The cinematic apparatus (Zeiss-Kinamo) was mounted on the turntable and images were taken during the rotation.

The recorded movie will be presented at the upcoming Physiology conference in Bonn (Pentecost 1931).[3]

CALORIC STIMULATION

More impressive is the deflection during caloric stimulation. The preparation was placed such that the semicircular canal was oriented vertically. At the lowest possible point of the semicircular canal, an electrically heated platinum loop (0.1 mm wire diameter) was placed. If current was passed through the platinum wire and as a result the platinum wire was heated, a deflection of the cupula, corresponding to the respective endolymph flow, became clearly visible under the microscope.

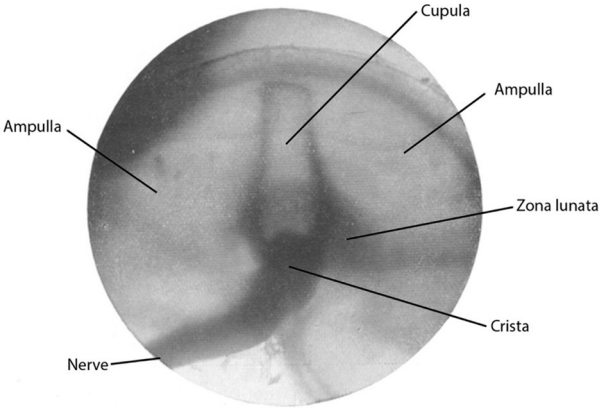

FIGURE 2 | Ink-stained freshly-produced cupula in the intact semicircular canal ampulla of the labyrinth of a pike. Magnification about 25x.

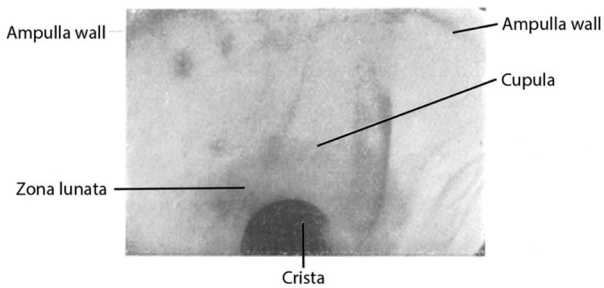

FIGURE 3 | Ink-stained cupula in the intact semicircular canal ampulla of the labyrinth of a pike (freshly-produced) *at rest* (the 4 edges of the cupula are particularly clearly stained).

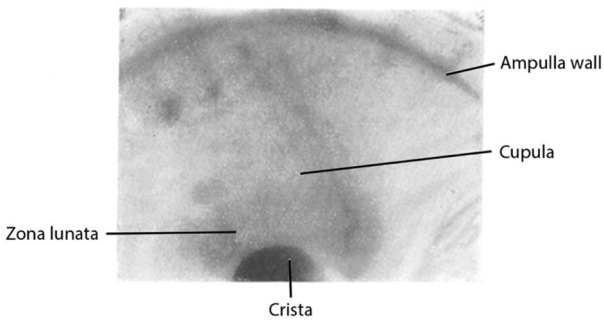

FIGURE 4 | Same preparation as in **Figure 3**. *Caloric stimulation*. Three different deflection positions are photographically superimposed on a stationary plate (see also text).

[3]Note edit in proof: has happened in the meantime.

The deflection lasted, in contrast to the rotatory stimulation, very long, and after switching off the current, the cupula did not return immediately, but on the contrary the deflection usually increased further, and only after some time the cupula slowly returned to its initial position. The return movement lasted from many seconds to several minutes, depending on the magnitude and duration of the applied heat.

Figures 3, **4** show two images, which demonstrate the success of the caloric stimulation, i.e., the deflection of the cupula. **Figure 3** shows a photographic image of the cupula at rest. The blackened edges indicate the prismatic shape of the cupula, which extends almost vertically above the crista in the intact ampulla. In **Figure 4**, an endolymph flow is generated by heating and the cupula is photographed on a stationary plate in three different positions. **Figure 4** provides, as I hope, clear evidence for the large displacements of the cupula that can occur during caloric stimulation.

Cinematographic images were also made of the deflections caused by caloric stimulation, which will also be shown at the Physiology conference in Bonn.[4]

[4]Note edit in proof: has happened in the meantime.

CONCLUSION

From the described experiments I believe I should see that the theory of *Mach-Breuer-Brown* on the function of the cupula has finally been proven experimentally. The observed deflections are in perfect agreement with calculations made by Mr. *Schmaltz* and the results about which he recently informed me.

SUMMARY

An improvement of the earlier reported method for visualizing the cupula in the semicircular canal ampullae of the labyrinth is described, which allows observations of the cupula in the *intact* semicircular canal ampulla and to study its behavior during physiological rotatory and caloric stimulation. This allowed producing a decision between the different theories on the function of the cupula.

I am very grateful for the loan of a micromanipulator, a preparation microscope and a stereo camera by the *Notgemeinschaft Deutscher Wissenschaften* and for the donation of a ball-bearing turntable by the *Vereinigte Kugellagerwerke* Fichtel & Sachs, Berlin-Schweinfurt.

On the Observation of the Cupula in the Semicircular Canal Ampullae of the Labyrinth in the Living Pike

Wilhelm Steinhausen

Physiological Institute of the University Greifswald (Received February 23, 1933)

After the method for dissection and visualization of the cupula had been established in freshly-produced preparations,[1] it could, at least in principle, not be difficult to prepare the cupula also in the *living animal*. In the following, the method for preparing the cupula in the living animal[2] and the results obtained with it shall be described. Subsequently, a theory of the cupula movement, which can be established based on the observations, shall be presented. All observations are made on the cupula of the left horizontal semicircular canal ampulla in the living pike, and the theory also applies only to the processes in this semicircular canal. It is very probable that for the other semicircular canals, certain differences in these processes with respect to those in the horizontal semicircular canal will be found. These differences, however, will likely not be of fundamental nature.

METHOD OF PREPARING THE CUPULA IN THE LIVING ANIMAL

As experimental animals, pikes were used, which originated from the Greifswald Bodden (*Note by the translators: shallow basin in the southwestern Baltic Sea, off the shore of Greifswald*) and therefore were adapted to saline water. The body weight of the animals was 750–1,000 g. For the preparation, an absolutely necessary requirement was a strict mechanical fixation of the skull while preserving the viability of the whole animal. This is achieved as follows: the animal is placed in a C-shaped *fish cradle* (*Note by the translators: custom-made mechanical fixation device to restrain the fish body for experimental manipulations*), similar to the construction used by *Tschermak*.[3] Instead of movable arms of the *fish cradle* used by *Tschermak*, fixed bars are attached to a base rail. The bars are interconnected with wire mesh, which is covered with felt and cotton wool. This causes the fish body to be tightly wrapped by the padding except for the head and anus region. The opening on the top is secured by wide rubber bands, such that the animal is unable to make any movements, while on the other hand the bondage does not cause a compression: the head is clamped to a bite board and the skull is fixed laterally by 2 additional clamps. Bite board and clamps are firmly connected to the base rail of the fish cradle. This ensures a complete mechanical immobilization of the skull, without much struggling of the animal by the fixation. The cradle with the animal is placed in a container with isotonic Ringer's solution (1.4-fold Frog Ringer), aerated with oxygen. The animal breathes itself and remains completely calm.

Also, during surgery, no strong arousal occurs, provided the intervention progresses slowly. The *left horizontal ampulla* and a larger part of the corresponding semicircular canal are exposed. With some practice, the surgery is successful without collateral injuries and major bleeding. Once the ampulla and semicircular canal have been sufficiently exposed, one can either burn a hole into the semicircular canal with the thermo cauterizer, as described earlier on a freshly-produced specimen,[4] or cut through the semicircular canal with a Gillette splinter knife. I lately came to prefer the latter method because it produces smooth cut surfaces and facilitates the insertion of cannulas (see below). When cutting through the semicircular canal, I put a very small piece of rubber underneath. When cutting, of course a strong ampullary stimulation occurs, which however subsides shortly after.

For *staining*, a small, ink-filled cannula is inserted into the semicircular canal. By applying pressure to a tube, connected to the cannula, ink can be introduced into the semicircular canal. After ink has been introduced into the semicircular canal, the cannula is withdrawn and the pike cradle is reoriented such that the ink can flow into the ampulla. Thereby the cupula is stained, precisely as described previously in freshly-produced specimen.[5] If the staining is successful, the semicircular canal side of the cupula is made visible just as in the staining performed in the freshly-produced specimen; either as a sharp black line or more or less diffusely stained area.

Until the beginning of the staining procedure, *illumination* aspects pose no problem. During dissection and staining, very small optical magnifications are sufficient. Accordingly, the distance between object and lens is very large and illumination can be provided

[1] *Steinhausen, W.*: Pflügers Arch. 217, 747–755 (1927); 228, 322–328 (1931); Z. Zellforsch. 7, 513–518; Z. Laryng. etc. 17, 410–415 (1928); Z. Hals- usw. Heilk. 29, 211–214 (1931).

[2] In Arch. Ohr. etc. Heilk. 132, 147 (1932) I have reported the successful visualization of the cupula in the living animal already in February 1932. If the detailed publication only takes place now, then external reasons (illness and other adversities that kept me from working) were decisive for the delay.

[3] *Tschermak, A. v.*: Pflügers Arch. 222, 439–444 (1929).

[4] See *W. Steinhausen*: Pfügers Arch. 228, 322–328 (1931).

[5] Occasionally, the staining has to be carried out several times, because as a result of the reverse cupula movement (see later), the amount of injected ink is washed out, causing pulsations that are in synchrony with the respiratory rhythm.

from above by strong microscopy lamps. When observing the cupula, in particular at higher magnifications, the illumination is insufficient and adequate illumination becomes a difficult task. This problem could be solved, however, if the newly developed top-light illumination methods (*Ultropak-Leitz*, episcopic illumination—*Zeiss*, *Busch*, etc.) could be applied to the observation of the cupula. Unfortunately, that is not possible. This is due to the fact that all of these illumination methods are designed exclusively for surface observations. However, the cupula is located deep inside the tissue, in a tissue funnel. The opening of the funnel cannot be sufficiently enlarged such that the wide lens sockets of the illumination devices in question can be positioned sufficiently close. Until the size of the sockets of the top-light illumination devices can be made smaller, any application in physiology remains limited.

One might think of generating a picture of the cupula through a suitable photographic lens, which is then observed microscopically.[6] My own experiments have shown that this method likely allows a better observation, which is why this method should be tested further.

Good observation of the cupula in the living animal has so far only been achieved by providing illumination through the pharynx. A strong low-voltage lamp was inserted into the pharynx allowing observation by translucent light. For subjective observation, the achieved light intensity is entirely sufficient. Photographic and especially cinematographic recordings, such as those made during the observation of the cupula in the freshly-produced specimen,[7] have not yet been successful in the living animal. This is due to the thick layer of tissue between the horizontal ampulla and the pharynx, which cannot be removed without damaging the labyrinth or harming the animal. Since this layer of tissue absorbs a very large amount of light, the brightness is insufficient for photographic image acquisition.

For the time being, it was thus necessary to limit the focus in the living animal to subjective observations. This however, suffices to clearly ask the essential questions. When creating a flow in the semicircular canal, it is possible to subjectively observe very well the deflection of the cupula and the reaction of the animal (eye movements etc.). As described earlier,[8] one can observe the cupula and the eye simultaneously with the help of a drawing mirror. However, a simpler and better approach is the use of multiple observers; one observer for the behavior of the cupula and the other for e.g., the eye movements.

RESULTS

Rotatory Stimulation

It would have been most desirable to apply the same stimulation methods also in the living animal as used to observe the cupula movement in the freshly-produced specimen.[9] So, the most obvious procedure would have been to put the animal on a turntable and to observe how the cupula behaves and how the animal reacts, i.e., which eye movements, etc. occur. However, a simple consideration shows that this would not have been the most straightforward approach to obtain information about the more detailed mechanism of the semicircular canal excitation. First, the technical task of rotating the living animal together with the surrounding water tank and the rest of the device, while simultaneously observing eye and cupula movement in detail, would have been rather difficult to achieve given our limited resources. But even if we had succeeded in solving this task, the result would not have been unequivocal. In fact, rotation would not only cause the expected deflection of the cupula of the observed ampulla (in our case the left horizontal ampulla), but also rotational effects in other parts of the same labyrinth, in particular of the cupula in the horizontal ampulla of the other, right labyrinth. Eye movements observed during rotation (so far, we restricted our observations to eye movements) could therefore not be simply assigned to the movement of the cupula in the observed ampulla. It would thus well be possible that the observed eye movements would have been caused by rotational effects at the other, unobserved sites.

DIRECT MECHANICAL STIMULATION OF THE LEFT HORIZONTAL SEMICIRCULAR CANAL

The currently best approach to make a particular statement about the detailed mechanism of the cupula activation rather derives from the direct, isolated stimulation of an ampulla with a concurrent observation of the cupula and the eyes. The method is indeed applicable because the rotational effect on the cupula has already been demonstrated by the observations on the isolated preparation. As shown in previous studies,[10] rotation causes deflections of the cupula as predicted by the *Mach-Breuer-Brown* theory. The goal is now to investigate how cupula movements are linked with eye movements. So, it is sufficient to cause a cupula movement by the simplest means and to observe the corresponding eye movements.

Isolated stimulation of individual ampullae (of course without observation of the cupula) have been carried out quite frequently (*Flourens, Breuer, Ewald* and many others.[11]) A particularly elegant method of isolated stimulation of semicircular canals in the pigeon was applied by *Ewald*[12] in his famous experiments using the pneumatic hammer.

Fishes have been used by *Bethe,*[13] *Lee,*[14] *Kubo,*[15] *Maxwell*[16] and others to conduct stimulation experiments. The results of all these experiments have not yet led to a consolidated opinion

[6] Herr Prof. *Seeliger* indicated that for the microscopic observation of filaments, this procedure is very successful.

[7] See *W. Steinhausen*: ibid.

[8] Arch. Ohr. etc. Heilk. 132, 148 (1932).

[9] *Steinhausen*: See literature in footnote 1, previous page.

[10] *Steinhausen, W.*: ibid.

[11] With respect to literature, see e.g., *Bethes* Handbook Vol. 11 1, Rezeptionsorgane. 1926; and Vol. 15 1, Correlations 1930 and Vol. 18. Supplement 1932. In particular, the articles by *M. H. Fischer* und *Magnus und de Kleijn*.

[12] *Ewald, I. R.*: Physiologische Untersuchungen über das Endorgan des Nervus octavus. Wiesbaden 1892.

[13] *Bethe, A.*: Biol. Zbl. 14, 97–114, 563–582 (1894).

[14] *Lee, F. S.*: J. of Physiol. 15, 311–348; 17, 192–210 (1894).

[15] *Kubo, I.*: Plügers Arch. 115, 457–482 (1906).

[16] *Maxwell, S. S.*: Labyrinth and equilibrium. 1923.

about the function of the semicircular canal system. For example, *Maxwell*[17] writes about E*wald's* experiments that indeed the latter confirmed the fact of a linkage between an ampulla with movements of the eyes in a particular plane. Further implications of his experiments that endolymph movement in one direction causes excitation, and inhibition in the other are "open to criticism." Many contradictions, contained in the literature on semicircular canal excitation can be resolved by observations of the cupula during isolated semicircular excitation. Since this has not been possible so far, it explains, in my view, the uncertainty in the interpretation of the hitherto existing experimental results.

To determine the dependency of eye movements on the movement of the cupula, the *left horizontal ampulla* is mechanically stimulated in isolation while the movement of the cupula and the eyes are observed.

The isolated mechanical stimulation of the cupula was performed as follows: a cannula is inserted into the semicircular canal.[18] The cannula is connected to a tube system, which allows applying a shorter or longer lasting pressure pulse to the other end using an appropriate device. *Breuer*[19] has already inserted cannulas into the semicircular canals but failed to obtain reliable results. *Bethe*[20] has also made experiments with the insertion of cannulas into the semicircular canal, which, however, as he states, were unsuccessful.

If the cannula is positioned in the ampullary part of the semicircular canal, generation of pressure in the tube system should cause an endolymph movement in the semicircular canal directed toward the ampulla (i.e., ampullopetal flow.[21]) Observation of the cupula, reveals a deflection in the direction of the utricle. It is possible now to adjust the magnitude and timing of pressure application *such that a clearly visible*, but small *deflection of the cupula becomes visible*. Such a small, rapidly fading deflection of the cupula causes a *horizontal deviation of both eyes to the right*. The eyes remain in the new position and only return to their normal position after a while. If the deflection of the cupula is maintained for a longer period of time (continuous pressure exerted onto the tube connected to the semicircular canal cannula), the deviation changes into a *horizontal nystagmus of both eyes with the fast component directed to the left*.

During a *reverse deflection of the cupula*, i.e., toward the semicircular canal (ampullofugal flow), *there is no effect on the eye position*. The eyes remain in their normal resting position.

A dependency of semicircular canal excitation on the flow direction of the endolymph has already been found by *Ewald*[22] in his experiments with the pneumatic hammer in pigeons. *Ewald* discovered that an ampullopetal endolymph flow caused a strong excitation, and an ampullofugal endolymph flow caused a weak excitation. He did of course not investigate the behavior of the cupula.

These observations indicate that in fact cupula movements cause the excitation of semicircular canals during endolymph flow rather than other changes of the state of the cupula (direct pressure effects, osmotic changes, ion shifts or the like).

ELECTRICAL STIMULATION

Flow in the left horizontal ampulla in ampullofugal direction, i.e., anode on the utricular side of the ampulla and cathode on the semicircular canal side, cause *deviation of both eyes to the right* (current threshold magnitude about 0.6 mA). Current flow in the opposite direction *fails to provoke any eye movements* (even not at magnitudes beyond 5 mA). During current stimulation, the *cupula remains completely at rest*. *Brüning's* theory[23] on the cataphoretic effect of the electric current on the cupula thus fails to explain the facts.

Switching to faradaic stimulation by using a large sled inductor, while maintaining the same position of the electrodes, yields no semicircular canal excitation. Augmenting the current magnitude by increasing the overlap of the coils of the inductor, causes the impact of the current loops to more likely evoke a general excitation of the surrounding muscle tissue than to produce a distinct semicircular canal excitation. This suggests that the chronaxie of the semicircular canals must be unusually large. For the entirety of the vestibular apparatus, *Bourguignon*[24] has already stated a particularly large chronaxie.

GENERAL CONCLUSIONS FROM THE OBSERVATIONS

Since the cupula, as demonstrated, remains immobile during electrical stimulation, the electrical stimulation of the semicircular canal system must result from a direct stimulation of the sensory epithelium or of the ampullary nerve itself. The following will therefore only discuss the processes during rotational stimulation. It has been shown that a movement of the cupula of the left horizontal ampulla toward the utricle causes a deviation of both eyes to the right or, during a prolonged deflection of the cupula, causes a nystagmus to the left. This result complies with the prediction of the *Mach-Breuer-Brown* theory of semicircular canal excitation.

Figure 1 schematically illustrates the relationship between the cupula of the left horizontal semicircular canal (l.h.s.c.) and eye movements.

At the onset of a leftward rotation from a static position (large arrow), according to the theory by *Mach-Breuer-Brown,* the endolymph, due to its inertia will lag the motion of the semicircular canal wall. This will cause a relative motion of the endolymph in the direction indicated by the small arrow.

[17] *Maxwell*: ibid. S. 67.

[18] It does not matter whether the cannula is inserted into the duct or the ampullar part of the transected semicircular canal. It only matters that the cupula is moved in the same direction to achieve the same effect. In the one case a suction effect, in the other case a pressure effect would be the cause for the same movement.

[19] *Breuer, J.*: Med. Jb. 1874, H. 1; 1875 H. 1.

[20] *Bethe, A.*: Biol. Zbl. 14, 579 (1894).

[21] Ampullopetal semicircular canal flow generally indicates a flow from the semicircular canal toward the ampulla into the utricle, the reverse flow is denoted as ampullofugal semicircular canal flow.

[22] *Ewald, I. R.*: Physiologische Untersuchungen über das Endorgan des Nervus octavus, S. 259. Wiesbaden 1892.

[23] *Brünings*: Verh. dtsch, otol. Ges. Dresden 1910, 192.

[24] See *A. Kreindler*: Z. Neur. 138, 699–703 (1932) und *P. Vogel*: Pflügers Arch. 230, 16–32 (1932).

Accordingly, an ampullopetal flow must be caused in the semicircular canal. This ampullopetal flow induces a deflection of the cupula[25] in the direction of the utricle.

To avoid a shift of the point of fixation on the retina, the eyes will perform a rightward counter-rotation. Ampullopetal endolymph flow in the left horizontal semicircular canal and consequent deflection of the left horizontal cupula toward the utricle must therefore be associated with a rightward deviation of the eyes. Since an artificial deflection of the cupula toward the utricle causes a rightward eye deviation, it follows that the *cupula deflection during rotation represents the actual stimulus that triggers the eye deviation*.

In the same way, it can be demonstrated that during a *prolonged leftward rotation*, a long-lasting deflection of the left horizontal cupula toward the utricle must occur. During prolonged leftward rotation, a *nystagmus to the left* can be observed in the intact animal. Since prolonged artificial deflection of the cupula of the left horizontal ampulla provokes a nystagmus to the left, it can be concluded that the nystagmus to the left during prolonged rotation derives from a deflection of the cupula of the left horizontal ampulla during the ampullopetal endolymph flow toward the utricle.

Finally, the same line of arguments allows concluding that the *after-nystagmus to the left*, which is observed after a longer, rightward rotation in the intact animal, is triggered by a continuing endolymph motion, as must be deduced from the theory by *Mach-Breuer-Brown* and my own experimentally verified deflection of the cupula of the left horizontal ampulla toward the utricle (see also below).

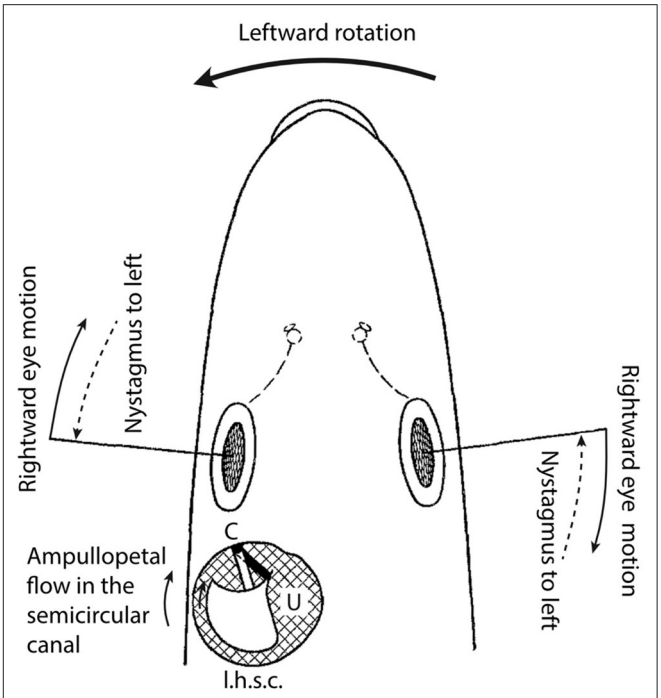

FIGURE 1 | Head of a pike viewed from dorsal with delineated left horizontal semicircular canal and utricle (schematic).

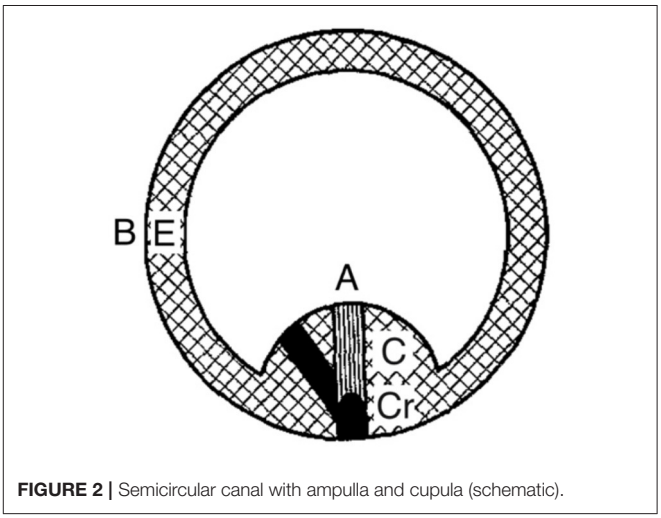

FIGURE 2 | Semicircular canal with ampulla and cupula (schematic).

ON THE THEORY OF CUPULA MOVEMENT

There thus is a clear dependency of the labyrinthine symptoms (eye movements) on the *deflections of the cupula*. The reported observations are thus definitive proof for the validity of the *Mach-Breuer-Brown* theory. In addition, the results of the experimental study allow formulating a theory of the cupula deflection, which will be described following the theoretical work of *Gaede*, *Rohrer,* and *Schmaltz*[26] below.

Figure 2 shows schematic drawings of the semicircular canal, ampulla and cupula. B is the semicircular canal, E, the endolymph within the semicircular canal, A, the ampulla, and C, the mobile cupula, with the crista (Cr) as pivotal point. Because of the endolymph-tight closure, any endolymph movement must induce a cupula movement and *vice versa*. The endolymph is thus mechanically tightly coupled to the cupula[27]. This tight coupling can be accurately demonstrated in experiments. If the semicircular canal cannula (see above) is tightly inserted into the semicircular canal, the cupula will remain in any possible position, depending on the pressure, produced by the tubular system connected to the cannula. Only when the endolymph is given an evasion alternative e.g., by inserting the cannula only loosely into the semicircular canal, the cupula, due to its mechanical force, returns to the average resting position by shifting the endolymph.

Due to the mechanical force of the cupula, the system has a null position from which it can deviate by rotation in the plane of the semicircular canal. The mechanical force of the cupula causes a return to its null position. This theory thus leads to *harmonic*

[25]The deviation during normal rotatory stimulation was observed by *Steinhausen* [see Plügers Arch. 228, 322 (1931)] for the first time in freshly prepared preparations.

[26]*Gaede*: Arch. Ohr. etc. Heilk. 110, 6 (1922). *Rohrer*: See *Rohrer* u. *Masuda*, *Bethes* Handbuch der Physiologie, Bd. 11, S. 985–1101. 1927. *Schmaltz*: Proc. Roy. Soc. Med. sec. otol. Sitzung vom 1. Mai 1931, 374.

[27]See also *Steinhausen*: Arch. Ohr. etc. Heilk. 132, 155 (1932).

equations. The exact equation can be written as follows:

$$m\frac{d^2x}{dt^2} + k\left(\frac{dx}{dt} - \frac{d\xi}{dt}\right) = -a^2\,(x - \xi) \tag{1}$$

In this equation, x is the motion coordinate of the cupula (or rather of the endolymph), ξ the motion coordinate of the wall, *t*, time, m, mass of the endolymph including the relatively small mass of the cupula, *k*, the friction coefficient and a^2, the constant of the mechano-elastic force that causes the cupula to return to the null position. If $a^2 = 0$, this is neglecting the influence of the mechano-elastic force of the cupula on the movement, then:

$$m\frac{d^2x}{dt^2} + k\left(\frac{dx}{dt} - \frac{d\xi}{dt}\right) = 0 \tag{2}$$

Equation (2) is the equation of pure endolymph movement, assumed by *Gaede*[28] and which was at length discussed with respect to rotatory and caloric stimulation by *Schmaltz*.[29]

The equation for the cupula movement Equation (1) can be written as follows:

$$m\frac{d^2x}{dt^2} + k\frac{dx}{dt} = -a^2x + a^2\xi + k\frac{d\xi}{dt} \tag{3}$$

This is the equation of a forced, damped oscillation in which the term $a^2\xi + k\frac{d\xi}{dt}$ can be interpreted as a disturbance function. In order to be able to solve the equation, first of all the disturbance function must be known. The simplest usable case for our purpose is obtained by setting $\frac{d\xi}{dt}$ = constant = *w*.[30] In this case $\xi = \int w dt = wt$. This indicates that during the period in question the rotation velocity of the wall is constant. Thus, for the semicircular canal wall a sudden transition from rest into a movement with constant speed, or *vice versa*, is assumed, an assumption that can be practically met with sufficient approximation.

The equation for the cupula movement Equation (3) for this case is:

$$m\frac{d^2x}{dt^2} + k\frac{dx}{dt} = -a^2x + a^2wt + kw \tag{4}$$

According to the experimental findings, *k* is very large and a^2 is small. The general solution[31] of Equation (4) therefore is:

$$x = \frac{u_0 - w + x_0\beta_2}{\beta_2 - \beta_1} \bullet e^{-\beta_1 t} - \frac{u_0 - w + x_0\beta_1}{\beta_2 - \beta_1} \bullet e^{-\beta_2 t} + w \bullet t \tag{5}$$

Therein, x_0 is the cupula coordinate at the time $t = 0$, u_0 the velocity of the cupula at time t = 0, β_1 and β_2 have the following values:

$$\beta_1 = \frac{k}{2m} + \sqrt{\frac{k^2}{4m^2} - \frac{a^2}{m}}$$

$$\beta_2 = \frac{k}{2m} - \sqrt{\frac{k^2}{4m^2} - \frac{a^2}{m}}$$

Since ξ (i.e., the motion constant of the semicircular canal wall) = *wt* (see above), it follows for the relative motion of the cupula (*z*) with respect to the wall z = x - ξ:

$$Z = \frac{u_0 - w + x_0\beta_2}{\beta_2 - \beta_1} \bullet e^{-\beta_1 t} - \frac{u_0 - w + x_0\beta_1}{\beta_2 - \beta_1} \bullet e^{-\beta_2 t} \tag{6}$$

It is only necessary to insert into this equation the values β_1, β_2 and w and for the initial conditions x_0 and u_0 in order to obtain z, i.e., the cupula deflection as a function of the time *t*.

In the following, the *general character of the cupula movement* will be examined, in particular regarding the dependency on the rotation time or rather the turning angle. Assuming that the rotation is always performed at the same velocity, the rotation times are a direct indicator for the turning angle. It shall therefore be investigated how the cupula movement changes when the turning angle (or the rotation time) changes. In particular, the question is how the cupula movement during small turning angles, i.e., short rotations, differs from those during large turning angles, i.e., long-lasting rotations. Short rotations form in fact the normal way of operation of the vestibular apparatus, as occurs in daily life, while longer-lasting rotations occur only under exceptional circumstances. During short rotations, appropriate compensatory movements, for example the illustrated eye movements are triggered, while during abnormal, longer-lasting rotations a nystagmus and subjective dizziness is provoked. In the calculation, 20 s (=15 divisions in **Figure 3**) is assumed as the longest rotation time, completing 10 full turns. 1 scale mark therefore indicates 240° turn angle. Concerning the cupula movement, only relative

[28] *Gaede, W.*: Arch. Ohr. etc. Heilk. 110, 9 (1922).

[29] *Schmaltz, G.*: Proc. Roy. Soc. Med. sec. otol. Sitzung vom 1. Mai 1931, 374.

[30] *Schmaltz* discusses for the pure endolymph equation [Equation (2) above] (i.e., without consideration of the cupula effect) the case $\frac{d^2\xi}{dt^2} = const$, whereby a homogeneously accelerated motion is thus assumed for the motion of the wall (*Schmaltz:* l.c., p. 371). For constant acceleration (g = const.) the equation is as following: $m\frac{d^2x}{dt^2} + k\frac{dx}{dt} = -a^2x + \frac{a^2}{2}\gamma t^2 + k\gamma t$
The solution of this equation is:

$$x = \frac{u_0 + x_0\beta_2 + \frac{m}{a^2}\gamma\beta_2}{\beta_2 - \beta_1} e^{-\beta_1 t} - \frac{u_0 + x_0\beta_1 + \frac{m}{a^2}\gamma\beta_1}{\beta_2 - \beta_1} e^{-\beta_2 t} + \frac{1}{2}\gamma t^2 - \frac{m}{a^2}\gamma$$

for $a^2 = 0$ (i.e., without consideration of the cupula) the motion equation of the endolymph results in the equation of Schmaltz (*Schmaltz:* l.c., p. 371):

$$m\frac{d^2x}{dt^2} + k\frac{dx}{dt} = k\gamma t$$

and the solution translates into:

$$x = \frac{1}{2}\gamma t^2 + \gamma\frac{m^2}{k^2} - \frac{m}{k}\gamma t - \frac{m^2}{k^2}\gamma e^{-\frac{k}{m}t}$$

[31] See text books on theoretic physics, e.g., *Clemens Schäfer*.

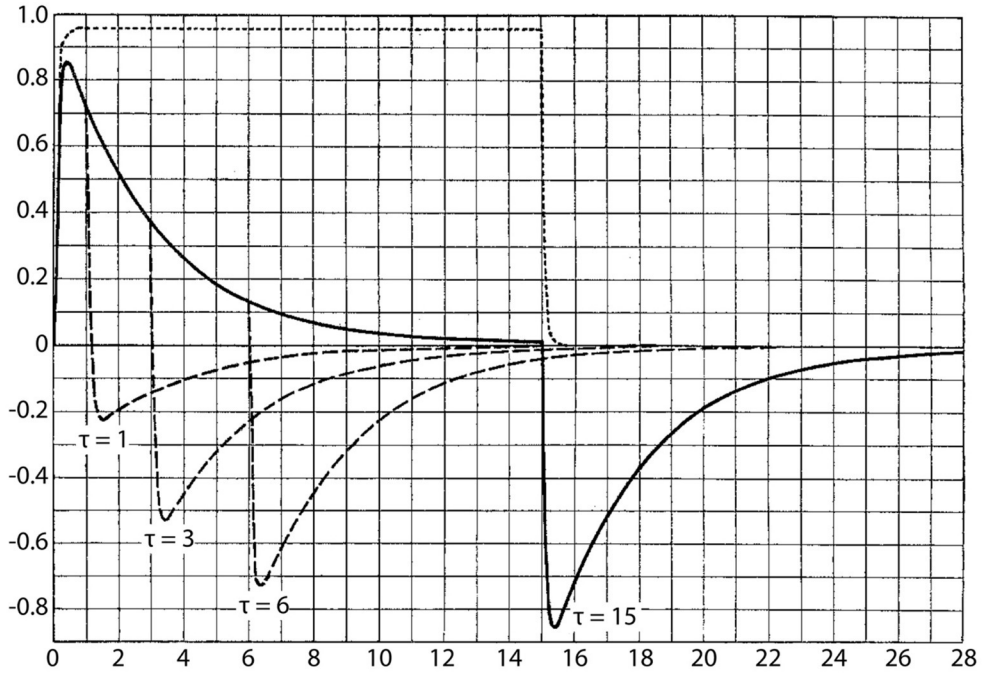

FIGURE 3 | Cupula movement during long rotation periods. Abscissa: time (scale marks 30 = 40 seconds); ordinate, cupula movement as arbitrary scale.

numbers are calculated. From the above indicated prerequisites, the following result, illustrated in **Figure 3**, is obtained.

In **Figure 3**, the abscissa represents time from 0 to 30 (corresponding to 40 s), the ordinate indicates the cupula deflections, plotted arbitrarily from 0 to 1. The assumption is made that the semicircular canal at time t = 0 is put into a uniform rotation at the speed u_0. The solid curve indicates the cupula movement. As can be seen, the cupula very quickly reaches maximum deflection, which in the indicated case assumes a value of 0.85, and then returns very slowly to the resting position. At time 15, i.e., after 20 s, this resting position is essentially reached (theoretically the cupula returns to its resting position only after an infinite amount of time). At time 15, the movement is stopped, i.e., the rotation is suddenly terminated. The solid line indicates the movement of the cupula when stopping. This causes a rapid deflection of the cupula to the other side, with the same magnitude as during the rotation onset, followed by a slow return motion to the resting position, resulting in the same curve as following the onset of the rotation.

Long rotations cause in fact a long-lasting cupula deflection, which is followed by a similar deflection to the other side when the rotation is stopped. Long-lasting cupula deflections are associated with a nystagmus. By additionally considering the events in the corresponding semicircular canal on the other side, the curves demonstrate that a rotational nystagmus during turning is followed after stopping by an oppositely-directed nystagmus.

The curves also explain the long duration of the rotational nystagmus as well as that of the after-nystagmus. The plot also contains the curve representing the endolymph movement (dotted line), as can be deducted from *Gaede*'s theory, assuming i.e., that the mechanical force of the cupula is zero (see above). The endolymph movement is pulsatile, both at the time of rotation onset and at stopping, and thus by itself cannot explain the long duration of the after-effect. Only when considering the cupula, the long duration of the nystagmus and the after-nystagmus becomes explainable.

Figure 3 also shows the cupula movement under the conditions that the stopping occurs before the cupula has reached null position. For example, the curve $\tau = 6$ indicates that at time 6 the rotation is interrupted and corresponding curves after stops at shorter periods are indicated.

For very short rotation periods, the curves would be densely overlapping, thus preventing an overview.

Therefore, **Figure 4** illustrates separately the curves for cupula movements during short rotation periods. Accordingly, the curve $\tau = 0.1$ indicates the cupula deflection calculated when the rotation was stopped after the time $\tau = 0.1$, corresponding to a turning angle of 24°. Such small turning angles, only cause a very brief cupula deflection (a nystagmus can therefore not be triggered) and the post-rotational movement (as well as the after-nystagmus) becomes smaller and smaller and finally imperceptible. Small turning angles thus cause a very different form of cupula movement as large rotation angles: the cupula movement during small turning angles mainly consist of a short deflection with a magnitude that decreases with decreasing turning angles. The analysis thus explains the fact that during small rotations (representing normal

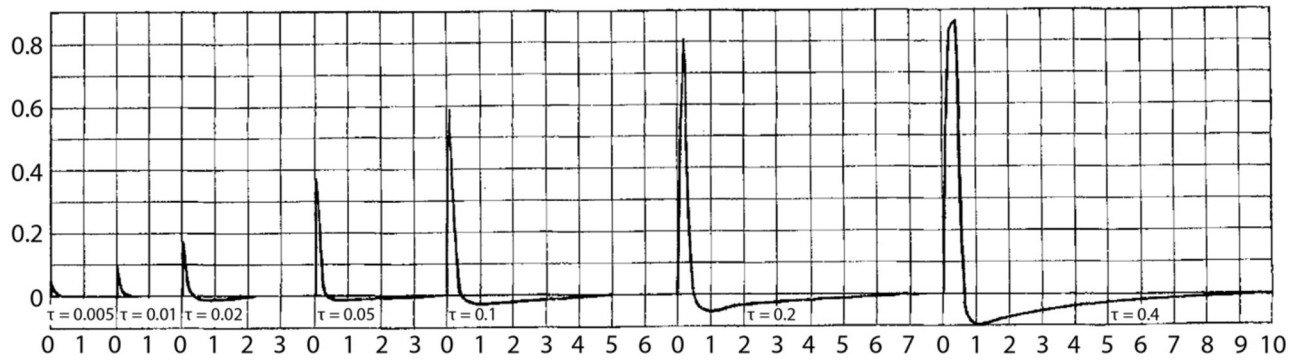

FIGURE 4 | Cupula movement during short rotation periods. Descriptions as in **Figure 3**.

semicircular canal stimuli) it is exclusively the magnitude of the rotation that is differentially perceived. Only during longer-lasting rotations (abnormal semicircular canal stimuli) the perception of the rotation is superimposed and impaired by the gradual return movement of the cupula (nystagmus) as well as by the oppositely-directed negative deflection of the cupula (after-nystagmus) after stopping of the rotation. The curves also show how the duration of the nystagmus and after-nystagmus increases with increasing rotation period and which quantitative relationship can be deduced. Experimentally, this dependency has been particularly well-studied by *Masuda*[32] (see *Rohrer*).

The theory described here only explains the processes in the semicircular canals of the pike. It is well possible that in other animals including humans, adaptations might exist and influence the processes, such as for example different constants compared to those obtained by the experimental observations on the pike labyrinth.

SUMMARY

1. The method, described in earlier studies, also allows visualizing the *cupula* in the *living* pike by ink staining and to determine its mechanical behavior.
2. *Electrical stimulation* does not elicit cupula movements, although the typical labyrinthine symptoms are present, of which only eye movements were observed in the present study. *Brüning's* theory of the cataphoretic deflection of the cupula by electric current does not meet the facts.

   The electric current is effective only in utricle-semicircular canal direction, an inverse direction fails to yield an excitation *(Note by the translators: the asymmetric effect of current stimulation is likely related to the placement of one electrode close to the cupula and the other at a distance; reversal of the polarity would thus yield only a single effective configuration).*
3. Isolated mechanical stimulation of the *left horizontal ampulla* in the living pike while observing the cupula was made as follows: a cannula, connected to a tubing system was inserted into the semicircular canal. Application of pressure to the tube caused a displacement of the endolymph in the semicircular canal. The result was the following:

   (a) The cupula is tightly coupled to the endolymph. Deflections of the cupula can only be reversed if the endolymph moves.
   (b) Deflection of the cupula toward the utricle causes a *movement of both eyes to the right* if the cupula deviation is brief, and a *nystagmus of both eyes to the left*, if the cupula deviation is longer-lasting. Deflection of the cupula toward the semicircular canal fails to yield an excitation.
4. Based on the experimental results, a theory of the cupula movement is established, which closely follows the work of *Gaede, Rohrer* and *Schmaltz* on the theory of endolymph movement.

I am very grateful to Dr. *Erdmann*, Medizinalpraktikant *Ulrich,* and Medizinalpraktikant Dr. *des. Wünn* for their help with the preparations. I also thank the *Notgemeinschaft der Deutschen Wissenschaft* for providing a micromanipulator and a dissecting microscope.

[32]Masuda: Pflügers Arch. 107, 1–65 (1922).

DISCUSSION

In his quest to resolve questions regarding how the semicircular canal cristae transform head motion, through the action of the endolymph, into neuronal signals and eventually into motor commands for eye movements, Steinhausen provided several key features of the mechanism:

(1) he demonstrated that rotational head movements result in relative endolymph flow and a force exerted upon the semicircular canal cupula producing its displacement;
(2) he demonstrated a tight coupling of the cupula with the endolymph;
(3) he demonstrated that, in the pike, unilateral (i.e., *via* a cannula in the left horizontal semicircular canal) small cupula deflections in the ampullopetal direction (toward the utricle) caused compensatory movements of both eyes; oppositely directed (i.e., ampullofugal) unilateral cupula displacements did not produce detectable eye movements.

Collectively, these findings were interpreted to refute other hypotheses concerning endolymph and cupula function that prominently circulated at that time. This was clearly expressed in the summary of the '33 monograph (23): "*These observations indicate that in fact cupula movements cause the excitation of semicircular canals during endolymph flow rather than other changes of the state of the cupula (direct pressure effects, osmotic changes, ion shifts or the like).*" These observations represented hallmark features of the vestibular periphery, which were experimentally demonstrated for the first time (despite limitations concerning the exact mechanical behavior of the cupula, see below). Through these observations Steinhausen recognized the similarity to harmonic oscillations and advanced the quantitative relationship between the force induced by rotational head movements and the mechanical factors influencing cupula motion. In doing so, he conceptualized the sensory transformation of angular head movements. While it wasn't until more than a decade later that van Egmond et al. (25) applied the *torsion pendulum* label to this transformation, it is readily traced back to Steinhausen's seminal observations culminating in the '33 paper (23). This formulation had a tremendous impact on the field of peripheral vestibular physiology by ushering in the first quantitative model of peripheral vestibular function, representing the seed from which numerous quantitative descriptions have grown [reviewed in (29)]. Therefore, while Steinhausen did not originally refer to his model as a torsion-pendulum, he was the first to apply a rigorous mechanical analysis to semicircular canal function and proposed the essential form of the mathematical model that shortly thereafter came to be known by that metaphor (23).

Despite the significance of Steinhausen's biomechanical model of endolymph-cupular interaction (23), the experimental results and subsequent interpretations are associated with significant irony. The principal conclusions regarding endolymph movement and tight coupling with the cupula were based upon the readily-observed cupula displacements. These were documented in the photograph taken during caloric stimulation [Figure 4; in (21)] and the summary schematics illustrating the *swinging-gate* cupula motion profile [Figures 1, 2; in (23)]. However, more recent investigations demonstrated cupular displacements exhibiting much more modest profiles resembling a diaphragm, with its perimeter attached to the ampullary walls and coupled to laminar flow profiles of the endolymph exhibiting considerably smaller magnitudes (30, 31). This discrepancy may be explained by cupulae that became detached from the ampullary walls during Steinhausen's manipulations (e.g., creating the window to observe cupular motion, or during creation of the fenestra through which ink particles were introduced into the endolymph). The irony in Steinhausen's interpretations, then, rests in the strong likelihood that the observations were derived from the non-physiologic condition represented by detached cupulae.

Meanwhile, as a champion of the concept advocating the fundamental importance of interstitial hydrostatic pressure to physiologic function, Witmaack (22) challenged the veracity of Steinhausen's findings from the *in vitro* preparations. Witmaack argued that this turgescence would be lost in the *in vitro* condition, casting the analogy of the cupula to a balloon, and the flaccid condition resulting from the loss of turgor or surface rupture (22). Consequently, Steinhausen worked to improve his methods of preparation so that the observations were closer to the *in vivo* condition. Indeed, the observations from the living pike, being similar to those from the earlier *in vitro* preparations, argued against Witmaack's (22) challenge and supported Steinhausen's claim that large cupula displacements were not a consequence of the *in vitro* condition, *per se*. However, it appears highly likely that his interpretations were based upon observations of detached cupulae, independent of whether they were made under *in vivo* or *in vitro* conditions.

Despite the likelihood that Steinhausen's conclusions were derived from observations of detached (and, therefore, non-physiologic) cupulae, this condition resulted in an overall positive impact on the understanding of the biomechanical characteristics contributing to semicircular canal function. To be sure, cupula detachment would have a profound impact on these characteristics. For example, Rabbitt et al. (31) reported a dramatic reduction in the adaptation time constant in cupulae similarly detached as depicted by Steinhausen (21). However, the detached cupulae actually made it possible for him to observe the rotation-evoked endolymph displacement and coupling with the cupula, fostering the postulates regarding the application of harmonic oscillations and the mechanical factors contributing to endolymph displacement. Ironically, had the preparation been made to retain the normal *in situ* attachments, it is highly unlikely that Steinhausen would have observed the displacement of the central cupula that has been shown to be far less than 1 μm (31). Without these observations, Steinhausen would likely have conceded that sensory transduction was founded in other mechanisms under consideration at that time.

Of course, the alternative mechanism of which Steinhausen was eminently aware was advocated by Mach (10), whereby angular head movements generated pressures acting on the cupula, and implied that the cupula was an integral component of a pressure transducer. We now appreciate that these "competing" hypotheses (e.g., endolymph displacement and pressure generation) are not mutually exclusive, and that pressure differentials across the cupula lead to small

displacements. For example, Oman and Young provided an analytical formulation of pressure generation resulting from angular head movements, which was consistent with human vestibular subjective thresholds (32). They also predicted that pressures acting on the cupula would result in diaphragm-like cupular displacements, profiles that were observed experimentallys shortly thereafter (30). The pressures leading to small cupular displacements (33), in the range of millipascals, have been shown to be sufficient to modulate the discharge in vestibular afferent neurons (34). Therefore, while Steinhausen's view of cupular movement was overzealous, the logic of the generative biomechanical model laid the foundation for decades of vestibular physiology research.

AUTHOR CONTRIBUTIONS

HS translated the original German text to English, contributed to the writing, and editing of the Introduction and Discussion. MGP edited the translations, Introduction, and Discussion. LFH contributed to the writing of the Introduction and Discussion and edited the translations. All authors contributed to the article and approved the submitted version.

FUNDING

This work was supported by the German Science Foundation (Deutsche Forschungsgemeinschaft, CRC 870, B12, Ref. nr. 118803580; STR 478/3-1). The funder had no input to the content or decision to submit for publication.

ACKNOWLEDGMENTS

Permissions for each of the original publications are provided below.

Translated by permission from Springer Nature Customer Service Center GmbH: Springer Nature, Pflüger's Archiv für die gesamte Physiologie des Menschen und der Tiere, Über Sichtbarmachung und Funktionsprüfung der Cupula terminalis in den Bogengangsanipullen des Labyrinthes, Wilhelm Steinhausen, 1927.

Translated by permission from Springer Nature Customer Service Center GmbH: Springer Nature, Pflüger's Archiv für die gesamte Physiologie des Menschen und der Tiere, Über den Nachweis der Bewegung der Cupula in der intakten Bogengangsampulle des Labyrinthes bei der natürlichen rotatorischen und calorischen Reizung, Wilhelm Steinhausen, 1931.

Translated by permission from Springer Nature Customer Service Center GmbH: Springer Nature, Pflüger's Archiv für die gesamte Physiologie des Menschen und der Tiere, Über die Beobachtung der Cupula in den Bogengangsampullen des Labyrinths des lebenden Hechts, Wilhelm Steinhausen, 1933.

REFERENCES

1. Van de Water TR. Historical aspects of inner ear anatomy and biology that undelie the design of hearing and balance prosthetic devices. *Anatomical Rec.* (2012) 295:1741–59. doi: 10.1002/ar.22598
2. Canalis RF, Mira E, Bonandrini L, Hinojosa R. Antonio Scarpa and the discovery of the membranous inner ear. *Otol Neurotol.* (2001) 22:105–12. doi: 10.1097/00129492-200101000-00020
3. Breuer J. Über die function der bogengänge des ohrlabyrinths. *Med Jahrbücher*. (1874) 4:72–124.
4. Retzius G. *Das Gehörorgan der Wirbelthiere*. Stockholm: Samson & Wallin (1881).
5. Bechterew W. Ergebnisse der Durchschneidung des N. acusticus, nebst Erörterung der Bedeutung der semicirculären Canäle für das Körpergleichgewicht. *Archiv Gesamte Phys Menschen Tiere.* (1883) 30:312–47. doi: 10.1007/BF01674334
6. Berthold E. Ueber die Function der Bogengänge des Ohrlabyrinths. *Archiv Ohrenheilkunde.* (1874) 9:77–95. doi: 10.1007/BF01803958
7. Crum Brown A. The sense of rotation and the anatomy and physiology of the semicircular canals of the internal ear. *J Anat Physiol.* (1874) 8(Pt 2):327–31.
8. Ewald JR. *Physiologische Untersuchungen üBer das Endorgan des N. Oktavus*. Wiesbaden: Bergmann (1892).
9. Goltz F. Ueber die physiologische Bedeutung der Bogengänge des Ohrlabyrinths. *Archiv Gesamte Phys Menschen Tiere.* (1870) 3:172–92. doi: 10.1007/BF01855753
10. Mach E. Über den Gleichgewichtssinn. *Mitt Akad Wiss Wien*. (1874) 69:44–51.
11. Lee FS. Study of the senses of equilibrium. *J Physiol.* (1894) 15:311–48.
12. Kubo I. Über die vom N. acusticus ausgelösten Augenbewegungen. II. Mitteilung: Versuche an Fischen. *Pflügers Arch Physiol.* (1906) 115:457–82. doi: 10.1007/BF01677353
13. McNally WJ, Tait J. Ablation experiments on the labyrinth of the frog. *Am J Physiol*. (1925) 75:155–79. doi: 10.1152/ajplegacy.1925.75.1.155
14. Tait J, McNally WJ. Some features of the action of the utricular maculæ (and of the associated action of the semicircular canals) of the frog. *Philos Trans R Soc London Ser B Biol Sci.* (1934) 224:241–86. doi: 10.1098/rstb.1934.0019
15. McNally WJ, Tait J. Some results of section of particular nerve branches to the ampullae of the four vertical semicircular canals of the frog. *Q J Exp Physiol*. (1933) 23:147–96. doi: 10.1113/expphysiol.1933.sp000593
16. Mowrer OH. The electrical response of the vestibular nerve during adequate stimulation. *Science.* (1935) 81:180–1. doi: 10.1126/science.81.2094.180-a
17. Ross DA. Electrical studies on the frog's labyrinth. *J Physiol.* (1936) 86:117–46. doi: 10.1113/jphysiol.1936.sp003348
18. Henn V, Young LR. Ernst Mach on the vestibular organ 100 years ago. *Otorhinolaryngol Relat Spec*. (1975) 37:138–48. doi: 10.1159/000275218
19. Wiest G, Baloh RW. The pioneering work of Josef Breuer on the vestibular system. *Arch Neurol.* (2002) 59:1647–53. doi: 10.1001/archneur.59.10.1647
20. Steinhausen W. Über Sichtbarmachung und Funktionsprüfung der Cupula terminalis in den Bogengangsanipullen des Labyrinthes. *Pflüger's Archiv Gesamte Physiol Menschen Tiere.* (1927) 217:747–55. doi: 10.1007/BF01723723
21. Steinhausen W. Über den Nachweis der Bewegung der Cupula in der intakten Bogengangsampulle des Labyrinthes. *Pflüger's Archiv Gesamte Physiol Menschen Tiere.* (1931) 228:807. doi: 10.1007/BF01755546
22. Wittmaack K. Über den Tonus der Sinnesendstellen des Innenohres. *Archiv Ohren Nasen Kehlkopfheilkunde.* (1929) 120:256–96. doi: 10.1007/BF01583294
23. Steinhausen W. Über die Beobachtung der Cupula in den Bogengangsampullen des Labyrinths des lebenden Hechts. *Pflügers Archiv Euro J Physiol.* (1933) 232:500–12. doi: 10.1007/BF01754806
24. Mayne R. The dynamic characteristics of the semicircular canals. *J Comp Physiol Psychol*. (1950) 43:309–19. doi: 10.1037/h0054827
25. Van Egmond AA, Groen JJ, Jongkees LB. The mechanics of the semicircular canal. *J Physiol*. (1949) 110:1–17. doi: 10.1113/jphysiol.1949.sp004416
26. Goldberg JM, Fernandez C. Physiology of peripheral neurons innervating semicircular canals of the squirrel monkey. 3. Variations

among units in their discharge properties. *J Neurophysiol.* (1971) 34:676–84. doi: 10.1152/jn.1971.34.4.676
27. Groen JJ, Lowenstein O, Vendrik JH. The mechanical analysis of the responses from the end-organs of the horizontal semicircular canal in the isolated elasmobranch labyrinth. *J Physiol.* (1952) 117:329–46. doi: 10.1113/jphysiol.1952.sp004752
28. O'Leary DP, Dunn RF, Honrubia V. Functional and anatomical correlation of afferent responses from the isolated semicircular canal. *Nature.* (1974) 251:225–7. doi: 10.1038/251225a0
29. Paulin MG, Hoffman LF. Models of vestibular semicircular canal afferent neuron firing activity. *J Neurophysiol.* (2019) 122:2548–67. doi: 10.1152/jn.00087.2019
30. McLaren JW, Hillman DE. Displacement of the semicircular canal cupula during sinusoidal rotation. *Neuroscience.* (1979) 4:2001–8. doi: 10.1016/0306-4522(79)90071-X
31. Rabbitt RD, Breneman KD, King C, Yamauchi AM, Boyle R, Highstein SM. Dynamic displacement of normal and detached semicircular canal cupula. *J Assoc Res Otolaryngol.* (2009) 10:497–509. doi: 10.1007/s10162-009-0174-y
32. Oman CM, Young LR. The physiological range of pressure difference and cupula deflections in the human semicircular canal. Theoretical considerations. *Acta Otolaryngol.* (1972) 74:324–31. doi: 10.3109/00016487209128458
33. Yamauchi A, Rabbitt RD, Boyle R, Highstein SM. Relationship between inner-ear fluid pressure and semicircular canal afferent nerve discharge. *J Assoc Res Otolaryngol.* (2002) 3:26–44. doi: 10.1007/s101620010088
34. Rabbitt RD, Yamauchi AM, Boyle R, Highstein SM. How endolymph pressure modulates semicircular canal primary afferent discharge. *Ann N Y Acad Sci.* (2001) 942:313–21. doi: 10.1111/j.1749-6632.2001.tb03756.x

Conflict of Interest: The authors declare that the research was conducted in the absence of any commercial or financial relationships that could be construed as a potential conflict of interest.

frontiers in Neurology

BRIEF RESEARCH REPORT
published: 01 July 2021
doi: 10.3389/fneur.2021.693963

Dizziness and Driving From a Patient Perspective

Roeland B. van Leeuwen[1], Tjard R. Schermer[2], Carla Colijn[3] and Tjasse D. Bruintjes[4,5]*

[1] Department of Neurology Gelre Hospitals, Apeldoorn Dizziness Centre, Gelre Hospitals, Apeldoorn, Netherlands, [2] Department of Epidemiology and Statistics, Apeldoorn Dizziness Centre, Gelre Hospitals, Apeldoorn, Netherlands, [3] Apeldoorn Dizziness Centre, Gelre Hospitals, Apeldoorn, Netherlands, [4] Department of Otorhinolaryngology, Apeldoorn Dizziness Centre, Gelre Hospitals, Apeldoorn, Netherlands, [5] Department of Otorhinolaryngology, Leiden University Medical Center, Leiden, Netherlands

Background: People with dizziness may experience driving-related limitations. Few data are available about the impact of dizziness on driving.

Aim: The aim of this study is to investigate the impact of dizziness on driving, factors related to impairment (age, gender, and type of diagnosis), and the potential consequences for patients' ability to work. We also investigated whether the patients expected and actually received information about their dizziness-related fitness to drive from their physician.

Methods: A cross-sectional, observational study was conducted in the Apeldoorn Dizziness Centre, a tertiary care referral centre for patients with dizziness. A consecutive cohort of patients was asked to complete a study-specific questionnaire about driving.

Results: Between January 1, 2020, and December 20, 2020, 432 patients were included. Fifty-six percent of the patients in this group were female. The average age of patients was 58.3 years (SD 16). Overall, 191 of the 432 patients (44%) experienced limitations related to driving, and 40% of the patients who experienced limitations also experienced limitations to work related to their inability to drive. The subject of fitness to drive had not been discussed with their physician in 92% of the patients, and 24% of the whole patient group indicated that they would have liked to discuss this topic. The following factors, independently from each other, increased the chance of experiencing driving-related limitations: younger age, female sex, and the diagnosis of Meniere's disease.

Conclusion: Dizzy patients, especially younger patients, women, and patients with Meniere's disease, regularly experience limitations related to driving, and this often means that they are unable to work. Driving is hardly ever discussed during a medical consultation. In our opinion, the topic of driving and dizziness should always be addressed during medical consultations in dizzy patients.

Keywords: dizziness, driving, patient perspective, fitness to drive, vertigo

OPEN ACCESS

Edited by:
Michael Strupp, Ludwig Maximilian University of Munich, Germany

Reviewed by:
Jasmine Menant, Neuroscience Research Australia, Australia
Jeremy Hornibrook, University of Canterbury, New Zealand
Louisa Murdin, Guy's and St Thomas' NHS Foundation Trust, United Kingdom

****Correspondence:***
Roeland B. van Leeuwen
r.b.van.leeuwen@gelre.nl

Specialty section:
This article was submitted to Neuro-Otology, a section of the journal Frontiers in Neurology

Received: *12 April 2021*
Accepted: *26 May 2021*
Published: *01 July 2021*

Citation:
van Leeuwen RB, Schermer TR, Colijn C and Bruintjes TD (2021) Dizziness and Driving From a Patient Perspective. Front. Neurol. 12:693963. doi: 10.3389/fneur.2021.693963

INTRODUCTION

Dizziness is a common presenting complaint in patients, both in primary care and in the hospital. Dizziness and vertigo may be associated with significant morbidity and may have a profound impact on the quality of life, especially in the older population (1) This means that it is important to establish an accurate diagnosis and treatment plan quickly, even though dizziness and vertigo often has a benign origin.

Few data are available about the impact of dizziness on driving in patients with dizziness (2–4). At the same time, the (in)ability to drive can have a large impact on the quality of life of these patients (5). A number of factors play a role in deciding whether a patient with dizziness and vertigo should be allowed to drive. What does the national law say about driving restrictions? Are these restrictions known by the health professionals and/or the patients? Are patients informed by health professionals about the potential restrictions? Which considerations play a role in the patient's decision whether or not to drive?

As far as we know, the question how patients with dizziness deal with driving has only been investigated in three previous studies (2–4). Because we wanted to know what percentage of dizzy patients experience inability to drive, we performed an observational study in this patient group. The research questions focused on the frequency of impairment to driving in patients with dizziness, factors related to impairment (age, gender and type of diagnosis), and the potential consequences for the patients' ability to work. Furthermore, we wanted to investigate whether the patients expected and actually received information about fitness to drive from their physician.

METHODS

A cross-sectional, observational study was conducted in the Apeldoorn Dizziness Centre—a tertiary care referral centre for patients with dizziness as their main complaint. We used the term "dizziness" to describe the complaint from a patient perspective. The terms "dizziness and vertigo" were used as an umbrella term to describe the symptoms from a doctor's point of view (6).

In our centre, all patients routinely complete several questionnaires and undergo a physical examination and advanced audiovestibular testing. During a joint consultation with an ENT surgeon and a neurologist, the diagnosis is made in consensus between the two specialties. In the period between January 1, 2020, and December 20, 2020, a consecutive cohort of patient was asked to complete a study-specific questionnaire about driving. Only those patients who used to drive before their dizziness complaints started were included in the study. The questions that were asked are set out in **Table 1**. The entire patient sample was asked to respond to questions 1, 6, and 7. Questions 2, 3, 4, and 5 were only applicable for patients who experienced limitations related to driving. For all patients, the following data were collected from their medical records: sex, age, primary diagnosis, and (if applicable) a second diagnosis.

The local ethics committee of Gelre hospitals authorized the study and patients provided written informed consent for the use of information from their medical records and the completed questionnaires for the study.

Statistical Analysis

Demographic characteristics and diagnoses underlying the dizziness and vertigo were compared between two subgroups of patients (i.e., those with and those without driving limitations) using Student's *t*-test (for age) and Chi-square tests (for sex and diagnoses). Multivariate logistic regression analysis was performed to calculate odds ratios (ORs) for experiencing limitations due to dizziness related to driving as the dichotomous dependent variable and the patient's age, sex, and diagnoses underlying the dizziness as the independent variables. We categorized the patients in various age groups. Only diagnoses with a prevalence in the study population of at least five patients with and five patients without limitations due to dizziness while driving were included in the logistic regression model (i.e., vestibular migraine, unknown unilateral vestibular hypofunction, bilateral vestibular hypofunction, vestibular paroxysmia, Meniere's disease, vestibular neuritis, BPPV, and anxiety disorder/hyperventilation syndrome). Using likelihood ratio-based backward stepwise elimination of variables, the initial full model was reduced to a final model. Goodness of fit of the logistic regression models was assessed using Hosmer and Lemeshow test. All analyses were performed using SPSS (IBM SPSS Statistics for Windows, Version 25.0. Armonk, NY: IBM Corp.). $p < 0.05$ were considered statistically significant in all analyses.

RESULTS

Overall, 432 patients were included in the study. Fifty-six percent of the patients in this group was female. The average age of patients was 58.3 years (SD 16).

The most frequent diagnoses were hyperventilation/anxiety (34%), benign paroxysmal positional vertigo (BPPV, 22%), Meniere's disease (7%), vestibular migraine (6%), vestibular neuritis (5%), vestibular paroxysm (4%), bilateral vestibular hypofunction (3%), and benign recurrent vertigo (2%). No diagnosis could be made in 13% of the patients. A second diagnosis was made in 22.5% of the patients.

The answers to the questions in the questionnaire are set out in **Table 1**. Overall, 191 of the 432 patients (44%) experienced limitations related to drive, and 40% of the patients who experienced limitations also experienced limitations to work related to their inability to drive. The subject of driving had not been discussed with their physician in 92% of the patients, and 24% of the whole patient group indicated that they would have liked to discuss this topic.

The data of the groups without and with limitations are presented in **Table 2**.

The following factors, independently from each other, influenced the chance of experiencing driving limitations: age [compared to patients aged ≥71 years, the three subgroups below the age of 60 all showed statistically significant ORs > 3; being 1 year older reduced the risk (i.e., OR = 0.96; 95% CI 0.95 to 0.98)], sex {being a female increased the risk [OR = 1.99

TABLE 1 | Answers to questionnaire about limitations in driving in 432 dizziness patients of the tertiary care referral center.

	Questionnaire	*n*	
1	Did you experience driving-related limitations as a result of your dizziness?	432	Yes: 44.2% No: 55.8%
2	How many periods have you experienced in which you were unable to drive?	185	1–5 periods: 60% 6–10 periods: 11% >10 periods: 29%
3	For how long have you had dizziness complaints?	190	1–6 months: 25%, 6–12 months: 16% >12 months: 59%
4	What was the length of the longest period in which you were unable to drive?	184	1–6 days: 30% 1–4 weeks: 26% 1–3 months: 23% >3 months: 21%
5	Were you unable to work as a result of the inability to drive?	173	Yes: 40% No: 60%
6	Did your doctor inform you about potential restrictions on driving?	406	Yes: 8% No: 92%
7	Did you miss receiving information about dizziness and driving?	405	Yes: 24% No: 76%

TABLE 2 | Characteristics of the total study population and the subgroups with and without limitations in driving.

Variables	Total group (*n* = 432)	Group without limitations (*n* = 241)	Group with limitations (*n* = 191)	*p*-value
Female (%)	243 (56)	116 (48)	127 (67)	<0.001
Age in years (mean, SD)	58.3 (16)	62.6 (16)	52.9 (15)	<0.001
Age, in categories (%)				<0.001
≤40 years	68 (16)	26 (11)	42 (22)	
41–50 years	69 (16)	23 (10)	46 (24)	
51–60 years	83 (19)	41 (17)	42 (22)	
61–70 years	87 (20)	59 (24)	28 (15)	
≥71 years	125 (29)	92 (38)	33 (17)	
Meniere's disease (%)	29 (7)	10 (4)	19 (10)	0.020
Vestibular migraine (%)	26 (6)	9 (4)	17 9)	0.040
BPPV (%)	93 (22)	53 (22)	40 (21)	0.815
Hyperventilation/anxiety (%)	149 (34)	75 (31)	74 (39)	<0.001
Unknown unilateral vestibular hypofunction (%)	20 (5)	7 (4)	13 (3)	0.066
Benign recurrent vertigo (%)	9 (2)	7 (3)	2 (1)	0.310
Bilateral vestibular hypofunction (%)	13 (3)	6 (3)	7 (4)	0.575
Vestibular paroxysmia (%)	15 (4)	9 (4)	6 (3)	0.797
Vestibular neuritis (%)	23 (5)	13 (5)	10 (5)	1.000

BPPV, Benign paroxysmal positional vertigo; SD, standard deviation.

(95%CI 1.30 to 3.05)]}, and Meniere's disease {being diagnosed with Meniere's disease increased the risk [OR = 3.90 (95%CI 1.70 to 8.94) compared to other diagnoses underlying the dizziness; see **Table 3**]}.

DISCUSSION

Our study shows that a rather high percentage of patients with dizziness and vertigo (44%), who have been seen in a tertiary care centre, experience limitations related to driving. Limitations were more frequent among younger patients, women, and patients diagnosed with Meniere's disease. In only a few cases had the subject of driving been discussed with the health professional.

It is not clear why younger patients experience more limitations than elderly patients. It is possible that younger patients use their car more frequently than elderly patients for work, leisure, or both. Furthermore, they might make more use of the motorway. We cannot explain why women experience more limitations while driving. Perhaps, because women generally drive more carefully than men, dizzy women may experience

TABLE 3 | Results of the multivariate logistic regression model for associations between experiencing driving limitations due to dizziness and vertigo and patient demographic characteristics and underlying diagnoses ($n = 432$).

	Reference	OR	95% CI	*p*-value
Full model				
Female	Male	1.92	1.24, 2.97	0.004
Age categories				
≤40 years	≥71 years	4.70	2.34, 9.44	<0.001
41–50 years	≥71 years	6.52	3.22, 13.20	<0.001
51–60 years	≥71 years	3.15	1.67, 5.94	<0.001
61–70 years	≥71 years	1.28	0.68, 2.41	0.441
Meniere's disease	No Meniere's disease	4.99	2.08, 11.95	<0.001
Vestibular migraine (VM)	No VM	1.90	0.83, 4.38	0.131
BPPV	No BPPV	1.65	0.94, 2.89	0.078
Anxiety disorder	No anxiety disorder	1.84	0.83, 4.06	0.131
Hyperventilation	No hyperventilation	0.99	0.61, 1.63	0.977
Unknown unilateral vestibular hypofunction (UUVH)	No UUVH	0.88	0.34, 2.28	0.796
Bilateral vestibular hypofunction (BVH)	No BVH	2.38	0.80, 7.10	0.121
Vestibular paroxysmia (VP)	No VP	1.84	0.61, 5.49	0.277
Vestibular neuritis (VN)	No VN	1.24	0.49, 3.11	0.654
Reduced model*				
Age categories				
≤40 years	≥71 years	4.33	2.26, 8.29	<0.001
41–50 years	≥71 years	5.51	2.86, 10.63	<0.001
51–60 years	≥71 years	2.89	1.58, 5.30	0.001
61–70 years	≥71 years	1.32	0.71, 2.45	0.378
Female	Male	1.99	1.30, 3.05	0.002
Meniere's disease	No Meniere's disease	3.90	1.70, 8.94	0.001

CI, confidence interval; OR, odds ratio.

**Using backward stepwise elimination of variables from the full model.*

more limitations in driving than men (7). The percentage of patients with driving limitations in our study is higher than found in previous studies (14–35%) (2–4). It should be noted that in one of these studies, only patients with Meniere's disease were included (4). The higher prevalence of experiencing driving-related limitations among patients with Meniere's disease confirms the findings reported by Cohen et al. (3).

In 40% of the patients with limitations related to driving, this resulted in absence from work. Therefore, the inability to drive has major consequences for a large group of patients with dizziness and vertigo. We have been unable to find data in other published studies on the impact of not being able to drive for the patient's ability to work.

In only 8% of the patients, the topic of fitness to drive had been discussed with the patient's physician. Sindwani's study shows that 10% of dizzy patients received a negative advice about driving (2). While a significant number of patients in our study indicated that they would have liked more clarity on this, and while the Dutch government assumes that health professionals are under an obligation to inform patients about potential limitations related to driving, in 92% of the patients with dizziness and vertigo in our study, the topic of driving was not discussed. This could be because doctors are not aware of the requirements imposed by national law (8, 9). Another explanation could be that doctors in the Netherlands regard the current legislation as too strict. As a result, they might decide not to discuss this topic with their patients. Previous studies have shown that many patients (50–60%) do not intend to comply with the imposed restrictions on driving (2, 3).

A limitation of our study may be that it was conducted in a tertiary centre. This means that we see a selection of patients with often more severe complaints. Moreover, our study does not show why patients with dizziness and vertigo often experience the inability to drive. This could be because of physical complaints or because of insecurity or anxiety. Our study did not aim at getting more clarity about these or other potential explanations. As to the question about inability to work, we do not know how many patients were in fact employed or self-employed.

Further research on the reasons for the limitations with respect to driving and the possibility of dealing with these limitations through advice or treatment is warranted.

In conclusion, dizzy patients, especially younger patients, women, and patients with Meniere's disease, regularly experience limitations related to driving, and this often means that they are unable to work. Driving is hardly ever discussed during the medical consultation. As such, doctors should always discuss the

topic of driving and dizziness as part of their management of dizzy patients.

DATA AVAILABILITY STATEMENT

The original contributions presented in the study are included in the article/supplementary material, further inquiries can be directed to the corresponding author/s.

AUTHOR CONTRIBUTIONS

RL, TS, and TB contributed to conception and design of the study. CC organized the database. TS performed the statistical analysis. RL wrote the first draft of the manuscript. TS, CC, and TB wrote sections of the manuscript. All authors contributed to manuscript revision, read, and approved the submitted version.

REFERENCES

1. Dros J, Maarsingh OR, Beem L, van der Horst HE, ter Riet G, Schellevis FG, et al. Impact of dizziness on everyday life in older primary care patients: a cross-sectional study. *Health Qual Life Outcomes.* (2011) 9:44. doi: 10.1186/1477-7525-9-44
2. Sindwani RAJ, Parnes LS, Goebel JA, Cass SP. Approach to the vestibular patient and driving: a patient perspective. *Otolaryngol Head Neck Surg.* (1999) 121:13–7. doi: 10.1016/S0194-5998(99)70115-4
3. Cohen HS, Wells J, Kimball T, Owsley C. Driving disability and dizziness. *J Safety Res.* (2003) 34:361–9. doi: 10.1016/j.jsr.2003.09.009
4. Pyykkö I, Manchaiah V, Zou J, Levo H, Kentala E. Driving habits and risk of traffic accidents among people with Meniere's disease in Finland. *J Int Adv Otol.* (2019) 5:289–95. doi: 10.5152/iao.2019.5915
5. Chihuri S, Mielenz TJ, DiMaggio CJ, Betz ME, DiGuiseppi C, Jones VC, et al. Driving cessation and health outcomes in older patients. *J Am Geriatr Soc.* (2016) 64:332–41. doi: 10.1111/jgs.13931
6. Bisdorff A, Von Brever M, Lempert, T, Newman-Toker, DE. Classification of vestibular symptoms: towards an international classification of vestibular disorders. *J Vestib Res.* (2009) 19:1–3. doi: 10.3233/VES-2009-0343
7. Aldred R, Johnson R, Jackson C, Woodcock J. How does mode of travel affect risks posed to other road users? An analysis of English road fatality data, incorporating gender and road type. *Inj. Prev.* (2021) 27:71–6. doi: 10.1136/injuryprev-2019-043534
8. Caruana P, Hughes AR, Lea RA, Lueck CJ. Australian driving restrictions: how well do neurologists know them? *Intern Med J.* (2018) 48:1144–9. doi: 10.1111/imj.14026
9. Evans AS, Eng CY. Driving and otolaryngology: do we know the rules? *J Laryngol Otol.* (2006) 120:181–4. doi: 10.1017/S0022215105006663

Conflict of Interest: The authors declare that the research was conducted in the absence of any commercial or financial relationships that could be construed as a potential conflict of interest.

Advantages of publishing in Frontiers

OPEN ACCESS
Articles are free to read for greatest visibility and readership

FAST PUBLICATION
Around 90 days from submission to decision

HIGH QUALITY PEER-REVIEW
Rigorous, collaborative, and constructive peer-review

TRANSPARENT PEER-REVIEW
Editors and reviewers acknowledged by name on published articles

Frontiers
Avenue du Tribunal-Fédéral 34
1005 Lausanne | Switzerland

Visit us: www.frontiersin.org
Contact us: frontiersin.org/about/contact

REPRODUCIBILITY OF RESEARCH
Support open data and methods to enhance research reproducibility

DIGITAL PUBLISHING
Articles designed for optimal readership across devices

FOLLOW US
@frontiersin

IMPACT METRICS
Advanced article metrics track visibility across digital media

EXTENSIVE PROMOTION
Marketing and promotion of impactful research

LOOP RESEARCH NETWORK
Our network increases your article's readership